

30 NOV 1999

Final Report
AFOSR Grant F49620-6-1-0462

September 1, 1996 – August 31, 1999

HIERARCHICAL ADAPTIVE MODELING

Submitted to:

Department of the Air Force
Air Force Office of Scientific Research
801 North Randolph Street, Room 732
Washington, DC 20011

Attention: Major Brian Sanders

Submitted by:

Ahmed K. Noor
Ferman W. Perry Professor of
Aerospace Structures and Applied Mechanics

SEAS Report No. UVA/525856/CE00/101
November 1999

DEPARTMENT OF CIVIL ENGINEERING

5388a

Reproduced From
Best Available Copy

SCHOOL OF
ENGINEERING 
& APPLIED SCIENCE

University of Virginia
Thornton Hall
Charlottesville, VA 22903

DTIC QUALITY INSPECTED 3

19991215 092

UNIVERSITY OF VIRGINIA
School of Engineering and Applied Science

The University of Virginia's School of Engineering and Applied Science has an undergraduate enrollment of approximately 1,500 students with a graduate enrollment of approximately 600. There are 160 faculty members, a majority of whom conduct research in addition to teaching.

Research is a vital part of the educational program and interests parallel academic specialties. These range from the classical engineering disciplines of Chemical, Civil, Electrical, and Mechanical and Aerospace to newer, more specialized fields of Applied Mechanics, Biomedical Engineering, Systems Engineering, Materials Science, Nuclear Engineering and Engineering Physics, Applied Mathematics and Computer Science. Within these disciplines there are well equipped laboratories for conducting highly specialized research. All departments offer the doctorate; Biomedical and Materials Science grant only graduate degrees. In addition, courses in the humanities are offered within the School.

The University of Virginia (which includes approximately 2,000 faculty and a total of full-time student enrollment of about 17,000), also offers professional degrees under the schools of Architecture, Law, Medicine, Nursing, Commerce, Business Administration, and Education. In addition, the College of Arts and Sciences houses departments of Mathematics, Physics, Chemistry and others relevant to the engineering research program. The School of Engineering and Applied Science is an integral part of this University community which provides opportunities for interdisciplinary work in pursuit of the basic goals of education, research, and public service.

REPORT DOCUMENTATION PAGE

AFRL-SR-BL-TR-99-

Public reporting burden for this collection of information is estimated to average 1 hour per response, including the time for gathering and maintaining the data needed, and completing and reviewing the collection of information. Send comments regarding this burden estimate or any other aspect of this collection of information, including suggestions for reducing this burden, to Washington Headquarters Services, Directorate for Information Operations and Reports, 1215 Jefferson Davis Highway, Suite 1204, Arlington, VA 22202-4302, and to the Office of Management and Budget, Paperwork Reduction Project (0334-0187).

0283

1. AGENCY USE ONLY (Leave Blank)		2. REPORT DATE November 1999	3. REPORT TYPE AND DATES COVERED Final Report - September 1, 1996 - August 31, 1999	
4. TITLE AND SUBTITLE Hierarchical Adaptive Modeling			5. FUNDING NUMBERS F49620-6-1-0462	
6. AUTHORS Ahmed K. Noor				
7. PERFORMING ORGANIZATION NAME(S) AND ADDRESS(ES) University of Virginia School of Engineering and Applied Science Dept. of Civil Engineering Charlottesville, VA 22903-2442			8. PERFORMING ORGANIZATION REPORT NUMBER SEAS Report No. UVA/525856/CE00/101	
9. SPONSORING / MONITORING AGENCY NAME(S) AND ADDRESS(ES) Air Force Office of Scientific Research 801 North Randolph Street, Room 732 Washington, DC 20011			10. SPONSORING / MONITORING AGENCY REPORT NUMBER	
11. SUPPLEMENTARY NOTES				
12a. DISTRIBUTION STATEMENT A DISTRIBUTION STATEMENT A Approved for Public Release Distribution Unlimited			12b. DISTRIBUTION CODE	
13. ABSTRACT (Maximum 200 words) See Report Text.				
14. SUBJECT TERMS			15. NUMBER OF PAGES	
			16. PRICE CODE	
17. SECURITY CLASSIFICATION OF REPORT None	18. SECURITY CLASSIFICATION OF THIS PAGE None	19. SECURITY CLASSIFICATION OF ABSTRACT UL	20. LIMITATION OF ABSTRACT UL	

TABLE OF CONTENTS

ABSTRACT	3
RESEARCH OBJECTIVES	3
RESEARCH ACCOMPLISHMENTS	3
APPENDIX I - Abstracts of Papers	
APPENDIX II - List of Presentations	

HIERARCHICAL ADAPTIVE MODELING

AFOSR Grant F49620-96-1-0462

Abstract

Computational procedures are developed for evaluating the hierarchical sensitivity coefficients of the nonlinear response of composite and sandwich structures. The hierarchical sensitivity coefficients measure the sensitivity of the response to three sets of interrelated parameters; namely, panels (or shells), layer and micromechanical parameters. The computational procedure is applied to the nonlinear static and postbuckling responses of composite shells and panels, as well as to sandwich structures with composite face sheets. The sensitivity coefficients are used in conjunction with fuzzy set techniques to study the range of variation of various response quantities associated with pre-selected variations of the major parameters.

Research Objectives

The overall goal of this research is to develop effective hierarchical adaptive modeling strategies for predicting the response and failure of complex structures. The strategies are used in simulating phenomena occurring at disparate spatial and time scales taking account of the uncertainties in material and other system properties, and using reasonable computer resources. The strategies are based on: a) developing practical methods for the accurate calculation of transverse stresses; b) evaluating the sensitivity of the structural response to variations in material parameters associated with a hierarchy of models used in describing phenomena occurring at different length scales, and identifying the material parameters which have the most impact on the response quantities of interest; c) studying the range of variation of various response quantities associated with pre-selected variations of the major parameters; and d) using multiple mathematical models, as well as hybrid deterministic/non-deterministic models, in different regions of the structure to take advantage of efficiencies gained by matching the model to the expected response in each region.

The scope of the work includes nonlinear and postbuckling responses of composite and sandwich panels. Stiffened and unstiffened panels with and without cutouts are considered.

Research Accomplishments

The results of the research conducted under this grant are included in sixteen publications. The abstracts of the papers are given in Appendix I. Eight technical presentations were made based on the studies made under this grant and are listed in Appendix II.

The research activities can be grouped into three categories:

Practical Methods for the Accurate Determination of Transverse Normal Stresses.

A two-stage computational procedure has been developed for the accurate determination of transverse normal stresses in composite and sandwich panels. The procedure is based on a posteriori determination of the shape of the displacement variation in the thickness direction. In the first stage, a first-order shear deformation theory is used for evaluating the average through-the-thickness displacements and strains as well as the in-plane stress components.

Three-dimensional continuum equations are then used to evaluate the transverse shear and normal stresses and strains. In the second stage, the strains are integrated to obtain the distributions of the displacement components in the thickness direction. The Rayleigh-Ritz technique is applied to

obtain a modified displacement field in the panel. The in-plane stresses are calculated and the transverse shear and normal stresses are determined from the equations of equilibrium. The second stage is repeated until convergence of the transverse normal stresses is achieved.

The effectiveness of the procedure is demonstrated by means of numerical examples of flat rectangular sandwich panels with composite face sheets, subjected to thermomechanical loadings. The results obtained by using the foregoing computational procedure, with a single application of Rayleigh-Ritz technique, were found to be in close agreement with those obtained by using three-dimensional continuum models for each of the face sheet layers and the core.

Evaluation of Hierarchical Sensitivity Coefficients.

An efficient computational procedure has been developed for evaluating the hierarchical sensitivity coefficients of sandwich panels with composite face sheets. The computational procedure consists of evaluating the sensitivity coefficients with respect to each of the stiffnesses of the sandwich structure. The sensitivity coefficients with respect to the effective material parameters of the face sheets and core layers, and micromechanical properties (viz., fiber, matrix, core and interface properties) are then computed as linear combinations of the sensitivity coefficients with respect to the structural stiffnesses. If the panel stiffnesses are uniform, and the constitutive relations of the panel, layer and the constituents are linear, the coefficients in the linear combinations are constants and need to be generated only once for each panel, even when the response is linear.

Uncertainty Analysis.

A computational procedure has been developed for uncertainty analysis. The procedure is based on treating the major parameters of the structure (identified by the hierarchical sensitivity coefficients) as fuzzy parameters, and using fuzzy set techniques to provide information about the range and variation of possible responses, associated with selected ranges and variations of the major structural parameters.

The procedure developed after improvements will allow commercial deterministic analysis codes to perform uncertainty analysis. This can be accomplished by modifying the input (to include the variation in the major parameters) and adding a postprocessor to generate the range of variation of the response quantities. The resulting program can serve as a designer's tool kit. See Fig. 1.

Summary of Recent Accomplishments/New Findings

1. Transverse normal and shear stresses are important for predicting the onset of some of the damage mechanisms in composite and sandwich panels. Until now, no practical method was available for the accurate determination of transverse normal stresses, particularly for thermal loading. The computational procedure developed in this study is a step towards meeting this need. The procedure can be incorporated, as a post-processing module, in commercial finite element programs.
2. The design of future complex air vehicles envisioned by the Air Force must take uncertainties and risk into consideration. The procedure developed in this study will allow commercial deterministic analysis codes to perform uncertainty analysis. This can be accomplished by modifying the input (to include the variation in the major structural and material parameters), and adding a post-processor to generate the range of variation of the response quantities.

Proposed Future Studies

Based on the work completed under this grant, the following research tasks are proposed:

- Extending the hierarchical sensitivity analysis to the sub-component and component levels - see Fig. 2.
- Application of hierarchical sensitivity coefficients to smart materials/structures with strong coupling between mechanical, electrical, thermal and possibly magnetic field.
- Improving the efficiency of the uncertainty analysis, through the use of rapid reanalysis techniques, in conjunction with the hierarchical sensitivity coefficients, in generating the responses associated with variations in the major structural parameters. The procedure will be applied to stiffened composite and sandwich panels with and without cutouts.
- Incorporation of the hierarchical sensitivity analysis into a hierarchical adaptive modeling strategy, based on using multiple mathematical models in different regions of the structure to take advantage of efficiencies gained by matching the model to the expected response in each region.

Publications

List peer-reviewed publications submitted and/or accepted during the period October 1, 1996-September 30, 1999 period :

1. Karaoglan, L., Noor, A. K. and Kim, Y. H., "Frictional Contact/Impact Response of Textile Composite Structures," *Composite Structures*, Vol. 37, No. 2, Feb. 1997, pp. 269-280.
2. Noor, A. K., Starnes, Jr., J. H. and Peters, J. M., "Thermomechanical Buckling and Postbuckling Responses of Composite Panels with Skewed Stiffeners," *Finite Elements in Analysis and Design*, Vol. 27, No. 2, Oct. 1997, pp. 193-214.
3. Burton, W. S. and Noor, A. K., "Assessment of Continuum Models for Sandwich Panel Honeycomb Cores," *Computer Methods in Applied Mechanics and Engineering*, Vol. 145, 1997, pp. 341-360.
4. Karaoglan, L. and Noor, A. K., "Space Time Finite Element Methods for the Sensitivity Analysis of Contact/Impact Response of Axisymmetric Composite Structures," *Computer Methods in Applied Mechanics and Engineering*, Vol. 144, Nos. 3-4, May 1997, pp. 371-389.
5. Noor, A. K., Starnes, Jr., J. H. and Peters, J. M., "Curved Sandwich Panels Subjected to Temperature Gradient and Mechanical Loads," *Journal of Aerospace Division, ASCE*, Vol. 10, No. 4, Oct. 1997, pp. 143-161.
6. Xu, K. and Noor, A. K., "Predictor-Corrector Finite Element Approach for Electroelastic Analysis of Hybrid Composite Plates," *Computer Methods in Applied Mechanics and Engineering*, Vol. 147, Nos. 1-2, July 1997, pp. 139-145.
7. Noor, A. K., "Computational Structures Technology - Leap Frogging into the Twenty-First Century," in *Advances in Computational Structures Technology*, B.H.V. Topping (ed.), Civil-Comp Press, Edinburgh, U.K., 1996, pp. 1-18; also, *Computers and Structures*, Vol. 73, Nos. 1-5, Sept. 1999, pp. 1-31.

8. Noor, A. K., "Some Future Directions of Computational Structures Technology," in *Advances in Computational Engineering Science*, S. N. Atluri and G. Yagawa (eds.), Tech Science Press, Forsyth, GA, 1997, pp. 502-507.
9. Rolfes, R., Noor, A. K. and Sparr, H., "Evaluation of Transverse Thermal Stresses in Composite Plates Based on First-Order Shear Deformation Theory," *Computer Methods in Applied Mechanics and Engineering*, Vol. 167, Nos. 3-4, Dec. 1998, pp. 355-368.
10. Noor, A. K., "Recent Advances in Sensitivity Analysis for Nonlinear Structural Mechanics Problems," in *Discretization Methods in Structural Mechanics*, Proc. IUTAM/IACM Symposium on Discretization Methods in Structural Mechanics II, Vienna, Austria, June 2-6, 1997, H. A. Mang and F. G. Rammerstorfer (eds.), Kluwer Academic Publishers, Dordrecht, The Netherlands, 1999, pp. 207-216.
11. Noor, A. K. and Peters, J. M., "Analysis of Curved Sandwich Panels with Cutouts Subjected to Combined Temperature Gradient and Mechanical Loads," in *Analysis and Design Issues for Modern Aerospace Vehicles - 1997*, G. J. Simitses (ed.), Proc., ASME International Congress and Exposition, Dallas, TX, Nov. 17-21, 1997, AD Vol. 55, ASME, 1997, pp. 293-310; also *Journal of Sandwich Structures and Materials*, Vol. 1, Jan. 1999, pp. 42-59.
12. Noor, A. K. and Peters, J. M., "Nonlinear Analysis of Curved Composite Panels Subjected to Combined Temperature Gradient and Mechanical Loads," in *Analysis and Design Issues for Modern Aerospace Vehicles - 1997*, G. J. Simitses (ed.), Proc., ASME International Congress and Exposition, Dallas, TX, Nov. 17-21, 1997, AD Vol. 55, ASME, 1997, pp. 143-158; also, with different title, "Analysis of Composite Panels Subjected to Thermo-mechanical Loads," *Journal of Aerospace Engineering*, ASCE, Vol. 12, No. 1, Jan. 1999, pp. 1-17.
13. Noor, A. K., Starnes, Jr., J. H. and Peters, J. M., "Uncertainty Analysis of Composite Structures," in *Recent Advances and Future Trends in Composite Materials and Structures*, special issue of *Computer Methods in Applied Mechanics and Engineering* (to appear).
14. Noor, A. K. and Malik, M., "Accurate Determination of Transverse Normal Stresses in Sandwich Panels Subjected to Thermomechanical Loadings," *Computer Methods in Applied Mechanics and Engineering*, Vol. 178, 1999, pp. 431-443.
15. Malik, M. and Noor, A. K., "Accurate Determination of Transverse Normal Stresses in Hybrid Laminated Panels Subjected to Electro-thermo-mechanical Loadings," *International Journal for Numerical Methods in Engineering* (to appear).
16. Noor, A. K. and Malik, M., "An Assessment of Five Modeling Approaches for Thermo-mechanical Stress Analysis of Laminated Composite Panels," *Computational Mechanics* (to appear).

Appendix I

Abstracts of Publications

Frictional Contact/Impact Response of Textile Composite Structures

Levent Karaoglan, A. K. Noor and Y. H. Kim

Composite Structures, Vol. 37, No. 2, Feb. 1997, pp. 269-280.

The results of a detailed study of the frictional contact/impact response of axisymmetric textile composite structures are presented. The structures are assumed to consist of an arbitrary number of perfectly bonded layers of woven fabric or braided preforms. The material of each layer is assumed to be hyperelastic and the effect of geometric nonlinearity is included. The equations of motion of the structure are established in the current configuration and a displacement finite element model is used for the spatial discretization. A Coulomb friction model is used and the temporal integration is performed by using an explicit central difference scheme. Both the dynamic response and the sensitivity coefficients are evaluated. The sensitivity coefficients measure the sensitivity of the response to variations in the effective layer properties. Numerical results are presented for the frictional contact/impact response of a spherical cap made of textile (woven and braided) composite material, impacting a rigid surface. Results are compared with those of a spherical cap made of tape laminate.

Thermomechanical Buckling and Postbuckling Responses of Composite Panels with Skewed Stiffeners

Ahmed K. Noor, James H. Starnes, Jr. and Jeanne M. Peters

Finite Elements in Analysis and Design, Vol. 27, No. 2, Oct. 1997, pp. 193-214.

The results of a detailed study of the buckling and postbuckling responses of composite panels with skewed stiffeners are presented. The panels are subjected to applied edge displacements and temperature changes. A first-order shear-deformation geometrically nonlinear shallow-shell theory that includes the effects of laminated anisotropic material behavior is used to model each section of the stiffeners and the skin. A mixed formulation is used in the analysis with the fundamental unknowns consisting of the generalized displacements and the stress resultants of the panel. The nonlinear displacements, strain energy, transverse shear stresses, transverse shear strain energy density, and their hierarchical sensitivity coefficients are evaluated. The hierarchical sensitivity coefficients measure the sensitivity of the buckling and postbuckling responses to variations in three sets of interrelated parameters; namely, the panel stiffnesses; the effective material properties of the individual layers; and the constituent material parameters (fibers, matrix, interface and interphase). Numerical results are presented for rectangular panels with open section I-stiffeners, subjected to edge shortening and uniform temperature change.

The results show the effects of variations in the material properties of the skin and the stiffener on the buckling and postbuckling responses of the panel, as well as on the sensitivity coefficients.

Assessment of Continuum Models for Sandwich Panel Honeycomb Cores

W. Scott Burton and A. K. Noor

Computer Methods in Applied Mechanics and Engineering, Vol. 145, 1997, pp. 341-360

Detailed finite element models are used for predicting the free-vibration response of infinitely long and rectangular sandwich panels. The panels considered have square-cell honeycomb core and simply supported edges. The sandwich core and face sheets are modeled by using three-dimensional solid elements and two-dimensional plate elements. The predictions of the finite element models are compared with those obtained by using higher-order sandwich theory for

panels with the core replaced by an effective (equivalent) continuum. Three different approaches are used for estimating the effective material properties of the equivalent continuum layer.

Space-Time Finite Element Methods for the Sensitivity Analysis of Contact/Impact Response of Axisymmetric Composite Structures

Levent Karaoglan and A. K. Noor

Computer Methods in Applied Mechanics and Engineering, Vol. 144, 1997, pp. 371-389

Space-time finite element methods are applied to the sensitivity analysis of frictional contact/impact response of axisymmetric composite structures. The structures are assumed to consist of an arbitrary number of perfectly bonded homogeneous anisotropic layers. Only small displacements are considered and the material of each layer is assumed to be hyperelastic. The sensitivity coefficients measure the sensitivity of the response to variations in material parameters of the structure.

A displacement finite element model is used for the spatial discretization. The temporal integration is performed by using the time-discontinuous Galerkin method. Least-squares stabilizing operators are added to the governing equations to enhance the stability by smoothing out the high frequency modes, without degrading the accuracy. A quasi-explicit iterative technique is used for generating the response and evaluating the sensitivity coefficients. The normal contact conditions are incorporated within the iterative process. Numerical results are presented for the sensitivity analysis of contact/impact response of a composite spherical cap impacting a rigid plate.

Curved Sandwich Panels Subjected to Temperature Gradient and Mechanical Loads

Ahmed K. Noor, James H. Starnes, Jr. and Jeanne M. Peters

Journal of Aerospace Division, ASCE, Vol. 10, No. 4, Oct. 1997, pp. 143-161.

The results of a detailed study of the nonlinear response of curved sandwich panels with composite face sheets subjected to a temperature gradient through-the-thickness combined with mechanical loadings are presented. The analysis is based on a first-order shear-deformation Sanders-Budiansky type theory with the effects of large displacements, moderate rotations, transverse shear deformation and laminated anisotropic material behavior included. A mixed formulation is used with the fundamental unknowns consisting of the generalized displacements and the stress resultants of the panel. The nonlinear displacements, strain energy, principal strains, transverse shear stresses, transverse shear strain energy density, and their hierarchical sensitivity coefficients are evaluated. The hierarchical sensitivity coefficients measure the sensitivity of the nonlinear response to variations in the panel parameters, the effective properties of the face sheet layers and the core, and the micromechanical parameters. Numerical results are presented for cylindrical panels subjected to combined pressure loading, edge shortening or extension, edge shear and a temperature gradient through the thickness. The results show the effects of variations in the loading and the panel aspect ratio, on the nonlinear response and its sensitivity to changes in the various panel, effective layer and micromechanical parameters.

Predictor-Corrector Finite Element Approach for Electroelastic Analysis of Hybrid Composite Plates

Kangming Xu and A. K. Noor

Computer Methods in Applied Mechanics and Engineering, Vol. 147, Nos. 1-2, July 1997, pp. 139-145

A predictor-corrector finite element approach is presented for the steady-state (static) electroelastic

analysis of multilayered hybrid composite plates. The plates consist of a combination of fiber-reinforced and piezoelectric layers (or patches). The problem is formulated in terms of the displacement components and the electric potential. Two-dimensional finite element model is used in the predictor phase. Linear displacement variation and quadratic electric potential variation are assumed in the thickness direction (five displacement parameters and three electric potential parameters). The functional dependence of the displacement components and the electric potential are then calculated using three-dimensional equations. The corrected quantities are used to obtain better estimates for the different response quantities. The effectiveness of the predictor-corrector approach is demonstrated by numerical examples of five-layer plates consisting of four graphite-epoxy layers and one piezoelectric layer, subjected to transverse mechanical loading and electric potential.

Computational Structures Technology - Leap Frogging into the Twenty-First Century

Ahmed K. Noor

In *Advances in Computational Structures Technology*, B.H.V. Topping (ed.), Civil-Comp Press, Edinburgh, U.K., 1996, pp. 1-18

The history, recent developments and trends in computational structures technology (CST) are summarized. Discussion focuses on development of CST software and goals of CST activities. Some recent advances in a number of CST areas are described, including discretization techniques and element technology; computational material modeling; modeling of composite and sandwich structures; life prediction methodology; transient response analysis; numerical simulation of frictional contact/impact response; articulated structural dynamics; non-deterministic modeling and analysis methods; hybrid techniques; error estimation and adaptive improvement strategies; strategies for solution of coupled problems; sensitivity analysis; integrated analysis and design; strategies and numerical algorithms for new computing systems; model generation facilities; and application of object-oriented technology. Research areas in CST which have high potential for meeting the future technological needs are identified.

Some Future Directions of Computational Structures Technology

Ahmed K. Noor

In *Advances in Computational Engineering Science*, S. N. Atluri and G. Yagawa (eds.), Tech Science Press, Forsyth, GA, 1997, pp. 502-507

Some of the research areas of computational structures technology (CST) which have high potential for meeting the needs of future high-tech engineering systems are identified. Discussion focuses on the characteristics of future engineering systems; drivers for the technology; characteristics of future computing environment; and role of CST in future CAD/CAM/CAE systems and design environment. Future research areas include high fidelity modeling of the structure and its components; failure and life prediction methodologies; hierarchical, integrated methods and adaptive modeling strategies; non-deterministic analysis, soft computing and risk assessment; fully-coupled analysis and optimization problems associated with intelligent and modular structures; and validation of numerical simulations.

Evaluation of Transverse Thermal Stresses in Composite Plates Based on First-Order Shear Deformation Theory

Raimund Rolfes, A. K. Noor and H. Sparr

Computer Methods in Applied Mechanics and Engineering, Vol. 167, Nos. 3-4, Dec. 1988, pp. 355-368

A post-processing procedure is presented for the evaluation of the transverse thermal stresses in laminated plates. The analytical formulation is based on the first-order shear deformation theory and the plate is discretized by using a single-field displacement finite element model. The procedure is based on neglecting the derivatives of the in-plane forces and the twisting moments, as well as the mixed derivatives of the bending moments, with respect to the in-plane coordinates. The calculated transverse shear stiffnesses reflect the actual stacking sequence of the composite plate. The distributions of the transverse stresses through-the-thickness are evaluated by using only the transverse shear forces and the thermal effects resulting from the finite element analysis. The procedure is implemented into a post-processing routine which can be easily incorporated into existing commercial finite element codes. Numerical results are presented for four- and ten-layer cross-ply laminates subjected to mechanical and thermal loads.

Recent Advances in Sensitivity Analysis for Nonlinear Structural Mechanics Problems

Ahmed K. Noor

In Discretization Methods in Structural Mechanics, H. A. Mang and F. G. Rammerstorfer (eds.), Proc. IUTAM/IACM Symposium on Discretization Methods in Structural Mechanics II, Vienna, Austria, June 2-6, 1997, Kluwer Academic Publishers, Dordrecht, The Netherlands, 1999, pp. 207-216

Recent developments in the sensitivity analysis for nonlinear structural mechanics and dynamics problems are reviewed. The activities are grouped into two general categories, namely, computational strategies and facilities for evaluating the sensitivity coefficients, and new applications. Brief description is given of the activities pertaining to the first category. More detailed discussion is presented for two recent applications: a) hierarchical sensitivity coefficients of the various response quantities of sandwich panels with composite face sheets with respect to the different laminate, layer and micromechanical characteristics of the face sheets and core; and b) sensitivity analysis of the large strain response of visco-plastic solids subjected to dynamic loading. Sample numerical results are presented and some of the future directions for research on sensitivity analysis of large-scale nonlinear structures are outlined.

Analysis of Curved Sandwich Panels with Cutouts Subjected to Combined Temperature Gradient and Mechanical Loads

Ahmed K. Noor and Jeanne M. Peters

In Analysis and Design Issues for Modern Aerospace Vehicles - 1997, Jack R. Vinson (ed.), Proc. of a symposium held at the ASME International Congress and Exposition, Dallas, TX, Nov. 17-21, 1997, AD Vol. 55, ASME, 1997, pp. 293-310; also in Journal of Sandwich Structures and Materials, Vol. 1, Jan. 1999, pp. 42-59.

The results of a detailed study of the effect of the cutout on the response of curved sandwich panels are presented. The panels have honeycomb core composite face sheets. The loading consists of a temperature gradient through-the-thickness combined with pressure loading and edge shortening or edge shear. The analysis is based on a first-order shear-deformation Sanders-Budiansky type theory with the effects of large displacements, moderate rotations, transverse shear deformation and laminated anisotropic material behavior included. A mixed formulation is used with the fundamental unknowns consisting of the generalized displacements and the stress resultants of the panel. The nonlinear displacements, strain energy, principal strains, transverse shear stresses, transverse shear strain energy density, and their hierarchical sensitivity coefficients are evaluated. The hierarchical sensitivity coefficients measure the sensitivity of the nonlinear response to variations in the panel parameters, the effective properties of the face sheet layers and the core, and the micromechanical parameters. Numerical results are presented for cylindrical sandwich panels and show the effects of variations in the loading and the size of the cutout on the global and local

response quantities and their sensitivity to changes in the various panel, effective layer and micromechanical parameters.

Nonlinear Analysis of Curved Composite Panels Subjected to Combined Temperature Gradient and Mechanical Loads

Ahmed K. Noor and Jeanne M. Peters

In *Analysis and Design Issues for Modern Aerospace Vehicles - 1997*, L. Librescu (ed.), Proc. of a symposium held at the ASME International Congress and Exposition, Dallas, TX, Nov. 17-21, 1997, AD Vol. 55, ASME, 1997, pp. 143-158; also w/different title: *Analysis of Composite Panels Subjected to Thermo-mechanical Loads*, in *Journal of Aerospace Engineering*, ASCE, Vol. 12, Jan. 1999, pp. 1-7.

The results of a detailed study of the effect of the cutout on the nonlinear response of curved unstiffened panels are presented. The panels are subjected to combined temperature gradient through-the-thickness combined with pressure loading and edge shortening or edge shear. The analysis is based on a first-order shear-deformation Sanders-Budiansky type shell theory with the effects of large displacements, moderate rotations, transverse shear deformation and laminated anisotropic material behavior included. A mixed formulation is used with the fundamental unknowns consisting of the generalized displacements and the stress resultants of the panel. The nonlinear displacements, strain energy, principal strains, transverse shear stresses, transverse shear strain energy density, and their hierarchical sensitivity coefficients are evaluated. The hierarchical sensitivity coefficients measure the sensitivity of the nonlinear response to variations in the panel parameters, as well as in the material properties of the individual layers. Numerical results are presented for cylindrical panels and show the effects of variations in the loading and the size of the cutout on the global and local response quantities and their sensitivity to changes in the various panel, layer and micromechanical parameters.

Uncertainty Analysis of Composite Panels

Ahmed K. Noor, James H. Starnes, Jr. and Jeanne M. Peters, J. M.

In *Recent Advances and Future Trends in Composite Materials and Structures*, special issue of *Computer Methods in Applied Mechanics and Engineering* (to appear).

A two-phase approach and a computational procedure are presented for predicting the variability in the nonlinear response of composite structures associated with variations in the geometric and material parameters of the structure. In the first phase, hierarchical sensitivity analysis is used to identify the major parameters, which have the most effect on the response quantities of interest. In the second phase, the major parameters are taken to be fuzzy parameters, and a fuzzy set analysis is used to determine the range of variation of the response, associated with pre-selected variations in the major parameters. The effectiveness of the procedure is demonstrated by means of a numerical example of a cylindrical panel with four T-shaped stiffeners and a circular cutout.

Accurate Determination of Transverse Normal Stresses in Sandwich Panels Subjected to Thermomechanical Loadings

Ahmed K. Noor and M. Malik

Computer Methods in Applied Mechanics and Engineering, Vol. 178, 1999, pp. 431-443.

A two-stage computational procedure is presented for the accurate determination of transverse normal stresses in sandwich panels subjected to thermomechanical loadings. The procedure involves the use of a first-order shear deformation model in the first stage, and an iterational process for successive improvement of the accuracy of the displacement and stress fields in the

second stage. The effectiveness of the procedure is demonstrated by means of numerical studies of thin and moderately thick flat rectangular sandwich panels. Two sets of boundary conditions are considered; namely, one with all edges simply supported, and the other with two opposite edges simply supported and the remaining two clamped. The displacement components and the transverse shear and normal stresses obtained by the proposed computational procedure are found to be in close agreement with the solutions of the three dimensional continuum models.

Accurate Determination of Transverse Normal Stresses in Hybrid Laminated Panels Subjected to Electro-thermo-mechanical Loadings

Moinuddin Malik and A. K. Noor

International Journal for Numerical Methods in Engineering (to appear).

A computational procedure is presented for the accurate determination of transverse normal stresses in hybrid laminated panels consisting of fiber-reinforced composite and piezoelectric layers, and subjected to mechanical, thermal and electrical loadings. The three key elements of the procedure are: a) using through-the-thickness distributions of the response quantities of a simpler problem to effect a dimensional reduction in the given problem, b) adaptive improvement of the thickness distributions of the response quantities through successive applications of the Rayleigh-Ritz technique, in conjunction with the three-dimensional electro-thermo-elasticity equations for each layer, and c) using three dimensional divergence equations for evaluating the transverse stresses and the transverse component of the electric field.

The effectiveness of the procedure is demonstrated by means of two numerical examples of rectangular, hybrid laminated panels. The panels had two opposite edges clamped and the other two either simply supported or clamped. In both cases, the simpler panels were the panels of the same lamination and geometry as the example problems, but with all edges simply supported.

An Assessment of Five Modeling Approaches for Thermo-mechanical Stress Analysis of Laminated Composite Panels

Noor, A. K. and Malik, M.

Computational Mechanics (to appear).

A study is made of the effects of variation in the lamination and geometric parameters, and boundary conditions of multi-layered composite panels on the accuracy of the detailed response characteristics obtained by five different modeling approaches. The modeling approaches considered include four two-dimensional models, each with five parameters to characterize the deformation in the thickness direction, and a predictor-corrector approach with twelve displacement parameters. The two-dimensional models are first-order shear deformation theory, third-order theory, a theory based on trigonometric variation of the transverse shear stresses through the thickness, and a discrete layer theory. The combination of the following four key elements distinguishes the present study from previous studies reported in the literature: 1) the standard of comparison is taken to be the solutions obtained by using three-dimensional continuum models for each of the individual layers; 2) both mechanical and thermal loadings are considered; 3) boundary conditions other than simply supported edges are considered; and 4) quantities compared include detailed through-the-thickness distributions of transverse shear and transverse normal stresses.

Based on the numerical studies conducted, the predictor-corrector approach appears to be the most effective technique for obtaining accurate transverse stresses, and for thermal loading, none of the two-dimensional models is adequate for calculating transverse normal stresses, even when used in conjunction with three-dimensional equilibrium equations.

Appendix II
List of Technical Presentations Made Based
on the Studies Made Under This Grant

1. "Analysis of Curved Sandwich Panels Subjected to Combined Temperature Gradient and Mechanical Loads," 38th AIAA/ASME/ASCE/AHS/ASC Structures, Structural Dynamics and Materials Conference, April 7-10, 1997, Kissimmee, FL.
2. "Some Future Directions of Computational Structures Technology," International Conference on Computational Engineering Science (ICES '97), May 4-9, 1997, Costa Rica.
3. "Recent Advances in Sensitivity Analysis for Nonlinear Structural Mechanics Problems," IUTAM/IACM Symposium on Discretization Methods in Structural Mechanics II, June 2-6, 1997, Vienna, Austria.
4. "Nonlinear Analysis of Curved Composite Panels Subjected to Combined Temperature Gradient and Mechanical Loads," ASME International Mechanical Engineering Congress and Exposition, Dallas, TX, Nov. 16-21, 1997.
5. "Analysis of Curved Sandwich Panels with Cutouts Subjected to Combined Temperature Gradient and Mechanical Loads," ASME International Mechanical Engineering Congress and Exposition, Dallas, TX, Nov. 16-21, 1997.
6. "Evaluation of Transverse Thermal Stresses in Composite Plates Based on First-Order Shear Deformation Theory," ASME International Mechanical Engineering Congress and Exposition, Dallas, TX, Nov. 16-21, 1997.
7. Keynote address to Second Symposium on Multidisciplinary Environments and Applications (MAPINT '98), Wright Patterson Air Force Base, Dayton, Ohio, Aug. 25-26, 1998.
8. "Uncertainty Analysis of Composite Structures," 40th AIAA/ASME/ASCE/ AHS/ASC Structures, Structural Dynamics and Materials Conference, St. Louis, MO, April 12-15, 1999.

Frictional contact/impact response of textile composite structures

Levent Karaoğlu, Ahmed K. Noor

Center for Advanced Computational Technology, University of Virginia, Mail Stop 369, NASA Langley Research Center,
 Hampton, VA 23681, USA

&

Yong H. Kim

Seoul National University, Seoul, Korea

The results of a detailed study of the frictional contact/impact response of axisymmetric textile composite structures are presented. The structures are assumed to consist of an arbitrary number of perfectly bonded layers of woven fabric or braided preforms. The material of each layer is assumed to be hyperelastic and the effect of geometric nonlinearity is included. The equations of motion of the structure are established in the current configuration and a displacement finite element model is used for the spatial discretization. A Coulomb friction model is used and the temporal integration is performed by using an explicit central difference scheme.

Both the dynamic response and the sensitivity coefficients are evaluated. The sensitivity coefficients measure the sensitivity of the response to variations in the textile preform architecture and constituent properties, as well as to variations in the effective layer properties. Numerical results are presented for the frictional contact/impact response of a spherical cap made of textile (woven and braided) composite material, impacting a rigid surface. Results are compared with those of a spherical cap made of tape laminate. © 1997 Published by Elsevier Science Ltd.

NOTATION

	nodal acceleration vector	g	gap vector associated with a contact node
	yarn spacing	G_{f12}	shear modulus of the fiber
	filament diameter	G_{xy}, G_{xz}, G_{yz}	shear moduli of the individual layers in the planes xy , xz , and yz , respectively (see Fig. 1)
$1, E_{y2}$	elastic moduli of the yarn in the longitudinal and transverse directions, respectively	G_{y12}, G_m	shear moduli of the yarn and matrix, respectively
$1, E_{f2}$	elastic moduli of the fiber in the longitudinal and transverse directions, respectively	h	total thickness of the structure
	elastic modulus of the matrix	M	lumped mass matrix
n, E_y, E_z	effective elastic moduli of the individual layers in the x , y , and z directions, respectively (see Fig. 1)	n_a, n_b	yarn filament counts for the axial and braided yarns
		P_{d_n}	yarn packing density
		s	meridional distance
on, F^{ext}, F^{int}	vectors of contact, external and internal forces, respectively	t_N	normal component of contact tractions (pressures)
		t_r, t_θ	tangential components of contact tractions (pressures) in the radial

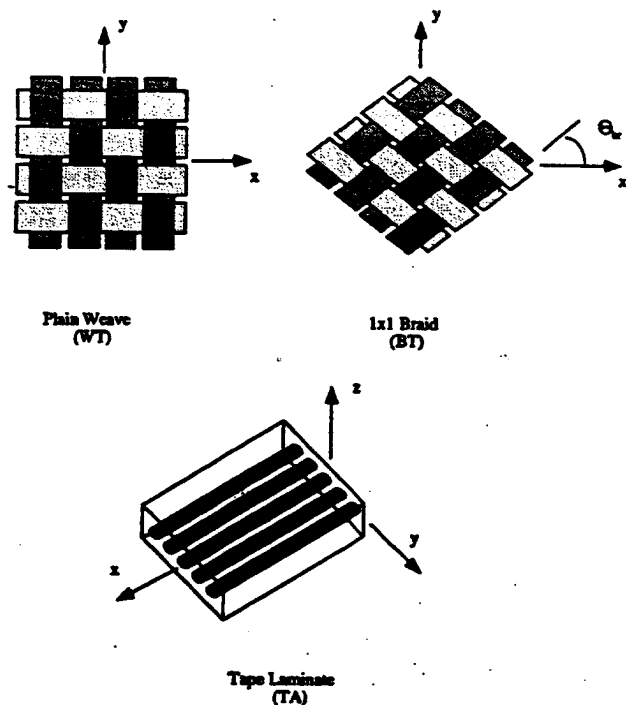


Fig. 1. Typical layer of plain weave, one-by-one braid and tape laminate.

u, v, w

v_f

V

X

x, y, z

Δt

$\lambda_i^{(l)}$

$\lambda_k^{(m)}$

$\nu_{xy}, \nu_{xz}, \nu_{yz}$

ν_{y12}, ν_{y23}

ν_{f12}, ν_{f23}

ν_m

θ_{br}

and circumferential directions, respectively

displacement components in the radial, circumferential and axial directions, respectively

overall fiber volume fraction

nodal velocity vector

nodal displacement vector

orthogonal local coordinate system (see Figs 1 and 2)

time step increment

typical layer parameter (e.g. layer thickness, and effective material properties of the layer)

typical micromechanical parameter (e.g. constituent properties, and textile preform architecture)

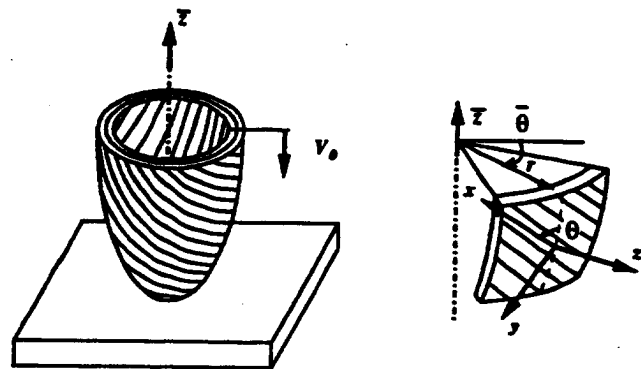
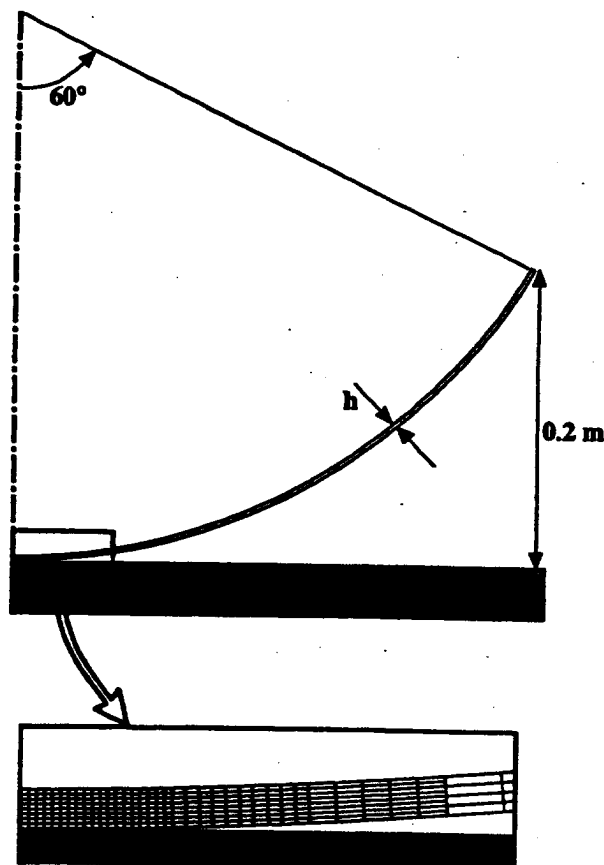
Poisson's ratios of the individual layers

Poisson's ratios of the yarn

Poisson's ratios of the fibers

Poisson's ratio of the matrix

braid angle



	WB and BT	TA
Number of Layers	40	24
Fiber Orientation	$[45_s / -45_s]_4$	$[45_s / -45_s]_4$

Thickness $h = 0.003$ m

Friction Coefficient $\mu = 0.3$

Fig. 2. Geometric and material characteristics of the spherical cap, and the finite element model used in the present study.

subscripts

current time step
initial conditions at $t = 0$
half time step

/2

superscripts

) layer quantities
n) micromechanical quantities

INTRODUCTION

In recent years, considerable attention has been devoted to textile composites. The main motiva-

Table 1. Micromechanical material properties for woven and braided textile composites

γ_1 (GPa)	144.8
γ_2 (GPa)	11.73
γ_{12} (GPa)	5.516
γ_{12}	0.23
γ_{23}	0.3
γ_m (GPa)	3.448
γ_m (GPa)	1.276
γ_n	0.35
γ_0 (mm)	6.1
γ_n	0.75
γ_r (mm) > 3 levels	0.007
γ_r	0.54
γ_b	12,000
γ_w	60°

Table 2. Micromechanical material properties for tape laminate composite

γ_1 (GPa)	250
γ_2 (GPa)	14.7
γ_{12} (GPa)	25
γ_{12}	0.2
γ_{23}	0.3
γ_m (GPa)	5.5
γ_n	0.35
γ_r	0.6

Table 3. Material properties for woven, braided textile and tape laminate composites

	WT	BT	TA
(kg/m ³)	1600	1600	1600
γ_1 (GPa)	57.66	39.80	152.23
γ_2 (GPa)	57.66	10.03	10.05
γ_3 (GPa)	10.48	10.11	10.05
γ_{xy} (GPa)	4.33	2.18	5.93
γ_{yz} (GPa)	3.97	4.15	5.93
γ_{xz} (GPa)	3.97	3.79	3.55
γ_{xy}	0.04	1.23	0.26
γ_{yz}	0.32	0	0.26
γ_{xz}	0.32	0.23	0.41

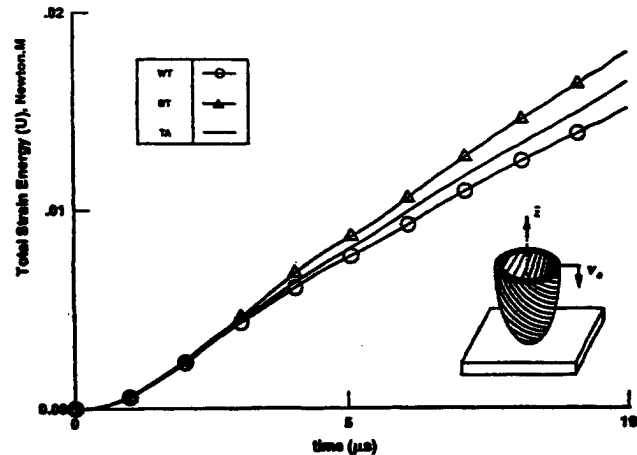


Fig. 3. Time histories of total strain energy U for the three material systems WT, BT and TA.

tion has primarily been the reduced cost of manufacturing. In addition, textile composites offer better dimensional stability over a large range of temperatures; better impact resistance and tolerance; subtle conformability and deep draw moldability/shapability. A variety of fabric structures have been proposed including wovens, knits, braids and nonwovens. Orthogonal woven fabrics are made by interlacing two or more yarn systems at a 90° angle; knits are made by interlooping one or more yarns; braids are formed by intertwining yarn systems; and nonwovens are formed by stitch binding or adhesive binding of fibers and/or yarns. The braids and weaves have emerged as promising approaches for cost-effective composite structures. Micromechanical models have been developed to predict the effects of textile preform architecture and constituent properties on the layer properties. Also, tests were proposed for measuring material properties and for identifying the damage mechanisms for braided and woven preform composites. Review of these activities is contained in two monographs [1,2], and a recent conference proceedings [3]. Despite the advantages of textile composites, their application has mostly been limited to secondary structural components. The main impediment to the use of textile composites in primary structures is the lack of understanding of their structural and dynamic responses.

The overall goal of the present study is to provide insight into the dynamic response of textile composite structures and compare these responses with those of tape laminates. Specifically, the objective of this paper is to study the frictional contact/impact response of axisym-

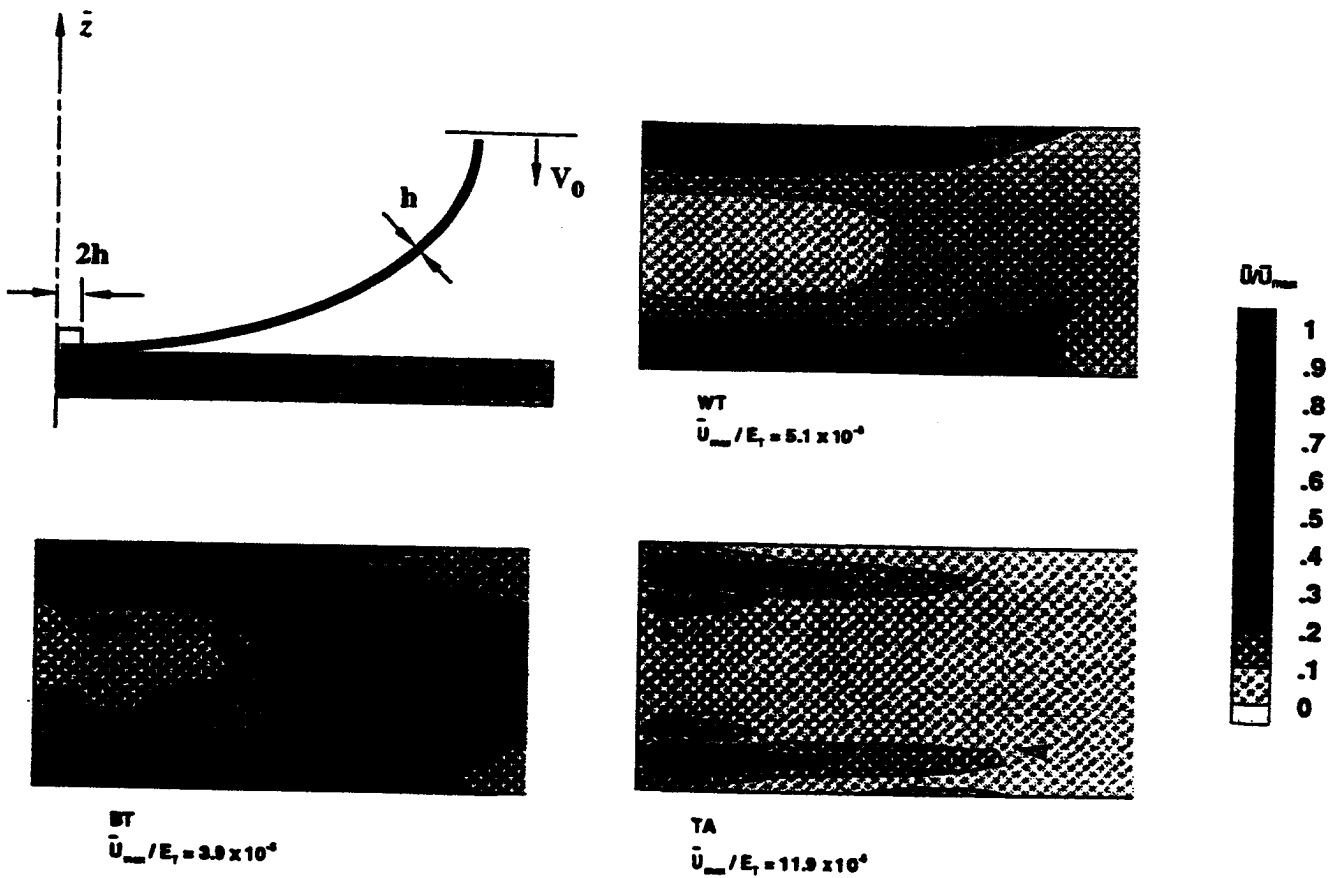


Fig. 4. Strain energy density contours at $t = 10 \mu s$ for the three material systems WT, BT and TA.

metric textile composite structures, and its sensitivity to variations in both the various textile preform architecture (braids and weaves) and the constituent properties. Also, comparisons are made between the responses of the textile and tape laminate composites.

FINITE ELEMENT FORMULATION

The analytical formulation is based on the dynamic nonlinear theory of axisymmetric solids of revolution. A hyperelastic material model is used and the equations of motion of the structure are established in the current configuration. The deformation is described by using the Green-Lagrange strain tensor and the associated second Piola-Kirchhoff stress tensor. The spatial discretization is performed by finite elements, with the fundamental unknowns consisting of the three displacement components u , v , w at each node. An explicit central difference scheme is used for temporal integration of the semi-discrete equations of motion. The Coulomb friction model is used, and the contact conditions are enforced by using the Lagrange

multipliers. A brief summary of the fundamental equations is given subsequently. The details of the computational procedure, along with other temporal integration and contact algorithms, are discussed in Ref. [4].

The semi-discrete equations of motion at time t_n , and the associated central difference equations can be written in the following form

$$M A_n = F_n^{ext} - F_n^{int} - F_n^{con} \quad (1)$$

$$A_n = \ddot{g}_n \quad (2)$$

$$V_{n+1/2} = V_{n-1/2} + A_n \Delta t \quad (3)$$

$$X_{n+1} = X_n + V_{n+1/2} \Delta t \quad (4)$$

Initially,

$$V_{1/2} = V_0 \quad (5)$$

$$X_1 = X_0 + V_{1/2} \Delta t \quad (6)$$

where M is the lumped mass matrix; X , V , A are the nodal displacement, velocity and acceleration vectors, respectively; M , A , F_n^{int} , F_n^{ext} and F_n^{con} are the inertial, internal, external and contact force vectors, respectively; and subscripts refer to the time steps. The sensitivity analysis involves differentiation of eqns (1)–(6) with respect to two interrelated sets of parameters,

iz., the effective layer parameters $\lambda_i^{(l)}$, and the micromechanical parameters $\lambda_k^{(m)}$. A direct differentiation approach is used for evaluating the sensitivity coefficients with respect to layer properties. The resulting equations can be written in the following form

$$M \frac{\partial A_n}{\partial \lambda_i^{(l)}} = - \frac{\partial F_n^{int}}{\partial \lambda_i^{(l)}} - \frac{\partial F_n^{ext}}{\partial \lambda_i^{(l)}} \quad (7)$$

$$\frac{\partial A_n}{\partial \lambda_i^{(l)}} = \frac{\partial \bar{g}_n}{\partial \lambda_i^{(l)}} \quad (8)$$

$$\frac{\partial V_{n+1/2}}{\partial \lambda_i^{(l)}} = \frac{\partial V_{n-1/2}}{\partial \lambda_i^{(l)}} + \frac{\partial A_n}{\partial \lambda_i^{(l)}} \Delta t \quad (9)$$

$$\frac{\partial X_{n+1}}{\partial \lambda_i^{(l)}} = \frac{\partial X_n}{\partial \lambda_i^{(l)}} + \frac{\partial V_{n+1/2}}{\partial \lambda_i^{(l)}} \Delta t \quad (10)$$

After the sensitivity coefficients with respect to the layer parameters $\lambda_i^{(l)}$ are evaluated, the sensitivity coefficients with respect to micromechanical parameters (preform architectural parameters and constituent properties) $\lambda_k^{(m)}$ are calculated by using the following relations (see Ref. [5])

$$\frac{\partial z}{\partial \lambda_k^{(m)}} = \frac{\partial \lambda_i^{(l)}}{\partial \lambda_k^{(m)}} \frac{\partial z}{\partial \lambda_i^{(l)}} \quad (11)$$

where z refers to any of the response quantities and the quantities $\partial \lambda_i^{(l)} / \partial \lambda_k^{(m)}$ are evaluated by

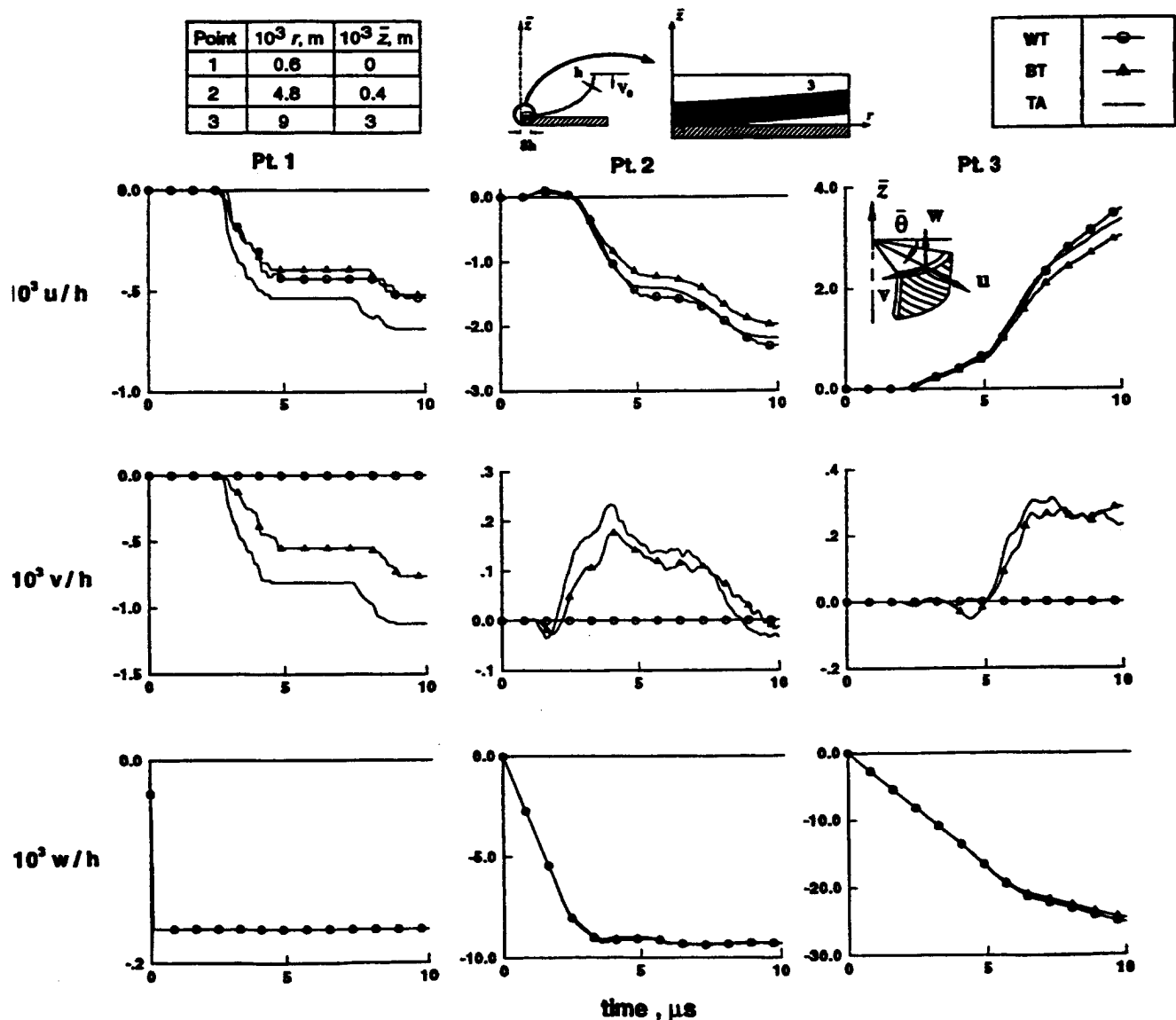


Fig. 5. Time histories of radial, circumferential and axial displacement components.

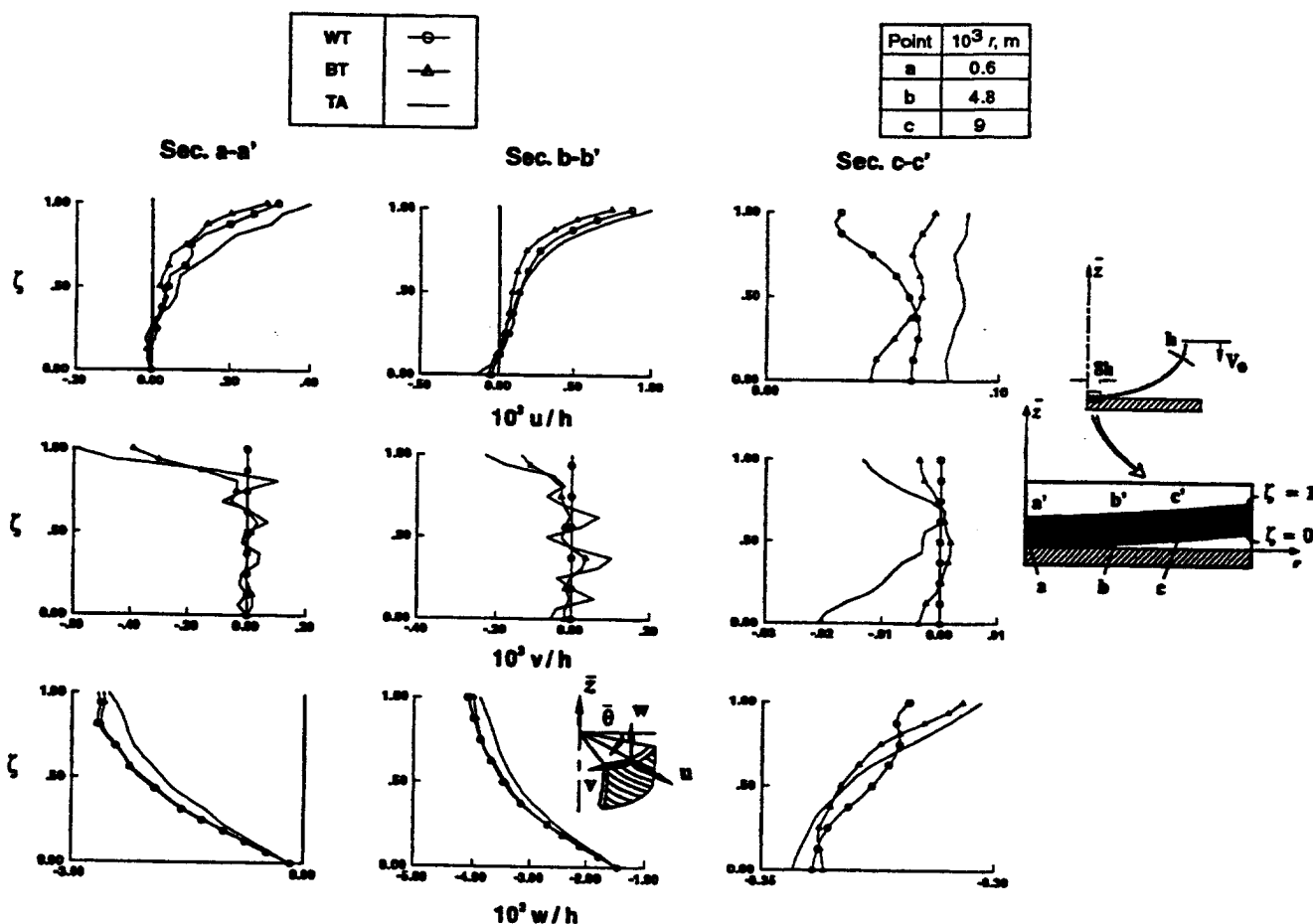


Fig. 6. Through-the-thickness distributions of the axial, circumferential and radial displacement components at time $t = 2.5 \mu s$ for the three material systems WT, BT and TA. (The points a, b, c are on the bottom surface.)

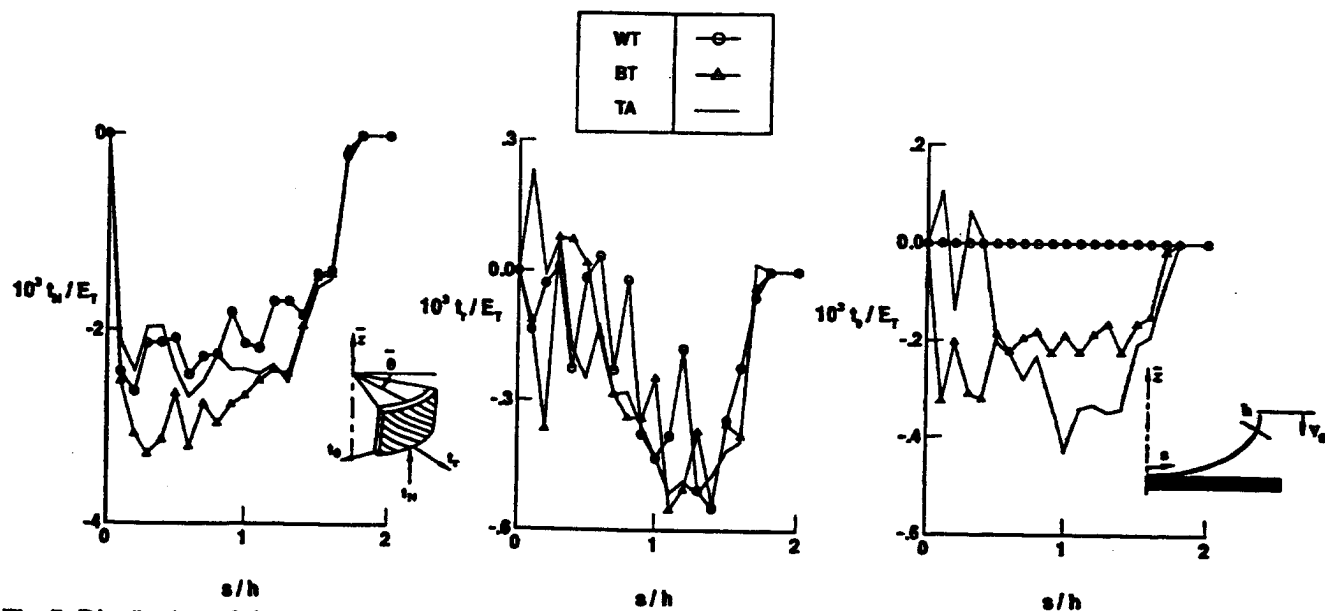


Fig. 7. Distribution of the normal and tangential contact pressures at $t = 10 \mu s$ for the three material systems WT, BT and TA.

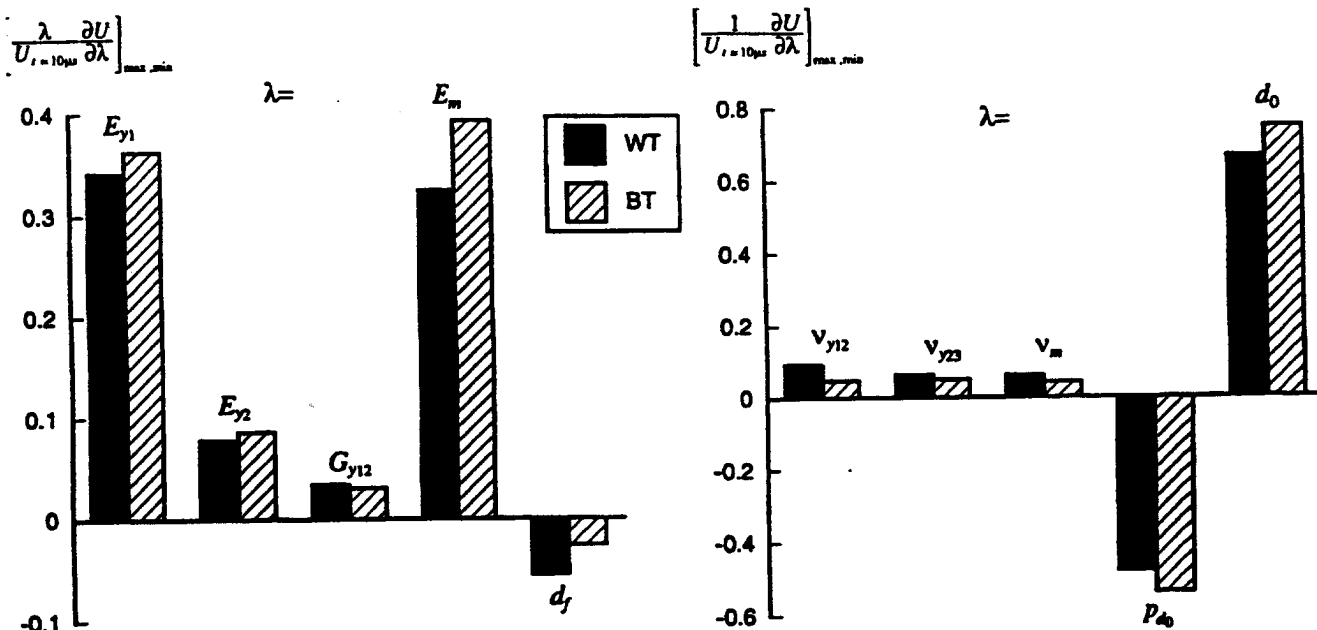


Fig. 8. Sensitivity coefficients of total strain energy, with respect to micromechanical properties of textile materials WT and BT, at $t = 10 \mu s$.

sing a micromechanical model, as described subsequently.

MICROMECHANICAL MODEL

In the present study two-dimensional woven and braided composites are considered. The woven composites consist of interlaced, mutually orthogonal warp and fill yarns which are

then impregnated with a matrix material and then cured. The plain weave, 5- and 8-harness satin weaves are considered. The braided composites contain axial yarns and braided yarns which are oriented at an angle θ_{br} to the axial yarns. Both one-by-one and two-by-two braid patterns are considered.

The micromechanical model uses the periodicity of the textile architecture to isolate a representative unit cell. Overall properties are

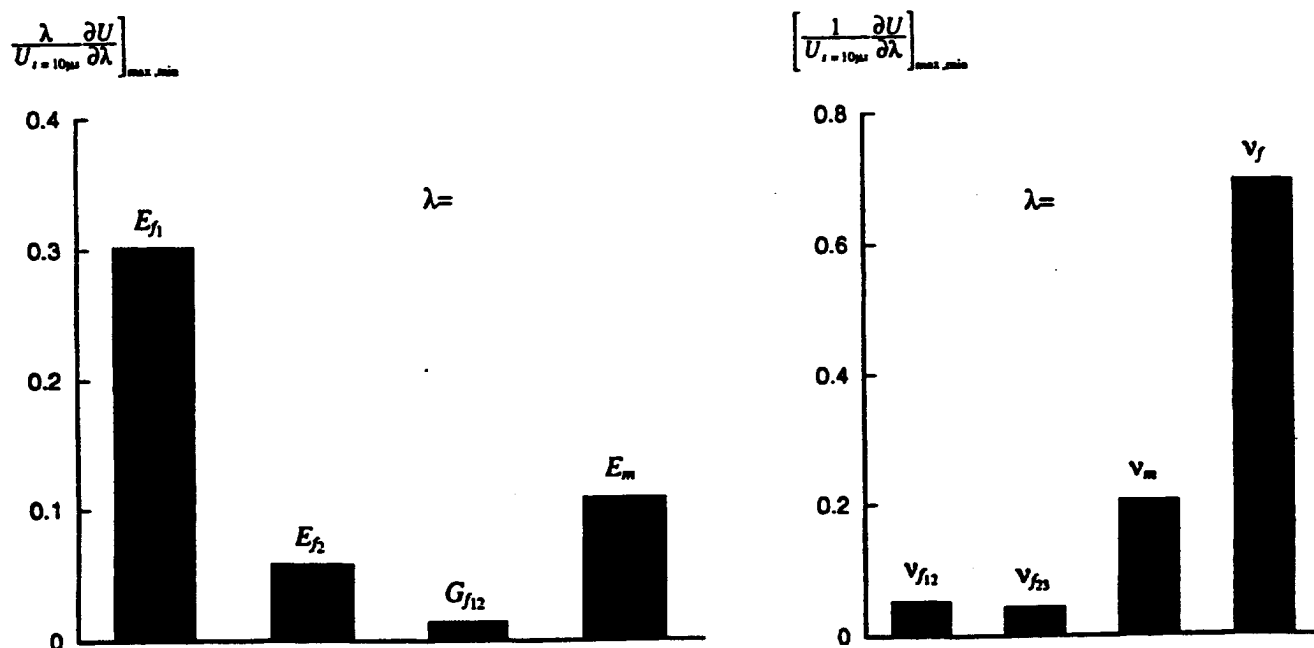


Fig. 9. Sensitivity coefficients of total strain energy, with respect to micromechanical properties of tape laminate TA, at $t = 10 \mu s$.

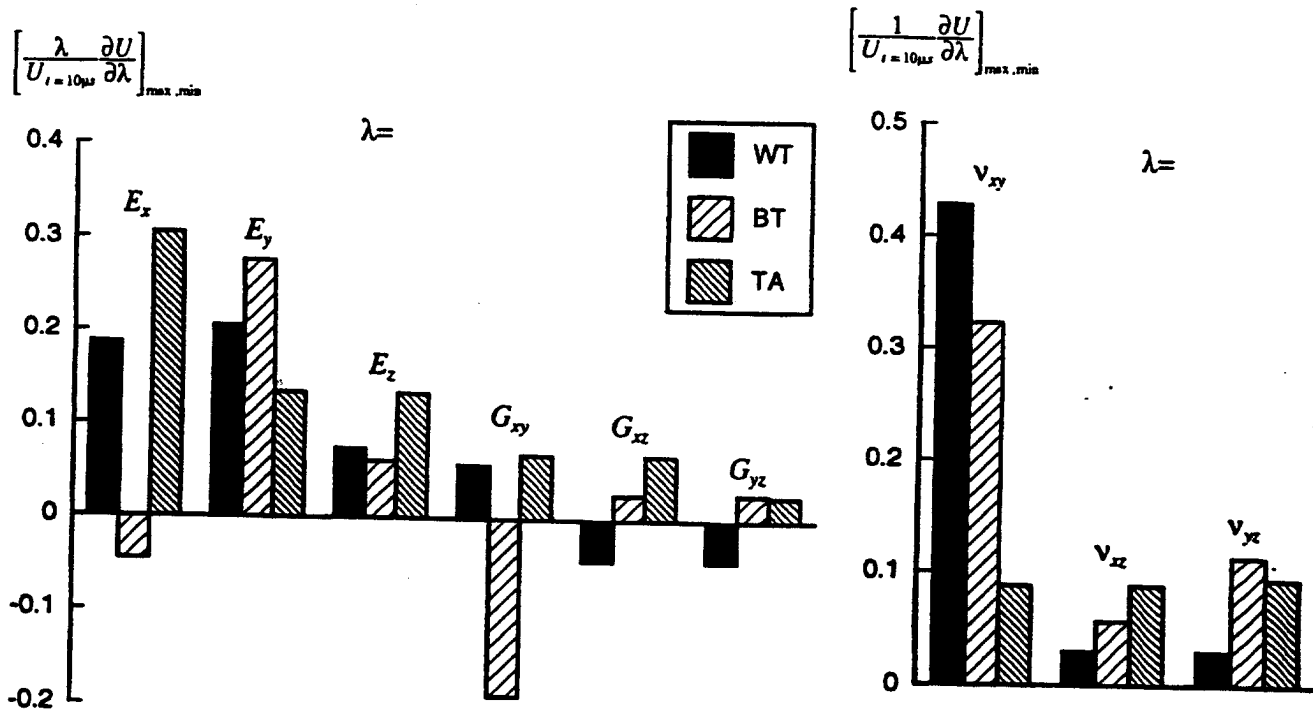


Fig. 10. Sensitivity coefficients of total strain energy, with respect to layer properties at $t = 10 \mu s$ for the three material systems WT, BT and TA.

calculated by making simplifying assumptions about the unit cell geometry and the deformation field, together with a stress averaging technique. The TEXCAD (Textile Composite Analysis for Design) program [6–8] was used for calculating the effective layer properties. The typical micromechanical parameters needed to calculate layer properties in woven and braided composites are the following

$$\lambda_k^{(m)} = \{E_{y1}, E_{y2}, G_{y12}, \nu_{y12}, \nu_{y23}, E_m, \nu_m, d_0, P_{d0}, d_f, \nu_f, n_a, n_b, \theta_{br}\} \quad (12)$$

where E_{y1} , E_{y2} are the elastic moduli of the yarn in the longitudinal and transverse directions; E_m is the elastic modulus of the matrix; G_{y12} is the shear modulus of the yarn; ν_{y12} , ν_{y23} are Poisson's ratios of the yarn; ν_m is Poisson's ratio of the matrix; d_0 is the yarn spacing; P_{d0} is the yarn packing density; d_f is the filament diameter; ν_f is the overall fiber volume fraction; n_a , n_b are the yarn filament counts for the axial and braided yarns; and θ_{br} is the braid angle.

Aboudi's method of cells was used for evaluating the effective layer properties for the tape laminate. The method is based on the assumption that the fibers are continuous and are arranged in a doubly periodic array, and therefore, only a representative cell is analyzed

[9,10]. Typical micromechanical parameters for the tape laminate are the following

$$\lambda_k^{(m)} = \{E_{f1}, E_{f2}, G_{f12}, \nu_{f12}, \nu_{f23}, E_m, \nu_m, \nu_f\} \quad (13)$$

where E_{f1} , E_{f2} are the elastic moduli of the fiber in the longitudinal and transverse directions; G_{f12} is the shear moduli of the fiber; ν_{f12} , ν_{f23} are Poisson's ratios of the fibers; E_m is the elastic modulus of the matrix; and ν_m is Poisson's ratio of the tape matrix.

NUMERICAL STUDIES

Numerical studies were performed to gain insight into the frictional contact/impact response of axisymmetric textile composites and to compare it with structures made of tape laminate. Herein, the results for a 40-layer spherical textile composite cap impacting a rigid plate with an initial axial velocity of 10 m/s are discussed. The problem was selected to assess the potential of using textile composites in dynamically loaded structures and to identify the differences in the dynamic response between laminated, woven and braided composites. Results are compared with those of a 24-layer cap made from tape laminate, with the

same total thickness. The geometric characteristics of the structure are given in Fig. 2. Two different textile composites are considered; namely woven textile (WT), and braided textile (BT) composites. The yarns are made of Hercules AS4 graphite fibers and are impregnated with Hercules 3501-6 epoxy matrix. The reform architectural properties and constituent properties for the textile composites are given in Table 1; the constituent properties for the tape laminate are given in Table 2. The effective layer properties for both the textile composite and the tape laminate are given in Table 3.

The structures were discretized by using 327 two-dimensional elements (a total of 4307 displacement degrees of freedom). Biquadratic

interpolation functions are used for approximating the displacement components. The number of elements in the thickness direction is gradually reduced from eight in the contact region to one away from that region. The finite element model used is shown in Fig. 2.

Sensitivity analyses were conducted to identify which material and lamination parameters most affected the frictional contact/impact response of the structure. Sensitivity coefficients with respect to both the material parameters of the individual layers and the micromechanical parameters are evaluated.

The effect of the weave architectures and braid patterns on the dynamic response was found to be not significant. Therefore, only the results for the plain weave and for the one-by-

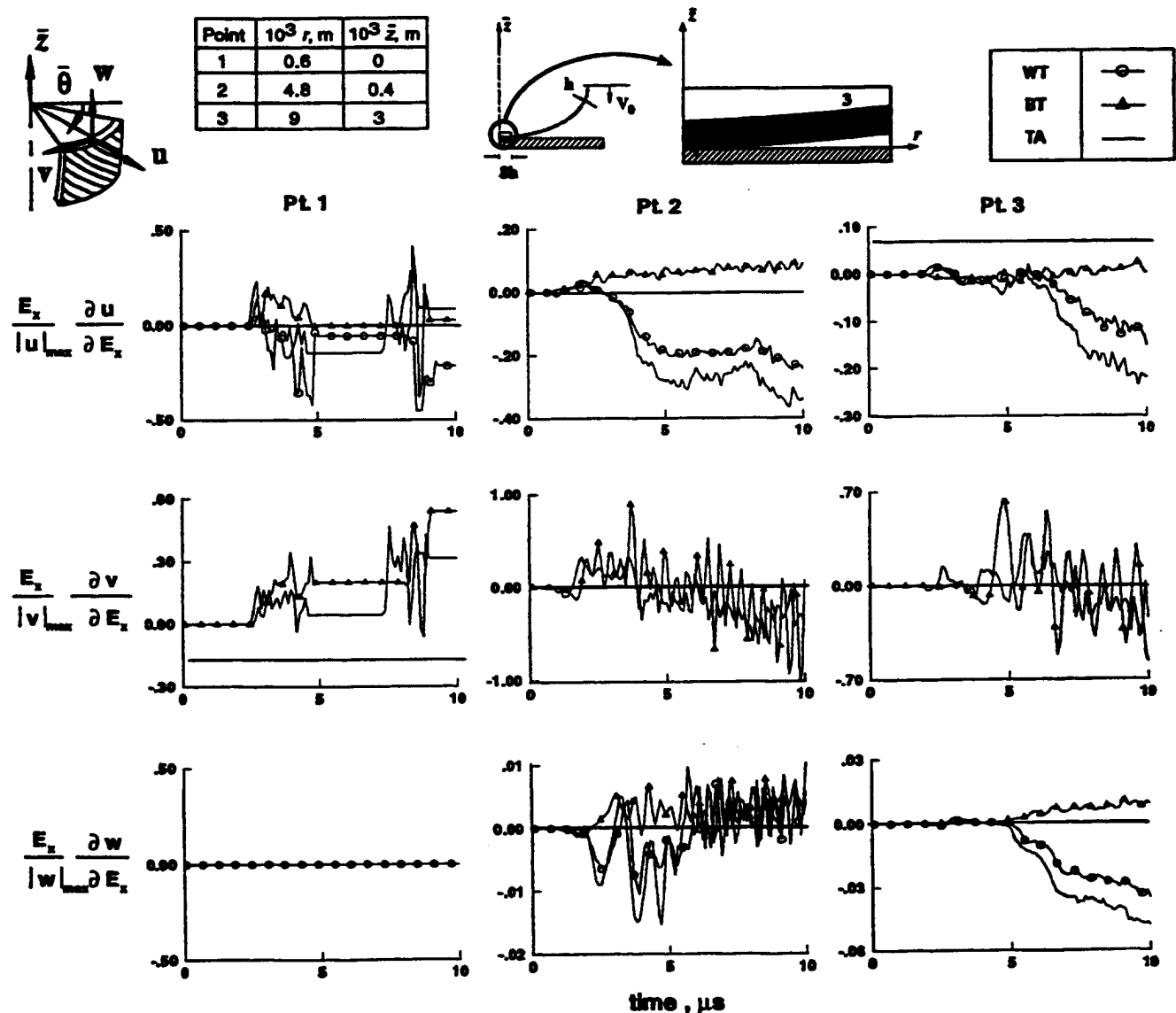


Fig. 11. Time histories of the normalized sensitivity coefficients of the displacement components with respect to E_x for the three material systems WT, BT and TA.

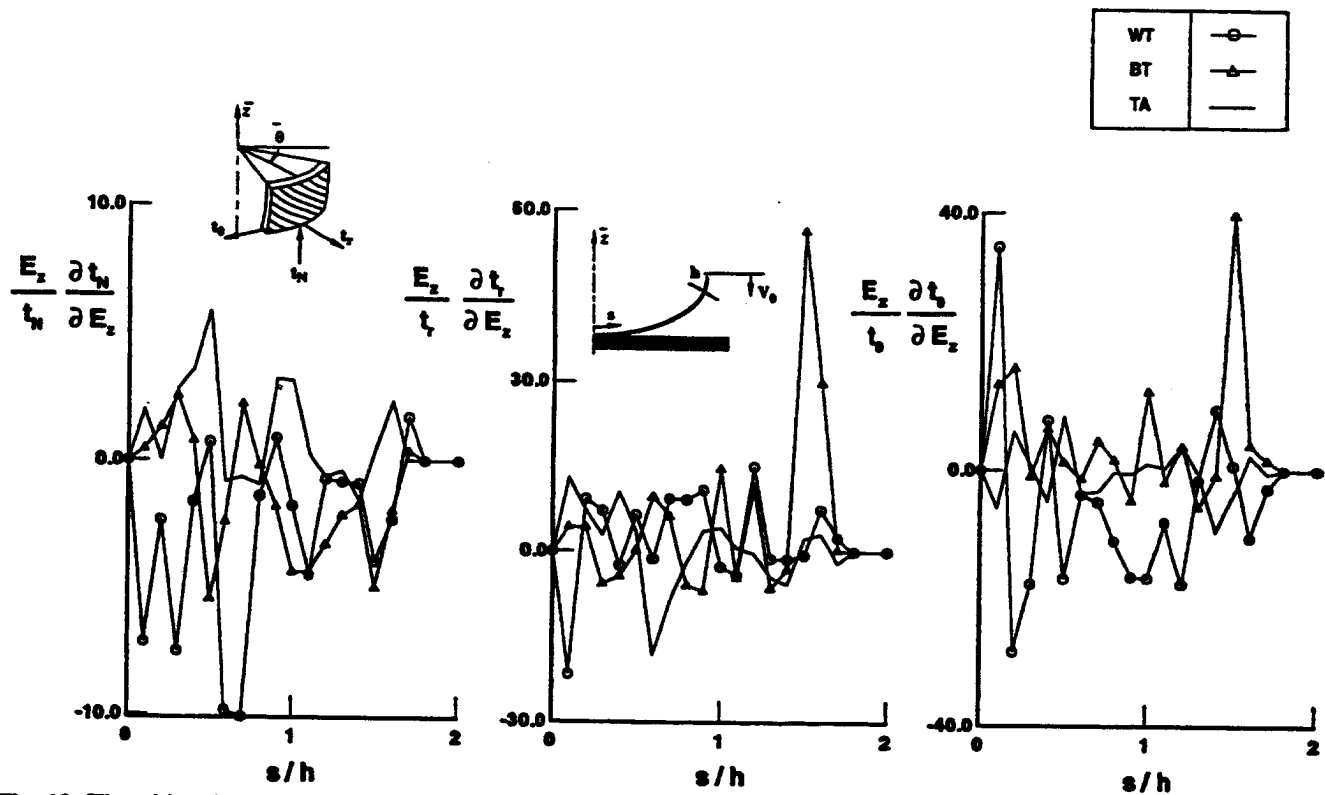


Fig. 12. Time histories of the normalized sensitivity coefficients of the contact traction components with respect to E_z for the three material systems WT, BT and TA.

one braided textile composites are presented herein. The plain weave, the one-by-one braided textile and the tape laminate will henceforth be denoted by WT, BT and TA, respectively.

Response studies

The time histories of the total strain energy U for the three different material models WT, BT and TA are shown in Fig. 3. At any time, the total strain energy U is largest for the braided textile (BT) and smallest for the woven textile (WT) composites. The total strain energy provides insight into the overall deformation level in the structure. Local response characteristics such as displacement field, strain energy density and contact traction distribution are needed in the failure analysis. The normalized contour plots for the strain energy density \bar{U} in the contact region of the structure are shown in Fig. 4 at time $t = 10 \mu s$. The contour plots are normalized by dividing by the maximum value of the strain energy density in each case. An examination of Fig. 4 reveals a localization (high gradients) of the strain energy density at the inner and outer (contact) surface for material

WT; and at the interfaces between layers of $\bar{\theta} = +45^\circ$ and $\bar{\theta} = -45^\circ$ for materials BT and TA. Higher gradients occur for material TA than for textile materials.

The time histories of the radial, circumferential and axial displacement components u , v , w at three points (points 1, 2, 3) are shown in Fig. 5. Point 1 is a contact node, point 2 is close to the contact region, and point 3 is outside the contact region. Since the initial velocity is in the axial direction, the axial displacement component w at points 2 and 3 is larger than the corresponding radial and circumferential components. Since point 1 remains in contact, it has a very small w component. Initially, the contact region is in a sticking contact state and the tangential displacements are very small. Then the tangential motion and the tangential tractions become large and sliding starts at the contact surface. Note that the displacement time histories for the three material systems are qualitatively similar. However, the circumferential displacement component v for material WT is very small compared to the others.

The distributions of the displacement components in thickness direction at three different sections (sections $a-a'$, $b-b'$, $c-c'$) at time

$= 2.5 \mu\text{s}$ are shown in Fig. 6. The displacement components are normalized by dividing each by the thickness. The axial displacement component w is the largest one and does not vary linearly through the thickness. The radial and circumferential displacement components in the contact region (sections $a-a'$ and $b-b'$) are fairly complicated. Outside the contact region (section $c-c'$), the axial displacement component w is almost constant and the radial and circumferential displacement components are almost zero through the thickness. The circumferential displacement component is very small for material WT. The use of eight elements through the thickness in the contact region was intended to capture the correct thickness distribution of the displacement components. The thickness distributions of displacements for the three material models are not significantly different.

The distributions of the normal, radial and circumferential contact pressures, t_N , t_r and t_θ at the bottom surface of the structure are shown in Fig. 7 at time $t = 10 \mu\text{s}$. Each of the contact pressures is normalized by dividing by E_T . As expected, the magnitudes of the normal contact pressures are considerably larger than those of the corresponding radial and circumferential pressures. Normal contact pressures for material BT are larger than those for materials WT and TA. On the other hand, the circumferential contact pressures are very small for material WT.

Sensitivity studies

To simplify the assessment of the effects of various material parameters on the frictional contact/impact response, the sensitivity coefficients are normalized by multiplying each by the material parameter, and dividing by the maximum value of the response quantity.

The maximum value of normalized sensitivity coefficients of the total strain energy U with respect to micromechanical properties are given in Figs 8 and 9 for textile and tape laminate composites, respectively. For materials WT and BT the dynamic response is more sensitive to variations in E_y , E_m than to variations in other parameters. For material TA the response is sensitive to variations in E_f and E_m .

The maximum values of normalized sensitivity coefficients of the total strain energy U with respect to layer properties are shown in

Fig. 10. The total strain energy is more sensitive to variations in E_x , E_y and ν_{xy} for material WT; E_y , G_{xy} and ν_{xy} for material BT; and E_x for material TA than to variations in other parameters.

The time histories of the normalized sensitivity coefficients of the displacement components u , v , w with respect to E_x at points 1, 2 and 3 are shown in Fig. 11. The axial displacement w is shown to be considerably less sensitive to variations in E_x than the corresponding radial and circumferential displacements. Since v is very small for material WT, the normalized sensitivities of v are much larger compared to those of the other two, and it is not shown in the figure. The displacement components are more sensitive to variations in E_x for the TA material than for the WT and BT materials. The sensitivity coefficients of the displacements for the BT material have different signs from the corresponding ones for the TA and WT materials.

The distributions of the normalized sensitivity coefficient of the normal and tangential contact pressures t_N , t_r and t_θ with respect to E_x at time $t = 10 \mu\text{s}$ are shown in Fig. 12.

Since t_θ is very small for material WT, the normalized sensitivity coefficients of t_θ are much larger than those of the other two, and it is not shown in the figure. Traction components are more sensitive to variations in E_x for the material WT than for the materials BT and TA.

CONCLUDING REMARKS

The results of a detailed study of the frictional contact/impact response of axisymmetric textile composite structures are presented. The structures are assumed to consist of an arbitrary number of perfectly bonded layers of woven fabric or braided preforms. The material of each layer is assumed to be hyperelastic and the effect of geometric nonlinearity is included. The deformation is described by using the Green-Lagrange strain tensor and the associated second Piola-Kirchhoff stress tensor. The equations of motion of the structure are established in the current configuration and a displacement finite element model is used. The Coulomb friction model is used and the contact conditions are enforced by using the Lagrange multipliers. An explicit central difference scheme is employed for the temporal integration of the

equations of motion. The sensitivity coefficients are evaluated by using a direct differentiation approach. The sensitivity coefficients measure the sensitivity of the response to variations in the textile preform architecture and constituent properties, as well as to variations in the effective layer properties.

Numerical results are presented for the frictional contact/impact response of a 40-layer spherical cap made of textile (woven and braided) composite material, impacting a rigid surface. Results are compared with those of a spherical cap made of tape laminate, and having approximately the same thickness. On the basis of the numerical results, the following conclusions are justified:

- (1) The global response-time histories of the textile composite cap are similar to those of the corresponding cap made of tape laminate. However, the strain energy density exhibits higher gradients in the tape laminate than in the textile composites.
- (2) The thickness distributions of the displacement components and their sensitivity coefficients in the contact region are not linear for both textile and tape laminate composites.
- (3) The dynamic frictional contact response of textile composites is relatively more sensitive to variations in the elastic moduli of the layers in the longitudinal and transverse directions, elastic modulus of the yarn in the longitudinal direction, elastic modulus of the matrix, volume fractions in yarn and composite; and somewhat sensitive to variations in the other material parameters. The response of tape laminate composites is more sensitive to variations in elastic modulus of the layers in the longitudinal direction,

elastic modulus of the fiber and Poisson's ratio of the tape matrix than to variations in other material parameters.

ACKNOWLEDGEMENTS

The present research is partially supported by NASA Cooperative Agreement NCCW 0011, NASA Grant NAG-1-1162 and by Air Force Office of Scientific Research Grant 49620-96-1-0462.

REFERENCES

1. Tarnopol'skii, Yu. M., Zhigun, I. G. and Polyakov, V. A., *Spatially Reinforced Composites*. Technomic, Lancaster, 1992.
2. Naik, N. K., *Woven Fabric Composites*. Technomic, Lancaster, 1994.
3. Poe, C. C. and Harris, C. E., editors., *Mechanics of Textile Composites Conference*. NASA. Conference Publication 3311, Parts 1 and 2, 1995.
4. Karaoğlu, L. and Noor, A.K., Assessment of temporal integration schemes for the sensitivity analysis of frictional contact/impact response of axisymmetric composite structures. *Comput. Methods Appl. Mech. Engng* 1996, 130, 369-93.
5. Noor, A. K., Recent advances in sensitivity analysis for the thermomechanical postbuckling of composite panels, in Thornton, E. A., editor, *Aerospace Thermal Structures and Materials for a New Era*, AIAA Series Progress in Astronautics and Aeronautics, 1995, Vol. 168, pp. 218-39.
6. Naik, R. A., Analysis of woven and braided fabric reinforced composites. NASA Contractor Report 194930, 1994.
7. Naik, R. A., Texcad-textile composite analysis for design; version 1.0 user's manual. NASA Contractor Report 4639, 1994.
8. Naik, R. A., Ifju, P. G. and Masres, J. E., Effect of fiber architecture parameters on deformation fields and elastic moduli of 2-d braided composites. *J. Comp. Mats* 1994, 28 (7), 656-81.
9. Noor, A. K. and Shah, R. S., Effective thermoelastic and thermal properties of unidirectional fiber-reinforced composites and their sensitivity coefficients. *Composite Structures* 1993, 26, 7-23.
10. Aboudi, J., *Mechanics of Composite Materials — A Unified Micromechanical Approach*. Elsevier, Amsterdam, 1991.

Reprinted from

FINITE ELEMENTS IN ANALYSIS AND DESIGN

Finite Elements in Analysis and Design 27 (1997) 193–214

Thermomechanical buckling and postbuckling responses of composite panels with skewed stiffeners

Ahmed K. Noor*, James H. Starnes, Jr., Jeanne M. Peters

*Center for Advanced Computational Technology, University of Virginia, NASA Langley Research Center,
Hampton, VA 23681, USA*



FINITE ELEMENTS IN ANALYSIS AND DESIGN

The International Journal of Applied Finite Elements and Computer Aided Engineering

Editor-in-Chief

Harry G. Schaeffer, *Mechanical Engineering Department, University of Louisville, Louisville, KY 40292, U.S.A.*
Tel: 502-852-6099. Fax: 502-852-6053. E-mail: hgscha01@starbase.spd.louisville.edu

Associate Editors

Bert Spreeuw, *Mechanics Software Enterprises B.V., The Netherlands*
K.Y. Sze, *City University of Hong Kong, Hong Kong*

Editorial Board

J.F. Abel, *Cornell University, NY, U.S.A.*
Michael Apostol, *Jordan, Apostol, Ritter Associates, Inc., RI, U.S.A.*
K.J. Bathe, *MIT, MA, U.S.A.*
Michel Bernadou, *INRIA, Le Chesnay, France*
Wei-Zang Chien, *Shanghai University of Technology, People's Republic of China*
Carlos A. Felippa, *University of Colorado, CO, U.S.A.*
G. Hofstetter, *University of Innsbruck, Austria*
G.M. Hulbert, *University of Michigan, MI, U.S.A.*
S.H. Lo, *The University of Hong Kong, Hong Kong*
Richard H. MacNeal, *The MacNeal-Schwendler Corporation, CA, U.S.A.*

H.A. Mang, *Technical University of Vienna, Austria*
Robert Melosh, *Duke University, NC, U.S.A.*
A. Nagamatsu, *Tokyo Institute of Technology, Japan*
Theodore H.H. Pian, *MIT, MA, U.S.A.*
E. Ramm, *University of Stuttgart, Germany*
Limin Tang, *Dalian Institute of Technology, People's Republic of China*
A.O. Tay, *National University of Singapore, Singapore*
O.C. Zienkiewicz, *University of Wales, United Kingdom*
Founding Editor
Walter D. Pilkey, *University of Virginia, VA, U.S.A.*

Subscription Information

Finite Elements in Analysis and Design (ISSN 0168-874X) is published monthly. For 1997 volumes 25-27 are scheduled for publication. Back volumes and subscription prices are available on request. Subscriptions are accepted on a prepaid basis only and are entered on a calendar year basis. Issues are sent by surface mail except to the following countries where air delivery (S.A.L. - Surface Air Lifted) is ensured: Argentina, Australia, Brazil, Canada, China, Hong Kong, India, Israel, Malaysia, Mexico, New Zealand, Pakistan, Singapore, South Africa, South Korea, Taiwan, Thailand, and the U.S.A. For all other countries airmail rates are available upon request. Claims for missing issues must be made within six months of our publication date of the issues. For orders, claims, product enquiries (no manuscript enquiries) please contact the Customer Support Department at the Regional Sales Office nearest to you: **New York**, Elsevier Science, P.O. Box 945, New York, NY 10159-0945, USA. Tel: (+1) 212-633-3730, [Toll Free number for North American Customers: 1-888-4ES-INFO (437-4636)], Fax: (+1) 212-633-3680, E-mail: usinfo-f@elsevier.com; **Amsterdam**, Elsevier Science, P.O. Box 211, 1000 AE Amsterdam, The Netherlands. Tel: (+31) 20-485-3757, Fax: (+31) 20-485-3432, E-mail: nlinfo-f@elsevier.nl; **Tokyo**, Elsevier Science, 9-15, Higashi-Azabu 1-chome, Minato-ku, Tokyo 106, Japan. Tel: (+81) 3-5561-5033, Fax: (+81) 3-5561-5047, E-mail: kyf04035@niftyserve.or.jp; **Singapore**, Elsevier Science, No. 1 Temasek Avenue, # 17-01 Millenia Tower, Singapore 039192. Tel: (+65) 434-3727, Fax: (+65) 337-2230, E-mail: asiainfo@elsevier.com.sg.

Copyright © 1997, Elsevier Science B.V. All rights reserved.

This journal and the individual contributions contained in it are protected by the copyright of Elsevier Science B.V., and the following terms and conditions apply to their use: **Photocopying** Single photocopies of single articles may be made for personal use as allowed by national copyright laws. Permission of the publisher and payment of a fee is required for all other photocopying, including multiple or systematic copying, copying for advertising or promotional purposes, resale, and all forms of document delivery. Special rates are available for educational institutions that wish to make photocopies for non-profit educational classroom use. In the USA, users may clear permissions and make payment through the Copyright Clearance Center, 222 Rosewood Drive, Danvers, MA 01923, USA. In the UK, users may clear permissions and make payment through the Copyright Licensing Agency Rapid Clearance Service (CLARCS), 90 Tottenham Court Road, London W1P 0LP, U.K. In other countries where a local copyright clearance centre exists, please contact it for information on required permissions and payments. **Derivative Works** Subscribers may reproduce tables of contents or prepare lists of articles including abstracts for internal circulation within their institutions. Permission of the publisher is required for resale or distribution outside the institution. Permission of the publisher is required for all other derivative works, including compilations and translations. **Electronic Storage** Permission of the publisher is required to store electronically any material contained in this journal, including any article or part of an article. Contact the publisher at the address indicated. *Except as outlined above, no part of this publication may be reproduced, stored in a retrieval system or transmitted in any form or by any means, electronic, mechanical, photocopying, recording or otherwise, without prior written permission of the publisher.* No responsibility is assumed by the Publisher for any injury and/or damage to persons or property as a matter of products liability, negligence or otherwise, or from any use or operation of any methods, products, instructions or ideas contained in the material herein. Although all advertising material is expected to conform to ethical (medical) standards, inclusion in this publication does not constitute a guarantee or endorsement of the quality or value of such product or of the claims made of it by its manufacturer.

0168-874X/97/\$17.00

Printed in The Netherlands

Ⓢ The paper used in this publication meets the requirements of ANSI/NISO Z39.48-1992 (Permanence of Paper)



ELSEVIER

Finite Elements in Analysis and Design 27 (1997) 193-214

FINITE ELEMENTS
IN ANALYSIS
AND DESIGN

Thermomechanical buckling and postbuckling responses of composite panels with skewed stiffeners

Ahmed K. Noor*, James H. Starnes, Jr., Jeanne M. Peters

*Center for Advanced Computational Technology, University of Virginia, NASA Langley Research Center,
Hampton, VA 23681, U.S.A*

Abstract

The results of a detailed study of the buckling and postbuckling responses of composite panels with skewed stiffeners are presented. The panels are subjected to applied edge displacements and temperature changes. A first-order shear-deformation geometrically nonlinear shallow-shell theory that includes the effects of laminated anisotropic material behavior is used to model each section of the stiffeners and the skin. A mixed formulation is used in the analysis with the fundamental unknowns consisting of the generalized displacements and the stress resultants of the panel. The nonlinear displacements, strain energy, transverse shear stresses, transverse shear strain energy density, and their hierarchical sensitivity coefficients are evaluated. The hierarchical sensitivity coefficients measure the sensitivity of the buckling and postbuckling responses to variations in three sets of interrelated parameters; namely, the panel stiffnesses; the effective material properties of the individual layers; and the constituent material parameters (fibers, matrix, interface and interphase). Numerical results are presented for rectangular panels with open section I-stiffeners, subjected to edge shortening and uniform temperature change.

The results show the effects of variations in the material properties of the skin and the stiffener on the buckling and postbuckling responses of the panel, as well as on the sensitivity coefficients. © Elsevier Science B.V.

Keywords: Buckling; Composite panels; Finite elements; Hierarchical sensitivity coefficients; Postbuckling; Skewed stiffener; Thermomechanical loads

1. Introduction

The potential of using the directional dependence of composite properties in designing tailored structures to improve structural performance has received increasing attention in recent years (see, for example [1, 2]). Structural tailoring can be achieved by using the bending-torsional stiffness coupling of composite structures, as has been demonstrated in the X-29 wing. It can also be achieved in metallic-stiffened panels by skewing the stiffeners with respect to the axes of the panel, thereby introducing extensional-shear stiffness coupling. A recent numerical and experimental study has been reported on the combined effects of tailoring both skin laminate anisotropy and stiffener orientation

* Corresponding author.

on the buckling and postbuckling of composite panels, subjected to edge displacements [3]. The present paper is an extension of the study reported in the cited reference. The extensions include: (a) study of the effect of uniform temperature change; and (b) development of hierarchical sensitivity coefficients of the buckling and postbuckling responses.

The panels considered are rectangular and flat with a single centrally located I-shaped stiffener. Both the skin and the stiffener consist of a number of perfectly bonded layers. The individual layers are assumed to be homogeneous and anisotropic. A plane of thermoelastic symmetry exists, at each point of the skin and the stiffener sections, parallel to the middle plane of the section. The loading consists of an applied edge displacement and a uniform temperature change. The skin and each section of the stiffener are modeled as plate elements.

The hierarchical sensitivity coefficients (derivatives of the response quantities with respect to the laminate, layer and micromechanical parameters) are used for the following:

- (a) determine a search direction in the direct application of nonlinear mathematical programming algorithms;
- (b) generate an approximation for the buckling and postbuckling responses of a modified panel (along with a rapid reanalysis technique);
- (c) assess the effects of uncertainties in the material and geometric parameters of the computational model of the panel on the responses; and
- (d) predict the changes in the buckling and postbuckling responses due to changes in these parameters.

2. Mathematical formulation

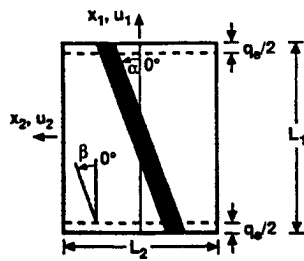
The analytical formulation is based on a first-order shear-deformation shallow-shell theory, with the effects of large displacements and laminated anisotropic material behavior included. A linear Duhamel–Neumann-type constitutive model is used and the material properties are assumed to be independent of temperature. The thermoelastic constitutive relations used in the present study are given in the appendix. The panel is discretized by using two-field mixed finite element models. The fundamental unknowns consist of the nodal displacements and the stress resultant parameters. The stress resultants are allowed to be discontinuous at interelement boundaries in the model. The sign convention for the generalized displacements is shown in Fig. 1. The external loading consists of an applied edge displacement q_e and a uniform temperature change T (independent of the coordinates x_1, x_2 and x_3).

2.1. Governing finite element equations

The governing finite element equations describing the postbuckling response of the panel can be written in the following compact form:

$$\{f(Z)\} = [K]\{Z\} + \{G(Z)\} - q_1\{Q^{(1)}\} - q_2\{Q^{(2)}\} = 0, \quad (1)$$

where $[K]$ is the global linear structure matrix which includes the flexibility and the linear strain-displacement matrices, $\{Z\}$ is the response vector which includes both unknown (free) nodal displacements and stress-resultant parameters, $\{G(Z)\}$ is the vector of nonlinear terms, q_1 and q_2 are

**Laminate properties**

$$E_L = 19.625 \text{ Msi}$$

$$E_T = 1.455 \text{ Msi}$$

$$G_{LT} = 0.82 \text{ Msi}$$

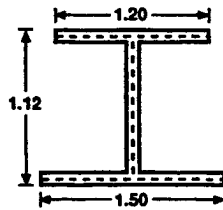
$$G_{TT} = 0.49 \text{ Msi}$$

$$\nu_{LT} = 0.295$$

$$\text{Thickness of individual layers} = .005 \text{ in.}$$

$$L_1 = 24 \text{ in.}$$

$$L_2 = 16.5 \text{ in.}$$

Stiffener**Boundary conditions**

$$\text{At } x_1 = \pm L_1/2$$

$$u_1 = \pm q_e/2$$

$$u_2 = w = \phi_1 = \phi_2 = \phi_3 = 0$$

$$\text{At } x_1 = \pm .4375 L_1 \text{ and at } x_2 = \pm .4848 L_2$$

$$w = 0$$

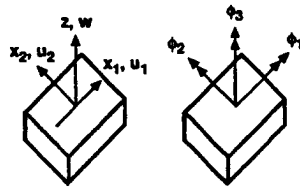


Fig. 1. Panels considered and stiffener geometry.

edge displacement and thermal strain parameters, respectively, $\{Q^{(1)}\}$ is the vector of normalized mechanical strains, and $\{Q^{(2)}\}$ is the vector of normalized thermal strains. The form of the arrays $[K]$, $\{G(Z)\}$, $\{Q^{(1)}\}$ and $\{Q^{(2)}\}$ is given in Ref. [4].

The procedures for determining the stability boundary, and the postbifurcation equilibrium configurations, corresponding to specified values of the parameters q_1 and q_2 are described in Ref. [4]. If an incremental-iterative technique such as the Newton–Raphson method is used, the recursion formula for the r th iteration can be written in the following form:

$$\left[[K] + \left[\frac{\partial G_i}{\partial Z_j} \right] \right] \{\Delta Z\}^{(r)} = -\{f(Z)\}^{(r)} \quad (2)$$

and

$$\{Z\}^{(r+1)} = \{Z\}^{(r)} + \{\Delta Z\}^{(r)}, \quad (3)$$

where $\{\Delta Z\}^{(r)}$ is the change in the response vector during the r th iteration cycle, and the range of I, J is the total number of components of the response vector $\{Z\}$.

2.2. Sensitivity of the postbuckling response

The derivatives of the postbuckling response with respect to the laminate, layer and micro-mechanical parameters are obtained by differentiating Eqs. (1). The resulting linear algebraic equations have the following form:

$$\left[[K] + \left[\frac{\partial G_I}{\partial Z_J} \right] \right] \left\{ \frac{\partial Z}{\partial \lambda} \right\} = - \left[\frac{\partial K}{\partial \lambda} \right] \{Z\} + q_1 \left\{ \frac{\partial Q^{(1)}}{\partial \lambda} \right\} + q_2 \left\{ \frac{\partial Q^{(2)}}{\partial \lambda} \right\}. \quad (4)$$

Note that the matrix on the left-hand side of Eqs. (4) is identical to that used in the Newton–Raphson iterative process (see Eq. (2)). Therefore, if the Newton–Raphson technique is used in generating the postbuckling response, the evaluation of each sensitivity coefficient requires the generation of the right-hand side of Eqs. (4), and a forward-reduction/back-substitution operation only (no decomposition of the left-hand side matrix is required). The explicit form of the arrays $\{\partial Q^{(1)}/\partial \lambda\}$ and $\{\partial Q^{(2)}/\partial \lambda\}$ is given in Ref. [4].

Multiple-parameter reduction methods have been developed for substantially reducing the number of degrees of freedom used in the initial discretization in order to reduce the cost of generating the stability boundary, the postbifurcation equilibrium configurations and the sensitivity coefficients [5, 6]. The methods are based on successive applications of the finite element method and the classical Rayleigh–Ritz technique. The finite element method is used to generate a few global approximation vectors (or modes) for approximating each of the nonlinear equations (1), and the equations for the sensitivity coefficients (4). The Rayleigh–Ritz technique is then used to generate the reduced sets of equations in terms of the amplitudes of these modes.

An effective set of modes for approximating the nonlinear equations was found to be the path derivatives of the response quantities with respect to the parameters q_1 and q_2 . The modes used in approximating the equations for the sensitivity coefficients include both the path derivatives and their derivatives with respect to λ . The equations used in evaluating the path derivatives, and their derivatives with respect to λ are obtained by successive differentiation of the original nonlinear equations (1), with respect to q_1, q_2 and λ . The left-hand side matrix in these equations is the same as that of Eqs. (2). The details of applying reduction methods to the generation of the stability boundary, and the postbifurcation equilibrium path are given in Refs. [5, 6], and their application to the evaluation of the sensitivity coefficients is described in Refs. [7, 8].

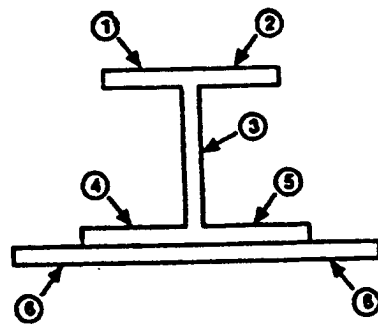
3. Numerical studies

Extensive numerical studies were performed to determine the effects of the stiffener skew angle and fiber orientation of the skin and the stiffener sections on the buckling and postbuckling responses and their sensitivity coefficients. The loading on the panels consisted of an applied edge shortening q_e and a uniform temperature change T . Hierarchical sensitivity coefficients were evaluated for each problem. The sensitivity coefficients are the derivatives of the different response quantities with respect to (a) skin and stiffener stiffnesses, and (b) material properties and fiber angles of the

Table 1
Number of layers and fiber orientations in the different sections

	Section	Number of layers	Fiber orientation
Top flange	1	16	$[\pm 45/0/90/\pm 45/0/90/90/0/\pm 45/90/0/\mp 45]$
	2	16	$[\mp 45/0/90/\mp 45/0/90/90/\pm 45/90/0/\mp 45]$
Web	3	16	$[\pm 45/0/90]_{2s}$
Bottom flange	4	16	$[\pm 45/0/90/\mp 45/0/90/90/0/\pm 45/90/0/\pm 45]$
	5	16	$[\pm 45/0/90/\mp 45/0/90/90/0/\mp 45/90/0/\mp 45]$
Skin	6	16	$[\pm 45/\mp 45/0_3/90]_s^*$

*Note: The laminate reference angle β° should be added to all fiber angles of the skin



individual layers. The material properties and geometric characteristics for the panels considered in the present study are given in Fig. 1. The material properties, the fiber orientations and the stacking sequence selected are those typical of composite panels considered for modern aircraft. The number of layers and fiber orientation in the different sections of the panel are given in Table 1. The skin and each section of the stiffener are modeled as plate elements. The middle planes of each of the top flange, web and skin are taken as their respective reference planes. For the bottom flange, the middle plane of the skin is taken as its reference plane.

Two parameters were varied in the present study, namely, the skew angle of the stiffener, α , and the fiber reference angle of the skin, β . The stiffener skew angle and the laminate reference angle for the five panels considered in the present study are given in Table 2. Mixed finite element models were used for the discretization of each section of the stiffener and the skin. A typical finite element model used in the analysis is shown in Fig. 2. Biquadratic shape functions were used for approximating each of the generalized displacements, and bilinear shape functions were used for approximating each of the stress resultants. The characteristics of the finite element model are given in Ref. [9]. The model had a total of 638 finite elements (12,229 nonzero displacement degrees of freedom). For each panel, the multiple parameter reduction methods outlined in Refs. [5, 8] were used for generating the buckling and postbuckling responses, and evaluating the sensitivity coefficients. Comparisons were made with available experimental results [3, 10]. Typical results are presented in Table 3, in Figs. 3–9 for the buckling response and in Figs. 10–16 for the postbuckling response, and are described subsequently.

Table 2
Panels considered in the present study






	Panel				
	1	2	3	4	5
Stiffener skew angle, α°	0	0	20	20	20
Laminate reference angle β°	0	20	0	20	20
					

Table 3
Critical values of q_c and T for the different panels

		Panel				
		1	2	3	4	5
$10^2 \times \frac{q_{cr}}{h_{skin}}$	Experiment [3]	12.36	12.28	11.86	10.58	10.49
	STAGS [8]	14.46	13.6	10.98	11.25	10.49
	Present	14.19	13.38	10.95	11.25	10.44
$T_{cr} (^\circ F)$ (Present)		408.8	333.0	292.6	240.6	287.7

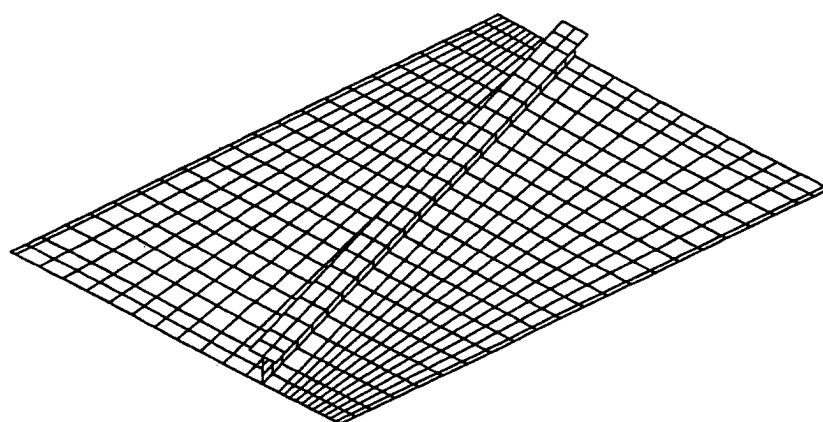


Fig. 2. Typical finite element model used.

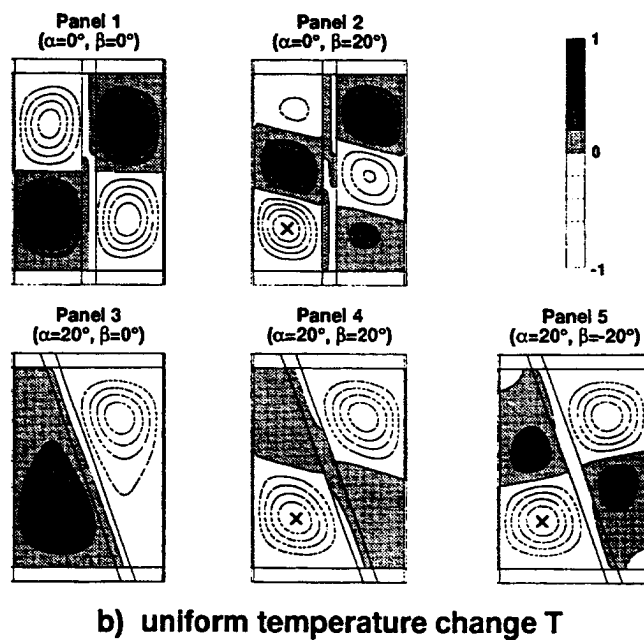
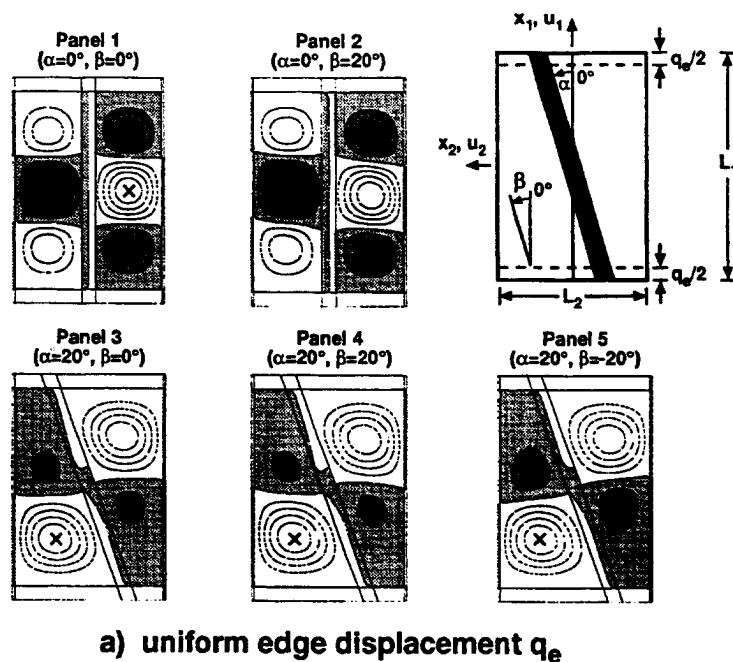


Fig. 3. Contour plots of transverse displacement w depicting the buckling mode shapes for panels subjected to uniform edge displacement q_e and uniform temperature change T . Spacing of contour lines is 0.2. Dashed lines refer to negative contours. Location of maximum values identified by \times .

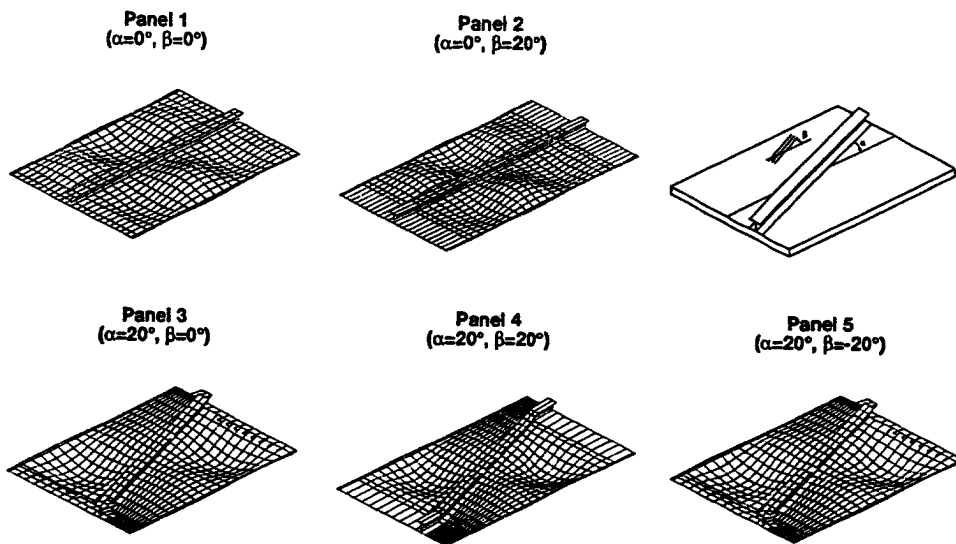
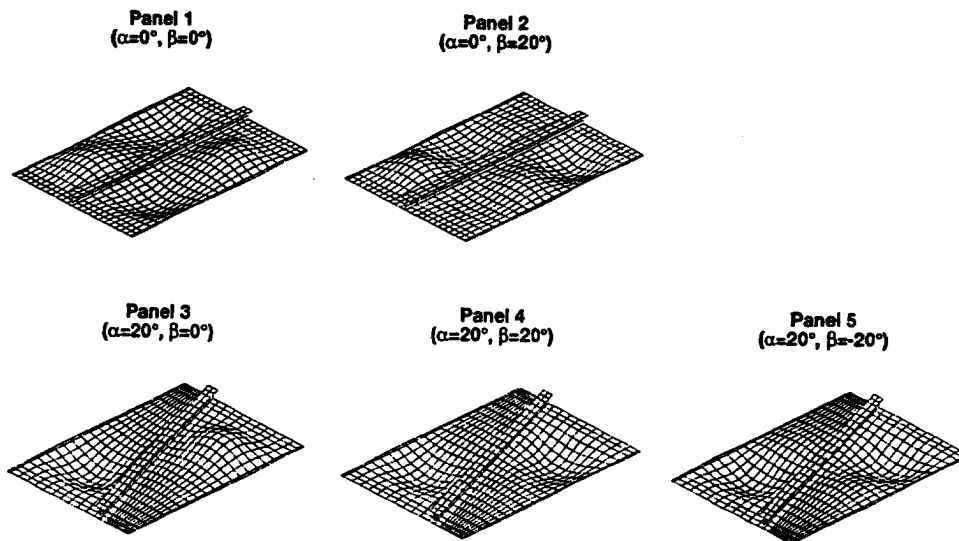
a) uniform edge displacement q_e b) uniform temperature change T

Fig. 4. Surface plots depicting the buckling modes for panels subjected to uniform edge displacement q_e and uniform temperature change T .

3.1. Bifurcation buckling

The critical values of q_c and T obtained by the present finite element model are given in Table 3. The critical values of q_c are compared with both the experimental values reported in Ref. [3], and the values obtained by the STAGS finite element program [10].

As can be seen from Table 3, rotating the stiffener has a more pronounced effect on the critical values of q_c and T than changing the reference angle of the skin. Panel 1 has the largest values of q_{cr} and T_{cr} ; panel 3 has the smallest value for q_{cr} and panel 4 has the smallest value of T_{cr} .

Contour plots of the transverse displacement w , and surface plots depicting the mode shapes associated with the critical values of q_c and T for the five panels, are shown in Figs. 3 and 4. Note that all the mode shapes satisfy the following inversion symmetry (or antisymmetry) conditions:

$$f(x_1, x_2) = \pm f(-x_1, -x_2),$$

where f refers to any of the generalized displacement components.

For all the panels considered, the lowest critical values of q_c and T are associated with two half-waves in the x_2 -direction. For the q_c -case, when $\alpha = 0^\circ$, the lowest buckling load is associated with three half-waves in the axial direction. This result is to be contrasted with two half-waves for the case $\alpha = 20^\circ$. For panels with $\beta = 0^\circ$, the buckling modes associated with q_{cr} and T_{cr} are different (exhibiting a different number of half-waves in the axial direction).

The normal and tangential edge forces associated with the critical values of q_c (with $T = 0, 100$ and 200°F), and T ($q_c = 0$) are shown in Fig. 5 for the five panels. For the q_c case, an increase in the temperature from 0 to 200°F reduces the total normal force \bar{N}_t in panels 1–4. For panel 4, an increase in T results in a decrease in the magnitude of the tangential force \bar{N}_s . An opposite trend is observed in panel 5 for which an increase in T increases the magnitudes of both \bar{N}_t and \bar{N}_s .

For the T case, increasing the magnitude of either α or β or both results in decreasing the total axial force \bar{N}_t . The tangential forces for positive nonzero α and β are of opposite signs. Therefore, the values of \bar{N}_s for panels 4 and 5 are less than, and greater than, respectively, those for panels 2 and 3.

An indication of the sensitivity of the critical values of q_c and T to variations in the material properties of the individual layers and the skin reference angle β is given in Figs. 6 and 7, respectively. The sensitivity coefficients of q_c and T are evaluated at $T = 0^\circ\text{F}$ and $q_c = 0$, respectively. For the q_c case, panels 2 and 5 are more sensitive to variations in E_L than the other panels; panel 1 is more sensitive to variations in G_{LT} than the other panels; panel 5 is insensitive to variations in G_{LT} ; and as to be expected, all panels are sensitive to variations in β . For the T case, panels 1 and 4 are more sensitive to variations in E_L than the other panels, and panel 5 is more sensitive to variations in β than the other panels.

An indication of the sensitivity of the critical values of q_c and T to variations in the skin, web and flange stiffnesses is given in Figs. 8 and 9. For the q_c case, the panels are more sensitive to variations in A_{11} of the skin and D_{22} of the web than to variations in the other extensional and bending stiffnesses of the panel. By contrast, for the T case, the panels are more sensitive to variations in the thermal force N_{T11} of the skin and the thermal moment M_{T21} of the bottom flange (see Eqs. (A.10) in the appendix).

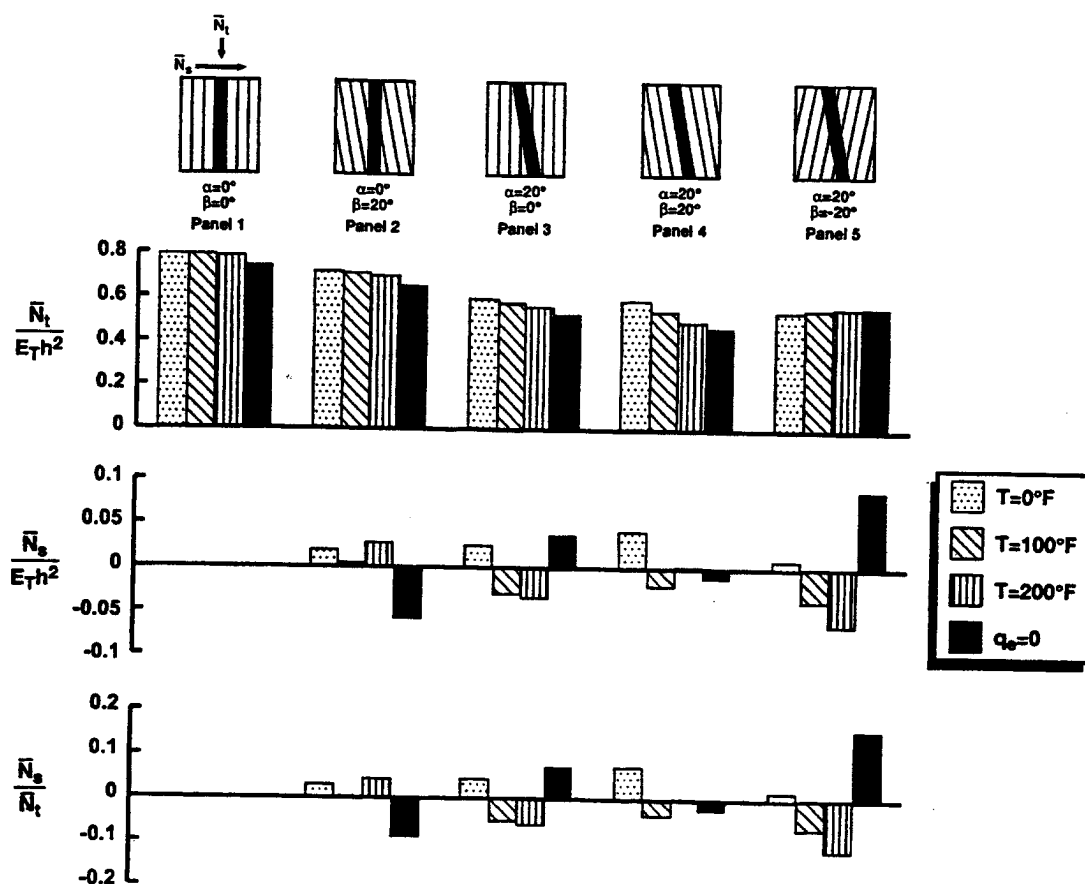


Fig. 5. Normal and tangential edge forces associated with the critical values of q_e and T for the different panels.

3.2. Postbuckling response

The postbuckling response of the different panels subjected to combined edge shortening q_e , and uniform temperature change $T = 100^\circ\text{F}$ is shown in Fig. 10. Plots of the total axial force \bar{N}_t versus the applied edge shortening q_e and the total strain energy U are shown. Also shown are the ratios of the tangential force to the axial force \bar{N}_s/\bar{N}_t versus q_e for the different panels. The bottom right section of Fig. 10 shows the corresponding plot of \bar{N}_s versus q_e normalized by dividing \bar{N}_s and q_e by the critical values $\bar{N}_{t,cr}$ and $q_{e,cr}$ for panel 1 ($\alpha = 0^\circ, \beta = 0^\circ$). The normalized plots of $\bar{N}_s/\bar{N}_{t,cr}$ versus $q_e/q_{e,cr}$ are almost linear.

As can be seen from Fig. 10, the \bar{N}_t versus q_e and \bar{N}_t versus U plots for the different panels are close to each other. For a given \bar{N}_t , both q_e and U have their smallest and largest values for panels 1 and 5, respectively. The panels with the rotated stiffener (panels 3-5) have higher shear stiffness than those with the unrotated stiffener (panels 1 and 2). The tangential force \bar{N}_s for panel 1 is equal to zero, and \bar{N}_s for panel 2 is smaller than \bar{N}_s for other panels. In the advanced postbuckling stage, the ratio \bar{N}_s/\bar{N}_t for panel 4 is higher than that for all other panels.

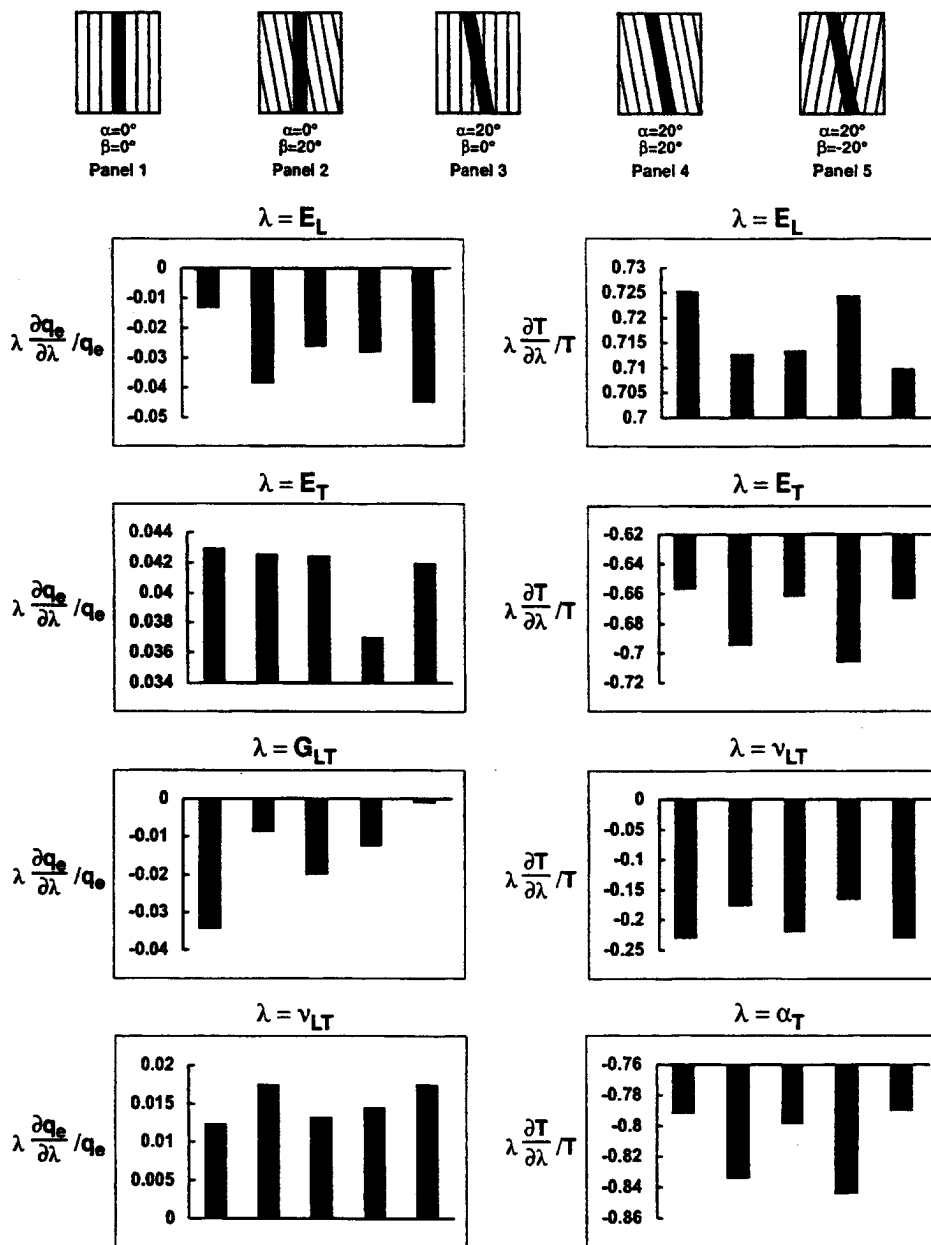


Fig. 6. Sensitivity of the critical values of q_c and T to variations in the material properties of individual layers.

An indication of the effect of temperature on the postbuckling response of the different panels is given in Fig. 11. An increase in temperature results in a parallel shift of the \bar{N}_t versus q_c plots. The same is true for the \bar{N}_t versus U plots (results not shown).

Normalized contour plots for the transverse displacement w of the skin and the total strain energy density \bar{U} , at two different values of \bar{N}_t , namely, $\bar{N}_t/(E_T h^2) = 0.8$ and $\bar{N}_t/(E_T h^2) = 1.6$, are shown in

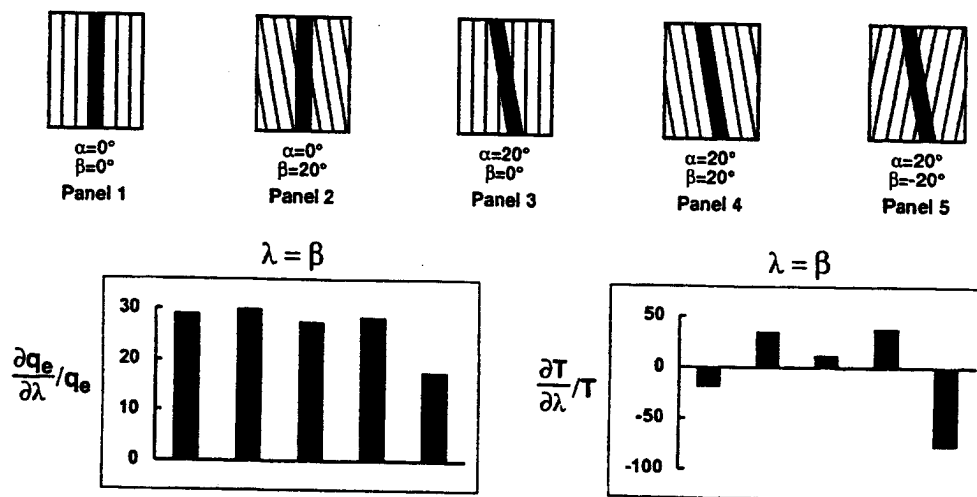


Fig. 7. Sensitivity of the critical values of q_e and T to variations in the skin reference angle β .

Figs. 12 and 13. As can be seen from Fig. 12, a mode change occurs in the advanced postbuckling stage for panel 1. The distributions of the total strain energy density are different in different panels. For each panel the distributions change in the advanced postbuckling stage. For the two panels with $\alpha = 0$ (panels 1 and 2), the distributions of \bar{U} are similar. The same applies to the three panels with $\alpha = 2$ (panels 3–5).

The sensitivity coefficients of the total strain energy U for the different panels with respect to the layer properties $E_L, E_T, G_{LT}, G_{TT}, \alpha_L$ and α_T ; and the skin reference angle β are shown in Figs. 14 and 15 for different temperatures. As can be seen from Figs. 14 and 15, the sensitivity of the total strain energy to variations in E_L increases rapidly with the increase in q_e . Other sensitivity coefficients exhibit smaller variation with changes in q_e . For $T \leq 100^\circ\text{F}$, the normalized sensitivity coefficient $E_L(\partial U / \partial E_L)$ becomes the dominant sensitivity coefficient in the advanced postbuckling stage. For $T \geq 100^\circ\text{F}$, the total strain energy is very sensitive to variations in α_T and E_T and somewhat sensitive to variations in E_L in the initial postbuckling stage.

Fig. 15 shows that for $T = 0^\circ\text{F}$, the panels with $\beta \neq 0^\circ$ (panels 2, 4 and 5) are considerably more sensitive to variations in β than the two panels with $\beta = 0^\circ$ (panels 1 and 3). In the advanced postbuckling stage, an increase in temperature results in decreasing $\partial U / \partial \beta$ (for a given value of q_e).

Normalized contour plots for the sensitivity coefficient of the total strain energy density with respect to E_L and β , for two different values of \bar{N}_t , namely, $\bar{N}_t / (E_T h^2) = 0.8$ and $\bar{N}_t / (E_T h^2) = 1.6$, are shown in Fig. 16. Each contour plot is normalized by dividing by the maximum value of the sensitivity coefficient. The contour plots for the different sensitivity coefficients are different. The contour plots for each of the sensitivity coefficients change with changing \bar{N}_t .

4. Concluding remarks

A study is made of the buckling and postbuckling responses of composite panels with skewed stiffeners. The panels are subjected to applied edge displacements and temperature changes. Each section of the stiffeners and skin is modeled by using a first-order shear-deformation shallow-shell

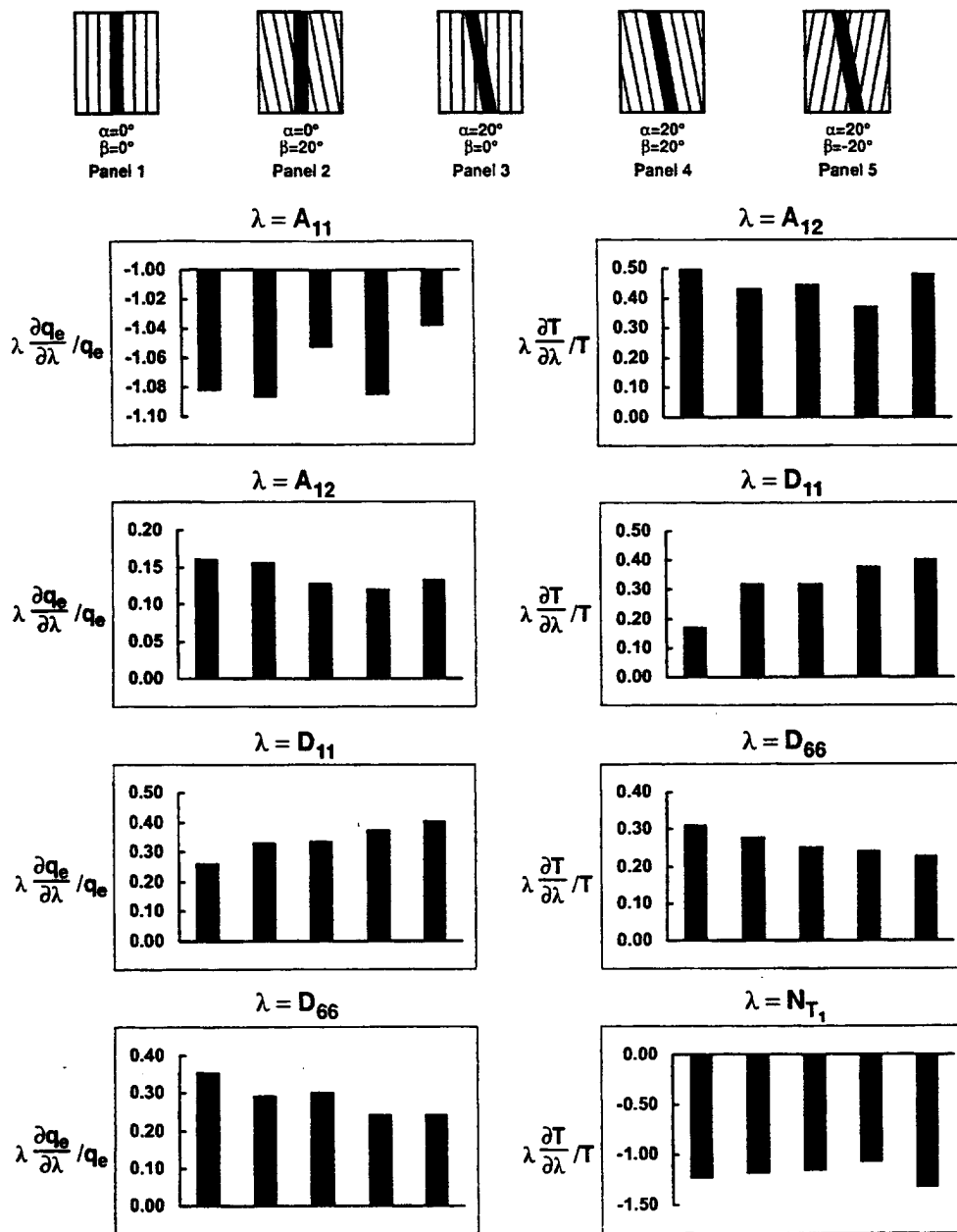


Fig. 8. Sensitivity of the critical values of q_e and T to variations in the skin stiffnesses of the panels.

theory, with the effects of large displacements and laminated anisotropic material behavior included. A linear, Duhamel–Neumann-type constitutive model is used and the material properties are assumed to be independent of temperature. The different sections of the stiffeners and skin are discretized by using two-field mixed finite element models with the fundamental unknowns consisting of the nodal

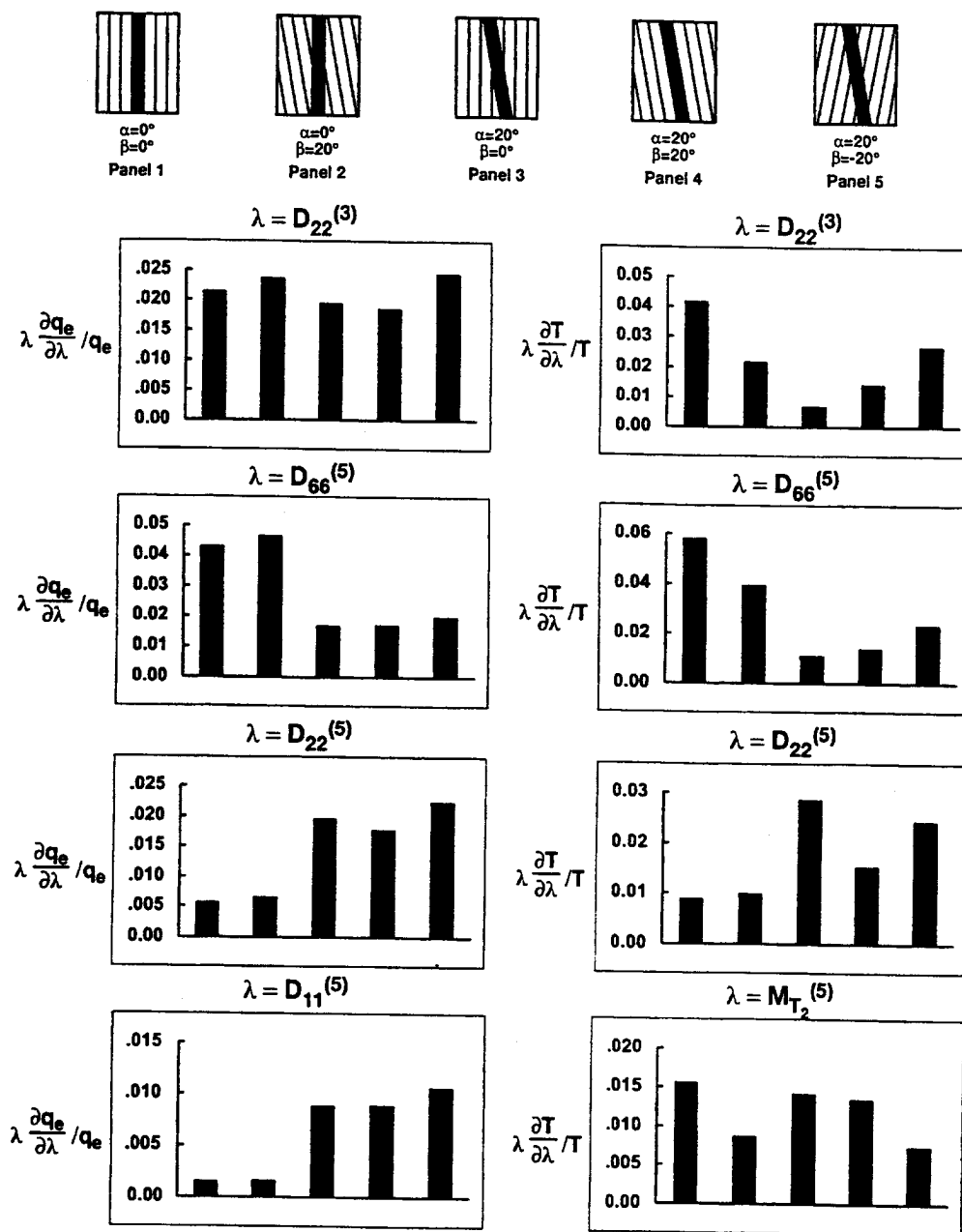


Fig. 9. Sensitivity of the critical values of q_c and T to variations in the web and flange stiffnesses of the panels. Superscripts refer to the stiffener section (see Table 1).

displacements and stress-resultant parameters. The stress resultants are allowed to be discontinuous at interelement boundaries.

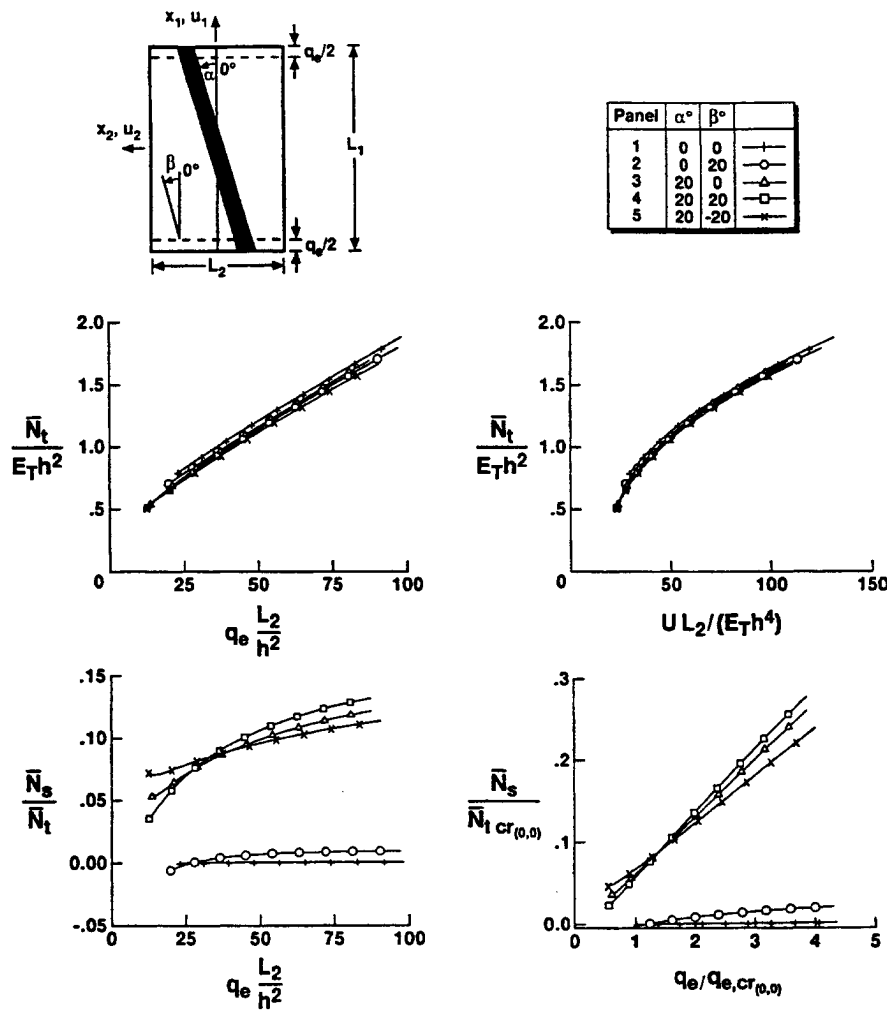


Fig. 10. Postbuckling responses for the different panels when subjected to edge displacement q_e , and uniform temperature change $T=100^\circ\text{F}$.

The buckling, postbuckling responses and hierarchical sensitivity coefficients are generated. The hierarchical sensitivity coefficients measure the sensitivity of the different response quantities to variations in three sets of interrelated parameters; namely, laminate, layer and constituent (fiber, matrix and interface or interphase) parameters. An efficient multiple-parameter reduction method is used for generating the buckling and postbuckling responses, and evaluating the sensitivity coefficients.

Numerical studies are presented which show the effects of variations in the stiffener skew angle and the fiber orientation of the skin on the buckling and postbuckling responses, and the sensitivity coefficients.

The results show that rotating the stiffener has a more pronounced effect on the critical values of the edge shortening and temperature than changing the material reference angle of the skin. Also, rotating the stiffener increases the shear stiffness of the panels in the postbuckling range.

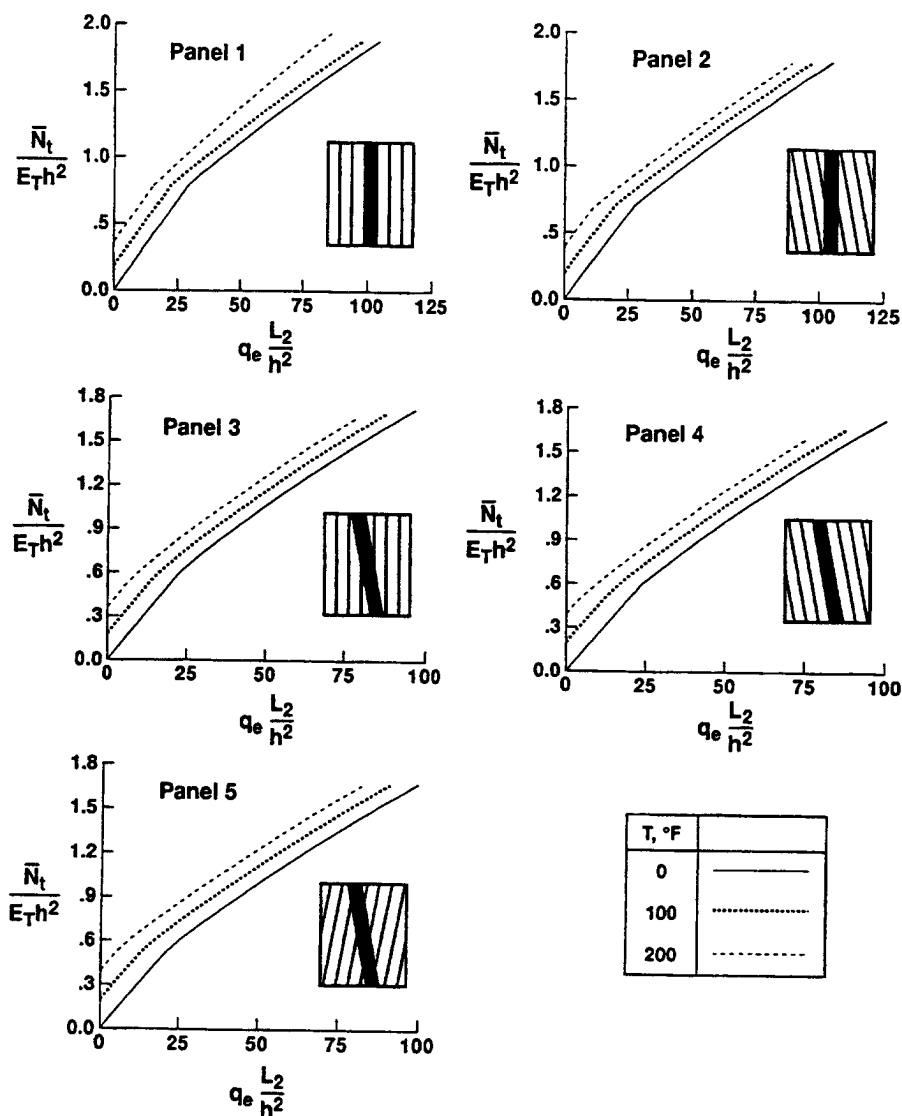


Fig. 11. Effect of temperature change on the postbuckling response of different panels subjected to edge displacement q_e .

Acknowledgments

This work was partially supported by NASA Grant NAG-1-1162 and AFOSR Grant F49620-96-1-0462. The numerical studies were performed on the CRAY C-90 computer at NASA Ames Research Center. The authors acknowledge the assistance of Catherine Richter of the University of Virginia in preparing the final manuscript and improving the figures.

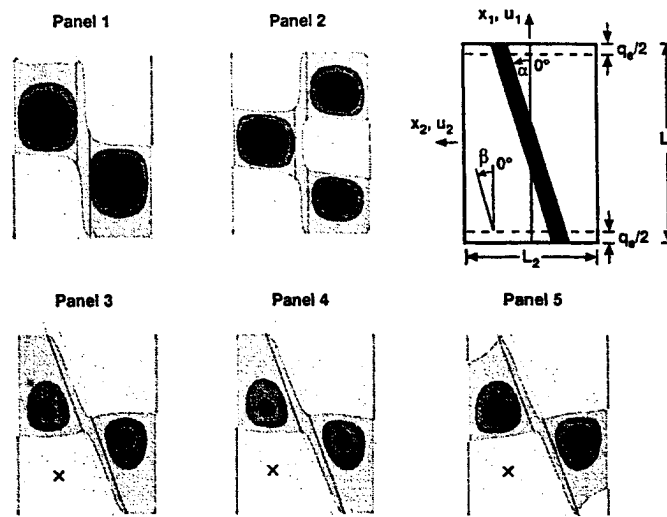
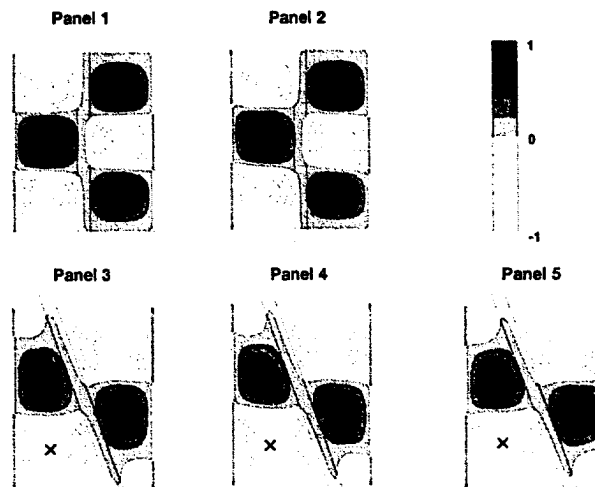
a) total edge force $\bar{N}_t/(E_T h^2) = 0.8$ b) total edge force $\bar{N}_t/(E_T h^2) = 1.6$

Fig. 12. Normalized contour plots depicting the effects of the stiffener skew angle α and skin reference angle β on the transverse displacement w of the skin. Combined edge displacement q_e and uniform temperature change $T=100^\circ\text{F}$. Spacing of contour lines is 0.2. Dashed lines refer to negative contours. Location of maximum values identified by x .

Appendix. Thermoelastic constitutive relations for the laminate

The thermoelastic model used in the present study is based on the following assumptions:

- (1) The laminates are composed of a number of perfectly bonded layers.
- (2) Every point of the laminate is assumed to possess a single plane of thermoelastic symmetry parallel to the middle plane.

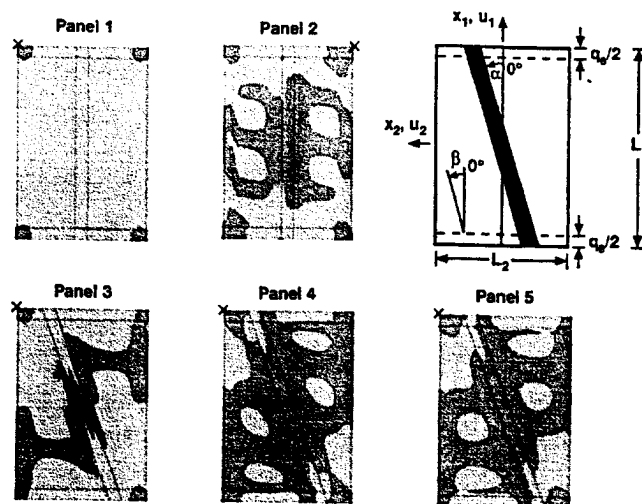
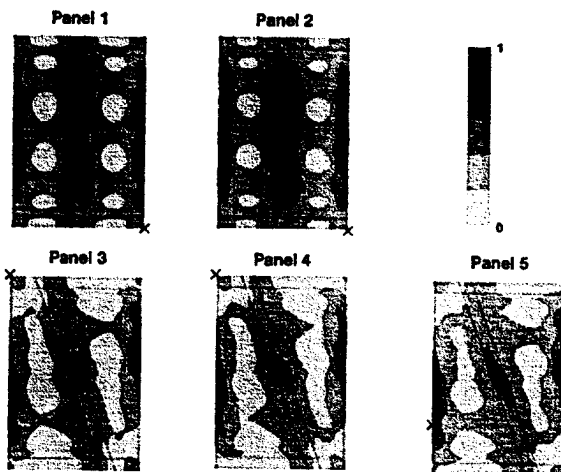
a) total edge force $\bar{N}_t / (E_T h^2) = .8$ b) total edge force $\bar{N}_t / (E_T h^2) = 1.6$

Fig. 13. Normalized contour plots depicting the effects of the stiffener skew angle α and skin reference angle β on the total strain energy density in the skin. Combined edge displacement q_e and uniform temperature change $T = 100^\circ\text{F}$. Spacing of contour lines is 0.2. Dashed lines refer to negative contours. Location of maximum values identified by \times .

- (3) The material properties are independent of temperature.
- (4) The constitutive relations are described by lamination theory, and can be written in the following compact form:

$$\begin{Bmatrix} N \\ M \\ Q \end{Bmatrix} = \begin{bmatrix} [A] & [B] & 0 \\ [B]^T & [D] & 0 \\ 0 & 0 & [A_s] \end{bmatrix} \begin{Bmatrix} \epsilon \\ \kappa \\ \gamma \end{Bmatrix} - \begin{Bmatrix} N_T \\ M_T \\ 0 \end{Bmatrix}, \quad (\text{A.1})$$

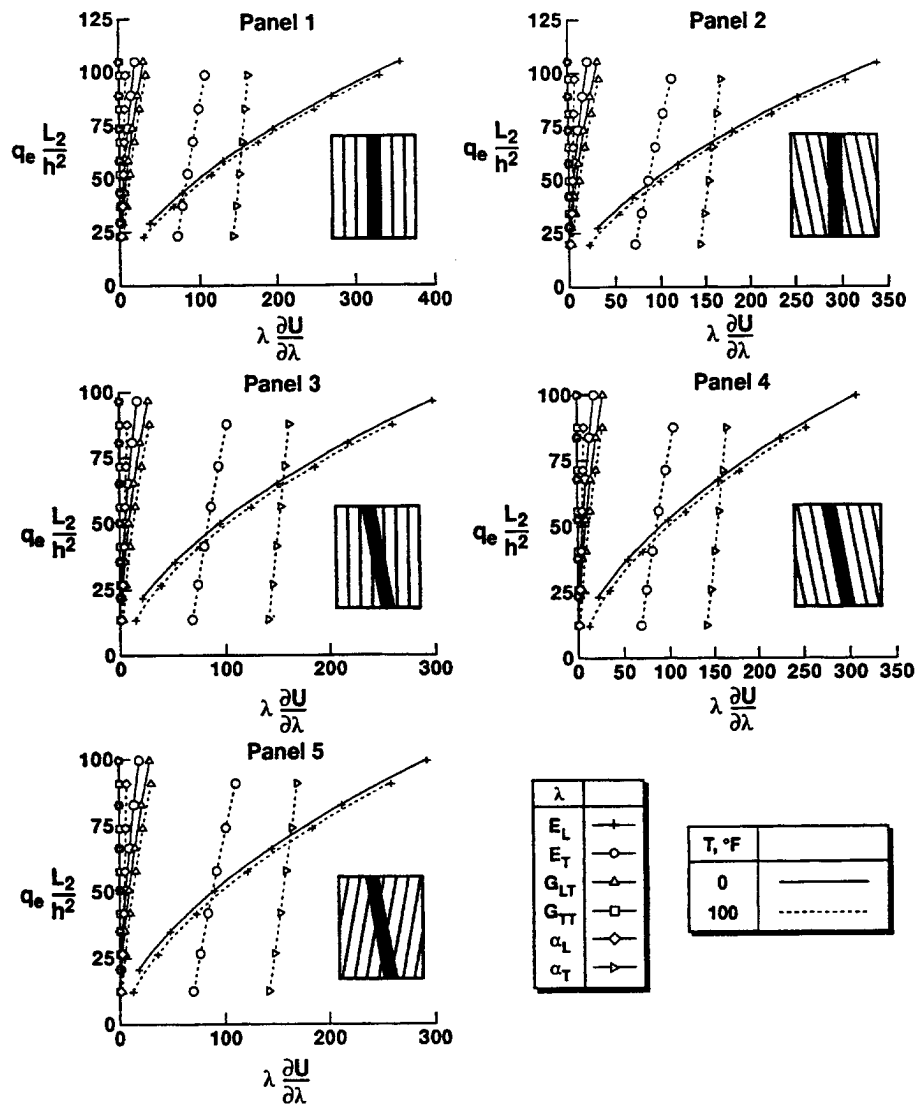


Fig. 14. Sensitivity of the postbuckling responses of the different panels to variations in the material properties of the individual layers. Combined edge displacement q_e and uniform temperature change $T = 0^\circ$ and $100^\circ F$.

where $\{N\}$, $\{M\}$, $\{Q\}$ and $\{\epsilon\}$, $\{\kappa\}$, $\{\gamma\}$ are the vectors of extensional, bending and transverse shear stress resultants and strain components of the laminate given by

$$\{N\}^t = [N_1 \quad N_2 \quad N_{12}], \quad (A.2)$$

$$\{M\}^t = [M_1 \quad M_2 \quad M_{12}], \quad (A.3)$$

$$\{Q\}^t = [Q_1 \quad Q_2], \quad (A.4)$$

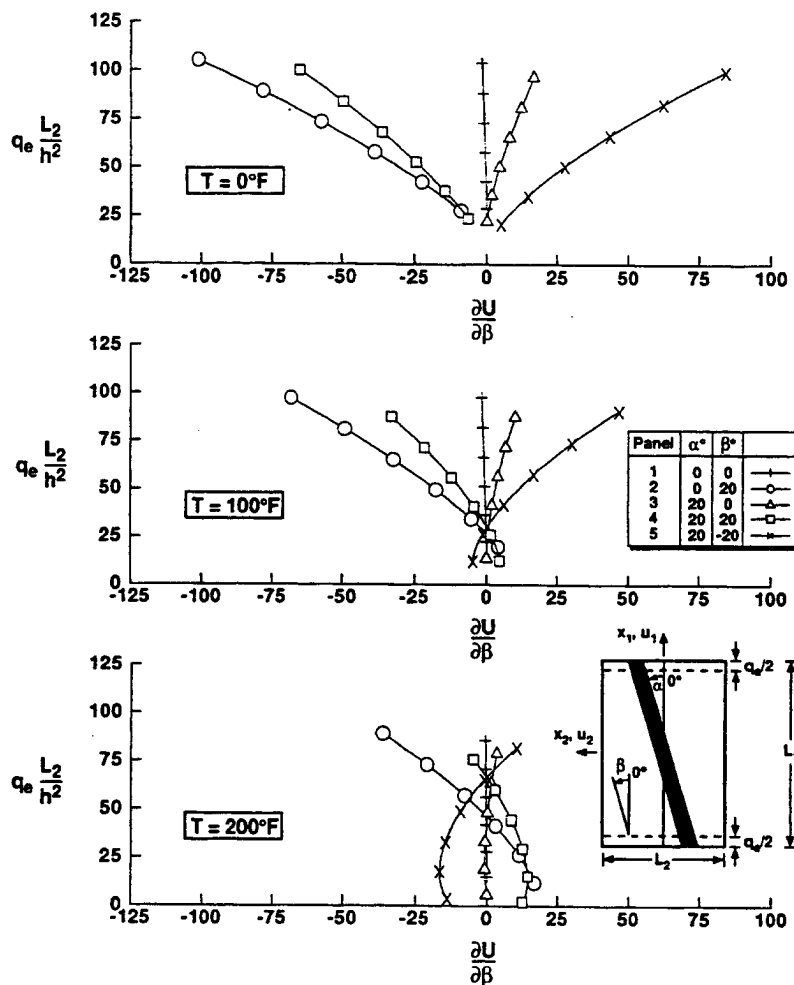


Fig. 15. Sensitivity of the postbuckling responses of the different panels to variations in the skin reference angle β . Combined edge displacement q_e and uniform temperature change $T = 0^\circ, 100^\circ$ and 200°F .

$$\{\varepsilon\}^t = [\varepsilon_1 \quad \varepsilon_2 \quad 2\varepsilon_{12}], \quad (\text{A.5})$$

$$\{\kappa\}^t = [\kappa_1 \quad \kappa_2 \quad 2\kappa_{12}], \quad (\text{A.6})$$

and

$$\{\gamma\}^t = [2\varepsilon_{31} \quad 2\varepsilon_{32}]. \quad (\text{A.7})$$

The matrices $[A]$, $[B]$, $[D]$ and $[A_s]$ contain the extensional, coupling, bending and transverse shear stiffnesses of the laminate which can be expressed in terms of the layer stiffnesses as follows:

$$[[A] \quad [B] \quad [D]] = \sum_{k=1}^{NL} \int_{h_{k-1}}^{h_k} [\bar{Q}]^{(k)} [[I] \quad x_3[I] \quad (x_3)^2[I]] dx_3, \quad (\text{A.8})$$

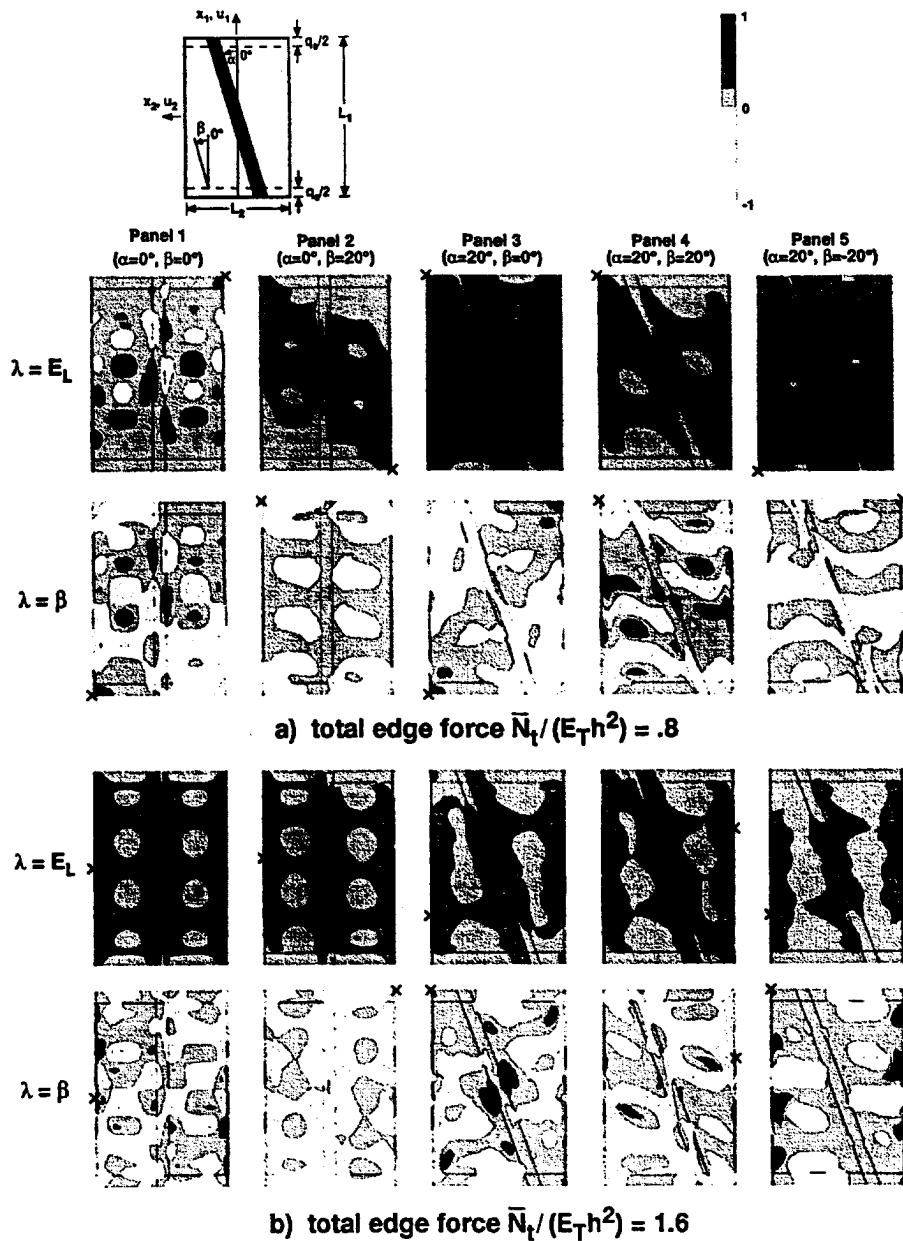


Fig. 16. Normalized contour plots depicting the effects of the stiffener skew angle α and skin reference angle β on the sensitivity coefficients of the total strain energy density in the skin. Combined edge displacement q_c and uniform temperature change $T = 100^\circ\text{F}$. Spacing of contour lines is 0.2. Dashed lines refer to negative contours. Location of maximum values identified by \times .

$$[A_s] = \sum_{k=1}^{NL} \int_{h_{k-1}}^{h_k} [\bar{Q}_s]^{(k)} dx_3, \quad (A.9)$$

where $[\bar{Q}]^{(k)}$ and $[\bar{Q}_s]^{(k)}$ are the extensional and transverse shear stiffnesses of the k th layer, $[I]$ is the identity matrix, h_k and h_{k-1} are the distances from the top and bottom surfaces of the k th layer to the middle surface, and NL is the total number of layers in the laminate. The expressions for the different coefficients of the matrices $[\bar{Q}]^{(k)}$ and $[\bar{Q}_s]^{(k)}$ in terms of the material and geometric properties of the constituents (fiber and matrix) are given in Refs. [11, 12].

The vectors of thermal effects, $\{N_T\}$ and $\{M_T\}$, are given by

$$[\{N_T\} \quad \{M_T\}] = \sum_{k=1}^{NL} \int_{h_{k-1}}^{h_k} [\bar{Q}]^{(k)} \{\alpha\}^{(k)} [1 \quad x_3] T dx_3, \quad (A.10)$$

where $\{\alpha\}$ is the vector of coefficients of thermal expansion (referred to the coordinates x_1, x_2 and x_3 – see, for example, Refs. [13, 14]). Note that the skin and the bottom flange stiffnesses and thermal effects are referred to the middle plane of the skin. The top flange and web section stiffnesses and thermal effects are referred to their respective middle plane.

References

- [1] D.W. Gimmestad, An aeroelastic optimization procedure for composite high aspect ratio wings, Proc. 20th ASME/ASCE/AIAA/AHS/ASC Structures, Structural Dynamics and Materials Conf., 1979, pp. 79–86, AIAA Paper No. 79-0726.
- [2] E.H. Mansfield, Some structural parameters for aero-isoclinic wings, Aircraft Eng. 24 (1952) 283.
- [3] R.D. Young, J.H. Starnes, Jr., M.W. Hyer, Effects of skewed stiffeners and anisotropic skins on the response of compression-loaded composite panels, Proc. 10th DoD/NASA/FAA Conference on Fibrous Composites in Structural Design, Hilton Head Island, SC, 1–4 November 1993, Naval Air Warfare Center Report No. NAWACADWAR-94096-60, Vol. 1, April 1994, pp. II-109 to II-123.
- [4] A.K. Noor, Finite element buckling and postbuckling analyses, in: G.J. Turvey, I.H. Marshall (Eds.), Buckling and Postbuckling of Composite Plates, Chapman & Hall, London, 1995, pp. 58–107.
- [5] A.K. Noor, J.M. Peters, Multiple-parameter reduced basis technique for bifurcation and postbuckling analyses of composite plates, Int. J. Numer. Methods Eng. 19 (1983) 1783–1803.
- [6] A.K. Noor, J.M. Peters, Recent advances in reduction methods for instability analysis of structures, Comput. Struct. 16 (1–4) (1983) 67–80.
- [7] A.K. Noor, J.M. Peters, Reduced basis technique for calculating sensitivity coefficients of nonlinear structural response, AIAA J. 30(7) (1992) 1840–1847.
- [8] A.K. Noor, Recent advances in the sensitivity analysis for the thermomechanical postbuckling of composite panels, J. Eng. Mech. ASCE 122(4) (1996) 300–307.
- [9] A.K. Noor, C.M. Andersen, Mixed models and reduced/selective integration displacement models for nonlinear shell analysis, Int. J. Numer. Methods Eng. 18 (1982) 1429–1454.
- [10] R.D. Young, private communication.
- [11] R.M. Jones, Mechanics of Composite Materials, McGraw-Hill, New York, 1975.
- [12] S.W. Tsai, H.T. Hahn, Introduction to Composite Materials, Technomic Publishing Co., Westport, CT, 1980.
- [13] J. Padovan, Anisotropic thermal stress analysis, in: R.B. Hetnarski (Ed.), Thermal Stresses I, Elsevier Science Publishers, Amsterdam, 1986, pp. 143–262.
- [14] C.W. Bert, Analysis of Plates, in: C.C. Chamis (Ed.), Structural Design and Analysis, Part I, Vol. 7, Composite Materials, Academic, New York, 1975, pp. 149–206.

FINITE ELEMENTS IN ANALYSIS AND DESIGN

Editorial Policy

To provide ideas and information involving the use of the finite element method, including CAD/CAM, in professional practice, with an emphasis on structural, fluid and mechanical technologies.

Scope

Subjects presented by this journal will include static and dynamic, thermal and nonthermal, linear and nonlinear analysis and design associated with structural, fluid and mechanical engineering systems. Areas covered will be finite and boundary elements in heat transfer, solid, and fluid mechanics, with industrial, chemical, electronic, power generation, and aerospace applications. A particular emphasis will be in design-oriented finite element technology, especially integration into computer aided design and computer-aided manufacturing. Interaction problems of interest will include numerical analysis methods for simulating structure-structure, structure-thermal, structure-fluid, and structure-electrical field interaction. Contributions will be welcomed dealing with micro, mini, and main frame computers and their software related to solving finite element problems, as well as computer-aided design methods, optimal design algorithms, programming techniques, and programming reviews.

Descriptions of new concepts, algorithms, computing systems, physical data processing procedures, optimization and sensitivity routines, capabilities, modeling techniques, benchmark problems, and applications will be accepted.

The journal will also provide information on available software, including summaries and critical evaluations. Authoritative state-of-the-art reviews of appropriate computational mechanics technology will be published. In addition, there will be book reviews of new texts and treatises as well as information on useful databases.

Information for Contributors

Submission of papers: Papers to be submitted for publication should be sent in quadruplicate to the Editor-in-Chief: Dr. Harry G. Schaeffer, Mechanical Engineering Department, University of Louisville, Louisville, KY 40292, U.S.A. (Tel: 502-852-6099; Fax: 502-852-6053; E-mail: hgscha01@starbase.spd.louisville.edu), or communicated via a member of the Editorial Board who is most closely associated with the content of the work. In the latter case, one copy of the manuscript should be sent to the office of the Editor-in-Chief. All contributions should be written in English. Manuscripts submitted in other languages may be considered at the discretion of the Editorial Board.

Upon acceptance of an article, the author(s) will be asked to transfer copyright of the article to the publisher. This transfer will ensure the widest possible dissemination of information.

The corresponding author will receive *proofs*, which should be corrected and returned to the publisher by airmail within three days of receipt. Please note that typesetting costs of extensive corrections in proofs, other than printer's errors, will be charged to the author. *No page charge* is being made. *Fifty offprints* of each paper will be provided free of charge, and sent to the communicating author. Additional offprints can be ordered at cost.

Preparation of manuscript: Manuscripts should be typed double-spaced with wide margins and on one side of the page only. The first page of the manuscript should contain: title, name(s) of author(s), affiliation(s), complete mailing address(es), and a short abstract. Use this journal to see examples of correctly formatted papers. All mathematical symbols which are not typewritten should be specified and listed separately. Unusual symbols of notations should be identified in the margins. An explanation of notation in the text is highly preferred to the publication of a list of symbols. Do not use awkward mathematical notations which require special typesetting procedures. The numbers identifying displayed mathematical expressions should be placed in parentheses. (1), (2), The use of metric units of the SI (Système Internationale) form is preferred.

Footnotes should be brief, and their number should be kept to a minimum.

Originally drawn *figures* and glossy prints of photographs should be provided in a form suitable for photographic reproduction and reduction. The lettering should be done carefully; the captions should be given on a separate sheet. Complex diagrams should be referred to as figures and should be numbered consecutively; simple diagrams can be typeset. Each figure should have a number and should accompany the manuscript on a separate sheet. Reference to all figures should be made in the text.

Tables must be numbered, and typed on separate sheets in ample spacing.

Acknowledgements should be given before the references.

References to (un)published literature should be referred to consecutively in the text in square brackets [] and grouped together at the end of the paper in numerical order. Journal titles should be abbreviated in the style of the World List of Scientific Periodicals. References should be cited in the following style:

- | | |
|------------------------|--|
| Journal | [1] R.V. Southwell, "On the analogues relating flexure and extension of flat plates", <i>Q. J. Mech. Appl. Math.</i> 3 (3), pp. 257-270, 1950. |
| Book | [2] M.G. Salvadori, and M.L. Baron, <i>Numerical Methods in Engineering</i> , Prentice-Hall, Englewood Cliffs, NJ, 1961. |
| Conference proceedings | [3] Y.Q. Liu and H. Wu, A general computer program for two-dimensional thermal flows. <i>Proc. 1st Light Metallic Structures Conf.</i> , University Press of Virginia, Charlottesville, VA, pp. 310-315, 1990. |
| or | [4] G.C. Hsiao and J.F. Porter, "The coupling of BEM and FEM for exterior boundary value problems", in: D. Qinghua (ed.), <i>Boundary Elements</i> , (Proc. Int. Conf. on Boundary Element Methods in Engineering, Beijing, China, 1986), Pergamon Press, Oxford, pp. 77-86, 1986. |

Instructions for LaTeX Manuscripts

Papers that have been accepted for publication may be sent as an electronic file to the Publisher by E-mail or on a diskette. If the electronic file is suitable for processing by the Publisher, proofs will be produced without rekeying the full text. The article should be encoded in Elsevier-LaTeX or in standard LaTeX (in document style 'article'). The Elsevier-LaTeX package, together with more detailed instructions on how to prepare a file, is available from the Publisher upon request. This package can also be obtained through the Elsevier WWW homepage (<http://www.elsevier.nl/>), or using anonymous FTP from the Comprehensive TeX Archive Network (CTAN). The host-names are: ftp.dante.de, ftp.tex.ac.uk, ftp.shsu.edu; the directory is: /tex-archive/macros/latex/contrib/supported/elsevier.

No changes from the version accepted by the Editor of the journal are permissible, without the prior and explicit approval of the Editor. The Publisher reserves the right to decide whether to process a manuscript from authors' files or not. Articles coded in a simple manner with no user-defined macros are most likely to be handled this way.

If sent via electronic mail, files should be accompanied by a clear identification of the article (name of Journal, Editor's reference number) in the "subject field" of your electronic mail message. Authors should include an ASCII table (available from the Publisher) in their files to enable any transmission errors to be detected. For diskettes, allowed formats are 3.5" or 5.25" MS-DOS or 3.5" Macintosh.

E-mail: r.meesters@elsevier.nl.

Reprinted from

Computer methods in applied mechanics and engineering

Comput. Methods Appl. Mech. Engrg. 145 (1997) 341-360

Assessment of continuum models for sandwich panel honeycomb cores

W.S. Burton, A.K. Noor*

Center for Advanced Computational Technology, University of Virginia, NASA Langley Research Center, Hampton, VA USA

Received 9 June 1996; revised 18 September 1996



ELSEVIER

COMPUTER METHODS IN APPLIED MECHANICS AND ENGINEERING

EDITORS: J.H. ARGYRIS, STUTTGART and LONDON

T.J.R. HUGHES, STANFORD, CA

J.T. ODEN, AUSTIN, TX

W. PRAGER

Founding Editor

(deceased 1980)

EDITORIAL ADDRESSES

John H. ARGYRIS
Institut für Computer Anwendungen
Pfaffenwaldring 27
D-70569 STUTTGART
Germany
(Editorial Office)

Thomas J.R. HUGHES
Division of
Applied Mechanics
Durand Building
Room No. 281
Stanford University
STANFORD
CA 94305-4040, USA

J. Tinsley ODEN
The University of Texas
The Texas Institute for
Computational and
Applied Mathematics
Taylor Hall 2.400
AUSTIN
TX 78712, USA

ASSOCIATE EDITORS

K. APPA, Hawthorne, CA
I. BABUŠKA, Austin, TX
A.J. BAKER, Knoxville, TN
T. BELYTSCHKO, Evanston, IL
L. DEMKOWICZ, Austin, TX
R.E. EWING, College Station, TX
M. FEINGOLD, Marly-le-Roy

R.H. GALLAGHER, Potsdam, NY
R. GLOWINSKI, Houston, TX
H.-O. KREISS, Los Angeles, CA
J.L. LIONS, Paris
H. LOMAX, Moffet Field, CA
C.E. MASSONNET, Liège

L.S.D. MORLEY, Farnborough
K.S. PISTER, Berkeley, CA
G. STRANG, Cambridge, MA
G.P. VOSKRESENSKY, Moscow
W.H. YANG, Ann Arbor, MI
O.C. ZIENKIEWICZ, Swansea

ADVISORY EDITORS

J.F. ABEL, Ithaca, NY
H. ARMEN, Bethpage, NY
K.J. BATHE, Cambridge, MA
P.G. BERGAN, Høvik
J.F. BESSELING, Delft
G. BORM, Potsdam
H. BUFLER, Stuttgart
H. CABANNES, Paris
C. CANUTO, Torino
G.F. CARRIER, Cambridge, MA
T. CEBECI, Long Beach, CA
A.S.L. CHAN, London
J.L. CHENOT, Valbonne
H. CHRISTIANSEN, Provo, UT
T.J. CHUNG, Huntsville, AL
P.G. CIARLET, Paris
H. COHEN, New York, NY
M.Z. COHN, Waterloo, Ont.
J. DONEA, Ispra
P.R. EISEMAN, New York, NY
B. ENGQUIST, Los Angeles, CA
C.A. FELIPPA, Boulder, CO
K. FENG, Beijing
I. FRIED, Boston, MA
Editorial Secretary: Marties PARSONS

R.A. GELLATLY, San Leandro, CA
M. GERADIN, Liège
R. GRUBER, Manno
K.K. GUPTA, Edwards, CA
R.W. HAMMING, Monterey, CA
F.H. HARLOW, Los Alamos, NM
E.J. HAUG, Iowa City, IA
J.C. HEINRICH, Tucson, AZ
M. HOGGE, Liège
I. HOLAND, Trondheim
C. JOHNSON, Göteborg
B.Z. KAPLAN, Beer-Sheva
T. KAWAI, Tokyo
J. KESTENS, Brussels
S.W. KEY, La Cañada-Flintridge, CA
W.C. KNUDSON, Sunnyvale, CA
F.A. LECKIE, Santa Barbara, CA
R.W. LEWIS, Swansea
K. LINKWITZ, Stuttgart
LUO Shi-jun, Xi'an
G. MAIER, Milano
J.L. MEEK, St. Lucia, Queensland
A.J. MORRIS, Cranfield
A. NEEDLEMAN, Providence, RI
M.P. NIELSEN, Lyngby

A.K. NOOR, Hampton, VA
R. OHAYON, Paris
P.J. PAHL, Berlin
B. PAUL, Philadelphia, PA
R. PEYRET, Nice
J. PLANCHARD, Clamart
A.R.S. PONTER, Leicester
V.F. POTERASU, Iasi
QIAN Ling-xi (L.H. Tsien), Dalian
A.K. RAO, Bangalore
M. REISER, Rorschlikon
E. RIKS, Delft
P.J. ROACHE, Albuquerque, NM
G.I.N. ROZVANY, Essen
W. SCHIEHLEN, Stuttgart
B. SCHÖNUNG, Baden
P.S. SYMONDS, Providence, RI
A.B. TEMPLEMAN, Liverpool
C.W. TROWBRIDGE, Kidlington
J.R. WHITEMAN, Uxbridge
K.J. WILLAM, Boulder, CO
Y. YAMADA, Tokyo
Th. ZIMMERMANN, Lausanne

International Standard Serial Number 0045-7825

Copyright © 1997 Elsevier Science S.A. All rights reserved.

0045-7825/97/\$17.00

This journal and the individual contributions contained in it are protected by the copyright of Elsevier Science S.A., and the following terms and conditions apply to their use:

Photocopying

Single photocopies of single articles may be made for personal use as allowed by national copyright laws. Permission of the publisher and payment of a fee is required for all other photocopying, including multiple or systematic copying, copying for advertising or promotional purposes, resale, and all forms of document delivery. Special rates are available for educational institutions that wish to make photocopies for non-profit educational classroom use.

In the USA, users may clear permissions and make payment through the Copyright Clearance Center, 222 Rosewood Drive, Danvers, MA 01923, USA. In the UK, users may clear permissions and make payment through the Copyright Licensing Agency Rapid Clearance Service (CLARCS), 90 Tottenham Court Road, London, W1P 0LP. In other countries where a local copyright clearance centre exists, please contact it for information on required permissions and payments.

Derivative Works

Subscribers may reproduce tables of contents or prepare lists of articles including abstracts for internal circulation within their institutions. Permission of the publisher is required for resale or distribution outside the institution.

Permission of the publisher is required for all other derivative works, including compilations and translations.

Electronic Storage

Permission of the publisher is required to store electronically any material contained in this journal, including any article or part of an article. Contact the publisher at the address indicated.

Except as outlined above, no part of this publication may be reproduced, stored in a retrieval system or transmitted in any form or by any means, electronic, mechanical, photocopying, recording or otherwise, without prior written permission of the publisher.

Disclaimers

No responsibility is assumed by the publisher for any injury and/or damage to persons or property as a matter of products liability, negligence or otherwise, or from any use or operation of any methods, products, instructions or ideas contained in the materials herein.

Although all advertising material is expected to conform to ethical (medical) standards, inclusion in this publication does not constitute a guarantee or endorsement of the quality or value of such product or of the claims made of it by its manufacturer.

© The paper used in this publication meets the requirements of ANSI/NISO Z39.48-1992 (Permanence of Paper).

Printed in The Netherlands



ELSEVIER

Comput. Methods Appl. Mech. Engrg. 145 (1997) 341-360

**Computer methods
in applied
mechanics and
engineering**

Assessment of continuum models for sandwich panel honeycomb cores

W.S. Burton, A.K. Noor*

Center for Advanced Computational Technology, University of Virginia, NASA Langley Research Center, Hampton, VA USA

Received 9 June 1996; revised 18 September 1996

Abstract

Detailed finite element models are used for predicting the free-vibration response of infinitely long and rectangular sandwich panels. The panels considered have square-cell honeycomb core and simply supported edges. The sandwich core and face sheets are modeled by using three-dimensional solid elements and two-dimensional plate elements. The predictions of the finite element models are compared with those obtained by using higher-order sandwich theory for panels with the core replaced by an effective (equivalent) continuum. Three different approaches are used for estimating the effective material properties of the equivalent continuum layer.

1. Introduction

A considerable body of literature exists on the modeling, analysis and design of sandwich panels. Much of the early work focused primarily on sandwich structures with thin isotropic face sheets. Recent applications of sandwich structures, which demand both light weight and high performance (e.g. higher strength, damage tolerance and thermal resistance) have motivated the development of sandwich structures with composite face sheets and the use of advanced manufacturing techniques. Sandwich panels with composite face sheets are candidates for use in future high-speed aircraft, hypersonic aerospacecraft, and spacecraft with stringent precision requirements (e.g. communication satellite antennas and reflectors of terrestrial systems). Review of recent applications of sandwich structures is included in a recent monograph, [1], and review articles [2,3].

Structural efficiency of sandwich structures relies heavily on the lightweight core to separate the face sheets and provide the necessary stiffness. A variety of core configurations have been proposed. The most commonly-used core configurations can be classified in three groups: cellular, corrugated and honeycomb (see Fig. 1). Cellular core materials include natural products such as balsa wood and foams manufactured from modern plastics. Cellular cores are often the least expensive among core materials and offer some advantages in machineability and sandwich manufacture. Corrugated core materials include a large variety of geometries, often providing a highly directional core stiffness for certain applications. Ordinary cardboard is a common example of corrugated core sandwich. Stiffened panels, as well as web core and truss, can be considered as corrugated core structures. Honeycomb core sandwich structures are widely used in the aerospace industry and are the focus of the present study. Honeycomb cores can possess a very high stiffness to weight ratio, can be manufactured from a wide

* Corresponding author.

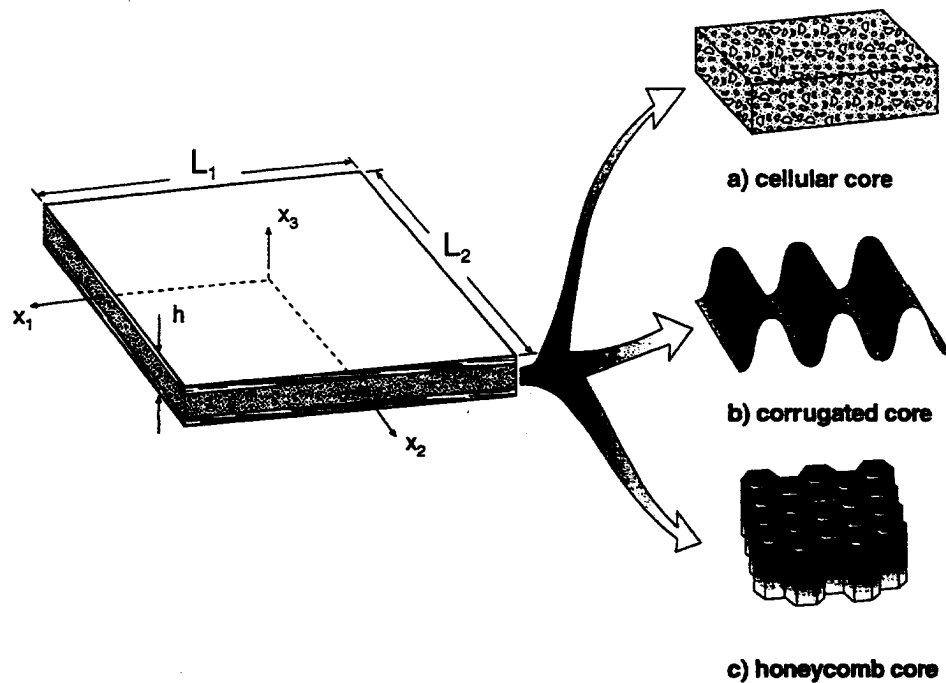


Fig. 1. Sandwich core materials and global geometry of sandwich panel.

range of materials such as aluminum, titanium, fiber reinforced plastics or even resin impregnated paper, and can be manufactured with a variety of geometric shapes. Some common geometries include: hexagonal cell, square cell and flex-core. Honeycomb cell size can be chosen to provide cores with different stiffness and density properties. Different cell shapes, such as that of flex-core, can allow the core to bend appropriately when constructing sandwiches with complex curvature.

The accuracy of response quantities predicted by different computational models of sandwich structures depends on a large number of material, lamination and geometric parameters of the face sheets and the core. The computational effort associated with detailed finite element models of honeycomb sandwich panels increases very rapidly with the increase in the number of cells in the panel core. For this reason, the analysis of sandwich panels is usually carried out by replacing the core structure with an equivalent continuum layer. The static and free vibration responses of a range of honeycomb sandwich panels were shown to be highly sensitive to variations in the equivalent continuum transverse shear stiffnesses of the core (see [3,4]). Therefore, the accurate prediction of the sandwich response requires accurate characterization of the transverse shear moduli. An assessment of the accuracy of static, mechanical and thermomechanical responses predicted by using continuum core models has been reported in [5–7], respectively. To the authors' knowledge, no assessment has been made on the accuracy of free-vibration responses predicted by continuum core models using detailed finite element models as the standard of comparison. The present study focuses on the accuracy of the vibrational response obtained by different continuum core models.

Specifically, comparisons are made between free-vibration responses predicted by equivalent continuum models and detailed finite element models. The finite element models are constructed using three-dimensional solid and two-dimensional plate elements. The equivalent properties for the continuum core model are obtained by using three different approaches which are described in the succeeding sections. In addition to the free-vibration frequencies, the associated strain energy components, local core stresses, strains and strain energy densities are used to assess the core property estimation techniques, and to gain insight into the limitations of these models.

Each of the sandwich panels considered in this study is composed of eight layer cross-ply composite face sheets perfectly bonded to a lightweight titanium square cell honeycomb core. Each sandwich panels' edges are simply supported, the outer faces are traction free, and the body is free from initial

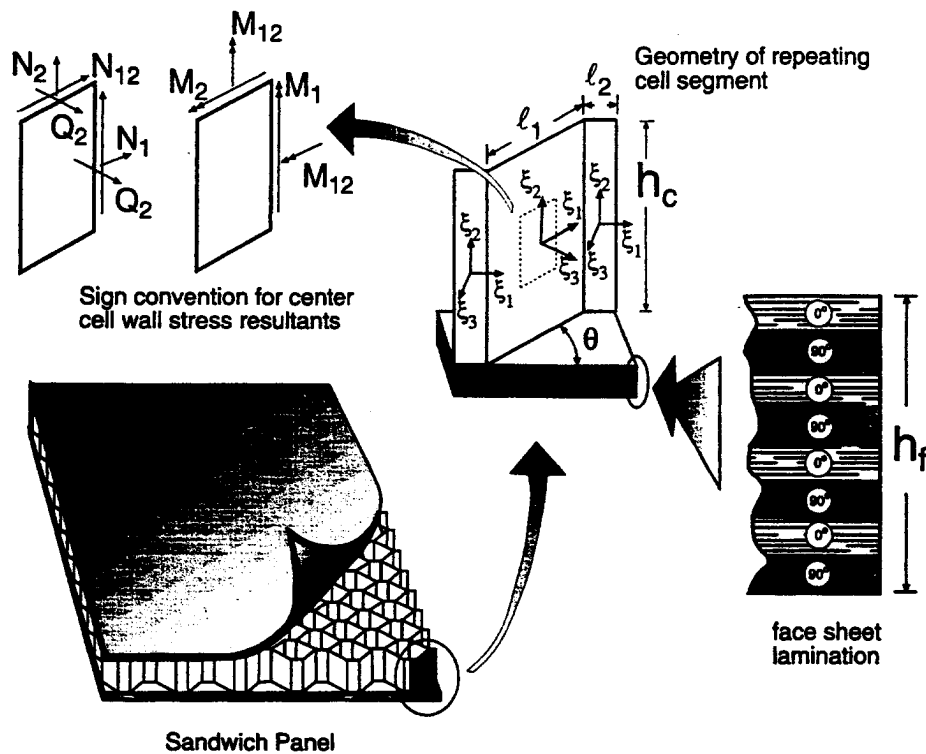


Fig. 2. Honeycomb panel segment geometry, face sheet lamination and cell wall local coordinates.

stresses. The geometric characteristics of the panels are shown in Figs. 1 and 2, and are described in rectangular Cartesian coordinates (x_1, x_2, x_3) , where x_1 and x_2 lie on the sandwich middle surface and x_3 is normal to that surface; L_1 and L_2 are the side lengths of the panels; and $h = 2h_f + h_c$ is the total thickness of the sandwich panel, where h_f and h_c refer to the face sheet and core thicknesses, respectively. The fiber directions of the layers in the face sheets are in either the x_1 or x_2 directions. The square cell honeycomb core structure is oriented with its ribbon direction parallel to the x_1 direction and its cell walls parallel to the x_3 coordinate axis and is characterized by the following dimensions: cell height, h_c ; cell wall thickness, t_c ; cell wall width, l_1 ; cell joint width, $2l_2$; and cell corrugation angle, θ . For convenience, the additional parameters, $d = l_1 + l_2/\cos \theta$, and $\eta = 2l_2/l_1$ are also used to describe the honeycomb cell.

The core property estimation techniques considered, as well as the finite element and continuum models used in this analysis, are discussed in the succeeding sections.

2. Equivalent continuum honeycomb core properties

A number of experimental and analytical techniques have been proposed for predicting the effective properties of honeycomb sandwich cores in terms of their geometric and material characteristics. The procedures vary in their level of sophistication and can be divided into test methods and analytical techniques. Test methods include those described in ASTM C273-61 [8], MIL-STD-401B [9], and other NDE techniques described in [10–13]. Analytical techniques which include energy methods (see, for example, [14–22]); homogenization techniques (see, for example, [23]); and mechanics of materials and other simplified models (see, for example, [24–25]). Some of the analytical methods require simplifying assumptions in order to obtain an elasticity solution on a repeating cell segment. Discrete element approaches, such as the finite element models used in [5,6,26–28], help overcome this limitation by providing more realistic distributions of stresses and strains in the detailed core structure. A large list of

references on the determination of effective in-plane, transverse shear, and transverse normal characteristics of sandwich core structures, are given in [3].

In the present study, the detailed finite element models are not used to generate improved estimates of equivalent core layer properties. Instead, the finite element free-vibration responses are used as the standard for assessing the accuracy of the predictions of an equivalent core model, with the shear stiffnesses estimated by three approaches: a lower bound energy approach; an upper bound energy approach; and design data obtained by direct test methods. The upper and lower bound energy approaches referred to in the literature as unit displacement and unit force methods, are essentially potential and complementary potential energy methods, respectively. The application of these approaches to honeycomb core structures are reported in many publications, including an early study [14] for hexagonal honeycomb cells. The equivalent transverse shear stiffnesses, $G_{\alpha 3}^{LB}$ and $G_{\alpha 3}^{UB}$, can be calculated by applying the following inequalities to the repeating cell and the associated continuum core segments (see Fig. 3).

$$\frac{1}{2} \frac{\tau_{\alpha 3}^2 V}{G_{\alpha 3}^{LB}} \leq \frac{1}{2} \sum_i \left(\frac{\tau_i^2}{G_c} V_i \right), \quad (\alpha = 1, 2), \quad (1)$$

for lower bound estimates, and

$$\frac{1}{2} G_{\alpha 3}^{UB} \gamma_{\alpha 3}^2 V \leq \frac{1}{2} \sum_i (G_c \gamma_i^2 V_i), \quad (\alpha = 1, 2) \quad (2)$$

for upper bound estimates, where τ_i and γ_i are the assumed, uniform equilibrium stress and compatible strain states in the i th cell walls of the representative cell segment; V_i is the volume of the i th cell wall; and G_c is the isotropic shear modulus of the core cell material. The shear stress, shear strain and transverse shear moduli, $\tau_{\alpha 3}$, $\gamma_{\alpha 3}$ and $G_{\alpha 3}$, respectively, are associated with the equivalent core material of volume, V . Details of the application of this approach to honeycomb cores similar to those used in this study can be found in [20]. The only difference is the thickness of the cell wall (along the length, l_2), where adjacent formed foil ribbons are joined together to form the honeycomb core. This thickness is twice the core foil thickness of the wall with length, l_1 . Expressions for the equivalent transverse shear stiffnesses used in this study are given in Appendix A.

The equivalent transverse shear stiffnesses obtained from design data were calculated in accordance

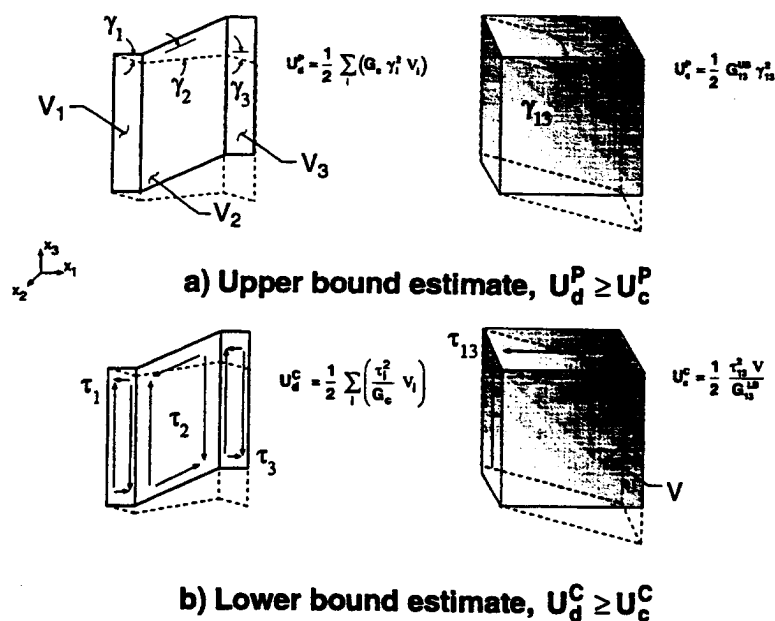


Fig. 3. Honeycomb core segment used in calculating lower-bound and upper-bound equivalent continuum material properties.

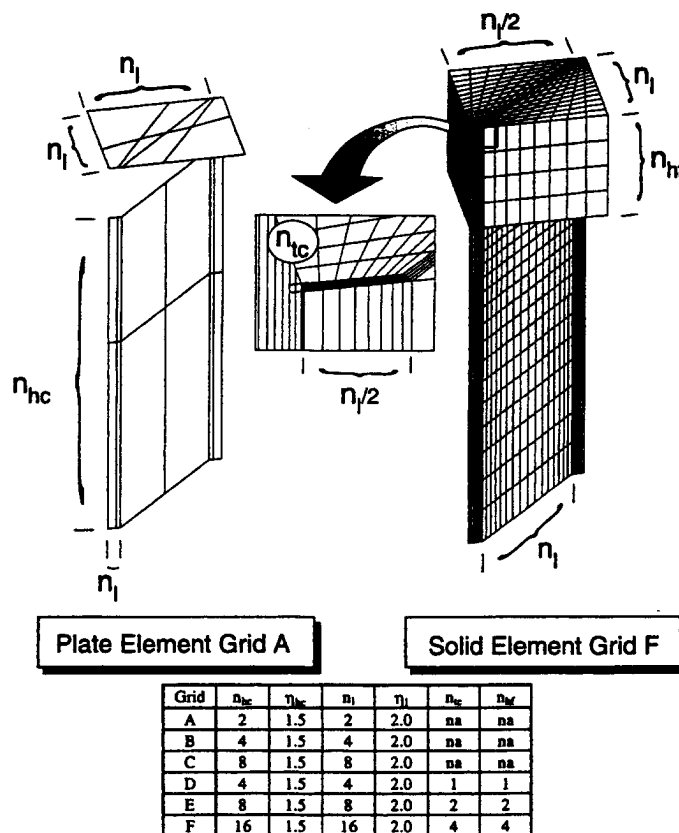
with MIL-STD-401B [9]. Different estimation methods for calculating the remaining equivalent continuum elastic properties are not assessed herein. Rather, the equivalent in-plane properties are calculated using strength of materials methods similar to those presented in [20]. The equivalent transverse normal stiffness and equivalent core density are each proportional to their respective core material values in the same ratio as the volumes, $\Sigma_{i=1}^3 V_i/V$. Expressions for these additional components are also given in Appendix A.

3. Sandwich models used in the present study

3.1 Two- and three-dimensional finite element models

The finite element models used in the present study were constructed using the commercial code ANSYS [29]. Both eight-node, two-dimensional plate elements, with quadratic interpolation functions, and eight-node, three-dimensional elements with trilinear interpolation functions are used. Each of the finite element models in this study was constructed by reflecting or translating the cell segment shown in Fig. 4.

The finite element grids for the two- and three-dimensional elements are identical in the surface directions of the cell walls and are characterized by the number of divisions in the core half height, n_{hc} , and the number of divisions in the cell wall widths, n_l . For the three-dimensional element models, the number of uniform thickness elements in the directions of the cell wall and the face sheet thickness are n_{lc} and n_{hf} , respectively. The number of element divisions on opposite edges of the cell segment are



Note: n refers to number of subdivisions,
 η refers to ratio of largest to smallest element
edge length along subdivision.

Fig. 4. Typical finite element grids and table of grid parameters for the sandwich panel segment.

equal, producing quadrilateral and hexahedral grids for the two- and three-dimensional elements, respectively. The number of divisions on the edges of the face sheet are determined by adjacent cell wall divisions. An additional characteristic of the finite element model is the ratio of the smallest to largest element side length along a geometrical segment. The grid parameters along with typical two- and three-dimensional finite element grids for the repeating sandwich cell segment are shown in Fig. 4.

3.2 Discrete higher-order continuum-core model

Discrete, higher-order two-dimensional sandwich theory was used to assess the equivalent core properties chosen to simulate the elastic response of the honeycomb sandwich core. For a wide range of geometric parameters, the free-vibration responses obtained by these models was found [3,4] to be in close agreement with those predicted by the associated three-dimensional elasticity solutions. The details of the derivation and computational procedure used in obtaining the higher-order theory and three-dimensional elasticity solutions are given in the aforementioned references and are highlighted subsequently:

- (1) Each of the displacement components is expressed as a series of products of functions of the thickness coordinate x_3 and trigonometric functions of the surface coordinates, x_1 and x_2 . The surface displacements are represented by quadratic functions in each of the faces and the core with the continuity enforced at their interfaces. The transverse displacement is assumed to be constant through the entire sandwich thickness.
- (2) For each pair of harmonics, substitution of the displacement expansions into the governing differential equations, and integrating in the thickness coordinate, x_3 , produces a system of homogeneous algebraic equations with coefficients representing the amplitudes of the assumed thickness distribution of the displacement.
- (3) These algebraic equations are solved to obtain the free-vibration frequencies and the associated eigenfunctions.

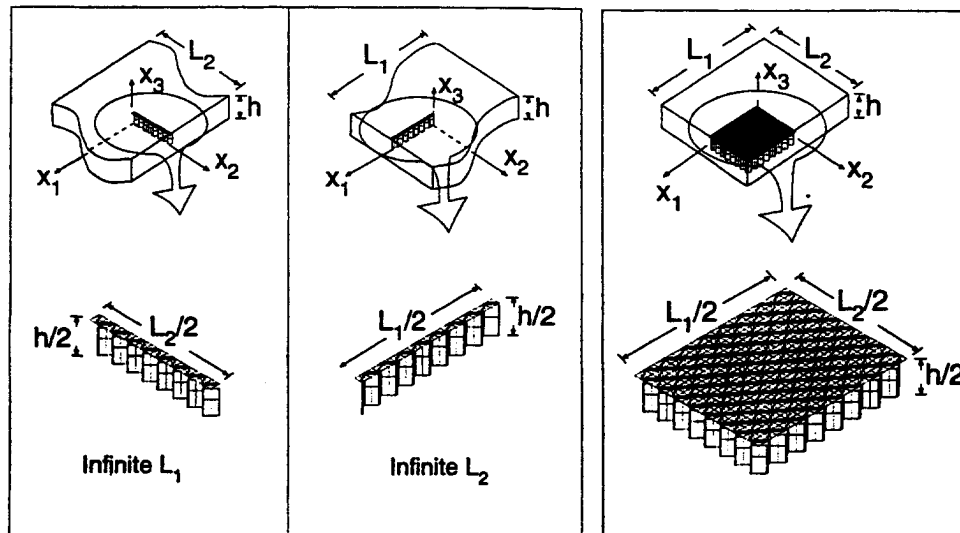
The effective properties for the equivalent continuum core layer were determined by the three approaches described in the preceding section, namely, a lower bound energy approach, an upper bound energy approach, and a design-data, test-based approach. Henceforth, the continuum models based on these approaches will be referred to as UB, LB and T models, respectively.

4. Numerical studies

4.1 Sandwich panels considered

The sandwich panels considered in this study are shown in Fig. 5. Both infinitely long panels, with either L_1 or L_2 infinite, and rectangular panels are studied. The in-plane displacements and in-plane stress components are assumed to be antisymmetric with respect to the middle plane ($x_3 = 0$). Infinitely long panels in both the x_1 and x_2 directions are considered because the geometric characteristics and the estimated shear properties, G_{13}^c and G_{23}^c , are different in the two directions. For infinitely-long panels the response quantities are periodic in the finite-length direction, but are assumed to be independent of the coordinate in the direction of infinite length. These conditions correspond to simple supports at the edges normal to the finite length direction, and a state of plane strain in the direction of infinite length. For rectangular panels, each of the stress and displacement components are assumed to be periodic in both x_1 and x_2 with periods $2L_1$ and $2L_2$. The complete boundary conditions are listed in Appendix B. Because of the symmetries of the panel geometries, only a quadrant of the infinitely long panels, and an octant of the rectangular panels are modeled (see Fig. 5).

Three sets of square-cell titanium alloy honeycomb cell configurations are considered in the present study. In the first set, the cell wall thickness, $t_c = 0.002$ in., is fixed as the cell characteristic dimension, d , is varied, with $d = 3/16$ in., $1/4$ in. and $3/8$ in. In the second set, the average density is kept constant by varying the wall thicknesses, t_c , and cell dimension d , together. Three wall-thickness, cell-size pairs



a) Infinitely Long Panels

b) Rectangular Panel

Fig. 5. Simply-supported panels and example finite element grids used in the present study. (a) 16 cell panels in x_2 and x_1 coordinate directions with infinite L_1 and L_2 , respectively; (b) 16×16 cell, rectangular sandwich panel.

are considered, namely: ($t_c = 0.002$ in., $d = 3/16$ in.); ($t_c = 0.0026667$ in., $d = 1/4$ in.); and ($t_c = 0.004$ in., $d = 3/8$ in.). In the third set, the cell characteristic dimension is fixed, $d = 3/16$ in., as the cell wall thickness, t_c , is varied, with $t_c = 0.0015$ in., 0.002 in., and 0.003 in. For each cell configuration, the cell wall side length ratio and cell opening angle were fixed, with $\eta = 0.1621$ and $\theta = 45^\circ$. Note that a base configuration with $t_c = 0.002$ in. and $d = 3/16$ in. is common to each set. The procedure described in Section 2 was used for calculating the equivalent continuum properties associated with these core configurations. The equivalent transverse shear stiffness properties, calculated using the three approaches discussed previously, are listed in Table 1(a). The remaining equivalent continuum properties are listed in Table 1(b). The principal material directions of the equivalent continuum coincide with the global Cartesian coordinate system. The equivalent continuum core is oriented with the direction associated with the corrugated cell ribbon at 0° to the x_1 axis. The material properties of the titanium alloy, Ti-5Al-2.5V, used for the honeycomb core are $E' = 15.5 \times 10^6$ psi, $\nu' = 0.31$, and $\rho' = 0.162$ lbf/in³. Note that the material stiffness matrices of the equivalent continuum are positive-definite.

The elastic properties of the face-sheet layers are selected to be typical of a high-modulus transversely isotropic composite material, namely:

$$\begin{aligned} E_L^f &= 22.9 \times 10^6 \text{ psi}, & E_T^f &= 1.39 \times 10^6 \text{ psi}, & G_{LT}^f &= 0.86 \times 10^6 \text{ psi}, \\ G_{TT}^f &= 0.468 \times 10^6 \text{ psi}, & \nu_{LT}^f &= 0.32, & \nu_{TT}^f &= 0.49, & \text{and } \rho^f &= 0.058 \text{ lbf/in}^3 \end{aligned}$$

where subscripts L and T refer to the fiber and transverse directions, respectively, and superscript f refers to the face sheets. The fiber orientations of the layers of the top face sheet are $[90^\circ/0^\circ]_4$, with the fibers of the top layer making 90° with the x_1 coordinate axis. Two face sheet thicknesses are considered, $h_f = 0.04$ in. and $h_f = 0.12$ in. Since the total sandwich thickness is fixed at $h = 1.0$ in., the corresponding core thicknesses are $h_c = 0.92$ in. and $h_c = 0.76$ in.

Four parameters are varied in this study, namely: the two core parameters, t_c and d , the face sheet thickness, h_f , and the number of honeycomb core cells in the panels. For infinitely long panels, the number of cells in the direction of finite length, L_1 or L_2 , was varied from 6 to 192. For rectangular panels, the number of cells in the x_1 and x_2 directions was varied from 8 to 48.

Table 1
Equivalent continuum core properties, square cell Ti-5Al-2.5V titanium sandwich core

(a) Transverse shear moduli

	Cell size d (in.)	Cell wall thickness t_c (in.)	G_{13}^c (psi)			G_{23}^c (psi)		
			Upper bound	Lower bound	Test	Upper bound	Lower bound	Test
Constant Cell	3/16	0.002	51997	75108	93000	56723	56723	73000
Wall	1/4		38998	56331	60000	42523	42523	47000
Thickness	3/8		25999	37554	39000	28362	28362	31000
Constant Cell Size	3/16	0.0015	38998	56331	63000	42542	42542	50000
		0.002	51997	75108	93000	56723	56723	73000
		0.003	77996	112662	175000	85085	85085	130000
Constant Equivalent	3/16	0.002	51997	75108	93000	56723	56723	73000
Core density	1/4	0.0026667						
	3/8	0.004						

(b) Elastic moduli, in-plane shear modulus, Poisson's ratios and density

	Cell size d (in.)	Cell wall thickness t_c (in.)	E_1^c (psi)	E_2^c (psi)	E_3^c (psi)	G_{12}^c (psi)	ν_{23}^c ($\times 10^{-5}$)	ν_{13}^c ($\times 10^{-5}$)	ν_{12}^c	ρ^c (lb/ft ³)
Constant Cell	3/16	0.002	62.365	41.279	345400	1141.1	3.7048	5.5973	1.2288	6.2381
Wall	1/4		26.312	17.416	259050	481.53	2.0841	3.1487	1.2290	4.6785
Thickness	3/8		7.7967	5.1605	172700	142.68	0.9263	1.3995	1.2232	3.1190
Constant Cell Size	3/16	0.0015	26.312	174.16	259050	481.53	2.0841	3.1487	1.2290	4.6785
		0.0020	62.365	412.79	345400	1141.1	3.7048	5.5973	1.2288	6.2381
		0.0030	210.04	139.29	518100	3852.3	8.3345	12.591	1.2283	9.3571
Constant Equivalent	3/16	0.002	62.365	412.79	345400	1141.1	3.7048	5.5973	1.2288	6.2381
Core density	1/4	0.0026667								
	3/8	0.004								

4.2 Strain energy components

As a step towards establishing the range of validity of the different approaches for obtaining the equivalent core properties, the total strain energy of the continuum core sandwich panels, associated with each of the vibration modes, was decomposed into six components as follows:

$$\begin{aligned}
 U_1^f &= \frac{1}{2} \int_{V_{\text{face}}} \sigma_{\alpha\beta} \epsilon_{\alpha\beta} dV, & U_1^c &= \frac{1}{2} \int_{V_{\text{core}}} \sigma_{\alpha\beta} \epsilon_{\alpha\beta} dV, \\
 U_2^f &= \frac{1}{2} \int_{V_{\text{face}}} \sigma_{\alpha 3} \gamma_{\alpha 3} dV, & U_2^c &= \frac{1}{2} \int_{V_{\text{core}}} \sigma_{\alpha 3} \gamma_{\alpha 3} dV, \\
 U_3^f &= \frac{1}{2} \int_{V_{\text{face}}} \sigma_{33} \epsilon_{33} dV, & U_3^c &= \frac{1}{2} \int_{V_{\text{core}}} \sigma_{33} \epsilon_{33} dV.
 \end{aligned} \tag{3}$$

In Eq. (3) a repeated index α or β denotes summation over the range 1, 2; superscripts f and c denote face sheet and continuum core quantities, respectively; and V_{face} and V_{core} refer to the face sheet and continuum core volumes, respectively. The total strain energy of the sandwich, $U = U^f + U^c$, where U^f and U^c are the strain energies in the face sheets and core, respectively, i.e., $U^f = U_1^f + U_2^f + U_3^f$ and $U^c = U_1^c + U_2^c + U_3^c$.

The total strain energy of the sandwich panels with the core modeled using plate finite elements is decomposed into six components. The three components associated with the face sheets are the same as

those defined in Eq. (3). The three components associated with the core are expressed in terms of the generalized strains and stress resultants in the cell wall local coordinates as follows (see Fig. 2):

$$\begin{aligned} U_1^d &= \frac{1}{2} \int_{V_{\text{core}}} (N_1 \varepsilon_1^0 + M_1 \kappa_2^0 + M_2 \kappa_2^0 + Q_1 \gamma_1^0) dV, \\ U_2^d &= \frac{1}{2} \int_{V_{\text{core}}} (N_{12} \gamma_{12}^0 + M_{12} \kappa_{12}^0 + Q_2 \gamma_2^0) dV, \\ U_3^d &= \frac{1}{2} \int_{V_{\text{core}}} (N_2 \varepsilon_2^0) dV. \end{aligned} \quad (4)$$

The total strain energy in the core is $U^d = U_1^d + U_2^d + U_3^d$. In Eq. (4), V_{core} is the volume of the titanium core material. The energy component U_1^d is associated with bending, stretching and transverse shear of the cell walls in cell wall coordinates (see Fig. 2); the energy component U_2^d is associated with the in-plane shear of the cell walls in cell wall coordinates, which corresponds to the transverse shear strain energy in the global Cartesian system; and the energy component U_3^d represents the transverse normal deformation of the sandwich core in the global Cartesian system.

4.3 Infinitely long panels

Solid finite element models. Free vibration responses were calculated using three-dimensional solid elements and two-dimensional plate elements for panels with face thickness, $h_f = 0.04$ in.; 8 to 48 cells in x_1 ; and infinite L_2 . Two finite element grids were considered for the plate element model, and three grids were considered for the solid element model. The grid parameters for the repeating cell segments are shown in Fig. 4. Note that each successive grid is obtained by doubling the number of elements in each direction of the previous grid. As an example, a finite element grid with plate elements is shown in Fig. 5 for an infinitely long panel, with 16 cells in the x_1 direction. Typical results are shown in Table 2. As can be seen from this table, the frequencies obtained by the different plate and solid finite element models are within one percent of each other. Consequently, in subsequent sections, only the frequencies obtained by the plate finite element models with grid A are presented.

Comparison between continuum core model and plate finite element model results. Comparisons between the vibration frequencies obtained by using continuum core models with three different estimates for transverse shear properties, ω_{CM} , and the detailed finite element frequencies, ω_{FE} , are shown in Figs. 6 and 7. The differences between the frequencies predicted by each of the continuum models and the finite element model are normalized by dividing by the corresponding frequencies of the finite element model. The results shown in Figs. 6 and 7 are for infinitely long sandwich panels in either the x_1 and x_2 direction. Two face thicknesses and three cell wall thicknesses are considered, namely; $h_f = 0.04$ in. and $h_f = 0.12$ in.; and $t_c = 0.0015$ in., 0.002 in. and 0.003 in. The number of cells was

Table 2

Minimum vibration frequencies, ω , predicted by models with three-dimensional solid and two-dimensional plate finite elements. Symmetric sandwich panels with cross-ply, composite face sheets. $h = 1.0$ in., $h_f = 0.04$ in., infinite L_2 , and the edges in the x_1 direction simply supported. Cell dimensions: $d = 3/16$ in., $\theta = 45^\circ$, $\eta = 0.1621$ and $t_c = 0.002$ in.

Number of Cells in x_1 Direction	FE Model with Plate Elements		FE Model with Solid Elements		
	Mesh A	Mesh B	Mesh D	Mesh E	Mesh F
4	3325.7	3325.7	3355.6	3343.5	3333.2
6	2033.1	2032.9	2048.7	2042.9	2037.8
8	1378.4	1378.3	1387.3	1384.2	1381.4
12	745.59	745.55	749.15	748.05	
16	460.32	460.30	462.03	461.56	
24	221.58	221.57	221.16	222.03	

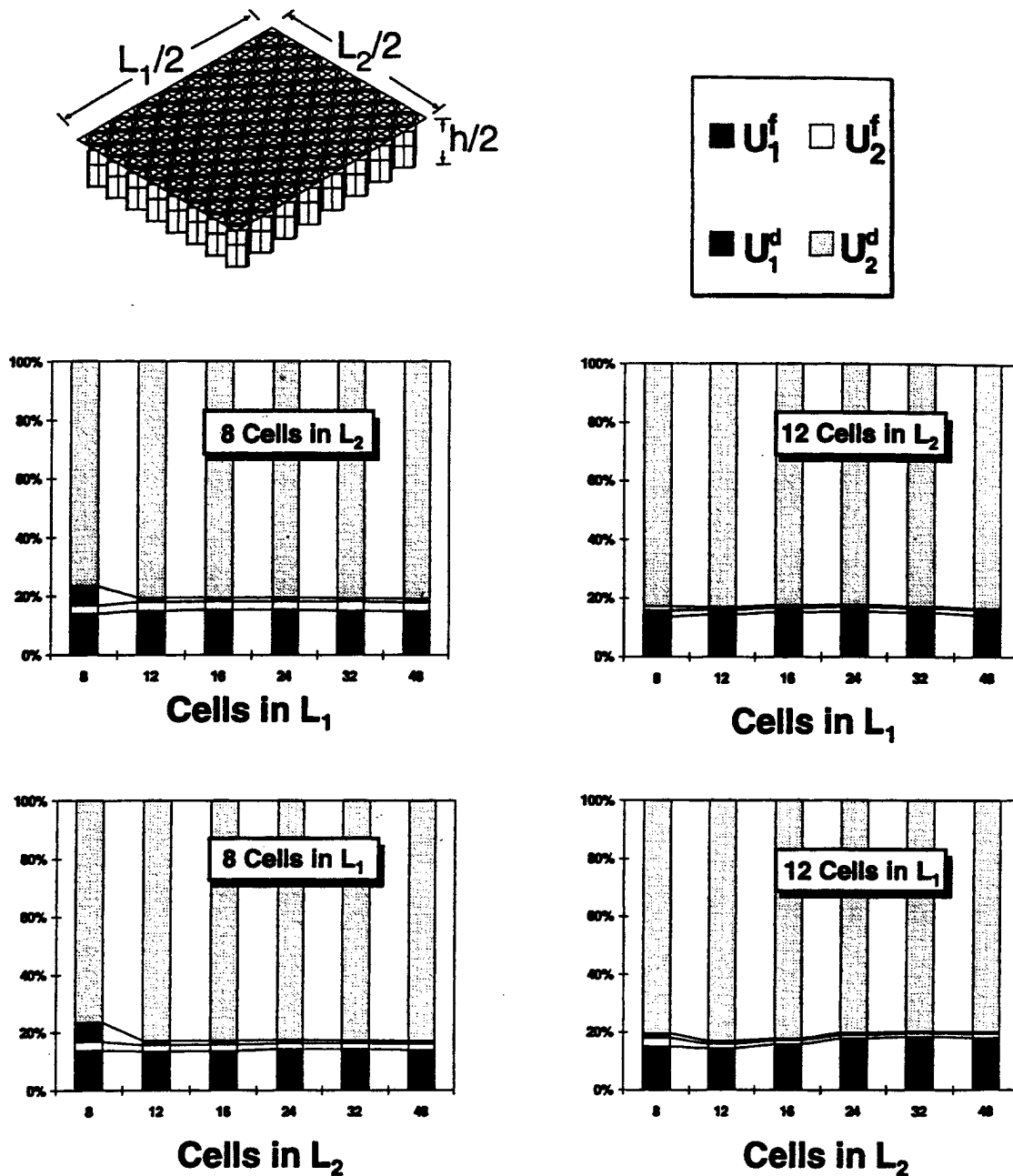


Fig. 6. Percent differences between the lowest vibration frequencies predicted by the two-dimensional finite element models (grid A) and those predicted by equivalent continuum core models. Symmetric sandwich panels, $h = 1$ in., with cross-ply, composite face sheets, infinite L_2 and edges in x_1 direction simply supported. Cell dimensions, $d = 3/16$ in., $\theta = 45^\circ$ and $\eta = 0.1621$.

varied from 10 to 192 in the x_2 direction, and from 6 to 192 in the x_1 direction. An examination of Figs. 6 and 7 reveals:

- (1) The frequencies predicted by the UB model are in close agreement with those predicted by the finite element model, for panels with infinite L_2 . The largest difference over the range of panels considered is less than two percent. On the other hand, the frequencies predicted by the LB

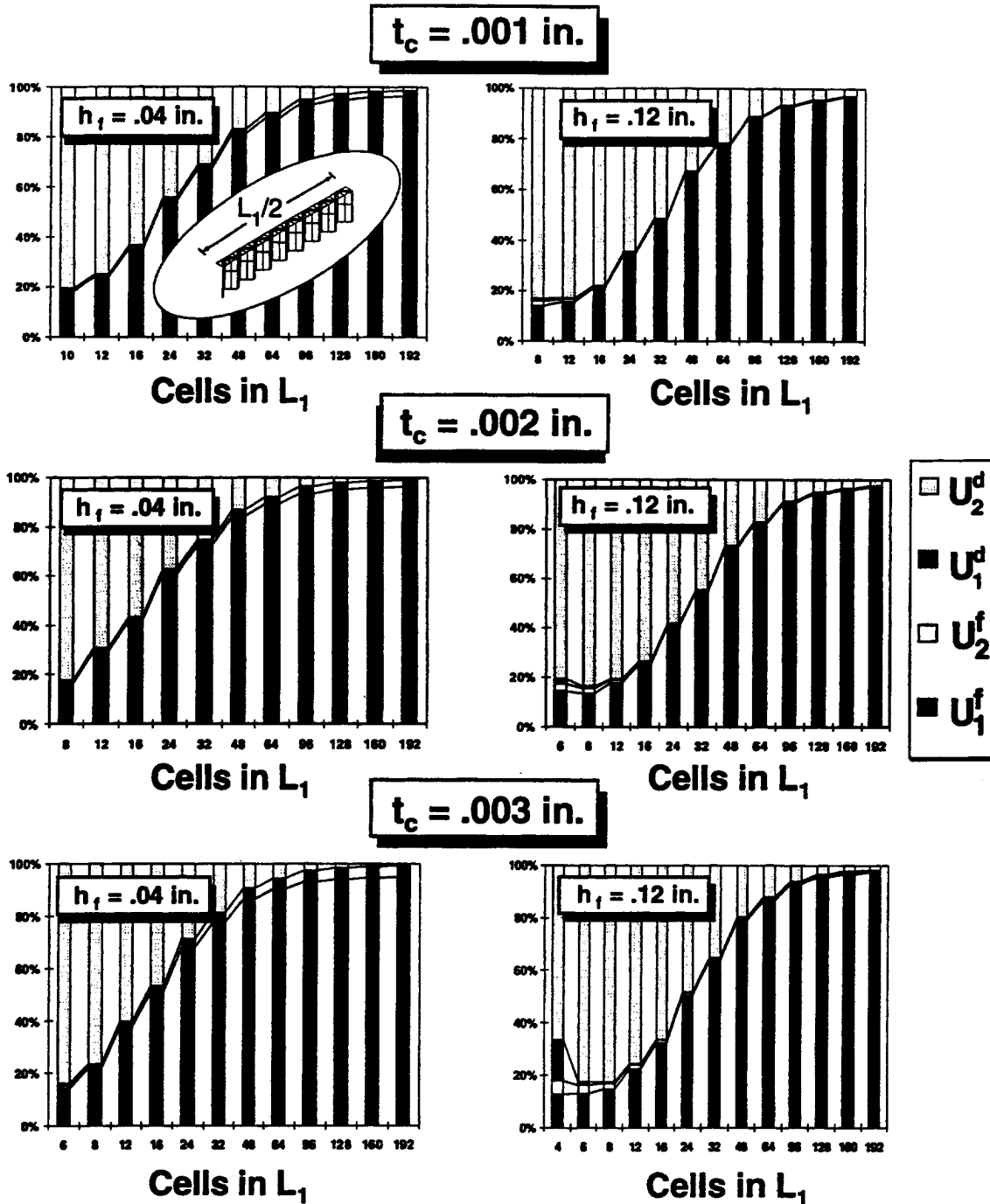


Fig. 7. Percent differences between the lowest vibration frequencies predicted by the two-dimensional finite element models (grid A) and those predicted by equivalent continuum core models. Symmetric sandwich panels, $h = 1$ in., with cross-ply, composite face sheets, infinite L_1 and edges in x_2 direction simply supported. Cell dimensions, $d = 3/16$ in., $\theta = 45^\circ$, $\eta = 0.1621$ and $r_c = 0.002$ in.

model are lower than those of the finite element model by up to 20%. For infinitely long panels, the T model overestimates the frequency by up to 11%.

- (2) For a fixed number of cells, the error in the frequencies predicted by the LB model is generally greater for sandwiches with thick face sheets ($h_f = 0.12$ in.), than for thin face sheets ($h_f = 0.04$ in.).

- (3) The error in the frequencies predicted by the T model increases with both face sheet thickness and cell wall thickness.
- (4) For panels with infinite length in the x_1 direction, the upper and lower bound estimates for the shear modulus G_{23}^c , are identical. Since there is no shearing in the $x_1 - x_3$ plane and hence no dependence on G_{13}^c , the associated frequency predictions are within one percent of those predicted by the finite element models (see Fig. 7).
- (5) For all the panels considered, the face sheet thickness does not appear to have a significant effect on the accuracy of the predictions based on any of the continuum core models considered herein.

In addition to the free vibration frequencies, the strain energy components (Eqs. (3) and (4)) from the detailed finite element models are calculated and are shown in Fig. 8. Comparison between the strain energy components predicted by the detailed finite element models (Eq. (4)) and the continuum core models (Eq. (3)) is given in Fig. 9. An examination of Fig. 8 reveals:

- (1) The total strain energy U , predicted by the finite element models is dominated by U_1^f and U_2^d . Contributions from the transverse shear strain energy in the face sheets, U_2^f , and the bending and stretching energies of the cell walls, U_1^d , are small. The transverse normal component U_3^f is not included in the plate element formulation and is assumed to be negligible. The component, U_3^d , is

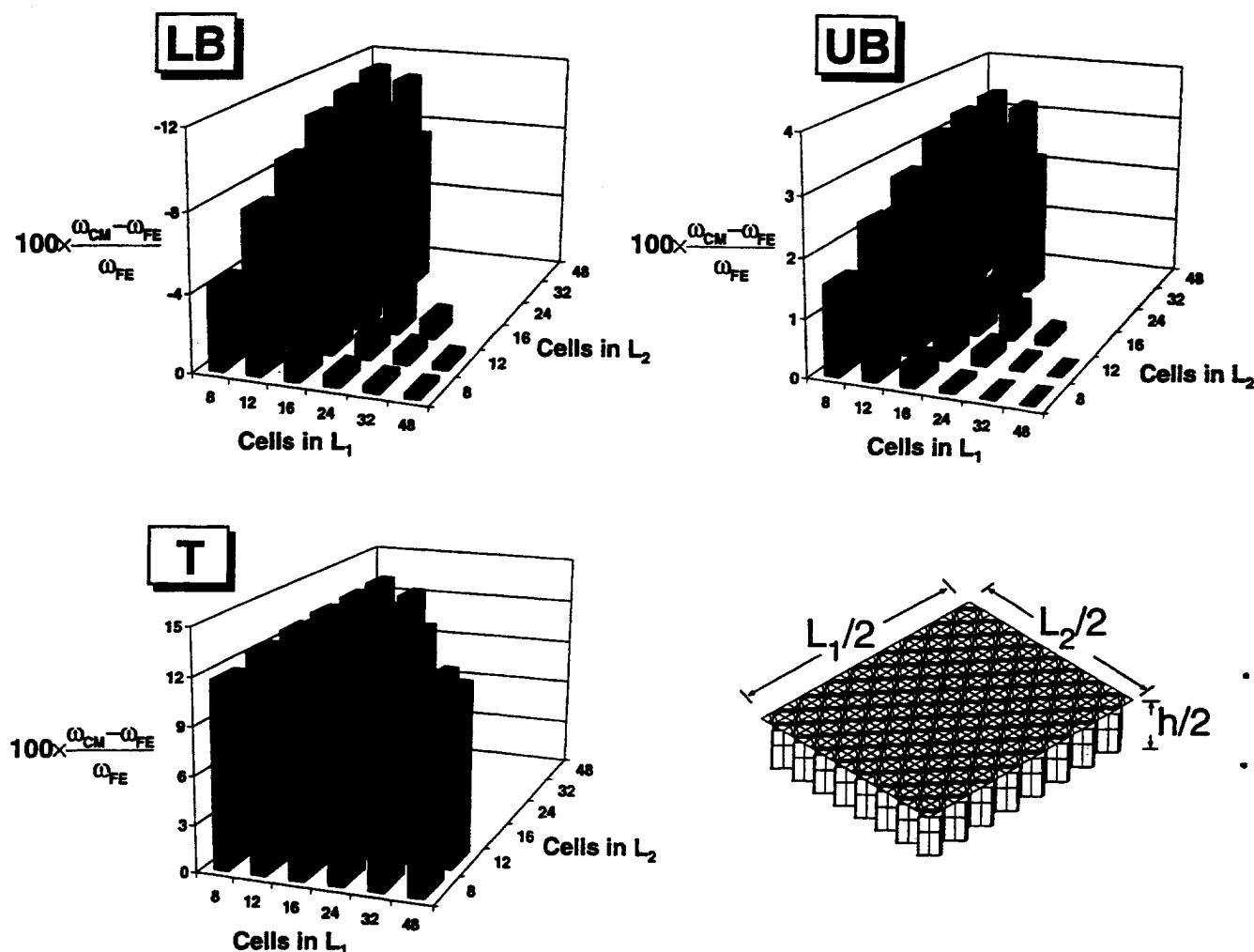


Fig. 8. Variation of the strain energy density components associated with the lowest free-vibration mode predicted by the two-dimensional finite element models (grid A). Symmetric sandwich panels, $h = 1$ in., with cross-ply, composite face sheets, infinite L_2 and edges in x_1 direction simply supported. Cell dimensions, $d = 3/16$ in., $\theta = 45^\circ$ and $\eta = 0.1621$.

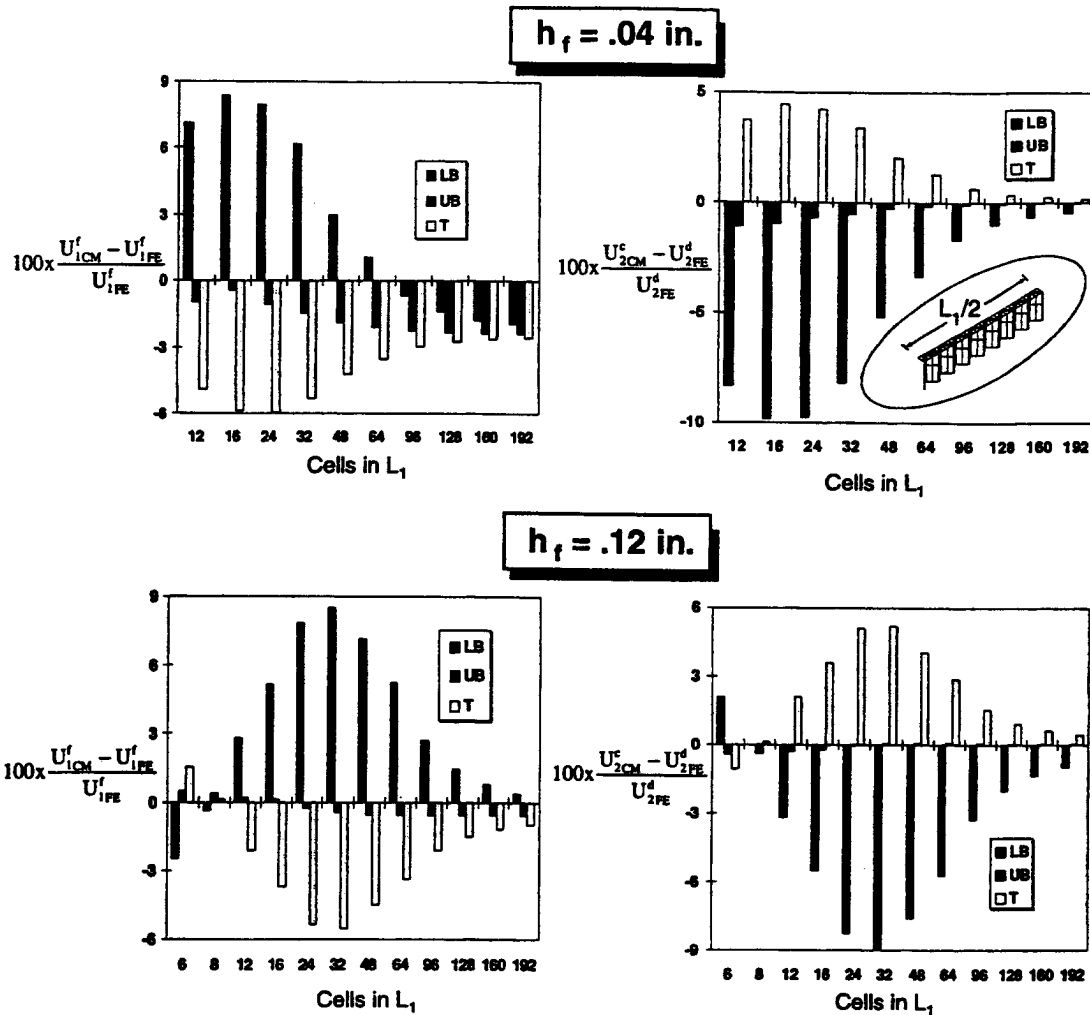


Fig. 9. Percent differences between the energy components associated with the lowest free-vibration mode predicted by the two-dimensional finite element models (grid A) and those associated with equivalent continuum core exact elasticity models (see Eqs. (3) and (4)). Symmetric sandwich panels, $h = 1$ in., with cross-ply, composite face sheets, infinite L_1 and edges in x_2 direction simply supported. Cell dimensions, $d = 3/16$ in., $\theta = 45^\circ$, $\eta = 0.1621$ and $t_c = 0.002$ in.

also negligible. Consequently, an increase in the number of cells in the length L_1 results in an increase in U_1^f and a nearly proportionate decrease in U_2^d .

- (2) The sandwich panels with thick face sheets have a slightly higher ratio of U_2^d/U than that for the corresponding panels with thin face sheets (and the same number of cells).
- (3) For a given average core density, the strain energy components are insensitive to variations in the core size and the wall thickness.
- (4) For sandwich panels with a given number of cells, the strain energy associated with the global transverse shear in the core increases significantly with the increase in the thickness of the face sheets. In contrast, the proportion of transverse shear strain energy decreases almost insignificantly with increases in cell wall thickness.

The dominant strain energy components for the continuum core models were found to be U_1^f and U_2^c . The differences between these components and the corresponding dominant components for the finite element model (U_1^f and U_2^d), are shown in Fig. 9. An examination of Fig. 9 reveals:

- (1) The strain energy components predicted by the UB continuum core model are closer to the finite element model strain energy components than those predicted by the other continuum core models. The largest difference over the range of problems considered is slightly above 2%.

- (2) The maximum differences between the strain energy components predicted by the LB and T continuum core models and those predicted by the finite element model are about 6% and 8%, respectively.
- (3) The strain energy components for infinitely long panels in the x_1 direction (not shown) predicted by the UB and T models are similar to those for the infinitely long panels in the x_2 direction. The predictions of the UB and LB models are identical since the upper and lower bound estimates of the equivalent core properties are identical.

The following comments can be made regarding the predictions of the finite element models and associated continuum core models for panels with honeycomb core cells of constant thickness and varying cell size; and for panels with constant average density, but varying wall thickness and cell size (results not shown).

- (1) The trends in the frequency and energy component predictions for sandwich panels with constant cell wall thickness and decreasing cell size are quantitatively similar to the predictions for panels with constant cell size and increasing cell wall thickness. This can be expected since the equivalent transverse shear stiffnesses shown in Appendix A are directly proportional to t_c/l_1 .
- (2) The frequencies predicted by the finite element models using characteristic cell size and cell wall thickness combinations of equal average density are nearly indistinguishable. Since each of the equal core density combinations produces the same estimates for the equivalent continuum core properties, the accuracy of the frequency predictions by the continuum models was observed to be the same for cell geometries with equivalent core density.

4.4 Rectangular panels

The free-vibration frequencies and associated strain energy components were calculated using plate finite element models for rectangular sandwich panels with the base cell configuration, $d = 3/16$ in. and $t_c = 0.002$ in., and face sheet thickness, $h_f = 0.12$. The number of cell segments in each of the x_1 and x_2 directions was varied between 8 to 48. The finite element grid for a typical rectangular panel is shown in Fig. 5. Since the computational effort increases rapidly with increasing the number of cells in both directions, panels with 24 or more cells in each direction were not analyzed in this study. Fig. 10 shows the percent differences between the frequencies predicted by each of the continuum models and the finite element model. Fig. 11 shows the dominant strain energy components, U_1^t , U_2^d , U_2^t and, U_1^d , for some of the rectangular panels considered. An examination of the differences between the frequencies predicted by the finite element and continuum models (see Fig. 10) shows:

- (1) The frequencies predicted by the UB model are in close agreement with those predicted by the

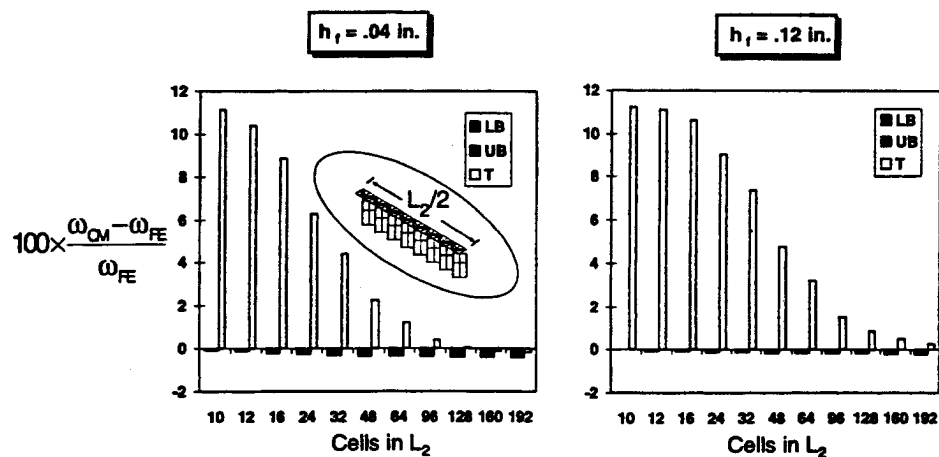


Fig. 10. Percent differences between the lowest vibration frequencies predicted by the two-dimensional finite element models (grid A) and those predicted by equivalent continuum core models. Symmetric, rectangular sandwich panels, $h = 1$ in., with cross-ply, composite face sheets, and edges in x_1 and x_2 directions simply supported. Cell dimensions, $d = 3/16$ in., $\theta = 45^\circ$, $\eta = 0.1621$ and $t_c = 0.002$ in.

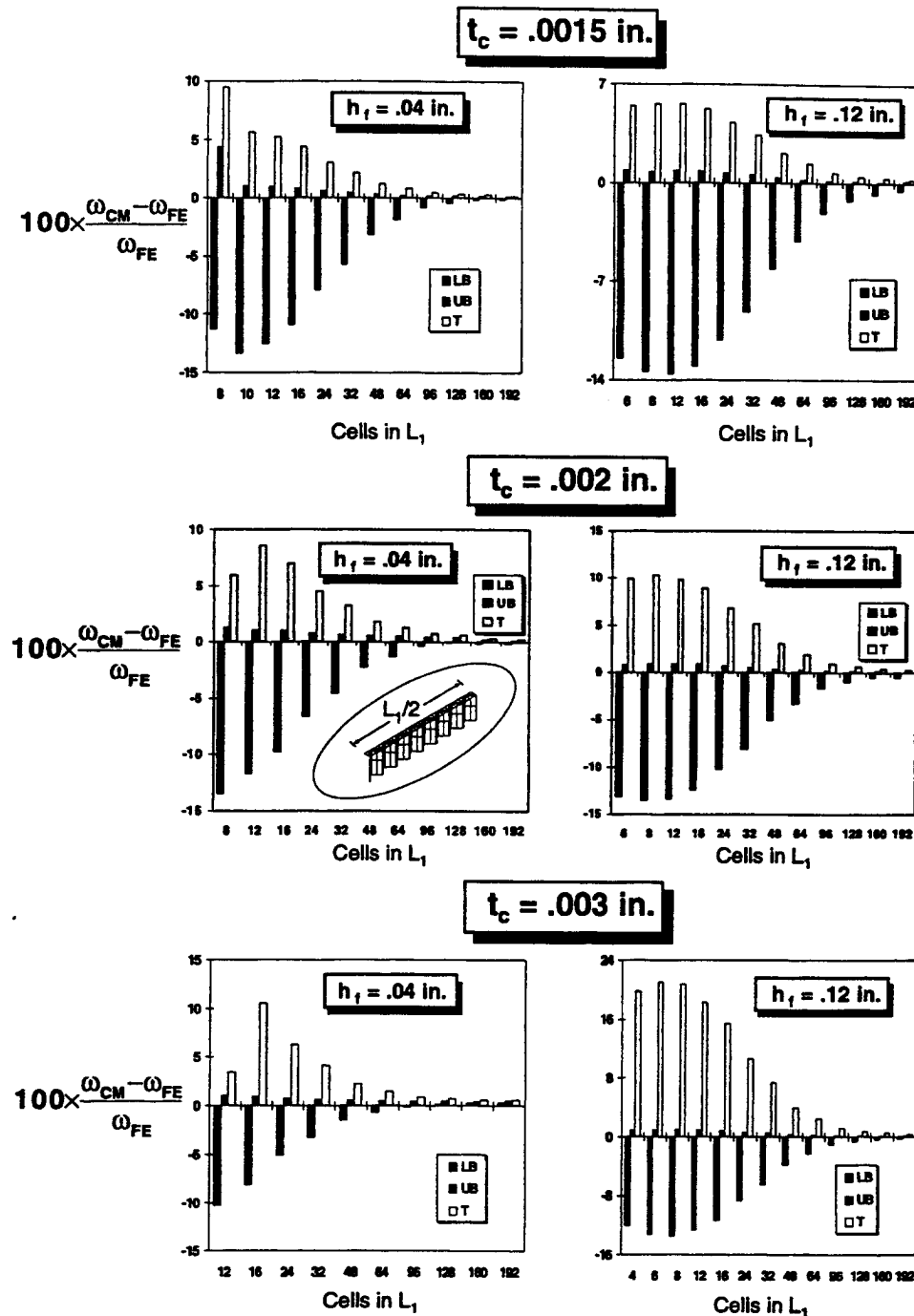


Fig. 11. Variation of the strain energy density components associated with the lowest free-vibration mode predicted by the two-dimensional finite element models (grid A). Symmetric, rectangular sandwich panels, $h = 1$ in., with cross-ply, composite face sheets, and edges in x_1 and x_2 directions simply supported. Cell dimensions, $d = 3/16$ in., $\theta = 45^\circ$, $\eta = 0.1621$ and $t_c = 0.002$ in.

finite element models. For the panels considered, the largest difference is less than 3.5%. The frequencies predicted by the LB model are lower than those of the finite element model. The differences reach nearly 11% for panels with large L_1/L_2 ratios (i.e. small numbers of cells in the x_1 direction, and larger numbers of cells in the x_2 direction). By contrast, for large L_1/L_2 ratio (few cells in the x_2 direction and a large number of cells in the x_1 direction), the frequencies

predicted by the UB continuum model are in close agreement with those of the finite element model. These results are consistent with those of infinitely long panels in either the x_1 or x_2 directions.

- (2) The frequencies obtained by the T continuum model are higher than those of the finite element model by up to 11% for the rectangular panels considered. The differences in the frequencies are fairly uniform for the panels considered. For large L_2/L_1 and L_1/L_2 the frequencies predicted by the T model are consistent with those of infinitely long plates.

The total strain energy associated with the minimum frequency predicted by the finite element model is dominated by the transverse shear energy in the core structure, U_2^d . As can be seen from Fig. 11, the ratio, U_2^d/U is fairly uniform for the panels considered. Differences in the predictions of the energy components, U_1^t and U_2^d , by the continuum models, are quantitatively similar to, although generally smaller than, the maximum differences observed for the infinitely long panels with small numbers of cells. Consequently, these results are not shown. Unfortunately, rectangular panels with more cells in each direction than considered herein may be required in order to provide additional information regarding the accuracy of the continuum models.

Supplementing the quantitative measures discussed thus far, some qualitative results, such as cell wall shear stress, shear strain and shear strain energy distributions, are available to provide insight into the energy estimation methods considered herein. These are presented in the following section.

4.5 Shear strain energy distribution in honeycomb cell walls

For panels with L_1 or L_2 infinite and ten cells in the finite-length direction, contour plots of the shear strain energy, U_{12} , are shown in Fig. 12. The strain energy U_{12} is referred to the local cell wall coordinates (see Fig. 2). Grid C (see Fig. 4) was used to discretize each sandwich panel. An examination of Fig. 12 reveals that, for the panels with infinite L_1 or L_2 , the distribution of the cell wall shear strain energy density, U_{12} , exhibits a small variation in the sandwich thickness, ξ_2 direction and a slow change along the length (local ξ_1) direction. The distributions of U_{12} are qualitatively similar to those of the resultant, N_{12} , and the generalized strain, ϵ_{12}^0 . The estimates of the shear stiffness coefficients using the lower and upper bound energy methods are based on assumed constant states of

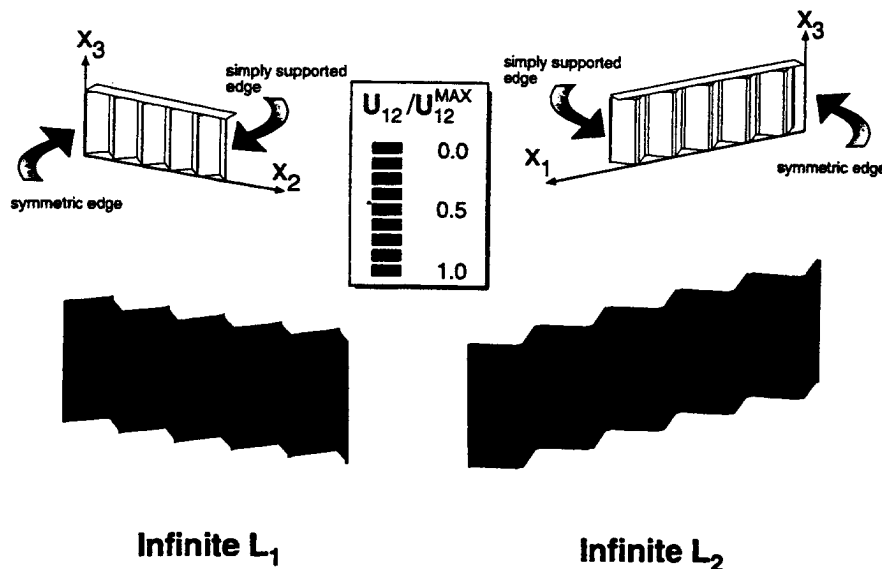


Fig. 12. Typical distribution of cell wall strain energy density component $U_{12} = (N_{12})^2 / G_c t_c$ (see Fig. 2), associated with the lowest free-vibration mode. Symmetric sandwich panels, $h = 1$ in., $h_f = 0.12$ in., with cross-ply, composite face sheets. Ten cells in each of the finite length directions and edges simply supported. Cell dimensions, $d = 3/16$ in., $\theta = 45^\circ$, $\eta = 6.12^\circ$ and $t_c = 0.002$ in.

stress and strain in the sandwich core structure, respectively. An examination of Fig. 12 does not show a difference in these stress and strain distributions that would explain the difference in the predictions of the UB and LB models.

5. Concluding remarks

Detailed finite element models are used for predicting the free-vibration response of infinitely long and rectangular sandwich panels. The panels considered have square-cell honeycomb core and simply supported edges. The sandwich core and face sheets are modeled by using three-dimensional solid elements, and two-dimensional plate finite elements. The predictions of the finite element models are compared with those obtained by using higher-order sandwich theory for panels, with the core replaced by an effective (equivalent) continuum. Three different approaches are used for estimating the effective material properties of the equivalent continuum layer: a lower bound energy approach; an upper bound energy approach; and a design-data test based approach. For all the sandwich panels considered in this study, the vibration frequencies and associated strain energy components predicted by the continuum models using the upper bound core property estimations were close to those calculated by using detailed two-dimensional plate finite element models. The frequencies predicted by the continuum models using the lower bound estimates of the shear stiffnesses were higher than those of the detailed finite element model. By contrast, the predictions of the continuum models with test-based equivalent properties were lower than those of the finite element model. The distributions of the in-plane shear stresses, strains and strain energy densities in the cell walls obtained by the detailed finite element models do not confirm either of the underlying constant strain or constant stress hypotheses used in the upper bound or lower bound energy estimation approaches, respectively.

Acknowledgment

The present work is partially supported by NASA Cooperative Agreement NCCW-0011, by NASA Grant NAG-1-1162 and by Air Force Office of Scientific Research Grant AFOSR-F49620-96-1-0462. The authors gratefully acknowledge Jim Starnes of NASA Langley Research Center, Joe Solecki and Shah Yunus of ANSYS, Inc., David Dietrich of Mallett Technology, Inc. and Eric Creggor and Patrick Roark of the Boeing Aircraft Company.

Appendix A. Equivalent (effective) properties of the continuum core model

The equivalent (effective) continuum properties of the continuum layer, replacing the actual honeycomb core, are calculated by using models similar to those in [20]. Fig. 2 shows the geometric characteristics of the honeycomb cell as follows: l_1 is the cell wall width; $2l_2$ is the joined (to the adjacent formed ribbon) width; θ is the opening angle of the cell; t_c is the cell wall foil thickness. For convenience, the ratio of the cell wall widths is represented by the parameter $\eta = 2l_2/l_1$. The expressions for the equivalent continuum core properties are given subsequently in terms of the three material parameters: Young's and shear moduli E_s and G_s , and material density ρ_s ; and the four geometric parameters l_1 , θ , t_c and η .

Continuum core density:

$$\frac{\rho_c}{\rho_s} = \frac{(1 + \eta)}{(\eta + \cos \theta) \sin \theta} \left(\frac{t_c}{l_1} \right)$$

In-plane continuum core properties:

$$E_1^c = E_s \left\{ \frac{1}{(\sin \theta)(\lambda \sin^2 \theta / (\eta + \cos \theta)(t_c/l_1)^3 + (\eta + \cos^2 \theta) / (\eta + \sin \theta)(t_c/l_1))} \right\}$$

$$E_2^c = E_s \left\{ \frac{\sin \theta}{(\eta + \cos \theta)(\lambda \cos^2 \theta / (t_c/l_1)^3 + \sin^2 \theta / (t_c/l_1))} \right\}$$

$$\nu_{12}^c = \left\{ -\cos \theta \left\{ \frac{(-\lambda / (t_c/l_1)^3 + 1 / (t_c/l_1))}{(\lambda \sin^2 \theta / (t_c/l_1)^3 (\eta + \cos \theta) + \cos^2 \theta / (t_c/l_1)(\eta + \sin \theta))} \right\} \right\}$$

$$G_{12}^c = E_s \left(\frac{t_c}{l_1} \right)^3 \frac{(\eta + \cos \theta)}{\eta^2 (1 + \eta/4) \sin \theta}$$

Transverse Young's modulus and transverse Poisson's ratios:

$$E_3^c = E_s \frac{(1 + \eta)}{(\eta + \cos \theta) \sin \theta} \left(\frac{t_c}{l_1} \right)$$

$$\nu_{31}^c = \nu_{32}^c = \nu_s$$

$$\nu_{13}^c = \frac{E_1^c}{E_3^c} \nu_s$$

$$\nu_{23}^c = \frac{E_2^c}{E_3^c} \nu_s$$

Upper and lower bounds of the transverse shear moduli:

$$G_{23}^c \text{ LB} = G_{23}^c \text{ UB} = G_{23}^c = G_s \frac{\sin \theta}{(\eta + \cos \theta)} \left(\frac{t_c}{l_1} \right)$$

$$G_{13}^c \text{ LB} = G_s \frac{(\eta + \cos \theta)}{(1 + 4\eta) \sin \theta} \left(\frac{t_c}{l_1} \right)$$

$$G_{13}^c \text{ UB} = G_s \frac{(\eta + \cos^2 \theta)}{(\eta + \cos \theta) \sin \theta} \left(\frac{t_c}{l_1} \right)$$

The effects of double-thickness cell walls resulting from cell assembly were incorporated in the preceding expressions. In the present study λ was selected to be 1. Note that the upper and lower bound shear stiffnesses are different in the x_1 direction but are equal in the x_2 direction. Also note that the equivalent continuum properties are independent of the honeycomb core thickness, h_c .

Appendix B. Boundary conditions used in the present study

B.1 - Infinitely long panels

For the infinitely long sandwich panels with either infinite L_1 or L_2 , the displacement and stress responses are assumed to be antisymmetric with respect to the midplane ($x_3 = 0$), and periodic in the x_2 or x_1 directions, with periods $2L_2$ or $2L_1$, respectively. For panels with infinite L_2 , the periodic response can be represented by modeling a quadrant of a plane section of the infinitely long panel and applying the following symmetry and antisymmetry conditions:

$$\begin{aligned} u_2 = w = 0, \quad \sigma_{11} = 0 \quad \text{at } x_1 = L_1/2, \quad -L_2 < x_2 < L_2, \quad 0 < x_3 < h/2, \\ u_1 = 0, \quad \sigma_{12} = \sigma_{13} = 0 \quad \text{at } x_1 = 0, \quad -L_2 < x_2 < L_2, \quad 0 < x_3 < h/2, \end{aligned} \quad (\text{B.1})$$

and

$$u_1 = u_2 = 0, \quad \sigma_{33} = 0 \quad \text{at } x_3 = 0, \quad 0 < x_1 < L_1/2, \quad -L_2 < x_2 < L_2. \quad (\text{B.2})$$

In addition, the required plane strain conditions for the direction extending to infinity are

$$u_2 = 0, \quad \sigma_{12} = \sigma_{23} = 0 \quad \text{for } 0 < x_1 = L_1, \quad -L_2 < x_2 < L_2, \quad 0 < x_3 < h/2. \quad (\text{B.3})$$

The corresponding symmetry and antisymmetry conditions for panels with infinite L_1 are obtained by interchanging subscripts 1 and 2 in Eqs. (B.1)–(B.3).

B.2. Rectangular panels

For the rectangular sandwich panels, the displacement and stress responses are assumed to be antisymmetric with respect to the midplane ($x_3 = 0$) and periodic in both the x_1 and x_2 directions with periods $2L_1$ and $2L_2$. The periodic response can be represented by modeling only one octant of the rectangular panel and applying the following symmetry and antisymmetry conditions:

$$u_1 = u_2 = 0, \quad \sigma_{33} = 0 \quad \text{at } x_3 = 0, \quad 0 < x_1 < L_1/2, \quad 0 < x_2 < L_2/2, \quad (\text{B.4})$$

and

$$\begin{aligned} u_1 &= 0, & \sigma_{12} &= \sigma_{13} = 0 & \text{at } x_1 &= 0, & 0 < x_2 < L_2/2, & 0 < x_3 < h/2, \\ u_2 &= w = 0, & \sigma_{11} &= 0 & \text{at } x_1 &= L_1/2, & 0 < x_2 < L_2/2, & 0 < x_3 < h/2, \\ u_2 &= 0, & \sigma_{12} &= \sigma_{23} = 0 & \text{at } x_2 &= 0, & 0 < x_1 < L_1/2, & 0 < x_3 < h/2, \\ u_1 &= w = 0, & \sigma_{22} &= 0 & \text{at } x_2 &= L_2/2, & 0 < x_1 < L_1/2, & 0 < x_3 < h/2. \end{aligned} \quad (\text{B.5})$$

References

- [1] D. Zenkert, *An Introduction to Sandwich Construction* (Chameleon Press, London, 1995).
- [2] C.W. Bert, Shear deformation and sandwich configuration, in: G.I. Turvey and I.H. Marshall, eds., *Buckling and Postbuckling of Composite Plates* (Chapman and Hall, London, 1995) 157–189.
- [3] A.K. Noor, W.S. Burton and C.W. Bert, Computational models for sandwich panels and shells, *Appl. Mech. Rev.* 155(3) (1995) 155–199.
- [4] W.S. Burton and A.K. Noor, Assessment of computational models for sandwich panels and shells, *Comput. Methods Appl. Mech. Engrg.* 124(1–2) (1995) 125–151.
- [5] C.C. Chamis, R.A. Aiello and P.L.N. Murthy, Composite sandwich thermostructural behavior: Computational simulation, *Proceedings of the 27th AIAA/ASME/ASCE/AHS/ASC Structures, Structural Dynamics and Materials Conference*, San Antonio, TX, May 19–21, 1986, Technical Papers, Part 1 (1986) 370–381.
- [6] C.C. Chamis, R.A. Aiello and P.L.N. Murthy, Fiber composite sandwich thermostructural behavior: Computational simulation, *J. Composites Tech. Res.* 10(3) (1988) 93–99.
- [7] W. Elspass and M. Flemming, Analysis of precision sandwich structures under thermal loading, *ICAS Proceedings, 1990, 17th Congress of the International Council on Aeronautical Sciences (ICAS-90-4.8.1)*, Stockholm, Sweden, Sept. 9–14, 1990, 2 (1990) 1513–1518.
- [8] *Annual Book of ASTM Standards*, ASTM 673–61, Vol. 15.03 (1988).
- [9] *Sandwich Constructions and Core Materials: General Test Methods*, MIL-STD-401B, Military Standard (1967).
- [10] H. Smullen and W.F. Roberts, Properties of stainless steel sandwich using low-density honeycomb cores, *Welding J.* 40(2) (1961) 90s–96s.
- [11] V. Weissberg and S. Cioclia, Test method for evaluation of shear modulus of low-stiffness material, *Exper. Tech.* 8 (1984) 34.
- [12] K.A. Feichtinger, Test methods and performance of structural core materials—1. Static Properties, *J. Reinforced Plastics Composit.* 8 (1989) 334–357.
- [13] R.D. Adams and M.R. Maheri, The dynamic shear properties of structural honeycomb materials, *Comput. Sci. Tech.* 47(1) (1993) 15–23.
- [14] S. Kelsey, R.A. Gellatly and B.W. Clark, The shear modulus of foil honeycomb cores, *Aircraft Engrg.* 30(356) (1958) 294–302.
- [15] C.C. Chang and I.K. Ebcioğlu, Effect of cell geometry on the shear modulus and on density of sandwich panel cores, *J. Basic Engrg.* ASME 83(D4) (1961) 513–518.
- [16] J. Penzien and T. Didriksson, Effective shear modulus of honeycomb cellular structure, *AIAA J.* 2(3) (1964) 531–535.

- [17] F.K. Abd El-Sayed, A.R. Jones and I.W. Burgess, A theoretical approach to the deformation of honeycomb based composite materials, *Composites* (1979) 209–214.
- [18] C.E.S. Ueng, Mechanical properties of superplastically formed core materials, *Proceedings 24th AIAA/ASME/ASCE/AHS/ASE Structures, Structural Dynamics and Materials Conference*, Lake Tahoe, NV, May 2–4, 1983, AIAA, Part I, (1983) 569–577.
- [19] C.E.S. Ueng and T.D. Kim, Shear modulus of core materials with arbitrary polygonal shape, *Comput. Struct.* 16(1–4) (1983) 21–25.
- [20] L.J. Gibson and M.F. Ashby, *Cellular Solids, Structures and Properties* (Pergamon Press, Oxford, 1988).
- [21] K.J. Bowles and R.D. Vannucci, Mechanical properties characterization of composite sandwich materials intended for space antenna applications, in: C. Chamis, ed., *Test Methods and Design Allowables for Fibrous Composites*, Vol. 2 (American Society of Testing and Materials, Philadelphia, PA, (ASTM STP-1003, 1989) 31–44.
- [22] B.T. Bhat and T.G. Wang, A comparison of mechanical properties of some foams and honeycombs, *J. Mat. Sci.* 25 (1990) 5157–5162.
- [23] G. Shi and P. Tong, Equivalent transverse shear stiffness of honeycomb cores, *Int. J. Solids Struct.* 32(10) (1995) 1383–1393.
- [24] L.J. Gibson, M.F. Ashby, G.S. Schajer and C.I. Robertson, The mechanics of two-dimensional cellular materials, *Proceedings of the Royal Society of London*, A382 (1982) 25–42.
- [25] K.E. Evans, The design of doubly curved sandwich panels with honeycomb cores, *Composite Struct.* 17(2) (1991) 95–111.
- [26] C.A. Ginty and N.M. Endres, Composite space antenna structures: Properties and environmental effects. In: *Materials for Space—The Gathering* (Proceedings 18th International SAMPE Technical Conference), J. Hoggatt, S. Hill and J. Johnson, eds., Seattle, WA, Oct. 7–9, 1986, Society for the Advancement of Material and Process Engineering, Covina, CA, 18 (1986) 545–560.
- [27] D.J. Chang and W.H. Kao, SiC reinforced titanium corrugated structures for high temperature application, *SAMPE J.* 24 (1988) 13–17.
- [28] M. Grediac, A finite element study of the transverse shear in honeycomb cores, *Int. J. Solids Struct.* 30(13) (1993) 1777–1788.
- [29] ANSYS, Version 5.1, ANSYS, Inc., Houston, PA. (1995).

INFORMATION FOR CONTRIBUTORS

Manuscripts should be sent in triplicate to one of the Editors. All manuscripts will be refereed. Manuscripts should preferably be in English. They should be typewritten, double-spaced, first copies (or clear Xerox copies thereof) with a wide margin. Abstracts, footnotes and lists of references should also be double-spaced. All pages should be numbered (also those containing references, tables and figure captions). Upon acceptance of an article, author(s) will be asked to transfer copyright of the article to the publisher. This transfer will ensure the widest possible dissemination of information.

Abstracts

The text of a paper should be preceded by a summary in English. This should be short, but should mention all essential points of the paper.

Figures and tables

The drawings for the figures must be originals, drawn in black India ink in large size and carefully lettered, or printed on a high-quality laser printer. The lettering as well as the details should have proportionate dimensions, so as not to become illegible or unclear after the usual reduction by the printers; in general, the figures should be designed for a reduction factor of two or three. Mathematical symbols should be entered in italics, where appropriate. Each figure should have a number and a caption; the captions should be collected on a separate sheet. The appropriate place of a figure should be indicated in the margin. Tables should be typed on separate sheets. Each table should have a number and a title. The appropriate places for the insertion of tables should be indicated in the margin. Colour illustrations can be included and will be printed in colour at no charge if, in the opinion of the Editors, the colour is essential. If this is not the case, the figures will be printed in black and white unless the author is prepared to pay the extra costs arising from colour reproduction.

Formulae

Displayed formulae should be numbered and typed or clearly written by hand. Symbols should be identified in the margin, where they occur for the first time.

References

In the text, reference to other parts of the paper should be made by section (or equation) number, but not by page number. References should be listed on a separate sheet in the order in which they appear in the text.

COMPLETE INSTRUCTIONS TO AUTHORS are published in every last issue of a volume, and copies can also be obtained from the Editors and the Publisher, Elsevier Science B.V., P.O. Box 1991, 1000 BZ Amsterdam, The Netherlands.

Instructions for LaTeX manuscripts

The LaTeX files of papers that have been accepted for publication may be sent to the Publisher by e-mail or on a diskette (3.5" or 5.25" MS-DOS). If the file is suitable, proofs will be produced without rekeying the text. The article should be encoded in Elsevier-LaTeX, standard LaTeX, or AMS-LaTeX (in document style "article"). The Elsevier-LaTeX package, together with instructions on how to prepare a file, is available from the Publisher. This package can also be obtained through the Elsevier WWW home page (<http://www.elsevier.nl/>), or using anonymous FTP from the Comprehensive TeX Archive Network (CTAN). The host-names are: `ftp.dante.de`, `ftp.tex.ac.uk`, `ftp.shsu.edu`; the CTAN directories are: `/pub/tex/macros/latex209/contrib/elsevier`, `/pub/archive/macros/latex209/contrib/elsevier`, `/tex-archive/macros/latex209/contrib/elsevier`, respectively. No changes from the accepted version are permissible, without the explicit approval of the Editor. The Publisher reserves the right to decide whether to use the author's file or not. If the file is sent by e-mail, the name of the journal should be mentioned in the "subject field" of the message to identify the paper. Authors should include an ASCII table (available from the Publisher) in their files to enable the detection of transmission errors.

The files should be mailed to: Elsevier Editorial Services, Mayfield House, 256 Banbury Road, Oxford OX2 7DH, UK. Fax: +44-1865-314990. E-mail: ees@elsevier.co.uk.

Publication information:

Computer Methods in Applied Mechanics and Engineering (ISSN 0045-7825). For 1997 volumes 140-150 are scheduled for publication. Subscription prices are available upon request from the Publisher. Subscriptions are accepted on a prepaid basis only and are entered on a calendar year basis. Issues are sent by surface mail except to the following countries where Air delivery via SAL mail is ensured: Argentina, Australia, Brazil, Canada, Hong Kong, India, Israel, Japan, Malaysia, Mexico, New Zealand, Pakistan, PR China, Singapore, South Africa, South Korea, Taiwan, Thailand, USA. For all other countries airmail rates are available upon request. Claims for missing issues should be made within six months of our publication (mailing) date.

Orders, claims, and product enquiries

Please contact the Customer Support Department at the Regional Sales Office nearest you:

New York
Elsevier Science
P.O. Box 945
New York, NY 10159-0945
USA
Tel. (+1)212-633-3730
[Toll free number for North American customers:
1-888-4ES-INFO (437-4636)]
Fax (+1)212-633-3680
e-mail usinfo-f@elsevier.com

Amsterdam
Elsevier Science
P.O. Box 211
1000 AE Amsterdam
The Netherlands
Tel. (+31)20-4853757
Fax (+31)20-4853432
e-mail nlinfo-f@elsevier.nl

Tokyo
Elsevier Science
9-15 Higashi-Azabu 1-chome
Minato-ku, Tokyo 106
Japan
Tel. (+81)3-5561-5033
Fax (+81)3-5561-5047
e-mail kyf04035@niftyserve.or.jp

Singapore
Elsevier Science
No. 1 Temasek Avenue
#17-01 Millenia Tower
Singapore 039192
Tel. (+65)434-3727
Fax (+65)337-2230
e-mail asiainfo@elsevier.com.sg

Advertising information

Advertising orders and enquiries may be sent to: **International:** Elsevier Science, Advertising Department, The Boulevard, Langford Lane, Kidlington, Oxford OX5 1GB, UK. Tel. (+44)(0)1865 843565, Fax (+44)(0)1865 843976. **USA and Canada:** Weston Media Associates, Daniel Lipner, P.O. Box 1110, Greens Farms, CT 06436-1110, USA. Tel. (+1)(203)261-2500, Fax (+1)(203)261-0101. **Japan:** Elsevier Science Japan, Marketing Services, 1-9-15 Higashi-Azabu, Minato-ku, Tokyo 106, Japan. Tel. (+81)3-5561-5033; Fax (+81)3-5561-5047.

Reprinted from

Computer methods in applied mechanics and engineering

Comput. Methods Appl. Mech. Engrg. 144 (1997) 371–389

**Space–time finite element methods for the sensitivity
analysis of contact/impact response of axisymmetric
composite structures**

Levent Karaoğlu, Ahmed K. Noor*

Center for Advanced Computational Technology, University of Virginia, Hampton, VA 23681, USA

Received 9 June 1996; revised 7 August 1996



COMPUTER METHODS IN APPLIED MECHANICS AND ENGINEERING

EDITORS: J.H. ARGYRIS, STUTTGART and LONDON

T.J.R. HUGHES, STANFORD, CA

J.T. ODEN, AUSTIN, TX

W. PRAGER
Founding Editor
(deceased 1980)

EDITORIAL ADDRESSES

John H. ARGYRIS
Institut für Computer Anwendungen
Pfaffenwaldring 27
D-70569 STUTTGART
Germany
(Editorial Office)

Thomas J.R. HUGHES
Division of
Applied Mechanics
Durand Building
Room No. 281
Stanford University
STANFORD
CA 94305-4040, USA

J. Tinsley ODEN
The University of Texas
The Texas Institute for
Computational and
Applied Mathematics
Taylor Hall 2.400
AUSTIN
TX 78712, USA

ASSOCIATE EDITORS

K. APPA, Hawthorne, CA
I. BABUŠKA, Austin, TX
A.J. BAKER, Knoxville, TN
T. BELYTSCHKO, Evanston, IL
L. DEMKOWICZ, Austin, TX
R.E. EWING, College Station, TX
M. FEINGOLD, Marly-le-Roy

R.H. GALLAGHER, Potsdam, NY
R. GLOWINSKI, Houston, TX
H.-O. KREISS, Los Angeles, CA
J.L. LIONS, Paris
H. LOMAX, Moffet Field, CA
C.E. MASSONNET, Liège

L.S.D. MORLEY, Farnborough
K.S. PISTER, Berkeley, CA
G. STRANG, Cambridge, MA
G.P. VOSKRESENSKY, Moscow
W.H. YANG, Ann Arbor, MI
O.C. ZIENKIEWICZ, Swansea

ADVISORY EDITORS

J.F. ABEL, Ithaca, NY
H. ARMEN, Bethpage, NY
K.J. BATHE, Cambridge, MA
P.G. BERGAN, Høvik
J.F. BESSELING, Delft
G. BORM, Potsdam
H. BUFLER, Stuttgart
H. CABANNES, Paris
C. CANUTO, Torino
G.F. CARRIER, Cambridge, MA
T. CEBECI, Long Beach, CA
A.S.L. CHAN, London
J.L. CHENOT, Valbonne
H. CHRISTIANSEN, Provo, UT
T.J. CHUNG, Huntsville, AL
P.G. CIARLET, Paris
H. COHEN, New York, NY
M.Z. COHN, Waterloo, Ont.
J. DONEA, Ispra
P.R. EISEMAN, New York, NY
B. ENGQUIST, Los Angeles, CA
C.A. FELIPPA, Boulder, CO
K. FENG, Beijing
I. FRIED, Boston, MA
Editorial Secretary: Marlies PARSONS

R.A. GELLATLY, San Leandro, CA
M. GERADIN, Liège
R. GRUBER, Manno
K.K. GUPTA, Edwards, CA
R.W. HAMMING, Monterey, CA
F.H. HARLOW, Los Alamos, NM
E.J. HAUG, Iowa City, IA
J.C. HEINRICH, Tucson, AZ
M. HOGGE, Liège
I. HOLAND, Trondheim
C. JOHNSON, Göteborg
B.Z. KAPLAN, Beer-Sheva
T. KAWAI, Tokyo
J. KESTENS, Brussels
S.W. KEY, La Cañada-Flintridge, CA
W.C. KNUDSON, Sunnyvale, CA
F.A. LECKIE, Santa Barbara, CA
R.W. LEWIS, Swansea
K. LINKWITZ, Stuttgart
LUO Shi-jun, Xi'an
G. MAIER, Milano
J.L. MEEK, St. Lucia, Queensland
A.J. MORRIS, Cranfield
A. NEEDLEMAN, Providence, RI
M.P. NIELSEN, Lyngby

A.K. NOOR, Hampton, VA
R. OHAYON, Paris
P.J. PAHL, Berlin
B. PAUL, Philadelphia, PA
R. PEYRET, Nice
J. PLANCHARD, Clamart
A.R.S. PONTER, Leicester
V.F. POTERASU, Iasi
QIAN Ling-xi (L.H. Tsien), Dalian
A.K. RAO, Bangalore
M. REISER, Rorschlikon
E. RIKS, Delft
P.J. ROACHE, Albuquerque, NM
G.I.N. ROZVANY, Essen
W. SCHIEHLEN, Stuttgart
B. SCHÖNUNG, Baden
P.S. SYMONDS, Providence, RI
A.B. TEMPLEMAN, Liverpool
C.W. TROWBRIDGE, Kidlington
J.R. WHITEMAN, Uxbridge
K.J. WILLAM, Boulder, CO
Y. YAMADA, Tokyo
Th. ZIMMERMANN, Lausanne

International Standard Serial Number 0045-7825

Copyright © 1997 Elsevier Science S.A. All rights reserved.

0045-7825/97/\$17.00

This journal and the individual contributions contained in it are protected by the copyright of Elsevier Science S.A., and the following terms and conditions apply to their use:

Photocopying

Single photocopies of single articles may be made for personal use as allowed by national copyright laws. Permission of the publisher and payment of a fee is required for all other photocopying, including multiple or systematic copying, copying for advertising or promotional purposes, resale, and all forms of document delivery. Special rates are available for educational institutions that wish to make photocopies for non-profit educational classroom use.

In the USA, users may clear permissions and make payment through the Copyright Clearance Center, 222 Rosewood Drive, Danvers, MA 01923, USA. In the UK, users may clear permissions and make payment through the Copyright Licensing Agency Rapid Clearance Service (CLARCS), 90 Tottenham Court Road, London, W1P 0LP. In other countries where a local copyright clearance centre exists, please contact it for information on required permissions and payments.

Derivative Works

Subscribers may reproduce tables of contents or prepare lists of articles including abstracts for internal circulation within their institutions. Permission of the publisher is required for resale or distribution outside the institution.

Permission of the publisher is required for all other derivative works, including compilations and translations.

Electronic Storage

Permission of the publisher is required to store electronically any material contained in this journal, including any article or part of an article. Contact the publisher at the address indicated.

Except as outlined above, no part of this publication may be reproduced, stored in a retrieval system or transmitted in any form or by any means, electronic, mechanical, photocopying, recording or otherwise, without prior written permission of the publisher.

Disclaimers

No responsibility is assumed by the publisher for any injury and/or damage to persons or property as a matter of products liability, negligence or otherwise, or from any use or operation of any methods, products, instructions or ideas contained in the materials herein.

Although all advertising material is expected to conform to ethical (medical) standards, inclusion in this publication does not constitute a guarantee or endorsement of the quality or value of such product or of the claims made of it by its manufacturer.

© The paper used in this publication meets the requirements of ANSI/NISO Z39.48-1992 (Permanence of Paper).

Printed in The Netherlands



ELSEVIER

Comput. Methods Appl. Mech. Engrg. 144 (1997) 371-389

Computer methods
in applied
mechanics and
engineering

Space-time finite element methods for the sensitivity analysis of contact/impact response of axisymmetric composite structures

Levent Karaoğlu, Ahmed K. Noor*

Center for Advanced Computational Technology, University of Virginia, Hampton, VA 23681, USA

Received 9 June 1996; revised 7 August 1996

Abstract

Space-time finite element methods are applied to the sensitivity analysis of frictional contact/impact response of axisymmetric composite structures. The structures are assumed to consist of an arbitrary number of perfectly bonded homogeneous anisotropic layers. Only small displacements are considered and the material of each layer is assumed to be hyperelastic. The sensitivity coefficients measure the sensitivity of the response to variations in material parameters of the structure.

A displacement finite element model is used for the spatial discretization. The temporal integration is performed by using the time-discontinuous Galerkin method. Least-squares stabilizing operators are added to the governing equations to enhance the stability by smoothing out the high frequency modes, without degrading the accuracy. A quasi-explicit iterative technique is used for generating the response and evaluating the sensitivity coefficients. The normal contact conditions are incorporated within the iterative process. Numerical results are presented for the sensitivity analysis of contact/impact response of a composite spherical cap impacting a rigid plate.

Nomenclature

E_L, E_T	elastic moduli of the individual layers in the fiber and transverse directions, respectively
F^{con}, F	vectors of contact and external forces, respectively
$f_{G/GL}$	combined force vector for Galerkin or Galerkin/least-square formulation
g_0	initial axial gap associated with a contact node
G_{LT}, G_{TT}	shear moduli of the individual layers in the plane of fibers and normal to it, respectively
h	total thickness of the structure
K	tangent stiffness matrix
$K_{G/GL}$	combined stiffness matrix for Galerkin or Galerkin/least-square formulation
$\tilde{K}_{G/GL}$	combined stiffness matrix for Galerkin or Galerkin/least-square formulation which includes terms related to K
M	lumped mass matrix
$\tilde{M}_{G/GL}$	combined mass matrix for Galerkin or Galerkin/least-square formulation which includes terms related to M
q	displacement vector at specified time levels
Q	displacement vector at specified levels in the absence of contact
r, z, θ	orthogonal coordinate system, see Fig. 1

*Corresponding author.

s	meridional distance
t	time
t_N	normal component of contact tractions (pressures)
u, v, w	displacement components in the radial, circumferential and axial directions, respectively
u	displacement vector
w	virtual displacement vector
Δt	time step size
τ	intrinsic time-scale parameter
$\bar{\tau}$	normalized intrinsic time-scale parameter
$\bar{\theta}_k$	fiber orientation angle of the k th layer
λ	typical lamination or material parameter of the structure
ν_{LT}, ν_{TT}	Poisson's ratios of the individual layers
ζ	normalized time step size

Subscripts

n	current time step
0	initial conditions at $t = 0$

Superscripts

i	iteration cycle
$+$	response and sensitivity quantities just after the time period starts
$-$	response and sensitivity quantities just before the time period starts

Other mathematical symbols

(\cdot)	time derivative
$\frac{\partial(\cdot)}{\partial(\cdot)}$	partial derivative

1. Introduction

Two general approaches have been applied to the solution of the time-dependent contact/impact problems. The first approach is widely used, and is based on employing the finite element techniques for the spatial discretization and a temporal integration scheme for integrating the semi-discrete equations (see review paper [1]). In the second approach a finite element technique is used for both the spatial discretization and the temporal integration. However, the numerical problems associated with the localized oscillations and the discontinuities associated with contact/impact conditions have only been addressed in a few studies. Also, few studies have attempted to identify the proper temporal integration schemes for use in conjunction with different formulations. A systematic and detailed study of the interplay between the integration scheme and the contact/impact formulation is discussed in [2]. The difficulties associated with the use of temporal integration schemes and suggested modifications are also discussed in [3–5]. Numerous research efforts have concentrated on the use of time discretization schemes [6,7]. In the present paper the time-discontinuous Galerkin/least-squares method ([7–11]) is applied to contact/impact problems. The time-discontinuous Galerkin method permits the unknown fields to be discontinuous with respect to time and leads to stable, higher-order accurate finite element methods. The least-squares methods were shown to enhance the stability of the Galerkin method without degrading accuracy and it is included to better capture the discontinuities which occur in contact/impact problems.

The present study focuses on the application of the space–time finite element method to the sensitivity analysis of the dynamic response of axisymmetric composite structures (see review paper [12]). The governing semi-discrete equations for the sensitivity coefficients are obtained by direct differentiation of the corresponding equations for the response with respect to material properties. The time-discontinuous Galerkin method is used for the response and evaluating the sensitivity coefficients. To fix ideas only small displacements and linear elastic response are considered. Numerical results are presented to verify the

proposed model and to demonstrate the effectiveness of the time-discontinuous Galerkin/least-squares method in contact/impact problems.

2. Mathematical formulation

The structures considered are assumed to consist of an arbitrary number of perfectly-bonded homogeneous anisotropic layers. Only small displacements are considered and the material of each layer is assumed to be hyperelastic. The analytical formulation is based on the linear dynamic theory of axisymmetric solids of revolution [13]. A displacement formulation is used and the fundamental unknowns consist of the three displacement components, u , v , w at each point. The sign convention for the displacements is shown in Fig. 1.

2.1. Governing equations for response

In the absence of damping the semi-discrete equations and the initial conditions governing the linear elastodynamic response of the structure can be written in the following compact form:

$$M\ddot{u} + Ku = F \quad (1)$$

$$\dot{u}_0 = v_0 \quad (2)$$

$$u_0 = d_0 \quad (3)$$

where u is the displacement vector; v_0 , d_0 are the initial velocity and initial displacement vectors, respectively; F is the external force vector; and K and M are the stiffness and the diagonal lumped mass matrices, respectively. The global arrays K , M and F are obtained by assembling the spatial element arrays. Each spatial finite element can accommodate more than one anisotropic layer by employing numerical integration points at each layer. Mass lumping is performed by using the technique proposed in [14].

The temporal integration is performed by using typical finite element interpolation functions defined in terms of Lagrange polynomials. A k th order polynomial in time can be expressed in terms of nodal values at $k + 1$ time levels (see Appendix A for quadratic-in-time interpolation functions).

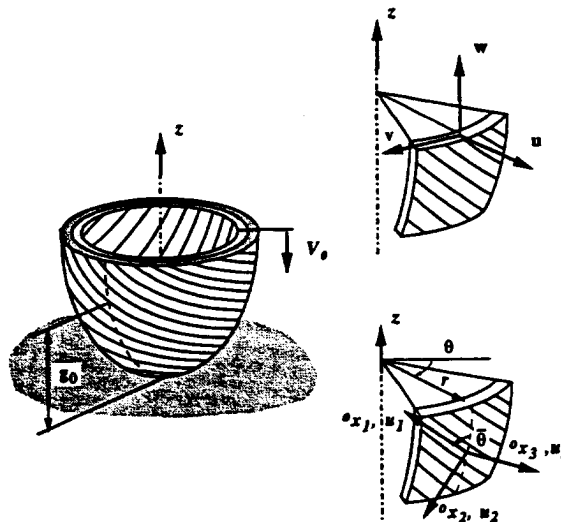


Fig. 1. Characteristics of frictional contact of an axisymmetric composite structure impacting a rigid plate and sign convention for displacements.

2.1.1. Time-discontinuous Galerkin method

The displacement field is allowed to be discontinuous in time, and the displacement continuity is weakly enforced via the strain energy inner product (see [10]). The following definitions are made:

$$u_n^+ = u(t_n^+) = \lim_{\epsilon \rightarrow 0} u(t_n + \epsilon) \quad (4)$$

$$u_n^- = u(t_n^-) = \lim_{\epsilon \rightarrow 0} u(t_n - \epsilon) \quad (5)$$

The time-discontinuous Galerkin method attempts to find u such that for all w the following is satisfied:

$$B(w, u)_n = L(w)_n \quad n = 1, 2, \dots, N \quad (6)$$

where

$$B(w, u)_n = \int_{I_n} \dot{w} \cdot (M\ddot{u} + Ku) dt + \dot{w}_{n-1}^+ \cdot M\dot{u}_{n-1}^+ + w_{n-1}^+ \cdot Ku_{n-1}^+ \quad (7)$$

$$L(w)_n = \int_{I_n} \dot{w} \cdot F dt + \dot{w}_{n-1}^+ \cdot M\dot{u}_{n-1}^- + w_{n-1}^+ \cdot Ku_{n-1}^- \quad (8)$$

$$L(w)_1 = \int_{I_1} \dot{w} \cdot F dt + \dot{w}_0^+ \cdot Mv_0 + w_0^+ \cdot Kd_0 \quad (9)$$

The last two terms in Eqs. (7) and (8) weakly enforce the initial conditions for each time interval. Substitution of the interpolation functions in Eqs. (6) lead to a system of linear algebraic equations of the form:

$$K_G q = f_G \quad (10)$$

where K_G and f_G are the combined stiffness matrix and the force vector, respectively, and are given in Appendix A for quadratic-in-time interpolation functions.

2.1.2. Time-discontinuous Galerkin/least-squares method

This method was developed to reduce the oscillations in the computer response and to ensure convergence for arbitrary space-time discretization and higher order element interpolations. To achieve these goals, stabilizing operators in least-squares form are added to Eq. (6) (see [10]). The resulting equation can be written in the following form:

$$\begin{aligned} B(w, u)_n + \int_{I_n} [(M\ddot{w} + Kw) \cdot \tau M^{-1} (M\ddot{u} + Ku)] dt \\ = L(w)_n + \int_{I_n} [(M\ddot{w} + Kw) \cdot \tau M^{-1} F] dt \quad n = 1, 2, \dots, N \end{aligned} \quad (11)$$

where τ is a parameter which has the dimension of time and is referred to as the intrinsic time scale. The least-squares terms in Eq. (12) add stability without degrading the accuracy of the underlying time-discontinuous Galerkin method.

The resulting system of algebraic equations (corresponding to Eq. (6)) can be written in the following form:

$$K_{GL} q = f_{GL} \quad (12)$$

where K_{GL} , q and f_{GL} are given in Appendix A for quadratic-in-time interpolation functions.

2.2. Governing equations for the sensitivity coefficients

The sensitivity coefficients of the response quantities with respect to the material parameters of the structure are obtained by differentiating the semi-discrete equations governing the contact/impact re-

sponse, Eqs. (3), with respect to each of the parameters. The resulting equations can be written in the following form:

$$M \frac{\partial \ddot{u}}{\partial \lambda} + K \frac{\partial u}{\partial \lambda} = -\frac{\partial K}{\partial \lambda} u \quad (13)$$

where λ is a typical material parameter of the structure. In Eq. (13) the external load vector and mass matrix are assumed to be independent of λ . The product $(\partial K / \partial \lambda) u$ on the right-hand side is evaluated on the element level. The resulting vectors are assembled to obtain the global vector.

If quadratic-in-time interpolation functions are used, the governing algebraic equations for the sensitivity coefficients for either the Galerkin or the Galerkin least-squares method can be written in the following form:

$$K_{G/GL} \frac{\partial q}{\partial \lambda} = \frac{\partial f_{G/GL}}{\partial \lambda} - \frac{\partial K_{G/GL}}{\partial \lambda} q \quad (14)$$

Note that the matrix on the left-hand side of Eq. (14) is the same as the one used in the response analysis. Therefore, the generation of the sensitivity coefficients involves only the evaluation of the right-hand sides and forward-reduction back substitution, and no matrix decomposition.

3. Computational procedure

3.1. Solution of the equations

The stiffness matrices of Galerkin and Galerkin least-squares methods are full and nonsymmetric. Since the direct solution of the full system of nonsymmetric equations is not desirable, a quasi-explicit technique is used in conjunction with an iterative method for the solution of Eqs. (10) and (12). The stiffness matrix for either Galerkin or Galerkin least-squares is decomposed into two parts as follows:

$$K_{G/GL} = \tilde{M}_{G/GL} + \tilde{K}_{G/GL} \quad (15)$$

where the \tilde{M} and \tilde{K} include the terms associated with the M and K , respectively. The explicit forms of the \tilde{M} and \tilde{K} are given in Appendix A. The iterative process used in generating the response vector q is described by the following equation:

$$q^i = \tilde{M}_{G/GL}^{-1} (f_{G/GL} - \tilde{K}_{G/GL} q^{i-1}) \quad (16)$$

where i refers to the i th iteration cycle. For the case of quadratic-in-time interpolation functions, the computational procedures for the Galerkin and the Galerkin least/squares methods are given in Appendix B.

The iterative process used in evaluating the sensitivity coefficients is described by the following equation:

$$\frac{\partial q^i}{\partial \lambda} = \tilde{M}_{G/GL}^{-1} \left(\frac{\partial f_{G/GL}}{\partial \lambda} - \frac{\partial K_{G/GL}}{\partial \lambda} q - \tilde{K}_{G/GL} \frac{\partial q^{i-1}}{\partial \lambda} \right) \quad (17)$$

The computational procedure used for evaluating the sensitivity coefficients are similar to those used in generating the response.

3.2. Contact analysis

The normal contact conditions are incorporated within the iterative process. The flat-rigid surface contact equations in the axial direction are

$$q_z \leq -g_0 \quad (18)$$

where g_0 is the initial gap distance. First, Eq. (16) is solved with contact constraints (q) and then without imposing any constraints (Q). The contact forces are calculated at each step as follows:

$$F^{\text{con}} = K_G (q - Q) \quad (19)$$

4. Numerical studies

Numerical studies are performed to validate the proposed time-discontinuous Galerkin method; and to show the effect of least-squares smoothing on both the contact/impact response, and the sensitivity coefficients for axisymmetric composite structures.

Herein, typical results are presented for a spherical cap impacting a rigid plate with an initial axial velocity of 10 m/s (see Fig. 1). The cap is made of twenty-four layers of graphite-epoxy composite. The properties for the composite material are given in Table 1.

Nine-noded elements with biquadratic interpolation functions are used for spatial discretization (a total of 4307 displacement degrees of freedom). Quadratic interpolation functions are used for the temporal integration. The sensitivity coefficients are evaluated by using Eqs. (14).

Since the dynamic frictional contact response was found to be more sensitive to variations in Young's modulus in the fiber direction E_L than to variations in other material parameters (see [5]), numerical results are presented herein for the sensitivity coefficients with respect to E_L .

4.1. Time-discontinuous Galerkin method

The predictions of the time-discontinuous Galerkin finite element method (TDG) are validated by comparing them with the predictions of the explicit central difference temporal integration scheme (CD).

The time histories of the radial, circumferential and axial displacement components u, v, w and their normalized sensitivity coefficients at two points (points 1, 2) are shown in Figs. 2 and 3, respectively. The sensitivity coefficients are normalized by multiplying each by the material parameter, and dividing by the maximum value of the response quantity. The displacements and sensitivities have strong oscillations at point 1.

The distributions of the normal contact pressure, t_N and its sensitivity coefficient at the bottom surface of the structure are shown in Fig. 4 at time $t = 5 \mu\text{s}$. The contact pressures are normalized by dividing by E_T . Both response and sensitivity distributions exhibit rapid changes in the contact region.

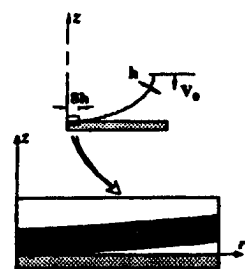
Figs. 2-4 show the close agreement between the TDG and CD predictions for both the response and sensitivity quantities.

4.2. Time-discontinuous Galerkin/least-squares method

The least square correction to the discontinuous Galerkin method is characterized by the parameter τ . The value $\tau = 0$ corresponds to the original time-discontinuous Galerkin method.

Table 1
Material properties for composite structure used in the present analysis.

ρ (kg/m^3)	1600
E_L (GPa)	151.68
E_T (GPa)	9.65
G_{LT} (GPa)	5.93
G_{TT} (GPa)	3.65
ν_{LT}	0.32
ν_{TT}	0.32



Point	$10^3 \times r, \text{ m}$	$10^3 \times z, \text{ m}$
1	0.62	0
2	4.8	0.4

Point 1

Point 2

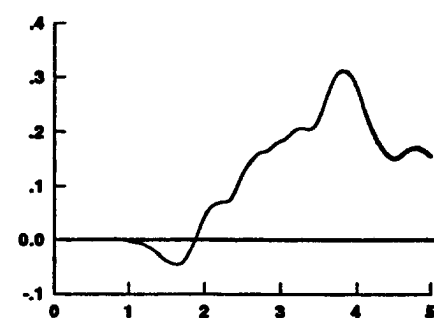
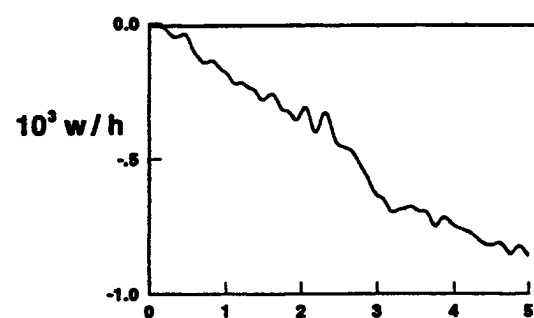
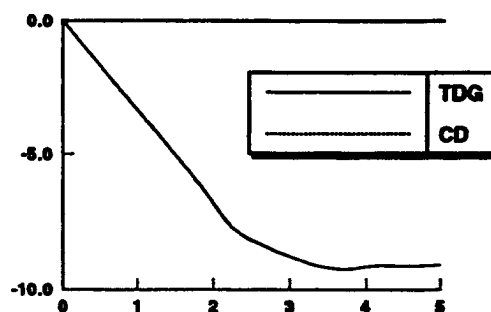
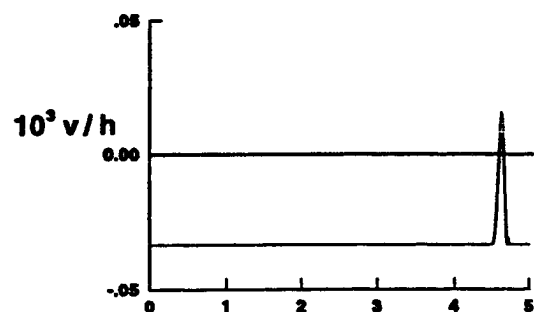
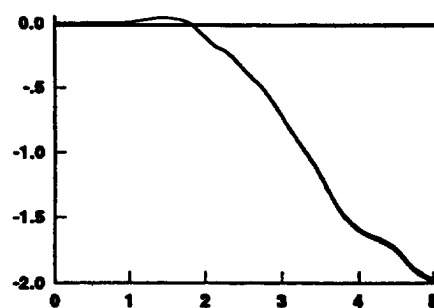
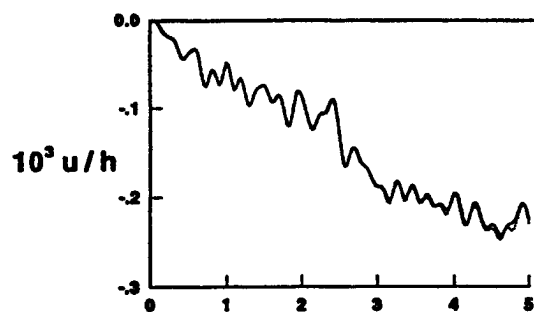
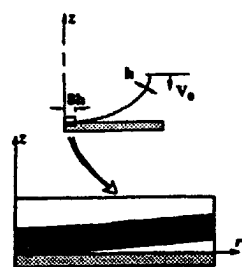
time, μs time, μs

Fig. 2. Time histories of radial, circumferential and axial displacement components for the time-discontinuous Galerkin (TDG) and central difference (CD) methods.



Point	$10^3 \times r, \text{m}$	$10^3 \times z, \text{m}$
1	0.62	0
2	4.8	0.4

Point 1

Point 2

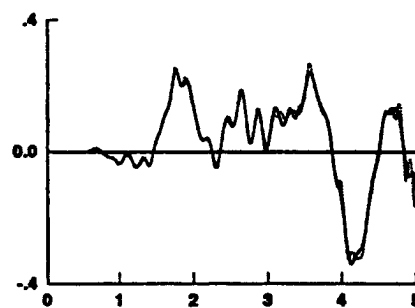
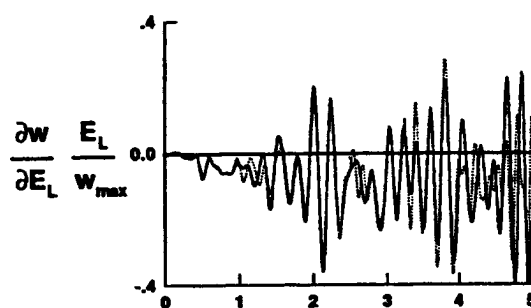
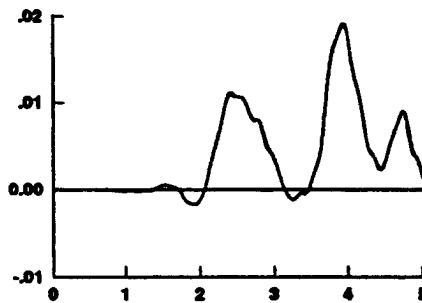
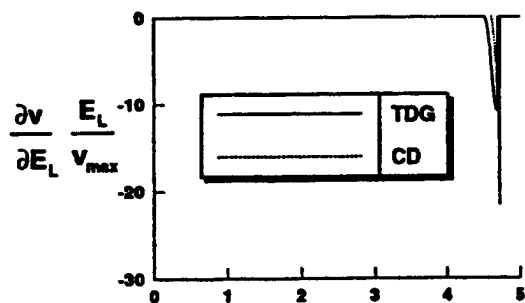
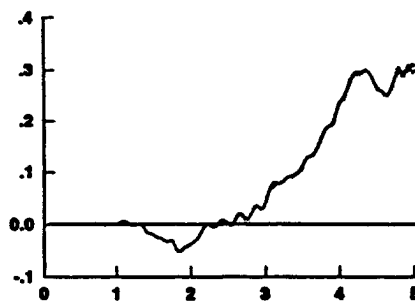
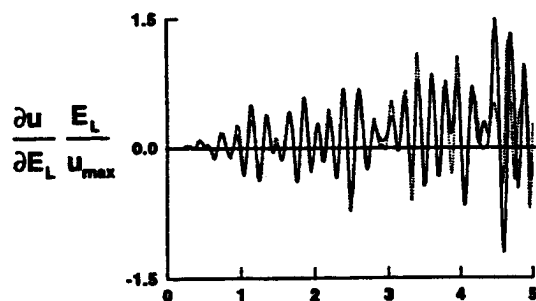
time, μs time, μs

Fig. 3. Time histories of the sensitivity coefficients of the displacement components for the time-discontinuous Galerkin (TDG) and central difference (CD) methods.

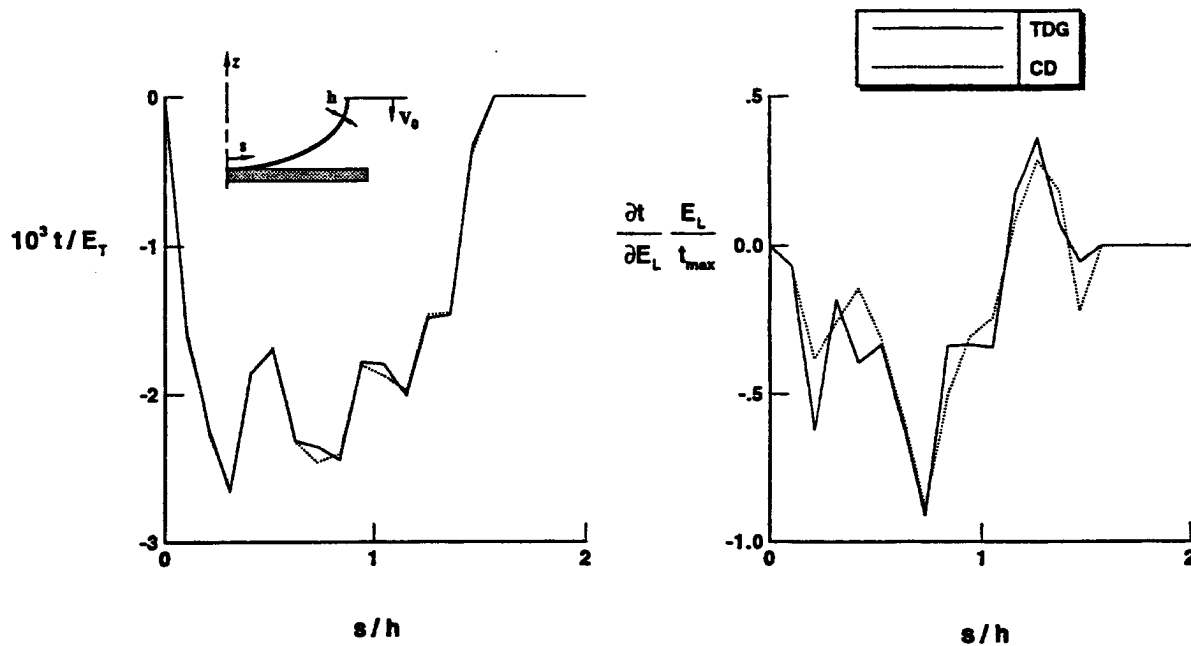


Fig. 4. Distribution of the normal contact pressure and its sensitivity coefficient at $t = 5 \mu\text{s}$ for the time-discontinuous Galerkin (TDG) and central difference (CD) methods.

To study the effect of the normalized intrinsic time-scale parameter $\bar{\tau} = \tau/\Delta t$ on the accuracy of the response and the sensitivity coefficients predicted by time-discontinuous Galerkin/least-squares method, solutions are obtained using different values of $\bar{\tau}$. The results are presented herein for two different time step increments, namely $\Delta t = 0.01$ and $0.025 \mu\text{s}$, and are discussed subsequently.

$\Delta t = 0.01 \mu\text{s}$

The time histories of the radial, circumferential and axial displacement components u, v, w and their normalized sensitivity coefficients are shown in Figs. 5 and 6, respectively, for four different values of $\bar{\tau}$, namely, $\bar{\tau} = 0, 0.4, 0.5$ and 1.5 . Examination of Figs. 5 and 6 reveals that for certain $\bar{\tau}$ values the least-squares method can annihilate the high frequency modes while minimizing the dissipation in the low frequency modes. While the accuracy of the displacement components and their sensitivity coefficients at point 1 show significant improvement, the corresponding quantities at point 2 are not affected much by choice of $\bar{\tau}$. The optimal choice of $\bar{\tau}$ appears to be between 0.4 and 0.5. Larger values of $\bar{\tau}$ result in degrading the accuracy.

The distributions of the normal contact pressure, t_N and its sensitivity coefficient are given in Fig. 7 at time $t = 5 \mu\text{s}$. The response, and especially sensitivity results, are smoothed out and exhibit much less oscillations for $\bar{\tau}$ values between 0.4 and 0.5.

$\Delta t = 0.025 \mu\text{s}$

The time histories of the radial, circumferential and axial displacement components u, v, w and their normalized sensitivity coefficients are shown in Figs. 8 and 9, respectively. The distributions of the normal contact pressure, t_N and its sensitivity coefficient are shown in Fig. 10 at time $t = 5 \mu\text{s}$. Figs. 8-10 show that the optimal value of $\bar{\tau}$ is between 0.1 and 0.15. For larger time step increments, the optimal value of the $\bar{\tau}$ parameter is expected to be smaller than 0.1.

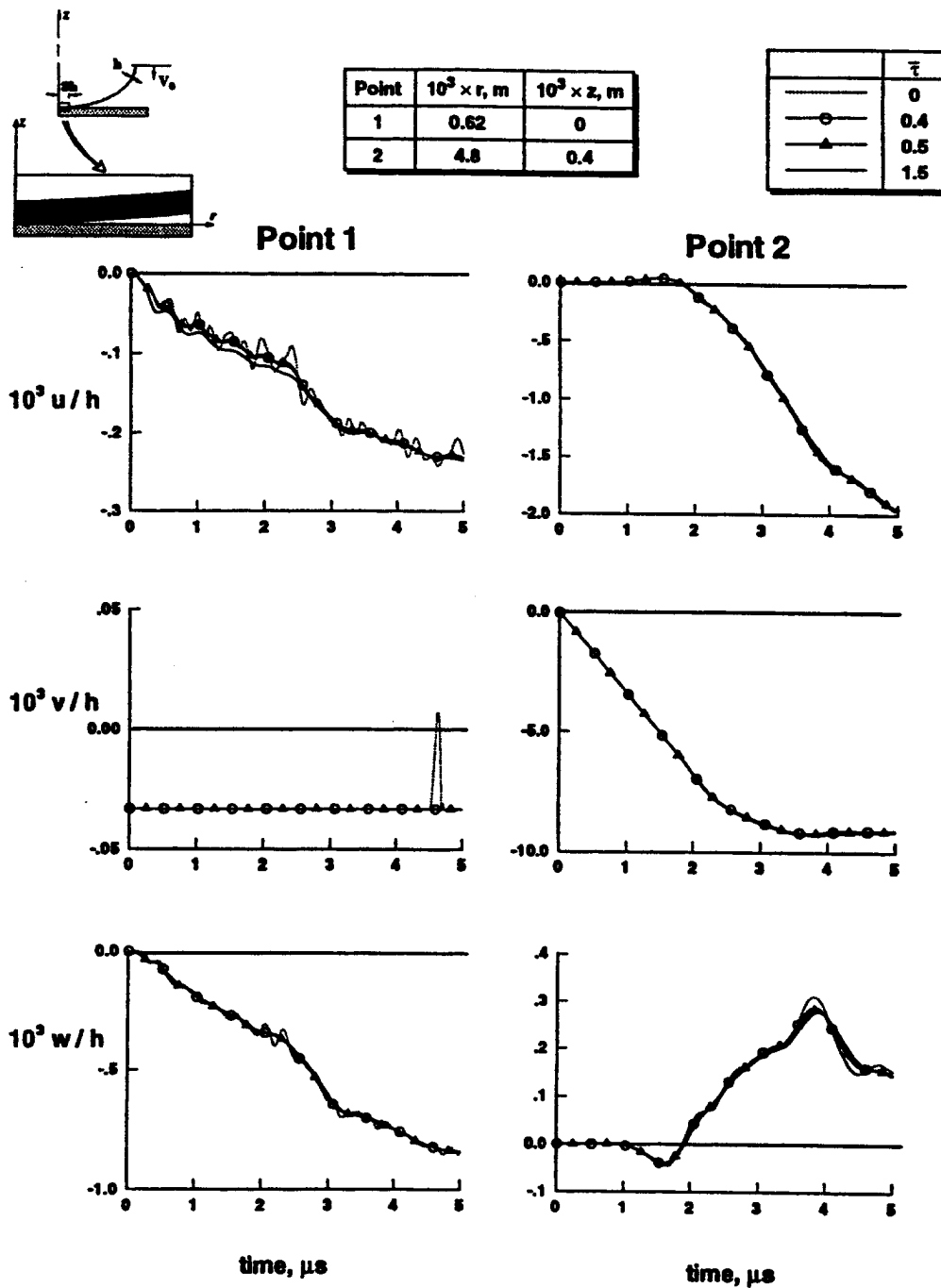


Fig. 5. Effect of the normalized intrinsic time-scale parameter values on the time histories of radial, circumferential and axial displacement components for $\Delta t = 0.01 \mu\text{s}$.

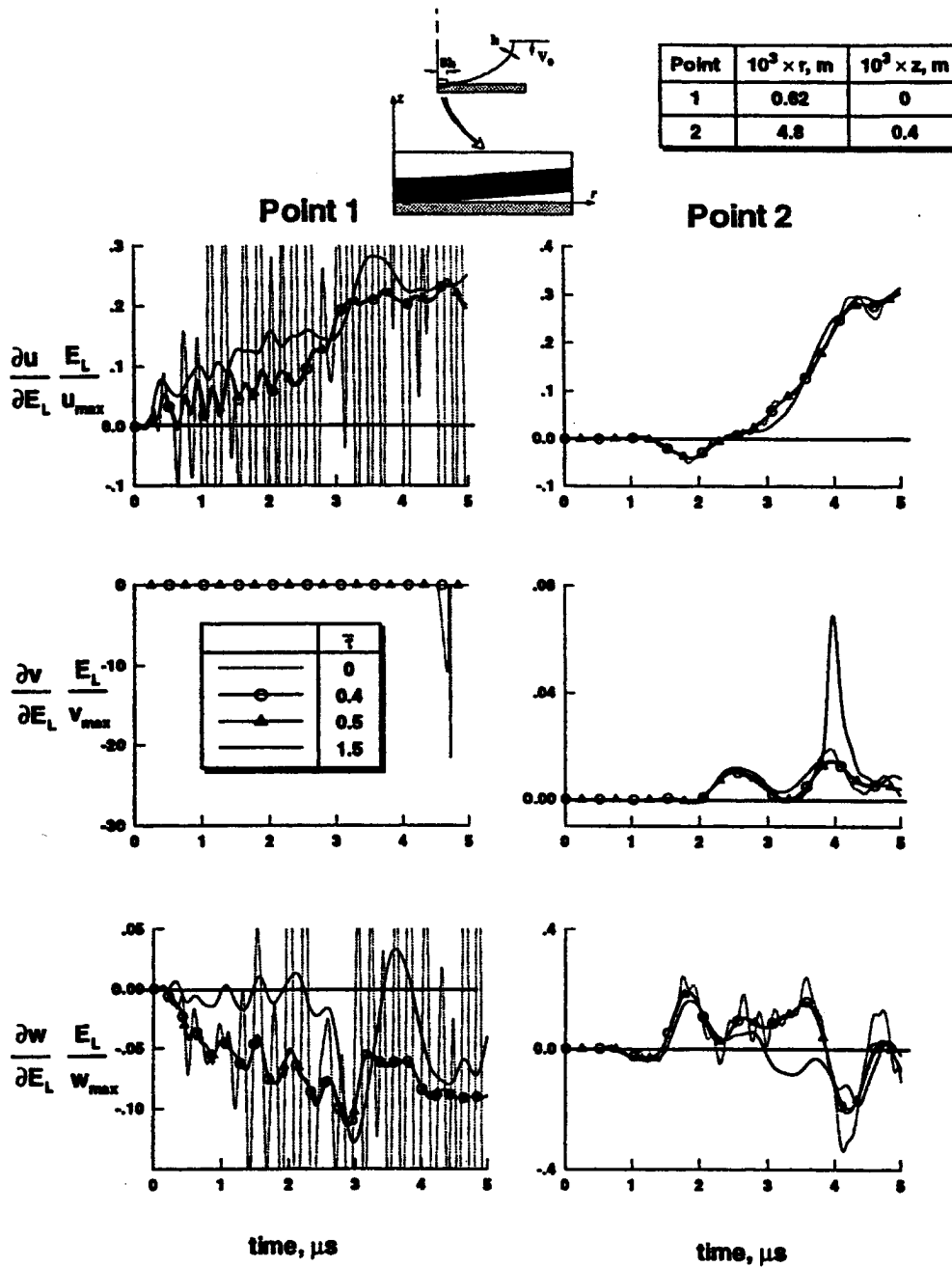


Fig. 6. Effect of the normalized intrinsic time-scale parameter values on the time histories of the sensitivity coefficients of radial, circumferential and axial displacement components for $\Delta t = 0.01 \mu\text{s}$.

To show the effect of τ on the global response quantities and their sensitivity coefficients, the following quantities are introduced:

$$p_1(\tau) = t_1(\tau)/\max(t_1(\tau)), \quad t_1(\tau) = \sum_{i=1}^{nnode} (u_i(\tau) - u_i(\tau + \Delta\tau))^2 \quad (20)$$

$$p_2(\tau) = t_2(\tau)/\max(t_2(\tau)), \quad t_2(\tau) = \sum_{i=1}^{nnode} \left(\frac{\partial u_i(\tau)}{\partial \lambda} - \frac{\partial u_i(\tau + \Delta\tau)}{\partial \lambda} \right)^2 \quad (21)$$

where p_1 and p_2 show the change in the overall response resulting from incrementing current τ for the displacements and their sensitivity coefficients, respectively. Fig. 11 gives the relation between τ and the p_1 , p_2 coefficients for time increments of 0.01 and 0.025 μs . The most accurate global response and sensitivity quantities are associated with τ in the range $0.4 \times 10^{-8} \leq \tau \leq 0.6 \times 10^{-8}$.

4.3. Comments on the numerical studies

In previous studies it was found that for the rigid surface contact/impact problems, the use of explicit temporal integration schemes, in conjunction with the Lagrange multiplier contact formulation, is more efficient than the use of implicit schemes (see [2]). For the problem considered herein the total analysis times (for generating the response and evaluating the sensitivity coefficients) for the time-discontinuous Galerkin and central difference methods are approximately the same. The response and sensitivity coefficients predicted by both methods are in close agreement.

Even though the time-discontinuous Galerkin method is not more efficient than the central difference method, addition of the least-squares terms to time-discontinuous Galerkin methods enhances the stability by smoothing out the high frequency modes while not degrading the accuracy. The time-discontinuous Galerkin/least-squares method better captures contact/impact discontinuities compared to the central difference technique.

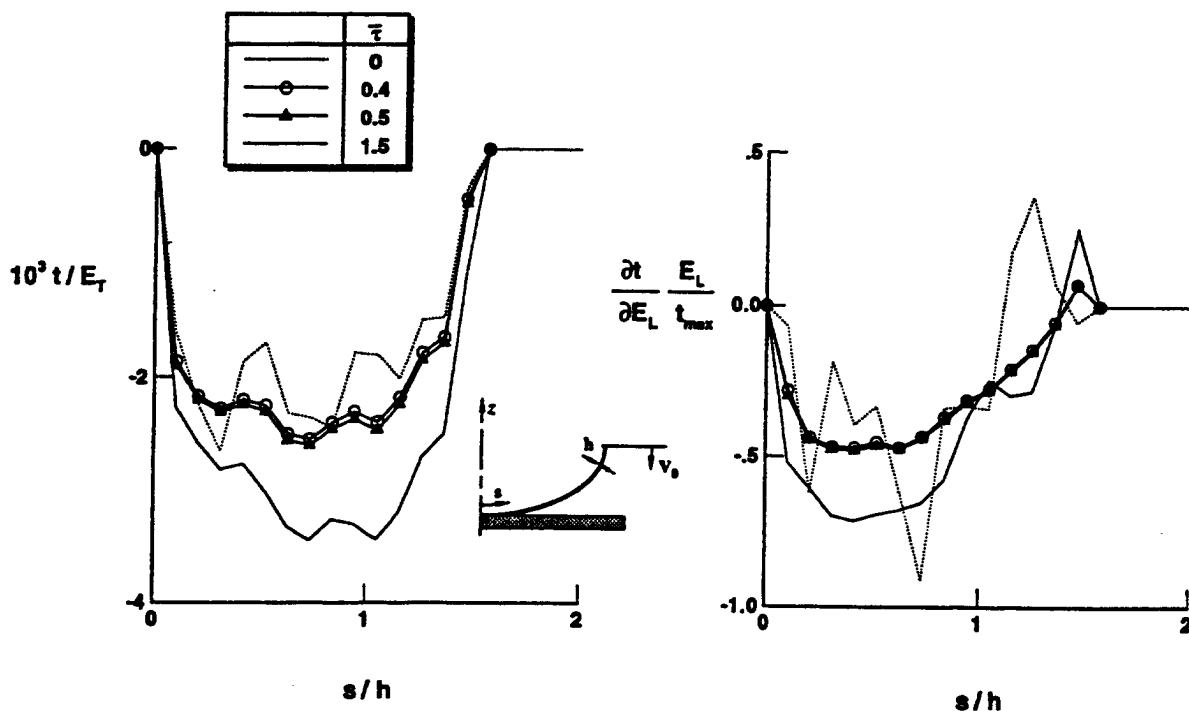


Fig. 7. Effect of the normalized intrinsic time-scale parameter values on the distribution of the normal contact pressure and its sensitivity coefficient at $t = 5 \mu\text{s}$ for $\Delta t = 0.01 \mu\text{s}$.

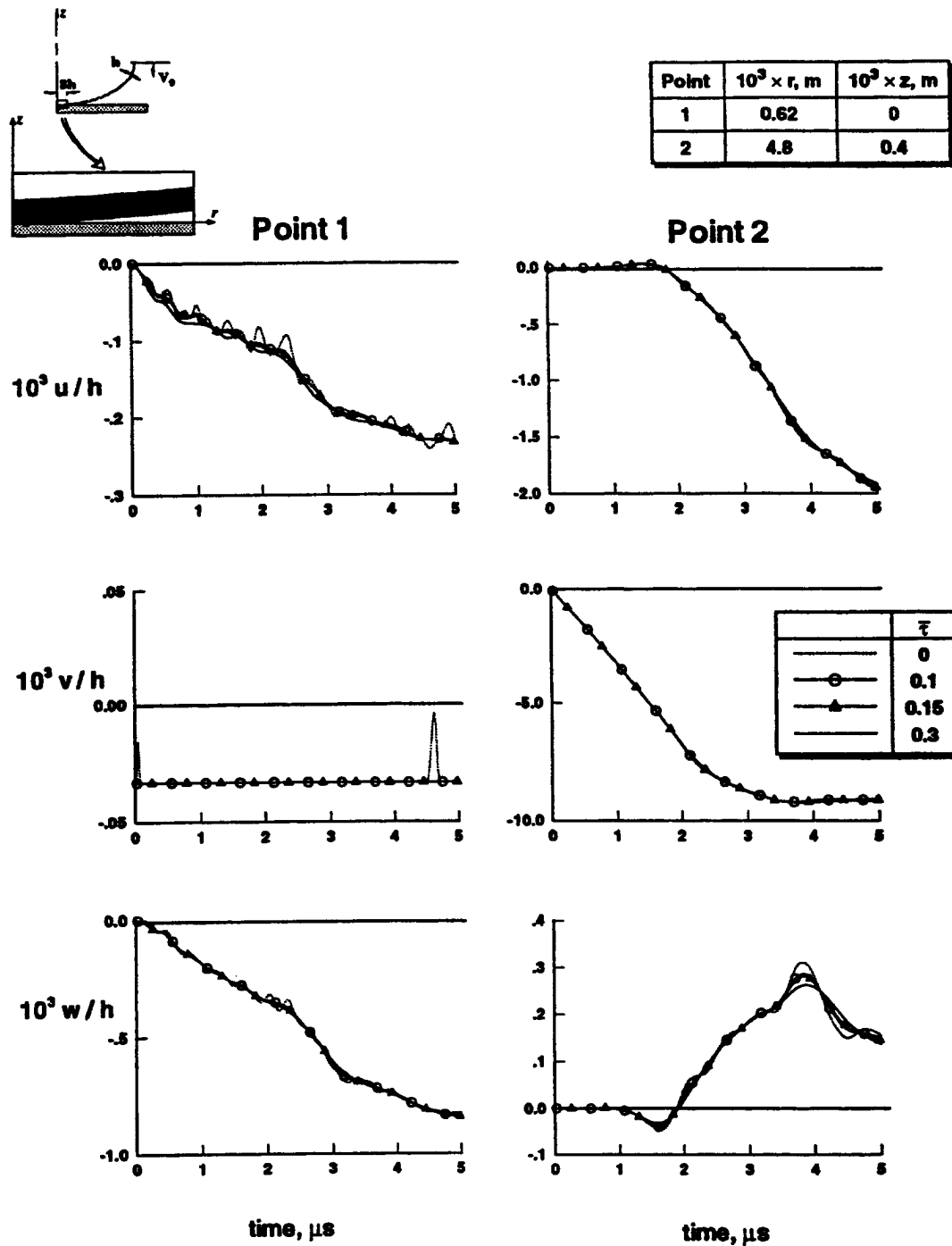


Fig. 8. Effect of the normalized intrinsic time-scale parameter values on the time histories of radial, circumferential and axial displacement components for $\Delta t = 0.025 \mu\text{s}$.

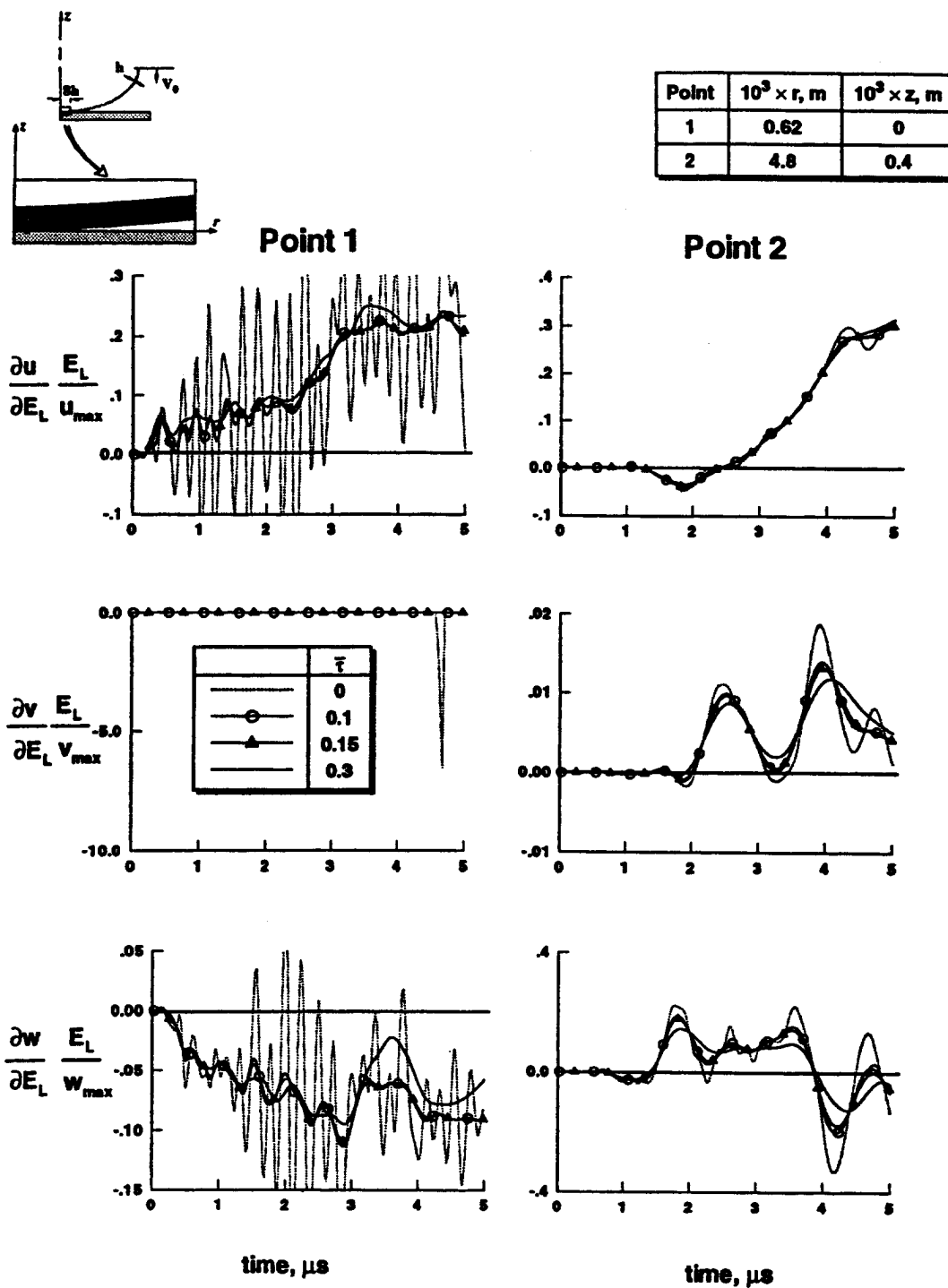


Fig. 9. Effect of the normalized intrinsic time-scale parameter values on the time histories of the sensitivity coefficients of radial, circumferential and axial displacement components for $\Delta t = 0.025 \mu s$.

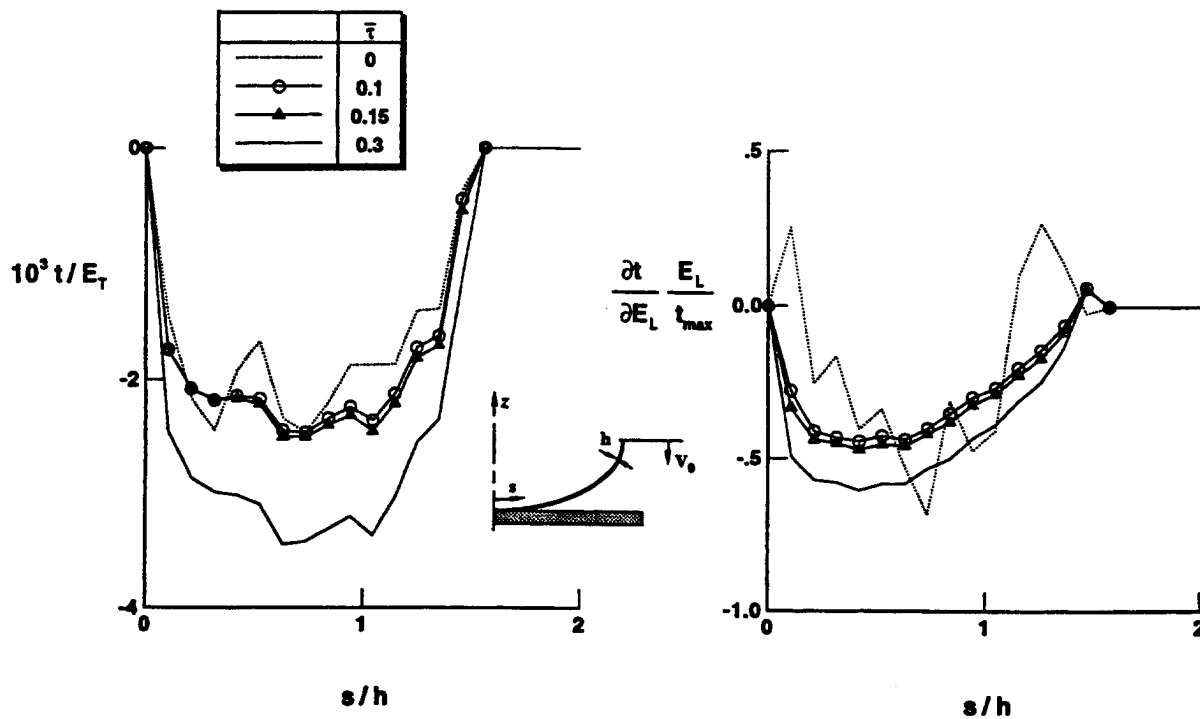


Fig. 10. Effect of the normalized intrinsic time-scale parameter values on the distribution of the normal contact pressure and its sensitivity coefficient at $t = 5 \mu s$ for $\Delta t = 0.025 \mu s$.

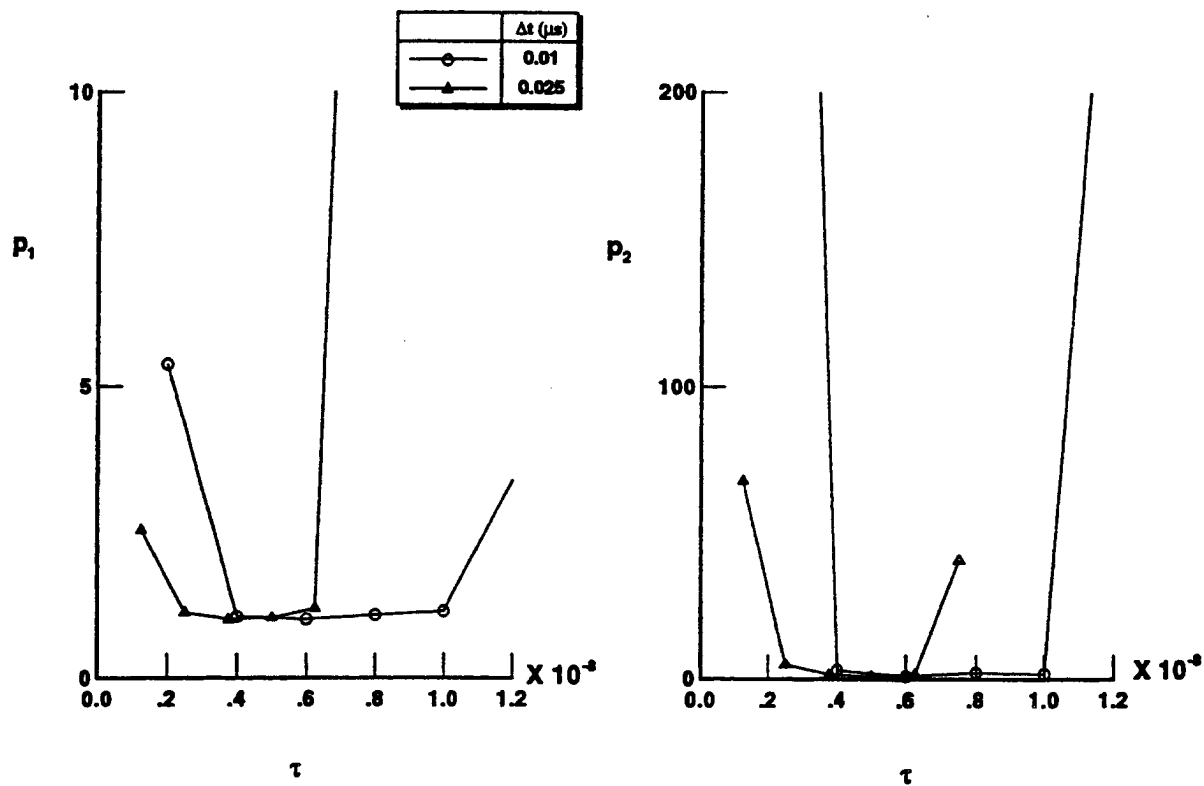


Fig. 11. Effect of the normalized intrinsic time-scale parameter values on the global response and sensitivity quantities at $t = 5 \mu s$ for $\Delta t = 0.01$ and $0.025 \mu s$.

5. Concluding remarks

Space-time finite element methods are applied to the sensitivity analysis of frictional contact/impact response of axisymmetric composite structures. The structures are assumed to consist of an arbitrary number of perfectly bonded homogeneous anisotropic layers. Only small displacements are considered and the material of each layer is assumed to be hyperelastic. The sensitivity coefficients measure the sensitivity of the response to variations in material parameters of the structure.

A displacement finite element model is used for the spatial discretization. The temporal integration is performed by using time-discontinuous Galerkin method. Least-squares stabilizing operators are added to enhance the stability by smoothing out the high frequency modes, without degrading the accuracy. A quasi-explicit iterative technique is used for generating the response and evaluating the sensitivity coefficients. The normal contact conditions are incorporated within the iterative process.

Numerical results are presented for the sensitivity analysis of contact/impact response of a composite spherical cap impacting a rigid plate. On the basis of the numerical results, it is concluded that the time-discontinuous Galerkin/least-squares method is more suitable than the central difference technique for contact/impact problems. While total analysis times for both methods are comparable, the Galerkin/least-squares method improves the results in the contact region.

Acknowledgment

The present research is partially supported by NASA Cooperative Agreement NCCW-0011 and Air Force Office of Scientific Research Grant No. 49620-96-1-0462.

Appendix A. Formulas for the time-discontinuous Galerkin/least-squares method

If the quadratic-in-time interpolation functions are employed for the unknowns at t_n^- , $t_{n-1/2}$ and t_{n-1}^+ , the displacements can be written as

$$u = \frac{1}{2} \zeta (\zeta + 1) u_n^- + (1 - \zeta^2) u_{n-1/2} + \frac{1}{2} \zeta (\zeta - 1) u_{n-1}^+ \quad (\text{A.1})$$

where

$$\zeta = t - t_{n-1/2} / (\Delta t / 2) \quad (\text{A.2})$$

The velocities and accelerations are

$$\dot{u} = \frac{2}{\Delta t} \left[\left(\zeta + \frac{1}{2} \right) u_n^- + (-2\zeta) u_{n-1/2} + \left(\zeta - \frac{1}{2} \right) u_{n-1}^+ \right] \quad (\text{A.3})$$

$$\ddot{u} = \frac{4}{\Delta t^2} [u_n^- - 2u_{n-1/2} + u_{n-1}^+] \quad (\text{A.4})$$

The displacement vector at t_n^- , $t_{n-1/2}$ and t_{n-1}^+ are

$$q = [u_n^- \quad u_{n-1/2} \quad u_{n-1}^+]^T \quad (\text{A.5})$$

The expressions for the terms in Eqs. (7) and (8) are given by

$$\int_{t_n} \dot{w} \cdot (M \ddot{u} + K u) dt = q^T \begin{bmatrix} 4/\Delta t^2 M + 1/2K & -8/\Delta t^2 M + 2/3K & 4/\Delta t^2 M - 1/6K \\ -2/3K & 0 & 2/3K \\ -4/\Delta t^2 M + 1/6K & 8/\Delta t^2 M - 2/3K & -4/\Delta t^2 M - 1/2K \end{bmatrix} q \quad (\text{A.6})$$

$$\dot{w}_{n-1}^+ \cdot M \dot{u}_{n-1}^+ = q^T \begin{bmatrix} 1/\Delta t^2 M & -4/\Delta t^2 M & 3/\Delta t^2 M \\ -4/\Delta t^2 M & 16/\Delta t^2 M & -12/\Delta t^2 M \\ 3/\Delta t^2 M & -12/\Delta t^2 M & 9/\Delta t^2 M \end{bmatrix} q \quad (\text{A.7})$$

$$w_{n-1}^+ \cdot Ku_{n-1}^+ = q^T \begin{bmatrix} 0 & 0 & 0 \\ 0 & 0 & 0 \\ 0 & 0 & K \end{bmatrix} q \quad (\text{A.8})$$

$$\dot{w}_{n-1}^+ \cdot M \dot{u}_{n-1}^- = q^T \begin{bmatrix} -1/\Delta t M \dot{u}_{n-1} \\ 4/\Delta t M \dot{u}_{n-1} \\ -3/\Delta t M \dot{u}_{n-1} \end{bmatrix} \quad (\text{A.9})$$

$$w_{n-1}^+ \cdot Ku_{n-1}^- = q^T \begin{bmatrix} 0 \\ 0 \\ Ku_{n-1}^- \end{bmatrix} \quad (\text{A.10})$$

The expressions of K_G and f_G are obtained by combining and rearranging constituent terms. The resulting expressions can be written in the following form:

$$K_G = \begin{bmatrix} 5/\Delta t^2 M + 1/2K & -12/\Delta t^2 M + 2/3K & 7/\Delta t^2 M - 1/6K \\ -4/\Delta t^2 M - 2/3K & 16/\Delta t^2 M & -12/\Delta t^2 M + 2/3K \\ 0 & 0 & K \end{bmatrix} \quad (\text{A.11})$$

$$f_G = \begin{bmatrix} f_n^- \\ f_{n-1/2} \\ f_{n-1}^+ \end{bmatrix} = \begin{bmatrix} -1/\Delta t M \dot{u}_{n-1} + F \\ 4/\Delta t M \dot{u}_{n-1} \\ Ku_{n-1}^- \end{bmatrix} \quad (\text{A.12})$$

For the Galerkin/least-squares method the expressions for K_{GL} and f_{GL} are given by

$$K_{GL} = K_G + K_{GLA} \quad (\text{A.13})$$

$$f_{GL} = f_G + f_{GLA} \quad (\text{A.14})$$

where

$$K_{GLA} = \tau \begin{bmatrix} \frac{16M}{\Delta t^3} + \frac{4K}{3\Delta t} + \frac{2KM^{-1}K\Delta t}{15} & -\frac{32M}{\Delta t^3} + \frac{4K}{3\Delta t} + \frac{KM^{-1}K\Delta t}{15} & \frac{16M}{\Delta t^3} + \frac{4K}{3\Delta t} - \frac{KM^{-1}K\Delta t}{30} \\ -\frac{32M}{\Delta t^3} + \frac{4K}{3\Delta t} + \frac{KM^{-1}K\Delta t}{15} & \frac{64M}{\Delta t^3} - \frac{32K}{3\Delta t} + \frac{8KM^{-1}K\Delta t}{15} & -\frac{32M}{\Delta t^3} + \frac{4K}{3\Delta t} + \frac{KM^{-1}K\Delta t}{15} \\ \frac{4K}{\Delta t} + \frac{KM^{-1}K\Delta t}{6} & -\frac{8K}{\Delta t} + \frac{2KM^{-1}K\Delta t}{3} & \frac{4K}{\Delta t} + \frac{KM^{-1}K\Delta t}{6} \end{bmatrix} \quad (\text{A.15})$$

and

$$f_{GLA} = \tau \begin{bmatrix} \frac{8F}{\Delta t^2} + \frac{KM^{-1}F\Delta t}{6} \\ -\frac{16F}{\Delta t^2} + \frac{2KM^{-1}F\Delta t}{3} \\ KM^{-1}F\Delta t \end{bmatrix} \quad (\text{A.16})$$

The \tilde{M} and \tilde{K} matrices in Eq. (15) are given by

$$\tilde{M}_{GL} = \begin{bmatrix} \left(5 + \frac{16\tau}{\Delta t}\right)M & \left(-12 - \frac{32\tau}{\Delta t}\right)M & \left(7 + \frac{16\tau}{\Delta t}\right)M \\ \left(-4 - \frac{32\tau}{\Delta t}\right)M & \left(16 + \frac{64\tau}{\Delta t}\right)M & \left(-12 - \frac{32\tau}{\Delta t}\right)M \\ 0 & 0 & 0 \end{bmatrix} \frac{1}{\Delta t^2} \quad (A.17)$$

$$\tilde{K}_{GL} = \begin{bmatrix} 1/2K & 2/3K & -1/6K \\ -2/3K & 0 & 2/3K \\ 0 & 0 & K \end{bmatrix} + \tau \begin{bmatrix} \frac{4K}{3\Delta t} + \frac{2KM^{-1}K\Delta t}{15} & \frac{4K}{3\Delta t} + \frac{KM^{-1}K\Delta t}{15} & \frac{4K}{3\Delta t} - \frac{KM^{-1}K\Delta t}{30} \\ \frac{4K}{3\Delta t} + \frac{KM^{-1}K\Delta t}{15} & -\frac{32K}{3\Delta t} + \frac{8KM^{-1}K\Delta t}{15} & \frac{4K}{3\Delta t} + \frac{KM^{-1}K\Delta t}{15} \\ \frac{4K}{\Delta t} + \frac{KM^{-1}K\Delta t}{6} & -\frac{8K}{\Delta t} + \frac{2KM^{-1}K\Delta t}{3} & \frac{4K}{\Delta t} + \frac{KM^{-1}K\Delta t}{6} \end{bmatrix} \quad (A.18)$$

Note that because of the structure of the matrix \tilde{M} , its inverse involves the inversion of the diagonal matrix M and adjustment of the coefficients of \tilde{M} in Eqs. (A.17).

Appendix B. Computational procedure for the time-discontinuous Galerkin/least-squares method

$$u_0^- = u_0$$

Do $n = 1, \dots, N$

$$u_{n-1(0)}^+ = u_{n-1}^-$$

$$u_{n(0)}^- = u_{n-1}^-$$

$$u_{n-1/2(0)} = u_{n-3/2}$$

While $\text{Res}_{(k)} \leq \text{tol}$

$$u_{n-1(k)}^+ = \frac{1}{4 + \bar{\tau}} \left[u_{n-1} - \bar{\tau} \left(4 + \frac{\bar{K}}{6} \right) u_{n(k-1)} - \bar{\tau} \left(-8 + 2\frac{\bar{K}}{3} \right) u_{n-1/2(k-1)} - \bar{\tau} \frac{\bar{K}}{6} u_{n-1(k-1)}^+ \right]$$

While $\text{Res}^{(i)} \leq \text{tol}$

$$u_n^{-(i)} = u_{n-1(k)}^+ + M^{-1} (l_{11}f_n^- + l_{12}f_{n-1/2}) - \bar{K} (l_{11}t_1^{(i-1)} + l_{12}t_2^{(i-1)}) - \bar{K}\bar{K} (l_{11}t_3^{(i-1)} + l_{12}t_4^{(i-1)})$$

$$u_{n-1/2}^{(i)} = u_{n-1(k)}^+ + M^{-1} (l_{21}f_n^- + l_{22}f_{n-1/2}) - \bar{K} (l_{21}t_1^{(i-1)} + l_{22}t_2^{(i-1)}) - \bar{K}\bar{K} (l_{21}t_3^{(i-1)} + l_{22}t_4^{(i-1)})$$

Continue i

$$u_{n(k)}^- = u_n^{-(i)}$$

$$u_{n-1/2(k)} = u_{n-1/2}^{(i)}$$

Continue k

Continue n

where

$$\tau = \bar{\tau} \Delta t$$

$$\bar{K} = M^{-1} K \Delta t^2$$

$$t_1 = (1/2 + 4\bar{\tau}/3)u_n^- + (2/3 + 4\bar{\tau}/3)u_{n-1/2} + (-1/6 + 4\bar{\tau}/3)u_{n-1}^+$$

$$t_2 = (-2/3 + 4\bar{\tau}/3)u_n^- - 32/3\bar{\tau}/3u_{n-1/2} + (2/3 + 4\bar{\tau}/3)u_{n-1}^+$$

$$t_3 = (2/15u_n^- + 1/15\bar{\tau}/3u_{n-1/2} - 1/30\bar{\tau}u_{n-1}^+)\bar{\tau}$$

$$t_4 = (1/15u_n^- + 8/15\bar{\tau}/3u_{n-1/2} + 1/15\bar{\tau}u_{n-1}^+)\bar{\tau}$$

$$l_{11} = (1 + 4\bar{\tau})/(2 + 4\bar{\tau})$$

$$l_{12} = (3/4 + 2\bar{\tau})/(2 + 4\bar{\tau})$$

$$l_{21} = (1/4 + 2\bar{\tau})/(2 + 4\bar{\tau})$$

$$l_{22} = (5/16 + \bar{\tau})/(2 + 4\bar{\tau})$$

References

- [1] Z.-H. Zhong and J. Mackerie, Contact-impact problems: A review with bibliography, *Appl. Mech. Rev.* 47(2) (1994) 55–76.
- [2] L. Karaoglan and A.K. Noor, Assessment of temporal integration schemes for the sensitivity analysis of frictional contact/impact response of axisymmetric composite structures. *Comput. Methods Appl. Mech. Engrg.* 130 (1996) 369–393.
- [3] T.J.R. Hughes, R.L. Taylor, J.L. Sackman, A. Curnier and W. Kanoknukulchai, A finite element method for a class of contact-impact problems, *Comput. Methods Appl. Mech. Engrg.* 8 (1976) 249–276.
- [4] R.L. Taylor and P. Papadopoulos, On a finite element method for dynamic contact/impact problems, *Int. J. Numer. Methods Engrg.* 26 (1993) 2123–2140.
- [5] L. Karaoglan and A.K. Noor, Dynamic sensitivity analysis of frictional contact/impact response of axisymmetric composite structures, *Comput. Methods Appl. Mech. Engrg.* 128 (1995) 169–190.
- [6] J.H. Argyris and D.W. Scharpf, Finite elements in time and space, *Nuclear Engrg. Des.* 10 (1969) 456–464.
- [7] G.M. Hulbert and T.J.R. Hughes, Space-time finite element methods for second-order hyperbolic equations, *Comput. Methods Appl. Mech. Engrg.* 84 (1990) 327–348.
- [8] O. Pironneau, J. Liou, and T. Tezduyar, Characteristic-Galerkin and Galerkin/least-squares space-time formulations for the advection diffusion equation with time-dependent domains. *Comput. Methods Appl. Mech. Engrg.* 100 (1992) 117–141.
- [9] F. Shakib and T.J.R. Hughes, A new finite element method for computational fluid dynamics: Ix. Fourier analysis of space-time Galerkin/least-squares algorithms, *Comput. Methods Appl. Mech. Engrg.* 87 (1991) 35–58.
- [10] G.M. Hulbert, Time finite element methods for structural dynamics, *Int. J. Numer. Methods Engrg.* 33 (1992) 307–331.
- [11] G.M. Hulbert, P.F. Leopoldo, and T.J.R. Hughes, A new finite element formulation for computational fluid dynamics: Viii. The Galerkin/least-squares method for advective-diffusive equations. *Comput. Methods Appl. Mech. Engrg.* 73 (1989) 173–189.
- [12] R.T. Haftka and H.M. Adelman, Recent developments in structural sensitivity analysis, *Struct. Optimiz.* 1(3) (1989) 137–151.
- [13] T.J.R. Hughes, *The Finite Element Method* (Prentice-Hall, Englewood Cliffs, NJ 1987).
- [14] E. Hinton, T. Rock and O.C. Zienkiewicz, A note on mass lumping and related process in the finite element method, *Earthquake Engrg. Struct. Dyna.* 4 (1976) 245–249.

INFORMATION FOR CONTRIBUTORS

Manuscripts should be sent in triplicate to one of the Editors. All manuscripts will be refereed. Manuscripts should preferably be in English. They should be typewritten, double-spaced, first copies (or clear Xerox copies thereof) with a wide margin. Abstracts, footnotes and lists of references should also be double-spaced. All pages should be numbered (also those containing references, tables and figure captions). Upon acceptance of an article, author(s) will be asked to transfer copyright of the article to the publisher. This transfer will ensure the widest possible dissemination of information.

Abstracts

The text of a paper should be preceded by a summary in English. This should be short, but should mention all essential points of the paper.

Figures and tables

The drawings for the figures must be originals, drawn in black India ink in large size and carefully lettered, or printed on a high-quality laser printer. The lettering as well as the details should have proportionate dimensions, so as not to become illegible or unclear after the usual reduction by the printers; in general, the figures should be designed for a reduction factor of two or three. Mathematical symbols should be entered in italics, where appropriate. Each figure should have a number and a caption; the captions should be collected on a separate sheet. The appropriate place of a figure should be indicated in the margin. Tables should be typed on separate sheets. Each table should have a number and a title. The appropriate places for the insertion of tables should be indicated in the margin. Colour illustrations can be included and will be printed in colour at no charge if, in the opinion of the Editors, the colour is essential. If this is not the case, the figures will be printed in black and white unless the author is prepared to pay the extra costs arising from colour reproduction.

Formulae

Displayed formulae should be numbered and typed or clearly written by hand. Symbols should be identified in the margin, where they occur for the first time.

References

In the text, reference to other parts of the paper should be made by section (or equation) number, but not by page number. References should be listed on a separate sheet in the order in which they appear in the text.

COMPLETE INSTRUCTIONS TO AUTHORS are published in every last issue of a volume, and copies can also be obtained from the Editors and the Publisher, Elsevier Science B.V., P.O. Box 1991, 1000 BZ Amsterdam, The Netherlands.

Instructions for LaTeX manuscripts

The LaTeX files of papers that have been accepted for publication may be sent to the Publisher by e-mail or on a diskette (3.5" or 5.25" MS-DOS). If the file is suitable, proofs will be produced without rekeying the text. The article should be encoded in Elsevier-LaTeX, standard LaTeX, or AMS-LaTeX (in document style "article"). The Elsevier-LaTeX package, together with instructions on how to prepare a file, is available from the Publisher. This package can also be obtained through the Elsevier WWW home page (<http://www.elsevier.nl/>), or using anonymous FTP from the Comprehensive TeX Archive Network (CTAN). The host-names are: <ftp.dante.de>, <ftp.tex.ac.uk>, <ftp.shsu.edu>; the CTAN directories are: [/pub/tex/macros/latex209/contrib/elsevier](#), [/pub/archive/macros/latex209/contrib/elsevier](#), [/tex-archive/macros/latex209/contrib/elsevier](#), respectively. No changes from the accepted version are permissible, without the explicit approval of the Editor. The Publisher reserves the right to decide whether to use the author's file or not. If the file is sent by e-mail, the name of the journal should be mentioned in the "subject field" of the message to identify the paper. Authors should include an ASCII table (available from the Publisher) in their files to enable the detection of transmission errors.

The files should be mailed to: Elsevier Editorial Services, Mayfield House, 256 Banbury Road, Oxford OX2 7DH, UK. Fax: +44-1865-314990. E-mail: ees@elsevier.co.uk.

Publication information:

Computer Methods in Applied Mechanics and Engineering (ISSN 0045-7825). For 1997 volumes 140-150 are scheduled for publication. Subscription prices are available upon request from the Publisher. Subscriptions are accepted on a prepaid basis only and are entered on a calendar year basis. Issues are sent by surface mail except to the following countries where Air delivery via SAL mail is ensured: Argentina, Australia, Brazil, Canada, Hong Kong, India, Israel, Japan, Malaysia, Mexico, New Zealand, Pakistan, PR China, Singapore, South Africa, South Korea, Taiwan, Thailand, USA. For all other countries airmail rates are available upon request. Claims for missing issues should be made within six months of our publication (mailing) date.

Orders, claims, and product enquiries

Please contact the Customer Support Department at the Regional Sales Office nearest you:

New York
Elsevier Science
P.O. Box 945
New York, NY 10159-0945
USA
Tel. (+1)212-633-3730
[Toll free number for North
American customers:
1-888-4ES-INFO (437-4636)]
Fax (+1)212-633-3680
e-mail usinfo-f@elsevier.com

Amsterdam
Elsevier Science
P.O. Box 211
1000 AE Amsterdam
The Netherlands
Tel. (+31)20-4853757
Fax (+31)20-4853432
e-mail nlinfo-f@elsevier.nl

Tokyo
Elsevier Science
9-15 Higashi-Azabu 1-chome
Minato-ku, Tokyo 106
Japan
Tel. (+81)3-5561-5033
Fax (+81)3-5561-5047
e-mail kyf04035@niftyserve.or.jp

Singapore
Elsevier Science
No. 1 Temasek Avenue
#17-01 Millenia Tower
Singapore 039192
Tel. (+65)434-3727
Fax (+65)337-2230
e-mail asiainfo@elsevier.com.sg

Advertising information

Advertising orders and enquiries may be sent to: **International:** Elsevier Science, Advertising Department, The Boulevard, Langford Lane, Kidlington, Oxford OX5 1GB, UK. Tel. (+44)(0)1865 843565, Fax (+44)(0)1865 843976. **USA and Canada:** Weston Media Associates, Daniel Lipner, P.O. Box 1110, Greens Farms, CT 06436-1110, USA. Tel. (+1)(203)261-2500, Fax (+1)(203)261-0101. **Japan:** Elsevier Science Japan, Marketing Services, 1-9-15 Higashi-Azabu, Minato-ku, Tokyo 106, Japan. Tel. (+81)3-5561-5033; Fax (+81)3-5561-5047.

CURVED SANDWICH PANELS SUBJECTED TO TEMPERATURE GRADIENT AND MECHANICAL LOADS

By Ahmed K. Noor,¹ Fellow, ASCE, James H. Starnes Jr.,² Member, ASCE, and Jeanne M. Peters³

ABSTRACT: The results of a detailed study of the nonlinear response of curved sandwich panels with composite face sheets, subjected to a temperature gradient through the thickness combined with mechanical loadings, are presented. The analysis is based on a first-order shear-deformation Sanders-Budiansky-type theory, including the effects of large displacements, moderate rotations, transverse shear deformation, and laminated anisotropic material behavior. A mixed formulation is used with the fundamental unknowns consisting of the generalized displacements and the stress resultants of the panel. The nonlinear displacements, strain energy, principal strains, transverse shear stresses, transverse shear strain energy density, and their hierarchical sensitivity coefficients are evaluated. The hierarchical sensitivity coefficients measure the sensitivity of the nonlinear response to variations in the panel parameters, the effective properties of the face sheet layers and the core, and the micromechanical parameters. Numerical results are presented for cylindrical panels subjected to combined pressure loading, edge shortening or extension, edge shear, and a temperature gradient through the thickness. The results show the effects of variations in the loading and the panel aspect ratio, on the nonlinear response, and its sensitivity to changes in the various panel, effective layer, and micromechanical parameters.

INTRODUCTION

In recent years, considerable work has been devoted to the study of thermomechanical nonlinear and postbuckling responses of composite and sandwich plates and shells. Attempts have been made to identify the differences between the isothermal and thermal responses. Reviews of recent contributions are contained in four survey papers (Noor and Burton 1992; Noor and Peters 1994; Bert 1995; Noor et al. 1996), and four monographs (Hoff 1986; Noor 1994; Zenkert 1995; Turvey and Marshall 1995). Only a few of the reported studies considered the nonlinear response of curved panels subjected to temperature gradient through-the-thickness (see, for example, Librescu and Souza 1993; Librescu et al. 1995), and to the authors' knowledge, none considered sandwich panels with composite face sheets, or boundary conditions other than simple supports. Because curved sandwich panels have many applications in aircraft structures, including fuselage, wing, and empennage components of high-speed aircraft, an understanding of their nonlinear response when subjected to a temperature gradient through-the-thickness combined with a mechanical loading is desirable. Moreover, a study of the sensitivity of the nonlinear response to variations in the material, lamination, and geometric parameters of these panels is needed to provide an indication of the effects of changes in these parameters on the structural response.

The present study focuses on understanding the detailed nonlinear response characteristics of cylindrical sandwich panels with composite face sheets subjected to a temperature gradient through-the-thickness combined with mechanical loadings. Sensitivity coefficients are evaluated that measure the sensitivity of the various response quantities to variations in the panel stiffnesses, the effective material properties of the

individual face sheet layers and core, and the micromechanical parameters.

The sandwich panels considered in the study consist of a number of perfectly bonded composite face sheet layers and a honeycomb core. The layers of the top and bottom face sheets are symmetrically distributed with respect to the middle surface. The individual layers of the face sheets and the core are assumed to be homogeneous and anisotropic. A plane of thermoelastic symmetry exists at each point of the panel, parallel to the middle surface. The loading is selected to simulate that of a typical fuselage panel of a high-speed aircraft.

MATHEMATICAL FORMULATION

Finite Element Equations Governing Panel Response

The analytical formulation is based on a first-order shear-deformation Sanders-Budiansky-type shell theory with the effects of large displacements, moderate rotations, average transverse shear deformation through-the-thickness, and laminated anisotropic material behavior. For simplicity, a linear Duhamel-Neumann-type constitutive model is used and the material properties are assumed to be independent of temperature. The constitutive relations for the panel are given in Appendix I. A total Lagrangian formulation is used, and the panel deformations, at different values of the applied loading, are referred to the original undeformed configuration. The panel is discretized by using two-field mixed finite-element models. The fundamental unknowns consist of the nodal displacements and the stress resultant parameters. The stress resultants are allowed to be discontinuous at interelement boundaries in the model. The sign convention for the generalized displacements and the stress resultants for the model are shown in Fig. 1. The external loading consists of a uniform pressure loading p ; monotonically increasing edge displacement q , (either normal or tangential to the edge); and a temperature gradient through-the-thickness q_T [linear through-the-thickness temperature variation, $q_T = (T_1 - T_2)/h$, where T_1 and T_2 are the changes in the top and bottom surface temperatures, see Fig. 2].

The governing finite-element equations describing the nonlinear and postbuckling responses of the sandwich panel can be written in the following compact form:

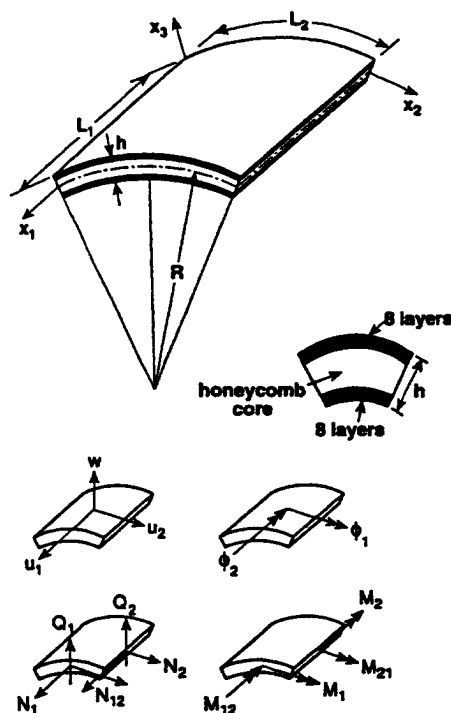
$$\{f(Z)\} = [K]\{Z\} + \{G(Z)\} - p\{Q^{(1)}\} - q\{Q^{(2)}\} - q_T\{Q^{(3)}\} = 0 \quad (1)$$

¹Ferman W. Perry Prof. of Aerospace Structures and Applied Mechanics; and Dir., Ctr. for Advanced Computational Technol., Univ. of Virginia, NASA Langley Res. Ctr., Hampton, VA 23681.

²NASA Langley Res. Ctr., Hampton, VA.

³Ctr. for Advanced Computational Technol., Univ. of Virginia, NASA Langley Res. Ctr., Hampton, VA.

Note. Discussion open until March 1, 1998. To extend the closing date one month, a written request must be filed with the ASCE Manager of Journals. The manuscript for this paper was submitted for review and possible publication on June 2, 1997. This paper is part of the *Journal of Aerospace Engineering*, Vol. 10, No. 4, October, 1997. ©ASCE, ISSN 0893-1321/97/0004-0143-0161/\$4.00 + \$.50 per page. Paper No. 15920.



Micromechanical Properties

Fiber
 $E_{11} = 226.5 \text{ GPa}$
 $E_{21} = 21.35 \text{ GPa}$
 $G_{12} = 20.37 \text{ GPa}$
 $\nu_{12} = .303$
 $\nu_{23} = .523$
 $\alpha_{11} = -6.94 \times 10^{-7}/^\circ\text{C}$
 $\alpha_{21} = 17.2 \times 10^{-6}/^\circ\text{C}$
 $\nu_1 = .6$

Matrix
 $E_m = 3.3 \text{ GPa}$
 $\nu_m = .35$
 $\alpha_m = 3.5 \times 10^{-5}/^\circ\text{C}$

Core
 $t_c = 5.08 \times 10^{-5} \text{ m}$
 $l_{1c} = 4.31 \times 10^{-3} \text{ m}$
 $l_{2c} = 6.99 \times 10^{-4} \text{ m}$
 $\theta_c = 45^\circ$
 $E_c = 107.6 \text{ GPa}$
 $G_c = 41.1 \text{ GPa}$
 $\nu_c = .31$
 $\alpha_c = 9.09 \times 10^{-6}/^\circ\text{C}$



Layer Properties

Face Sheets
 $E_L = 137.2 \text{ GPa}$
 $E_T = 8.62 \text{ GPa}$
 $G_{LT} = 3.76 \text{ GPa}$
 $G_{TT} = 2.89 \text{ GPa}$
 $\nu_{LT} = .32$
 $\alpha_L = -3.42 \times 10^{-7}/^\circ\text{C}$
 $\alpha_T = 27.9 \times 10^{-6}/^\circ\text{C}$
 $N_L = 8$
 Fiber Orientation $[\pm 45/0/90]_s$
 Thickness of individual layers
 $= 1.397 \times 10^{-4} \text{ m}$

Core
 $E_{1c} = .433 \text{ MPa}$
 $E_{2c} = .286 \text{ MPa}$
 $G_{12c} = 7.92 \text{ MPa}$
 $G_{13c} = .521 \text{ GPa}$
 $G_{23c} = .394 \text{ GPa}$
 $\nu_{12c} = 1.23$
 $\alpha_c = 9.09 \times 10^{-6}/^\circ\text{C}$
 $h(c) = .0254 \text{ m}$



Panel Geometric Parameters

$L_1 = .508 \text{ m}$
 $R = 2.54 \text{ m}$
 $L_1/L_2 = 1, 3, 1/3$



FIG. 1. Panels Considered in Present Study and Sign Convention for Generalized Displacements and Stress Resultants

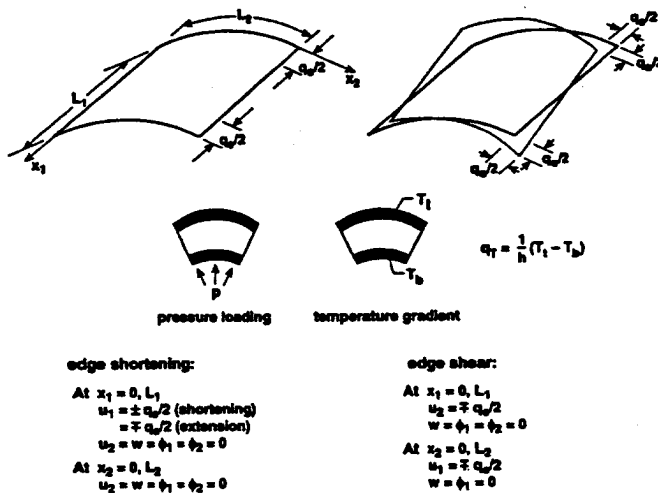


FIG. 2. Loadings and Boundary Conditions Considered in Numerical Studies

where $[K]$ = the global linear structural matrix that includes the flexibility and linear strain-displacement matrices; $\{Z\}$ = the response vector that includes both unknown (free) nodal displacements and stress-resultant parameters; $\{G(Z)\}$ = the vector of nonlinear terms; p , q , and q_T = the magnitudes of the internal pressure, applied edge displacement, and temperature gradient through-the-thickness, respectively; $\{Q^{(1)}\}$, $\{Q^{(2)}\}$, and $\{Q^{(3)}\}$ are normalized vectors corresponding to unit values of p , q , and q_T , respectively. The form of the arrays $[K]$, $\{G(Z)\}$, $\{Q^{(1)}\}$, and $\{Q^{(3)}\}$ is given in Appendix II.

The standard approach for the solution of (1) is to fix the value of two of the three parameters, p , q , and q_T and to vary the third, or to choose a functional relationship between the three parameters that is dependent on a single parameter q . In either case, the solution corresponding to the chosen combination of p , q , and q_T (which is effectively dependent on a single parameter), constitutes a curve on the equilibrium surface of the panel.

Governing Equations for Sensitivity Coefficients

The sensitivity coefficients are the derivatives of the various response quantities with respect to the different material, lamination, and geometric parameters of the panel. They can be used to study the sensitivity of the nonlinear and postbuckling responses to variations in the different parameters. The governing equations for the sensitivity coefficients are obtained by differentiating (1) with respect to a typical parameter λ . The resulting linear algebraic equations have the following form:

$$\left[[K] + \left[\frac{\partial G_i}{\partial Z_j} \right] \right] \left\{ \frac{\partial Z}{\partial \lambda} \right\} = - \left[\frac{\partial K}{\partial \lambda} \right] \{Z\} + q_T \left\{ \frac{\partial Q^{(3)}}{\partial \lambda} \right\} \quad (2)$$

where the range of the indices i and j is 1 to the total number of degrees of freedom in the model; and $\{Q^{(1)}\}$ and $\{Q^{(2)}\}$ are assumed to be independent of λ . Note that the matrix on the left-hand-side of (2) is identical to that used in the Newton-Raphson iterative process. Therefore, if the Newton-Raphson technique is used in generating the nonlinear response, the evaluation of the sensitivity coefficients requires the generation of the right-hand side of (2), and a forward-reduction/back-substitution operation only (no decomposition of the left-hand-side matrix is required).

Evaluation of Transverse Shear Stresses

The transverse shear stresses are evaluated by using piecewise integration, in the thickness direction, of the three-dimensional equilibrium equations. For optimum accuracy, the transverse shear stresses are computed as the numerical quadrature points and then interpolated to the center of the element. The same procedure is used for evaluating the thickness distributions of the sensitivity coefficients of the transverse shear stresses.

Hierarchical Sensitivity Coefficients

The nonlinear and postbuckling response characteristics of sandwich panels are dependent on a hierarchy of interrelated parameters including panel, effective layer, and micromechanical parameters. A study of the sensitivity of the response to

CURVED SANDWICH PANELS SUBJECTED TO TEMPERATURE GRADIENT AND MECHANICAL LOADS

By Ahmed K. Noor,¹ Fellow, ASCE, James H. Starnes Jr.,² Member, ASCE, and Jeanne M. Peters³

ABSTRACT: The results of a detailed study of the nonlinear response of curved sandwich panels with composite face sheets, subjected to a temperature gradient through the thickness combined with mechanical loadings, are presented. The analysis is based on a first-order shear-deformation Sanders-Budiansky-type theory, including the effects of large displacements, moderate rotations, transverse shear deformation, and laminated anisotropic material behavior. A mixed formulation is used with the fundamental unknowns consisting of the generalized displacements and the stress resultants of the panel. The nonlinear displacements, strain energy, principal strains, transverse shear stresses, transverse shear strain energy density, and their hierarchical sensitivity coefficients are evaluated. The hierarchical sensitivity coefficients measure the sensitivity of the nonlinear response to variations in the panel parameters, the effective properties of the face sheet layers and the core, and the micromechanical parameters. Numerical results are presented for cylindrical panels subjected to combined pressure loading, edge shortening or extension, edge shear, and a temperature gradient through the thickness. The results show the effects of variations in the loading and the panel aspect ratio, on the nonlinear response, and its sensitivity to changes in the various panel, effective layer, and micromechanical parameters.

INTRODUCTION

In recent years, considerable work has been devoted to the study of thermomechanical nonlinear and postbuckling responses of composite and sandwich plates and shells. Attempts have been made to identify the differences between the isothermal and thermal responses. Reviews of recent contributions are contained in four survey papers (Noor and Burton 1992; Noor and Peters 1994; Bert 1995; Noor et al. 1996), and four monographs (Hoff 1986; Noor 1994; Zenkert 1995; Turvey and Marshall 1995). Only a few of the reported studies considered the nonlinear response of curved panels subjected to temperature gradient through-the-thickness (see, for example, Librescu and Souza 1993; Librescu et al. 1995), and to the authors' knowledge, none considered sandwich panels with composite face sheets, or boundary conditions other than simple supports. Because curved sandwich panels have many applications in aircraft structures, including fuselage, wing, and empennage components of high-speed aircraft, an understanding of their nonlinear response when subjected to a temperature gradient through-the-thickness combined with a mechanical loading is desirable. Moreover, a study of the sensitivity of the nonlinear response to variations in the material, lamination, and geometric parameters of these panels is needed to provide an indication of the effects of changes in these parameters on the structural response.

The present study focuses on understanding the detailed nonlinear response characteristics of cylindrical sandwich panels with composite face sheets subjected to a temperature gradient through-the-thickness combined with mechanical loadings. Sensitivity coefficients are evaluated that measure the sensitivity of the various response quantities to variations in the panel stiffnesses, the effective material properties of the

individual face sheet layers and core, and the micromechanical parameters.

The sandwich panels considered in the study consist of a number of perfectly bonded composite face sheet layers and a honeycomb core. The layers of the top and bottom face sheets are symmetrically distributed with respect to the middle surface. The individual layers of the face sheets and the core are assumed to be homogeneous and anisotropic. A plane of thermoelastic symmetry exists at each point of the panel, parallel to the middle surface. The loading is selected to simulate that of a typical fuselage panel of a high-speed aircraft.

MATHEMATICAL FORMULATION

Finite Element Equations Governing Panel Response

The analytical formulation is based on a first-order shear-deformation Sanders-Budiansky-type shell theory with the effects of large displacements, moderate rotations, average transverse shear deformation through-the-thickness, and laminated anisotropic material behavior. For simplicity, a linear Duhamel-Neumann-type constitutive model is used and the material properties are assumed to be independent of temperature. The constitutive relations for the panel are given in Appendix I. A total Lagrangian formulation is used, and the panel deformations, at different values of the applied loading, are referred to the original undeformed configuration. The panel is discretized by using two-field mixed finite-element models. The fundamental unknowns consist of the nodal displacements and the stress resultant parameters. The stress resultants are allowed to be discontinuous at interelement boundaries in the model. The sign convention for the generalized displacements and the stress resultants for the model are shown in Fig. 1. The external loading consists of a uniform pressure loading p ; monotonically increasing edge displacement q , (either normal or tangential to the edge); and a temperature gradient through-the-thickness q_T [linear through-the-thickness temperature variation, $q_T = (T_t - T_b)/h$, where T_t and T_b are the changes in the top and bottom surface temperatures, see Fig. 2].

The governing finite-element equations describing the nonlinear and postbuckling responses of the sandwich panel can be written in the following compact form:

$$\{f(Z)\} = [K]\{Z\} + \{G(Z)\} - p\{Q^{(1)}\} - q_e\{Q^{(2)}\} - q_T\{Q^{(3)}\} = 0 \quad (1)$$

¹Ferman W. Perry Prof. of Aerospace Structures and Applied Mechanics; and Dir., Ctr. for Advanced Computational Technol., Univ. of Virginia, NASA Langley Res. Ctr., Hampton, VA 23681.

²NASA Langley Res. Ctr., Hampton, VA.

³Ctr. for Advanced Computational Technol., Univ. of Virginia, NASA Langley Res. Ctr., Hampton, VA.

Note. Discussion open until March 1, 1998. To extend the closing date one month, a written request must be filed with the ASCE Manager of Journals. The manuscript for this paper was submitted for review and possible publication on June 2, 1997. This paper is part of the *Journal of Aerospace Engineering*, Vol. 10, No. 4, October, 1997. ©ASCE, ISSN 0893-1321/97/0004-0143-0161/\$4.00 + \$.50 per page. Paper No. 15920.

variations in each of these parameters provides insight into the importance of the parameters and helps in the development of materials to meet certain performance requirements.

Three sets of sandwich parameters are considered herein: (1) panel; (2) effective layer; and (3) micromechanical parameters. The panel parameters include the extensional, bending-extensional, bending and transverse shear stiffnesses [components of the matrices $[A]$, $[B]$, $[D]$ and $[A_s]$, see (17) and (18) in Appendix I], and the vectors of thermal effects $\{N_T\}$ and $\{M_T\}$, [see (19) Appendix I]. The layer parameters include the individual face sheet layer properties: elastic moduli E_L , E_T ; shear moduli G_{LT} , G_{TT} ; major Poisson's ratio ν_{LT} ; coefficients of thermal expansion α_L , α_T ; fiber-orientation angle $\theta^{(l)}$; layer thickness $h^{(l)}$, where subscripts L and T refer to the longitudinal (fiber) and transverse directions, respectively. The parameters also include the effective core properties: elastic moduli E_{1c} , E_{2c} ; shear moduli G_{12c} , G_{13c} , G_{23c} ; Poisson's ratios ν_{12c} , ν_{13c} , ν_{23c} ; coefficient of thermal expansion α_c , and core thickness $h^{(c)}$. The micromechanical parameters refer to the fiber, matrix, and core material moduli E_{1f} , E_{2f} , E_m , E_c , G_{12f} , G_m , G_c ; Poisson's ratios ν_{12f} , ν_{23f} , ν_m , ν_c ; coefficients of thermal expansion α_{1f} , α_{2f} , α_m , α_c ; the fiber volume fraction v_f of the face sheet layers; and the geometric parameters of the core l_{1c} , l_{2c} , t_c , θ_c . The subscripts f , m , and c denote the fiber, matrix, and core property, respectively. The three sets of parameters will henceforth be referred to as $\lambda_i^{(p)}$, $\lambda_j^{(l)}$, $\lambda_k^{(m)}$, where superscripts p , l , and m refer to the panel, effective layer and micromechanical parameters, respectively; and the indices i , j , and k range from 1 to the number of parameters in each category.

The computational procedure consists of evaluating the sensitivity coefficients with respect to each of the panel parameters $\{\partial Z / \partial \lambda_i^{(p)}\}$, using (2). The sensitivity coefficients with respect to the effective layer and micromechanical parameters are then obtained by forming the following linear combinations:

$$\left\{ \frac{\partial Z}{\partial \lambda_j^{(l)}} \right\} = \sum_i a_{ij} \left\{ \frac{\partial Z}{\partial \lambda_i^{(p)}} \right\} \quad (3)$$

and

$$\left\{ \frac{\partial Z}{\partial \lambda_k^{(m)}} \right\} = \sum_j b_{jk} \left\{ \frac{\partial Z}{\partial \lambda_j^{(l)}} \right\} = \sum_i c_{ik} \left\{ \frac{\partial Z}{\partial \lambda_i^{(p)}} \right\} \quad (4)$$

where

$$a_{ij} = \left\{ \frac{\partial \lambda_j^{(l)}}{\partial \lambda_i^{(p)}} \right\}; \quad b_{jk} = \left\{ \frac{\partial \lambda_k^{(m)}}{\partial \lambda_j^{(l)}} \right\} \quad (5, 6)$$

$$c_{ik} = \left\{ \frac{\partial \lambda_k^{(m)}}{\partial \lambda_i^{(p)}} \right\} = \sum_j a_{ij} b_{jk} \quad (7)$$

The a_{ij} coefficients relate the panel stiffnesses to the effective properties of the individual layers and are obtained from the lamination theory. The b_{jk} coefficients relate the effective layer properties to the constituent properties and are obtained from the micromechanical and core models; and the c_{ik} coefficients relate the panel stiffnesses to the micromechanical properties (see Fig. 2). If the panel stiffnesses are uniform, and the constitutive relations of the panel, layer, and the constituents are linear, then the a_{ij} , b_{jk} , c_{ik} coefficients are constants and need to be generated only once for each panel, even when the response is nonlinear.

NUMERICAL STUDIES

Numerical studies were performed to determine the effects of variations in the loading, the panel aspect ratio, and the stacking sequence of the face sheet layers on the nonlinear response and the sensitivity coefficients of cylindrical sandwich panels. The panels considered have composite, eight-layer quasi-isotropic face sheets and a titanium honeycomb core with hexagonal cells. The material properties and geometric characteristics for the panels considered in the present study are given in Fig. 1. The material properties, fiber orientation, and stacking sequences selected are those typical of sandwich panels considered for high-speed aircraft applications. The loading on the panels consisted of a sequence of mechanical and thermal loadings: uniform pressure loading $p = 6.894 \times 10^4$ Pa, followed by monotonically increasing edge displacement q_e , and then a temperature gradient through-the-thickness q_T [linear through-the-thickness temperature varia-

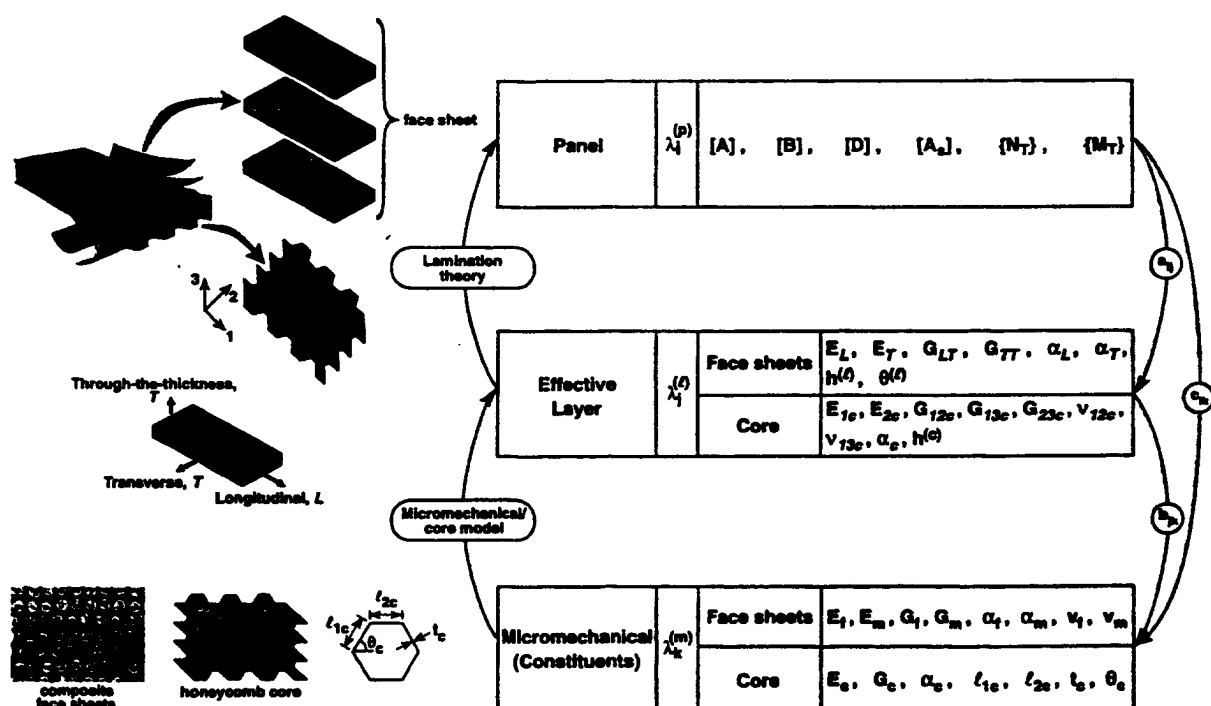


FIG. 3. Hierarchical Sensitivity Coefficients for Sandwich Panels with Composite Face Sheets

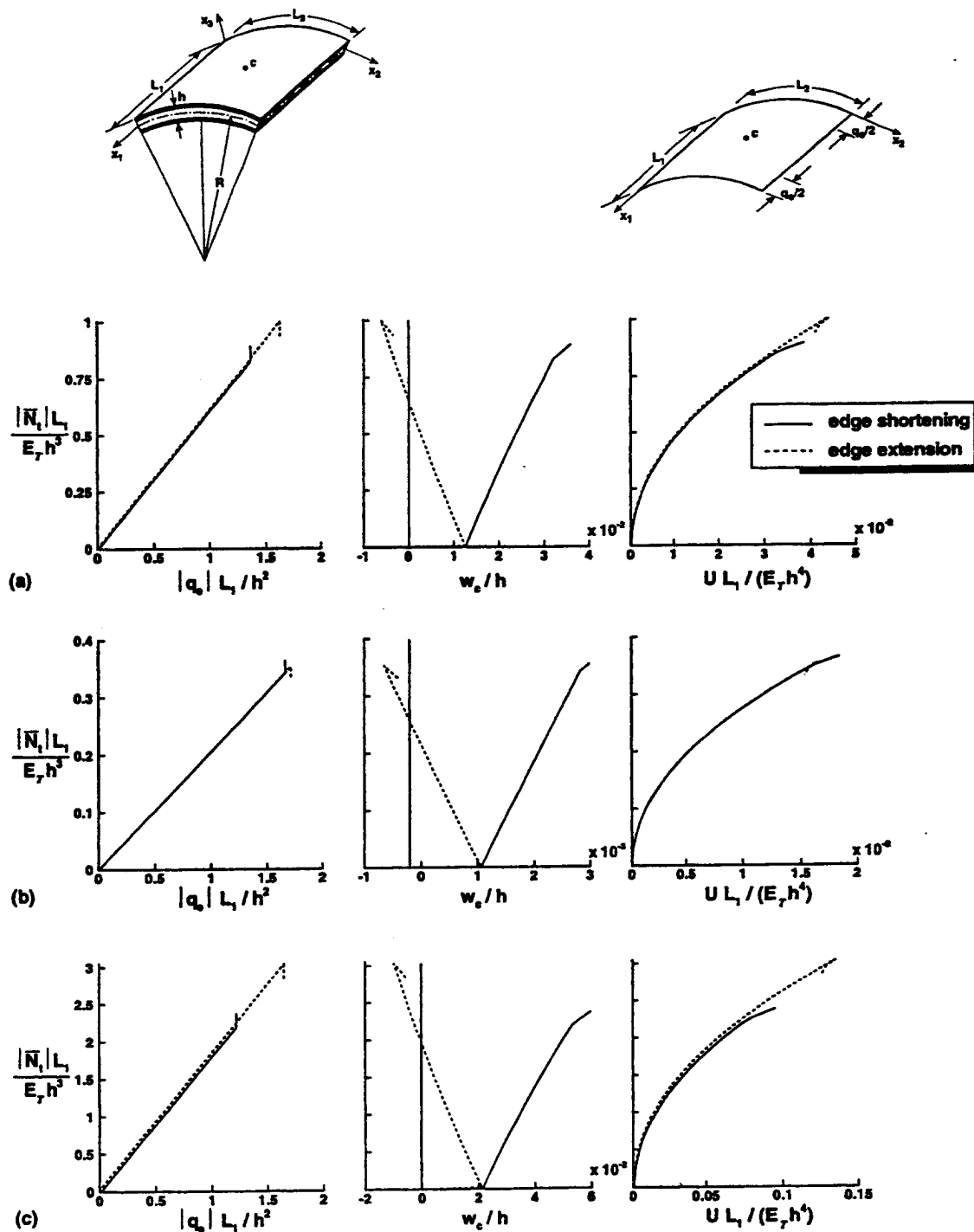


FIG. 4. Effect of Loading and Aspect Ratio on Nonlinear Response of Cylindrical Sandwich Panels with Honeycomb Core and Composite Eight-Layer Face Sheets Subjected to Combined Pressure Loading, Edge Shortening, or Extension and Temperature Gradient through Thickness [$L_1/L_2 =$ (a) 1; (b) 3; (c) 1/3]

tion, $q_T = (T_1 - T_2)/h$, where T_1 and T_2 are the changes in the top and bottom surface temperatures]. The value of T_2 was zero, and T_1 was increased to 137.8°C. Three different types of edge displacements were applied, namely, edge shortening, edge extension, and edge shear. The boundary conditions selected for the cases of edge shortening or extension and edge shear are shown in Fig. 2. In each loading case, the maximum value of q , was selected in such a way that the maximum principal strains on the surfaces do not exceed 0.005. Three different values of the panel aspect ratio are considered; namely, $L_1/L_2 = 1, 3$, and $1/3$. For each problem, hierarchical sensitivity coefficients are evaluated (Fig. 3). The hierarchical

sensitivity coefficients are the derivatives of the different response quantities with respect to panel stiffnesses, material parameters, and fiber angles of the individual face sheet layers; effective and actual properties of the core; and micromechanical parameters of the face sheet layers.

Mixed finite-element models were used for the discretization of each panel. Biquadratic shape functions were used for approximating each of the generalized displacements, and bilinear shape functions were used for approximating each of the stress resultants. The characteristics of the finite-element model are given by Noor and Andersen (1982). For each panel, the multiple parameter reduction methods described by

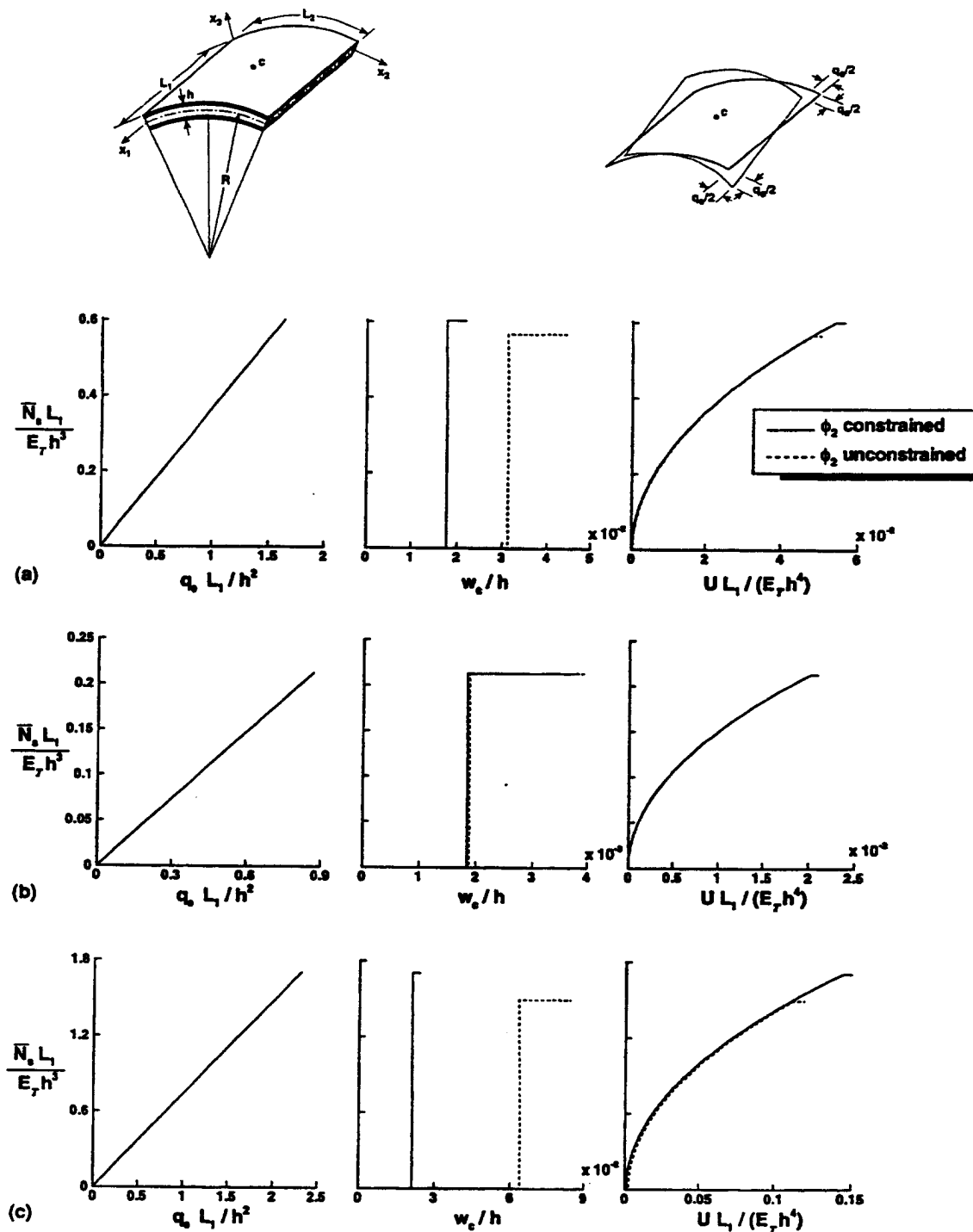


FIG. 5. Effect of Loading and Aspect Ratio on Nonlinear Response of Cylindrical Sandwich Panels with Honeycomb Core and Composite Eight-Layer Face Sheets, Subjected to Combined Pressure Loading, Edge Shear, and Temperature Gradient through Thickness [$L_1/L_2 =$ (a) 1; (b) 3; (c) 1/3]

Noor and Peters (1983a,b, 1992) were used in generating the nonlinear and postbuckling responses, and evaluating the sensitivity coefficients. Typical results are presented in Figs. 4–8 for the response studies, and in Figs. 9–17 for the sensitivity studies, and are described subsequently.

Response Studies

The responses of the sandwich panels considered are shown in Figs. 4–8. Plots of the total axial force \bar{N}_x versus the applied end shortening or extension q_e , the transverse displacement w_e , and the total strain energy U , are shown in Fig. 4 for panels with $L_1/L_2 = 1, 3$, and $1/3$. Similar plots of the total edge shear

force \bar{N}_y (at $x_1 = 0, L_1$) versus the applied edge shear q_e , w_e , and U are shown in Fig. 5. Normalized contour plots for the transverse displacement w , the total strain energy density \bar{U} , and the transverse shear strain energy density \bar{U}_{sh} at the end of the loading stage $p + q_e + q_r$, are shown in Figs. 6 and 7 for the panels with $L_1/L_2 = 1, 3$, and $1/3$. The effect of loading and aspect ratio on the distribution of the transverse shear strain energy density \bar{U}_{sh} at the location of maximum \bar{U}_{sh} , is shown in Fig. 8. The nonlinear response studies can be summarized as follows:

1. The stacking sequence of the face sheet layers (i.e., the relative locations of the $+45^\circ$ and -45° layers) has no

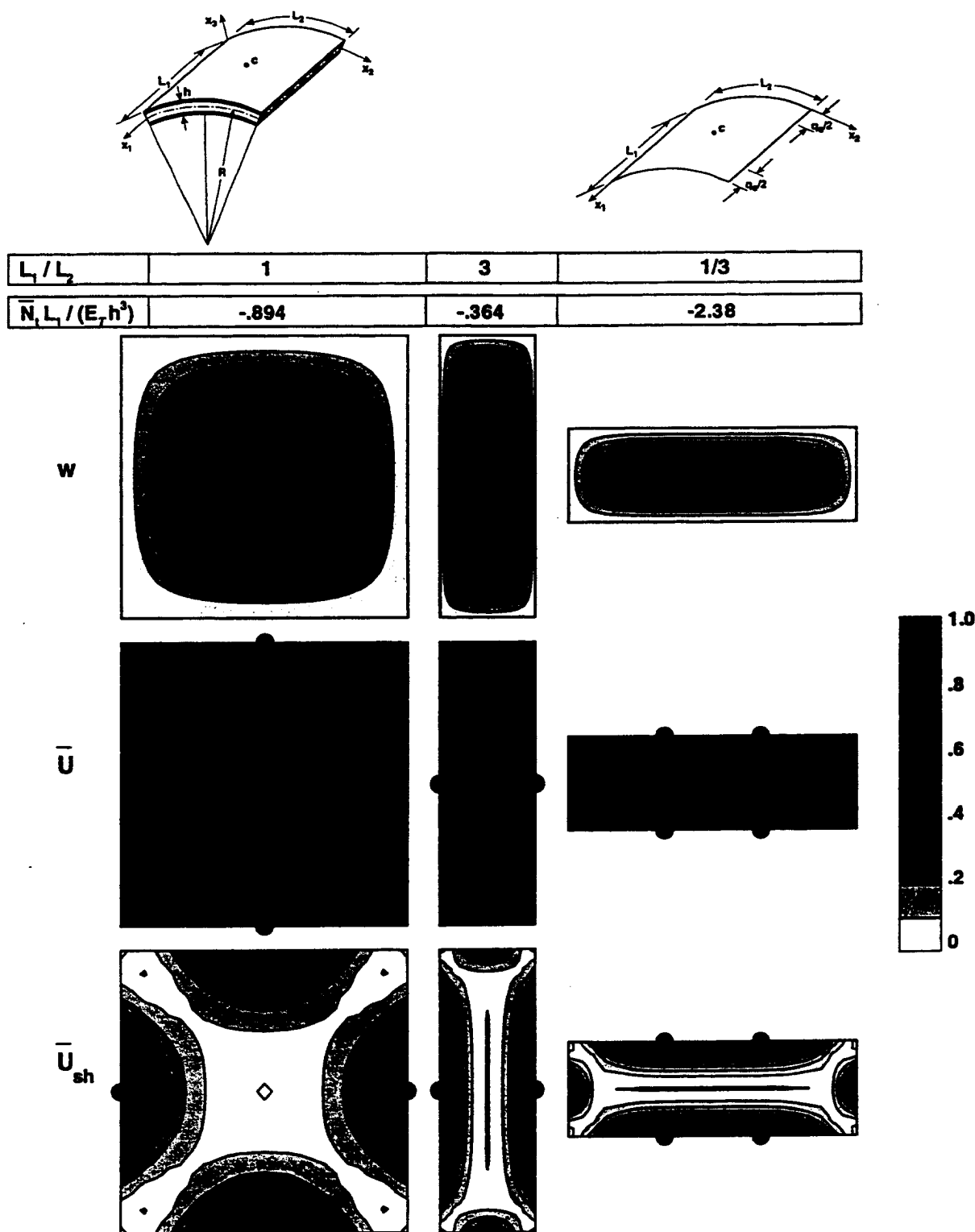


FIG. 6. Normalized Contour Plots Depicting Effect of Aspect Ratio on Transverse Displacement w , Total Strain Energy Density \bar{U} , and Transverse Shear Strain Energy Density \bar{U}_{sh} for Cylindrical Panels, with Honeycomb Core and Composite Eight-Layer Face Sheets, Subjected to Combined Pressure Loading, Edge Shortening, and Temperature Gradient through Thickness (e = Location of Maximum Values)

- noticeable effect on the global response characteristics of the panel.
- For all of the panels considered, the pressure loading p had the least effect on the global response characteristics, and the edge displacement q_r had the most effect on the global response. By contrast, the edge shear q_s had the least effect on the transverse shear strain energy density \bar{U}_{sh} at the location of maximum \bar{U}_{sh} .

- For all of the panels considered, no mode change occurs from the first to the second and third loading stages (p , $p + q_r$, $p + q_r + q_s$). However, the distribution of the strain energy density \bar{U} in the panel changes significantly from being nonuniform after the application of p to being nearly uniform after the application of $p + q_r$, and remains nearly uniform after the application of q_s .
- For the case of edge shear, relaxing the constraint $\phi_1 =$

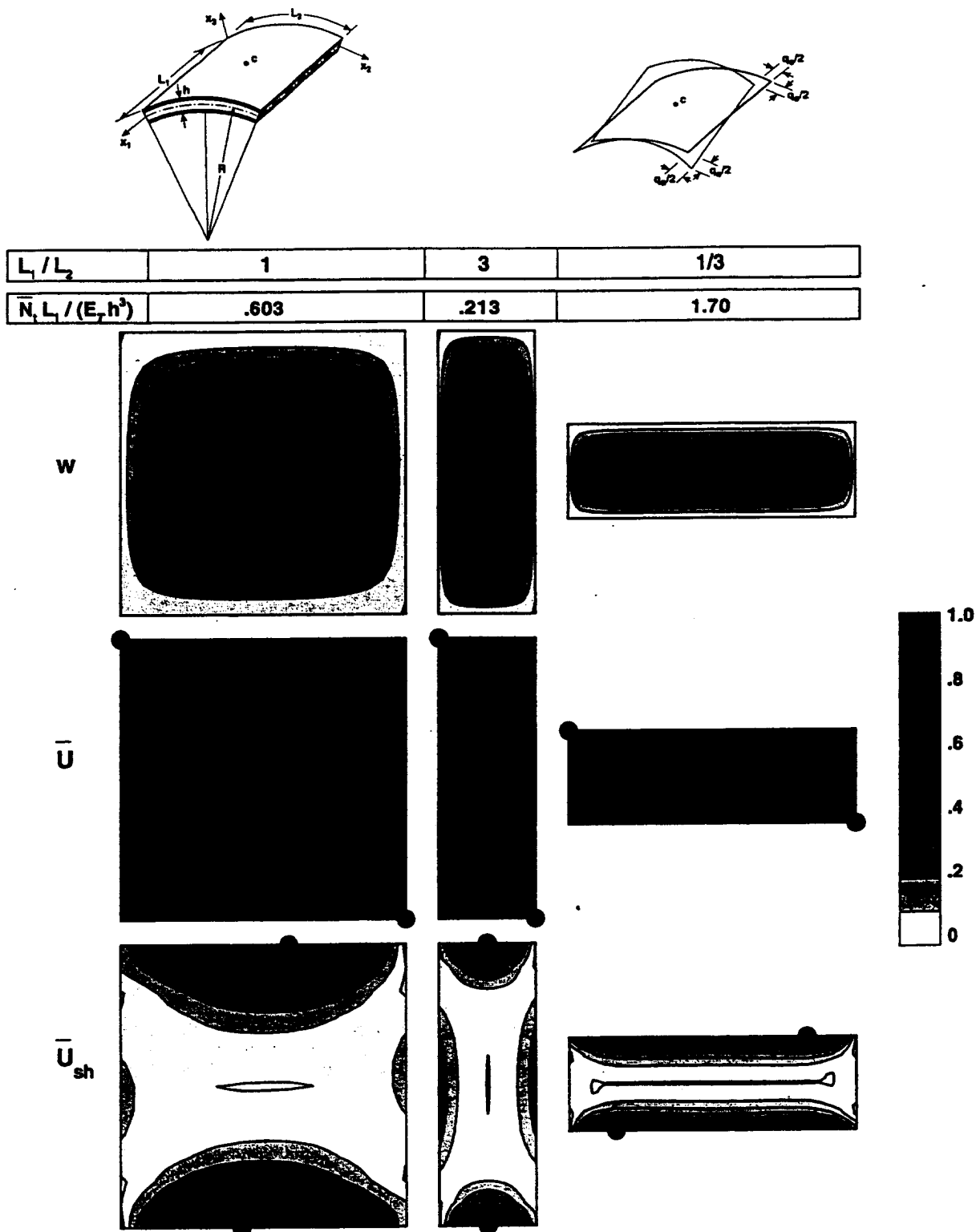


FIG. 7. Normalized Contour Plots Depicting Effect of Aspect Ratio on Transverse Displacement w , Total Strain Energy Density \bar{U} , and Transverse Shear Strain Energy Density \bar{U}_{sh} , for Cylindrical Panels, with Honeycomb Core and Composite Eight-Layer Face Sheets, Subjected to Combined Pressure Loading, Edge Shear, and Temperature Gradient through Thickness (• = Location of Maximum Values)

0 at $x_1 = 0$, L_1 has no noticeable effect on the in-plane shear stiffness or on the total strain energy of the panels. However, it results in increasing the center displacement w_c , particularly for panels with $L_1/L_2 \leq 1$.

- For the case of edge shear q_s , the location of the maximum strain energy density \bar{U} was different in each loading stage. By contrast, for the case of edge extension, the location of maximum \bar{U} was the same after the application p as after $p + q_s$, but was different after $p +$

$q_s + q_T$; and for the case of edge compression, only the panels with $L_1/L_2 = 1$ had the location of maximum \bar{U} after p the same as that after $p + q_s + q_T$, but different from the location of maximum \bar{U} after $p + q_s$.

Sensitivity Studies

Sensitivity studies were conducted to identify which of the panel parameters, effective face sheet and core properties, and

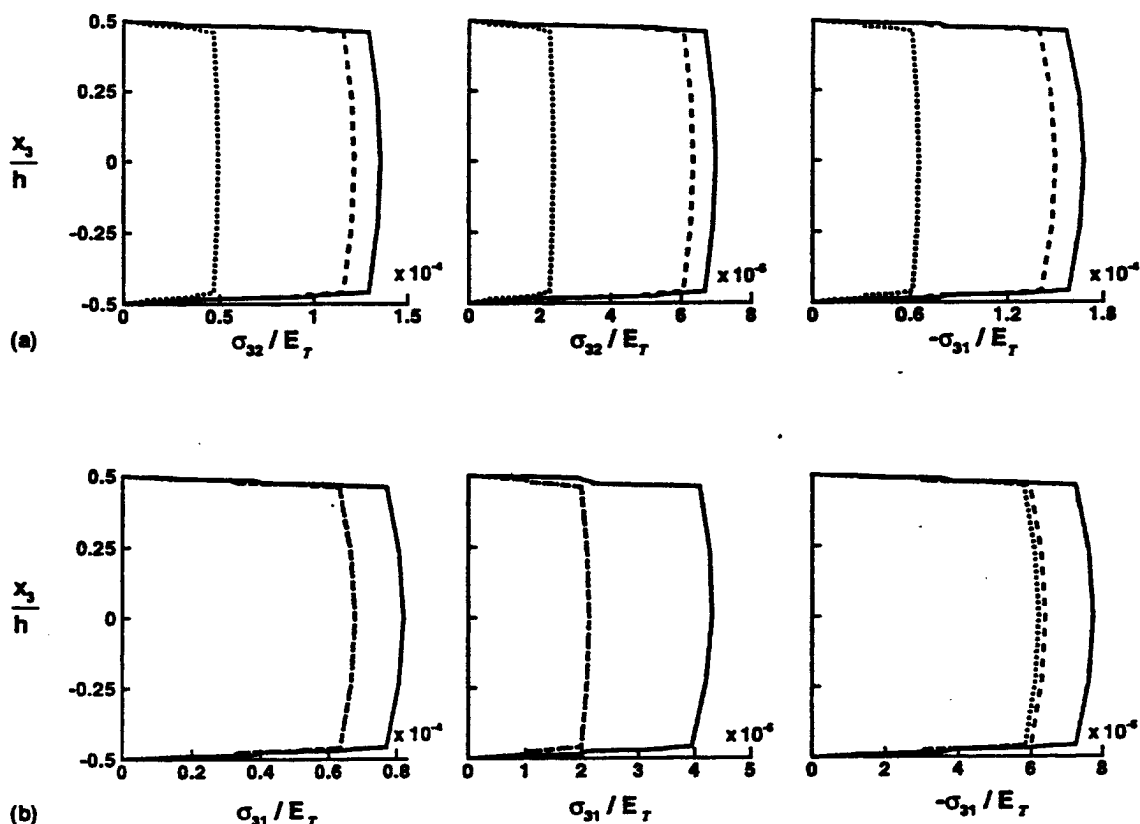
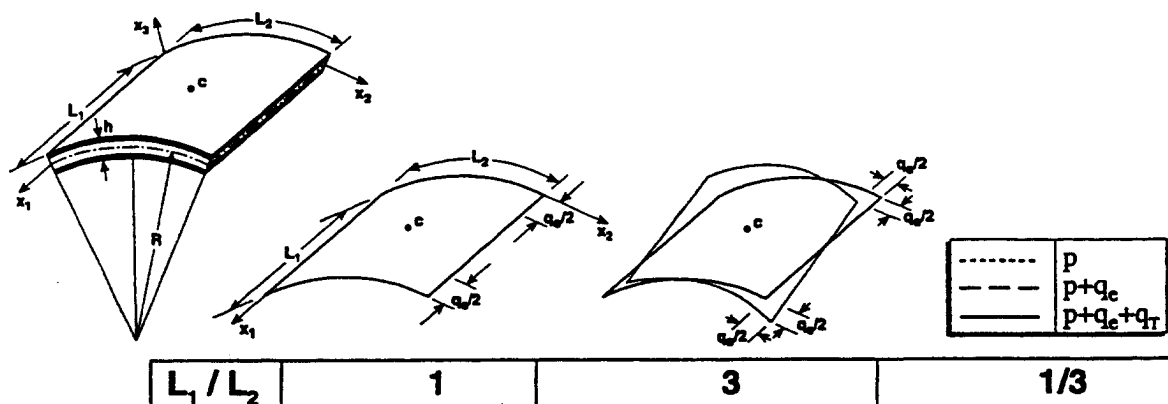


FIG. 8. Effect of Loading and Aspect Ratio on Distribution of Transverse Shear Strain Energy Density \bar{U}_s through Thickness, at Point of Maximum Transverse Shear Strain Energy Density \bar{U}_s (see Fig. 6); Cylindrical Sandwich Panels, with Honeycomb Core and Composite Eight-Layer Face Sheets, Subjected to Combined Pressure Loading, Prescribed Edge Displacement, and Temperature Gradient through Thickness; (a) Edge Shortening; (b) Edge Shear

micromechanical parameters most affect the nonlinear response. For the case of edge shortening or extension, typical results showing the sensitivity of the total strain energy U with respect to the extensional, bending, transverse shear stiffnesses, and the thermal forces and moments in the panel are presented in Fig. 9. Sensitivity coefficients of U with respect to effective material properties of individual face sheet layers are shown in Fig. 10; with respect to effective and actual core parameters, they are presented in Fig. 11; and with respect to micromechanical parameters of the face sheet layers, they are shown in Fig. 12. Corresponding results for the case of edge shear are shown in Figs. 13–16. For all of the loading cases and the panels considered, the stacking sequence of the face sheet layers has no noticeable effect on the sensitivity coefficients. Normalized contour plots for the largest sensitivity coefficients of the total strain energy density \bar{U} with respect to panel, core, and face sheet parameters at the end of each load-

ing stage (p only, $p + q$, and $p + q + q_T$) are shown in Fig. 17. An examination of Figs. 9–17 reveals the following facts.

Case of Edge Shortening or Extension

The total strain energy U is considerably more sensitive to variations in A_{11} than to variations in the other extensional stiffnesses. For the panels with $L_1/L_2 = 1$, U is more sensitive to variations in D_{11} and D_{22} than to variations in the other bending stiffnesses. For the panels with $L_1/L_2 = 3$, U is more sensitive to variations in D_{22} than to variations in the other bending stiffnesses, and for panels with $L_1/L_2 = 1/3$, U is more sensitive to variations in D_{11} .

The sensitivity of U to variations in A_{11} increases with an increase in q . For the case of edge shortening, the addition of the temperature gradient does not change the sensitivity with respect to A_{11} , but increases the sensitivity with respect

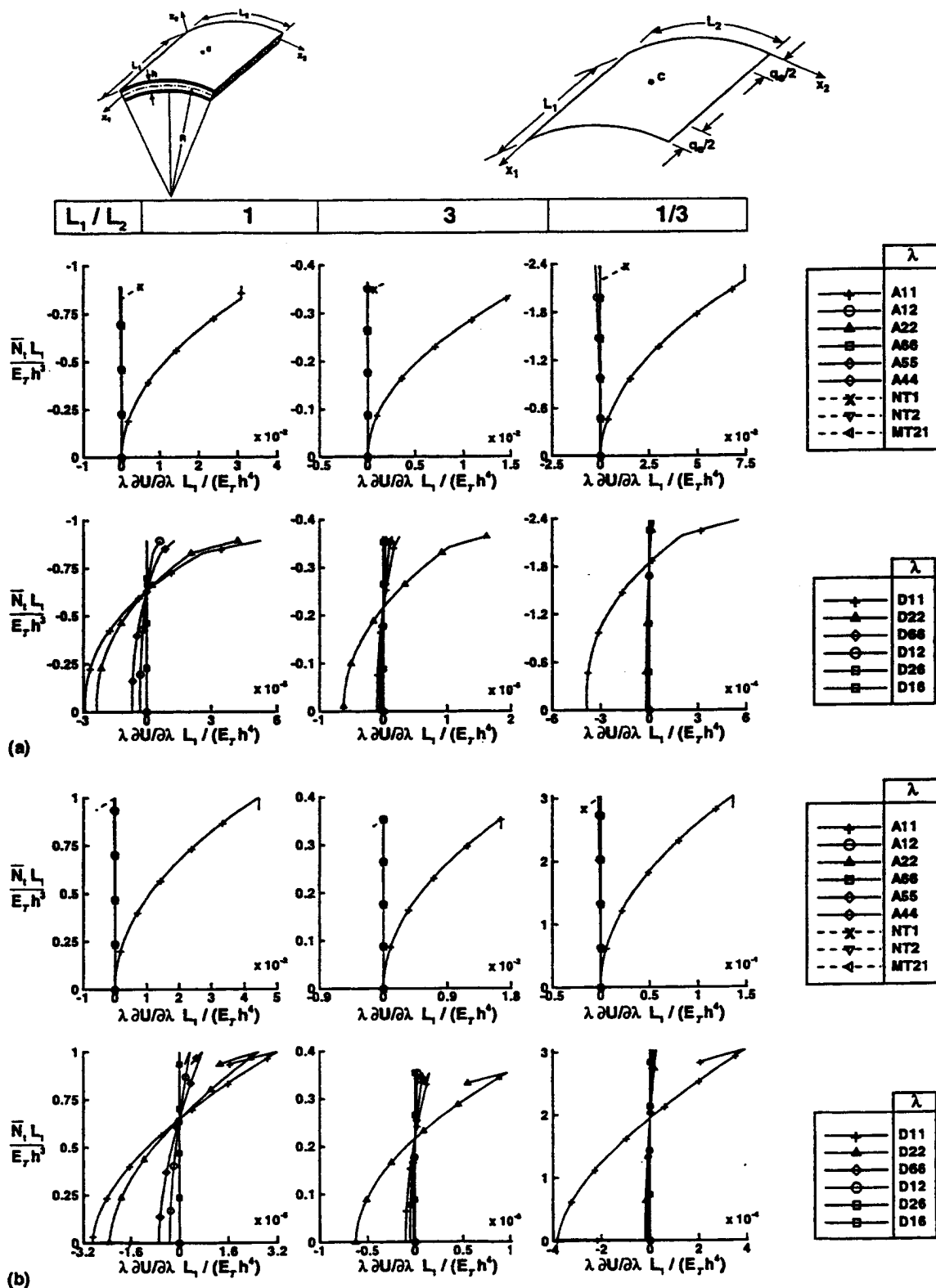


FIG. 9. Effect of Loading and Aspect Ratio on Normalized Sensitivity Coefficients of Total Strain Energy U with Respect to Panel Stiffnesses; Cylindrical Sandwich Panels, with Honeycomb Core and Composite Eight-Layer Face Sheets, Subjected to Combined Pressure Loading, Edge Shortening, and Temperature Gradient through Thickness; (a) Edge Shortening; (b) Edge Extension

to D_{11} (and with respect to D_{22} for the panels with $L_1/L_2 \geq 1$). For the case of edge extension, the addition of temperature gradient does not change the sensitivity with respect to A_{11} , but decreases the sensitivity with respect to D_{11} (and with respect to D_{22} for the panels with $L_1/L_2 \geq 1$).

The total strain energy is considerably more sensitive to variations in the following parameters than to each of the other

parameters in the same category: (1) The effective elastic modulus of the face sheets E_L ; (2) the fiber angles $+45^\circ$ and -45° ; (3) effective core properties ν_{12c} , E_{1c} , E_{2c} ; (4) the four core parameters θ_c , l_{1c} , E_c , and t_c ; and (5) micromechanical parameters of the face sheets ν_f , E_{1f} , E_{2f} , ν_m , and α_m . The sensitivity of U to variations in each of the parameters listed increases with the increase in q_c . For the edge shortening,

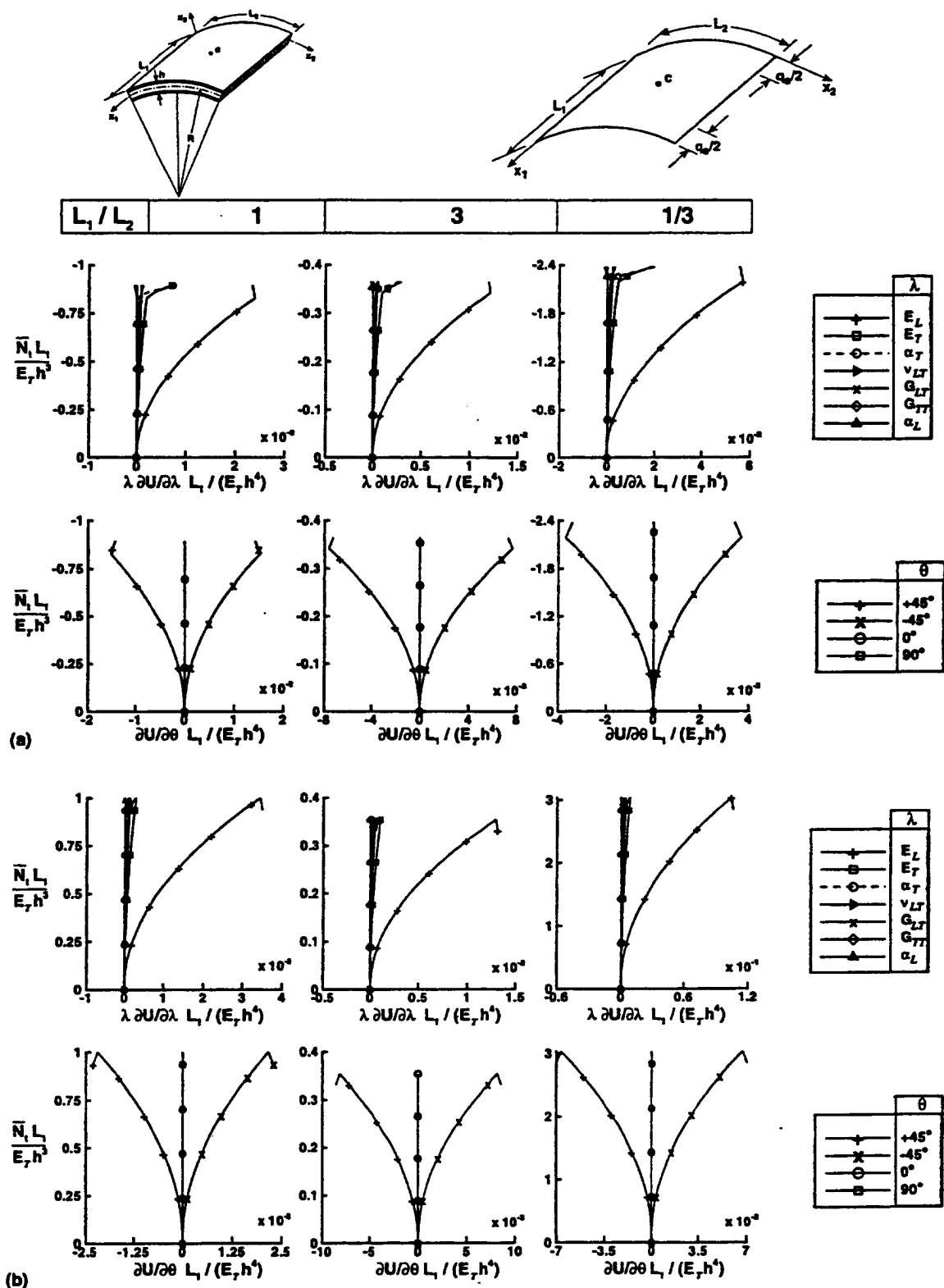


FIG. 10. Effect of Loading and Aspect Ratio on Normalized Sensitivity Coefficients of Total Strain Energy U with Respect to Effective Face Sheet Layer Properties; Cylindrical Sandwich Panels, with Honeycomb Core and Composite Eight-Layer Face Sheets, Subjected to Combined Pressure Loading, Edge Shortening, and Temperature Gradient through Thickness; (a) Edge Shortening; (b) Edge Extension

the addition of q_T increases the sensitivity of U to variations in v_{12c} , E_{1c} , E_{2c} , θ_c , l_{1c} , E_c , t_c , E_m , v_m , and α_m ; slightly decreases the sensitivity to variations in E_L , fiber angles $+45^\circ$, -45° , E_{1f} , and v_f . For the edge extension case, the addition of q_T has an opposite effect to that described for edge shortening.

The distribution of the sensitivity coefficients of the strain energy density \bar{U} with respect to all the parameters considered be-

comes nearly uniform throughout the panel after the application of $p + q_s$. Exceptions to that are the sensitivity coefficients of \bar{U} with respect to D_{11} and the fiber angles $+45^\circ$ and -45° .

Case of Edge Shear

The total strain energy U is considerably more sensitive to variations in the following parameters than to each of the other

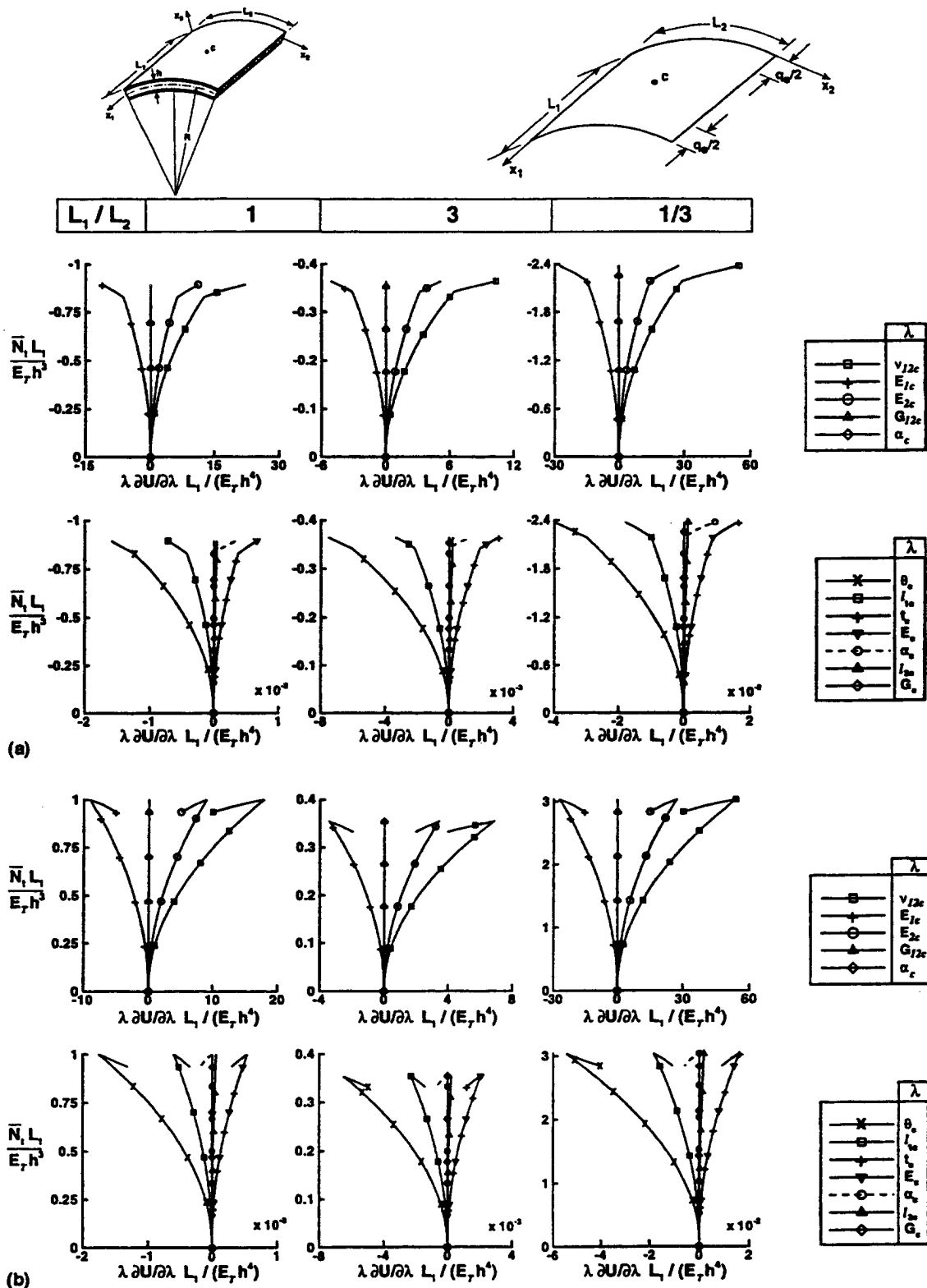


FIG. 11. Effect of Loading and Aspect Ratio on Normalized Sensitivity Coefficients of Total Strain Energy U with Respect to Core Properties; Cylindrical Sandwich Panels, with Honeycomb Core and Composite Eight-Layer Face Sheets, Subjected to Combined Pressure Loading, Edge Shortening, and Temperature Gradient through Thickness; (a) Edge Shortening; (b) Edge Extension

parameters in the same category: (1) Extensional stiffness A_{66} , and bending stiffness D_{11} (for the panels with $L_1/L_2 \leq 1$); (2) the effective modulus of the face sheets E_L ; (3) fiber angles 0° and 90° (after the application of q_T); (4) effective core parameters ν_{12c} , E_{1c} , E_{2c} (after the application of q_T); (5) core parameters t_c , α_c , E_c , l_c , and θ_c ; and (6) micromechanical parameters of the face sheets ν_f , E_{1f} , E_m , and α_m .

The sensitivity of U to variations in A_{66} , E_L , t_c , θ_c , E_c , l_c ,

ν_f , E_{1f} , and E_m increases with the increase of q_c . The sensitivity of U to variations in the other parameters listed in the first paragraph of this subsection does not change with changes in q_c . The addition of q_T significantly changes the sensitivity of U to variations in D_{22} , fiber angles 0° , 90° , and the parameters ν_{12c} , E_{1c} , E_{2c} , l_c , t_c , E_c , α_c , E_m , and α_m .

The distribution of the sensitivity coefficients of the strain energy density \bar{U} with respect to A_{66} , E_L , and ν_f becomes

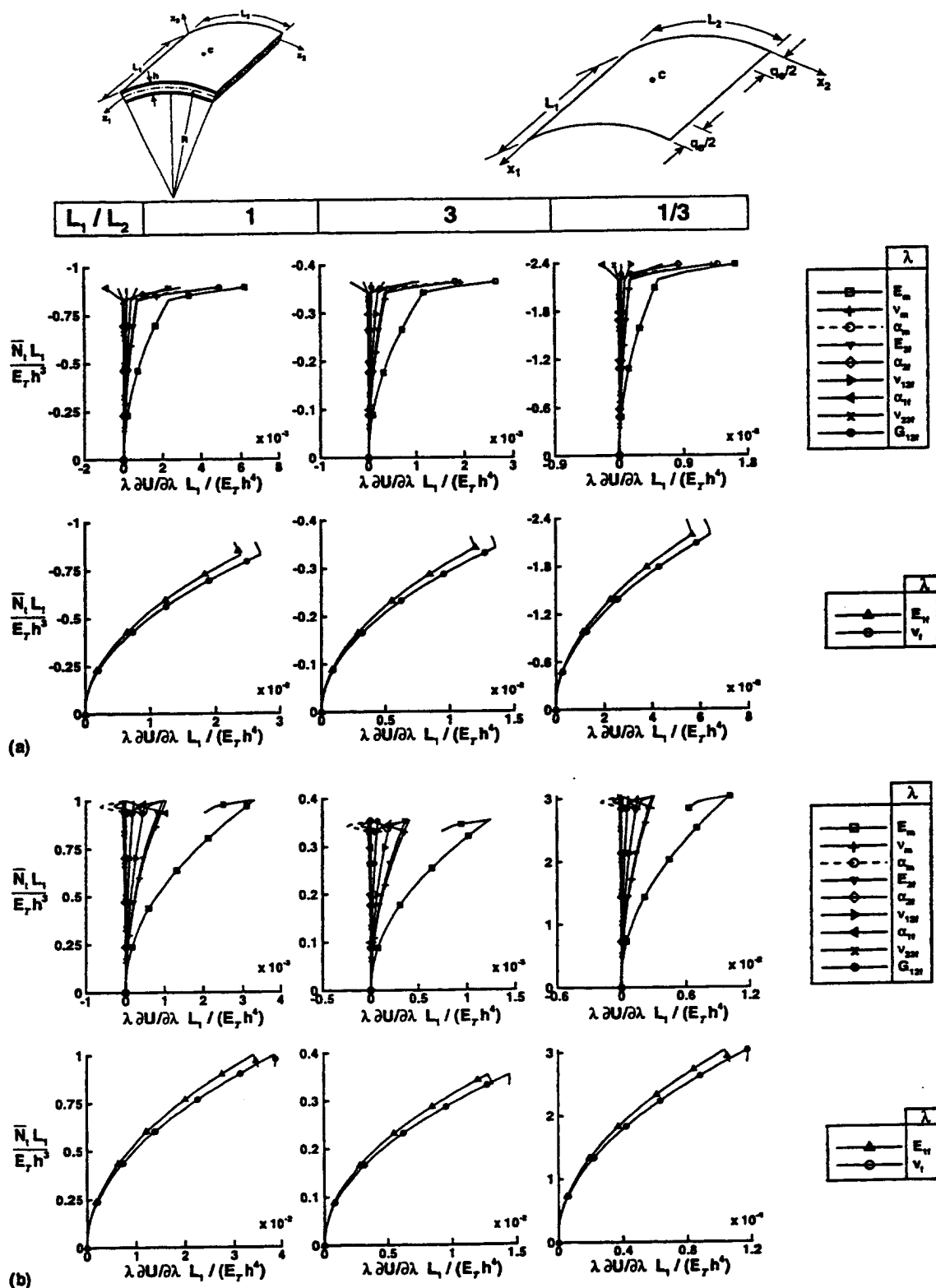


FIG. 12. Effect of Loading and Aspect Ratio on Normalized Sensitivity Coefficients of Total Strain Energy U with Respect to Micro-mechanical Properties of Face Sheet Layers; Cylindrical Sandwich Panels, with Honeycomb Core and Composite Eight-Layer Face Sheets, Subjected to Combined Pressure Loading, Edge Shortening, and Temperature Gradient through Thickness; (a) Edge Shortening; (b) Edge Extension

nearly uniform after the application of $p + q_s$, and remains uniform after the addition of q_T .

CONCLUDING REMARKS

A study is made of the nonlinear response of curved sandwich panels with composite face sheets subjected to a temperature gradient through the thickness combined with me-

chanical loadings. The panels are composed of perfectly bonded layers (face sheet layers and core), and the core is replaced by an equivalent homogeneous anisotropic layer. The analysis is based on a first-order shear-deformation Sanders-Budiansky-type theory, including the effects of large displacements, moderate rotations, average transverse shear deformation through the thickness, and laminated anisotropic material

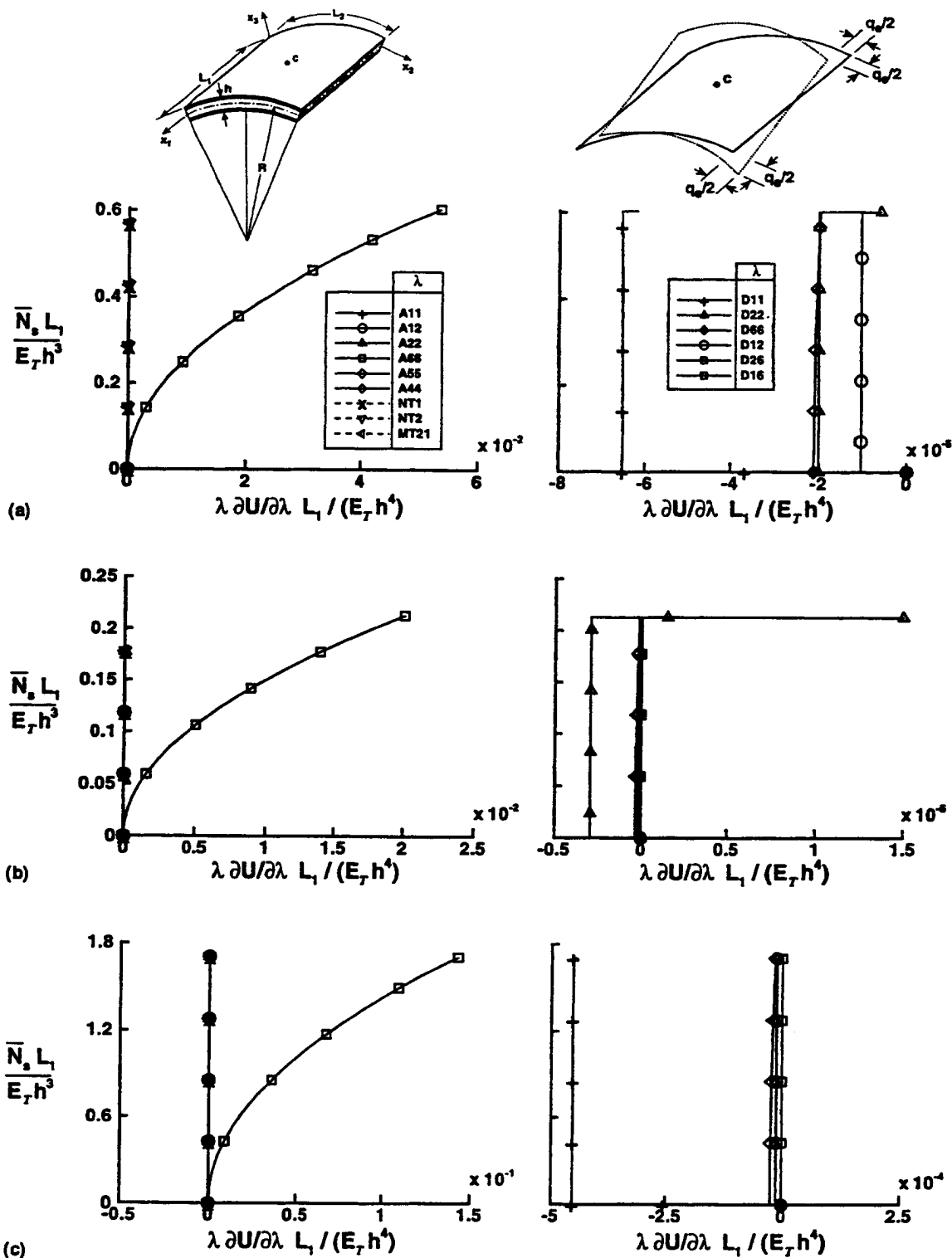


FIG. 13. Effect of Loading and Aspect Ratio on Normalized Sensitivity Coefficients of Total Strain Energy U with Respect to Panel Stiffnesses; Cylindrical Sandwich Panels, with Honeycomb Core and Composite Eight-Layer Face Sheets, Subjected to Combined Pressure Loading, Edge Shear, and Temperature Gradient through Thickness [$L_1/L_2 =$ (a) 1; (b) 3; (c) 1/3]

behavior. A linear, Duhamel-Neumann-type constitutive model is used and the material properties are assumed to be independent of temperature. The panels are discretized by using two-field mixed finite-element models with the fundamental unknowns consisting of the nodal displacements and stress resultant parameters. The stress resultants are allowed to be discontinuous at interelement boundaries.

Both the nonlinear response of the panel as well as the hierarchical sensitivity coefficients are generated. The hierarchical sensitivity coefficients measure the sensitivity of the dif-

ferent response quantities to variations in three sets of interrelated parameters: (1) Panel stiffnesses; (2) effective properties of the face sheet layers and the core; and (3) micromechanical parameters of the face sheet layers and the core. An efficient multiple-parameter reduction method is used for generating the nonlinear response and evaluating the sensitivity coefficients.

The computational procedure for evaluating the hierarchical sensitivity coefficients consists of evaluating the sensitivity coefficients with respect to each of the panel stiffnesses, and then

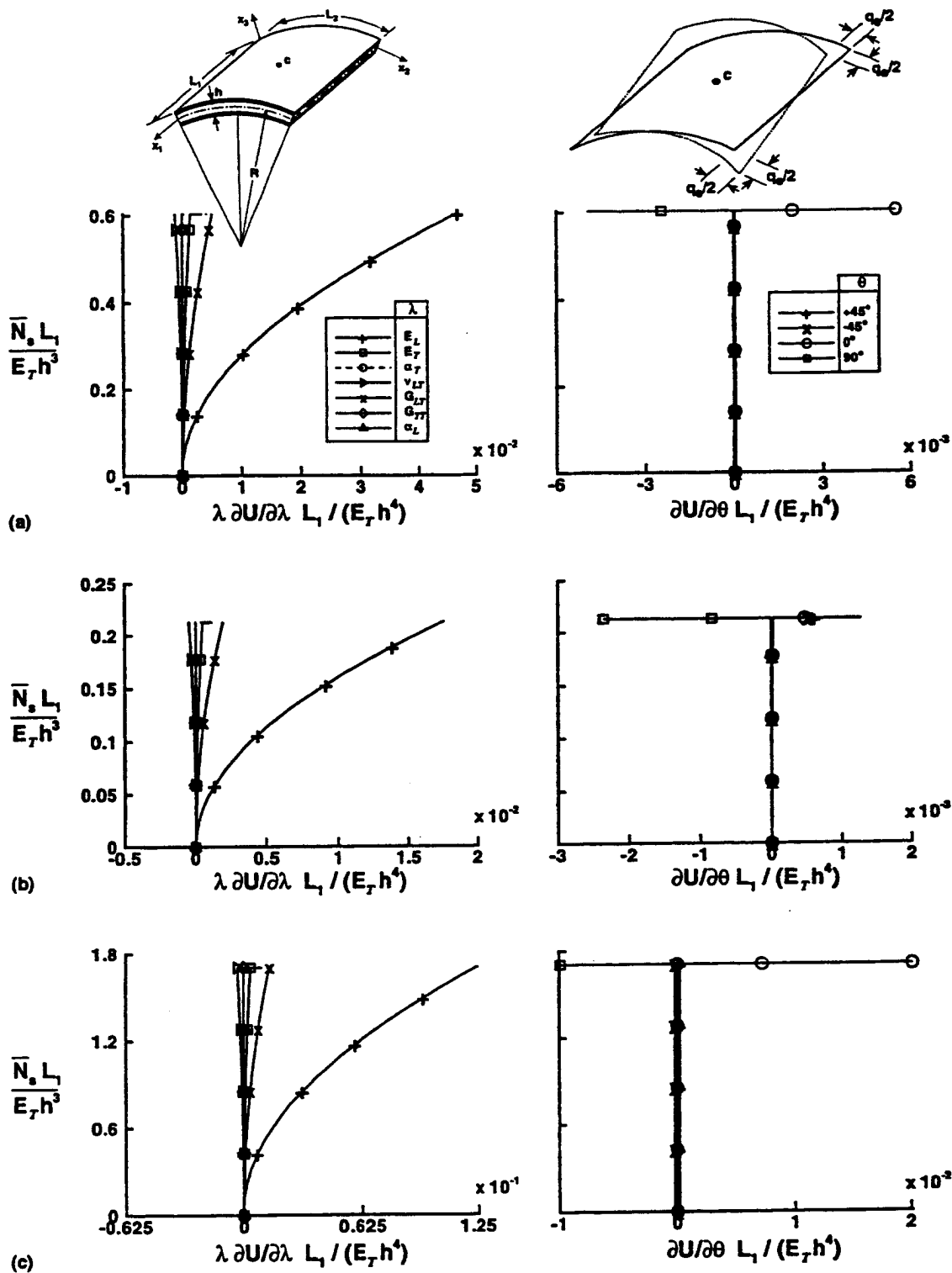


FIG. 14. Effect of Loading and Aspect Ratio on Normalized Sensitivity Coefficients of Total Strain Energy U with Respect to Effective Face Sheet Layer Properties; Cylindrical Sandwich Panels, with Honeycomb Core and Composite Eight-Layer Face Sheets, Subjected to Combined Pressure Loading, Edge Shear, and Temperature Gradient through Thickness [$L_1/L_2 =$ (a) 1; (b) 3; (c) 1/3]

generating the sensitivity coefficients with respect to the effective layer and micromechanical parameters as linear combinations of the sensitivity coefficients with respect to the panel parameters. Hierarchical sensitivity coefficients can be used to assess the effects of variations in the panel, face sheet layers, core, and micromechanical parameters on the nonlinear response. They can also help relate structural design and material development.

Numerical studies are presented that show the effects of variations in the loading, the panel aspect ratio, and in the

stacking sequence of the face sheet layers on the nonlinear response, and the sensitivity coefficients of cylindrical sandwich panels with eight-layer quasi-isotropic face sheets and titanium honeycomb core with hexagonal cells. The loading on the panels consisted of a sequence of mechanical and thermal loadings: uniform pressure loading, monotonically increasing-edge displacement, and then a temperature gradient through the thickness. Three types of edge displacements were considered: (1) Edge shortening; (2) edge extension; and (3) edge shear. In all cases considered, the stacking sequence of

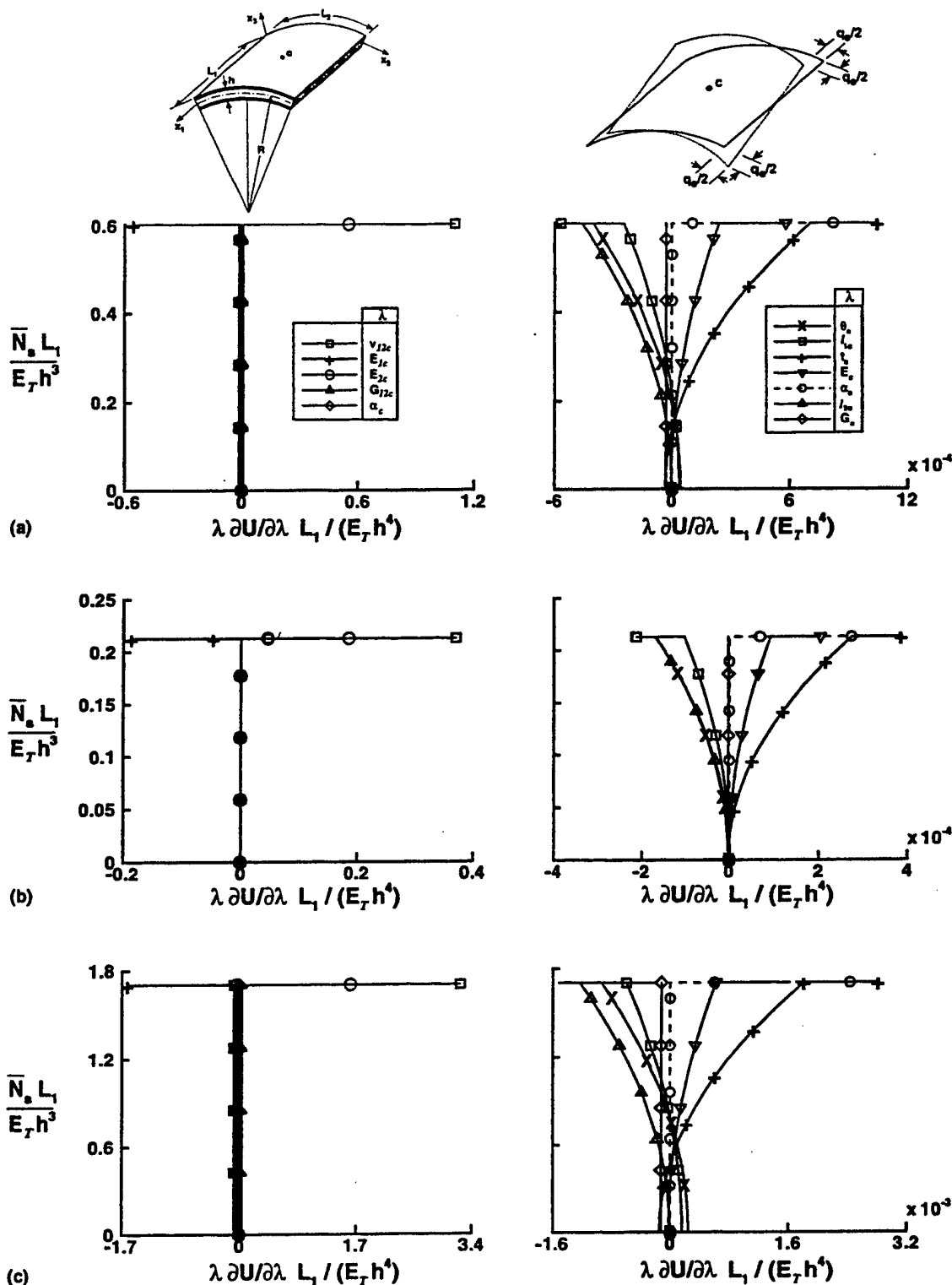


FIG. 15. Effect of Loading and Aspect Ratio on Normalized Sensitivity Coefficients of Total Strain Energy U with Respect to Core Properties; Cylindrical Sandwich Panels, with Honeycomb Core and Composite Eight-Layer Face Sheets, Subjected to Combined Pressure Loading, Edge Shear, and Temperature Gradient through Thickness [$L_1/L_2 =$ (a) 1; (b) 3; (c) 1/3]

the face sheet layers did not have a noticeable effect on either the nonlinear response or the sensitivity coefficients; and the edge displacement had the most pronounced effect on the response.

ACKNOWLEDGMENTS

This work was partially supported by NASA Grant NAG-1-1162 and AFOSR Grant F49620-96-1-0462. The numerical studies were performed on the Cray C-90 computer at NASA Ames Research Center. The authors

acknowledge the assistance of Thea Gaoe of the University of Virginia in preparing the final manuscript and improving the figures.

APPENDIX I. THERMOELASTIC CONSTITUTIVE RELATIONS FOR PANEL

The thermoelastic model used in the present study is based on the following assumptions:

1. The panels are composed of a number of perfectly bonded layers (face sheet layers and core).

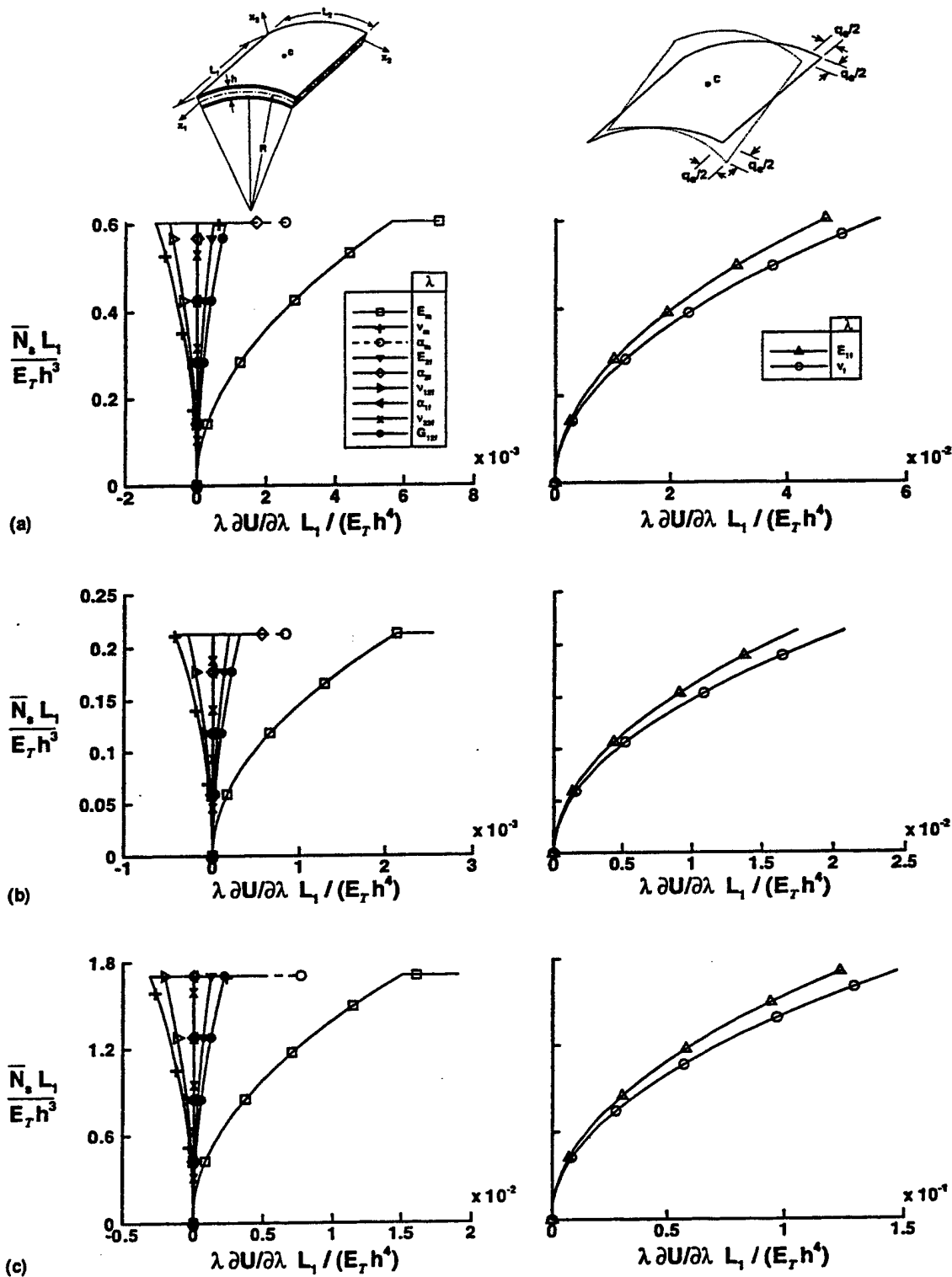


FIG. 16. Effect of Loading and Aspect Ratio on Normalized Sensitivity Coefficients of Total Strain Energy U with Respect to Micro-mechanical Properties of Face Sheet Layers; Cylindrical Sandwich Panels, with Honeycomb Core and Composite Eight-Layer Face Sheets, Subjected to Combined Pressure Loading, Edge Shear, and Temperature Gradient through Thickness [$L_1/L_2 =$ (a) 1; (b) 3; (c) 1/3]

2. A honeycomb core with hexagonal cells is used.
3. The Aboudi cell method is used to evaluate the effective properties of the face sheet layers (Aboudi 1991), and an upper-bound energy approach is used to evaluate the effective core properties (Gibson and Ashby 1988; Burton and Noor 1997).
4. Every point of the panel is assumed to possess a single plane of thermoelastic symmetry parallel to the middle surface of the panel.

5. The material properties are independent of temperature.
6. The constitutive relations for the panel are described by the lamination theory, and can be written in the following compact form:

$$\begin{Bmatrix} N \\ M \\ Q \end{Bmatrix} = \begin{bmatrix} [A] & [B] & 0 \\ [B]^T & [D] & 0 \\ 0 & 0 & [A_s] \end{bmatrix} \begin{Bmatrix} \epsilon \\ \kappa \\ \gamma \end{Bmatrix} - \begin{Bmatrix} N_T \\ M_T \\ 0 \end{Bmatrix} \quad (8)$$

where $\{N\}$, $\{M\}$, $\{Q\}$, $\{\epsilon\}$, $\{\kappa\}$, $\{\gamma\}$, $\{N_T\}$, $\{M_T\}$ = the

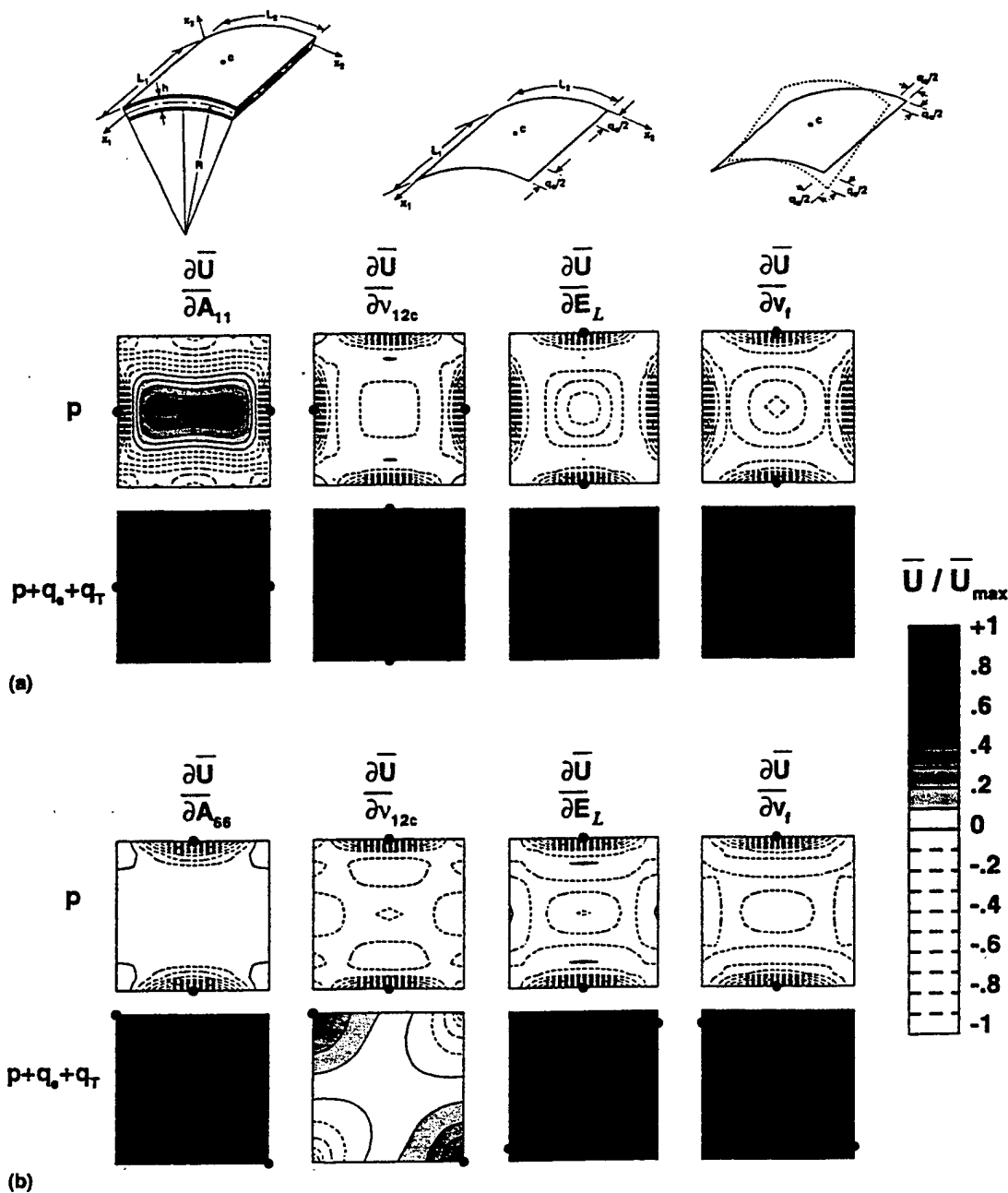


FIG. 17. Normalized Contour Plots Depicting Effect of Loading on Largest Sensitivity Coefficients of Total Strain Energy Density \bar{U} . Cylindrical Sandwich Panels, with Honeycomb Core and Composite Eight-Layer Face Sheets, Subjected to Combined Pressure Loading, Prescribed Edge Displacement, and Temperature Gradient through Thickness (\bullet = Location of Maximum Values); (a) Edge Shortening; (b) Edge Shear

vectors of extensional, bending, and transverse shear stress resultants; strain components and thermal effects of the panel are given by

$$\{N\}' = [N_1 \ N_2 \ N_{12}]; \quad \{M\}' = [M_1 \ M_2 \ M_{12}] \quad (9, 10)$$

$$\{Q\}' = [Q_1 \ Q_2]; \quad \{\epsilon\}' = [\epsilon_1 \ \epsilon_2 \ 2\epsilon_{12}] \quad (11, 12)$$

$$\{\kappa\}' = [\kappa_1 \ \kappa_2 \ 2\kappa_{12}]; \quad \{\gamma\}' = [2\epsilon_{31} \ 2\epsilon_{32}] \quad (13, 14)$$

$$\{N_T\}' = [N_{T1} \ N_{T2} \ N_{T12}] \quad (15)$$

and

$$\{M_T\}' = [M_{T1} \ M_{T2} \ M_{T12}] \quad (16)$$

The matrices $[A]$, $[B]$, $[D]$, and $[A_s]$ contain the extensional, coupling, bending, and transverse shear stiffnesses of the panel that can be expressed in terms of the effective layer stiffnesses as follows:

$$[[A][B][D]] = \sum_{l=1}^{NL} \int_{h_{l-1}}^{h_l} [\bar{Q}^{(l)}][I]x_3[I](x_3)^2[I] dx_3 \quad (17)$$

$$[A_s] = \sum_{l=1}^{NL} \int_{h_{l-1}}^{h_l} [\bar{Q}_s]^{(l)} dx_3 \quad (18)$$

where $[\bar{Q}]^{(l)}$ and $[\bar{Q}_s]^{(l)}$ = the extensional and transverse shear stiffnesses of the l th layer (referred to the x_1, x_2, x_3 coordinate system); $[I]$ = identity matrix; h_l and h_{l-1} are the distances from the top and bottom surfaces of the l th layer to the middle surface; and NL = the total number of layers in the laminate. The expressions for the different coefficients of the matrices $[\bar{Q}]^{(l)}$ and $[\bar{Q}_s]^{(l)}$ in terms of the material and geometric properties of the constituents of the composite face sheets (fiber and matrix) are given by Jones (1975) and Tsai and Hahn

(1980), and for the core they are given by Gibson and Ashby (1988) and Burton and Noor (1997).

The vectors of thermal effects $\{N_T\}$ and $\{M_T\}$ are given by

$$[\{N_T\} \{M_T\}] = \sum_{i=1}^{NL} \int_{h_{i-1}}^{h_i} [\bar{Q}]^{(i)} \{\alpha\}^{(i)} [1 \ x_3] T \, dx_3 \quad (19)$$

where $\{\alpha\}^{(i)}$ is the vector of coefficients of thermal expansion coefficients of the i th layer (referred to the coordinates x_1, x_2, x_3 ; e.g., Padovan 1986; Bert 1975).

APPENDIX II. FORM OF ARRAYS IN GOVERNING DISCRETE EQUATIONS OF PANEL

The governing discrete equations of the panel, (1), consist of both the constitutive relations and the equilibrium equations.

The response vector $\{Z\}$ can be partitioned into subvectors of stress-resultant parameters $\{H\}$, and free (unconstrained) nodal displacements $\{X\}$, as follows:

$$\{Z\} = \begin{Bmatrix} H \\ X \end{Bmatrix} \quad (20)$$

The difference arrays in (1) and (2) can be partitioned as follows:

$$[K] = \begin{bmatrix} F & S_1 \\ S_1^T & 0 \end{bmatrix}; \quad \{G(Z)\} = \begin{Bmatrix} M(X, \bar{X}_e) \\ N(H, X, \bar{X}_e) \end{Bmatrix} \quad (21, 22)$$

$$\{Q^{(2)}\} = \begin{Bmatrix} -[S_2]\{\bar{X}_e\} \\ 0 \end{Bmatrix}; \quad \{Q^{(3)}\} = \begin{Bmatrix} \epsilon_T \\ 0 \end{Bmatrix} \quad (23, 24)$$

$$\begin{bmatrix} \frac{\partial G_i}{\partial Z_j} \end{bmatrix} = \begin{bmatrix} 0 & \frac{\partial M_i}{\partial X_j} \\ \text{Sym} & \frac{\partial N_i}{\partial X_j} \end{bmatrix}; \quad \begin{bmatrix} \frac{\partial G_i}{\partial Z_j} \end{bmatrix} = \begin{bmatrix} -\frac{\partial F}{\partial \lambda} & 0 \\ 0 & 0 \end{bmatrix} \quad (25, 26)$$

$$\begin{bmatrix} \frac{\partial Q^{(2)}}{\partial \lambda} \end{bmatrix} = \begin{Bmatrix} \frac{\partial \epsilon_T}{\partial \lambda} \\ 0 \end{Bmatrix} \quad (27)$$

where $[F]$ = the linear flexibility matrix; $[S_1]$ and $[S_2]$ = the linear strain-displacement matrices associated with the free nodal displacements $\{X\}$, and the constrained (prescribed non-zero) edge displacements $q_e(\bar{X}_e)$; $\{M(X, \bar{X}_e)\}$ and $\{N(H, X, \bar{X}_e)\}$ = the subvectors of nonlinear terms; $\{\epsilon_T\}$ = the subvector of normalized thermal strains; 0 = a null matrix or vector; and superscript t = transposition. The explicit form of $\{\epsilon_T\}$ is given by Noor et al. (1993).

For the purpose of obtaining analytic derivatives with respect to lamination parameters (e.g., fiber orientation angles of different layers), it is convenient to express $\partial[F]/\partial\lambda$ in terms of $\partial[F]^{-1}/\partial\lambda$ as follows:

$$\frac{\partial[F]}{\partial\lambda} = -[F] \frac{\partial[F]^{-1}}{\partial\lambda} [F] \quad (28)$$

The explicit forms of $\partial[F]^{-1}/\partial\lambda$ and $\{\partial\epsilon_T/\partial\lambda\}$ are given by Noor et al. (1993).

Analytic expressions are given in Noor and Tenek (1992) for the laminate stiffnesses $[A]$, $[B]$, $[D]$, and $[A_s]$; the vectors of thermal effects $\{N_T\}$ and $\{M_T\}$; and their derivatives with respect to each of the material properties of the individual layers and fiber orientation angles.

APPENDIX III. REFERENCES

- Aboudi, J. (1991). *Mechanics of composite materials: a unified micro-mechanical approach*. Elsevier Science Publishers BV, Amsterdam, The Netherlands.
Bert, C. W. (1975). "Analysis of plates." Vol. 7—Structural design and

- analysis, part I, C. C. Chamis (ed.), *Composite Materials*, Academic Press, Inc., New York, 149–206.
Bert, C. W. (1995). "Shear deformation and sandwich configuration." *Buckling and postbuckling of composite plates*, G. J. Turvey and I. H. Marshall, eds., Chapman & Hall, Ltd., London, 157–189.
Burton, W. S., and Noor, A. K. (1977). "Assessment of continuum models for sandwich panel honeycomb cores." *Computer Methods in Appl. Mech. and Engrg.*, 145, 341–360.
Gibson, L. J., and Ashby, M. F. (1988). *Cellular solids, structures and properties*. Pergamon Press, Inc., Oxford.
Hoff, N. J. (1986). *Monocoque, sandwich, and composite aerospace structures*. Technomic Publishing Co., Lancaster, Pa.
Jones, R. M. (1975). *Mechanics of composite materials*. McGraw-Hill Inc., New York.
Librescu, L., Lin, W., Nemeth, M. P., and Starnes, J. H. (1995). "Thermomechanical postbuckling of geometrically imperfect flat and curved panels taking into account tangential edge constraints." *J. Thermal Stresses*, 18, 465–482.
Librescu, L., and Souza, M. A. (1993). "Postbuckling of geometrically imperfect shear-deformable flat panels under combined thermal and compressive edge loadings." *J. Appl. Mech.*, 60(June), 526–533.
Noor, A. K. (1994). "Buckling and postbuckling of composite structures." *Proc., Symp. on Buckling and Postbuckling of Compos. Struct.*, ASME Int. Mech. Engrg. Congr. and Exposition, Chicago, Ill., AD Vol. 41/PVP Vol. 293.
Noor, A. K., and Andersen, C. M. (1982). "Mixed models and reduced/selective integration displacement models for nonlinear shell analysis." *Int. J. Numer. Methods in Engrg.*, 18, 1429–1454.
Noor, A. K., and Burton, W. S. (1992). "Computational models for high-temperature multilayered composite plates and shells." *Appl. Mech. Rev.*, 45(10), 419–446.
Noor, A. K., Burton, W. S., and Bert, C. (1996). "Computational models for sandwich panels and shells." *Appl. Mech. Rev.*, 49(3), 155–199.
Noor, A. K., and Peters, J. M. (1983a). "Multiple-parameter reduced basis technique for bifurcation and postbuckling analyses of composite plates." *Int. J. Numer. Methods in Engrg.*, 19, 1783–1803.
Noor, A. K., and Peters, J. M. (1983b). "Recent advances in reduction methods for instability analysis of structures." *Comp. and Struct.*, 16(1–4), 67–80.
Noor, A. K., and Peters, J. M. (1992). "Reduced basis technique for calculating sensitivity coefficients of nonlinear structural response." *AIAA J.*, 30(7), 1840–1847.
Noor, A. K., and Peters, J. M. (1994). "Finite element buckling and postbuckling solutions for multilayered composite panels." *Finite Elements in Analysis and Design*, 15, 343–367.
Noor, A. K., Starnes, J. H. Jr., and Peters, J. M. (1993). "Thermomechanical buckling of multilayered composite panels with cutouts." *J. Compos. Struct.*, 23, 233–251.
Noor, A. K., and Tenek, L. H. (1992). "Stiffness and thermal coefficients for composite laminates." *J. Compos. Struct.*, 21(1), 57–66.
Padovan, J. (1986). "Anisotropic thermal stress analysis." *Thermal stresses I*, R. B. Hetnarski, ed., Elsevier Science Publishers BV, North Holland, Amsterdam, The Netherlands, 143–262.
Tsai, S. W., and Hahn, H. T. (1980). *Introduction to composite materials*. Technomic Publishing Co., Lancaster, Pa.
Turvey, G. J., and Marshall, I. H. (eds.) (1995). *Buckling and postbuckling of composite plates*. Chapman & Hall, Ltd., London.
Zenkert, D. (1995). *An introduction to sandwich construction*. Chameleon Press, London.

APPENDIX IV. NOTATION

The following symbols are used in this paper:

- $[A]$, $[B]$, $[D]$, $[A_s]$ = matrices of the extensional, bending-extensional coupling, bending and transverse shear stiffnesses of the panel, (17) and (18), Appendix I;
 a_{ij} , c_{ik} = coefficients relating panel stiffnesses to effective properties of individual layers, and micromechanical (constituent) properties, respectively, (3) and (4);
 b_{jk} = coefficients relating effective layer properties to the micromechanical properties, (4);
 E_c = elastic modulus of the core material;

E_L, E_T = effective elastic moduli of the individual face sheet layers in the direction of fibers and normal to it, respectively;
 E_m = elastic modulus of the matrix;
 E_{1c}, E_{2c} = effective elastic moduli of the core in the x_1 and x_2 directions;
 E_{1f}, E_{2f} = elastic moduli of the fibers in the longitudinal and transverse directions;
 $[F]$ = linear flexibility matrix of the panel, (21), Appendix II;
 G_c = shear modulus of the core material;
 G_{Lr}, G_{Tr} = effective shear moduli of the individual face sheet layers in the plane of the fibers and normal to it, respectively;
 $\{G(Z)\}$ = vector of nonlinear terms of the panel, (1);
 $G_{12c}, G_{13c}, G_{23c}$ = effective shear moduli of the core in the $x_1 - x_2, x_1 - x_3$, and $x_2 - x_3$ planes;
 G_{12f}, G_m = shear moduli of the fibers and matrix;
 $\{H\}$ = vector of stress-resultant parameters;
 h = total thickness of the sandwich panel;
 $h^{(c)}$ = core thickness;
 h_i, h_{i-1} = distances from the top and bottom surfaces of the i th layer to the middle surface;
 $[K]$ = global linear structural matrix, (1)
 L_1, L_2 = side lengths of the panel in the x_1 and x_2 coordinate directions;
 $l_{1c}, l_{2c}, t_c, \theta_c$ = characteristic lengths, thickness, and angle of a typical hexagonal honeycomb cell;
 $\{M(X, \bar{X}_c)\}$ = subvectors of nonlinear terms, (22), Appendix II;
 $\{N(H, X, \bar{X}_c)\}$ = bending stress resultants;
 M_1, M_2, M_{12}, M_{21} = bending stress resultants;
 $\{N\}, \{M\}$ = vectors of in-plane and bending stress resultants, (8), Appendix I;
 NL = total number of layers in the panel;
 $\{N_T\}, \{M_T\}$ = vectors of thermal forces and moments in the panel, (8), Appendix I;
 \bar{N}_i, \bar{N}_s = total axial force and total shear force on the curved edges of the panel;
 N_1, N_2, N_{12} = in-plane (extensional) stress resultants;
 p = intensity of uniform pressure loading;
 $\{Q\}$ = vector of transverse shear stress resultants;
 $[\bar{Q}]^{(n)}, [\bar{Q}_c]^{(n)}$ = matrices of the extensional and transverse shear stiffnesses of the i th layer of the panel (referred to the x_1, x_2, x_3 coordinate system);
 Q_1, Q_2 = transverse shear stress resultants;
 $\{Q^{(n)}\}, \{Q^{(n)}\}, \{Q^{(n)}\}$ = vectors of normalized mechanical loads, mechanical strains and thermal strains, (1);
 q_c = applied edge displacement;
 q_T = thermal strain parameter associated with $\{Q^{(n)}\}$;
 R = radius of curvature of the middle surface of the panel;
 $[S_1], [S_2]$ = linear strain-displacement matrices associated with the free nodal displacements, $\{X\}$, and the constrained (prescribed nonzero) edge displacements, $q_c, \{\bar{X}_c\}$;
 T_i, T_b = temperature changes at the top and bottom surfaces;
 U = total strain energy of the panel;
 \bar{U} = strain energy density (energy per unit surface area) of the panel;
 \bar{U}_h = transverse shear strain energy density (per unit surface area) of the panel;
 \hat{U}_h = transverse shear strain energy density per unit volume;
 u_1, u_2, w = displacement components in the coordinate directions, Fig. 1;
 v_f = fiber volume fraction;
 $\{X\}$ = vector of free (unknown) nodal displacements;

$\{\bar{X}_c\}$ = normalized vector of constrained (prescribed nonzero) edge displacements;
 x_1, x_2, x_3 = orthogonal coordinate system (x_3 is normal to the middle surface of the panel);
 $\{Z\}$ = response vector of the panel;
 α_c = coefficient of thermal expansion of the core material;
 $\{\alpha\}^{(n)}$ = vector of coefficients of thermal expansion of the i th layer of the panel (referred to the x_1, x_2, x_3 coordinate system);
 α_L, α_T = effective coefficients of thermal expansion of the individual layers of the face sheets in the direction of the fibers and normal to it, respectively;
 α_m = coefficient of thermal expansion of the matrix material;
 α_{1f}, α_{2f} = coefficients of thermal expansion of the fibers in the longitudinal and transverse directions;
 $\{\gamma\}$ = vector of transverse shear strain components of the panel, (8), Appendix I;
 $\{\epsilon\}$ = vector of extensional strain components of the panel, (8), Appendix I;
 $\{\epsilon_T\}$ = thermal strain subvector, (24), Appendix II;
 θ = fiber orientation angles of the individual face sheet layers;
 $\{\kappa\}$ = vector of bending strain components of the panel, (8), Appendix I;
 λ = typical panel, effective layer or micromechanical parameter;
 ν_c = Poisson's ratio of the core material;
 ν_{Lr} = effective major Poisson's ratio of the individual face sheet layers;
 ν_m = Poisson's ratio of the matrix;
 $\nu_{12c}, \nu_{13c}, \nu_{23c}$ = effective Poisson's ratios of the core;
 ν_{12f}, ν_{23f} = Poisson's ratios of the fibers; and
 ϕ_1, ϕ_2 = rotation components of the middle surface of the panel.

Subscripts

f = fiber;
 i' = 1 to the total number of stress-resultant parameters in the model (components of the vector $\{H\}$);
 I, J = 1 to the total number of free nodal displacement components in the model (components of the vector $\{X\}$);
 I, J = 1 to the total number of degrees of freedom (free nodal displacements and stress-resultant parameters) in the model;
 i = 1 to the total number of panel parameters;
 j = 1 to the total number of layer parameters;
 k = 1 to the total number of micromechanical parameters;
 L = direction of fibers;
 l = 1 to the total number of layers, NL ;
 m = matrix;
 T = transverse direction;
 T = thermal; and
 $\beta = 1, 2$.

Superscripts

l = layer;
 m = micromechanical property;
 p = panel property; and
 t = transposition.

Reprinted from

Computer methods in applied mechanics and engineering

Comput. Methods Appl. Mech. Engrg. 147 (1997) 139–145

Predictor–corrector finite element approach for electroelastic
analysis of hybrid composite plates

K. Xu¹, Ahmed K. Noor^{2,*}

*Center for Advanced Computational Technology, University of Virginia, Mail Stop 369, NASA Langley Research Center,
Hampton, VA 23681, USA*

Received 22 August 1996; revised 8 January 1997



COMPUTER METHODS IN APPLIED MECHANICS AND ENGINEERING

EDITORS: J.H. ARGYRIS, STUTTGART and LONDON

T.J.R. HUGHES, STANFORD, CA

J.T. ODEN, AUSTIN, TX

W. PRAGER

Founding Editor

(deceased 1980)

EDITORIAL ADDRESSES

John H. ARGYRIS
Institut für Computer Anwendungen
Pfaffenwaldring 27
D-70569 STUTTGART
Germany
(Editorial Office)

Thomas J.R. HUGHES
Division of
Applied Mechanics
Durand Building
Room No. 281
Stanford University
STANFORD
CA 94305-4040, USA

J. Tinsley ODEN
The University of Texas
The Texas Institute for
Computational and
Applied Mathematics
Taylor Hall 2.400
AUSTIN
TX 78712, USA

ASSOCIATE EDITORS

K. APPA, Hawthorne, CA
I. BABUŠKA, Austin, TX
A.J. BAKER, Knoxville, TN
T. BELYTSCHKO, Evanston, IL
L. DEMKOWICZ, Austin, TX
R.E. EWING, College Station, TX
M. FEINGOLD, Marty-le-Roy

R.H. GALLAGHER, Potsdam, NY
R. GLOWINSKI, Houston, TX
H.-O. KREISS, Los Angeles, CA
J.L. LIONS, Paris
H. LOMAX, Moffet Field, CA
C.E. MASSONNET, Liège

L.S.D. MORLEY, Farnborough
K.S. PISTER, Berkeley, CA
G. STRANG, Cambridge, MA
G.P. VOSKRESENSKY, Moscow
W.H. YANG, Ann Arbor, MI
O.C. ZIENKIEWICZ, Swansea

ADVISORY EDITORS

J.F. ABEL, Ithaca, NY
H. ARMEN, Bethpage, NY
K.J. BATHE, Cambridge, MA
P.G. BERGAN, Høvik
J.F. BESSELING, Delft
G. BORM, Potsdam
H. BUFLER, Stuttgart
H. CABANNES, Paris
C. CANUTO, Torino
G.F. CARRIER, Cambridge, MA
T. CEBECI, Long Beach, CA
A.S.L. CHAN, London
J.L. CHENOT, Valbonne
H. CHRISTIANSEN, Provo, UT
T.J. CHUNG, Huntsville, AL
P.G. CIARLET, Paris
H. COHEN, New York, NY
M.Z. COHN, Waterloo, Ont.
J. DONEA, Ispra
P.R. EISEMAN, New York, NY
B. ENGQUIST, Los Angeles, CA
C.A. FELIPPA, Boulder, CO
K. FENG, Beijing
I. FRIED, Boston, MA
Editorial Secretary: Marties PARSONS

R.A. GELLATLY, San Leandro, CA
M. GERADIN, Liège
R. GRUBER, Manno
K.K. GUPTA, Edwards, CA
R.W. HAMMING, Monterey, CA
F.H. HARLOW, Los Alamos, NM
E.J. HAUG, Iowa City, IA
J.C. HEINRICH, Tucson, AZ
M. HOGGE, Liège
I. HOLLAND, Trondheim
C. JOHNSON, Göteborg
B.Z. KAPLAN, Beer-Sheva
T. KAWAI, Tokyo
J. KESTENS, Brussels
S.W. KEY, La Cañada-Flintridge, CA
W.C. KNUDSON, Sunnyvale, CA
F.A. LECKIE, Santa Barbara, CA
R.W. LEWIS, Swansea
K. LINKWITZ, Stuttgart
LUO Shi-jun, Xi'an
G. MAIER, Milano
J.L. MEEK, St. Lucia, Queensland
A.J. MORRIS, Cranfield
A. NEEDLEMAN, Providence, RI
M.P. NIELSEN, Lyngby

A.K. NOOR, Hampton, VA
R. OHAYON, Paris
P.J. PAHL, Berlin
B. PAUL, Philadelphia, PA
R. PEYRET, Nice
J. PLANCHARD, Clamart
A.R.S. PONTER, Leicester
V.F. POTERASU, Iasi
QIAN Ling-xi (L.H. Tsien), Dalian
A.K. RAO, Bangalore
M. REISER, Rüsschlikon
E. RIKS, Delft
P.J. ROACHE, Albuquerque, NM
G.I.N. ROZVANY, Essen
W. SCHIEHLEN, Stuttgart
B. SCHÖNUNG, Baden
P.S. SYMONDS, Providence, RI
A.B. TEMPLEMAN, Liverpool
C.W. TROWBRIDGE, Kidlington
J.R. WHITEMAN, Uxbridge
K.J. WILLAM, Boulder, CO
Y. YAMADA, Tokyo
Th. ZIMMERMANN, Lausanne

International Standard Serial Number 0045-7825

Copyright © 1997 Elsevier Science S.A. All rights reserved.

0045-7825/97/\$17.00

This journal and the individual contributions contained in it are protected by the copyright of Elsevier Science S.A., and the following terms and conditions apply to their use:

Photocopying

Single photocopies of single articles may be made for personal use as allowed by national copyright laws. Permission of the publisher and payment of a fee is required for all other photocopying, including multiple or systematic copying, copying for advertising or promotional purposes, resale, and all forms of document delivery. Special rates are available for educational institutions that wish to make photocopies for non-profit educational classroom use.

In the USA, users may clear permissions and make payment through the Copyright Clearance Center, 222 Rosewood Drive, Danvers, MA 01923, USA. In the UK, users may clear permissions and make payment through the Copyright Licensing Agency Rapid Clearance Service (CLARCS), 90 Tottenham Court Road, London, W1P 0LP. In other countries where a local copyright clearance centre exists, please contact it for information on required permissions and payments.

Derivative Works

Subscribers may reproduce tables of contents or prepare lists of articles including abstracts for internal circulation within their institutions. Permission of the publisher is required for resale or distribution outside the institution.

Permission of the publisher is required for all other derivative works, including compilations and translations.

Electronic Storage

Permission of the publisher is required to store electronically any material contained in this journal, including any article or part of an article. Contact the publisher at the address indicated.

Except as outlined above, no part of this publication may be reproduced, stored in a retrieval system or transmitted in any form or by any means, electronic, mechanical, photocopying, recording or otherwise, without prior written permission of the publisher.

Disclaimers

No responsibility is assumed by the publisher for any injury and/or damage to persons or property as a matter of products liability, negligence or otherwise, or from any use or operation of any methods, products, instructions or ideas contained in the materials herein.

Although all advertising material is expected to conform to ethical (medical) standards, inclusion in this publication does not constitute a guarantee or endorsement of the quality or value of such product or of the claims made of it by its manufacturer.

© The paper used in this publication meets the requirements of ANSI/NISO Z39.48-1992 (Permanence of Paper).

Printed in The Netherlands



ELSEVIER

Comput. Methods Appl. Mech. Engrg. 147 (1997) 139–145

**Computer methods
in applied
mechanics and
engineering**

Predictor–corrector finite element approach for electroelastic analysis of hybrid composite plates

K. Xu¹, Ahmed K. Noor^{2,*}

Center for Advanced Computational Technology, University of Virginia, Mail Stop 369, NASA Langley Research Center, Hampton, VA 23681, USA

Received 22 August 1996; revised 8 January 1997

Abstract

A predictor–corrector finite element approach is presented for the steady-state (static) electroelastic analysis of multilayered hybrid composite plates. The plates consist of a combination of fiber-reinforced and piezoelectric layers (or patches). The problem is formulated in terms of the displacement components and the electric potential. A two-dimensional finite element model is used in the predictor phase. Linear displacement variation and quadratic electric potential variation are assumed in the thickness direction (five displacement parameters and three electric potential parameters). The functional dependence of the displacement components and the electric potential are then calculated using three-dimensional equations. The corrected quantities are used to obtain better estimates for the different response quantities. The effectiveness of the predictor–corrector approach is demonstrated by numerical examples of five-layer plates consisting of four graphite-epoxy layers and one piezoelectric layer, subjected to transverse mechanical loading and electric potential.

1. Introduction

The potential of combining piezoelectric layers and existing structures to alter the structure's responses through sensing, actuation and control has stimulated interest in the development of theories and computational models for hybrid composite plates consisting of a combination of fiber-reinforced and piezoelectric layers [1–5]. Finite element models have been used in predicting the response of hybrid composite plates. A number of different classifications of these finite element models can be made based on the continuum theories used (e.g. incorporating or neglecting the couplings between different fields), and the through-the-thickness approximations made. Some of the finite element models developed for hybrid composite plates are similar to those used for laminated fibrous composites and include: (a) three-dimensional electroelasticity models (see e.g. [6,7]); (b) two-dimensional models, which can be classified into: (1) global through-the-thickness approximation models (see e.g. [8–12]) and (2) discrete-layer models based on piecewise displacement/stress approximations in the thickness direction (see e.g. [13,14]).

The use of three-dimensional models for predicting the electroelastic response characteristics of plates with complicated geometry is computationally expensive and, therefore, may not be feasible for practical problems. Experience with two-dimensional models has shown them to be inadequate for the

* Corresponding author.

¹ Research Associate.

² Ferman W. Perry Professor of Aerospace Structures and Applied Mechanics, and Director.

accurate predictions of transverse response quantities. This is particularly true for the models based on low-order approximations of the response quantities in the thickness direction. The use of predictor-corrector approaches, in conjunction with analytic solutions, for electroelastic plates was shown to alleviate this problem [15]. The procedure uses a two-dimensional theory in the predictor phase. The functional dependence of the fundamental unknowns on the thickness coordinate is calculated using three-dimensional equations, and then is used in the corrector phase to obtain better estimates for the different response quantities.

The present study extends the predictor-corrector approach to finite element models. The plates considered consist of a combination of perfectly-bonded fiber-reinforced and piezoelectric layers. Numerical results are presented for five-layer plates consisting of four graphite-epoxy layers and one piezoelectric layer, subjected to transverse mechanical loading and electric potential.

2. Mathematical formulation

Fig. 1 shows the geometric characteristics of the hybrid multilayered plates considered herein as follows: L_1 and L_2 are the side lengths in the x_1 and x_2 directions, and h is the total thickness of the plate. The plate has combinations of anisotropic elastic layers and piezoelectric layers (or patches). The fundamental equations of the three-dimensional equations of electroelasticity theory for the piezoelectric materials are given in Appendix A.

2.1. Two-dimensional theory

A global-approximation, two-dimensional theory is used herein. The multilayered plate is replaced by an equivalent single-layer anisotropic plate. The displacement component is assumed to be independent of x_3 . The displacement components $\{u_1, u_2\}$ and the electric potential ϕ are assumed to have a linear and quadratic variation, respectively, in the thickness direction (see e.g. [4,5]) as follows:

$$u_1 = u_1^{(0)} + x_3 u_1^{(1)}, \quad u_2 = u_2^{(0)} + x_3 u_2^{(1)}, \quad u_3 = u_3^{(0)} \quad (1)$$

$$\phi = \phi^{(0)} + x_3 \phi^{(1)} + x_3^2 \phi^{(2)} \quad (2)$$

where the five displacement parameters $u_1^{(0)}, u_1^{(1)}, u_2^{(0)}, u_2^{(1)}, u_3^{(0)}$, and the three electric potential parameters $\phi^{(0)}, \phi^{(1)}$ and $\phi^{(2)}$ are functions of x_1 and x_2 only. Note that the five displacement parameters are the same ones used in the first-order shear deformation theory of plates. The eight parameters (five displacement and three electric potential parameters) are determined from the finite element analysis.

The predictor-corrector procedure used is an iterative process in which the information obtained in the first (predictor) phase of the analysis is used to correct the thickness distributions of the

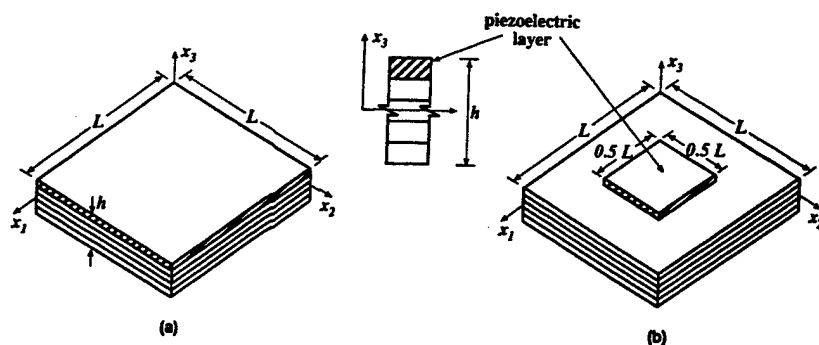


Fig. 1. Hybrid multilayered composite plates in the present study.

displacement components and the electric potential, and hence, improve the response predictions. The expressions for the fundamental unknowns are cast in the following compact form:

$$\begin{aligned} u_1 &= \sum_{j=1}^4 u_{1j} g_{1j}(x_3), & u_2 &= \sum_{j=1}^4 u_{2j} g_{2j}(x_3) \\ u_3 &= \sum_{l=1}^3 u_{3l} g_{3l}(x_3), & \phi &= \sum_{j=1}^4 \phi_j g_{4j}(x_3) \end{aligned} \quad (3)$$

where the functions $g_{KJ}(x_3)$ ($K=1, 2, 4$; $J=1, 2, 3, 4$) are the symmetric and antisymmetric components of the response functions in the two-dimensional theory used in the predictor phase, and the correction functions generated by using three-dimensional divergence equations and constitutive relations. The function $g_{3J}(x_3)$ ($J=1, 2, 3$) corresponds to the associated response function from the two-dimensional theory and the symmetric and antisymmetric components of the correction functions for u_3 . The fifteen parameters, u_{1j} , u_{2j} , ϕ_j ($J=1, 2, 3, 4$), and u_{3l} ($l=1, 2, 3$), are unknown functions of the coordinates x_1 and x_2 only, and are determined from the finite element analysis.

2.2. Finite element approximation

The weak (variational) form of the governing equations for the plate can be cast in the following form [16]

$$\int_V [\sigma_{ij,i} \delta u_j + d_{i,i} \delta \phi] dV - \int_S [(n_i \sigma_{ij} - t_j) \delta u_j + (n_i d_i - s) \delta \phi] dS = 0 \quad (4)$$

where σ_{ij} are the stress components; d_i are the electric displacement components; ϕ is the electric potential; t_i and s are the traction and electric charge on the surface of the electroelastic plate; δ is the variational operator; and the repeated indices i and j denote summation over their entire range (1 to 3). The relations between the electric potential ϕ and the electric field components E_i are given in Appendix A.

The stresses and electric displacement components in Eq. (4) are expressed in terms of the displacement and electric potential parameters of Eq. (1) using Eqs. (A.1)–(A.6) in Appendix A. The finite element discretization is performed by dividing the plate into elements and approximating each of the displacement and electric potential parameters by products of C^0 shape functions and nodal parameters. In the present study, biquadratic Lagrangian shape functions are used (a total of 72 nodal parameters for each element, in the predictor phase).

3. Numerical studies

To assess the effectiveness of the predictor–corrector finite element approach a number of hybrid composite plates were analyzed by using this approach. Herein, numerical results are presented for square five-layered plates ($L_1 = L_2 = L$), consisting of four graphite-epoxy layers with fiber orientation ($90^\circ/0^\circ/90^\circ/0^\circ$ —with the fibers of the bottom layer in the x_1 direction) and one PZT-5A piezoelectric layer (at the top). The layers are assumed to have equal thickness. The plates are shown in Fig. 1 and the material properties for the graphite-epoxy and piezoelectric layers are given in Table 1.

Two configurations of the piezoelectric layer are considered. In the first, the piezoelectric layer covers the entire composite plate (Fig. 1(a)) and in the second the piezoelectric layer partially covers the plate (Fig. 1(b)). The thickness ratio, h/L , of the plate was selected to be 0.1. Two different loadings with unit amplitude are applied to the plate, namely: transverse mechanical loading acting on the bottom surface $q = \sin(\pi x_1/L_1) \sin(\pi x_2/L_2)$ and electric potential acting on the bottom surface $\phi = \sin(\pi x_1/L_1) \sin(\pi x_2/L_2)$. Henceforth, for brevity, the two loading cases will be referred to as the q -case and the E -case, respectively.

The solutions obtained by the two-dimensional finite element (used in the predictor phase) and the predictor–corrector approach are compared with the exact three-dimensional solutions for plate

Table 1
Material properties of the graphite-epoxy and PZT-5A layers used in the present study

Graphite-epoxy layer		PZT-5A layer	
E_L (10^9 Pa)	181	\hat{E}_1 (10^9 Pa)	61.0
E_T (10^9 Pa)	10.3	\hat{E}_2 (10^9 Pa)	61.0
		\hat{E}_3 (10^6 Pa)	53.2
G_{LT} (10^9 Pa)	7.17	G_{12} (10^9 Pa)	22.6
		G_{13} (10^9 Pa)	21.1
G_{TT} (10^9 Pa)	2.87	G_{23} (10^9 Pa)	21.1
ν_{LT}	0.28	ν_{12}	0.35
		ν_{13}	0.38
ν_{TT}	0.33	ν_{23}	0.38
d_{31} (10^{-12} m/V)	0	d_{31} (10^{-12} m/V)	-171
d_{32} (10^{-12} m/V)	0	d_{32} (10^{-12} m/V)	-171
d_{33} (10^{-12} m/V)	0	d_{33} (10^{-12} m/V)	374
d_{24} (10^{-12} m/V)	0	d_{24} (10^{-12} m/V)	584
d_{15} (10^{-12} m/V)	0	d_{15} (10^{-12} m/V)	584
κ_{11} (10^{-8} farads/m)	1.53	κ_{11} (10^{-8} farads/m)	1.53
κ_{22} (10^{-8} farads/m)	1.53	κ_{22} (10^{-8} farads/m)	1.53
κ_{33} (10^{-8} farads/m)	1.53	κ_{33} (10^{-8} farads/m)	1.50

Note: The subscripts L and T refer to the fiber and transverse directions for each individual layer, respectively.

configuration 'a' (see [15]), and with the predictions of the ANSYS commercial finite element code (using solid 5 elements to model the plate) for plate configuration 'b'. The results are shown in Figs. 2–5, in which the two-dimensional finite element and predictor–corrector solutions are referred to as 2D and PC, respectively.

The thickness distributions of the electric potential ϕ , the electric field component E_3 , the stress components σ_{11} at $x_1 = L/2$ and $x_2 = L/2$, and σ_{13} at $x_1 = L/2$ and $x_2 = 0$ for plate configuration 'a' are shown in Figs. 2 and 3. The thickness distributions of ϕ and σ_{11} for plate configuration 'b' are shown in

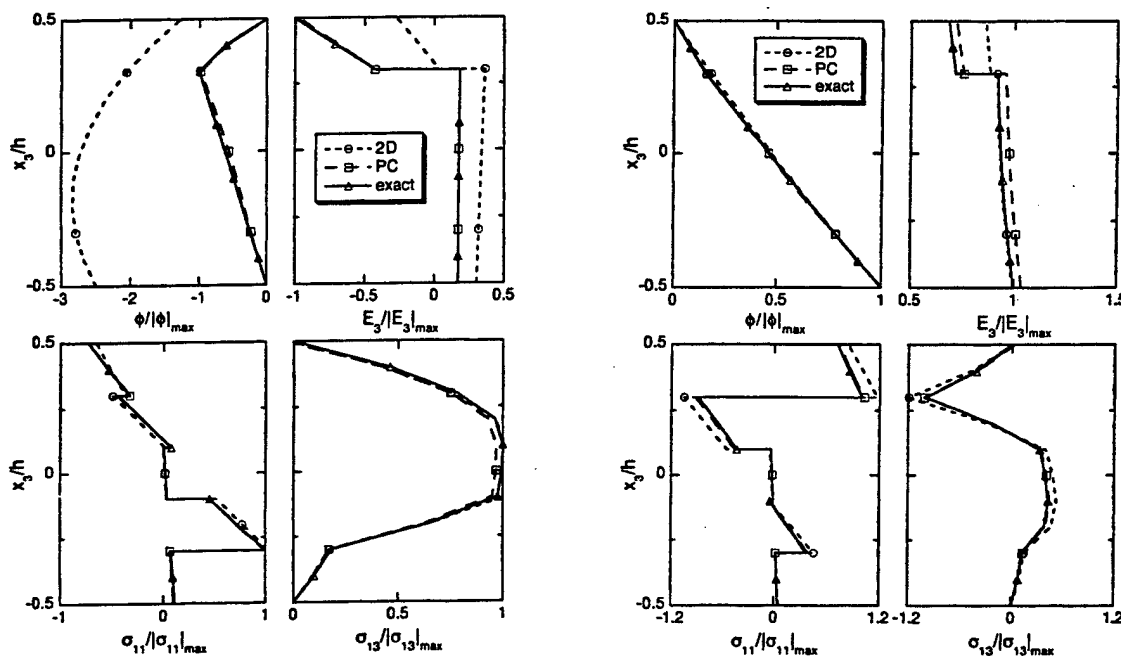


Fig. 2. Through-the-thickness distribution of electric potential ϕ , transverse electric field component E_3 , and stress components σ_{11} and σ_{13} . Hybrid multilayered plate subjected to mechanical load $q = \sin(\pi x_1/L_1) \sin(\pi x_2/L_2)$ shown in Fig. 1(a), $h/L = 0.1$.

Fig. 3. Through-the-thickness distribution of electric potential ϕ , transverse electric field component E_3 , and stress components σ_{11} and σ_{13} . Hybrid multilayered plate subjected to electric potential $\phi = \sin(\pi x_1/L_1) \sin(\pi x_2/L_2)$ shown in Fig. 1(a), $h/L = 0.1$.

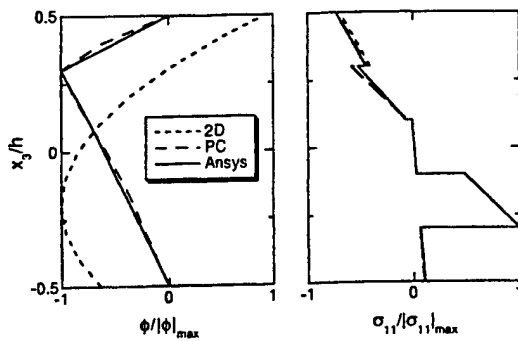


Fig. 4. Through-the-thickness distribution of electric potential ϕ and stress σ_{11} . Hybrid multilayered plate subjected to mechanical load $q = \sin(\pi x_1/L_1) \sin(\pi x_2/L_2)$ shown in Fig. 1(b) $h/L = 0.1$.

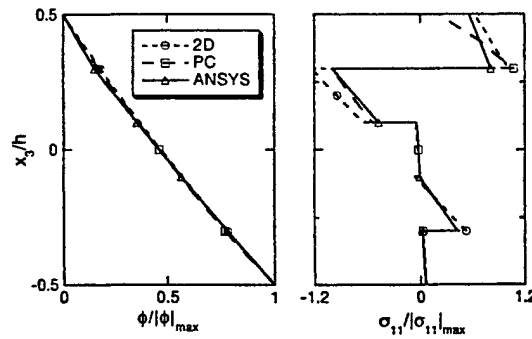


Fig. 5. Through-the-thickness variations of electric potential ϕ and stress σ_{11} . Hybrid multilayered plate subjected to electric potential $\phi = \sin(\pi x_1/L_1) \sin(\pi x_2/L_2)$ shown in Fig. 1(b) $h/L = 0.1$.

Figs. 4 and 5. Each of the response quantities is normalized by dividing it by its maximum absolute value, obtained from the three-dimensional solution for configuration 'a' or from the ANSYS finite element code (for configuration 'b'). An examination of Figs. 2–5 reveals:

- (1) The response quantities obtained by the predictor–corrector approach are in close agreement with the exact three-dimensional solution for plate configuration 'a' and with the ANSYS predictions for configuration 'b'.
- (2) For the q -case, the electric potential ϕ and electric field component E_3 obtained by the 2D finite element model (predictor phase) were grossly in error. The stress components σ_{11} and σ_{13} obtained by the 2D finite element model were qualitatively similar to the exact solution, though have noticeable error.
- (3) For the E -case of plate configuration 'a', the electric field component E_3 and the stress components σ_{11} and σ_{13} obtained by the 2D finite element model are inaccurate, particularly in the piezoelectric layer. The electric field component E_3 obtained by the predictor–corrector approach had a small but noticeable error. The accuracy of the transverse component of the electric field and the stress components can be improved by using more iterations in the corrector phase.
- (4) For configuration 'b', the electric potential obtained by the predictor–corrector approach is in close agreement with that obtained by the ANSYS finite element code for both loading cases. For the q -case, the electric potential obtained by the 2D finite element method is significantly different from those obtained by both the predictor–corrector approach and the ANSYS prediction.

4. Concluding remarks

A predictor–corrector finite element approach is presented for the steady-state (static) electroelastic analysis of multilayered hybrid composite plates. The plates consist of a combination of fiber-reinforced and piezoelectric layers (or patches). Two-dimensional finite element model with linear displacement variation and quadratic variation for the electric potential in the thickness direction is used in the predictor phase. The functional dependence of the displacement components and the electric potential are calculated using three-dimensional equations in corrector phase, and are then used to correct the different response quantities.

Numerical studies are presented for five-layer plates consisting of four graphite-epoxy layers and one piezoelectric layer. The solutions are compared with exact three-dimensional solutions and with the predictions of the ANSYS finite element code. Both the response quantities obtained in the predictor and corrector phases are presented. The transverse component of the electric field and electric potential obtained by the finite element model used in the predictor phase were inaccurate. By contrast, all the

response quantities obtained after the corrector phase are in close agreement with the exact three-dimensional solution and with the ANSYS predictions.

Acknowledgment

The present work is partially supported by NASA Cooperative Agreement NCCW-0011 and by Air Force Office of Scientific Research Grant F49620-96-1-0462. The authors acknowledge useful discussions with Samuel L. Venneri of NASA Headquarters. The material properties for PZT-5A used in the present study were obtained from Morgan Matroc, Inc., Bedford, Ohio.

Appendix A. Fundamental equations of the three-dimensional electroelasticity theory

The equations governing the steady-state (static) linear response of an electroelastic medium can be grouped into three sets of equations; namely, divergence equation, gradients relations, and constitutive relations, as follows [16]:

Divergence equations

$$\sigma_{ji,j} = 0 \quad (\text{A.1})$$

$$d_{i,j} = 0 \quad (\text{A.2})$$

Gradient relations

$$\epsilon_{ij} = \frac{1}{2} (u_{i,j} + u_{j,i}) \quad (\text{A.3})$$

$$E_j = -\phi_{,j} \quad (\text{A.4})$$

Constitutive relations

$$\sigma_{ij} = C_{ijkl}\epsilon_{kl} - e_{lij}E_l \quad (\text{A.5})$$

$$d_i = e_{ikl}\epsilon_{kl} + \kappa_{ii}E_l \quad (\text{A.6})$$

In Eqs. (A.1)–(A.6), σ_{ij} , ϵ_{ij} and u_i ($i = 1, 2, 3$) are the stress, strain and displacement components, respectively; d_i and E_i are the electric displacement and the electric field components, respectively; ϕ is the electric potential; C_{ijkl} are material stiffness coefficients; e_{lij} are piezoelectric coefficients; and κ_{ii} are permittivities.

References

- [1] T. Bailey and J.E. Hubbard, Distributed piezoelectric-polymer active vibration control of a cantilever beam, *J. Guid. Dynam. Control* 8(6) (1985) 605–611.
- [2] E. Crawley and J. de Luis, Use of piezoelectric actuators as element of intelligent structures, *AIAA J.* 25(10) (1987) 1373–1385.
- [3] C.K. Lee and F.C. Moon, Laminated piezopolymer plates for torsion and bending sensors and actuators, *J. Acoust. Soc. Am.* 85(6) (1989) 2432–2439.
- [4] N.N. Rogacheva, *The Theory of Piezoelectric Shells and Plates* (CPC Press, Boca Raton, FL, 1994).
- [5] M. Bernadou and C. Haenel, On the numerical analysis of general piezoelectric thin shells, in: S.N. Atluri et al., eds., *Proc. Int. Conf. on Computational Engineering Science*, July 30–August 3, 1995, HI.
- [6] H.S. Tzou and C.I. Tseng, Distributed piezoelectric sensor/actuator design for dynamic measurement/control of distributed parameter systems: A piezoelectric finite element approach, *J. Sound Vib.* 138(1) (1990) 17–34.
- [7] P. Gaudenzi and K.J. Bathe, Iterative finite element procedure for the analysis of piezoelectric continua, *J. Intelligent Material Systems and Structures* 6(2) (1995) 266–273.
- [8] K. Chandrashekhara and A.N. Agarwal, Active vibration control of laminated composite plates using piezoelectric devices: A finite element approach, *J. Intell. Mater. Syst. Struct.* 4 (1993) 496–508.

- [9] D.K. Shah, W.S. Chan and S.P. Joshi, Finite element analysis of plates with piezoelectric layers, AIAA-93-1678-CP (1993) 3189–3197.
- [10] W.S. Hwang, H.C. Park and W. Hwang, Vibration control of a laminated plate with piezoelectric sensor/actuator: Finite element formulation and modal analysis, *J. Intell. Mater. Syst. Struct.* 4 (1993) 317–329.
- [11] K.D. Jonnalagadda, G.E. Blandford and T.R. Tauchert, Piezothermoelastic composite plate analysis using first-order shear-deformation theory, *Comput. Struct.* 51 (1994) 79–89.
- [12] K.D. Jonnalagadda, T.R. Tauchert and G.E. Blandford, High-order displacement formulation for a piezothermoelastic laminate, *Mech. Electromag. Mater. Struct.*, ASME, AMD-Vol. 161/MD-Vol. 42 (1993) 145–159.
- [13] D.H. Robbins and J.N. Reddy, Analysis of piezoelectrically actuated beams using a layer-wise displacement theory, *Comput. Struct.* 41(2) (1991) 265–279.
- [14] P. Heyliger, G. Ramirez and D. Saravanos, Coupled discrete-layer finite elements for laminated piezoelectric plates, *Comm. Numer. Methods Engrg.* 10 (1994) 971–981.
- [15] Y.Y. Tang, A.K. Noor and K. Xu, Assessment of computational models for thermoelectroelastic multilayered plates, *Comput. Struct.* 61(5) (1996) 915–933.
- [16] R.D. Mindlin, High frequency vibrations of piezoelectric crystal plates, *Int. J. Sol. Struct.* 8 (1972) 895–906.

INFORMATION FOR CONTRIBUTORS

Manuscripts should be sent in triplicate to one of the Editors. All manuscripts will be refereed. Manuscripts should preferably be in English. They should be typewritten, double-spaced, first copies (or clear Xerox copies thereof) with a wide margin. Abstracts, footnotes and lists of references should also be double-spaced. All pages should be numbered (also those containing references, tables and figure captions). Upon acceptance of an article, author(s) will be asked to transfer copyright of the article to the publisher. This transfer will ensure the widest possible dissemination of information.

Abstracts

The text of a paper should be preceded by a summary in English. This should be short, but should mention all essential points of the paper.

Figures and tables

The drawings for the figures must be originals, drawn in black India ink in large size and carefully lettered, or printed on a high-quality laser printer. The lettering as well as the details should have proportionate dimensions, so as not to become illegible or unclear after the usual reduction by the printers; in general, the figures should be designed for a reduction factor of two or three. Mathematical symbols should be entered in italics, where appropriate. Each figure should have a number and a caption; the captions should be collected on a separate sheet. The appropriate place of a figure should be indicated in the margin. Tables should be typed on separate sheets. Each table should have a number and a title. The appropriate places for the insertion of tables should be indicated in the margin. Colour illustrations can be included and will be printed in colour at no charge if, in the opinion of the Editors, the colour is essential. If this is not the case, the figures will be printed in black and white unless the author is prepared to pay the extra costs arising from colour reproduction.

Formulae

Displayed formulae should be numbered and typed or clearly written by hand. Symbols should be identified in the margin, where they occur for the first time.

References

In the text, reference to other parts of the paper should be made by section (or equation) number, but not by page number. References should be listed on a separate sheet in the order in which they appear in the text.

COMPLETE INSTRUCTIONS TO AUTHORS are published in every last issue of a volume, and copies can also be obtained from the Editors and the Publisher, Elsevier Science B.V., P.O. Box 1991, 1000 BZ Amsterdam, The Netherlands.

Instructions for LaTeX manuscripts

The LaTeX files of papers that have been accepted for publication may be sent to the Publisher by e-mail or on a diskette (3.5" or 5.25" MS-DOS). If the file is suitable, proofs will be produced without rekeying the text. The article should be encoded in Elsevier-LaTeX, standard LaTeX, or AMS-LaTeX (in document style "article"). The Elsevier-LaTeX package, together with instructions on how to prepare a file, is available from the Publisher. This package can also be obtained through the Elsevier WWW home page (<http://www.elsevier.nl/>), or using anonymous FTP from the Comprehensive TeX Archive Network (CTAN). The host-names are: <ftp.dante.de>, <ftp.tex.ac.uk>, <ftp.shsu.edu>; the CTAN directories are: [/pub/tex/macros/latex209/contrib/elsevier](#), [/pub/archive/macros/latex209/contrib/elsevier](#), [/tex-archive/macros/latex209/contrib/elsevier](#), respectively. No changes from the accepted version are permissible, without the explicit approval of the Editor. The Publisher reserves the right to decide whether to use the author's file or not. If the file is sent by e-mail, the name of the journal should be mentioned in the "subject field" of the message to identify the paper. Authors should include an ASCII table (available from the Publisher) in their files to enable the detection of transmission errors.

The files should be mailed to: Elsevier Editorial Services, Mayfield House, 256 Banbury Road, Oxford OX2 7DH, UK. Fax: +44-1865-314990. E-mail: ees@elsevier.co.uk.

Publication information:

Computer Methods in Applied Mechanics and Engineering (ISSN 0045-7825). For 1997 volumes 140–150 are scheduled for publication. Subscription prices are available upon request from the Publisher. Subscriptions are accepted on a prepaid basis only and are entered on a calendar year basis. Issues are sent by surface mail except to the following countries where Air delivery via SAL mail is ensured: Argentina, Australia, Brazil, Canada, Hong Kong, India, Israel, Japan, Malaysia, Mexico, New Zealand, Pakistan, PR China, Singapore, South Africa, South Korea, Taiwan, Thailand, USA. For all other countries airmail rates are available upon request. Claims for missing issues should be made within six months of our publication (mailing) date.

Orders, claims, and product enquiries

Please contact the Customer Support Department at the Regional Sales Office nearest you:

New York
Elsevier Science
P.O. Box 945
New York, NY 10159-0945
USA
Tel. (+1)212-633-3730
[Toll free number for North
American customers:
1-888-4ES-INFO (437-4636)]
Fax (+1)212-633-3680
e-mail usinfo-f@elsevier.com

Amsterdam
Elsevier Science
P.O. Box 211
1000 AE Amsterdam
The Netherlands
Tel. (+31)20-4853757
Fax (+31)20-4853432
e-mail nlinfo-f@elsevier.nl

Tokyo
Elsevier Science
9-15 Higashi-Azabu 1-chome
Minato-ku, Tokyo 106
Japan
Tel. (+81)3-5561-5033
Fax (+81)3-5561-5047
e-mail kyf04035@niftyserve.or.jp

Singapore
Elsevier Science
No. 1 Temasek Avenue
#17-01 Millenia Tower
Singapore 039192
Tel. (+65)434-3727
Fax (+65)337-2230
e-mail asiainfo@elsevier.com.sg

Advertising information

Advertising orders and enquiries may be sent to: **International:** Elsevier Science, Advertising Department, The Boulevard, Langford Lane, Kidlington, Oxford OX5 1GB, UK, Tel. (+44)(0)1865 843565, Fax (+44)(0)1865 843976. **USA and Canada:** Weston Media Associates, Daniel Lipner, P.O. Box 1110, Greens Farms, CT 06436-1110, USA, Tel. (+1)(203)261-2500, Fax (+1)(203)261-0101. **Japan:** Elsevier Science Japan, Marketing Services, 1-9-15 Higashi-Azabu, Minato-ku, Tokyo 106, Japan, Tel. (+81)3-5561-5033; Fax (+81)3-5561-5047.



Computational structures technology: leap frogging into the twenty-first century

Ahmed K. Noor

Center for Advanced Computational Technology, University of Virginia, NASA Langley Research Center, Hampton, VA 23681, USA

Received 1 December 1998; accepted 10 March 1999

Abstract

The history, recent developments and trends in computational structures technology (CST) are summarized. Discussion focuses on development of CST software and goals of CST activities. Some recent advances in a number of CST areas are described, including discretization techniques and element technology; computational material modeling; modeling of composite, sandwich and smart structures; computational tools and methodologies for life management; transient response analysis; numerical simulation of frictional contact/impact response; articulated structural dynamics; non-deterministic modeling and analysis methods; qualitative analysis and simulation; neuro-computing; hybrid techniques; error estimation and adaptive improvement strategies; strategies for solution of coupled problems; sensitivity analysis; integrated analysis and design; strategies and numerical algorithms for new computing systems; model generation facilities; and application of object-oriented technology. Research areas in CST that have high potential for meeting the future technological needs are identified. Published by Elsevier Science Ltd.

1. Introduction

Computational structures technology (CST) blends the insightful modeling of structural response with the development of computational methods. CST is an outgrowth of matrix and finite element methods of structural analysis that were developed over the past five decades. Brief historical reviews of the finite element method are given in two articles [1,2]. Computing technology is the technological foundation of CST. The advances made in computer hardware, firmware and software have significantly impacted all aspects of CST development. Current CST activities include computational material modeling, computational methods for predicting the response, performance, failure and life of structures and their components, and automated methods of structural synthesis and optimization.

Application of CST to contemporary structures pro-

blems typically involves a sequence of five steps: observation of the response phenomena of interest; development of computational models for the numerical simulation of these phenomena; development and assembly of software and/or hardware to implement the computational models; post-processing and interpretation of the predictions of the computational models; and utilization of the computational models in the analysis and design of structures (Fig. 1).

Development of a computational model includes selection of the mathematical model that describes the phenomena; mathematical analysis of the model to ensure that the problem is properly formulated; testing the range of validity of the model; and development of a discrete model, computational strategy, and numerical algorithms to approximate the mathematical model. Successful computational models for structures are those based on thorough familiarity with the response phenomena being simulated and a good under-

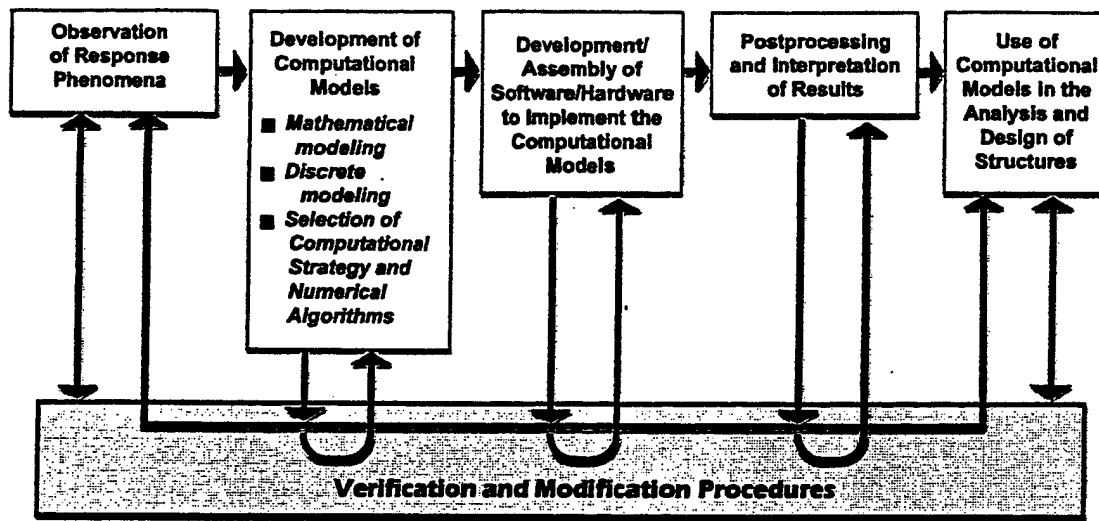


Fig. 1. Application of CST to practical structural problems.

standing of the mathematical models available to describe them.

Within the aforementioned general framework, CST is currently being used in a broad range of applications including aerospace, automotive, naval, and nuclear structures. Reviews of some of the activities in the US and European aerospace industries are given in Refs. [3,4]. Other industrial applications of CST are described in Refs. [5,6]. Large structural calculations performed to date account for complicated geometry, complex loading history and material behavior.

Computational structures technology represents one

of the most significant developments in the history of the structures field. Its use has transformed much of theoretical structural mechanics and materials science into practical tools that affect all phases of the design, fabrication and testing of engineering systems. Although CST led the way among computational aero-sciences until the 1970s, the emphasis has shifted in the early 1980s to other disciplines, particularly computational fluid dynamics. However, since the late 1980s, there has been renewed interest in CST. There are three compelling motivations for vigorously pursuing CST development: the practical problems awaiting sol-

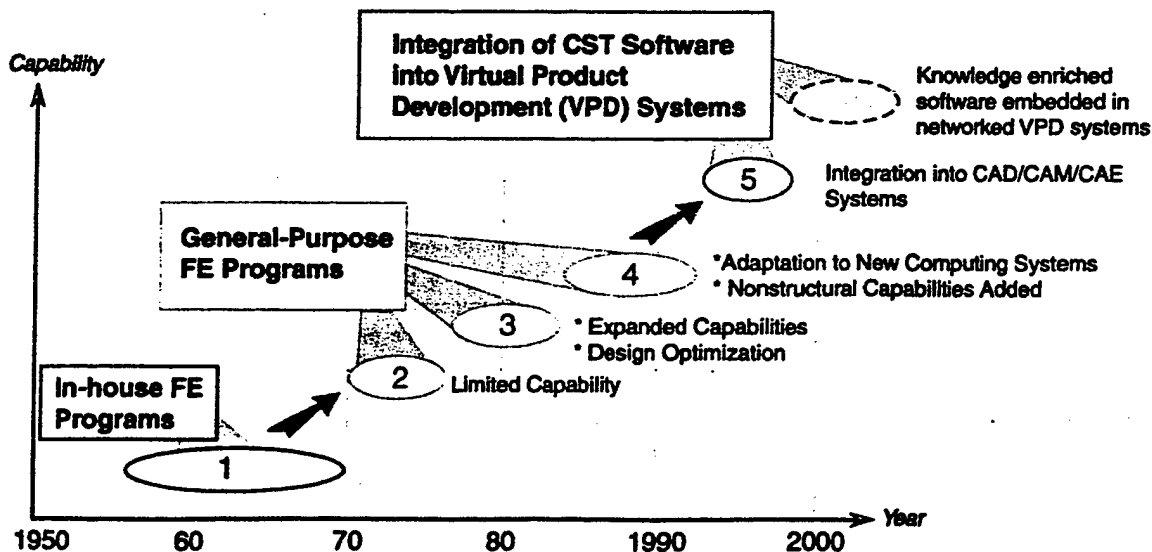


Fig. 2. Evolution of CST software.

utions; the need for reducing dependence on extensive and costly testing; and the desire to use the power of new and emerging computing paradigm in the design and operation of future engineering structures.

A number of survey papers and monographs have been written on various aspects of computational structures technology [7–10]. Also, a number of workshops and symposia have been devoted to CST and proceedings have been published (for example, Refs. [11–15]). The objectives of the present paper are to present a brief review of the history of the development of CST software, summarize some of the recent developments and trends in CST, and identify research areas in CST that have high potential for meeting future technological needs. The number of publications on CST has been steadily increasing, and a vast amount of literature currently exists on various aspects and applications of CST. The cited references illustrate the ideas presented and are not necessarily the only significant contributions to the subject. The discussion in this paper is kept on a descriptive level and for the details the reader is referred to the cited literature.

2. Brief history of the development of CST software

Development of CST software spans a period of less than fifty years and may be divided into five stages, each of the first four stages lasting approximately eight to twelve years, and the fifth stage lasting four to five years (Fig. 2). In the first stage (during the 1950s and 1960s) the aircraft industry pioneered development of in-house finite element programs. These programs were generally based on the force method of analysis and were used to automate analysis of highly redundant structural components. Subsequent efforts in industry and academia led to development of simple two- and three-dimensional finite elements based on the displacement formulation. The variational process for formulating the elemental matrices was also introduced during this period.

In the second stage, general-purpose finite element programs such as NASTRAN, ASKA, ANSYS, STARDYNE, MARC, SAP, SESAM and SAMCEF were released for public use in the U.S. and Europe. These programs brought a significant technology base that led to the development of numerous commercial finite element software systems. Technology development during the second stage included mixed and hybrid finite element models, with the fundamental unknowns consisting of stress and displacement parameters; efficient numerical algorithms for solution of algebraic equations and extraction of eigenvalues and substructuring and modal synthesis techniques for handling large problems. The finite element method's success in linear static problems has encouraged bolder

applications to nonlinear and transient response problems.

The third stage involved refining the commercial software codes and expanding their technology base. Design optimization techniques were also developed during this stage as were pre- and post-processing software and computer-aided design (CAD) systems. The technology development included singular elements for fracture mechanics applications; boundary element techniques; coupling of finite elements with other discretization techniques such as boundary elements; and quality assurance methods for both software and finite element models.

The fourth stage included the adaptation of CST software to new computing systems (vector, multiprocessor, and parallel machines); development of efficient computational strategies and numerical algorithms for these machines; widespread availability of CST software on workstations, personal computers and laptop computers; and the addition of substantial nonstructural modeling and analysis capabilities to CST software systems such as MSC/NASTRAN and ANSYS. The latter capabilities were added because current high-performance engineering systems (e.g., high performance aircraft and micro-sized spacecraft) require significant interactions between CST and other disciplines such as aerodynamics, controls, acoustics, electromagnetics, and optics.

Technology development in the fourth stage included introduction of advanced material models; development of stochastic models and probabilistic methods for structural analysis and design; and development of facilities for quality assessment and control of numerical simulations.

The fifth stage started around the mid-1990s and involved integration of CST and other simulation software into CAD/CAM/CAE systems to provide a complete virtual product facility. Parametric, variational and feature-based solid modeling methods are combined to generate a single 'smart' product model. This eliminates data transfers and data interfaces and allows detailed analyses from within the CAD system on the latest model throughout the design process. Technology development during the fifth stage included mesh automation, object-oriented tools and facilities, particularly in the user interfaces and databases. The object-oriented interface lets the users rapidly generate models by assembling and resizing components and then get immediate predictions of response, risk, cost and performance metrics.

The five stages of CST software development parallel the five stages of the computing environment's evolution: non-centralized mainframes; centralized mainframes; mainframe computing with timesharing; parallel computing; and heterogeneous metacomputing and metacenters (distributed computing and network-

ing). A summary of the major characteristics of currently used finite element systems is given in Ref. [16], and a guide to information sources on finite element methods is given in Ref. [17]. A finite element bibliography, including books and conference proceedings published since 1967, is available on the Internet. The URL address is <http://www.solid.ikp.liu.se/fe/index.html>.

3. Goals of CST activities

In general, five major goals can be identified for CST activities. The five goals are described subsequently for aerospace-related CST activities. However, most of the goals described also apply to structures in fields other than aeronautics and space. The *first* goal is to predict the response, performance, failure and life of structures and their components at actual operating conditions. Major advances in support of this goal continue to occur on a broad front. They include development of sophisticated computational models to simulate the mechanical, thermal, and electromagnetic responses of structures; efficient discretization techniques (namely, improved finite elements, boundary elements, and hybrid analytical/numerical methods); computational strategies for nonlinear static, dynamic, and fracture problems; quality assessment and adaptive refinement of numerical simulations; and versatile, powerful software systems for structural analysis.

Life prediction methods are required for performing structural integrity assessments of engineering systems. For metallic structures, empirical methods are being replaced by fracture-mechanics based computational methods. For composite structures, mechanistic approaches are being developed for predicting strength and life under sustained and cyclic mechanical, thermal, and chemical environments. Because of the difficulty of understanding and modeling damage and failure phenomena, computational methods for strength and failure predictions lag behind those for response predictions.

CST's *second* goal is to complement experiments and other tests involving structures and their components and to aid in the design of such experiments. The need for reducing dependence on extensive and costly testing gives this goal added importance. In some cases, computational techniques are the only tools available to the designer. Examples include hypersonic aerospacecraft, outer planetary entry probes, large space structures, and extraterrestrial bases.

Another important area pertaining to the second goal is development of computational models and methods used in support of nondestructive evaluation. Still another is the system identification (ID) methods

that allow the use of experiments to validate and improve the quality of numerical models. The ID methods have become particularly important in the control-structure area because they promise a control system that can automatically identify the structure it is trying to control.

The *third* goal is to study phenomena that are difficult to understand by means other than numerical simulations. Such studies involve the implications of various microstructural damage mechanisms on the macroscopic response and performance of structural components. Also included in this goal are nonlinear chaotic dynamics of structural systems whose history indicates sensitivity to initial conditions.

The *fourth* goal is to give material developers guidance, enabling them to improve material systems and thereby meet performance and design requirements. Examples of computations supporting this goal include simulating the effect of a fiber-matrix interface on residual stresses, and mechanical response of metal matrix composites.

The *fifth* goal of CST is to aid in the design process of engineering systems. Activities here include the development of efficient techniques for large-scale design optimization of structures; techniques for calculating the sensitivity of the structures' responses to design modifications; and inverse design problems. Sensitivity calculations are now part of many commercial software systems. Optimization techniques are gaining more acceptance in aerospace and automotive engineering [18] and are slowly but steadily changing all phases of the structural design process, from concept identification to the detailed design of components and flight vehicles. Inverse design problems attempt to identify design characteristics that produce the desired performance.

Current CST activities include the study of phenomena occurring at disparate spatial and time scales. Length scales range from the microscopic level to the structural level. Today no important design can be completed without CST, nor can any new theory be validated without it. Commercial programs for structural analysis have a rich variety of elements, and are widely used for performing structural calculations on large components and/or entire structures.

4. Recent advances in CST

The development of CST cuts across a number of disciplines including structural mechanics, materials science, discretization techniques, numerical analysis, and computer science. Advances in each of these disciplines can have a strong impact on CST. Some of the recent advances which have had, or promise to have, a strong impact on CST are listed subsequently. The

advances are grouped into the following categories: element technology and discretization techniques; computational material modeling; computational modeling of composite, sandwich and smart structures; life management computational tools and methodologies; transient response analysis; numerical simulation of frictional contact/impact response; computational methods for articulated structural dynamics; probabilistic analysis and stochastic modeling; qualitative analysis and simulation; neuro-computing; hybrid techniques; error estimation and adaptive improvement strategies; strategies for solution of coupled problems; sensitivity analysis; integrated analysis and design; strategies and numerical algorithms for new computing systems; model generation facilities; and application of object-oriented technology. This list is by no means complete or exhaustive. The intention is to make researchers aware of the full potential of CST in the analysis and design of engineering structures. Among the advances not covered herein are: computational methods in fracture and damage mechanics [19-21]; computational methods for inverse problems (e.g., parameter/system identification [22,23]); computational methods for material process modeling; and multidisciplinary optimization problems.

4.1. Element technology and discretization techniques

The establishment of reliable and efficient finite elements, boundary elements and other discretization techniques for modeling structures with complicated geometry has been, and continues to be, the focus of intense research effort. In this section, some of the recent advances are reviewed. These advances are grouped into six categories: formulative aspects of finite elements; spectral and wavelet and other non-classical elements; meshless methods (also referred to as element-free Galerkin methods or nodes without elements); finite volume method; generalized finite element methods; and finite elements for shell analysis. Recent advances in boundary element methods are reviewed in recent survey articles [24-26], and in a monograph [27].

4.1.1. Formulative aspects of finite elements

The desire to establish a variational basis for high-performance finite elements (viz., simple elements with few degrees of freedom—all physical, which delivers results of engineering accuracy on coarse meshes) has led to the development of generalized mixed variational principles (GMVPs) in the early-1980s [28,29] which were referred to as parametrized variational principles (PVP) by Felippa in 1989 [30,31]. For a discussion of the attributes of high-performance elements see Ref. [30]. The functional of a generalized multifield variational principle (GMVP) is a parametrized combi-

nation of canonical functionals, with each of the canonical functionals represented by a point in the parametric continuum.

Generalized multifield variational principles provide a framework by which classical variational principles may be embedded into a parametrizable continuum of functions. To date, GMVPs have been constructed for finite deformation elasticity, incompressible solids, micropolar elasticity and linear electrodynamics. Two of the important applications of GMVPs are: (a) selection of variational functionals for ill-conditioned problems [29]; and (b) development of finite element templates. A *template* is a parametrized algebraic form which yields a continuum of finite elements for a specific application, with a given element configuration, and a given number of degrees of freedom [31]. GMVPs provide a variational framework for some of the elements that lack such framework. Two notable examples are the scaled free formulation (SFF) elements, and the assumed natural deviatoric strains (ANDES) elements. The SFF element was shown to be associated with a multifield variational principle with one free parameter that interpolated between hybrid versions of the potential energy principles and Hellinger-Reissner principle. The ANDES element is associated with a one-parameter hybrid multifield functional that interpolated between the potential energy and the Hu-Washizu functionals. The development of GMVPs and the widespread availability of powerful computerized symbolic manipulation systems can help in the systematic construction of optimal finite elements by the template approach.

4.1.2. Spectral, wavelet and other non-classical elements

Over the past decade spectral element (p-type finite element) methods have proven to be an efficient and accurate way to solve partial differential equations, especially in the fluid mechanics area. Spectral element methods utilize the fast convergence and good phase properties inherent in singular Sturm-Liouville approximations, while allowing the solution domain to include complex geometries. Developments in the last five years included extension of spectral methods to triangular and tetrahedral elements in two- and three-dimensions, respectively [32-34].

Wavelets are functions with local support (i.e., functions that are local in time and frequency, or in space and wave number; see, for example, review articles, Refs. [35,36]). Several engineering applications of wavelets has been reported in the literature, especially in signal and image processing. However, only in the last five years have finite element application of wavelets to model localization phenomena become an active research area [37].

Recent work included: (a) evaluating the performance of hierarchical/wavelet formulations in terms of

convergence rate, dispersive behavior, and computational complexity, and (b) employing multiple scaling functions for multi-resolution analysis. The resulting techniques are referred to as multi-wavelet methods [38]. With multi-wavelet methods no special quadratures are needed in the generation of wavelet elements, and the difficulties associated with the application of wavelets to closed bounded domains are greatly alleviated [39].

Wavelet elements have the potential of computing multiscale solutions to partial differential equations with higher convergence rates than conventional finite element methods. Their built-in adaptive nature offers the possibility of automatic adaptivity [40]. They are well suited to preconditioning finite element approximations of boundary value problems. They also yield methodologies for obtaining sparse representations of boundary element formulations.

In addition to the spectral and wavelet elements, a number of other non-classical elements have been developed using a variety of approximation functions including digital Walsh functions, orthogonal and non-orthogonal polynomials, spline functions and fundamental solutions of elasto-static problems [41].

4.1.3. Meshless methods

One of the advantages of the methodology of meshless methods is that the model description is the same as that required by CAD systems. Recent work included development of: (a) an element-free Galerkin method which uses a moving least square interpolant [42]. The method has been applied to crack propagation problems and was found to possess the following advantages: avoiding the locking associated with compressible materials; providing high rates of convergence with low-order polynomials; and facilitating adaptivity, since it is only necessary to add extra nodes in the area where extra resolution is needed; and (b) reproducing kernel particle methods for structural dynamics problems [43], which are extensions of the smooth particle hydrodynamic method developed by Gingold and Monaghan to provide a mesh free environment [44]. It can be viewed as a continuous least square polynomial. Recently, a meshless local Petrov-Galerkin (MLPG) approach has been developed using the moving least squares approximation. The integrals in this method are evaluated only over regularly shaped sub-domains and their boundaries. The local boundary is selected to be the surface of a sphere centered at the node in question [45].

4.1.4. Finite volume method

Although attempts were made in the 1960s to use an integration technique (cell method) for generating finite difference approximations for plane elasticity, plates and elasto-plastic flow, it was not until the early-1970s

that the finite volume method evolved as a finite difference approximation on non-orthogonal grids. The method has been widely used in fluid dynamics and heat transfer applications, but it has not gained acceptance in structures applications. The method was shown to be a special case of the finite element method with non-Galerkin weighting [46-48]. One motivation for developing this method for structures is to solve fluid-structure interaction problems (such as simulation of flow induced vibration phenomena) using commercially popular finite volume-based CFD software [49]. The method has the advantage of computing element matrices and vectors using boundary integrals along the control volume sides [50,51]. Also, the potential of mixing finite element and finite volume methods for the discretization of complex domains needs to be investigated.

4.1.5. Generalized finite element methods

The high-fidelity modeling of complex three-dimensional structural components in high-tech industries by conventional finite element methods often requires an excessive number of elements in order to capture high gradients in the response quantities. To alleviate this problem several methods were proposed under the names, *finite element partition of unity*, *cloud-based hp finite element methods*, and *special finite element method* [52,53]. Recently, it was shown that these methods, and several of the meshless methods, can be considered as special cases of a generalized finite element method based on the use of a set of functions whose values sum to the unity at each point in the domain. The functions are defined over element patches.

4.1.6. Finite elements for shell analysis

Attempts to develop finite elements for shell analysis date back to the late-1960s. Since then a significant capability has been developed for modeling shell behavior. Fundamental considerations for, and reviews of, the development of some of the finite elements for shell analysis are included in two recent papers (see Refs. [54,55]) and a monograph [56]. Mixed shell elements which satisfy the fundamental condition for stability and optimality are reported in Refs. [57-59]. These elements are particularly useful for membrane dominated and bending dominated behavior. Despite the progress made to date, there is no mathematically validated approach for overcoming the difficulties associated with finite element shell analysis (such as complete removal of shear and membrane locking).

4.2. Computational material modeling

Considerable attention has recently been devoted to computational material modeling. In the context of CST, the objectives of this activity are: (a) to model

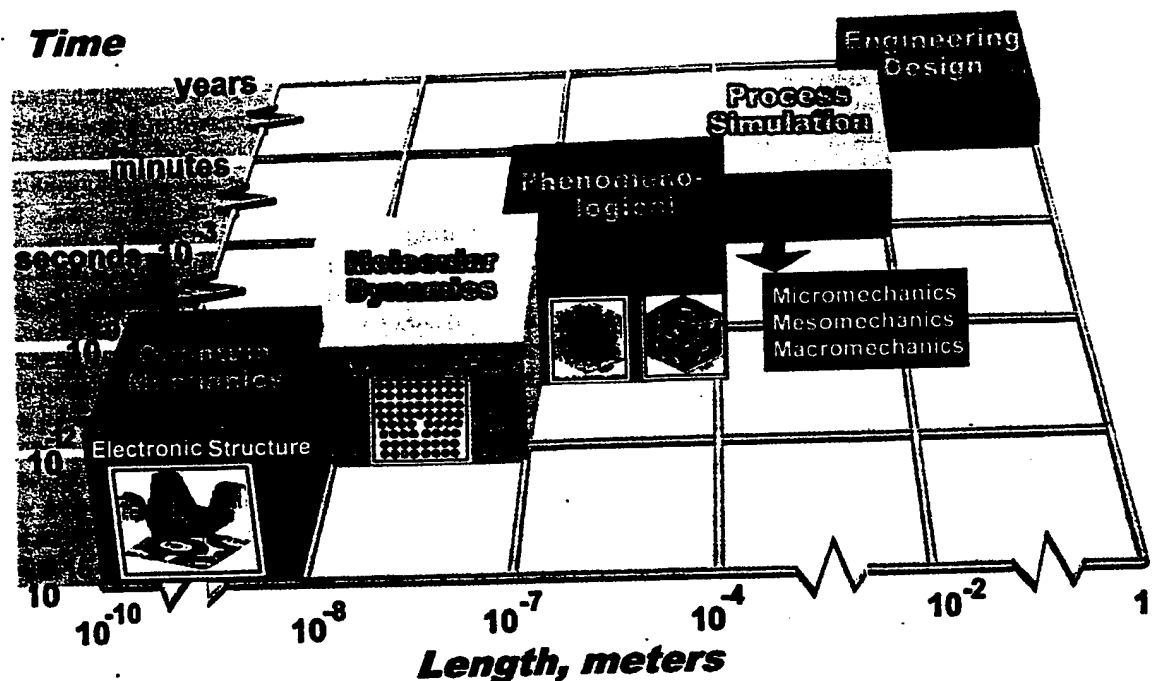




Fig. 3. Multiscale phenomena associated with computationally-driven material development.

realistic constitutive behavior by means of equations that represent the main physics and are capable of predicting results consistent with macroscopic observations [60-63]; and (b) to develop a hierarchy of material models (multilevel/multiscale) to describe the different phenomena associated with response, life and failure of structures.

A major consideration in the application of constitutive equations is the determination of material parameters from test data. This can be a difficult undertaking for the more complex equations with large numbers of parameters. In most formulations for metals, the parameters divide into a few that govern the overall strain rate and temperature dependence of

Table 1

Models	Discipline		Length scale, m	Phenomena
Phenomenological/ macromechanical	Computational structural mechanics		 10^{-2} to 10^{-0}	<ul style="list-style-type: none"> • Structural response • Metal forming
Micromechanical	Computational material science		 10^{-4} to 10^{-2}	<ul style="list-style-type: none"> • Plastic strain localization • Crack tip fields • Indentation fracture
Polycrystals (homogenized models)			10^{-6} to 10^{-4}	<ul style="list-style-type: none"> • Void growth • Polycrystalline slip • Microstructural effects
Single crystals			10^{-8} to 10^{-6}	<ul style="list-style-type: none"> • Dislocations • Particles and interfaces
Atomistic models	Molecular dynamics	Computa- tional chemistry	10^{-10} to 10^{-8}	<ul style="list-style-type: none"> • Creep diffusion • Cleavage • Discrete defects
	Quantum mechanics		10^{-10} to 10^{-10}	<ul style="list-style-type: none"> • Basic transport properties • Phase transformation

inelastic flow and would generally appear in the kinetic equation. A larger number of material parameters usually arise in the evolution equations for the hardening or possible softening properties. Attempts to rationalize and formalize the procedure have been made.

The multiscale material modeling activity has resulted in a gradual evolution from empirical models to physics-based models that predict the processing response and properties. The hierarchy of material models that has been developed is shown in Fig. 3 and Table 1. The models are arranged according to the phenomena they describe and the length scale at which the phenomena are studied (from 10^{-10} m to 1 m). The disciplines involved include computational chemistry that covers molecular dynamics and quantum mechanics, computational material science, and computational structural mechanics. The models used range from atomistic to single crystals to polycrystals to micromechanical and macromechanical models. However, many gaps still exist in the hierarchy of models, and to date no rational way exists to integrate these models and to couple them with experiments in order to relate the phenomena at the very small length scales with the macroscopic behavior.

The hierarchy of material models is an important element in the computationally driven material development activity which has been pursued at a number of research labs for over ten years [64,65]. The central paradigm of the computationally driven material development activity is the sequential interrelation of processing, structure, properties, and performance of materials. Ideally, the inner structure of the material is used to predict properties, then the properties are used to predict performance, and finally, a sequence of processing procedures are selected to yield the desired material and inner structure at a reasonable cost.

4.3. Computational modeling of composite, sandwich and smart structures

Increasing work has recently focused on the development of computational models for studying various phenomena associated with the response, life, failure, and performance of composite and sandwich structures. The phenomena involved cover a wide range of length scales, from microstructural to structural response. Recent noteworthy contributions can be grouped into the following five categories: accurate determination of inter-laminar stresses; multiscale modeling approaches; thermal and thermomechanical buckling and postbuckling; heat transfer analysis; specialized software for predicting the response and failure of high-temperature sandwich and composite structures; and modeling of smart structures. These categories are described subsequently.

4.3.1. Accurate determination of inter-laminar stresses

The importance of inter-laminar stresses in predicting the onset of some of the damage mechanisms in multilayered composite structures has long been recognized. Therefore, since the 1970s various techniques have been proposed for the accurate determination of transverse stresses in laminated composites. These include using [66,67]: (1) three-dimensional or quasi-three-dimensional finite elements; (2) two-dimensional finite elements based on higher-order shear deformation theories with either nonlinear or piecewise linear approximations for the displacements in the thickness direction; and (3) post-processing techniques, used in conjunction with two-dimensional finite elements based on the classical or first-order shear deformation theory (with linear displacement approximation through-the-thickness of the entire laminate).

Experience with most of the three-dimensional finite elements and two-dimensional finite elements based on higher-order shear deformation theories, has shown that unless the three-dimensional equilibrium equations are used in evaluating the thickness distribution of the transverse stresses, the resulting stresses are inaccurate. Since the finite element models based on the first-order shear deformation theory are considerably less expensive than those based on three-dimensional and higher order two-dimensional theories, their use in conjunction with post-processing techniques has received increasing attention in recent years. The post-processing techniques proposed for the evaluations of transverse stresses are based on the use of: (a) three-dimensional equilibrium equations; (b) predictor-corrector approaches; and (c) simplifying assumptions [68,69].

4.3.2. Multiscale modeling approaches

The global response and performance of composite and sandwich structures is governed by a number of local (constituent scale) phenomena such as fiber-matrix interface bonding, core-free sheet interface bonding, progressive damage and failure processes, and constitutive material behavior which exhibits cyclic nonlinear history dependence. An attempt has been made to develop an integrated multiscale modeling approach that incorporates nonlinear constituent material models and failure models; composite micromechanical models; and finite element global structural analysis models. The multiscale approach has been used to assess the performance and structural integrity of aircraft engine components.

4.3.3. Buckling and postbuckling

In recent years, considerable work has been devoted to the study of buckling and postbuckling responses of composite and sandwich plates and shells. Both thermal as well as combined thermal and mechanical load-

ing cases have been considered. Attempts have been made to identify the differences between the isothermal and thermal responses. Reviews of recent contributions are contained in three survey papers [66,67,70] and a monograph [71]. Of special interest is the study of the sensitivity of the buckling and postbuckling responses to variations in the material and lamination parameters of the composite [72-77].

4.3.4. Heat transfer

A number of approaches have been developed for the determination of the heat transfer characteristics and thermal response of composite structures. Some of these approaches are similar to the ones used in predicting the deformational response of composite structures. Recent developments include two-dimensional finite element models for heat transfer in multilayered composite panels [78,79].

Moderate intensity, short-duration radiant exposures of composites with organic matrices may result in processes such as pyrolysis, ablation, and diffusion of moisture or vapor. Only a few publications have addressed this subject.

4.3.5. Special-purpose analysis and design codes

A variety of special-purpose codes have been developed for assessing the structural integrity/durability and reliability of the high-temperature structures used in advanced propulsion systems. The codes developed fall into a number of categories including: (a) probabilistic structural analysis; (b) progressive fracture of composite structures; and (c) coupled structural/thermal/electromagnetic tailoring [80-83].

4.3.6. Smart structures

Smart structures sense external stimuli, process the sensed information, and respond with active control. Response can consist of deforming or deflecting the structure, or communicating the information to another control center [84]. Smart materials deform or deflect the structure by changing their physical properties when subjected to electric, magnetic, or thermal loads. The active elements in smart structures can be embedded in or attached to the structure. The computational models developed for predicting the thermo-mechanical response of laminated composites were extended to predict the electro-thermo mechanical response of anisotropic composite structures made of smart materials as well as hybrid fibrous composite/smart materials [85-89].

4.4. Computational tools and methodologies for life management

Life management tools range from those used in the initial design phase of new systems to those required

to make technology insertion and retain-or-retire decisions of aging systems. Among the computational needs for both new and aging aerospace systems are life prediction methods for performing structural integrity assessments. At high temperatures, life prediction involves a complex combination of processes that change the stress and material states of a structural component.

Structural life prediction procedures utilize material life models in conjunction with thermal, acoustic and structural analysis to quantify material response in identified local damage initiation-prone regions of a structure. A large number of high-temperature material life models have been proposed [90-92]. Acoustic fatigue life estimates have been made for simple structures only [93,94].

The complexity of life prediction for high-temperature structures may be attributed to a number of factors, including:

1. The processes experienced by the structural component are multidisciplinary in character. The mechanics, thermodynamics and chemistry aspects are coupled in such a way that classical representations such as fatigue (which attempts to isolate cycle-dependent mechanical behavior) and creep rupture (which attempts to isolate time-dependent behavior alone) are inadequate representations of the total performance of the structure.
2. Some of the inputs to the life prediction methods are random in time or are stochastically distributed. Cyclic or fatigue loading of high-temperature structural components is applied in a fairly random or stochastic sequence. Moreover, other variables such as corrosion, oxidation and chemical activities may occur in a random fashion; and
3. The rate equations that are used in representing the evolution of material properties are difficult to establish experimentally. Because of the complexity of the life prediction problem, it is common to represent changes in life by empirical or phenomenological descriptions that are limited to correlations of experimental observations. Recent work has focused on establishing mechanistic models for predicting remaining strength and life of structures. However, before these models can be used they have to be validated and calibrated by macroexperiments.

Performance simulation has been proposed as an approach for predicting the remaining strength and life of material systems [95,96]. The performance simulation approach is based on experimental determination of failure and damage modes, and the use of that information to establish critical elements of the materials that control the failure event. These representations are combined into a single integral equation that represents the remaining strength as a function of

time and loading history. The integral equation is discretized in time, and the physical behavior of the system at different times is estimated by accounting for the changes in the material state, and the stress state during the loading history. The approach has the potential of representing highly nonlinear and coupled phenomena such as creep, damage, oxidation, corrosion and thermodynamic variations.

Among the different projects aimed at developing life prediction methodologies for metallic structural components, the following four projects are noted:

1. Fracture-mechanics based techniques for metallic hypersonic airframes subjected to combined mechanical and thermal loads. These techniques, developed by McDonnell Douglas (currently part of Boeing Company) under Air Force support, are based on modeling crack growth behavior, and accounting for effects of temperature on yield strength and fracture toughness.
2. High temperature, crack-initiation fatigue models developed by Pratt and Whitney (a division of United Technologies) under NASA Glenn support for use in the aerospace propulsion industry. These models are based on cyclic damage accumulation (CDA) and use the output of finite element analysis as direct input.
3. Total strain version of strain range partitioning that has evolved at NASA Glenn over the past decade.
4. The damage mechanics approach promoted by Chaboche and colleagues at ONERA.

Further applications and refinements have been suggested by Arnold [97]. A symbolic computation program, SYMFRAC [98], has been developed at NASA Glenn for studying the damage growth in multi-cracked brittle materials. This program is useful for life prediction of brittle materials. For composite structures, an extensive research program was carried out by General Dynamics to develop life prediction techniques in a supersonic cruise environment. However, the predictions did not agree well with experiments (see Ref. [99]). Extensive analytical and experimental work is being carried out at NASA Langley and NASA Glenn to provide a basic understanding of the damage mechanisms and fatigue of composites at high temperatures. The work at Langley is primarily focused on continuous-fiber-metal matrix composites (see a review of this work in Ref. [100]). The controlling parameters identified for fatigue damage include relative strains to fatigue failure of the fiber and matrix, fiber/matrix interface strength, and thermal residual stresses. The NASA Glenn activities are part of the HiTEMP and EPM Projects and include:

1. Assessing life and fracture prediction methods for metal-matrix composites (MMC's-consisting of a

titanium alloy matrix and ceramic reinforcement) and evaluating different means of nondestructive evaluation (NDE). This work was done jointly with Pratt and Whitney and included determination of actual fracture strength and lives of MMC rings [101].

2. Prediction of the probability of failure of monolithic ceramic components as a function of time in service. A computer program, CARES/Life, has been developed that couples commercial finite element programs (used for determining the temperature and stress distributions) to reliability evaluation and fracture mechanics routines for modeling strength-limiting defects [102].

For aging air vehicles, fatigue damage, loss of corrosion protection and the subsequent occurrence of damaging corrosion can become a serious threat to their operational integrity. Better life prediction schemes (e.g., based on probabilistic analysis and stochastic modeling) are required in support of the alternate usage schedules, management techniques, corrosion protection refurbishment and affordable inspection and maintenance approaches. There is also a need for computational simulation of technology insertion processes and repair technologies.

4.5. Transient response analysis

The development of efficient computational strategies and numerical algorithms for simulating the transient response of structures has been, and continues to be, an active research area. Some of the advances made in this area are contained in Ref. [103]. Among the recent developments, the following three are cited:

1. Variable multi-step integration algorithms for first-order equations, that are extensions of multi-time step (subcycling) algorithms based on nodal or element partitions allowing each node to be integrated with a different time step [104]. A stability analysis for the algorithms is presented in Ref. [105].
2. Space-time finite elements, which include discontinuity-capturing operators to accurately resolve sharp gradients or discontinuities in wave propagation and impact problems [106-109]. Also, the time-discontinuous Galerkin method has been proposed to provide controllable numerical dissipation in the high-frequency response domain without introducing excessive algorithmic damping in the important low-frequency modes.
3. Multiple-scale finite element methods for linear structural dynamics problems, based on decomposing the response into fast and slow time scales using temporal shifting [110]. The slow time scale is solved by the direct time integration method with a reasonably large time step. The total response is then

recovered via a sampling theorem and superposition.

4.6. Numerical simulation of frictional contact/impact response

The numerical simulation of the nonlinear response of structures subject to impact loads has been the focus of intense efforts because of the pressing needs for collision protection, or crashworthiness, of transportation vehicles, nuclear reactors and containment vessels. Several software systems are currently available for frictional contact/impact analysis of structures, including ABAQUS, ADINA, DYCAST, DYNA, KRASH, LS/DYNA, McALOG/RADIOSS, MSC/DYTRAN, NIKE, PAMCRASH and PRONTO.

Recent activities included study of the mechanics of large dynamic deformation, and of material strain-rate sensitivity; development of friction models, contact/impact algorithms, and semi-empirical damage and failure mechanisms [111-119].

4.7. Computational methods for articulated structural dynamics

Flexible multi-body systems (FMS) have important applications in aircraft and space structures, including deployable space structures, space robots and manipulators, and aircraft landing gears. The response of FMS involves coupled effects of deformation, angular velocity and acceleration relative to an inertial reference frame. Considerable progress has been made in predicting the response of FMS [120-123]. The progress is manifested by the development of (a) efficient methods for solving differential-algebraic equations of motion of rigid and flexible multi-body systems; and (b) software systems and object-oriented tools for the numerical simulation of the transient dynamic response of FMS.

4.8. Non-deterministic modeling and analysis methods

In the past two decades there has been a growing realization among engineers that unavoidable uncertainties in geometry, material properties, boundary conditions, loading, operational environment, modeling and analysis assumptions must be taken into account to produce meaningful designs. Three possible approaches for handling uncertainty can be identified, depending on the type of uncertainty and the amount of information available about the structural characteristics and the operational environment. The three approaches are probabilistic analysis, fuzzy-logic approach, and set theoretical, convex (or anti-optimization) approach. Discussion of the three approaches

and their combinations are given in Refs. [124,125]. In probabilistic analysis, the structural characteristics and/or the source variables are assumed to be random variables (or functions), and the joint probability density functions of these variables are selected. The main objective of the analysis is the determination of the reliability of the system. Reliability is defined as the probability that the structure will adequately perform its intended mission for a specified interval of time when operating under specified environmental conditions.

Southwest Research Institute, under NASA funding, developed a code that combines a fast probability integration algorithm with general-purpose stress, free vibration, buckling and dynamic structural analysis programs, based on finite element and boundary element techniques. Output of the analysis consists of a user-defined region for the probability distribution function (or cumulative distribution function), together with confidence bands. A comparative study of probabilistic finite element methods of structures was reported in a journal article [126], and in a monograph [127].

If the uncertainty is due to vaguely defined structural and/or operational characteristics, imprecision of data and subjectivity of opinion or judgment, then fuzzy logic-based treatment is appropriate [128-130]. Randomness describes the uncertainty in the occurrence of an event (e.g., damage or failure of the structure). Fuzziness describes the ambiguity of the event (e.g., imprecisely defined criteria for failure or damage). When the information about the structural and/or operational characteristics is fragmentary (e.g., only a bound on a maximum possible response function is known), then convex modeling can be used. Convex modeling produces the maximum or least favorable response and the minimum or most favorable response of the structure under the constraints within the set-theoretical description [131].

4.9. Qualitative analysis and simulation

Many engineering structures are made up of several interconnected components. The complexity of the response of the components and/or the incomplete knowledge about the structure characteristics can make the prediction of the response of the system by traditional computational (quantitative) methods intractable. Qualitative analysis and simulation, a branch of AI, can help in this situation by building models that reflect the phenomena associated with the response of the actual system. Application of qualitative analysis to snap-through mechanics problems is described in Ref. [132]. Recent studies have focused on the application of interval methods to estimate the range of possible solutions, and on developing hybrid

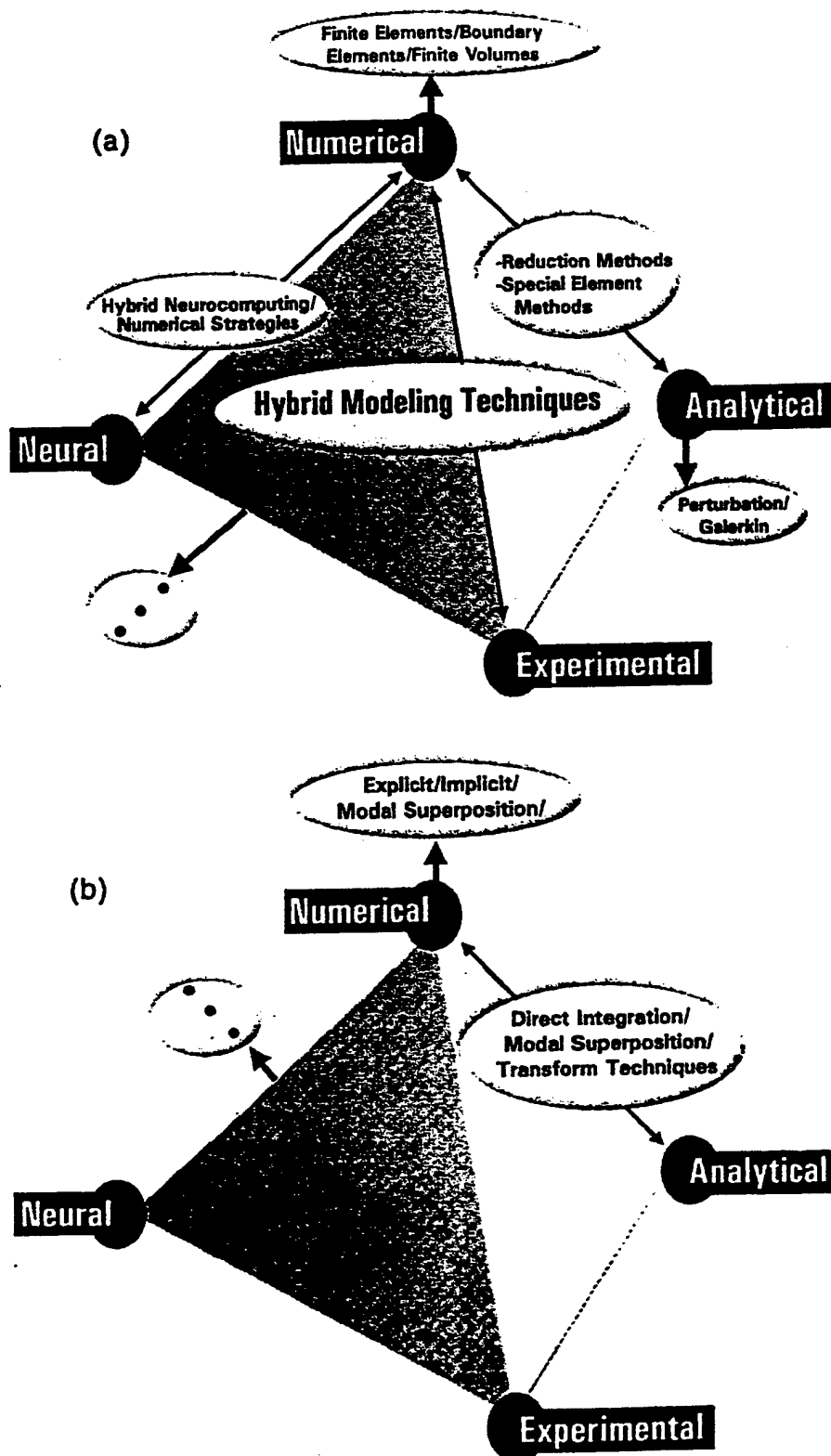


Fig. 4. Examples of hybrid analysis techniques.

approaches integrating qualitative, quantitative and rule-based analysis [133,134].

4.10. Neuro-computing

Neuro-computing is rooted in various disciplines, but the concept of artificial neural networks was inspired by biological networks. Neural networks are pattern computers—information processing devices (either algorithms or actual hardware). They use simplified mathematical functions to approximate the behavior of neurons in the brain. Biological neurons, as the structural constituents of the brain, are much slower than silicon logic gates. However, inferencing in biological neural networks is faster than the fastest computer. The brain compensates for the relatively slower electro-chemical operation by having an enormous number of massively interconnected neurons.

The application of artificial neural networks (ANNs) in structural mechanics has been gaining support in recent years. Operations performed by neural networks include classification, pattern matching, optimization, control and noise removal. Neural networks are particularly useful in situations where good analytic models are either unknown or extremely complex. When analytic models are either missing or incomplete, neural nets can be used to estimate a model from empirical data. They essentially work as interpolators: using partial input/output data about a system, a neural net can be used to estimate other output values. When good analytic models are available, neural networks are likely to be less accurate than numerical solution techniques. ANNs have been used as computational tools in various areas of structural mechanics, some of which are analysis, identification, simulation, design and optimization [135].

4.11. Hybrid techniques

The application of hybrid techniques to complicated structural problems can result in a dramatic saving in computational effort. Four groups of hybrid techniques can be identified in relation to the four groups of numerical, experimental, analytical and neural techniques: (1) hybrid analytical techniques [136]; (2) hybrid analytical/numerical techniques [137]; (3) hybrid numerical/experimental techniques [138]; and (4) hybrid neuro-computing/numerical techniques. Examples of the four groups are shown in Fig. 4. Recent work has focused on the coupling of different methods to generate effective hybrid techniques. Specifically: (a) applications of neuro-computing/numerical techniques include nonlinear structural and sensitivity analyses [139,140]; and (b) micro-mechanics based constitutive damage models [141]. In the second application, the finite element results, in the form of

equivalent inelastic stress-strain response, are used to train ANN. The finite element analyses are performed for a relatively small number of selected strain-paths, geometric and damage parameters. The ANN is used to construct a micromechanical damage model that can be applied in nonlinear analysis of composite structures.

4.12. Error estimation and adaptive improvement strategies

Assessment of the reliability of computational models has been the focus of intense efforts in recent years. These efforts can be grouped into three general categories [142-147]: a posteriori error estimation; super-convergent recovery techniques; and adaptive improvement strategies. A posteriori error estimates use information generated during the solution process to assess the discretization errors. In super-convergent recovery techniques more accurate values of certain response quantities (e.g., derivatives of fundamental unknowns) are calculated than those obtained by direct finite element calculations. Adaptive strategies attempt to improve the reliability of the computational model by controlling the discretization error.

4.12.1. Error estimation

Two broad classes of error estimation schemes are currently used: residual methods, and interpolation methods. Residual methods involve the use of local residuals, usually as data in a local auxiliary problem designed to generate the local error to an acceptable accuracy. A significant amount of computation may be required in implementing these methods. In interpolation methods the available approximate solution for a given mesh (or time step) is used to estimate higher derivatives locally (e.g., local gradients or second derivatives). The higher derivatives are used, in turn, to determine the local error. Although these error estimates can be very crude, they are portable: a subroutine for computing local estimates can be added to virtually any existing code that operates on unstructured meshes with some effort.

Although significant progress has been made in developing a posteriori error estimates for linear elliptic problems [148-151], the error estimates for nonlinear and time-dependent (parabolic and hyperbolic) problems are considerably less developed. This is particularly true for bifurcation problems, problems with multiple scales, and problems with resonance. Work on error estimation for highly nonlinear problems has mainly been a subject of ad hoc experimentation.

4.12.2. Super-convergent recovery techniques

Super-convergent recovery techniques refer to simple post-processing techniques that provide increased accu-

racy of the sought quantities at some isolated points (e.g., Gauss-Legendre, Jacobi, or Lobatto) in a sub-domain or even in the whole domain [152,153]. In the latter two cases, the techniques are referred to as local and global super-convergent recovery techniques, respectively. Recent work included development of local super-convergent patch derivative techniques for both interior and boundary (or material interface) points [154-161]. It was shown in Refs. [154,155] that the super-convergent recovery technique can be used to obtain a posteriori error estimates for the finite element solution.

4.12.3. Adaptive strategies

Different strategies have been used for adaptive improvement of the numerical solutions [147,162-166], including: (i) mesh refinement (or de-refinement) schemes, h methods; (ii) moving mesh (no redistribution) schemes, r methods; (iii) subspace enrichment schemes (selection of the local order of approximation), p methods; (iv) mesh superposition schemes (overlapping local finite element meshes on the global one), s methods; (v) hybrid (or combined) schemes. Examples of these schemes are: (a) simultaneous selection of the meshes and local order of approximation, h - p methods. Recent theoretical results have shown that the fastest possible convergence rates can be attained by optimally decreasing the mesh size h and increasing the degree of the polynomial degree p in a special way; (b) simultaneous selection of the meshes and node redistribution, h - r method. These methods can be effective in shock problems since an r method might align the mesh along discontinuities prior to a mesh refinement. Although all the aforementioned strategies can be applied to structural and non-structural problems, only the first strategy, h method, has been applied, in conjunction with unstructured grids, to thermal stress analysis (see Ref. [167]).

4.13. Strategies for solution of coupled problems

Two general strategies are used for solution of multifield problems, such as fluid flow/acoustic/thermal/structural problems; namely, the staged solution strategy, and the coupled solution strategy, which are briefly outlined subsequently.

4.13.1. Staged solution strategy

The multiple fields are treated separately. The discrete models for each of the fields may be developed separately. Coupling effects are viewed as information that must be transferred between the discrete models of the different fields. For thermal/fluid/structural problems, the heating rates are first predicted on aerodynamic surfaces using coupled fluid flow/thermal analysis. Then the structural temperatures are deter-

mined via thermal analysis. The structural response is then computed using the structural equations of motion and constitutive relations. The structural deformations can be used to correct the shape of the body and the whole process is repeated. This is depicted in an integrated fluid flow/thermal/structural analysis capability as presented in Refs. [168,169].

A modification of this strategy is the multi-stagger solution strategy in which a partial de-coupling is made of the full system of equations. The full system of coupled equations is partitioned into smaller subsystems of equations. Each subsystem is solved separately under the assumption that the variables of the other subsystems are frozen (temporarily) (see Ref. [170]). A staggered solution process is presented in Refs. [171,172] to analyze the coupling of incompressible and compressible fluid flows with structural motions.

4.13.2. Coupled solution strategy

The multiple-field problem is treated as an indivisible whole. The discrete models of the different fields are tightly coupled.

4.14. Sensitivity analysis

Sensitivity analysis refers to methods of calculating the rates of change of: (a) response quantities (e.g., displacements, stresses, vibration frequencies and buckling loads) with respect to changes in the structure characteristics (e.g., geometric and material parameters of the structure); and (b) the optimum design variable values with respect to changes in the structure parameters (e.g., applied loads and allowable stresses). The two types of calculations are usually designated by response and optimum design sensitivity analysis, and the rates of changes are referred to as sensitivity coefficients.

A number of techniques have been developed for evaluating the sensitivity coefficients of response quantities using either the governing discrete (e.g., finite element) equations or continuum equations of the structure. The techniques used with the discrete equations can be grouped into three categories: analytical direct differentiation methods, semi-analytical or quasi-analytical methods, and finite difference methods (see Refs. [173,174]). To avoid the subtractive cancellation errors inherent in the classical finite difference method, complex variables have been used to estimate derivatives of real functions [175].

Methods for computing sensitivity coefficients for linear structural response have been developed for over twenty years [176,177]. However, only in the last few years have attempts been made to extend the domain of sensitivity analysis to: (a) nonlinear structural response and to path-dependent problems, for which the sensitivity coefficients depend also on the deformation

history (e.g., visco-plastic response and frictional contact [178-181]); and (b) structural systems exhibiting probabilistic uncertainties.

Because of the importance of its role in structural optimization and in assessing the effect of uncertainties in the input parameters on the structural response, some commercial software systems have incorporated response sensitivity analysis into the systems. Also, an automatic differentiation facility has been developed for evaluating the derivatives of functions defined by computer programs, exactly to within machine precision. The facility has the acronym ADIFOR (Automatic Differentiation of FORTRAN), and is described in Refs. [182,183]. The use of ADIFOR to evaluate the sensitivity coefficients from incremental/iterative forms of three-dimensional fluid flow problems is discussed in Ref. [184] and the additional facilities needed for ADIFOR to become competitive with hand-differentiated code are listed in Ref. [183].

4.15. Integrated analysis and design

The design of vehicular and propulsion systems for future aerospace missions requires: (a) integration between the structures discipline and other traditionally separate disciplines such as aerodynamics, heat transfer, chemistry, materials and control; (b) integrated system analysis to couple subsystems, components, and sub-components at an appropriate level of detail; and (c) a simulation environment that provides a user-friendly interface between the analyst and the multitude of complex codes and computing systems that are required to perform the simulations. NASA Lewis has built a numerical propulsion system simulator (NPSS) to determine the system attributes such as performance, reliability, stability and life (see Ref. [185]).

4.16. Strategies and numerical algorithms for new computing systems

In recent years, intense efforts have been devoted to the development of efficient computational strategies and numerical algorithms which exploit the capabilities of new computing systems; in particular, the vector and parallel processing of the powerful high-performance computers [14,186]. Efficient direct and iterative numerical algorithms have been developed for solution of large sparse linear systems of equations.

Most parallel strategies are related to the 'divide and conquer' paradigm based on breaking a large problem into a number of smaller sub-problems that may be solved separately on individual processors. The degree of independence of the sub-problems is a measure of the effectiveness of the algorithm since it determines the amount and frequency of communication and syn-

chronization. The numerical algorithms developed for structural analysis can be classified into three major categories, namely: element-wise algorithms, node-wise algorithms, and domain-wise algorithms.

The element-wise parallel algorithms include element-by-element equation solvers and parallel frontal equation solvers. The node-wise parallel equation solvers include node-by-node iterative solvers as well as column-oriented direct solvers. The domain-wise algorithms include nested dissection-based (substructuring) techniques and domain decomposition methods. The first two categories of numerical algorithms allow only small granularity of the parallel tasks, and require frequent communication among the processors. By contrast, the third category allows a larger granularity that can result in improved performance for the algorithm.

Nested dissection ordering schemes have been found to be effective in reducing both the storage requirements and the total computational effort required of direct factorization. The performance of nested dissection-based linear solvers depends on balancing the computational load across processors in a way that minimizes inter-processor communication. Several nested dissection-ordering schemes have been developed which differ in the strategies used in partitioning the structure and selecting the separators. Among the proposed partitioning strategies are: recursive bisection strategies (e.g., spectral graph bisection, recursive coordinate bisection, and recursive graph bisection [187,188]; combinatorial and design-optimization based strategies (e.g., simulated annealing algorithm, genetic algorithm, and neural-network-based techniques [189]; heuristic strategies (e.g., methods based on geometric projections and mappings; and algorithms based on embedding the problem in Euclidean space). For highly irregular and/or three-dimensional structures, the effectiveness of nested dissection-based schemes may be reduced. However, this is also true for most other parallel numerical algorithms. Scalable parallel computational strategies for nonlinear, postbuckling and dynamic contact/impact problems are presented in Refs. [190,191].

4.17. Model generation facilities

It has long been recognized that for complex structures the task of generating the finite element model is both tedious and error prone. Moreover, the cost of the analysis directly depends on the size, shape and number of elements. Extensive research has been devoted to automatic and semi-automatic generation of finite element grids [192,193]. The techniques proposed for model generation include two-dimensional quadtree, three-dimensional octree, triangulation parameter space mapping, and substructuring. Among the

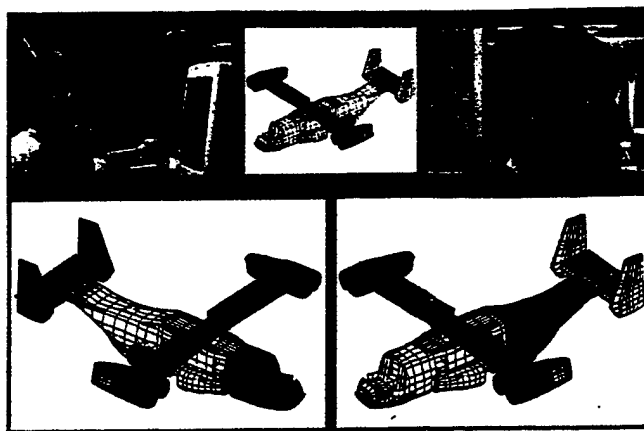


Fig. 5. Collaborative model development.

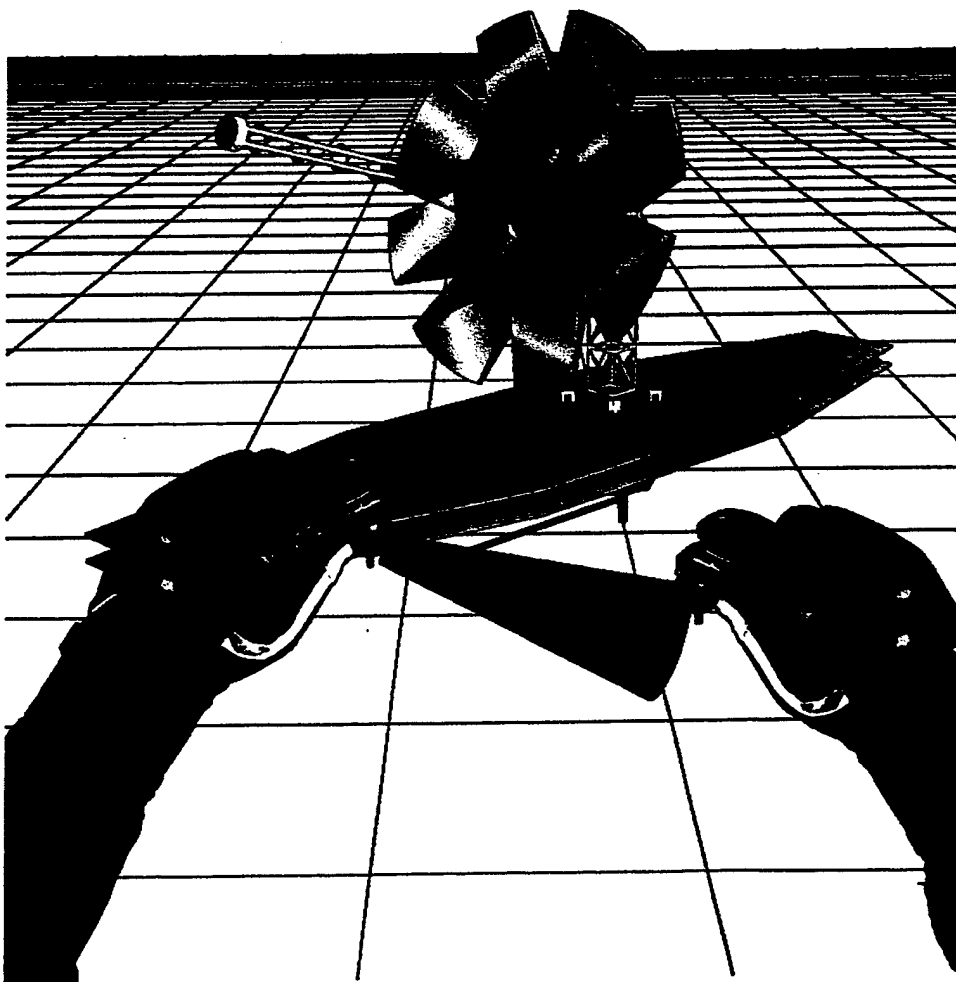


Fig. 6. Real-time model generation.

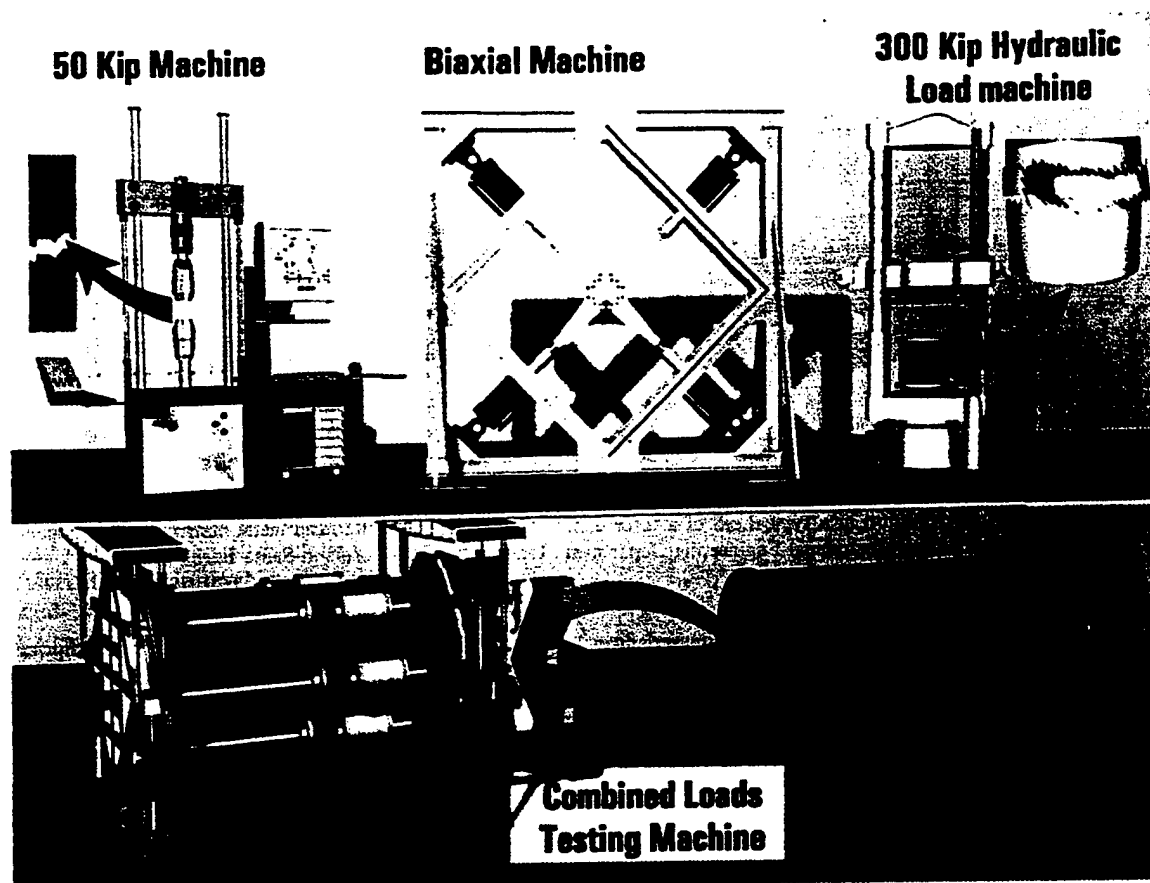


Fig. 7. Virtual structural laboratory.

recent studies on model generation are: (a) application of knowledge-based analysis assistance tools which allows a simple description of the analysis objectives and generates the corresponding discrete models appropriate for these objectives; (b) the development of a solid modeler-based preprocessor, CUBIT, for the automatic generation of well-formed quadrilateral and hexahedral finite element grids (with reasonably small distortion metric). CUBIT provides a combination of techniques, including paving, mapping, sweeping, and various other algorithms for discretizing the geometry into a finite element grid; (c) use of visual object-oriented technology facilities; (d) development of collaborative model generation (Fig. 5) (this also includes interactive assembly of finite element component models and stock parts); and (e) real-time model generation using immersive technologies, such as special gloves and VR facilities (Fig. 6). Such technologies enable interaction with complete or incomplete models, and allow interactive feedback to the model generation process. The capability is particularly useful for examining the finite element topology in certain spatial lo-

calities where the automated model generation facility may have produced certain complexities or anomalies.

4.18. Application of object-oriented technology

Because of the increasing size and complexity of analysis and design software systems, change in programming paradigm and a shift in software design strategy have occurred for developing easily readable, expandable and maintainable software systems. The change is from procedure-oriented to object-oriented programming, and the shift is towards object-oriented system development methodologies. The use of object-oriented technology can: (a) lead to smaller programs; (b) provide better management of data and procedures; and (c) simplify extensions of the system to cope with the advances in analysis methods, new materials and structural components and new computer architectures. Some of the recent structural and dynamic applications of object-oriented technology are reported in Refs. [194-201]. The efficiency issues in an object-

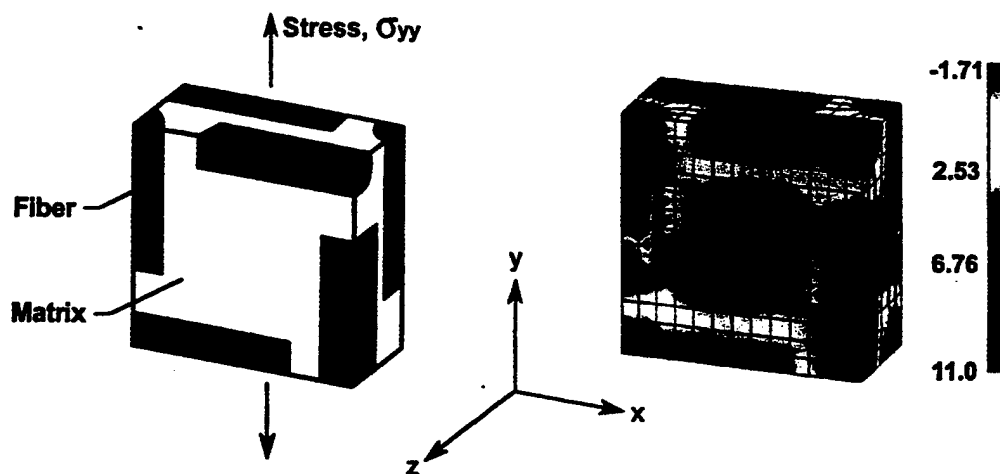


Fig. 8. Microstress σ_{yy} distribution in a typical cell of a three dimensional short fiber reinforced metal matrix composite loaded in the y -direction (courtesy of the Mechanical Engineering Department, University of California at Santa Barbara).

oriented programming environment are discussed in Ref. [202].

The current trend is to move from object-oriented to component-based software development (CBD). CBD allows developers to use and reuse code in applications that are written in any language and that run on any platform, almost anywhere on most networks. A prerequisite for the success of CBD is a standard infrastruc-

ture, with three main elements, for the components. The three elements are: uniform design notation, which can be achieved by using a uniform modeling language, UML; a standardized interface, which enables any application (in any language) to access component features by binding to the component model or interface definition language; and repositories, catalogues of available components with a

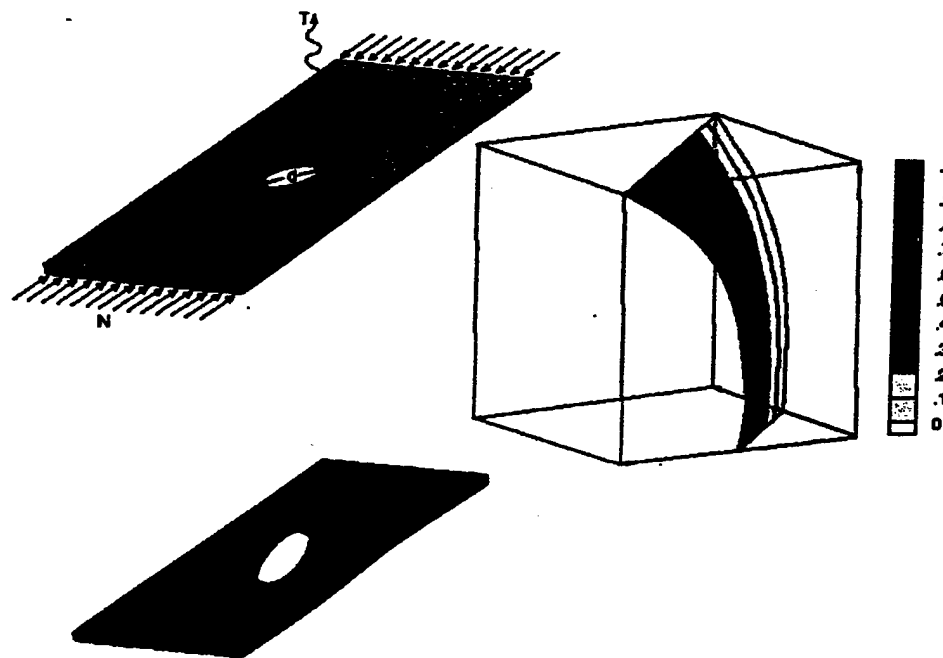


Fig. 9. Thermomechanical stability boundary for a composite panel with circular cutout.

description of the features that enable the developer to find the components appropriate for an application.

5. CST at universities and industry

Through their dual mission of teaching and research, universities have aided CST development. Their contributions started in the early days of finite element development and included new finite elements, numerical algorithms for solving equations and extracting eigenvalues, computational strategies for contact/impact, large deformation, buckling, postbuckling, and dynamic problems, and optimization techniques. Until recently, however, when high-performance computers and advanced workstations became widely available to university researchers, most university CST research focused on fundamental problems and did not involve very large-scale numerical simulations.

Universities began teaching finite element courses in the mid-1960s; since then a variety of CST-related and computer-aided engineering courses have been added to many undergraduate and graduate curricula. CST can significantly enhance structures education by allowing students to apply the basic principles to real (though scaled-down) structures. It can also provide a virtual experimental facility for simulating structural, dynamic and wind tunnel experiments. Although observations of real tests and experiments are invaluable, physical insight is rarely derived from a single experiment; CST provides a facility in which the student may change the design variables and study such changes' effects on the response characteristics of the structure. University of Virginia researchers are developing a virtual structural laboratory as part of a distributed learning environment (Fig. 7), that will be internet-centric and web-based with a virtual reality modeling language, multimedia, immersive facilities and multi-sensory interfaces.

Examples of university studies include micromechanical analysis of short-fiber composites (Fig. 8), and thermomechanical buckling of composite panels with cutouts (Fig. 9). The second example showed that, contrary to intuitive expectations, for certain boundary conditions both the critical load and critical temperature can increase as the size of the cutout increases.

In industry, recent CST activities include development of pre- and post-processors. The goal of this work is to reduce the efforts needed for creating the finite element model and to cut the time required for interpretation and visualization of results. Also, in-house special-purpose programs have been developed for detailed analysis of structural connections and joints.

Although the sophistication of computational models in industry has increased in the last decade, the

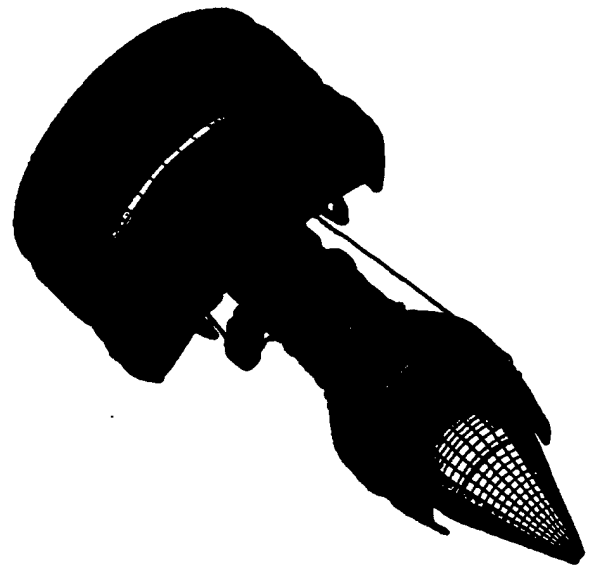


Fig. 10. MSC/NASTRAN model of GE engine, 180,000 degrees of freedom (courtesy of GE Aircraft Engines).

traditional role of computational structural analysis has not changed significantly in industry. In the aircraft industry, computational structural analysis is used to establish load paths and local stress levels. These are fed into separate analyses, or component tests, to predict strength, life, or other failure modes, and the whole process is then validated by full-scale tests. The level of detail in the finite element modeling currently used in the aircraft and automotive industries is provided by the three finite element models shown in Figs. 10-12 (GE-90 engine model, V-22 Osprey tilt rotor model, and car model used in crash simulation).

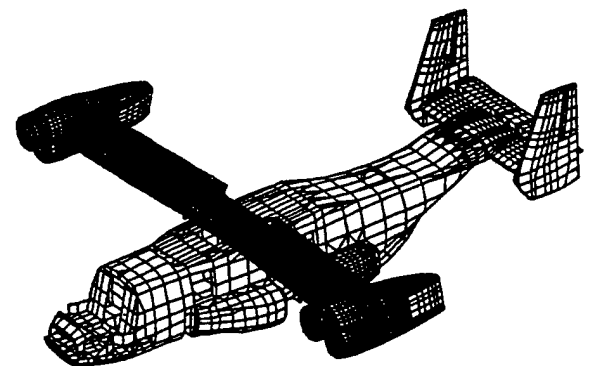


Fig. 11. MSC/NASTRAN finite element dynamics model of the V-22 Osprey Tiltrotor, 134,982 degrees of freedom (22,497 grid points), 44,006 elements (courtesy of Bell-Boeing).

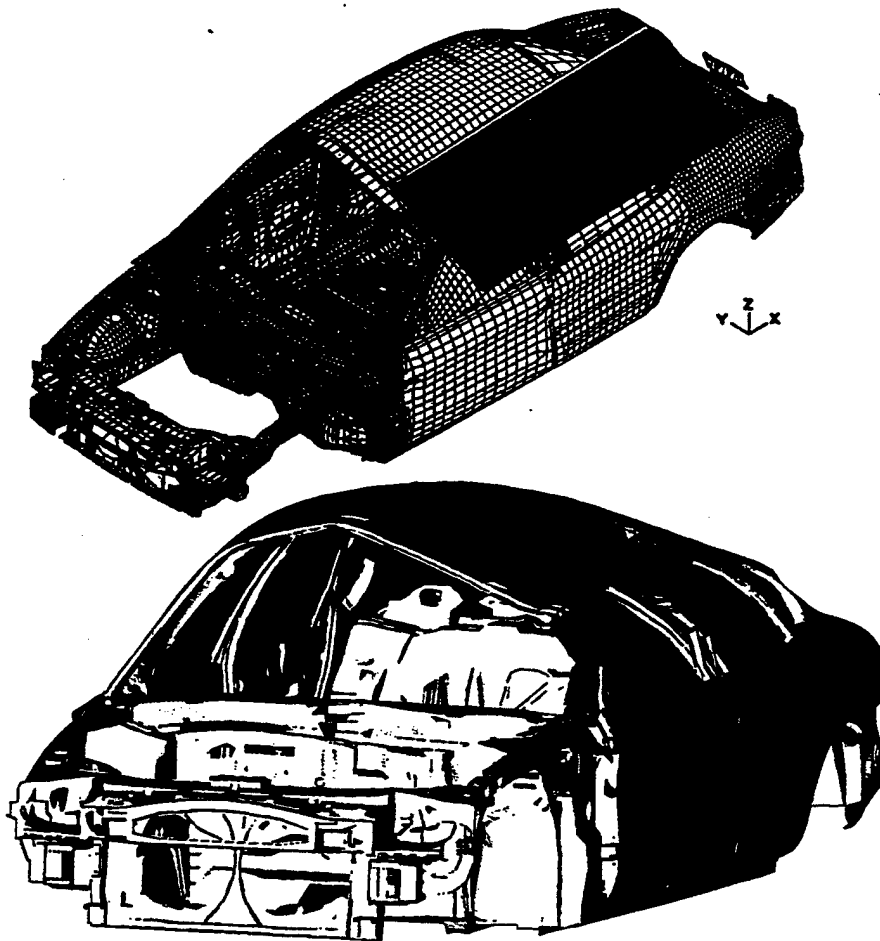


Fig. 12. Crush analysis of a Taurus car model performed by implicit dynamic finite element analysis (corresponding to an incremental static solution). A rigid plate moving at 10 mm/s is crushing the car (courtesy of ADINA R&D).

Today many of these calculations can be performed on powerful workstations in a matter of hours.

6. A look at the future

Economic stresses are forcing many industries to reduce cost and time to market, and to insert emerging technologies into their products. This trend is likely to continue and will require engineers to design faster, ever more complex systems. They must find globally optimal designs that take uncertainties and risk into consideration.

The realization of future cost-effective high-performance engineering systems requires: (a) technology advances in the materials and structures areas; (b) computational technologies and tools for solving complex problems with system uncertainties (e.g., computational intelligence and its associated tools, also called

soft computing); and (c) distributed integrated virtual environment for simulating the entire life cycle of an engineering system, from concept development to detailed design and prototyping to qualification testing and operations (see Fig. 13). The environment links scientists, design teams, manufacturers, suppliers, and consultants in the creation and operation of engineering systems. It enables a seamless integration of team processes and disciplines.

In order for CST to play a significant role in future development of structures technology, as well as in the design and certification of future engineering systems, major advances and new computational tools are needed in several key areas. To this end the research community must address several primary pacing items and related tasks. In identifying these pacing items, researchers must consider the characteristics of future engineering systems and their implications for the future computing paradigm and environment; as

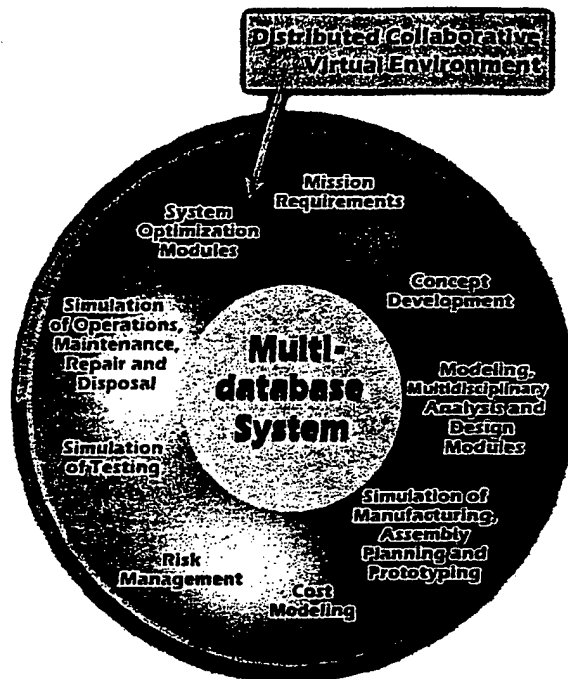


Fig. 13. Intelligent synthesis environment for aerospace systems.

developments in (a) other technologies that can impact CST (e.g., virtual product development, information technology and knowledge-based engineering); and (b) other fields of computational science and engineering that can be adapted to CST.

6.1. Characteristics of future engineering systems

The demands that future high-performance engineering systems place on CST will differ somewhat from those of current systems. The trend toward miniaturization, and the radically different and more unpredictable operational environments for many of the future systems, are two reasons for this difference. Another is the stringent design requirements for economy, high performance, lightweight, and rapid prototyping. The twenty-first century will see engineering systems made from computationally designed materials at the atomic/molecular level to accomplish a variety of missions. Programmable, multifunctional materials will be able to adjust their shape and their mechanical, electromagnetic, optical and acoustic properties on demand. The technical needs for future systems in the materials and structures areas include:

1. Development of new high-performance material systems such as smart/intelligent, multifunctional and bio-mimetic material systems;

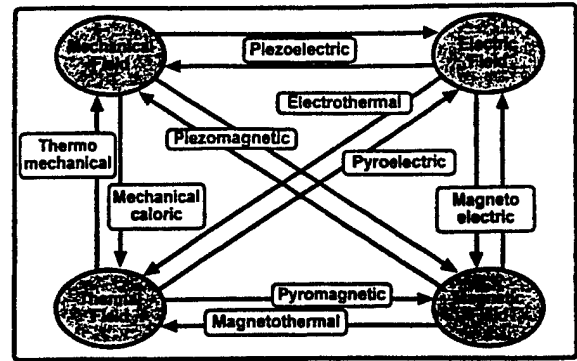


Fig. 14. Couplings between mechanical, electric, magnetic and thermal fields in smart materials.

2. Development of innovative materials processing technologies that enable low cost fabrication;
3. Development of novel structural concepts, such as structural tailoring and intelligent/smart structures, with active and/or passive adaptive control of dynamic deformations; and
4. Investigation of more complex phenomena and interdisciplinary couplings such as fluid flow/acoustics/thermal/control/electromagnetic/optics and structural couplings (see Fig. 14).

6.2. New and emerging computing paradigm and environment

Significant advances have been made and continue to be made in the entire spectrum of computing and communication technologies. The advances included fast microprocessors, parallel computer architectures, high-speed, high-capacity optical networks, communication protocols, distributed software structures and security mechanisms. A partial list of some the recent and projected advances in computing technology are given in Refs. [203,204]. The impact of these advances on the structures technology is given in Ref. [205], and are summarized subsequently. At one end of the spectrum are heterogeneous meta-computers and meta-centers. Meta-computers refer to an integrated (virtual) computing environment with geographically separated resources connected by one or more high-speed interconnectors. The middle-wire (a software layer) transforms a collection of independent hosts into a single, coherent virtual machine. Use of meta-computers has significantly affected CST by greatly alleviating the size limitations that current memory capacities impose on numerical simulations. Moreover, highly parallel systems and meta-computers have achieved sustained speeds in the tera-flop (trillion floating-point oper-

ations per second) range. The meta-computer hardware components are described in Refs. [204,205].

At the other end of the computing spectrum, small systems such as handheld computers (referred to as personal digital assistants), and wearable computers have emerged with cellular technology to support portable computing. Also, new powerful microprocessors such as Intel 500-MHz Pentium II Katami, Alpha 21364, AMD K7, Cyrix MII, IBM POWER3 and MIPS R12000 processors will be used as structural health monitoring systems for detecting and recording damage. The aforementioned advances have resulted in: (a) an explosive growth in computer power and connectivity which is reshaping relationships among researchers and organizations; and (b) the emergence of the new paradigm of *parallel, distributed, collaborative, immersive computing*. The implications of the new paradigm for engineering practice in general, and for CST in particular, are immense. The new paradigm, along with the advances in modeling and simulation, virtual product development, information technology and knowledge-based engineering, will enable dramatic changes in which engineering systems are designed, produced, operated, maintained, and disposed. Future environments will allow diverse, geographically dispersed teams to share and transform information into knowledge by combining and analyzing it in new ways. The interactive collaboration among experts in several disciplines will enable them to attack heretofore-intractable multi-physics problems involving phenomena at disparate length scales.

Realizing the full potential of new computing technology, however, requires new approaches for human-machine interfaces. The full power of creative artificial intelligence research should be brought to bear on the development of these interfaces, which should effectively link to as many of the human sensing and communication mechanisms as possible.

6.3. Virtual product development systems and information technology

Current virtual product development (VPD) systems have embedded simulation capabilities for the entire life cycle of the product. A description of the capabilities of over 120 CAD systems (including some VPD systems) is given in Ref. [206]. The addition of intelligent agents and networking facilities will transform the VPD systems into knowledge-enriched networked VPD systems. The benefits obtained include higher productivity, better product quality, and a broader design to provide an integrated system solution.

Information technology (IT) is concerned with the dissemination, processing, storage, retrieval and use of information [207]. IT will change product development from a sequence of distinct phases into a continuous

process covering the entire life cycle of the product with full interplay of information from beginning to end and everywhere throughout. IT will also be an important component of future distributed learning environments used for engineering training and education.

6.4. Primary pacing items

The primary pacing items for CST are: (1) high-fidelity modeling of the structure and its components; (2) failure and life prediction methodologies; (3) hierarchical, integrated methods and adaptive modeling techniques; (4) non-deterministic analysis, soft computing and risk assessment; (5) validation of numerical simulations; and (6) multidisciplinary analysis and design optimization. For each of the aforementioned items, attempts should be made to exploit the major characteristics of high-performance computing technologies, as well as future computing environments. The six primary pacing items are described subsequently. Note that some of the tasks within the pacing items are of a generic nature. Others are specific to either certain components of future engineering systems (e.g., propulsion systems or airframes of flight vehicles).

6.4.1. High-fidelity modeling of the structure

The reliability of the predictions of response, failure and life of structures is critically dependent on: (a) the accurate characterization and modeling of material behavior; (b) high-fidelity modeling of the critical details of the structure and its components (e.g., joints, damping, and for large deformations, frictional contact between the different parts of the structure). The simple material models used to date are inadequate for many of the future applications, especially those involving severe environment (e.g., high temperatures). Needed work on material modeling can be grouped in two general areas: (a) modeling the response and damage of advanced material systems in the actual operating environment of future engineering systems; and (b) numerical simulation of manufacturing (fabrication) processes.

Advanced material systems include functionally graded materials (FGMs), multifunctional materials, smart materials, bio-mimetic materials, textile and high-temperature composites and advanced metallics. For FGMs, novel processing techniques are used to produce engineered, gradual transitions in microstructure, composition, and properties to satisfy spatially varying functional performance requirements within a single component. Use of FGMs can alleviate the high gradients of internal stresses and strains resulting from the different local deformation fields induced when dissimilar materials are joined to form a component. This technology could allow researchers to develop compli-

cated structures without using conventional methods of joining. Besides being less costly, joint-less gradient materials are much more robust as stresses are distributed throughout the volume of the material rather than being concentrated at the joint. Multifunctional materials, in addition to supporting mechanical loads, may incorporate sensors to detect and evaluate loads or failure, and to interact with the surrounding electromagnetic environment. By contrast, materials as we know and use them at the present are largely 'mono-functional'.

Bio-mimetic technology aims at producing new materials by mimicking the synthesis, processing, and properties of materials found in biological systems. Among the unique and useful characteristics of such systems are multi-functionality, hierarchical organization, self-repair, adaptability and durability. Moreover, biological structural systems do not distinguish between materials and structures.

The length scale selected in the model must be adequate for capturing the response phenomena of interest (e.g., micro-mechanics, meso-mechanics, and macro-mechanics). For materials used in high-temperature applications, work is needed on the modeling of damage accumulation and propagation to fracture; modeling of thermoviscoplastic response, thermal-mechanical cycling and ratcheting; and prediction of long-term material behavior from short-term data, which are particularly important.

6.4.2. Failure and life management computational tools and methodologies

Practical numerical techniques are needed for predicting the life as well as the failure initiation and propagation in structural components made of new, high-performance materials in terms of measurable and controllable parameters. Examples of these materials are electronic, optical and smart materials for space applications; high-temperature materials for hypersonic vehicles; and piezoelectric composites. For some of the materials, accurate constitutive descriptions, failure criteria, damage theories, and fatigue data are needed, along with more realistic characterization of interface phenomena (such as contact and friction). The constitutive descriptions may require investigations at the microstructure level or even the atomic level, as well as carefully designed and conducted experiments. Failure and life prediction of structures made of these materials is difficult and numerical models often constructed under restricting assumptions may not capture the dominant and underlying physical failure mechanisms. Moreover, material failure and structural response (such as instability) often couple in the failure mechanism.

6.4.3. Hierarchical, integrated multiple methods and adaptive modeling techniques

The effective use of numerical simulations for predicting the response, life, performance and failure of future engineering structures requires strategies for treating phenomena occurring at disparate spatial and time scales, using reasonable computer resources. The strategies are based on using multiple mathematical models in different regions of the structure to take advantage of efficiencies gained by matching the model to the expected response in each region. To achieve the full potential of hierarchical modeling, there should be minimal reliance on a priori assumptions about the response. This is accomplished by adding adaptivity to the strategy. The key tasks of the research in this area are: (1) simple design-oriented models for use in the early stages of the design process; (2) rational selection of a set of nested mathematical models for different regions, and discretization techniques for use in conjunction with the mathematical models (this, in turn, requires the availability of a capability for holistic modeling from micro to structural response with varying degrees of accuracy); (3) simulation of local phenomena through global/local methodologies; (4) automated (or semi-automated) coupling of different mathematical/discrete models; (5) error estimation and adaptive modeling strategies; (6) efficient methods for coupling different components of structures (e.g., for flight vehicles coupling the engine, airframe and rotor/engine-frame); and (7) sensitivity analysis to assess the sensitivity of the response to each of the parameters neglected in the current mathematical model.

A variational multiscale method was presented for solution of multiscale problems in fluid mechanics, acoustics and electromagnetics [208,209]. The method is based on decomposing the solution into two parts: a course scale part represented by finite elements, and a fine scale part represented by Green's function. The two parts may overlap or be disjointed, and the fine scale part may be global or local. Application of this method to structural mechanics problems deserves attention.

6.4.4. Non-deterministic analysis, soft computing and risk assessment

The novel modes of computation which exploit tolerance for imprecision and uncertainty in geometry, material properties, boundary conditions, loading, and operational environment to achieve tractability, robustness, and low cost need to be extended to structural design. These facilities include neuro-computing, fuzzy logic and genetic algorithms, and have been collectively referred to as soft computing [210]. The distinction between expert systems (the most mature and resilient product of AI), soft computing paradigms, and conventional computational methods can be illustrated by

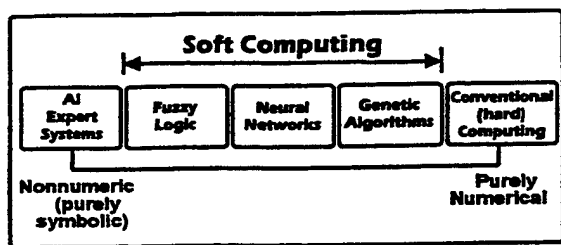


Fig. 15. Relationship between AI expert systems, soft computing paradigms and conventional (hard) computing.

the extent to which they use nonnumeric (symbolic) and numerical computations (see Fig. 15).

The ability to quantify inherent uncertainties in the response of the structure is obviously of great advantage. However, the principal benefit of using any of the soft computing tools consists of the insights into engineering, safety and economics that are gained in the process of arriving at those quantitative results and carrying out reliability analyses. As future engineering structures become more complicated, modeling of failure mechanisms will account for uncertainties from the beginning of the design process, and potential design improvements will be evaluated to assess their effects on reducing overall risk. The results, combined with economic considerations, will be used in systematic cost-benefit analyses (perhaps also done on a non-deterministic basis) to determine the structural design with the most acceptable balance of cost and risk.

6.4.5. Validation of numerical simulations

In addition to selecting a benchmark set of structures for assessing new computational strategies and numerical algorithms, a high degree of interaction and communication is needed between computational modelers and experimentalists. This is done on four different levels, namely: (1) laboratory tests on small specimens to obtain material data; (2) component tests to validate computational models; (3) full-scale tests to validate the modeling of details; and for flight vehicles and (4) flight tests to validate the entire modeling process. At each level, analysis of the computational model can be used to help set up the test, and the test data to help construct a more accurate computational model. For the first two levels, the use of flexible multi-body system codes allows the testing machine to be included in the analysis.

6.4.6. Multi-disciplinary analysis and design optimization

The realization of new complex engineering systems requires integration between the structures discipline and other traditionally separate disciplines such as aerodynamics, propulsion and control. This is man-

dated by significant interdisciplinary interactions and couplings that need to be accounted for in predicting response, as well as in optimal design of these vehicles. Examples are the couplings between the aerodynamic flow field, structural heat transfer, and structural response of high-speed aircraft and propulsion systems; and the couplings between the control system and structural response in control configured aircraft and spacecraft. This activity also includes design optimization with multi-objective functions (e.g., performance, durability, integrity, reliability and cost), and multi-scale structural tailoring (micro, local and global levels). For propulsion systems of flight vehicles it also includes design with damping for high-cycle, low-cycle, and acoustic fatigue.

Typically, in the design process questions arise regarding influence of design variable changes on system behavior. Answers to these questions, quantified by the derivatives of behavior with respect to the design variables or by parametric studies, guide design improvements toward a better overall system. In large applications this improvement process is executed by numerical optimization, combined with symbolic/AI techniques and human judgment aided by data visualization. Efficiency of the computations that provide data for such a process is decisive for the depth, breadth, and rate of progress achievable, and hence, ultimately, is critical for the final product quality.

6.5. Related tasks

For CST to impact the design process, the following tasks need to be addressed by the research community: (1) adaptation of CST software to the emerging parallel, distributed, collaborative, immersive computing paradigm. This includes exploiting the existing infrastructure for distributed visual problem solving environments (consisting of an integrated set of high level facilities and tools providing intelligence and expert assistance for solving problems from a prescribed domain); and development of: (a) real-time collaborative model and grid generation facilities; (b) interfaces between CST software and advanced visualization facilities (e.g., multimedia and virtual reality); and (c) infrastructure for component-based software development for facilitating the integration and reuse of diverse codes; and (2) development of intelligent software agents (simulation advisors) to enable the designers to use the CST software (embedded in the virtual product development systems) early in the design process.

CST's wide acceptance can affect the design and operation of future engineering systems and structures in three ways. It can provide a better understanding of the phenomena associated with response, failure and life, thereby identifying desirable structural design

attributes. CST can verify and certify designs and also allow low-cost modifications to be made during the design process. Finally, it can improve the design team's productivity and allow major improvements and innovations during the design phase, enabling a fully integrated simulation-based design environment. Such an environment allows computer simulation of the entire life cycle of the structure, including material selection and processing, multidisciplinary design, automated manufacturing and fabrication, quality assurance, certification, operation, health monitoring and control, retirement and disposal.

The outlook for CST is bright. Innovative structural concepts, advanced computational material models, intelligent computational tools for analysis and synthesis, along with the rapid convergence of computing, communications, and information technology should significantly enhance CST development and improve the performance of engineering systems.

Acknowledgements

The present work is partially supported by NASA Cooperative Agreement NCC-1-263, and by Air Force Office of Scientific Research Grant AFOSR-F49620-96-1-0462. The author acknowledges useful discussions and suggestions by many of his colleagues including S. Arnold, I. Babuska, J. Bathe, T. Belytschko, L. Berke, C. Chamis, C. Felippa, R. Haftka, G. Halford, C. Harris, D. Herting, D. Hopkins, J. Housner, R. Johns, W. Johnson, A. Kurdila, J. Mackerle, L. Pinson, J. Sobieski, S. Utku, A. Weiting and E. Wilson.

References

- [1] Clough RW. Original formulation of the finite element method. *Finite Elements in Analysis and Design* 1991;7:89-101.
- [2] Wilson EL. Automation of the finite element method: a personal historical review. *Finite Elements in Analysis and Design* 1993;13(2):91-104.
- [3] Focus '93: Computational Structures Technology. Aerospace America, February 1993.
- [4] Noor AK, et al. (compilers). Computational structures technology for airframes and propulsion systems. NASA CP-3142, 1992.
- [5] Goudreau GL. Computational structural mechanics: from national defense to national resource. *IEEE Computational Science and Engineering* 1994;1(1):33-42.
- [6] Argyris J, St Doltsinis I, Frik G, Tenek L. Computational structures technology in Europe: past, present and future. *IEEE Computational Science and Engineering* 1994;1(1):43-54.
- [7] Noor AK, Atluri SN. Advances and trends in computational structural mechanics. *AIAA Journal* 1987;25(7):977-95.
- [8] Noor AK, Venneri SL. A perspective on computational structures technology. *IEEE Computer Journal* 1993;26(10):38-46.
- [9] Noor AK, Venneri SL, editors. Computational structures technology. In: *Flight vehicle materials, structures and dynamics*, vol. 6. New York: American Society of Mechanical Engineers, 1995.
- [10] Ju JW, editor. Numerical methods in structural mechanics. New York: ASME Press, 1995.
- [11] Noor AK, Housner JM, Starnes Jr JH, Hopkins DA, Chamis CC (compilers). Computational structures technology for airframes and propulsion systems, NASA CP-3142, 1992.
- [12] Ladeveze P, Zienkiewicz OC, editors. New advances in computational structural mechanics, Proc. European Conf. on New Advances in Computational Structural Mechanics, Giens, France. Amsterdam: Elsevier, 1992.
- [13] Stein E, editor. Progress in computational analysis in inelastic structures. Vienna: Springer-Verlag, 1993.
- [14] Storaasli OO, editor. Large scale analysis and design on high performance computers and workstations, *Advances in Engineering Software* 1998;29(3-6).
- [15] Topping BHV, editor. Advances in computational structural mechanics. In: *Civil-Comp Press*. UK: Edinburgh, 1998.
- [16] Mackerle J, Fredriksson B. A handbook of finite element software: supercomputers, main-frames, minicomputers and microcomputers. Lund, Sweden: Studentlitteratur, 1988.
- [17] Mackerle J. Finite element methods: a guide to information sources. Amsterdam: Elsevier, 1991.
- [18] Proc. of the Seventh AIAA/USAF/NASA/ISSMO Symposium on Multidisciplinary Analysis and Optimization, September 2-4, 1998, St. Louis, MO, A Collection of Technical Papers, 3 volumes, Washington, DC: AIAA, 1998.
- [19] Petit J, de Fouquet J, Henaff G, Villechaise P, Dragon A, editors. ECF 11: mechanisms and mechanics of damage and failure, vol. 1, Proc. 11th Biennial European Conference on Fracture, Poitiers-Futuroscope, France. West Midlands, UK: Engineering Materials Advisory Services, 1996.
- [20] Nishioka T. Computational dynamic fracture mechanics. *International Journal of Fracture* 1997;86(1/2):127-59.
- [21] Aliabadi MH, editor. Nonlinear fracture and damage mechanics. In: *Advances in fracture mechanics*, vol. 4. Southampton, UK: WIT Press, 1999.
- [22] Trujillo DM, Busby HR. Practical inverse analysis in engineering. Boca Raton, FL: CRC Press, 1997.
- [23] Tanaka M, Dulikravich GS, editors. Inverse problems in engineering mechanics. New York: Elsevier Science, 1998.
- [24] Tanaka M, Sladek V, Sladek J. Regularization techniques applied to boundary element methods. *Applied Mechanics Reviews* 1994;47(10):457-99.
- [25] Beskos DE. Boundary element methods in dynamic analysis: part II (1986-1996). *Applied Mechanics Reviews*. ASME 1997;50:149-97.

- [26] Aliabadi MH. Boundary element formulations in fracture mechanics. *Applied Mechanics Reviews* 1997;50(2):83-96.
- [27] Banerjee PK. *Boundary element methods in engineering*. New York: McGraw-Hill, 1994.
- [28] Rong T-Y. Generalized mixed variational principles and new FEM models in solid mechanics. *International Journal of Solids and Structures* 1988;24(11):1131-40.
- [29] Rong T-Y, Lu A-Q. Parametrized Lagrange multiplier method and construction of generalized mixed variational principles for computational mechanics. *Computer Methods in Applied Mechanics and Engineering* 1998;164(3/4):287-96.
- [30] Felippa CA. A survey of parametrized variational principles and applications to computational mechanics. *Computer Methods in Applied Mechanics and Engineering* 1994;113:109-39.
- [31] Felippa CA, Haugen B, Militello C. From the individual element test to finite element templates: evolution of the patch test. *International Journal for Numerical Methods in Engineering* 1995;38:199-239.
- [32] Selected Papers From the Second International Conference on Spectral and High-Order Methods; special issue of *Computer Methods in Applied Mechanics and Engineering* 1994;116(1-4).
- [33] Sherwin SJ, Karniadakis GE. A triangular spectral element method: applications to the incompressible Navier-Stokes equations. *Computer Methods in Applied Mechanics and Engineering* 1995;123:189-229.
- [34] Sherwin SJ, Karniadakis GE. Tetrahedral hp finite elements: algorithms and flow simulations. *Journal of Computational Physics* 1996;124:14-45.
- [35] Strang G. Wavelets and dilation equations: a brief introduction. *SIAM Review* 1989;31(4):614-27.
- [36] Williams JR, Amaratunga K. Introduction to wavelets in engineering. *International Journal for Numerical Methods in Engineering* 1994;37(14):2365-88.
- [37] Ko J, Kurdila AJ, Pilant MS. A class of wavelet-based finite element methods for computational mechanics. In: *Proc. of the 35th AIAA/ASME/ASCE/AHS/ASC Structures, Structural Dynamics and Materials Conference*, Hilton Head, SC, April 18-20, 1994, Part 2, AIAA Paper 94-1388-CP, 1994.
- [38] Kurdila AJ, editor. *Wavelet and multiscale methods for partial differential equations*. San Diego, CA: Academic Press, 1997.
- [39] Ko J, Kurdila AJ, Pilant MS. Triangular wavelet based finite elements via multivalued scaling equations. *Computer Methods in Applied Mechanics and Engineering* 1997;146(1-2):1-17.
- [40] Vasilyev OV, Paolucci S. A dynamically adaptive multi-level wavelet collocation method for solving partial differential equations in a finite domain. *Journal of Computational Physics* 1996;125:498-512.
- [41] Teixeira de Freitas JA, Moitinho de Almeida JP, Ribeiro Pereira EMB. Non-conventional formulations for the finite element method. *Structural Engineering and Mechanics* 1996;4(6):655-78.
- [42] Belytschko T, Krongauz Y, Organ D, Fleming M. Meshless methods: an overview and recent developments. *Computer Methods in Applied Mechanics and Engineering* 1996;139:3-47.
- [43] Liu W-K, Jun S, Adee J, Belytschko T. Reproducing kernel particle methods for structural dynamics. *International Journal for Numerical Methods in Engineering* 1994;38(8):1655-79.
- [44] Gingold RA, Monaghan JJ. Smoothed particle hydrodynamics: theory and application to non-spherical stars. *Mon Nat Roy Astron Soc* 1977;181:375-89.
- [45] Atluri SN, Zhu T. A new meshless local Petrov-Galerkin (MLPG) approach in computational mechanics. *Computational Mechanics* 1998;22(2):117-27.
- [46] Zienkiewicz OC, Onate E. Finite volumes vs finite elements. Is there really a choice? In: Wriggers P, Wagner W, editors. *Nonlinear computational mechanics, state-of-the-art*. Berlin: Springer-Verlag, 1991. p. 240-54.
- [47] Onate E, Cervera M, Zienkiewicz OC. A finite volume format for structural mechanics. *International Journal for Numerical Methods in Engineering* 1994;37(2):181-201.
- [48] Bailey C, Cross M. A finite volume procedure to solve elastic solid mechanics problems in three dimensions on an unstructured mesh. *International Journal for Numerical Methods in Engineering* 1995;38:1757-76.
- [49] Demirdzic I, Muzaferija S. Numerical method for coupled fluid flow, heat transfer and stress analysis using unstructured moving meshes with cells of arbitrary topology. *Computer Methods in Applied Mechanics and Engineering* 1995;125:235-55.
- [50] Song Ch, Wolf JP. The scaled boundary finite-element method—alias consistent infinitesimal finite element cell method—for elastodynamics. *Computer Methods in Applied Mechanics and Engineering* 1997;147:329-55.
- [51] Demirdzic I, Muzaferija S, Peric M. Benchmark solutions of some structural analysis problems using finite volume method and multigrid acceleration. *International Journal for Numerical Methods in Engineering* 1997;40:1893-908.
- [52] Duarte CAM, Oden JT. Hp clouds: an hp meshless method. *Numerical Methods for Partial Differential Equations* 1996;12:673-705.
- [53] Babuska I, Melenk JM. The partition of unity finite element method. *International Journal for Numerical Methods in Engineering* 1997;40:727-58.
- [54] Chapelle D, Bathe KJ. Fundamental considerations for the finite element analysis of shell structures. *Computers and Structures* 1998;66(1):19-36.
- [55] MacNeal RH. Perspective on finite elements for shell analysis. *Finite Elements in Analysis and Design* 1998;30:175-86.
- [56] Noor AK, Belytschko T, Simo JC, editors. *Analytical and computational models for shells*. Proc. of the symposium, ASME Winter Annual Meeting, December 10-15, 1989, San Francisco, CA, CED vol. 3. ASME, New York, 1989.
- [57] Bathe KJ. *Finite element procedures*. Englewood Cliffs, NJ: Prentice-Hall, 1996.
- [58] Bathe KJ, Iosilevich A, Chapelle D. An evaluation of the MITC shell elements. *Computers and Structures*, in press.

- [59] Bathe KJ, Iosilevich A, Chapelle D. An inf-sup test for shell finite elements, *Computers and Structures*, in press.
- [60] Tvergaard V, Needleman A. Effects of non-local damage in porous plastic solids. *International Journal of Solids and Structures* 1995;32:1063-77.
- [61] Owen DRJ, et al. *Computational plasticity: fundamentals and applications*. Barcelona: CIMNE, 1997.
- [62] Simo JC, Hughes TJR. *Computational inelasticity*. New York: Springer-Verlag, 1998.
- [63] Ramaswamy S, Aravas N. Finite element implementation of gradient plasticity models. Part I: gradient-dependent yield functions. *Computer Methods in Applied Mechanics and Engineering* 1998;163(1-4):11-32.
- [64] Eberhardt JJ, Hay PJ, Carpenter JA. Materials by design: a hierarchical approach to the design of new materials. *Materials Research Society Symposium Proc* 1985;63:191-206.
- [65] U.S. Congressional Board, *Advanced materials by design*, Office of Technology Assessment, Washington, DC, 1988.
- [66] Noor AK, Burton WS. Computational models for high-temperature multilayered composite plates and shells. *Applied Mechanics Reviews* 1992;45(10):419-46.
- [67] Noor AK, Burton WS, Bert CW. Computational models for sandwich panels and shells. *Applied Mechanics Reviews* 1996;49(3):155-99.
- [68] Rolfes R, Noor AK, Sparr H. Evaluation of transverse thermal stresses in composite plates based on first-order shear deformation theory. *Computer Methods in Applied Mechanics and Engineering* 1998;167(3/4):355-68.
- [69] Rolfes R, Rohwer K, Ballerstaedt M. Efficient linear transverse normal stress analysis of layered composite plates. *Computers and Structures* 1998;68:643-52.
- [70] Noor AK. Finite element buckling and postbuckling analyses. In: Turvey GJ, Marshall IH, editors. *Buckling and postbuckling of composite plates*. London: Chapman and Hall, 1995. p. 58-107.
- [71] Noor AK, editor. *Buckling and postbuckling of composite structures*, Proc. of the Symposium on Buckling and Postbuckling of Composite Structures, ASME International Mechanical Engineering Congress and Exposition, Chicago, IL, November 6-11, 1994, AD-vol. 41/PVP-vol. 293. New York: The American Society of Mechanical Engineers, 1994.
- [72] Noor AK, Burton WS. Three dimensional solutions for the thermal buckling and sensitivity derivatives of temperature-sensitive multilayered angle-ply plates. *Journal of Applied Mechanics* 1992;59(4):848-56.
- [73] Noor AK, Starnes Jr JH, Peters JM. Nonlinear and postbuckling responses of curved composite panels with cutouts. *Composite Structures* 1996;34(2):213-40.
- [74] Noor AK, Kim YH. Buckling and postbuckling of composite panels with cutouts subjected to combined edge shear and temperature change. *Computers and Structures* 1996;60(2):203-22.
- [75] Noor AK, Starnes Jr JH, Peters JM. Thermomechanical buckling and postbuckling responses of composite panels with skewed stiffeners. *Finite Elements in Analysis and Design* 1997;27(2):193-214.
- [76] Noor AK, Starnes Jr JH, Peters JM. Curved sandwich panels subjected to temperature gradient and mechanical loads. *Journal of Aerospace Engineering, ASCE* 1997;10(4):143-61.
- [77] Noor AK, Peters JM. Analysis of curved sandwich panels with cutouts subjected to combined temperature gradient and mechanical loads. *Journal of Sandwich Structures and Materials* 1999;1:42-59.
- [78] Noor AK, Tenek LH. Steady-state nonlinear heat transfer in multilayered composite panels. *Journal of Engineering Mechanics, ASCE* 1992;118(8):1661-78.
- [79] Rolfes R. Higher-order theory and finite element for heat conduction in composites. In: Lewis RW, Chin JH, Homsy GM, editors. *Proc. of the Seventh International Conference on Numerical Methods in Thermal Problems*, Paris, vol. 7, 1991. p. 880-9.
- [80] Chamis CC, Hopkins DA. Probabilistic composite design. In: Hooper SJ, editor. *Composite materials: testing and design*, vol. 13, ASTM STP-1242, Philadelphia, PA: American Society for Testing and Materials, 1997. p. 23-42.
- [81] Chamis CC, Murthy PLN, Minnetyan L. Progressive fracture in composite structures. In: Armanios EA, editor. *Composite materials: fatigue and fracture*, vol. 6, ASTM STP-1285, Philadelphia, PA: American Society for Testing and Materials, 1997. p. 70-84.
- [82] Minnetyan L, Chamis CC, Murthy PLN. Structural behavior of composites with progressive fracture. *Journal of Reinforced Plastics and Composites* 1992;11(4):413-42.
- [83] Chamis CC, Abumeri GH, Patnaik SN. Multi-scale multi-level multidisciplinary analysis and design for engine structures. In: *Proc. 7th AIAA/USAF/ NASA/ ISSMO Symposium on Multidisciplinary Analysis and Optimization*, St. Louis, MO, September 2-4, 1998, Part 2, AIAA. 1998. p. 1187-97.
- [84] Tani J, Takagi T, Qiu J. Intelligent material systems: application of functional materials. *Applied Mechanics Reviews* 1998;51(8):505-21.
- [85] Brebbia CA, Marchetti M, Santini P, editors. *Smart structures '98. Computational methods for smart structures and materials*. Southampton, UK: WIT Press, 1998.
- [86] Tang YY, Noor AK, Xu K-M. Assessment of computational models for thermo-electro-elastic multilayered plates. *Computers and Structures* 1996;61(5):915-33.
- [87] Xu K-M, Noor AK, Tang YY. Three-dimensional solutions for free vibrations of initially-stressed thermo-electro-elastic multilayered plates. *Computer Methods in Applied Mechanics and Engineering* 1997;141(1/2):125-39.
- [88] Xu K-M, Noor AK. Three-dimensional analytical solutions for coupled thermo-electro-elastic response of multilayered cylindrical shells. *AIAA Journal* 1996;34(4):802-12.
- [89] Xu K-M, Noor AK. Predictor-corrector finite element approach for electro-elastic analysis of hybrid composite plates. *Computer Methods in Applied Mechanics and Engineering* 1997;147(1/2):139-45.

- [90] Halford GR. Cumulative fatigue damage modeling: crack nucleation and early growth. *International Journal of Fatigue* 1997;19(1):5253-60.
- [91] Mitchell MR, Landgraf RW, editors. *Advances in fatigue lifetime predictive techniques*, STP-1122. Philadelphia, PA: American Society for Testing and Materials, 1992.
- [92] Noor AK, et al. (compilers). *Computational methods for failure analysis and life prediction*. Proc. of the Workshop, NASA Langley Research Center, Hampton, VA, October 14-15, 1992, NASA CP-3230, 1993.
- [93] Sun JQ, Miles RN. Acoustic fatigue life prediction for nonlinear structure. *Journal of Sound and Vibration* 1991;150(3):531-5.
- [94] Miles RN. Effect of spectral shape on acoustic fatigue life estimates. *Journal of Sound and Vibration* 1992;153:376-86.
- [95] Reifsnider KL. Performance simulation: a new approach to the prediction of remaining strength and life of material systems. In: Kobayashi A, editor, *Achievement in composites in Japan and the United States*. Proc. of the Japan-U.S. CCM-V, Tokyo, 1990. p. 3-9.
- [96] Reifsnider KL, editor. *Fatigue of composite materials*. New York: Elsevier Science Publishers, 1990.
- [97] Arnold SM, Kruch S. Differential continuum damage mechanics models for creep and fatigue of unidirectional metal matrix composites, NASA TM-105213, November 1991.
- [98] Binienda WK, Arnold SM, Tan HQ. Application of symbolic computations to damage growth in multi-cracked brittle materials. *HITEMP Review* 1991;CP-10082:30(1/2).
- [99] Kerr JR, Haskins JF. Time temperature-stress capabilities of composite materials for advanced supersonic technology application, NASA CR-178272, May 1987.
- [100] Johnson WS. Damage development in titanium metal matrix composites subjected to cyclic loading, NASA TM-107597, April 1992.
- [101] Zaretsky EV, editor. *MMC life system development (Phase I): A NASA/Pratt and Whitney life prediction cooperative program*, NASA Reference Publication 1361, Nov. 1996.
- [102] Nemeth NN, et al. Durability evaluation of ceramic components using CARES/LIFE. *Journal of Engine Gas Turbines Power* 1996;118:150-8.
- [103] Belytschko T, Englemann BE, Liu WK. A review of recent developments in time integration. In: Noor AK, Oden JT, editors. *State-of-the-art surveys on computational mechanics*. New York: The American Society of Mechanical Engineers, 1989. p. 185-99.
- [104] Smolinski P. A variable multi-step method for transient heat conduction. *Computer Methods in Applied Mechanics and Engineering* 1991;86:61-71.
- [105] Smolinski P. Stability of variable explicit time integration for unsteady diffusion problems. *Computer Methods in Applied Mechanics and Engineering* 1991;93:247-52.
- [106] Hulbert GM, Hughes TJR. Space-time finite element methods for second-order hyperbolic equations. *Computer Methods in Applied Mechanics and Engineering* 1990;84:327-48.
- [107] Hulbert GM. Time finite element methods for structural dynamics. *International Journal for Numerical Methods in Engineering* 1992;33:307-31.
- [108] Hulbert GM. Discontinuity-capturing operators for elastodynamics. *Computer Methods in Applied Mechanics and Engineering* 1992;96:409-26.
- [109] Karaoglan L, Noor AK. Space-time finite element methods for the sensitivity analysis of contact/impact response of axisymmetric composite structures. *Computer Methods in Applied Mechanics and Engineering* 1997;144(3/4):371-89.
- [110] Liu WK, Zhang Y, Ramirez MR. Multiple scale finite element methods. *International Journal for Numerical Methods in Engineering* 1991;32:969-90.
- [111] Zhong Z-H, Mackerle J. *Contact-impact problems: a review with bibliography*. Applied Mechanics Reviews 1994;47(2):55-76.
- [112] Zhong Z-H. *Finite element procedures for contact-impact problems*. Oxford, UK: Oxford University Press, 1993.
- [113] Noor AK, Carden HD (compilers). *Computational methods for crashworthiness*, Proc. of the Workshop, Sept. 2-3, 1992, NASA Langley Research Center, Hampton, VA, NASA CP-3223, August 1993.
- [114] Wriggers P. Finite element algorithms for contact problems. *Archives of Computational Methods in Engineering* 1995;2(4):1-49.
- [115] Bathe KJ, Bouzinov PA. On the constraint function method for contact problems. *Computers and Structures* 1997;64(5/6):1069-85.
- [116] Bathe KJ, Guillermin O, Walczak J, Chen H-Y. Advances in nonlinear finite element analysis of automobiles. *Computers and Structures* 1997;64(5/6):881-91.
- [117] Mackerle J. *Contact mechanics—finite element and boundary element approaches: A bibliography (1995-1997)*. Finite elements in analysis and design 1998;29:275-85.
- [118] Brebbia CA, Jones N, Manolis GD, Talaslidis DG, editors. *SUSI 98. Structures under shock and impact V*. Southampton, UK: WIT Press, 1998.
- [119] Mamalis AG, Manolatos DE, Demosthenous GA, Ioannidis MB. *Crashworthiness of composite thin-walled structural components*. Lancaster, PA: Technomic, 1998.
- [120] Huston RL. Multibody dynamics: modeling and analysis methods. *Applied Mechanics Reviews* 1991;44(3):109-17.
- [121] Haug EJ. Dynamics of articulated structures. In: Noor AK, Venneri SL, editors. *Monograph on flight-vehicle materials, structures and dynamics: assessment and future directions*. Structural dynamics and aeroelasticity, vol. 5. New York: The American Society of Mechanical Engineers, 1993. p. 45-53 [chapter 5].
- [122] Huston RL. Multibody dynamics since 1990. *Applied Mechanics Reviews* 1996;49(10):S35-40.
- [123] Shabana AA. Flexible multi-body dynamics: review of past and recent developments. *Multi-body System Dynamics* 1997;1:189-222.

- [124] Elishakoff I. Essay on uncertainties in elastic and viscoelastic structures: from AM Freudenthal's criticism to modern convex modeling. *Computers and Structures* 1995;56(6):871-95.
- [125] Elishakoff I. Three versions of the finite element method based on concepts of either stochasticity, fuzziness, or anti-optimization. *Applied Mechanics Reviews* 1998;51(3):209-18.
- [126] Araujo JM, Awruch AM. Stochastic finite elements for structural analysis. *Computers and Structures* 1994;52(3):461-9.
- [127] Kleiber M, Hien TD. *The stochastic finite element method*. New York: Wiley, 1992.
- [128] Noor AK, Malone JB (compilers). Computational tools and facilities for the next-generation analysis and design environment. *Proc. of the Workshop*, September 17-18, 1996, Hampton, VA, NASA CP-3346, March 1997.
- [129] Wasfy TM, Noor AK. Application of fuzzy sets to transient analysis of space structures. *Finite Elements in Analysis and Design* 1998;29:153-71.
- [130] Abdel-Tawab K, Noor AK. A fuzzy-set analysis for a dynamic thermo-elasto-visco-plastic damage response. *Computers and Structures* 1999;70(1):91-107.
- [131] Qiu Z, Elishakoff I. Anti-optimization of structures with large uncertain but non-random parameters via interval analysis. *Computer Methods in Applied Mechanics and Engineering* 1998;152(3/4):361-72.
- [132] Kleiber M. Computer-assisted qualitative mechanics: an exemplary simulation of a 'Snap-Through' problem. *Computers and Structures* 1994;52(6):1261-8.
- [133] Kulpa Z, Pownuk A, Skalna I. Analysis of linear mechanical structures with uncertainties by means of interval methods. *Computer Assisted Mechanics and Engineering Sciences* 1998;5(4):1-38.
- [134] Kulpa Z, Radomski A, Gajl O, Kleiber M, Skalna I. Hybrid expert system for qualitative and quantitative analysis of mechanical structures. In: Ironi L, editor. *Qualitative Reasoning: 11th Int. Workshop*, Cortona, Italy, June 3-6, 1997, p. 287-93. Publ. No. 1036, Istituto di Analisi Numerica CNR, Pavia, Italy, 1997.
- [135] Topping BHV, Bahreininejad A. *Neural computing for structural mechanics*. Edinburgh, UK: Saxe-Coburg, 1997.
- [136] Noor AK, Andersen CM. Hybrid analytical technique for the nonlinear analysis of curved beams. *Computers and Structures* 1992;43(5):823-30.
- [137] Noor AK. Recent advances and applications of reduction methods. *Applied Mechanics Reviews* 1994;47(5):125-46.
- [138] Kobayashi AS. Hybrid experimental-numerical stress analysis. In: Kobayashi AS, editor. *Handbook of experimental mechanics*, 2nd ed. Weinheim, Berlin: Wiley-VCH, 1993, p. 751-83.
- [139] Szewczyk ZP, Noor AK. A hybrid neuro-computing/numerical strategy for nonlinear structural analysis. *Computers and Structures* 1996;58(4):661-78.
- [140] Szewczyk ZP, Noor AK. A hybrid neuro-computing strategy for sensitivity analysis of nonlinear structures. *Computers and Structures* 1997;65(6):869-80.
- [141] Ghaboussi J, Pecknold DA, Zhang M, Haj-Ali RM. Auto-progressive training of neural network constitutive models. *International Journal for Numerical Methods in Engineering* 1998;42:105-26.
- [142] Shephard MS, Weatherill NP, editors. Adaptive meshing: special issue of *International Journal for Numerical Methods in Engineering* 1991;32(4).
- [143] Noor AK, editor. Adaptive, multilevel and hierarchical computational strategies. *Proc. of the symposium, ASME Winter Annual Meeting*, Nov. 8-13, 1992, Anaheim, CA, AMD-157. New York: The American Society of Mechanical Engineers, 1992.
- [144] Demkowicz L, Oden JT, Babuska I. Reliability in computational mechanics: special issue of *Computer Methods in Applied Mechanics and Engineering* 1992;101(1-3).
- [145] Lee N-S, Bathe KJ. Error indicators and adaptive remeshing in large deformation finite element analysis. *Finite Elements in Analysis and Design* 1994;16:99-136.
- [146] Verfurth R. *A posteriori error estimation and adaptive mesh-refinement techniques*. Chichester, UK: Wiley, 1996.
- [147] Ladeveze P, Oden JT, editors. *Advances in adaptive computational methods*. New York: Elsevier Science, 1998.
- [148] Stewart JR, Hughes TJR. A tutorial in elementary finite element error analysis: a systematic presentation of a priori and a posteriori error estimates. *Computer Methods in Applied Mechanics and Engineering* 1998;158(1/2):1-22.
- [149] Zhu JZ. A posteriori error estimation: the relationship between different procedures. *Computer Methods in Applied Mechanics and Engineering* 1997;150(1-4):411-22.
- [150] Babuska I, Strouboulis T, Gangaraj SK, Upadhyay CS. Pollution error in the h-version of the finite element method and the local quality of the recovered derivatives. *Computer Methods in Applied Mechanics and Engineering* 1997;140(1/2):1-37.
- [151] Babuska I, Strouboulis T, Gangaraj SK, Copps K, Datta DK. Practical aspects of a-posteriori estimation for reliable finite element analysis. *Computers and Structures* 1998;66(5):627-64.
- [152] Krizek M, Neittaanmaki P. On super-convergence techniques. *Acta Applicandae Mathematicae* 1987;9:175-98.
- [153] Babuska I, Miller A. The postprocessing approach in the finite element method—part I: calculation of displacements, stresses and other higher derivatives of the displacements. *International Journal for Numerical Methods in Engineering* 1984;20:1085-109.
- [154] Zienkiewicz OC, Zhu JZ. The super-convergent patch recovery and a posteriori error estimates. part I: the recovery technique. *International Journal for Numerical Methods in Engineering* 1992;33:1331-64.
- [155] Zienkiewicz OC, Zhu JZ, Wu J. Super-convergent patch recovery techniques: some further tests. *Communications in Numerical Methods in Engineering* 1993;9(3):251-8.
- [156] Tabbara M, Blacker T, Belytschko T. Finite element derivative recovery by moving least square interpolants. *Computer Methods in Applied Mechanics and Engineering* 1994;117(1/2):211-23.
- [157] Zhang Z, Zhu JZ. Analysis of the super-convergent

- patch recovery technique and a posteriori error estimator in the finite element method (I). *Computer Methods in Applied Mechanics and Engineering* 1995;123:173-87.
- [158] Zhang Z, Zhu JZ. Analysis of the super-convergent patch recovery technique and a posteriori error estimator in the finite element method (II). *Computer Methods in Applied Mechanics and Engineering* 1998;163(1-4):159-70.
- [159] Lee T, Park HC, Lee SW. A super-convergent stress recovery technique with equilibrium constraint. *International Journal for Numerical Methods in Engineering* 1997;40(6):1139-60.
- [160] Tenchev RT. A study of the accuracy of some FEM stress recovery schemes for two dimensional stress concentration problems. *Finite Elements in Analysis and Design* 1998;29:105-19.
- [161] Yazdani AA, Gakwaya A, Dhatt G. An improved super-convergent patch recovery technique for the axisymmetrical problems. *Computers and Structures* 1998;66(6):799-821.
- [162] Fish J, Markolefas S. Adaptive s-method for linear elastostatics. *Computer Methods in Applied Mechanics and Engineering* 1993;104:363-96.
- [163] Fish J, Markolefas S. Adaptive global-local refinement strategy based on the interior error estimates of the h-method. *International Journal for Numerical Methods in Engineering* 1994;37:827-38.
- [164] Wiberg N-E, Li XD, Abdulwahab F. Adaptive finite element procedures in elasticity and plasticity. *Engineering with Computers* 1996;12:120-41.
- [165] Lee CK, Lo SH. Automatic adaptive three dimensional finite element refinement using different-order tetrahedral elements. *International Journal for Numerical Methods in Engineering* 1997;40:2195-226.
- [166] Rashid MM. The arbitrary local mesh replacement method: an alternative to remeshing for crack propagation analysis. *Computer Methods in Applied Mechanics and Engineering* 1998;154(1/2):133-50.
- [167] Dechaumphai P. Adaptive unstructured meshing for thermal stress analysis of built-up structures. In: *Proc. of the 33rd AIAA/ASME/ASCE/AHS/ASC Structures, Structural Dynamics and Materials Conference*, April 13-15, 1992, Dallas, TX, Part 2, 1992, p. 1069-77.
- [168] Dechaumphai P, Thornton EA, Weiting AR. Flow-thermal-structural study of aerodynamically heated leading edges. *Journal of Spacecraft* 1989;26(4):201-9.
- [169] Weiting AR, Dechaumphai P, Bey KS. Application of integrated fluid-thermal-structural analysis method. *Thin-Walled Structures* 1991;11:1-23.
- [170] Multiple Field Methods. In *Spectrum Solver Theory Manual*, Version 2.0, chap. 4. Centric Engineering Systems, Sunnyvale, CA, 1997.
- [171] Bathe KJ. Simulation of structural and fluid flow response in engineering practice. *Computer Modeling and Simulation in Engineering* 1996;1:47-77.
- [172] Bathe KJ, Zhang H, Zhang X. Some advances in the analysis of fluid flows. *Computers and Structures* 1997;64(5/6):909-30.
- [173] Kleiber M, Hisada T, editors. *Design-sensitivity analysis*. Atlanta, GA: Atlanta Technology Publications, 1993.
- [174] Hinton E, Sienz J. Aspects of adaptive finite element analysis and structural optimization. In: Topping BHV, Papadrakakis M, editors. *Advances in structural optimization*. Edinburgh: CIVIL-COMP, 1994, p. 1-25.
- [175] Squire W, Trapp G. Using complex variables to estimate derivatives of real functions. *SIAM Review* 1998;40(1):110-2.
- [176] Haber RB, Tortorelli DA, Vidal CA. Design sensitivity analysis of nonlinear structures—I: large deformation hyperelasticity and history dependent material response. In: Kamat MP, editor. *Structural optimization: status and promise*. Washington, DC: American Institute of Aeronautics and Astronautics, 1993, p. 369-406.
- [177] Kleiber M, Antunez H, Hien TD, Kowalczyk P. *Parameter sensitivity in nonlinear mechanics: theory and finite element computations*. New York: Wiley, 1997.
- [178] Kirsch U. Efficient sensitivity analysis for structural optimization. *Computer Methods in Applied Mechanics and Engineering* 1994;117(1/2):143-56.
- [179] Kleiber M, Hien TD, Postek E. Incremental finite element sensitivity analysis for nonlinear mechanics applications. *International Journal for Numerical Methods in Engineering* 1994;37(19):3291-308.
- [180] Kulkarni M, Noor AK. Sensitivity analysis of the nonlinear dynamic viscoplastic response of two dimensional structures with respect to material parameters. *International Journal for Numerical Methods in Engineering* 1995;38:183-98.
- [181] Noor AK, Needleman A, Peters JM. Sensitivity analysis for failure and damage in dynamically loaded tensile bars. *Computer Methods in Applied Mechanics and Engineering* 1998;151(3/4):461-78.
- [182] Chinchalker S. The application of automatic differentiation to problems in engineering analysis. *Computer Methods in Applied Mechanics and Engineering* 1994;118:197-207.
- [183] Green LL, Newman PA, Haigler KJ. Sensitivity derivatives for advanced CFD algorithm and viscous modeling parameters via automatic differentiation. *Journal of Computational Physics* 1996;125:313-24.
- [184] Sherman LL, Taylor III AC, Green LL, Newman PA, Hou GW, Korivi VM. First and second-order aerodynamic sensitivity derivatives via automatic differentiation with incremental iterative methods. *Journal of Computational Physics* 1996;129:307-31.
- [185] Follen G, Evans AL, Naiman C, Lopez I. Numerical propulsion system simulation's national cycle program. In: *AIAA/ASME/ASCE/SAE/ASEE 34th Joint Propulsion Conference and Exhibit*, Cleveland, OH, July 13-15, 1998. AIAA-98-3113.
- [186] Topping BHV, Khan AI. *Parallel finite element computations*. Edinburgh, UK: Saxe-Coburg, 1996.
- [187] Hendrickson B, Leland R. An improved spectral graph partitioning algorithm for mapping parallel computations. Sandia National Labs, TR-SAND92-1460, 1992.
- [188] Barnard ST, Simon H. A parallel implementation of multilevel recursive spectral bisection for application to

- adaptive unstructured meshes. Proc. of the Seventh SIAM Conference on Parallel Processing for Scientific Computing 1995;18:627-32.
- [189] Khan AI, Topping BHV. Sub-domain generation for parallel finite element analysis. *Computing Systems in Engineering* 1993;4(4-6):473-88.
- [190] Watson BC, Noor AK. Sensitivity analysis for large-deflection and postbuckling responses on distributed-memory computers. *Computer Methods in Applied Mechanics and Engineering* 1996;129:393-409.
- [191] Watson BC, Noor AK. Large scale contact/impact simulation and sensitivity analysis on distributed-memory computers. *Computer Methods in Applied Mechanics and Engineering* 1997;141(3-4):373-88.
- [192] George PL. Automatic mesh generation: application to finite element methods. New York: Wiley and Masson, 1991.
- [193] Frykestig J. Advancing front mesh generation techniques with application to the finite element method. Department of Structural Mechanics, Chalmers University of Technology, Rept. 94:10, Gotenborg, Sweden, 1994.
- [194] Tworzydło WW, Oden JT. Towards an automated environment in computational mechanics. *Computer Methods in Applied Mechanics and Engineering* 1993;104:87-143.
- [195] Chandra S, Woodman NJ, Blockley DI. An object-oriented structure for transient dynamics on concurrent computers. *Computers and Structures* 1994;51(4):437-52.
- [196] Kecskemethy A, Hiller M. An object-oriented approach for an effective formulation of multi-body dynamics. *Computer Methods in Applied Mechanics and Engineering* 1994;115(3-4):287-314.
- [197] Besson J, Foerch R. Large scale object-oriented finite element code design. *Computer Methods in Applied Mechanics and Engineering* 1997;142(1-2):165-87.
- [198] Mackie RI. Using objects to handle complexity in finite element software. *Engineering with Computers* 1997;13:99-111.
- [199] Eyheramendy D, Zimmermann Th. Object-oriented finite elements. III: theory and application of automatic programming. *Computer Methods in Applied Mechanics and Engineering* 1998;154(1-2):41-68.
- [200] Zimmermann Th, Bomme P, Eyheramendy D, Vernier L, Commend S. Aspects of an object-oriented finite element environment. *Computers and Structures* 1998;68(1-3):1-16.
- [201] Dubois-Pelerin Y, Pegon P. Object-oriented programming in nonlinear finite element analysis. *Computers and Structures* 1998;68(4):225-41.
- [202] Devloo PRB. Efficiency issues in an object-oriented programming environment. In: Topping BHV, Papadrakakis M, editors. *Artificial intelligence and object-oriented approaches for structural engineering*. Edinburgh: CIVIL-COMP, 1994. p. 147-51.
- [203] Denning PJ, Metcalfe RM. Beyond calculation: the next fifty years of computing. New York: Springer-Verlag, 1997.
- [204] Foster I, Kesselman C, editors. *The grid: blueprint for a new computing infrastructure*. San Francisco, CA: Morgan Kaufmann, 1999.
- [205] Noor AK. New computing systems and future high performance computing environments and their impact on structural analysis and design. *Computers and Structures* 1997;64(1-4):1-30.
- [206] Holtz WB. *The CAD rating guide*, 5th ed. Nashua, NH: PennWell, 1997.
- [207] Kumar B. (guest editor). Information technology in civil and structural engineering design, *Computers and Structures* (special issue) 1998;67(5).
- [208] Hughes TJR, Stewart J. A space time formulation for multi-scale phenomena. *Journal of Comput Applied Math* 1996;74:217-29.
- [209] Hughes TJR, Feijoo GR, Mazzei L, Quincy J-B. The variational multiscale method: a paradigm for computational mechanics. *Computer Methods in Applied Mechanics and Engineering* 1998;166(1/2):3-24.
- [210] Noor AK (compiler). Computational intelligence and its impact on future high performance engineering systems, Proc. of the Workshop, June 27-28, 1995, Hampton, VA, NASA GP-3323, January 1996.

Computers & Structures

An
International
Journal

vol. 73, no. 1-5

published September 1999

- | | | |
|---|-----|---|
| A. K. Noor | 1 | Computational structures technology: leap frogging into the twenty-first century |
| P. Saint-Georges,
G. Warzee, Y. Notay and
R. Beauwens | 33 | Problem-dependent preconditioners for iterative solvers in FE elastostatics |
| P. Ladevèze and N. Moës | 45 | Adaptive control for finite element analysis in plasticity |
| H. Cramer, M. Rudolph,
G. Steinl and W. Wunderlich | 61 | A hierarchical adaptive finite element strategy for elastic-plastic problems |
| C. Chinosi and C. Lovadina | 73 | Remarks on partial selective reduced integration method for Reissner-Mindlin plate problem |
| N.-E. Wiberg, R. Bausys and
P. Hager | 79 | Improved eigenfrequencies and eigenmodes in free vibration analysis |
| J. Aalto and M. Perälä | 91 | Built-in field equations for patch recovery procedures using weighted residuals |
| J. Aalto and M. Åman | 119 | Polynomial representations for patch recovery procedures |
| A. Lorenzana and
J. A. Garrido | 147 | Analysis of the elastic-plastic problem involving finite plastic strain using the boundary element method |
| V. Sladek and J. Sladek | 161 | Modified Overhauser elements for approximation of boundary densities in regularized BEM formulations |

(Contents continued on inside back cover)

INDEXED IN Appl Mech Rev, Curr Cont ASCA, Cam Sci Abstr, Curr Cont CompuMath, Curr Cont/Eng Tech & Applied Sci, Comput Cont, Eng Ind, Geo Struct Info, INSPEC Data, Int Civil Eng Abstr, Info Sci Abstr, Math R, Mechanics, Metals Abstr, PASCAL-CNRS Data, Curr Cont SCISEARCH Data, Soft Rev on File, SSSA/CISA/ECA/ISMEC.



PERGAMON



0045-7949(1999)73:1-5;1-0

ISSN 0045-7949

SOME FUTURE DIRECTIONS OF COMPUTATIONAL STRUCTURES TECHNOLOGY*

Ahmed K. Noor
Center for Advanced Computational Technology
University of Virginia
NASA Langley Research Center
Hampton, VA 23681

SUMMARY

Some of the research areas of computational structures technology (CST) which have high potential for meeting the needs of future high-tech engineering systems are identified. Discussion focuses on the characteristics of future engineering systems; drivers for the technology; characteristics of future computing environment; and role of CST in future CAD/CAM/CAE systems and design environment. Future research areas include high fidelity modeling of the structure and its components; failure and life prediction methodologies; hierarchical, integrated methods and adaptive modeling strategies; nondeterministic analysis, soft computing and risk assessment; fully-coupled analysis and optimization problems associated with intelligent and modular structures; and validation of numerical simulations.

INTRODUCTION

Computational structures technology blends the insightful modeling of structural response with the development of computational methods and represents one of the most significant developments in the history of the structures field. Its use over the past four decades has transformed much of theoretical structural mechanics and materials science into practical tools that affect all phases of the design, fabrication and testing of engineering systems.

Current CST activities include the study of phenomena occurring at disparate spatial and time scales. Length scales range from the microscopic level to the structural level. Today no important design can be completed without CST, nor can any new theory be validated without it. Commercial programs for structural analysis have a rich variety of elements, and are widely used for performing structural calculations on large components and/or entire structures. CST applications cover a broad range of industries, including aerospace, automotive, electronic, naval and nuclear industries. Reviews of recent activities in the U.S. and European aerospace industries are given in Noor, Housner, Starnes, Hopkins and Chamis (1992), and AIAA (1993). Other industrial applications of CST are described in Goudreau (1994), and Argyris, St. Doltsinis, Frik and Tenek (1994).

Although CST led the way among computational mechanics disciplines until the 1970's, the emphasis has since shifted to other computational science disciplines, particularly computational fluid dynamics. However, there is now renewed interest in CST. There are three compelling motivations for vigorously pursuing CST development: the radically different demands that future high-performance

*Work is partially supported by NASA Cooperative Agreement NCCW-0011, and by Air Force Office of Scientific Research Grant AFOSR-F49620-96-1-0462.

engineering systems place on CST, from those of current systems; the need for reducing the cost and development time of future systems and the associated need for reducing dependence on extensive and costly testing; and the desire to use the power of new and emerging computing, communication and networking technologies in the design and operation of future engineering structures.

In this paper an attempt is made to identify some of the promising research areas of CST which are likely to impact future high-tech engineering systems. In identifying these areas, the following four factors are considered: characteristics of future engineering systems, their design drivers, and their implications for CST; future computing, communication and networking environment; trends in CAD/CAM/CAE systems which will be used to integrate CST modules with other computational modules for product development; and developments that can be adapted to CST from other fields of computational sciences. The first three factors are discussed subsequently.

CHARACTERISTICS OF FUTURE STRUCTURES

Structures of future high-performance engineering systems (e.g., aerospace, automotive and electronic) will have a number of major characteristics which will significantly impact their design, including (see Figs. 1-3):

- a high degree of autonomy (thinking, self-healing structures) with embedded sensors, actuators and elaborate information processing systems;
- miniaturization of subcomponents and/or of the entire structure; and
- modularity - the system capabilities will be tailored through the use of modules for specific mission needs. Examples of modular systems are provided by modular aircraft and the multifunctional bus needed in a number of spacecraft.

The design drivers for future engineering systems include:

- affordability - emphasis will be on reducing the life-cycle cost;
- rapid prototyping - which requires reducing both the design cycle and development times; and
- improved performance - which can be accomplished through insertion of new and emerging technologies.

The design drivers can be accomplished by using intelligent simulation-based design environment for simulating the entire life-cycle of the engineering system, from concept development, detailed design and prototyping to qualification testing, operations and disposal (see Fig. 4).

NEW AND EMERGING COMPUTING, COMMUNICATION AND NETWORKING ENVIRONMENTS

Computer technology has always served as the technological foundation of CST. The current trend towards merging telecommunications and computer technologies, and the advances made in computing, communication and networking technologies, will significantly impact all aspects of CST given in Noor (1995). These advances include:

- ultrafast computers with sustained speeds in the teraflop range, such as the Intel/Sandia machine with 9072 Pentium Pro processors and a peak performance of 1.8 teraflops; and the IBM RS/6000 SP system, built for Lawrence Livermore Lab, with 4096 processors and a peak performance of 3 teraflops;
- intelligent distributed metacomputing environment in which the network of geographically dispersed computers acts as a single problem solving environment. Examples are the National MetaCenter for Computational Science and Engineering which connects the NSF supercomputer centers, and the DARPA Intelligent Metacomputing Center;

- special-purpose computers such as neural networks and embedded computers;
- infrastructure for collaborative computing among geographically dispersed teams. The Internet, with commercial and public domain software, provides the communication infrastructure between analysis and design teams using a mixed environment of hardware and operating systems. For very-large scale projects, Intranets (networks within individual organizations) are used for communicating design information among members of each organization, and Extranets are used to provide secured Internet connections between Intranets. The next-generation Internet is expected to alleviate the performance problems associated with constricted network bandwidth;
- high-bandwidth human-computer interaction facilities including multimedia, immersive synthetic environment with miniature wearable computing devices and wireless communications (see Figs. 5 and 6). Some of these facilities will enable a shared interactive experience in which multiple users coexist in the same virtual environment and in which users can actually interact with and modify the environment in real time.

TRENDS IN CAD/CAM/CAE SYSTEMS

In addition to new modeling functionality, fundamental changes in the architecture and facilities of CAD/CAM/CAE systems include:

- seamless integration of structural and other physics-based analysis codes into the CAE system, eliminating data transfers and interfaces and allowing detailed structural and other analyses to be performed from within the CAD system, on the most current product model throughout the design process (Fig. 7);
- incorporation of object-oriented technology, particularly in the user interface and databases for the CAE system, enabling a "plug-and-play" capability for rapid modeling. "Plug" refers to object-oriented user interface for the rapid assembly of component models. Model generation via assembly and resizing of parts and components can be performed rapidly. "Play" refers to immediately available predictions of structural and other response characteristics;
- incorporation of Internet-enabling software allowing structural analysts and designers to access the product model data without leaving their application and to move the data reliably on the Internet;
- incorporation of seamless interface (translation) from the CAE system to the virtual environment with a mathematically correct visualization of the structural model.

FUTURE RESEARCH AREAS

In order for CST to play a significant role in future development of structures technology, as well as in the design and certification of future engineering systems, major advances and new computational tools are needed in several key areas. To this end the research community must address several primary pacing items and related tasks. In identifying the pacing items, due consideration was given to the factors described in the preceding sections.

Primary Pacing Items

The primary pacing items for CST are: high-fidelity modeling of the structure and its components; failure and life prediction methodologies; hierarchical, integrated methods and adaptive modeling strategies; nondeterministic analysis, soft computing and risk assessment (Fig. 8); and fully-coupled analysis and optimization problems associated with intelligent and modular structures (Fig. 9). For each of the aforementioned items, attempts should be made to exploit the major characteristics of the future computing environment as well as the next-generation CAD/CAM/CAE systems. The five

primary pacing items are described in Noor (1996). Note that some of the tasks within the pacing items are of a generic nature. Others are specific to either certain components of future engineering systems (e.g., propulsion systems or airframes of flight vehicles).

Related Tasks

For CST to impact the design process, the following two tasks need to be addressed by the research community: a) development of automated or semi-automated model (and mesh) generation facilities, including real-time model generation; use of advanced visualization technology and emerging visualization paradigms, including multimedia, virtual reality facilities, interactive visualization (real-time visualization and simulation), and computational steering; and b) adaptation of object-oriented technology and AI tools (knowledge-based/expert systems and techniques for knowledge discovery in databases) to CST.

The outlook for CST is bright. Innovative structural concepts, advanced computational material models, intelligent computational tools for analysis and synthesis, future computing environment and CAE systems should significantly enhance CST development and improve the design of engineering systems.

REFERENCES

- Argyris, J., St. Doltsinis, I., Frik, G. and Tenek, L., "Computational Structures Technology in Europe - Past, Present and Future," *IEEE Computational Science and Engineering*, Vol. 1, No. 1, Spring 1994, pp. 43-54.
- American Institute of Aeronautics and Astronautics, Focus 93 - Computational Structures Technology, *Aerospace America*, February 1993.
- Goudreau, G. L., "Computational Structural Mechanics: From National Defense to National Resource," *IEEE Computational Science and Engineering*, Vol. 1, No. 1, Spring 1994, pp. 33-42.
- Noor, A. K., Housner, J. M., Starnes, J. H., Jr., Hopkins, D. A. and Chamis, C. C. (compilers), *Computational Structures Technology for Airframes and Propulsion Systems*, NASA CP-3142, May 1992.
- Noor, A. K., "Computational Structures Technology - Leap Frogging into the Twenty-First Century," in *Advances in Computational Structures Technology*, B.H.V. Topping (ed.), Civil-Comp Press, Edinburgh, U.K., 1996, pp. 1-18.
- Noor, A. K., "New Computing Systems and Future High-Performance Computing Environment," in *Monograph on Flight Vehicle Materials, Structures and Dynamics - Assessment and Future Directions*, Noor, A. K. and Venneri, S. L. (eds.), American Society of Mechanical Engineers, NY, 1995, Vol. 6, pp. 39-87.

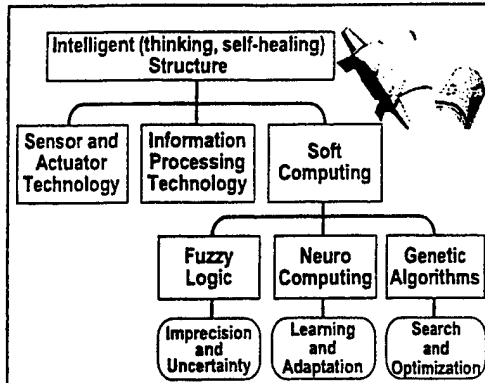


Figure 1. Intelligent (thinking, self-healing) structure.

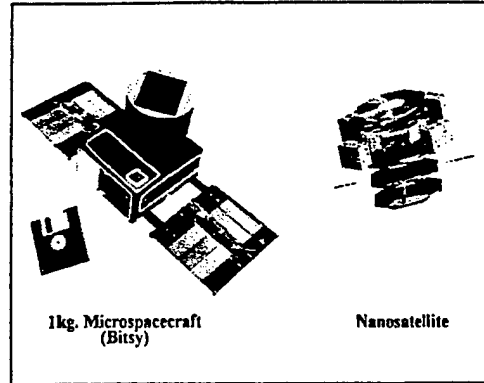


Figure 2. Miniature spacecraft.

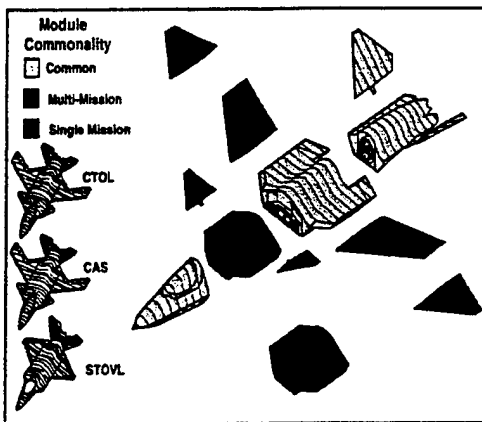


Figure 3. Modular aircraft.

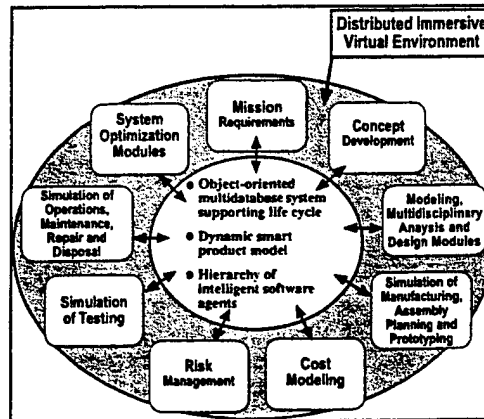


Figure 4. Schematic of a simulation based design environment for engineering systems.

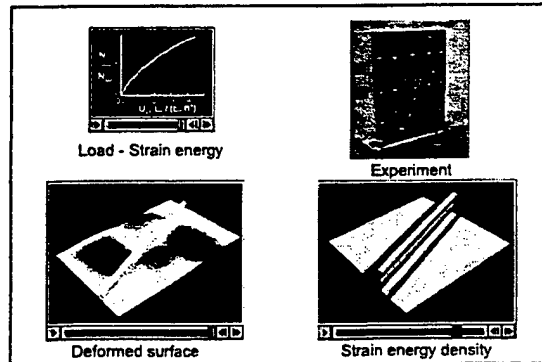


Figure 5. Multimedia facilities.

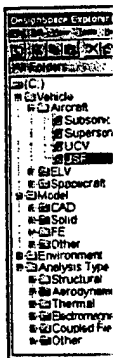


Figure 7. CAD system.

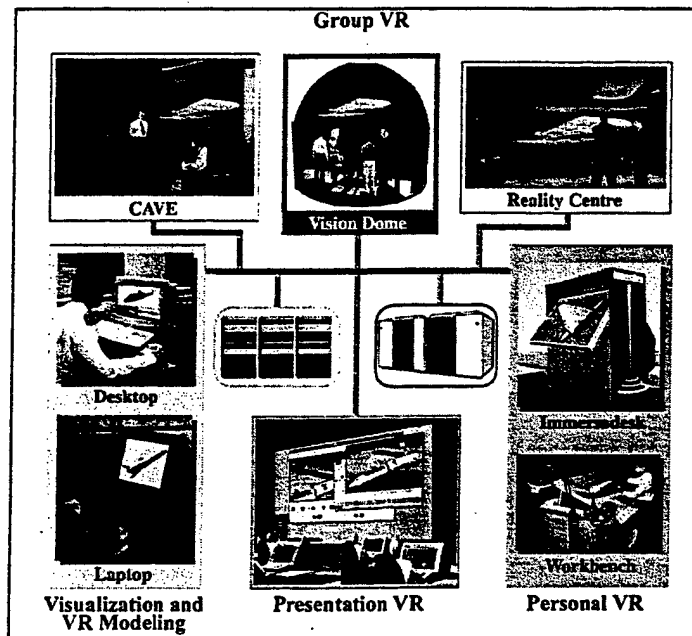


Figure 6. Integrated virtual reality facilities.

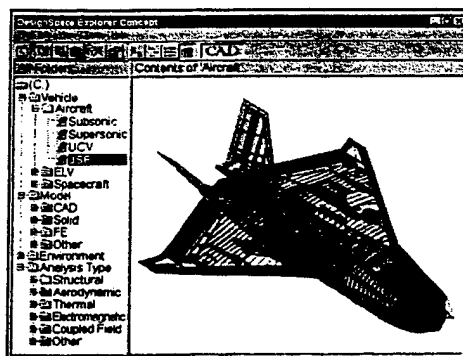


Figure 7. Concept of analysis-embedded CAD system.

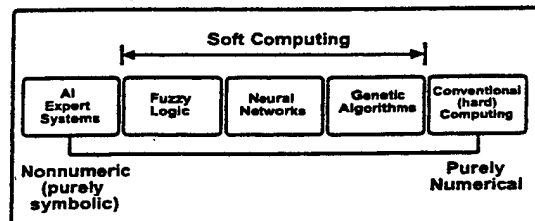


Figure 8. Relationship between soft computing, AI and conventional (hard) computing.

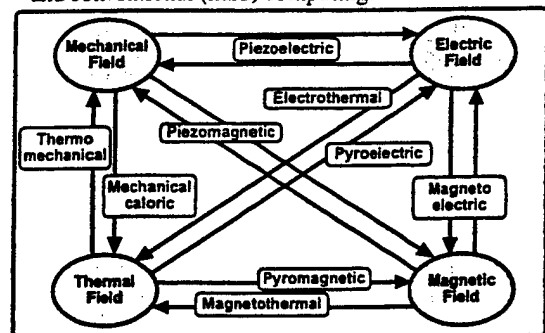


Figure 9. Couplings between mechanical, electric, magnetic and thermal fields in smart materials.

**Advances in
Computational Engineering Science**

**S.N. Atluri and G. Yagawa
Editors**

**Tech Science Press
81 E. Main Street
Forsyth, Georgia 31029
USA**

S.N. Atluri
Computational Modeling Center
Georgia Institute of Technology
Atlanta, Georgia 30332-0356, U.S.A.

G. Yagawa
Department of Quantum Engineering
& Systems Science
The University of Tokyo
7-3-1 Hongo, Bunkyo-ku
Tokyo 113, Japan

Published by Tech Science Press
81 E. Main Street
Forsyth, Georgia 31029
U.S.A.
tel/fax: 912-994-4051
e-mail: ksi@mylink.net

Copyright 1997 Tech Science Press

All rights reserved. No part of this publication may be reproduced or distributed in any form or by any means without written permission of the publisher.

All trademarks and brand names mentioned in this book are the property of their respective owners and in no way affiliated with the editors or publisher. The authors, editors and publisher will not accept any legal responsibility for any errors or omissions that may be made in this publication. The publisher makes no warranty, express or implied, with respect to the material contained herein.

Printed in the United States of America.

ISBN 0-96570001-0-0

Comput
years b
compute
relative
impact
papers

It is als
position
develop
applican
minusc
tools co

Thus, c
unargua
authors
and sim

Satya N
and
Genki Y

Satya N
Institute
of Engin
Comput
Georgia
Atlanta

Reprinted from

Computer methods in applied mechanics and engineering

Comput. Methods Appl. Mech. Engrg. 167 (1998) 355–368

Evaluation of transverse thermal stresses in composite plates based
on first-order shear deformation theory

R. Rolfes^a, A.K. Noor^{b,*}, H. Sparr^a

^a*Institute of Structural Mechanics, German Aerospace Research Establishment (DLR), Braunschweig, Germany*

^b*Center for Advanced Computational Technology, University of Virginia, NASA Langley Research Center, Hampton, VA 23681, USA*

Received 26 March 1998



ELSEVIER

COMPUTER METHODS IN APPLIED MECHANICS AND ENGINEERING

EDITORS: J.H. ARGYRIS, STUTTGART and LONDON

T.J.R. HUGHES, STANFORD, CA

J.T. ODEN, AUSTIN, TX

W. PRAGER
Founding Editor
(deceased 1980)

EDITORIAL ADDRESSES

John H. ARGYRIS
Institut für Computer Anwendungen
Pfaffenwaldring 27
D-70569 STUTTGART
Germany
(Editorial Office)

Thomas J.R. HUGHES
Division of
Applied Mechanics
Durand Building
Room No. 281
Stanford University
STANFORD
CA 94305-4040, USA

J. Tinsley ODEN
The University of Texas
The Texas Institute for
Computational and
Applied Mathematics
Taylor Hall 2.400
AUSTIN
TX 78712, USA

ASSOCIATE EDITORS

K. APPA, *Lake Forest, CA*
I. BABUŠKA, *Austin, TX*
A.J. BAKER, *Knoxville, TN*
T.B. BELYTSCHKO, *Evanston, IL*
F. BREZZI, *Pavia*
P.G. CIARLET, *Paris*
L. DEMKOWICZ, *Austin, TX*
R.E. EWING, *College Station, TX*
R. GLOWINSKI, *Houston, TX*

R.W. LEWIS, *Swansea*
J.L. LIONS, *Paris*
F.L. LITVIN, *Chicago, IL*
H. LOMAX, *Moffet Field, CA*
L.S.D. MORLEY, *Farnborough*
N. OLSHOFF, *Aalborg*
E. ONATE, *Barcelona*
M. PAPADRAKAKIS, *Athens*

J. PLANCHARD, *Clamart*
E. RAMM, *Stuttgart*
G. STRANG, *Cambridge, MA*
R.L. TAYLOR, *Berkeley, CA*
S.Ø. WILLE, *Oslo*
G. YAGAWA, *Tokyo*
D. ZHU, *Xi'an*
O.C. ZIENKIEWICZ, *Swansea*

ADVISORY EDITORS

M.P. ARNAL, *Baden*
J.S. ARORA, *Iowa City, IA*
K.J. BATHE, *Cambridge, MA*
P.G. BERGAN, *Høvik*
J.F. BESSELINE, *Delft*
M.O. BRISTEAU, *Le Chesnay*
C. CANUTO, *Turin*
J.L. CHENOT, *Valbonne*
Y.K. CHEUNG, *Hong Kong*
T.J. CHUNG, *Huntsville, AL*
T.A. CRUSE, *Nashville, TN*
E.R. DE ARANTES E OLIVEIRA, *Lisbon*
J. DONEA, *Ispra*
A. ERIKSSON, *Stockholm*
C. FARHAT, *Boulder, CO*
C.A. FELIPPA, *Boulder, CO*
C.J. FITZSIMONS, *Baden-Dattwil*
M. GERADIN, *Liège*
R. GRUBER, *Manno*
H.-Å. HÄGGBLAD, *Luleå*
E.J. HAUG, *Iowa City, IA*

J.C. HEINRICH, *Tucson, AZ*
U. HEISE, *Aachen*
J. HELLESAND, *Oslo*
C. HOEN, *Oslo*
M. HOGGE, *Liège*
S. IDELSOHN, *Santa Fe*
L. JOHANSSON, *Linköping*
C. JOHNSON, *Göteborg*
M. KAWAHARA, *Tokyo*
S.W. KEY, *Albuquerque, NM*
A. KLARBRING, *Linköping*
M. KLEIBER, *Warsaw*
P. LADEVEZE, *Chachan*
A. LEGER, *Clamart*
B.P. LEONARD, *Akron, OH*
P. LE TALLEC, *Paris*
W.K. LIU, *Evanston, IL*
G. MAIER, *Milan*
H.A. MANG, *Vienna*
A. NEEDLEMAN, *Providence, RI*
M.P. NIELSEN, *Lyngby*

A.K. NOOR, *Hampton, VA*
R. OHAYON, *Paris*
J. PERIAUX, *Saint Cloud*
QIAN Ling-xi (L.H. Tsien), *Dalian*
A.K. RAO, *Hyderabad*
B.D. REDDY, *Rondebosch*
J.N. REDDY, *College Station, TX*
E. RIKS, *Delft*
G.L.N. ROZVANY, *Essen*
W. SCHIEHLEN, *Stuttgart*
M.S. SHEPHARD, *Troy, NY*
E. STEIN, *Hannover*
P.K. SWEET, *Reading*
M. TANAKA, *Nagano*
T.E. TEZDUYAR, *Houston, TX*
C.W. TROWBRIDGE, *Kidlington*
H. VAN DER VORST, *Utrecht*
J.R. WHITEMAN, *Uxbridge*
K.J. WILLAM, *Boulder, CO*
T. ZIMMERMANN, *Lausanne*

Editorial Secretary: Marlies PARSONS

Advertising information. Advertising orders and enquiries can be sent to: **Europe and ROW:** Rachel Gresle-Farthing, Elsevier Science Ltd., Advertising Department, The Boulevard, Langford Lane, Kidlington, Oxford OX5 1GB, UK; phone: (+44) (1865) 843565; fax: (+44) (1865) 843976; e-mail: r.gresle-farthing@elsevier.co.uk. **USA and Canada:** Elsevier Science Inc., Mr Tino DeCarlo, 655 Avenue of the Americas, New York, NY 10010-5107, USA; phone: (+1) (212) 633 3815; fax: (+1) (212) 633 3820; e-mail: t.decarlo@elsevier.com. **Japan:** Elsevier Science K.K., Advertising Department, 9-15 Higashi-Azabu 1-chome, Minato-ku, Tokyo 106, Japan; phone: (+81) (3) 5561-5033; fax: (+81) (3) 5561 5047.

© The paper used in this publication meets the requirements of ANSI/NISO Z39.48-1992 (Permanence of Paper).



ELSEVIER

Comput. Methods Appl. Mech. Engrg. 167 (1998) 355–368

**Computer methods
in applied
mechanics and
engineering**

Evaluation of transverse thermal stresses in composite plates based on first-order shear deformation theory

R. Rolfes^a, A.K. Noor^{b,*}, H. Sparr^a

^a*Institute of Structural Mechanics, German Aerospace Research Establishment (DLR), Braunschweig, Germany*

^b*Center for Advanced Computational Technology, University of Virginia, NASA Langley Research Center, Hampton, VA 23681, USA*

Received 26 March 1998

Abstract

A postprocessing procedure is presented for the evaluation of the transverse thermal stresses in laminated plates. The analytical formulation is based on the first-order shear deformation theory and the plate is discretized by using a single-field displacement finite element model. The procedure is based on neglecting the derivatives of the in-plane forces and the twisting moments, as well as the mixed derivatives of the bending moments, with respect to the in-plane coordinates. The calculated transverse shear stiffnesses reflect the actual stacking sequence of the composite plate. The distributions of the transverse stresses through-the-thickness are evaluated by using only the transverse shear forces and the thermal effects resulting from the finite element analysis. The procedure is implemented into a postprocessing routine which can be easily incorporated into existing commercial finite element codes. Numerical results are presented for four- and ten-layer cross-ply laminates subjected to mechanical and thermal loads. Published by Elsevier Science S.A.

1. Introduction

The importance of interlaminar stresses in predicting the onset of some of the damage mechanisms in multilayered composite panels has long been recognized. Therefore, various techniques have been proposed for the accurate determination of transverse stresses in laminated composites. These include using: (1) three-dimensional, or quasi-three-dimensional, finite elements (see for example [1–4]); (2) two-dimensional finite elements based on higher-order shear deformation theories with either nonlinear or piecewise linear approximations for the displacements in the thickness direction (see for example [5–7]); and (3) post-processing techniques, used in conjunction with two-dimensional finite elements based on the classical or first-order shear deformation theory (with linear displacement approximation through-the-thickness of the entire laminate).

Experience with most of the three-dimensional finite elements and two-dimensional finite elements based on higher-order shear deformation theories, has shown that unless the three-dimensional equilibrium equations are used in evaluating the thickness distribution of the transverse stresses, the resulting stresses are inaccurate (see for example [5,8–11]). Since the finite element models based on the first-order shear deformation theory are considerably less expensive than those based on three-dimensional and higher-order two-dimensional theories, their use in conjunction with postprocessing techniques has received increasing attention in recent years. The postprocessing techniques proposed for the evaluation of transverse stresses are based on the use of: (a) three-dimensional equilibrium equations (see [9,12–14]); (b) predictor–corrector approaches (see [15]); and (c) simplifying assumptions [16,17].

Except for Noor et al. [14], which considered only transverse shear stresses, none of the cited references

* Corresponding author.

considered transverse stresses in thermally loaded laminates. The present study focuses on the accurate evaluation of both the transverse shear and the transverse normal stresses, in composite panels subjected to mechanical and thermal loads. The postprocessing technique, based on the use of simplifying assumptions and presented in [16,17], is extended herein to the case of thermal stresses. The effectiveness of the proposed procedure is demonstrated by means of numerical examples of cross-ply panels.

2. Mathematical formulation

The mathematical formulation is based on the first-order shear deformation theory, with linear displacement approximation through-the-thickness of the entire laminate. The basic assumptions, equilibrium equations and thermoelastic constitutive relations of this theory are summarized in Appendix A. The sign convention for displacements, stresses and stress resultants is shown in Fig. 1.

2.1. Basic idea

The present method has in common with other postprocessing techniques (e.g. [9,12–14]), the use of three-dimensional equilibrium conditions to calculate the transverse stresses using the derivatives of the in-plane stresses. However, in contradistinction to other approaches, the transverse shear stresses are expressed in terms of the shear forces and the first derivatives of the temperature field with respect to the in-plane coordinates only. This results in saving one order of differentiation of the shape functions compared to other methods. The idea goes back to Rohwer [18] who introduced the following two simplifying assumptions:

- (1) the effect of the in-plane stress resultants on the transverse shear stresses is neglected; and
- (2) a cylindrical bending mode is assumed in each direction.

Because of the reduction in the order of differentiation, the present method can, in many cases, provide a good approximation of the transverse normal stresses using only eight-noded finite elements.

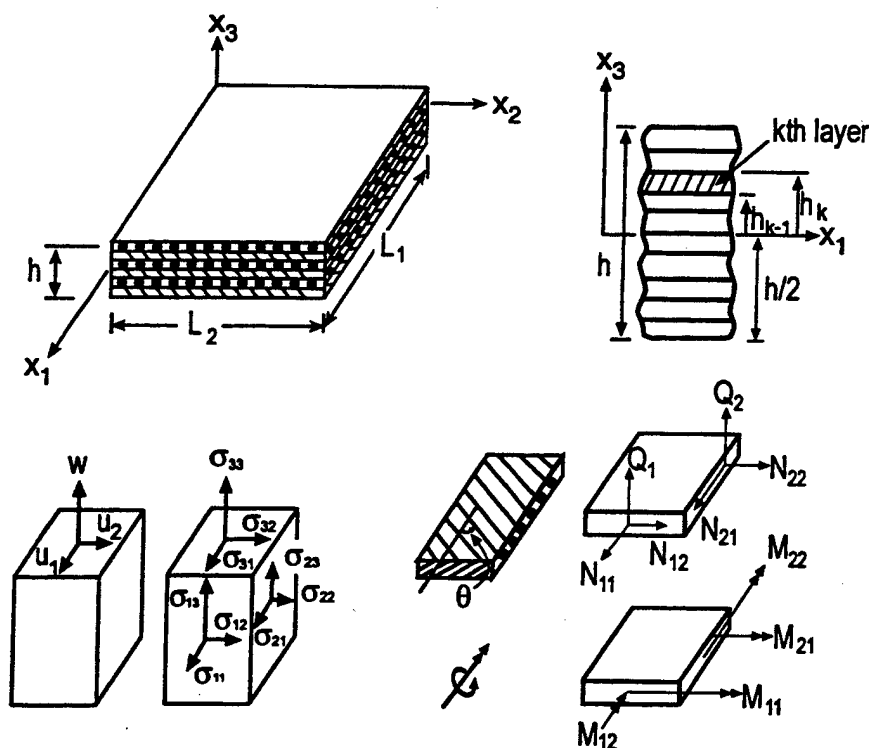


Fig. 1. Composite panels and sign convention for the displacements, stresses and stress resultants.

2.2. Transverse shear stresses

If Eqs. (A.1)–(A.3) of Appendix A are used, the expression for the transverse shear stresses $\sigma_{3\beta}$ at any point distance x_3 from the middle surface can be written in the following form:

$$\sigma_{3\beta} = - \int_{\zeta=-h/2}^{x_3} \bar{C}_{\alpha\beta\gamma\rho} (\varepsilon_{\gamma\rho,\alpha}^0 + \zeta \kappa_{\gamma\rho,\alpha} - \alpha_{\gamma\rho} \Delta T_{,\alpha}) d\zeta \quad (1)$$

where $\bar{C}_{\alpha\beta\gamma\rho}$ are the generalized plane-stress stiffness coefficients; $\varepsilon_{\gamma\rho}^0$ and $\kappa_{\gamma\rho}$ are the extensional strains and curvature changes of the middle surface of the laminate; ΔT is the temperature change; $\alpha_{\gamma\rho}$ are the coefficients of thermal expansion; ζ is the distance from the middle surface; the range of the Greek subscripts is 1, 2; a repeated subscript denotes summation; and $(\cdot)_{,\alpha}$ denotes derivative with respect to x_α (coordinates in the middle plane). Also, because of the possible discontinuity in the stiffness coefficients and the coefficients of thermal expansion at layer interfaces, piecewise integration is used in the evaluation of the right-hand side of Eq. (1).

If the laminate properties are independent of x_α and Eqs. (A.10) are used, $\sigma_{3\beta}$ can be expressed in terms of the stress resultants as follows:

$$\sigma_{3\beta} = - \int_{\zeta=-h/2}^{x_3} \bar{C}_{\alpha\beta\gamma\rho} [1 \quad \zeta] \begin{bmatrix} \bar{A}_{\gamma\rho\varepsilon\varphi} & \bar{B}_{\gamma\rho\varepsilon\varphi} \\ \bar{B}_{\gamma\rho\varepsilon\varphi} & \bar{D}_{\gamma\rho\varepsilon\varphi} \end{bmatrix} \left\{ \begin{Bmatrix} N_{\varepsilon\varphi,\alpha} \\ M_{\varepsilon\varphi,\alpha} \end{Bmatrix} + \begin{Bmatrix} N_{\varepsilon\varphi,\alpha}^{\text{th}} \\ M_{\varepsilon\varphi,\alpha}^{\text{th}} \end{Bmatrix} \right\} - \bar{C}_{\alpha\beta\gamma\rho} \alpha_{\gamma\rho} \Delta T_{,\alpha} d\zeta \quad (2)$$

where $\bar{A}_{\gamma\rho\varepsilon\varphi}$, $\bar{B}_{\gamma\rho\varepsilon\varphi}$, $\bar{D}_{\gamma\rho\varepsilon\varphi}$ are compliance coefficients of the panel (see Eq. (A.10)); $N_{\varepsilon\varphi}$, $M_{\varepsilon\varphi}$ are the extensional and bending stress resultants; and $N_{\varepsilon\varphi}^{\text{th}}$, $M_{\varepsilon\varphi}^{\text{th}}$ are thermal extensional and bending stress resultants (see Eq. (A.9)). If the temperature change ΔT is linear in the thickness direction, i.e. if

$$\Delta T = T^0 + x_3 T^1 \quad (3)$$

then, the expression for $\sigma_{3\beta}$ takes the following form:

$$\sigma_{3\beta} = [G_{\alpha\beta\gamma\rho} \quad F_{\alpha\beta\gamma\rho}] \left\{ \begin{Bmatrix} N_{\gamma\rho,\alpha} \\ M_{\gamma\rho,\alpha} \end{Bmatrix} + \begin{Bmatrix} N_{\gamma\rho,\alpha}^{\text{th}} \\ M_{\gamma\rho,\alpha}^{\text{th}} \end{Bmatrix} \right\} + [a_{\alpha\beta}^{\text{th}} \quad b_{\alpha\beta}^{\text{th}}] \begin{Bmatrix} T_{,\alpha}^0 \\ T_{,\alpha}^1 \end{Bmatrix} \quad (4)$$

where

$$\begin{Bmatrix} G_{\alpha\beta\gamma\rho} \\ F_{\alpha\beta\gamma\rho} \end{Bmatrix} = - \int_{\zeta=-h/2}^{x_3} \bar{C}_{\alpha\beta\varepsilon\varphi} \begin{bmatrix} \bar{A}_{\varepsilon\varphi\gamma\rho} & \bar{B}_{\varepsilon\varphi\gamma\rho} \\ \bar{B}_{\varepsilon\varphi\gamma\rho} & \bar{D}_{\varepsilon\varphi\gamma\rho} \end{bmatrix} \begin{Bmatrix} 1 \\ \zeta \end{Bmatrix} d\zeta \quad (5)$$

and

$$\begin{Bmatrix} a_{\alpha\beta}^{\text{th}} \\ b_{\alpha\beta}^{\text{th}} \end{Bmatrix} = \int_{\zeta=-h/2}^{x_3} \bar{C}_{\alpha\beta\gamma\rho} \alpha_{\gamma\rho} \begin{Bmatrix} 1 \\ \zeta \end{Bmatrix} d\zeta \quad (6)$$

The quantities $a_{\alpha\beta}^{\text{th}}$ and $b_{\alpha\beta}^{\text{th}}$ are integrals (over part of the laminate thickness) of products of material stiffnesses and coefficients of thermal expansion. Therefore, they can be thought of as *partial thermal stiffnesses*.

In order to simplify the calculation of the transverse shear stresses $\sigma_{3\beta}$, the following quantities in Eq. (2) (or its equivalent—Eq. (4)) are neglected:

- (1) $N_{\gamma\rho,\alpha}$
- (2) $M_{22,1}$, $M_{11,2}$, $M_{12,1}$ and $M_{12,2}$.

If the equilibrium equations of the laminate (Eqs. (A.7)) are used, the remaining derivatives of the bending stress resultants can be expressed in terms of the transverse shear stress resultants Q_α as follows:

$$M_{11,1} = Q_1 \quad (7)$$

$$M_{22,2} = Q_2 \quad (8)$$

Eqs. (7) and (8) represent the cylindrical bending assumptions in the x_1 and x_2 directions, respectively.

The expression for $\sigma_{3\beta}$, Eq. (4), reduces to:

$$\sigma_{3\beta} = f_{\alpha\beta} Q_{\alpha} + \left([G_{\alpha\beta\gamma\rho} \quad F_{\alpha\beta\gamma\rho}] \begin{bmatrix} A_{\gamma\rho}^{th} & B_{\gamma\rho}^{th} \\ B_{\gamma\rho}^{th} & D_{\gamma\rho}^{th} \end{bmatrix} + [a_{\alpha\beta}^{th} \quad b_{\alpha\beta}^{th}] \right) \begin{Bmatrix} T_{,\alpha}^0 \\ T_{,\alpha}^1 \end{Bmatrix} \quad (9)$$

where $f_{\alpha\beta}$ are the $F_{\alpha\beta\gamma\rho}$ terms multiplying the remaining derivatives of $M_{\gamma\rho}$, and Eqs. (A.12)—Appendix A, have been used.

Note that when using Eq. (9) in a finite element environment, the finite element code must only provide the transverse shear forces Q_{α} and the first derivatives of the uniform temperature T^0 and temperature gradient T^1 . These derivatives can be evaluated by using only bilinear shape functions for approximating the generalized displacements and the temperature distributions T^0 and T^1 . Thus, the required polynomial order is one lower than that of the standard equilibrium approach which uses Eq. (1). Furthermore, Eq. (9) allows the evaluation of improved transverse shear stiffnesses, which reflect the actual stacking sequence of the composite plate [18]. Thus, artificial shear correction factors are no longer necessary.

2.3. Transverse normal stresses

The foregoing methodology can also be applied to the evaluation of transverse normal stresses. Although the constitutive relations used in the FSDT neglect the transverse normal stress component, this component can be calculated a posteriori using the third equilibrium equation (Eq. (A.4)). If Eq. (9) is used, the expression for the transverse normal stress can be written in the following form:

$$\sigma_{33} = -f_{\alpha\beta}^* Q_{\alpha,\beta} - \left([G_{\alpha\beta\gamma\rho}^* \quad F_{\alpha\beta\gamma\rho}^*] \begin{bmatrix} A_{\gamma\rho}^{th} & B_{\gamma\rho}^{th} \\ B_{\gamma\rho}^{th} & D_{\gamma\rho}^{th} \end{bmatrix} + [a_{\alpha\beta}^{*th} \quad b_{\alpha\beta}^{*th}] \right) \begin{Bmatrix} T_{,\alpha\beta}^0 \\ T_{,\alpha\beta}^1 \end{Bmatrix} \quad (10)$$

where

$$\begin{Bmatrix} f_{\alpha\beta}^* \\ G_{\alpha\beta\gamma\rho}^* \\ F_{\alpha\beta\gamma\rho}^* \\ a_{\alpha\beta}^{*th} \\ b_{\alpha\beta}^{*th} \end{Bmatrix} = \int_{\zeta=-h/2}^{\zeta=x_3} \begin{Bmatrix} f_{\alpha\beta} \\ G_{\alpha\beta\gamma\rho} \\ F_{\alpha\beta\gamma\rho} \\ a_{\alpha\beta}^{th} \\ b_{\alpha\beta}^{th} \end{Bmatrix} d\zeta \quad (11)$$

In order to evaluate the transverse normal stress on element level, the finite element program must only provide the first derivatives of the transverse shear forces ($Q_{\alpha,\beta}$) and the second derivatives of the temperature field ($T_{,\alpha\beta}^0, T_{,\alpha\beta}^1$) with respect to the in-plane coordinates x_1 and x_2 . This can be accomplished by using biquadratic shape functions.

2.4. Boundary conditions

The boundary conditions for all transverse stresses at the top and bottom surfaces of the laminate are automatically satisfied in the present procedure. This is demonstrated in the subsequent subsections.

2.4.1. Transverse shear stresses

At the bottom surface of the laminate, $x_3 = -h/2$, the coefficients $G_{\alpha\beta\gamma\rho}$, $F_{\alpha\beta\gamma\rho}$, $a_{\alpha\beta}^{th}$ and $b_{\alpha\beta}^{th}$ are all zero and, therefore

$$\sigma_{3\beta}|_{x_3=-h/2} = 0 \quad (12)$$

At the top surface of the laminate, $x_3 = h/2$, the coefficients $F_{\alpha\beta\gamma\rho}$ and $G_{\alpha\beta\gamma\rho}$ are obtained by setting $x_3 = h/2$ in Eq. (5), i.e.

$$\begin{aligned}
 [G_{\alpha\beta\gamma\rho} \quad F_{\alpha\beta\gamma\rho}]|_{x_3=h/2} &= - \int_{\zeta=-h/2}^{\zeta=h/2} \bar{C}_{\alpha\beta\epsilon\varphi} [1 \quad \zeta] d\zeta \begin{bmatrix} \bar{A}_{\epsilon\varphi\gamma\rho} & \bar{B}_{\epsilon\varphi\gamma\rho} \\ \bar{B}_{\epsilon\varphi\gamma\rho} & \bar{D}_{\epsilon\varphi\gamma\rho} \end{bmatrix} \\
 &= - [A_{\alpha\beta\epsilon\varphi} \quad B_{\alpha\beta\epsilon\varphi}] \begin{bmatrix} \bar{A}_{\epsilon\varphi\gamma\rho} & \bar{B}_{\epsilon\varphi\gamma\rho} \\ \bar{B}_{\epsilon\varphi\gamma\rho} & \bar{D}_{\epsilon\varphi\gamma\rho} \end{bmatrix}
 \end{aligned} \quad (13)$$

Since the compliance matrix containing \bar{A} , \bar{B} , \bar{D} is the inverse of the stiffness matrix containing A , B , C , Eq. (13) reduces to

$$[G_{\alpha\beta\gamma\rho} \quad F_{\alpha\beta\gamma\rho}]|_{x_3=h/2} = -[\hat{\delta}_{\alpha\beta\gamma\rho} \quad 0] \quad (14)$$

where $\hat{\delta}_{\alpha\beta\gamma\rho} = \delta_{\alpha\gamma}\delta_{\beta\rho}$; δ 's are the Kronecker deltas ($\delta_{\alpha\gamma} = 1$ if $\alpha = \gamma$ and $\delta_{\alpha\gamma} = 0$ if $\alpha \neq \gamma$). Inserting Eq. (14) into Eq. (9), it follows that

$$\sigma_{3\beta}|_{x_3=h/2} = (-\hat{\delta}_{\alpha\beta\gamma\rho} A_{\gamma\rho}^{\text{th}} + A_{\alpha\beta}^{\text{th}}) T_{,\alpha}^0 + (\hat{\delta}_{\alpha\beta\gamma\rho} B_{\gamma\rho}^{\text{th}} + B_{\alpha\beta}^{\text{th}}) T_{,\alpha}^1 = 0 \quad (15)$$

i.e. the transverse shear stresses vanish at the upper surface of the laminate.

2.4.2. Transverse normal stress

If the definition of $F_{\alpha\beta\gamma\rho}$ given in Eq. (5) is used, the integrated tensor coefficients $F_{\alpha\beta\gamma\rho}^*$ can be expressed as follows:

$$F_{\alpha\beta\gamma\rho}^* = -a_{\alpha\beta\epsilon\varphi}^* \bar{B}_{\epsilon\varphi\gamma\rho} - b_{\alpha\beta\epsilon\varphi}^* \bar{D}_{\epsilon\varphi\gamma\rho} \quad (16)$$

$$a_{\alpha\beta\gamma\rho}^* = \int_{\zeta=-h/2}^{\zeta=x_3} \bar{C}_{\alpha\beta\gamma\rho} d\zeta \quad (17)$$

$$a_{\alpha\beta\gamma\rho}^* = \int_{\zeta=-h/2}^{\zeta=x_3} a_{\alpha\beta\gamma\rho} d\zeta = \sum_{i=1}^{n-1} \bar{C}_{\alpha\beta\gamma\rho}^{(i)} (h_i - h_{i-1}) \left(x_3 - \frac{1}{2} h_{i-1} - \frac{1}{2} h_i \right) + \frac{1}{2} \bar{C}_{\alpha\beta\gamma\rho}^{(n)} (x_3 - h_{n-1})^2 \quad (18)$$

$$b_{\alpha\beta\gamma\rho}^* = \int_{\zeta=-h/2}^{\zeta=x_3} \bar{C}_{\alpha\beta\gamma\rho} \zeta d\zeta \quad (19)$$

$$\begin{aligned}
 b_{\alpha\beta\gamma\rho}^* &= \int_{\zeta=-h/2}^{\zeta=x_3} b_{\alpha\beta\gamma\rho} d\zeta \\
 &= \sum_{i=1}^{n-1} \bar{C}_{\alpha\beta\gamma\rho}^{(i)} h_i^2 \left(\frac{1}{2} x_3 - \frac{1}{3} h_i \right) - \sum_{i=1}^n \bar{C}_{\alpha\beta\gamma\rho}^{(i)} h_{i-1}^2 \left(\frac{1}{2} x_3 - \frac{1}{3} h_{i-1} \right) + \frac{1}{6} \bar{C}_{\alpha\beta\gamma\rho}^{(n)} x_3^3
 \end{aligned} \quad (20)$$

where $a_{\alpha\beta\gamma\rho}$ and $b_{\alpha\beta\gamma\rho}$ denote the partial extension and coupling stiffnesses of the laminate, respectively; and n is the total number of layers in the panel. The stiffness coefficients $A_{\alpha\beta\gamma\rho}$ and $B_{\alpha\beta\gamma\rho}$ are obtained by setting the upper limit of the integrations in Eqs. (17) and (19) to $\zeta = h/2$. The values of the coefficients a^* and b are given by

$$\begin{aligned}
 a_{\alpha\beta\gamma\rho}^*|_{x_3=h/2} &= -\frac{1}{2} \sum_{i=1}^{n-1} \bar{C}_{\alpha\beta\gamma\rho} (h_i^2 - h_{i-1}^2) + \sum_{i=1}^{n-1} \bar{C}_{\alpha\beta\gamma\rho}^{(i)} (h_i - h_{i-1}) h_n - \frac{1}{2} \bar{C}_{\alpha\beta\gamma\rho}^{(n)} (h_n^2 - h_{n-1}^2) \\
 &\quad + \bar{C}_{\alpha\beta\gamma\rho}^{(n)} (h_n - h_{n-1}) h_n \\
 &= -\frac{1}{2} \sum_{i=1}^n \bar{C}_{\alpha\beta\gamma\rho}^{(i)} (h_i^2 - h_{i-1}^2) + h_n \sum_{i=1}^n \bar{C}_{\alpha\beta\gamma\rho}^{(i)} (h_i - h_{i-1}) = -B_{\alpha\beta\gamma\rho} + h_n A_{\alpha\beta\gamma\rho}
 \end{aligned} \quad (21)$$

Since the middle surface is assumed to be the reference surface, then

$$a_{\alpha\beta\gamma\rho}^*|_{x_3=h/2} = \frac{h}{2} A_{\alpha\beta\gamma\rho} - B_{\alpha\beta\gamma\rho} \quad (22)$$

$$b_{\alpha\beta\gamma\rho}^*|_{x_3=h/2} = \frac{h}{2} B_{\alpha\beta\gamma\rho} - D_{\alpha\beta\gamma\rho} \quad (23)$$

If Eqs. (22) and (23) are used, then

$$F_{\alpha\beta\gamma\rho}^*|_{x_3=-h/2} = -\frac{h}{2} A_{\alpha\beta\epsilon\phi} \bar{B}_{\epsilon\phi\gamma\rho} + B_{\alpha\beta\epsilon\phi} \bar{B}_{\epsilon\phi\gamma\rho} - \frac{h}{2} B_{\alpha\beta\epsilon\phi} \bar{D}_{\epsilon\phi\gamma\rho} + D_{\alpha\beta\epsilon\phi} \bar{D}_{\epsilon\phi\gamma\rho} = \hat{\delta}_{\alpha\beta\gamma\rho} \quad (24)$$

Again, it has been taken into account that the compliances are inverse to the stiffnesses.

Analogously, $G_{\alpha\beta\gamma\rho}^*$ can be evaluated at the top surface.

$$G_{\alpha\beta\gamma\rho}^*|_{x_3=h_n} = -\frac{h}{2} \hat{\delta}_{\alpha\beta\gamma\rho} \quad (25)$$

The expressions for the integrals of the partial thermal stiffnesses are similar to those of a^* and b^* —Eqs. (22) and (23), viz.

$$a_{\alpha\beta}^{*th}|_{x_3=h_n} = \frac{h}{2} A_{\alpha\beta}^{th} - B_{\alpha\beta}^{th} \quad (26)$$

$$b_{\alpha\beta}^{*th}|_{x_3=h_n} = \frac{h}{2} B_{\alpha\beta}^{th} - D_{\alpha\beta}^{th} \quad (27)$$

Therefore, the transverse normal stress at the upper surface appears as

$$\begin{aligned} \sigma_{33}|_{x_3=h_n} = & -\delta_{\alpha\beta} Q_{\alpha,\beta} - \left(-\frac{h}{2} \hat{\delta}_{\alpha\beta\gamma\rho} A_{\gamma\rho}^{th} + \hat{\delta}_{\alpha\beta\gamma\rho} B_{\gamma\rho}^{th} + \frac{h}{2} A_{\alpha\beta}^{th} - B_{\alpha\beta}^{th} \right) T_{,\alpha\beta}^0 \\ & - \left(-\frac{h}{2} \hat{\delta}_{\alpha\beta\gamma\rho} B_{\gamma\rho}^{th} + \hat{\delta}_{\alpha\beta\gamma\rho} D_{\gamma\rho}^{th} + \frac{h}{2} B_{\alpha\beta}^{th} - D_{\alpha\beta}^{th} \right) T_{,\alpha\beta}^1 = -\delta_{\alpha\beta} Q_{\alpha,\beta} = -Q_{\alpha,\alpha} \end{aligned} \quad (28)$$

Application of the equilibrium of forces at the upper surface (Eq. (A.6)) yields

$$\sigma_{33}|_{x_3=h/2} = -p \quad (29)$$

Therefore, the boundary condition is exactly satisfied. The boundary condition at the lower surface is also satisfied since all tensors appearing in Eq. (28) vanish at $x_3 = -h/2$.

2.5. Implementation

The present method is implemented into the finite element program B2000 and the postprocessor TRAVEST. The B2000 is a common research tool for a number of organizations, including NLR, CIRA, SMR, DLR, and some universities in the Netherland and Switzerland. Within B2000 a standard isoparametric eight-node element with reduced integration (2×2) is used. The same shape functions are used for interpolating the temperature distribution. Since the evaluation of transverse stresses requires the first derivative of the transverse shear forces ($Q_{\alpha,\beta}$), and the second derivatives of the temperature field ($T_{,\alpha\beta}^0$; $T_{,\alpha\beta}^1$), then second-order derivatives of the shape functions are required. These derivatives can be evaluated using the procedure outlined in [11]. The values for $Q_{\alpha,\beta}$, $T_{,\alpha\beta}^0$ and $T_{,\alpha\beta}^1$ are input to the postprocessor TRAVEST which calculates all quantities that depend on the transverse coordinate x_3 only, i.e. the tensors $f_{\alpha\beta}$, $G_{\alpha\beta\gamma\rho}$, $F_{\alpha\beta\gamma\rho}$, $a_{\alpha\beta}^{th}$, $b_{\alpha\beta}^{th}$, $A_{\alpha\beta}^{th}$, $B_{\alpha\beta}^{th}$ and $D_{\alpha\beta}^{th}$, and its integrals over x_3 which are denoted by stars. The integrations are carried out analytically. Thus, no additional numerical errors are introduced. If the material properties of each layer are uniform (i.e. independent of x_α and x_3), the additional computational effort is small since the aforementioned tensors have to be evaluated only once. The multiplications with $Q_{\alpha,\beta}$, $T_{,\alpha\beta}^0$ and $T_{,\alpha\beta}^1$ (according to Eqs. (9) and (10)) must be performed at each point where the transverse stresses are required.

3. Numerical studies

To assess the effectiveness of the foregoing postprocessing procedure for calculating transverse stresses in composite plates several multilayered composite panels were analyzed. The panels were subjected to transverse static loading or to a thermal loading, in the form of either a constant temperature change or a temperature gradient in the thickness direction. Typical results are presented herein for a ten-layered symmetric cross-ply laminate ($[0/90/0/90/0]_{sym}$) and a four-layered antisymmetric laminate ($[0/90/0/90]$), with the fibers of the

top layer parallel to the x_1 axis. The first laminate exhibits no bending-extensional coupling, and the second laminate exhibits a strong coupling. Two aspect ratios were selected; namely, $L_2/L_1 = 1$ and 2. Furthermore, two different thickness ratios, $h/L_1 = 0.05$ and 0.1, were considered. Each of the transverse loading, uniform temperature through the thickness, and the temperature gradient through-the-thickness, had a double sinusoidal variation in the $x_1 - x_2$ plane. The amplitudes of the transverse loading, uniform temperature and temperature gradient (p^0 , T^0 , T^1) were chosen to be one. The following boundary conditions which allow an exact three-dimensional solution to be obtained [19,14,20], were selected:

$$\begin{aligned} u_2 = 0, \quad w = 0, \quad \varphi_2 = 0, \quad \sigma_{11} = 0 \quad \text{at } x_1 = 0, L_1 \\ u_1 = 0, \quad w = 0, \quad \varphi_1 = 0, \quad \sigma_{22} = 0 \quad \text{at } x_2 = 0, L_2. \end{aligned}$$

The three-dimensional solution was used as the standard for comparison. Also, transverse stresses were calculated using the postprocessing technique based on the full three-dimensional equilibrium equations. This provided an assessment of the effect of neglecting $N_{\gamma p, \alpha}$, $M_{22,1}$, $M_{11,2}$, $M_{12,1}$, $M_{1,2}$ on the accuracy of the calculated transverse stresses. The material properties of the individual layers were taken to be those typical of high-modulus fibrous composites, namely:

$$\begin{aligned} E_L/E_T = 15, \quad G_{LT}/E_T = 0.5, \quad G_{TT}/E_T = 0.3378, \quad \nu_{LT} = 0.3, \quad \nu_{TT} = 0.48 \\ \alpha_L = 0.139 \times 10^{-6}, \quad \alpha_T = 9 \times 10^{-6} \end{aligned}$$

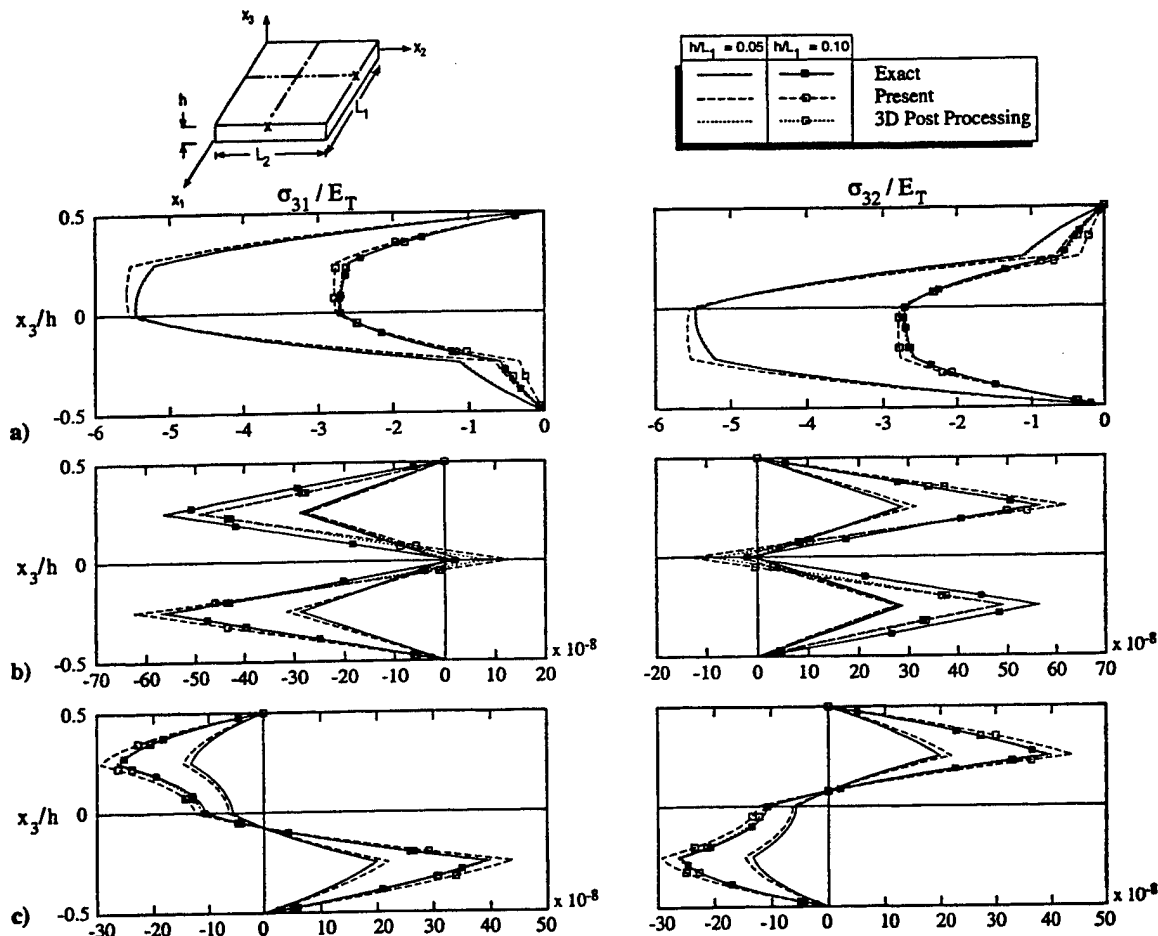


Fig. 2. Through-the-thickness distributions of transverse shear stresses (σ_{31} at $(L_1, L_2/2)$; σ_{32} at $(L_1/2, L_2)$). Four-layer antisymmetric cross-ply laminate with $L_2/L_1 = 1$ subjected to: (a) static loading p ; (b) uniform temperature T^0 ; (c) temperature gradient T^1 .

Typical results are shown in Figs. 2–4 for the transverse shear stresses and in Figs. 5 and 6 for the transverse normal stresses. The results are discussed subsequently.

3.1. Effect of laminate parameters and loading on the magnitude and distribution of transverse stresses through the thickness

- The transverse shear and normal stresses produced by the transverse loading p have a smooth variation in the thickness direction.
- The relative magnitudes of the transverse shear stresses, σ_{31} , σ_{32} , and of the transverse normal stresses, σ_{33} , is strongly influenced by the aspect ratio of the laminate. For square laminates, σ_{31} and σ_{32} have almost equal magnitudes, but opposite signs; and σ_{33} is very small. On the other hand, for rectangular laminates, the magnitudes of σ_{31} and σ_{32} are different and the ratio of $\max \sigma_{33} / \max \sigma_{3\beta}$ is larger than that for square laminates (see Table 1).

3.2. Accuracy of transverse shear stresses

- For all the laminates considered, the accuracy of the transverse shear stresses, $\sigma_{3\beta}$, predicted by the foregoing procedure, was at least satisfactory, often good or very good. The accuracy was higher for the static loading case than for the thermal loading cases.

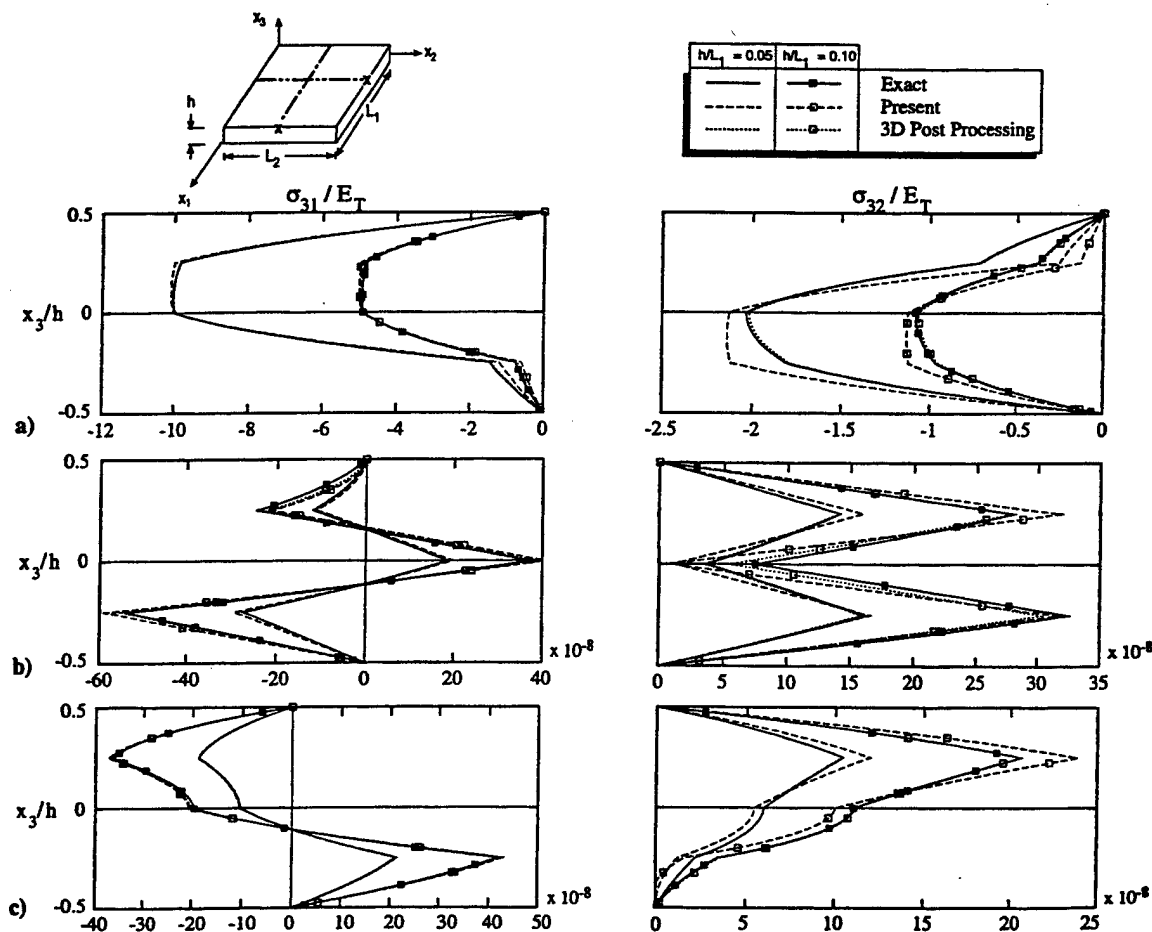


Fig. 3. Through-the-thickness distributions of transverse shear stresses (σ_{31} at $(L_1, L_2/2)$; σ_{32} at $(L_1/2, L_2)$). Four-layer antisymmetric cross-ply laminate with $L_2/L_1 = 2$ subjected to: (a) static loading p ; (b) uniform temperature T^0 ; (c) temperature gradient T^1 .

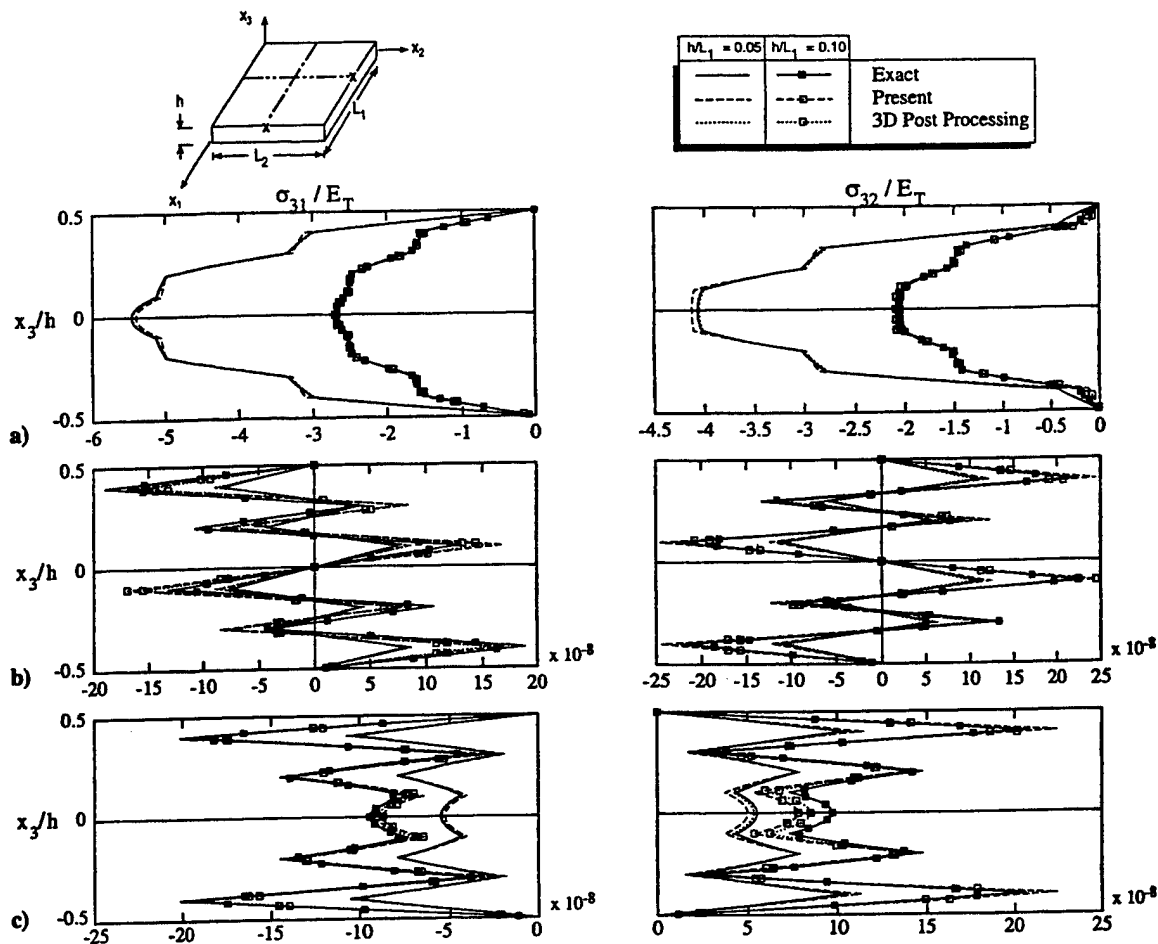


Fig. 4. Through-the-thickness distributions of transverse shear stresses (σ_{31} at $(L_1, L_2/2)$; σ_{32} at $(L_1/2, L_2)$). Ten-layer antisymmetric cross-ply laminate with $L_2/L_1 = 1$ subjected to: (a) static loading p ; (b) uniform temperature T^0 ; (c) temperature gradient T^1 .

- For the static loading case, the accuracy of $\sigma_{3\beta}$ was insensitive to the thickness ratio (h/L_1) . On the other hand, for the thermal loading cases, the accuracy increased with the decrease in (h/L_1) .
- For rectangular plates, the larger transverse shear stresses are predicted more accurately by the foregoing procedure than the smaller ones.
- The use of the full three-dimensional equilibrium equations in the postprocessing phase improved the accuracy of the transverse shear stress in all the cases considered. The improvement was more noticeable for the four-layer laminates.

3.3. Accuracy of transverse normal stresses

- The accuracy of the transverse normal stresses predicted by the foregoing procedure is strongly dependent on the relative magnitudes of the in-plane and bending stress resultants $(hN_{\alpha\beta}/M_{\alpha\beta})$, and the relative magnitudes of σ_{33} and $\sigma_{3\beta}$ which, in turn, are dependent on the loading, the lamination and the geometric parameters of the panel (see Table 1).
- For the static loading case, the accuracy of σ_{33} is, for all the panels considered, excellent. The accuracy is insensitive to variations in both (h/L_1) and L_2/L_1 .
- For the thermal loading cases, the accuracy of σ_{33} is satisfactory only when the ratio $hN_{\alpha\beta}/M_{\alpha\beta}$ is small and the ratio $(\max \sigma_{33}/\max \sigma_{3\beta})$ is larger than 0.01. For the case of uniform temperature through-the-thickness, the accuracy of σ_{33} is satisfactory for rectangular four-layer laminates, and is not satisfactory for all the other laminates considered. For the case of temperature gradient through-the-thickness, the accuracy

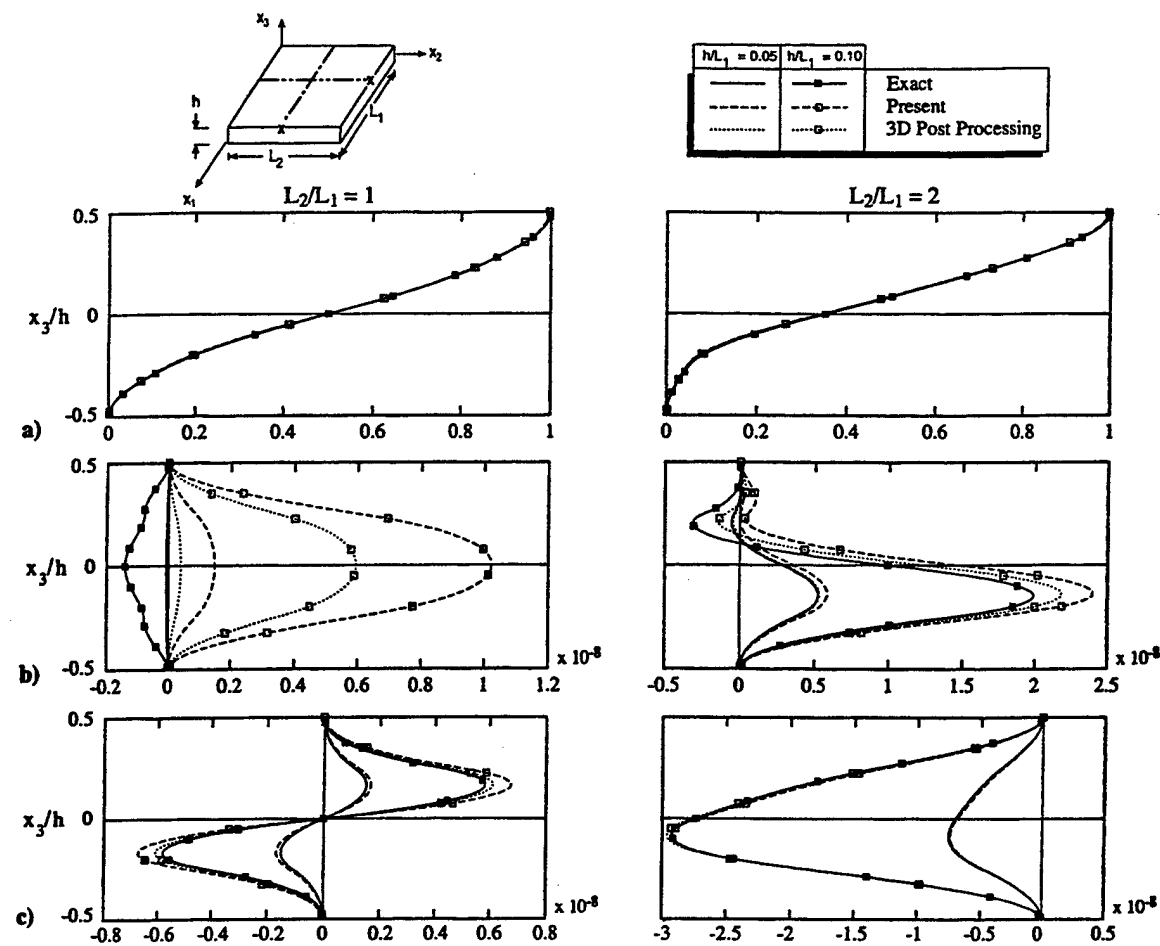


Fig. 5. Through-the-thickness distribution of transverse normal stress σ_{33} at $(L_1/2, L_2/2)$. Four-layer antisymmetric cross-ply laminate subjected to: (a) static loading p ; (b) uniform temperature T^0 ; (c) temperature gradient T^1 .

Table 1
Accuracy of the transverse normal stress component σ_{33} for the thermal loading cases T^0 and T^1

Laminate		Loading	Bending	$\frac{\max \sigma_{33}}{\max \sigma_{3p}}$	Accuracy of σ_{33}
n	L_2/L_1				
4	1	T^0	yes	2.5×10^{-3}	poor
	2		yes	3.6×10^{-2}	satisfactory
	1	T^1	yes	1.5×10^{-2}	good
	2		yes	7.0×10^{-2}	excellent
10	1	T^0	no	NA	poor
	2		no	NA	poor
	1	T^1	yes	5.8×10^{-4}	poor
	2		yes	1.8×10^{-2}	good

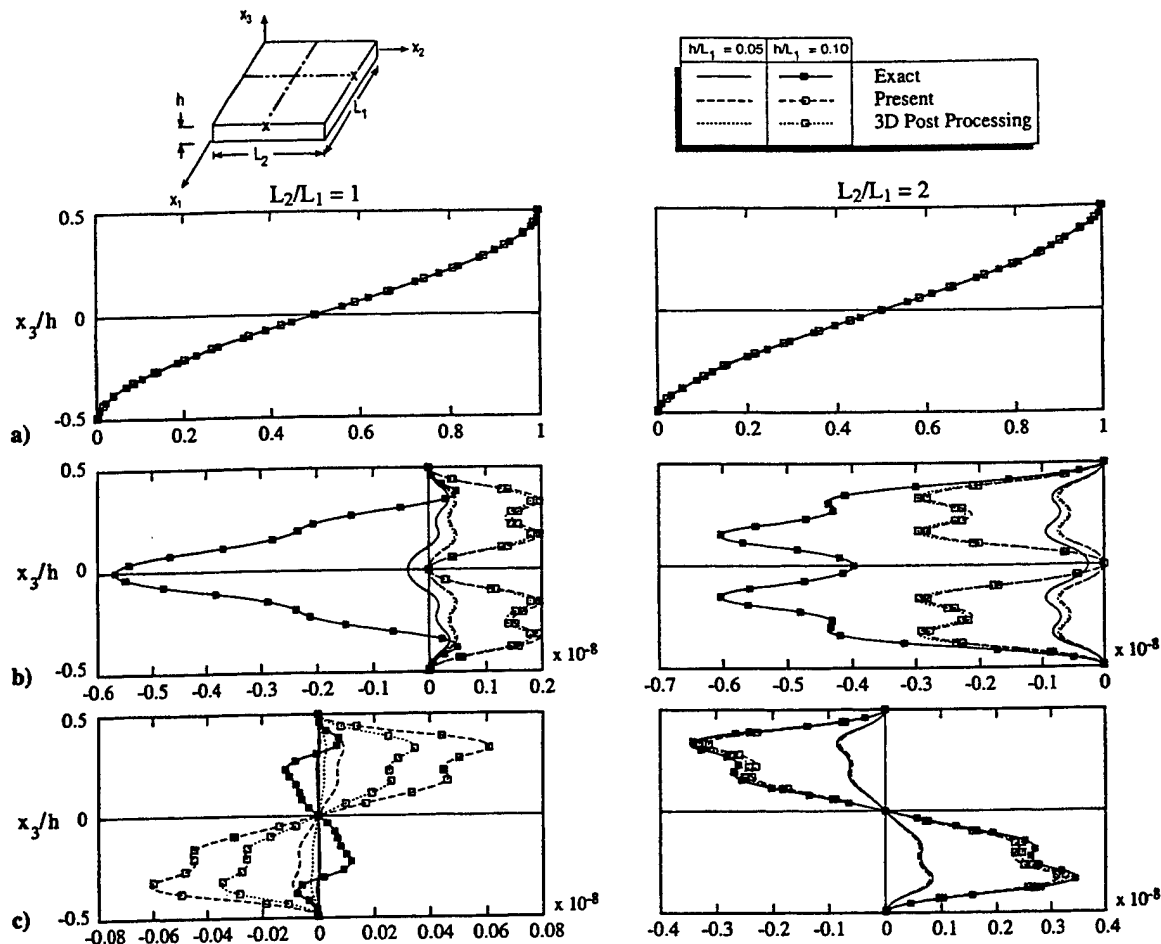


Fig. 6. Through-the-thickness distribution of transverse normal stress σ_{33} at $(L_1/2, L_2/2)$. Ten-layer symmetric cross-ply laminate subjected to: (a) static loading p ; (b) uniform temperature T^0 ; (c) temperature gradient T^1 .

of σ_{33} ranged from good to excellent, except for the square ten-layer laminate, where σ_{33} was less than three orders of magnitude smaller than $\sigma_{3\beta}$.

- The use of the full three-dimensional equilibrium equations in the postprocessing phase did not improve the accuracy of the transverse normal stresses significantly over those predicted by the foregoing procedure. For the cases where the transverse normal stresses predicted by the foregoing approach were unsatisfactory, the corresponding transverse normal stresses calculated by using the full three-dimensional equations were also unsatisfactory. For these cases, there is a need for another approach, such as the predictor–corrector approach presented in [15].

Acknowledgments

The work of A.K. Noor was partially supported by NASA Grant NAG-1-2016 and AFOSR Grant F49620-96-1-0462. The authors acknowledge the assistance of Jeanne M. Peters of the University of Virginia for generating the exact three-dimensional solutions, and Thea M. Ganoe of the University of Virginia in preparing the final manuscript and improving the figures.

Appendix A. Fundamental equations of the first-order shear deformation theory used in the present study

The first-order shear-deformation thermoelastic model used in the present study is based on the following assumptions:

- (1) The laminates are composed of a number of perfectly bonded layers.
- (2) The strains are linear in the thickness direction, i.e.

$$\varepsilon_{\alpha\beta} = \varepsilon_{\alpha\beta}^0 + x_3 \kappa_{\alpha\beta} \quad (\text{A.1})$$

where $\varepsilon_{\alpha\beta}^0$ and $\kappa_{\alpha\beta}$ are the extensional strains and curvature changes of the middle surface; x_3 is the thickness coordinate, and the range of the Greek indices is 1, 2.

- (3) Every point of the laminate is assumed to possess a single plane of thermoelastic symmetry parallel to the middle plane.

- (4) The material properties are independent of temperature.

- (5) The extensional stresses $\sigma_{\alpha\beta}$ and strains $\varepsilon_{\alpha\beta}$ are related by the plane stress constitutive relations:

$$\sigma_{\alpha\beta} = \bar{C}_{\alpha\beta\gamma\rho} (\varepsilon_{\gamma\rho} - \alpha_{\gamma\rho} \Delta T) \quad (\text{A.2})$$

where $\bar{C}_{\alpha\beta\gamma\rho}$ are the generalized plane-stress stiffness coefficients, $\alpha_{\gamma\rho}$ are the coefficients of thermal expansion, and ΔT is the temperature change. Henceforth, a repeated Greek index denotes summation over the range 1, 2.

A.1. Three-dimensional equilibrium equations

In the absence of body forces, the equilibrium equations can be written in the following form:

$$\sigma_{\alpha\beta,\alpha} + \sigma_{3\beta,3} = 0 \quad (\text{A.3})$$

$$\sigma_{3\beta,\beta} + \sigma_{33,3} = 0 \quad (\text{A.4})$$

where $\sigma_{3\beta}$ and σ_{33} are the transverse shear and transverse normal stresses, respectively.

A.2. Equilibrium equations for the laminate

The force and moment equilibrium equations for the laminate are given by

$$N_{\alpha\beta,\alpha} - p_\beta = 0 \quad (\text{A.5})$$

$$Q_{\alpha,\alpha} - p = 0 \quad (\text{A.6})$$

$$M_{\alpha\beta,\alpha} - Q_\beta = 0 \quad (\text{A.7})$$

where $N_{\alpha\beta}$, Q_α and $M_{\alpha\beta}$ are the extensional, transverse shear and bending stress resultants; p_β and p are the intensities of the external loadings in the x_β and x_3 directions, respectively.

A.3. Thermoelastic constitutive relations for the laminate

The thermoelastic constitutive relations of the laminate are given by

$$\begin{Bmatrix} N_{\alpha\beta} \\ M_{\alpha\beta} \end{Bmatrix} = \begin{bmatrix} A_{\alpha\beta\gamma\rho} & B_{\alpha\beta\gamma\rho} \\ B_{\alpha\beta\gamma\rho} & D_{\alpha\beta\gamma\rho} \end{bmatrix} \begin{Bmatrix} \varepsilon_{\gamma\rho}^0 \\ \kappa_{\gamma\rho} \end{Bmatrix} - \begin{Bmatrix} N_{\alpha\beta}^{\text{th}} \\ M_{\alpha\beta}^{\text{th}} \end{Bmatrix} \quad (\text{A.8})$$

where the A 's, D 's and B 's are the extensional, bending and bending-extensional coupling coefficients of the laminate; and $N_{\alpha\beta}^{\text{th}}$ and $M_{\alpha\beta}^{\text{th}}$ are thermal extensional and bending stress resultants given by

$$\begin{Bmatrix} N_{\alpha\beta}^{\text{th}} \\ M_{\alpha\beta}^{\text{th}} \end{Bmatrix} = \sum_{k=1}^n \int_{h_{k-1}}^{h_k} \bar{C}_{\alpha\beta\gamma\rho} \alpha_{\gamma\rho} \begin{Bmatrix} 1 \\ x_3 \end{Bmatrix} \Delta T \, dx_3 \quad (\text{A.9})$$

where n is the total number of layers, and h_{k-1} , h_k are the distances from the middle surface to the top and bottom faces of the k th layer (see Fig. 1).

The relations between the middle surface strains and stress resultants are given by

$$\begin{Bmatrix} \varepsilon_{\alpha\beta}^0 \\ \kappa_{\alpha\beta} \end{Bmatrix} = \begin{bmatrix} \bar{A}_{\alpha\beta\gamma\rho} & \bar{B}_{\alpha\beta\gamma\rho} \\ \bar{B}_{\alpha\beta\gamma\rho} & \bar{D}_{\alpha\beta\gamma\rho} \end{bmatrix} \begin{Bmatrix} N_{\gamma\rho} \\ M_{\gamma\rho} \end{Bmatrix} + \begin{Bmatrix} N_{\gamma\rho}^{\text{th}} \\ M_{\gamma\rho}^{\text{th}} \end{Bmatrix} \quad (\text{A.10})$$

where $\bar{A}_{\alpha\beta\gamma\rho}$, $\bar{B}_{\alpha\beta\gamma\rho}$ and $\bar{D}_{\alpha\beta\gamma\rho}$ are the compliance coefficients of the panel (inverse of the panel stiffness coefficients). Note that the constitutive relations for the transverse shears are not used in evaluating the transverse stresses.

If the temperature change has a linear variation through-the-thickness, viz.

$$\Delta T = T^0 + x_3 T^1 \quad (\text{A.11})$$

then the expressions for the thermal extensional and bending stress resultants reduce to

$$\begin{Bmatrix} N_{\alpha\beta}^{\text{th}} \\ M_{\alpha\beta}^{\text{th}} \end{Bmatrix} = \begin{bmatrix} A_{\alpha\beta}^{\text{th}} & B_{\alpha\beta}^{\text{th}} \\ B_{\alpha\beta}^{\text{th}} & D_{\alpha\beta}^{\text{th}} \end{bmatrix} \begin{Bmatrix} T^0 \\ T^1 \end{Bmatrix} \quad (\text{A.12})$$

where

$$\begin{Bmatrix} A_{\alpha\beta}^{\text{th}} \\ B_{\alpha\beta}^{\text{th}} \\ D_{\alpha\beta}^{\text{th}} \end{Bmatrix} = \sum_{k=1}^n \int_{h_{k-1}}^{h_k} \bar{C}_{\alpha\beta\gamma\rho} \alpha_{\gamma\rho} \begin{Bmatrix} 1 \\ x_3 \\ (x_3)^2 \end{Bmatrix} dx_3 \quad (\text{A.13})$$

References

- [1] S.T. Mau, P. Tong and T.H.H. Pian, Finite element solution for laminated thick plates, *J. Composite Mater.* 6 (1972) 304–311.
- [2] R.L. Spilker, S.C. Chou and O. Orringer, Alternate hybrid stress elements for analysis of multilayer composite plates, *J. Composite Mater.* 11 (1977) 51–70.
- [3] R.L. Spilker, Hybrid-stress eight-node elements for thin and thick multilayer laminated plates, *Int. J. Numer. Methods Engrg.* 18 (1982) 801–828.
- [4] D.R.J. Owen and Z.H. Li, A refined analysis of laminated plates by finite element displacement method—I: Fundamentals and static analysis, *Comput. Struct.* 26 (1987) 907–914.
- [5] R.A. Chaudhuri, An equilibrium method for prediction of transverse shear stresses in a thick laminated plate, *Comput. Struct.* 23 (1986) 139–146.
- [6] D.H. Robbins and J.N. Reddy Jr., Modeling of thick composites using a layerwise laminate theory, *Int. J. Numer. Methods Engrg.* 36 (1993) 655–677.
- [7] F. Gruttmann and W. Wagner, On the numerical analysis of local effects in composite structures, *Composite Struct.* 29 (1994) 1–12.
- [8] R.A. Chaudhuri and P. Seide, An approximate semi-analytical method for prediction of interlaminar shear stresses in an arbitrarily laminated thick plate, *Comput. Struct.* 25 (1987) 627–636.
- [9] J.J. Engblom and O.O. Ochoa, Through the thickness stress predictions for laminated plates of advanced composite materials, *Int. J. Numer. Methods Engrg.* 21 (1985) 1759–1776.
- [10] T. Kant and B.N. Pandya, A simple finite element formulation of a higher-order theory for unsymmetrically laminated composite plates, *Composite Struct.* 9 (1988) 215–246.
- [11] J.N. Reddy, E.J. Barbero and J.L. Teply, A plate bending element based on a generalized laminate plate theory, *Int. J. Numer. Methods Engrg.* 28 (1989) 2275–2292.
- [12] C.W. Pryor and R.M. Barker, A finite element analysis including transverse shear effects for application to laminated plates, *AIAA J.* 9 (1971) 912–917.
- [13] B.S. Manjunatha and S. Kant, On evaluation of transverse stresses in layered symmetric composite and sandwich laminates under flexure, *Engrg. Comput.* 10 (1993) 499–518.
- [14] A.K. Noor, Y.H. Kim and J.M. Peters, Transverse shear stresses and their sensitivity coefficients in multilayered composite panels, *AIAA J.* 32 (1994) 1259–1269.

- [15] A.K. Noor, W.S. Burton and J.M. Peters, Predictor–corrector procedure for stress and free vibration analyses of multilayered composite plates and shells, *Comput. Methods Appl. Mech. Engrg.* 82 (1990) 341–364.
- [16] R. Rolfes and K. Rohwer, Improved transverse shear stresses in composite finite elements based on first-order shear deformation theory, *Int. J. Numer. Methods in Engrg.* 40 (1997) 51–60.
- [17] R. Rolfes and K. Rohwer, Eine Einfache Methode zur Ermittlung aller Querspannungen in Faserverbundplatten als Voraussetzung einer Verbesserten Versagensanalyse, MSC Anwenderkonferenz, Bad Neuenahr, June 5–6, 1997.
- [18] K. Rohwer, Improved transverse shear stiffnesses for layered finite elements, DFVLR-FB-88-32, Braunschweig (1988).
- [19] A.K. Noor and W.S. Burton, Three-dimensional solutions for the free vibrations and buckling of thermally stressed multilayered angle-ply composite plates, *J. Appl. Mech.* 59 (1992) 868–877.
- [20] M. Savoia and J.N. Reddy, Three-dimensional thermal analysis of laminated composite plates, *Int. J. Solids Struct.* 32 (1995) 593–608.

INFORMATION FOR CONTRIBUTORS

Manuscripts should be sent in triplicate to one of the Editors. All manuscripts will be refereed. Manuscripts should preferably be in English. They should be typewritten, double-spaced, first copies (or clear Xerox copies thereof) with a wide margin. Abstracts, footnotes and lists of references should also be double-spaced. All pages should be numbered (also those containing references, tables and figure captions). Upon acceptance of an article, author(s) will be asked to transfer copyright of the article to the publisher. This transfer will ensure the widest possible dissemination of information.

Abstracts

The text of a paper should be preceded by a summary in English. This should be short, but should mention all essential points of the paper.

Figures and tables

The drawings for the figures must be originals, drawn in black India ink in large size and carefully lettered, or printed on a high-quality laser printer. The lettering as well as the details should have proportionate dimensions, so as not to become illegible or unclear after the usual reduction by the printers; in general, the figures should be designed for a reduction factor of two or three. Mathematical symbols should be entered in italics, where appropriate. Each figure should have a number and a caption; the captions should be collected on a separate sheet. The appropriate place of a figure should be indicated in the margin. Tables should be typed on separate sheets. Each table should have a number and a title. The appropriate places for the insertion of tables should be indicated in the margin. Colour illustrations can be included and will be printed in colour at no charge if, in the opinion of the Editors, the colour is essential. If this is not the case, the figures will be printed in black and white unless the author is prepared to pay the extra costs arising from colour reproduction.

Formulae

Displayed formulae should be numbered and typed or clearly written by hand. Symbols should be identified in the margin, where they occur for the first time.

References

In the text, reference to other parts of the paper should be made by section (or equation) number, but not by page number. References should be listed on a separate sheet in the order in which they appear in the text.

COMPLETE INSTRUCTIONS TO AUTHORS are published in every last issue of a volume, and copies can also be obtained from the Editors and the Publisher, Elsevier Science B.V., P.O. Box 1991, 1000 BZ Amsterdam, The Netherlands.

Instructions for LaTeX manuscripts

The LaTeX files of papers that have been accepted for publication may be sent to the Publisher by e-mail or on a diskette (3.5" or 5.25" MS-DOS). If the file is suitable, proofs will be produced without rekeying the text. The article should be encoded in Elsevier-LaTeX, standard LaTeX, or AMS-LaTeX (in document style "article"). The Elsevier-LaTeX package, together with instructions on how to prepare a file, is available from the Publisher. This package can also be obtained through the Elsevier WWW home page (<http://www.elsevier.nl/>), or using anonymous FTP from the Comprehensive TeX Archive Network (CTAN). The host-names are: <ftp.dante.de>, <ftp.tex.ac.uk>, <ftp.shsu.edu>; the CTAN directories are: [/pub/tex/macros/latex209/contrib/elsevier](#), [/pub/archive/macros/latex209/contrib/elsevier](#), [/tex-archive/macros/latex209/contrib/elsevier](#), respectively. *No changes from the accepted version are permissible, without the explicit approval of the Editor. The Publisher reserves the right to decide whether to use the author's file or not.* If the file is sent by e-mail, the name of the journal should be mentioned in the "subject field" of the message to identify the paper. Authors should include an ASCII table (available from the Publisher) in their files to enable the detection of transmission errors.

Publication information:

Computer Methods in Applied Mechanics and Engineering (ISSN 0045-7825). For 1998 volumes 151-163 are scheduled for publication. Subscription prices are available upon request from the Publisher. Subscriptions are accepted on a prepaid basis only and are entered on a calendar year basis. Issues are sent by surface mail except to the following countries where Air delivery via SAL mail is ensured: Argentina, Australia, Brazil, Canada, Hong Kong, India, Israel, Japan, Malaysia, Mexico, New Zealand, Pakistan, PR China, Singapore, South Africa, South Korea, Taiwan, Thailand, USA. For all other countries airmail rates are available upon request. Claims for missing issues should be made within six months of our publication (mailing) date.

Orders, claims, and product enquiries: please contact the Customer Support Department at the Regional Sales Office nearest you:

New York: Elsevier Science, PO Box 945, New York, NY 10159-0945, USA; phone: (+1) (212) 633 3730 [toll free number for North American customers: 1-888-4ES-INFO (437-4636)]; fax: (+1) (212) 633 3680; e-mail: usinfo-f@elsevier.com

Amsterdam: Elsevier Science, PO Box 211, 1000 AE Amsterdam, The Netherlands; phone: (+31) 20 4853757; fax: (+31) 20 4853432; e-mail: nlinfo-f@elsevier.nl

Tokyo: Elsevier Science K.K., 9-15 Higashi-Azabu 1-chome, Minato-ku, Tokyo 106, Japan; phone: (+81) (3) 5561 5033; fax: (+81) (3) 5561 5047; e-mail: info@elsevier.co.jp

Singapore: Elsevier Science, No. 1 Temasek Avenue, #17-01 Millenia Tower, Singapore 039192; phone: (+65) 434 3727; fax: (+65) 337 2230; e-mail: asiainfo@elsevier.com.sg

Rio de Janeiro: Elsevier Science, Rua Sete de Setembro 111/16 Andar, 20050-002 Centro, Rio de Janeiro - RJ, Brazil; phone: (+55) (21) 509 5340; fax: (+55) (21) 507 1991; e-mail: elsevier@campus.com.br [Note (Latin America): for orders, claims and help desk information, please contact the Regional Sales Office in New York as listed above]

References

- Antes, H. and Panagiotopoulos, P.D. (1992) *An integral equation approach to the static and dynamic contact problems. Equality and inequality methods*. Birkhäuser Verlag, Boston, Basel, Stuttgart.
- Brebbia, C.A. and Dominguez, J. (1989) *Boundary Elements. An introductory course*. Computational Mechanics Publications and McGraw-Hill Book Co.
- Luo, Z.-Q., Pang, J.-S. and Ralph, D. (1996) *Mathematical Programs with Equilibrium Constraints*. Cambridge University Press, 1996.
- Mellings S.C. and Aliabadi M.H. (1994) Three dimensional flow identification using sensitivity analysis. In: *Boundary Element Method XVI*, Brebbia, C.A. (ed), pp. 149-166, Computational Mechanics Publications, Southampton, Boston.
- Mitra, A.K. and Das, S. (1992) Solution of inverse problems by using the boundary element method. In: *Boundary Element Technology VII*, Brebbia, C.A., Inghier, M.S. (eds), pp. 721-731, Computational Mechanics Publ and Elsevier Appl. Science.
- Nashe H.G. (1991) *Einführung in Theorie und Praxis der Zeitreihen- und Modellanalyse*. 3rd Ed., Vieweg Verlag, Braunschweig, Wiesbaden.
- Nashe H.G. (1993) The state of the art of system identification. Emphasizing nonlinear systems and applications. In: *Structural Dynamics EURO-DYN'93*, Moen et al. (eds), Vol. 2, pp. 805-810, Balkema, Rotterdam.
- Nishimura N. and Kobayashi S. (1991) A boundary integral equation method for an inverse problem related to crack detection. *Intern. Journal for Numerical Methods in Engineering*, 32, pp. 1371-1387.
- Oishi, A., Yamada, K. and Yoshimura, A., Yagawa G. (1995) Quantitative nondestructive evaluation with ultrasonic method using neural networks and computational mechanics, *Computational Mechanics*, 15, pp. 521-533.
- Ostrata, J.V. and Zowe, J. (1993) A numerical approach to optimization problems with variational inequality constraints, *Mathematical Programming*, 68, pp. 105-130.
- Panagiotopoulos, P.D. (1995) *Inequality Problems in Mechanics and Applications, Convex and Nonconvex Energy Functions*, Birkhäuser Verlag, Basel.
- Rhim, J. and Lee S.W. (1995) A neural network approach for damage detection and identification of structures, *Computational Mechanics*, 16, pp. 437-443.
- Stavroulakis, G.E. (1995) Optimal prestress of cracked unilateral structures: finite element analysis of an optimal control problem for variational inequalities, *Computer Methods in Applied Mechanics and Engineering*, 123, pp. 231-246.
- Stavroulakis, G.E. and Antes, H. (1997) Nondestructive elastostatic identification of unilateral cracks through BEM and Neural Networks, *Computational Mechanics* (in press).
- Tanaka, M. and Masuda, Y. (1986) An integral equation approach to inverse problems in structural mechanics. In: *Computational Mechanics 86*, Yagawa, G., Atluri, S.N. (eds), Vol. 2, pp. XI-15, XI-24, Springer.
- Tanaka, M., Nakamura, M., Nakano, T., Ishikawa, H. (1991) Identification of defects by the elastodynamic boundary element method using noisy additional information. In: *Boundary Elements XIII*, Brebbia, C.A. Gipeon, G.S. (eds), pp. 799-810, Computational Mechanics Publ and Elsevier Appl. Science.
- Tsoka, N., Utani, A. and Takahashi, H. (1993) Unknown defect identification in elastic field by boundary element method with filtering procedure, *Engineering Analysis with Boundary Elements*, 15, pp. 207-215.
- Wu, X., Ghaboussi, J. and Garrett, Jr. J.H. (1992) Use of neural networks in detection of structural damage, *Computers and Structures*, 42, pp. 649-659.
- Yoshimura, S., Masuda, A. and Yagawa, G. (1996) New regularization by transformation for neural network based inverse analyses and its application to structure identification, *Intern. Journal of Numerical Methods in Engineering*, 39, pp. 3953-3968.

RECENT ADVANCES IN SENSITIVITY ANALYSIS FOR NONLINEAR STRUCTURAL MECHANICS PROBLEMS

AHMED K. NOOR AND JEANNE M. PETERS
Center for Advanced Computational Technology
University of Virginia
NASA Langley Research Center
Hampton, Virginia

1. Abstract

Recent developments in the sensitivity analysis for nonlinear structural mechanics and dynamics problems are reviewed. The activities are grouped into two general categories, namely, computational strategies and facilities for evaluating the sensitivity coefficients, and new applications. Brief description is given of the activities pertaining to the first category. More detailed discussion is presented for two recent applications: a) hierarchical sensitivity coefficients of the various response quantities of sandwich panels with composite face sheets with respect to the different laminate, layer and micromechanical characteristics of the face sheets and core; and b) sensitivity analysis of the large strain response of viscoplastic solids subjected to dynamic loading. Sample numerical results are presented and some of the future directions for research on sensitivity analysis of large-scale nonlinear structures are outlined.

2. Introduction

In recent years several attempts have been made to extend the domain of sensitivity analysis to nonlinear static and dynamic responses of structures. Some of these attempts are documented in a monograph [1], survey papers and conference proceedings [2-7]. The sensitivity information, in addition to being a necessary component in the automated optimum design of structures, is used to:

- 1) assess the effect of uncertainties, in the material and geometric parameters of the computational model, on the nonlinear response;
- 2) predict the changes in the nonlinear response due to changes in the parameters; and
- 3) generate an approximation for the nonlinear response of the structure (along with a rapid reanalysis technique). Other uses of sensitivity information will be outlined in subsequent sections.

The sensitivity analysis is performed by evaluating the derivatives of the response quantities with respect to the material and geometric coefficients of the structure. Henceforth, these derivatives will be referred to as sensitivity

coefficients. Two general procedures are currently used for calculating the sensitivity coefficients of the nonlinear response of structures. The two approaches are the direct differentiation method, and the adjoint variable method. The first procedure is based on the implicit differentiation of the equations that describe the nonlinear response with respect to the desired parameters, and the solution of the resulting sensitivity equations. In the adjoint variable method an adjoint physical system is introduced whose solution permits rapid evaluation of the desired sensitivity coefficients. Both procedures can be applied to the governing discrete, semi-discrete or continuum equations of the structure (with a consequent change in the order of spatial discretization, temporal integration, and implicit differentiation).

Recent activities on sensitivity analysis for nonlinear structural response can be grouped into two general categories: a) computational strategies and facilities for evaluating sensitivity coefficients; and b) new applications, including composite structures [8]; flexible multibody systems [9]; path dependent problems for which the sensitivity coefficients depend also on the deformation history (e.g., viscoplastic response and frictional contact) [10-16]; and structural systems exhibiting probabilistic uncertainties. The presence of inequality constraints in contact problems implies non-differentiability. As a consequence, only directional sensitivities of the structural response with respect to problem parameters can be expected. The persistent contact conditions and the use of the penalty method alleviate the discontinuity problem. The present paper provides a brief description of some of the recent developments in computational strategies and facilities for sensitivity analysis for nonlinear structural response. The two applications are: a) hierarchical sensitivity analysis for sandwich panels with composite face sheets, and b) sensitivity analysis of porous viscoplastic solids subjected to dynamic loading, and are described in succeeding sections.

3. Brief Review of Work on Computational Strategies and Facilities

An automatic differentiation facility has been developed for evaluating the derivatives of functions defined by computer programs, exactly to within machine precision. The facility has the acronym ADIFOR (Automatic Differentiation of FORtran), and is described in [17]. The use of ADIFOR to evaluate the sensitivity coefficients from incremental/iterative forms of three-dimensional fluid flow problems is discussed in [18], and the additional facilities needed for ADIFOR to become competitive with hand-differentiated codes are listed in [19].

For large deflection static problems, an efficient reduced basis technique for evaluating the sensitivity of the nonlinear response was developed by the authors and their colleagues. The technique is based on approximating each of the response vector and its various order sensitivity coefficients, by a small number of basis (or global approximation) vectors. The Bubnov-Galerkin technique is then used to approximate each of the finite element equations governing the response and the sensitivity coefficients, by a small number of algebraic equations in the amplitudes of these vectors. Path derivatives (derivatives of the response vector with respect to path parameters, e.g., load parameters) are used as basis vectors for approximating the response. A

combination of path derivatives and their derivatives with respect to the structural parameters is used for approximating the sensitivity coefficients. The technique was applied to geometrically nonlinear problems of composite panels and aircraft tires [20-21]. It was also extended to nonlinear vibration problems of composite panels [22].

Parallel computational strategies were developed for evaluating the sensitivity coefficients for static postbuckling and contact/impact response on distributed-memory computers. The strategies are applicable to any message-passing computational environment. The key elements of the strategy for geometrically nonlinear static problems are [23]: a) multiple-parameter reduced basis technique, b) a parallel sparse equation solver based on a nested dissection (or multilevel substructuring) node-ordering scheme, and c) a multilevel parallel procedure for evaluating the sensitivity coefficients. For contact/impact problems, an explicit central difference scheme is used for the temporal integration of the semi-discrete equations of motion, and the two key elements of the parallel strategy are [24]: a) an element-based domain decomposition technique, and b) a robust exchange algorithm for communicating information across subdomain interfaces.

Hybrid numerical/neurocomputing strategy has been developed for the evaluation of sensitivity coefficients of geometrically nonlinear structural response. In the hybrid strategy, multilayer feedforward neural networks are used to extend the range of validity of the sensitivity coefficients predicted by Pade' approximants [25].

4. Hierarchical Sensitivity Coefficients of Sandwich Panels with Composite Face Sheets

The response characteristics of sandwich panels with composite face sheets are dependent on a hierarchy of interrelated parameters including panel parameters, effective face sheet layer and core properties, and micromechanical (core and face sheet fiber, matrix, interphase and interface) parameters. A study of the sensitivity of the response to variations in each of these parameters provides an insight into the importance of the parameter and helps in the development of materials to meet certain performance requirements. Moreover, in multiscale analysis, the hierarchical sensitivity coefficients can be used for identifying the extent of the regions for which a micromechanical analysis is needed to capture the phenomena occurring at the small length scales.

Three sets of sandwich parameters are considered herein; namely, panel, effective layer, and micromechanical parameters. The panel parameters include the extensional, bending-extensional, bending and transverse shear stiffnesses (components of the matrices $[A]$, $[B]$, $[D]$ and $[A_s]$); and the thermal forces and moments (components of the vectors $\{N_T\}$ and $\{M_T\}$). The effective layer parameters include the individual face sheet layer properties; elastic moduli E_L, E_T ; shear moduli G_{LT}, G_{TT} ; major Poisson's ratio ν_L ; coefficients of thermal expansion α_L, α_T ; fiber orientation angle $\theta^{(i)}$; layer thickness $h^{(i)}$ where L and T refer to the longitudinal (fiber) and transverse

directions, respectively. The layer parameters also include the effective core properties: elastic moduli E_k, E_m ; shear moduli G_{12}, G_{13}, G_{23} ; Poisson's ratios $\nu_{12}, \nu_{13}, \nu_{23}$; coefficient of thermal expansion α_k and core thickness $h^{(c)}$. The micromechanical parameters refer to the fiber, matrix and core material moduli $E_f, E_m, E_c, G_{12}, G_{13}, G_{23}$; Poisson's ratios $\nu_{12}, \nu_{13}, \nu_{23}$; coefficients of thermal expansion $\alpha_f, \alpha_m, \alpha_c$; the fiber volume fraction V_f of the face sheet layers; and the geometric parameters of the core ℓ_k, ℓ_m, ℓ_c and θ . The subscripts f, m and c denote the fiber, matrix and core property, respectively. The three sets of parameters will henceforth be referred to as $\lambda_i^{(p)}, \lambda_j^{(m)}, \lambda_k^{(c)}$ where superscripts p, ℓ and m refer to the panel, layer, and micromechanical parameters, respectively; and the indices i, j and k range from 1 to the number of parameters in each category.

The governing equations for the sensitivity coefficients are obtained by differentiating the nonlinear equations describing with respect to a typical parameter λ . The resulting equations are linear in the sensitivity coefficients.

The computational procedure consists of evaluating the sensitivity coefficients with respect to each of the panel parameters $\left\{ \frac{\partial Z}{\partial \lambda_i^{(p)}} \right\}$. The sensitivity coefficients with respect to the effective layer and micromechanical parameters are then obtained by forming the following linear combinations:

$$\left\{ \frac{\partial Z}{\partial \lambda_j^{(m)}} \right\} = \sum_i a_{ij} \left\{ \frac{\partial Z}{\partial \lambda_i^{(p)}} \right\} \quad (1)$$

and

$$\left\{ \frac{\partial Z}{\partial \lambda_k^{(c)}} \right\} = \sum_j b_{jk} \left\{ \frac{\partial Z}{\partial \lambda_j^{(m)}} \right\} = \sum_i c_{ik} \left\{ \frac{\partial Z}{\partial \lambda_i^{(p)}} \right\} \quad (2)$$

where

$$a_{ij} = \left\{ \frac{\partial \lambda_j^{(m)}}{\partial \lambda_i^{(p)}} \right\} \quad (3)$$

$$b_{jk} = \left\{ \frac{\partial \lambda_k^{(c)}}{\partial \lambda_j^{(m)}} \right\} \quad (4)$$

$$c_{ik} = \left\{ \frac{\partial \lambda_k^{(c)}}{\partial \lambda_i^{(p)}} \right\} = \sum_j a_{ij} b_{jk} \quad (5)$$

The a_{ij} coefficients relate the panel stiffnesses to the effective properties of the individual layers and are obtained from the lamination theory. The b_{jk}

coefficients relate the effective layer properties to the constituent properties and are obtained from the micromechanical and core models; and the c_{ik} coefficients relate the panel stiffnesses to the micromechanical properties (see bottom part of Fig. 1). If the panel stiffnesses are uniform, and the constitutive relations of the panel, layer, and the constituents are linear, then the a_{ij}, b_{jk}, c_{ik} coefficients are constants and need to be generated only once for each panel, even when the response is nonlinear. For a curved sandwich panel with composite face sheets, the sensitivity coefficients with respect to panel stiffnesses, effective properties of the face sheets and core and micromechanical properties are shown in Fig. 2. The panel is subjected to a sequence of mechanical and thermal loadings: uniform pressure loading, monotonically increasing edge shortening, and then a temperature gradient through the thickness (see [26]).

5. Sensitivity Analysis of Porous Viscoplastic Solids Subjected to Dynamic Loading

The evaluation of the sensitivity coefficient of the nonlinear dynamic response entails the solution of an additional system of ordinary differential equations for the semi-discrete model. The sensitivity coefficients depend on the history of the response, the current values of the response quantities and the history of the sensitivity coefficients. Considerable simplification in the computational procedure results by exploiting the fact that response calculations are uncoupled from sensitivity calculations. If the response quantities are evaluated first, the sensitivity calculations reduce to solve a set of linear algebraic equations whose coefficients depend on the response quantities. For a rate problem such as that of porous viscoplastic solids with material strain and strain-rate hardening and thermal softening due to adiabatic heating, the increments of the sensitivity coefficients form a set of linear algebraic equations. This feature can be exploited in the sensitivity calculations of the constitutive model, wherein the increments of the matrix plastic strain are obtained in terms of response quantities and known sensitivity coefficients.

In the present study, the direct differentiation approach is used in conjunction with the automatic differentiation facility ADIFOR for evaluating the first- and second-order derivatives of the various response functions, with respect to the various geometric and material parameters. For complex material systems like the one considered herein, the sensitivity coefficients can be used in conjunction with experiments to refine the constitutive model and adjust the parameters used therein. For a notched specimen in a plane strain state subjected to an initial velocity, the first- and second-order sensitivity coefficients of the void volume fraction with respect to the material parameter q_1 , at three different times, are shown in Fig. 3 (see [27]).

6. Future Directions for Research

Among the different aspects of sensitivity analysis which have high potential for research are the following:

• Extension to structural systems with uncertainties. If fuzzy sets are used to represent the uncertain parameters, then possibility distributions of the various sensitivity coefficients with respect to these parameters can be generated and bounds on these coefficients can be obtained.

• Extension of hierarchical sensitivity analysis of composite and sandwich structures to the subcomponent and the component levels (see top part of Fig. 1). A stiffened panel is an example of a subcomponent. The parameters at that level include the stiffener dimensions and spacing. A fuselage barrel section is an example of a component. The potential of using hierarchical sensitivity analysis to bridge the gap between structural design and material development can then be realized.

• Application to coupled field problems (e.g., coupled mechanical, thermal and electromagnetic fields for smart materials). The sensitivity coefficients can be used to identify the coupling coefficients which have the most impact on the response quantities of interest. Experiments can then be designed to determine these coefficients.

• Application to multilevel strategies for simulating damage propagation in structures. Sensitivity coefficients can help in the automatic updating of the model as the damage propagates.

7. Acknowledgments

This work was partially supported by Office of Naval Research Grant N00014-96-1-0640, Air Force Office of Scientific Research Grant F49620-96-1-0462, and NASA Headquarters Cooperative Agreement NCCW-0011.

8. References

1. Kleiber, M. et al.: *Parameter Sensitivity in Nonlinear Mechanics - Theory and Finite Element Computations*, Wiley, NY, 1997.
2. Haftka, R.T. and Adelman, H.M.: Recent developments in structural sensitivity analysis, *Structural Optimization* 1(3) (1989), 137-151.
3. Haber, R.B., Tortorelli, D.A. and Vidal, C.A.: Design sensitivity analysis of nonlinear structures I: Large-deformation hyperelasticity and history-dependent material response, in M.P. Kamat (ed.), *Structural Optimization: Status and Promise*, Progress in Aeronautics and Astronautics Series, Vol. 150, American Institute of Aeronautics and Astronautics, Washington, DC, 1993, pp. 369-406.
4. Choi, K.K.: Design sensitivity of nonlinear structures - II, in M.P. Kamat (ed.), *Structural Optimization: Status and Promise*, Progress in Aeronautics and Astronautics Series, Vol. 150, American Institute of Aeronautics and Astronautics, Washington, DC, 1993, pp. 407-446.
5. Hinton, E. and Siens, J.: Aspects of adaptive finite element analysis and structural optimization, in B.H.V. Topping and M. Papadrakakis (eds.), *Advances in Structural Optimization*, CIVIL-COMP, Ltd., Edinburgh, Scotland, 1994, pp. 1-25.
6. Kirsch, U.: Efficient sensitivity analysis for structural optimization, *Comp. Meth. Appl. Mech. Eng.*, 117(1-2) (1994), 143-156.
7. Tortorelli, D.A. and Michaleris, P.: Design sensitivity analysis: overview and review, *Inverse Problems in Eng.* 1 (1994), 71-105.

8. Noor, A.K.: Recent advances in the sensitivity analysis for the thermomechanical postbuckling of composite panels, *ASCE J. Eng. Mech.* 122(4) (1996), 300-307.
9. Wasfy, T.M. and Noor, A.K.: Modeling and sensitivity analysis of multibody systems using new solid, shell and beam elements, *Comp. Meth. Appl. Mech. Eng.* 138 (1996), 187-211.
10. Tortorelli, D.A.: Sensitivity analysis for nonlinear constrained elastostatic systems, *Int. J. Num. Meth. Eng.* 33 (1992), 1643-1660.
11. Michaleris, P., Tortorelli, D.A. and Vidal, C.A.: Tangent operators and design sensitivity formulations for transient nonlinear coupled problems with applications to elastoplasticity, *Int. J. Num. Meth. Eng.* 37 (1994), 2471-2499.
12. Kulkarni, M. and Noor, A.K.: Sensitivity analysis of the nonlinear dynamic viscoplastic response of two-dimensional structures with respect to material parameters, *Int. J. Num. Meth. Eng.* 38 (1995), 183-198.
13. Kulkarni, M. and Noor, A.K.: Sensitivity analysis for the dynamic response of thermoviscoplastic shells of revolution, *Comp. Meth. Appl. Mech. Eng.* 129 (1996), 371-391.
14. Karagöglan, L. and Noor, A.K.: Dynamic sensitivity analysis of frictional contact/impact response of axisymmetric composite structures, *Comp. Meth. Appl. Mech. Eng.* 128 (1995), 169-190.
15. Kleiber, M. and Kowalczyk, P.: Sensitivity analysis in plane stress elasto-plasticity and elasto-viscoplasticity, *Comp. Meth. Appl. Mech. Eng.* 137 (1996), 395-409.
16. Kowalczyk, P. and Kleiber, M.: Parameter sensitivity for large deformation inelastic problems, *Comp. Assisted Mech. & Eng. Sci.* 4 (1997), 209-228.
17. Chinchalkar, S.: The application of automatic differentiation to problems in engineering analysis, *Comp. Meth. Appl. Mech. Eng.* 118 (1994), 197-207.
18. Carle, A., Green, L.L., Bischof, C.H. and Newman, P.A.: Application of automatic differentiation in CFD, *Proc. 25th AIAA Fluid Dynamics Conf.*, June 20-23, 1994, Colorado Springs, CO (1994), AIAA Paper 94-2197.
19. Sherman, L.L., Taylor, A.C., III, Green, L.L., Newman, P.A., Hou, G.J.-W. and Korivi, V.M.: First- and second-order aerodynamic sensitivity derivatives via automatic differentiation with incremental iterative methods, *Fifth AIAA/USF/NASA/ISSMO Symposium on Multidisciplinary Analysis and Optimization*, Sept. 7-9, 1994, Panama City Beach, FL (1994), AIAA Paper 94-4262.
20. Noor, A.K.: Recent advances and applications of reduction methods, *Applied Mechanics Reviews* 47(5) (1994), 125-146.
21. Noor, A.K., Tanner, J.A. and Peters, J.M.: Reduced-basis technique for evaluating the sensitivity coefficients of the nonlinear tire response, *AIAA J.* 31(2) (1993), 370-376.
22. Noor, A.K., Hadian, M.J. and Peters, J.M.: Reduced basis technique for evaluating the sensitivity of the nonlinear vibrational response of composite plates, *Comp. & Struct.* 52(6) (1994), 1097-1105.
23. Watson, B.C. and Noor, A.K.: Sensitivity analysis large-deflection and postbuckling responses on distributed-memory computers, *Comp. Meth. Appl. Mech. Eng.* 129 (1996), 393-409.
24. Watson, B.C. and Noor, A.K.: Large-scale contact/impact simulation and sensitivity analysis on distributed-memory computers, *Comp. Meth. Appl. Mech. Eng.* 141 (1997), 373-388.
25. Szwedzyk, Z.P. and Noor, A.K.: A hybrid numerical/neurocomputing strategy for sensitivity analysis of nonlinear structures, *Comp. & Struct.* 65(6) (1997), 869-880.
26. Noor, A.K., et al.: Curved sandwich panels subjected to temperature gradient and mechanical loads, *ASCE J. Aerospace Div.* 10(4) (1997), 143-161.

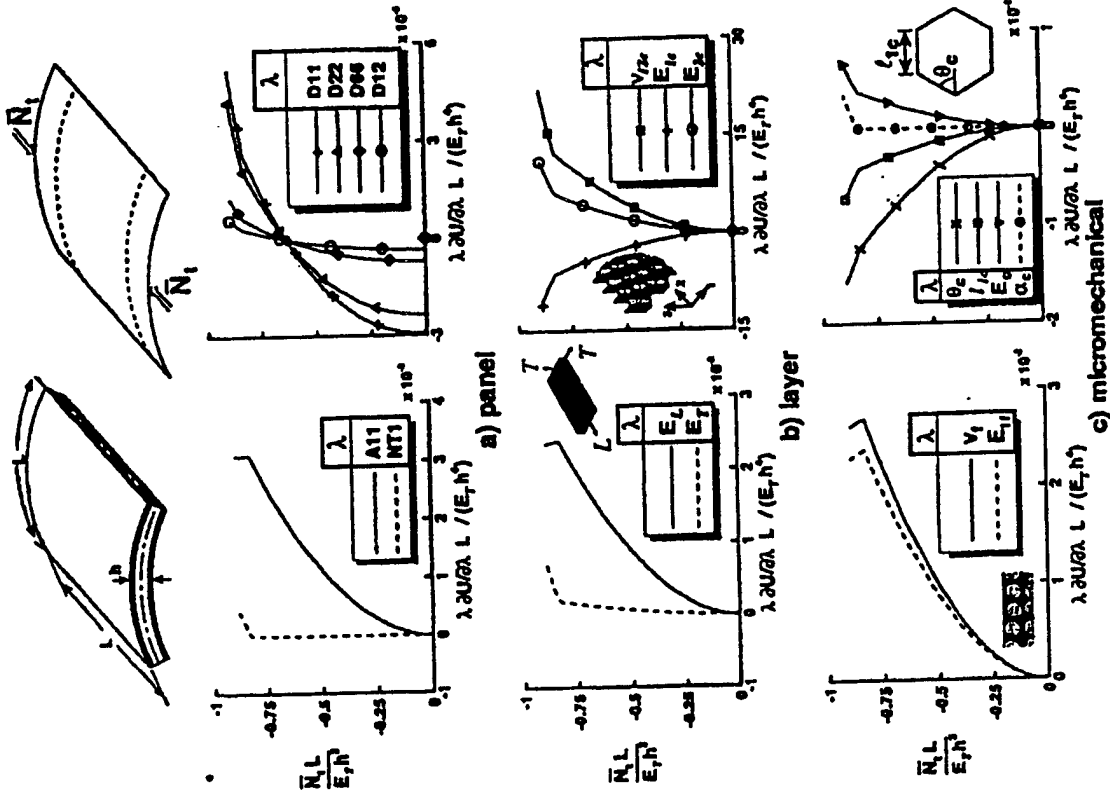


Figure 2 - Effect of loading on the normalized sensitivity coefficients of the total strain energy U with respect to panel, layer and micromechanical parameters. Cylindrical sandwich panels with honeycomb core and composite eight-layer face sheets, subjected to combined pressure loading, edge shortening and temperature gradient through the thickness (see [26]).

27. Noor, A.K., et al.: Sensitivity analysis for failure and damage in dynamically loaded tensile bars, *Comp. Meth. Appl. Mech. Eng.* 151(3-4) (1998), 461-478.

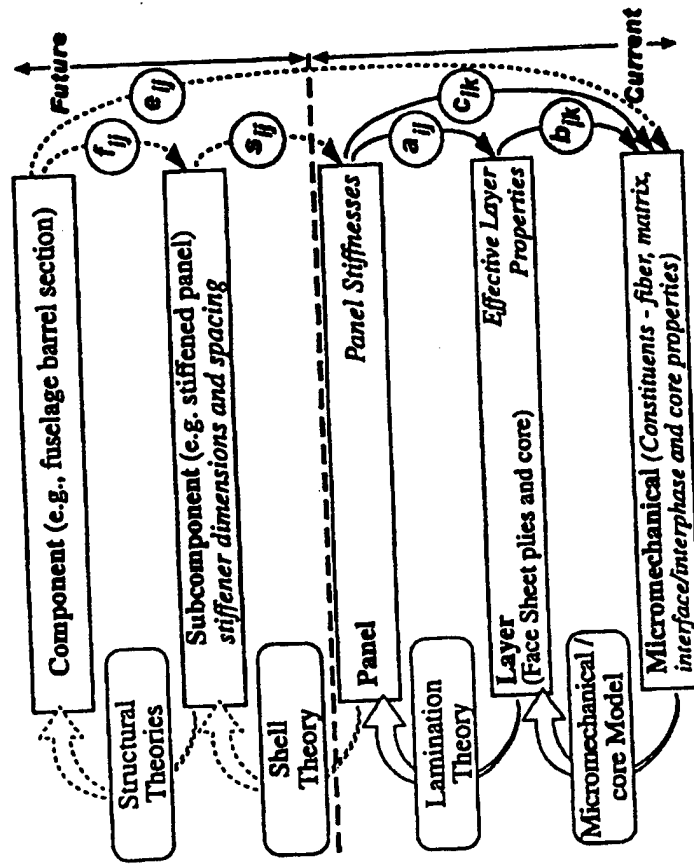


Figure 1 - Hierarchical sensitivity coefficients for sandwich structures with composite face sheets.

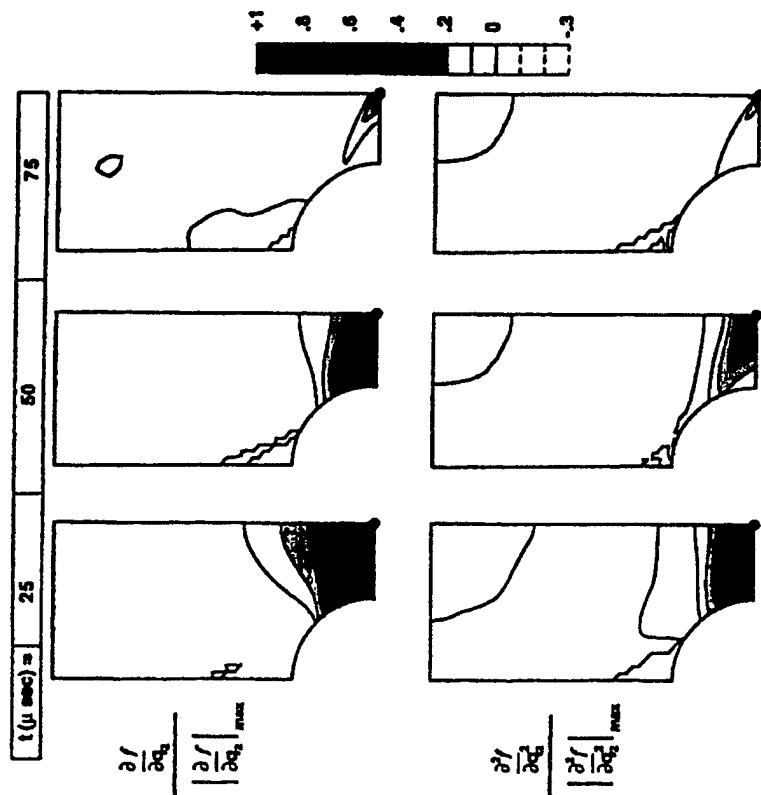


Figure 3 - Normalized contour plots for the first-order and second-order sensitivity coefficients of the void volume fraction f with respect to the material parameter q_1 . $\Phi = \frac{\sigma^2}{\bar{\sigma}^2} + 2q_1 f \cosh\left(\frac{2q_1 \sigma_1}{2\bar{\sigma}}\right) - 1 - q_1^2 f^2 = 0$, where $\bar{\sigma}$, σ , and σ_1 are the average strength of the matrix material, the macroscopic Mises stress and mean stress, respectively (see [27]).

SOME ASPECTS OF FEM APPLICATION FOR SENSITIVITY ANALYSIS OF QUASI-BRITTLE FRACTURE CONDITIONS

N.V. BANICHUK AND V.V. SAURIN

The Institute for Problems in Mechanics, Russian Academy of Sciences

Pr. Vernadskogo 101, 117526, Moscow, Russia

Abstract. In this paper continuum expressions of the shape design sensitivity analysis are derived for elastic bodies with cracks. Derived sensitivity analysis relations are implemented in FEM algorithm. Important aspects of sensitivity analysis and FEM effective applications are discussed.

1. Introduction

A substantial literature has been devoted to the field of shape design sensitivity analysis (SDSA) and optimization problems with integral and local functionals (see for example Haug et al., 1986 and Banichuk, 1992). Expressions for shape design sensitivity in terms of domain shape change have been derived in a continuous setting with the help of methods of classical calculus of variations and methods of optimization of distributed parameter systems. Shape design sensitivity information has been expressed as boundary integrals (boundary method of SDSA) or as domain integrals (domain method of SDSA) and evaluated using finite element analysis and boundary-element analysis. Fewer studies have been devoted to the important class of problems of construction and application of effective relations connecting the stress intensity factor and energy release rate with the variation of geometric parameters of the considered quasi-brittle bodies and structural elements with cracks. These relations and their implementation in FEM are of significant interest in fracture mechanics and optimal structural design. With their application it is possible to evaluate the sensitivity of a fracture criterion with respect to imperfect structural shape and non-ideal manufacture, to estimate structural parameters influence on crack

Analysis of Curved Sandwich Panels with Cutouts Subjected to Combined Temperature Gradient and Mechanical Loads

AHMED K. NOOR* AND JEANNE M. PETERS
Center for Advanced Computational Technology
University of Virginia
NASA Langley Research Center
Hampton, Virginia 23681

ABSTRACT: The results of detailed study of the effect of the cutout on the response of curved sandwich panels are presented. The panels have honeycomb core composite face sheets. The loading consists of a temperature gradient through-the-thickness combined with pressure loading and edge shortening or edge shear. The analysis is based on a first-order shear-deformation Sanders-Budiansky type theory with the effects of large displacements, moderate rotations, transverse shear deformation and laminated anisotropic material behavior included. A mixed formulation is used with the fundamental unknowns consisting of the generalized displacements and the stress resultants of the panel. The nonlinear displacement, strain energy, principal strains, transverse shear stresses, transverse shear strain energy density, and their hierarchical sensitivity coefficients are evaluated. The hierarchical sensitivity coefficients measure the sensitivity of the nonlinear response to variations in the panel parameters, the effective properties of the face sheet layers and the core, and the micromechanical parameters. Numerical results are presented for cylindrical sandwich panels and show the effects of variations in the loading and the size of the cutout on the global and local response quantities and their sensitivity to changes in the various panel, effective layer and micromechanical parameters.

INTRODUCTION

IN RECENT YEARS considerable work has been devoted to the study of thermomechanical nonlinear and postbuckling responses of sandwich plates and shells. Attempts have been made to identify the differences between the isothermal and thermal responses. Reviews of recent contributions are contained in two survey papers

* Author to whom correspondence should be addressed.

[2,8] and four monographs [5,6,13,14]. To the authors' knowledge, with the exception of Noor et al. [12], none of the reported studies considered the nonlinear response of curved sandwich panels subjected to temperature gradient through-the-thickness. The cited reference did not consider the effect of cutouts on the response of the panel. Since curved sandwich panels have many applications in aircraft structures, including fuselage, wing and empennage components of high-speed aircraft, an understanding of the nonlinear response of curved sandwich panels with cutouts, when subjected to a temperature gradient through-the-thickness combined with a mechanical loading, is desirable. Moreover, a study of the sensitivity of the nonlinear response to variations in the material, lamination and geometric parameters of these panels is needed to provide an indication of the effects of changes in these parameters on the structural response.

The present study focuses on understanding the detailed response characteristics of cylindrical sandwich panels with composite face sheets and circular cutouts subjected to a temperature gradient through-the-thickness combined with mechanical loadings. Sensitivity coefficients are evaluated which measure the sensitivity of the various response quantities to variations in the panel stiffnesses, the effective material properties of the individual face sheet layers and core, and the micromechanical parameters.

The sandwich panels considered in the study consist of a number of perfectly bonded composite face sheet layers, and a honeycomb core. The layers of the top and bottom face sheets are symmetrically distributed with respect to the middle surface. The individual layers of the face sheets and the core are assumed to be homogeneous and anisotropic. A plane of thermoelastic symmetry exists at each point of the panel, parallel to the middle surface. The loading is selected to simulate that of a typical fuselage panel of a high-speed aircraft.

MATHEMATICAL FORMULATION

The analytical formulation is based on a first-order shear-deformation Sanders-Budiansky type shell theory with the effects of large displacements, moderate rotations, average transverse shear deformation through-the-thickness, and laminated anisotropic material behavior included. For simplicity, a linear Duhamel-Neumann type constitutive model is used and the material properties are assumed to be independent of temperature. The constitutive relations for the panel are given in Noor et al. [12]. A total Lagrangian formulation is used and the panel deformations, at different values of the applied loadings, are referred to the original undeformed configuration. The panel is discretized by using two-field mixed finite element models. The fundamental unknowns consist of the nodal displacements and the stress resultant parameters. The stress resultants are allowed to be discontinuous at in-

terelement boundaries in the model. The sign convention for the generalized displacements and the stress resultants for the model are shown in Figure 1. The external loading consists of a uniform pressure loading p ; monotonically increasing edge displacement q_e (either normal or tangential to the edge); and a temperature gradient through-the-thickness q_T (linear through-the-thickness temperature variation, $q_T = (T_t - T_b)/h$, where T_t and T_b are the changes in the top and bottom surface temperatures, see Figure 2).

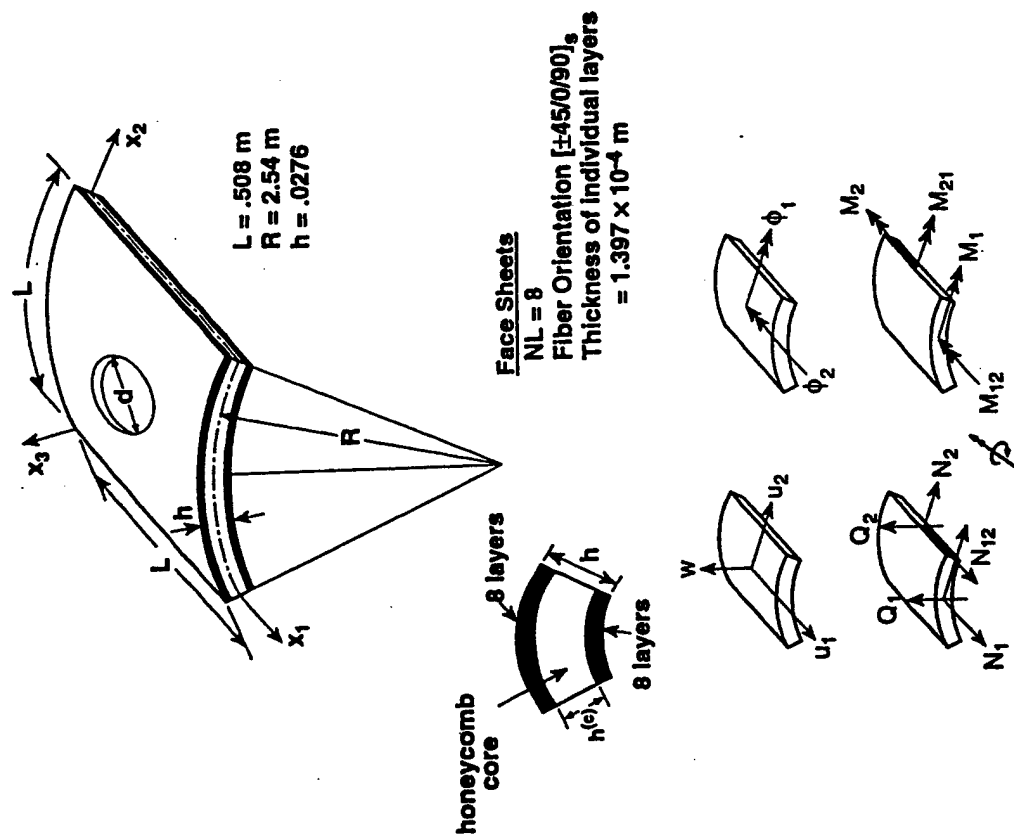


Figure 1. Panels considered in the present study and sign convention for generalized displacements and stress resultants.

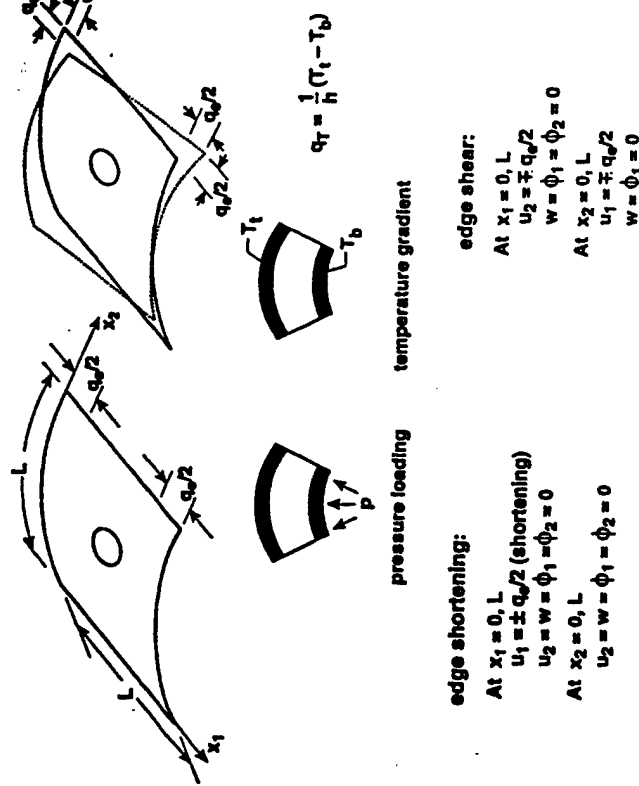


Figure 2. Loadings and boundary conditions considered in the numerical studies.

Governing Finite Element Equations

The governing equations for the response vector and its first-order sensitivity coefficients can be written in the following compact form:

$$\{f(Z)\} = [K]\{Z\} + \{G(Z)\} - p\{Q^{(1)}\} - q_e\{Q^{(2)}\} - q_T\{Q^{(3)}\} = 0 \quad (1)$$

$$\left[[K] + \left[\frac{\partial G_i}{\partial Z_j} \right] \right] \left\{ \frac{\partial Z}{\partial \lambda} \right\} = - \left[\frac{\partial K}{\partial \lambda} \right] \{Z\} + q_T \left\{ \frac{\partial Q^{(3)}}{\partial \lambda} \right\} \quad (2)$$

where $[K]$ is the global linear structural matrix which includes the flexibility and the linear strain-displacement matrices; $\{Z\}$ is the response vector which includes both unknown (free) nodal displacements and stress-resultant parameters; $\{G(Z)\}$ is the vector of nonlinear terms; p , q_e , and q_T are the magnitudes of the internal pressure, applied edge displacement and temperature gradient through-the-thickness; $\{Q^{(1)}\}$, $\{Q^{(2)}\}$, $\{Q^{(3)}\}$ are normalized vectors corresponding to unit values of p , q_e and q_T . λ is a typical parameter of the sandwich panel. The range of

indices \bar{I} and \bar{J} is 1 to the total number of degrees of freedom in the model; and $\{Q^{(1)}\}$ and $\{Q^{(2)}\}$ are assumed to be independent of λ . The form of the arrays $[K]$, $\{G(Z)\}$, $\{Q^{(1)}\}$ and $\{Q^{(2)}\}$ are given in Noor et al. [12]. Equation (1) is nonlinear in $\{Z\}$, but Equation (2) is identical to that used in the matrix on the left hand side of Equation (2) is identical to that used in the Newton-Raphson iterative process. Therefore, if the Newton-Raphson technique is used in generating the nonlinear response, the evaluation of the sensitivity coefficients requires the generation of the right-hand-side of Equation (2), and a forward-reduction/back-substitution operation only (no decomposition of the left-hand-side matrix is required).

Evaluation of the Transverse Shear Stresses

The transverse shear stresses are evaluated by using piecewise integration, in the thickness direction, of the three-dimensional equilibrium equations. For optimum accuracy, the transverse shear stresses are computed at the numerical quadrature points and then interpolated to the center of the element. The same procedure is used for evaluating the thickness distributions of the sensitivity coefficients of the transverse shear stresses.

Hierarchical Sensitivity Coefficients

The nonlinear and postbuckling response characteristics of sandwich panels are dependent on a hierarchy of interrelated parameters including panel, effective layer and micromechanical parameters. A study of the sensitivity of the response to variations in each of these parameters provides insight into the importance of the parameters and helps in the development of materials to meet certain performance requirements.

Three sets of sandwich parameters are considered herein; namely, panel, effective layer and micromechanical parameters. The panel parameters include the extensional, bending-extensional, bending and transverse shear stiffnesses [components of the matrices $[A]$, $[B]$, $[D]$ and $[A_s]$ (see Figure 3); and the vectors of the thermal effects $\{N_T\}$ and $\{M_T\}$ (see Reference [12]). The layer parameters include the individual face sheet layer properties: elastic moduli E_L , E_T ; shear moduli G_{LT} , G_{TT} ; major Poisson's ratio ν_{LT} ; coefficients of thermal expansion α_L , α_T ; fiber-orientation angle θ ; layer thickness h ; where subscripts L and T refer to the longitudinal (fiber) and transverse directions, respectively. The parameters also include the effective core properties: elastic moduli E_{1c} , E_{2c} ; shear moduli G_{12c} , G_{13c} , G_{23c} ; Poisson's ratios ν_{12c} , ν_{13c} , ν_{23c} ; coefficient of thermal expansion α_c ; and core thickness h_c . The micromechanical parameters refer to the fiber, matrix and core material moduli E_f , E_m , E_c , G_f , G_m , G_c ; Poisson's ratios ν_{12f} , ν_{23f} , ν_m ; coefficients of thermal expansion α_{1f} , α_{2f} , α_m ; and the fiber volume

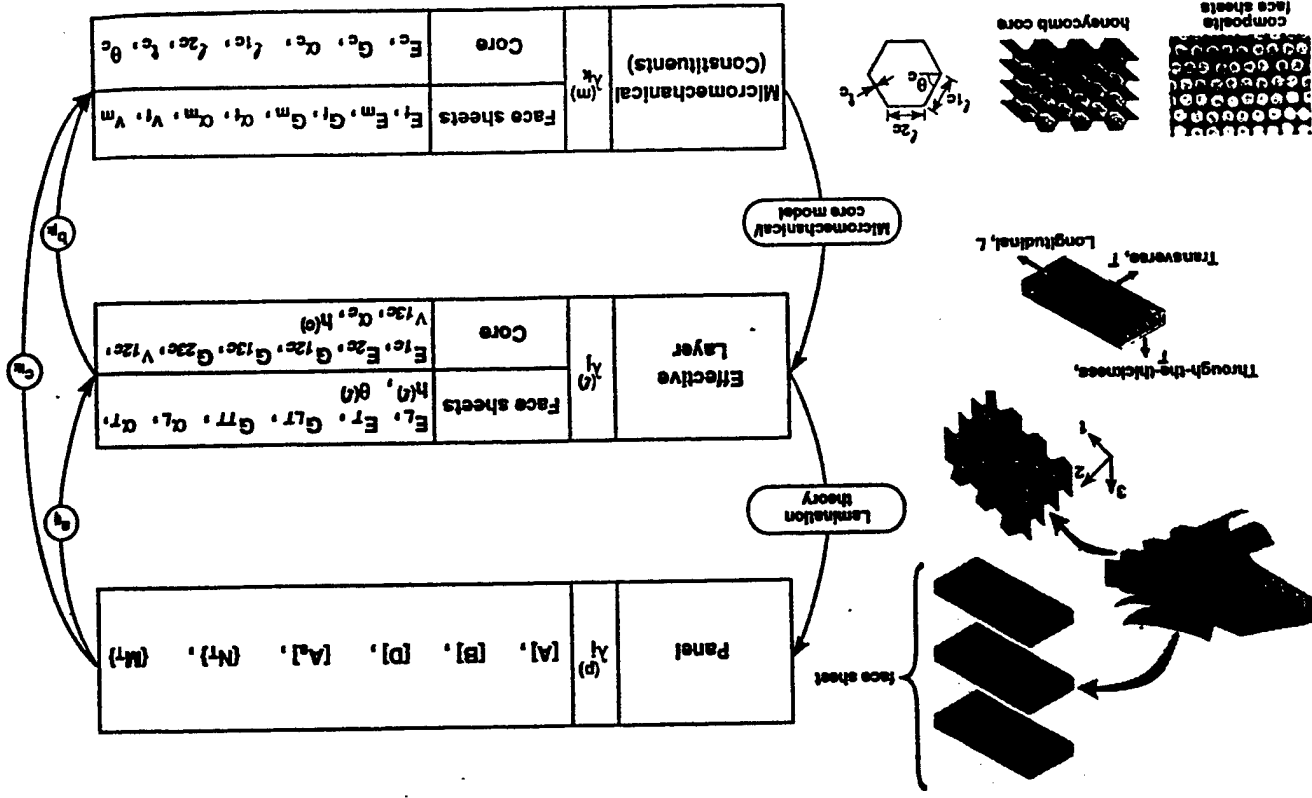


Figure 3. Hierarchical sensitivity coefficients for composite panels with composite face sheets.

fraction v_f of the face sheet layers. The subscripts f and m denote the fiber and matrix, respectively. The three sets of parameters will henceforth be referred to as $\lambda_i^{(p)}$, $\lambda_j^{(l)}$, $\lambda_k^{(m)}$ where superscripts p , l and m refer to the panel, effective layer, and micromechanical parameters, respectively; and the indices i , j and k range from 1 to the number of parameters in each category. In the present study, the Aboudi cell method [1] is used to evaluate the effective properties of the face sheet layers, and an upper bound energy approach is used to evaluate the effective core properties [3,4].

The computational procedure consists of evaluating the sensitivity coefficients with respect to each of the panel parameters $\{\partial Z/\partial \lambda_i^{(p)}\}$ using Equation (2). The sensitivity coefficients with respect to the effective layer parameters $\{\partial Z/\partial \lambda_j^{(l)}\}$ and micromechanical parameters $\{\partial Z/\partial \lambda_k^{(m)}\}$ are then obtained by forming linear combinations of them (see Reference [12]).

NUMERICAL STUDIES

Numerical studies were performed to determine the effects of variations in the loading and the diameter of the cutout on the response and the sensitivity coefficients of cylindrical sandwich panels with circular cutouts. The panels considered have composite, eight-layer quasi-isotropic face sheets and a titanium honeycomb core with hexagonal cells. The material properties and geometric characteristics for the panels considered in the present study are given in Table 1 and Figure 1. The material properties, the fiber orientation and the stacking sequences selected are those typical of sandwich panels considered for high-speed aircraft applications. The loading on the panels consisted of a sequence of mechanical and thermal loadings: uniform pressure loading $p = 6.894 \times 10^4$ Pa., followed by monotonically increasing edge displacement q_e , and then a temperature gradient through-the-thickness q_T (linear through-the-thickness temperature variation, $q_T = (T_t - T_b)/h$, where T_t and T_b are the changes in the top and bottom surface temperatures). The value of T_b was zero and T_t was increased to 137.8°C. Two different types of edge displacements were applied, namely, edge shortening and edge shear. The boundary conditions selected for the cases of edge shortening and edge shear are shown in Figure 2. In each loading case, the maximum value of q_e was selected in such a way that the maximum principal strains on the surfaces do not exceed 0.005. Four different values of the cutout diameter are considered; namely, $d/L = 0, 0.1, 0.3$ and 0.5 . For each problem, hierarchical sensitivity coefficients are evaluated (see Figure 3). The hierarchical sensitivity coefficients are the derivatives of the different response quantities with respect to panel stiffnesses, material parameters and fiber angles of the individual face sheet layers; effective and actual properties of the core; and micromechanical parameters of the face sheet layers.

Table 1. Micromechanical, effective layer, and panel properties of the sandwich panels considered in the present study.

(a) Micromechanical Properties

Fiber	Matrix	Core
E_{1f}	E_m	l_c
E_{2f}	ν_m	l_{1c}
G_{12f}	α_m	l_{2c}
ν_{12f}		θ_c
ν_{23f}		45°
α_{1f}		E_c
α_{2f}		G_c
ν_f		ν_c
		α_c

(b) Effective Layer Properties

Face Sheets	Core
E_L	E_{1c}
E_T	E_{2c}
G_{LT}	G_{12c}
G_{TT}	G_{13c}
ν_{LT}	G_{23c}
α_L	ν_{12c}
α_T	α_c
N_L	$h(c)$

(c) Panel Properties (Stiffnesses N/m)

Extensional	Bending	Transverse Shear
A_{11}	D_{11}	A_{55}
A_{12}	D_{12}	A_{44}
A_{22}	D_{22}	A_{45}
A_{66}	D_{66}	

Mixed finite element models were used for the discretization of each panel. Biquadratic shape functions were used for approximating each of the generalized displacements, and bilinear shape functions were used for approximating each of the stress resultants. The characteristics of the finite element model are given in Noor and Anderson [7]. For each panel, the multiple parameter reduction method described in Noor and Peters [9-11] were used in generating the nonlinear responses and evaluating the sensitivity coefficients. Typical results are presented in Figures 4-6 for the response studies and in Figures 7-9 for the sensitivity coefficients, and are described subsequently.

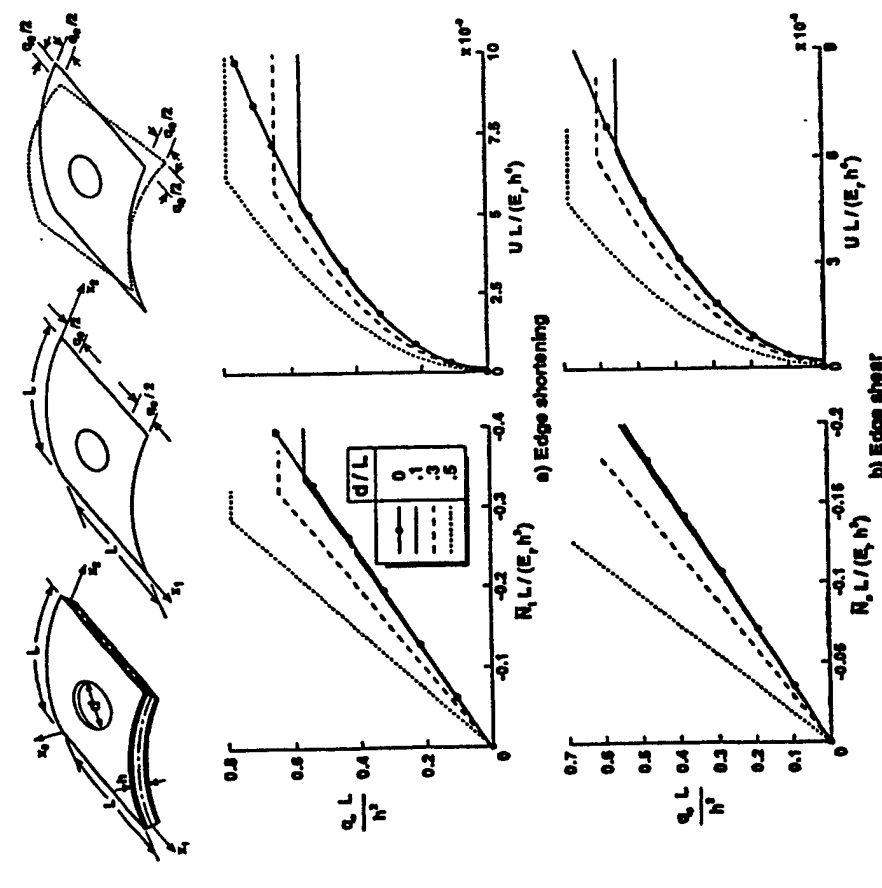


Figure 4. Effect of loading and hole diameter on the nonlinear response of cylindrical sandwich panels with honeycomb core and composite eight-layer face sheets subjected to combined pressure loading, prescribed edge displacement and temperature gradient through-the-thickness.

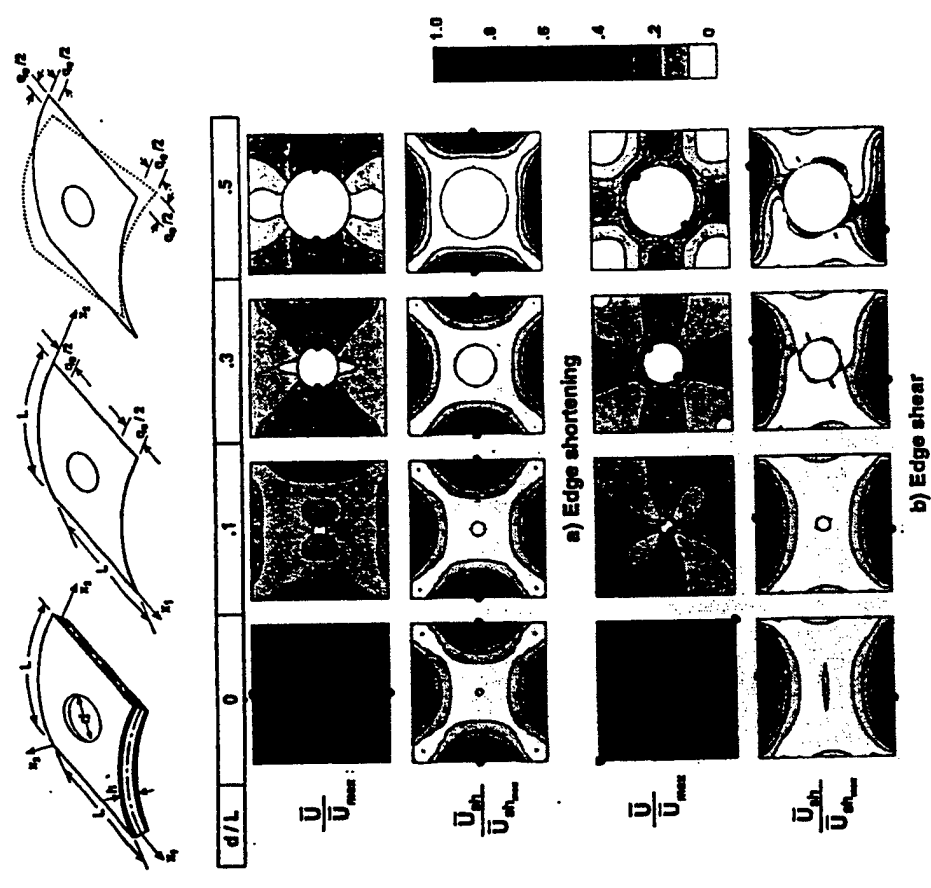


Figure 5. Normalized contour plots depicting the effect of loading and hole diameter on the total strain energy density U and the transverse shear strain energy density U_{sh} for cylindrical panels, with honeycomb core and composite eight-layer face sheets, subjected to combined pressure loading, prescribed edge displacement and temperature gradient through-the-thickness, $p + q_e + q_r$. Location of maximum values identified by a small solid circle.

Response Studies

Plots of the edge displacement q_e versus the total edge force \bar{N} , and the total strain energy U , are shown in Figure 4 for the four panels with $d/L = 0, 0.1, 0.3$ and 0.5 . Note that the horizontal lines in Figure 4 indicate that q_e was kept constant during the application of the temperature gradient. Normalized contour plots for the total strain energy density \bar{U} , and the transverse shear strain energy density \bar{U}_{sh} ,

for panels with and without cutouts, after the application of the total load $p + q_e + q_T$, are shown in Figure 5. The thickness distributions of the transverse shear strain energy density per unit volume, \dot{U}_{sh} , at the location of maximum \dot{U}_{sh} for the panels with and without cutouts are shown in Figure 6. In Figures 4-6 the two cases of edge shortening and edge shear are shown. The response studies can be summarized as follows:

- The effects of the cutout on the global and local response characteristics of the panel are very different. The presence of a small cutout, $d/L \leq 0.1$, reduces slightly the total edge force \bar{N} and total strain energy U . As d/L in-

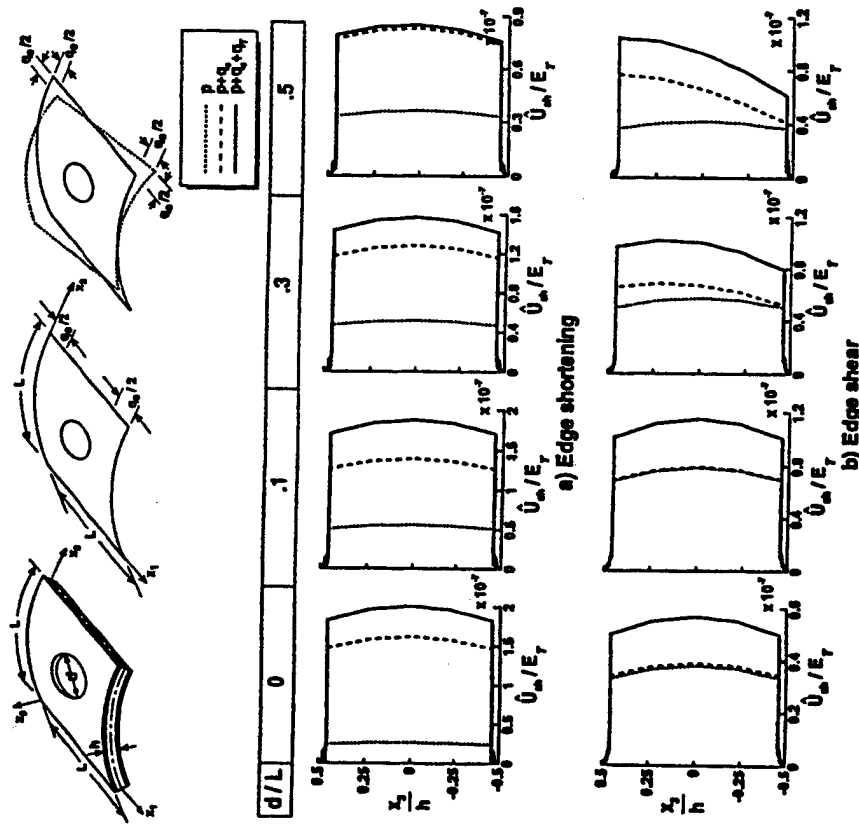


Figure 6. Effect of loading and hole diameter on the distribution of transverse shear strain energy density through-the-thickness, at the point of maximum transverse shear strain energy density \dot{U}_{sh} (see Figure 5). Cylindrical sandwich panels, with honeycomb core and composite eight-layer face sheets, subjected to combined pressure loading, prescribed edge displacement and temperature gradient through-the-thickness.

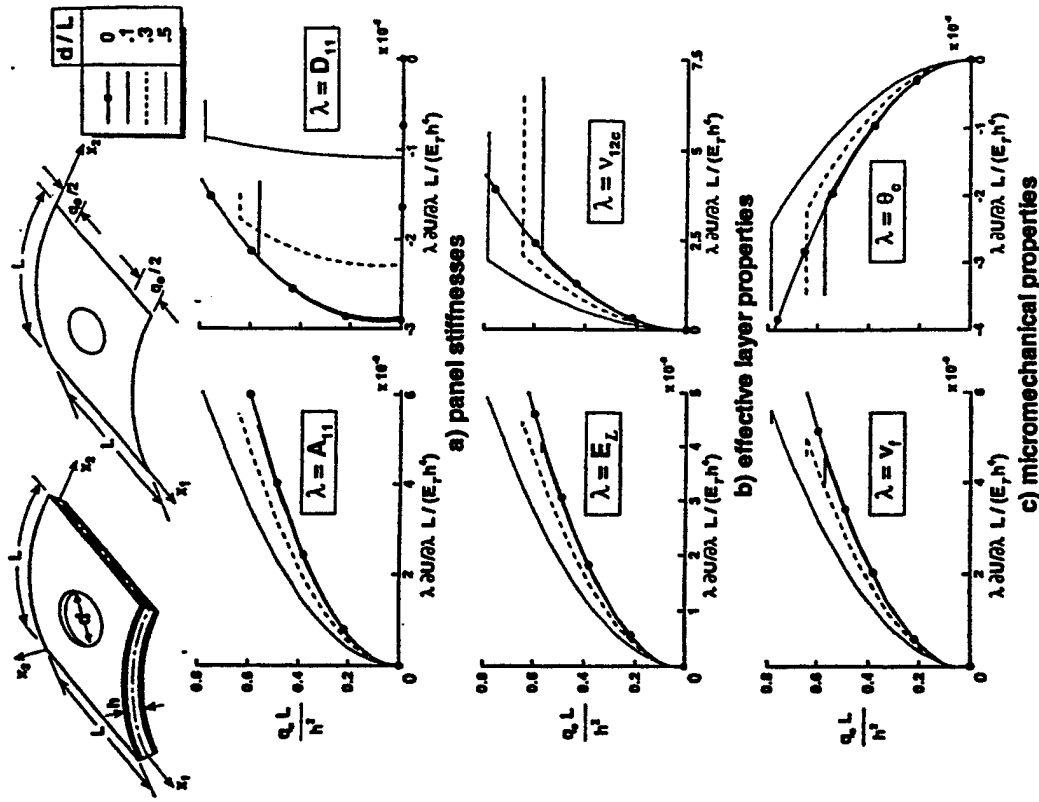


Figure 7. Effect of loading and hole diameter on the normalized sensitivity coefficients of the total strain energy U with respect to panel stiffness, effective layer properties, and micromechanical properties. Cylindrical sandwich panels, with honeycomb core and composite eight-layer face sheets, subjected to combined pressure loading, edge shortening and temperature gradient through-the-thickness.

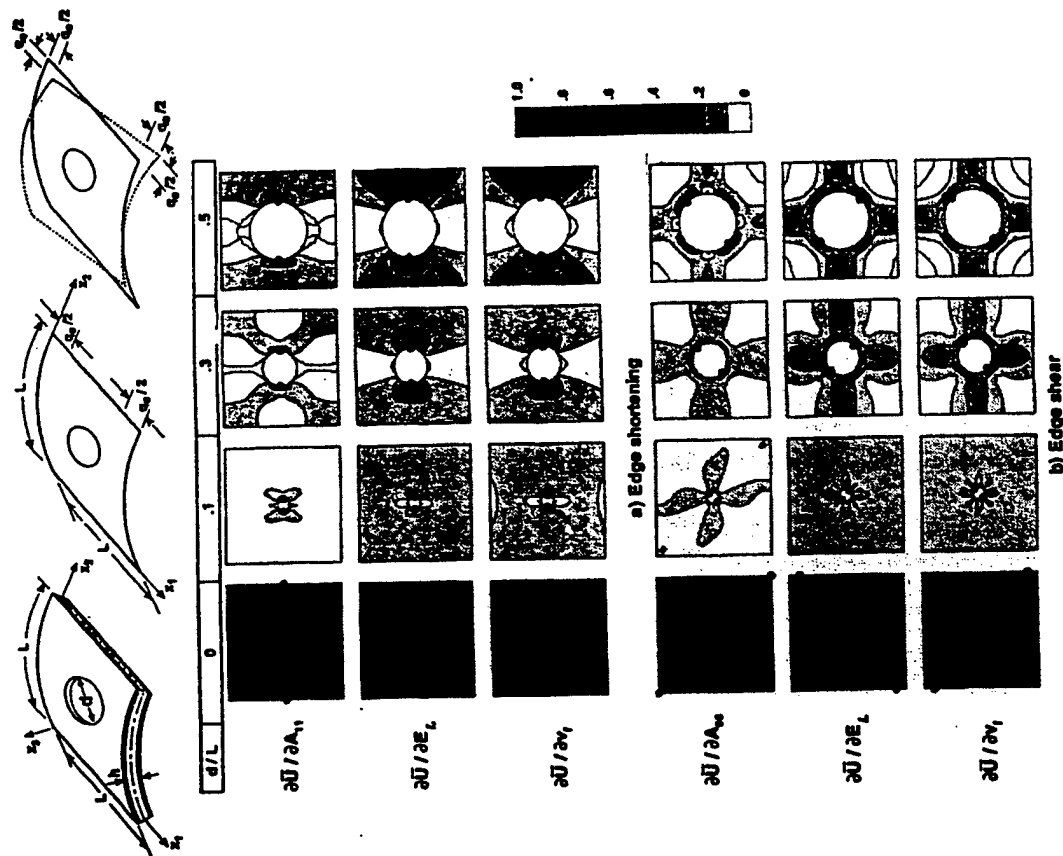


Figure 9. Normalized contour plots depicting the effect of loading on the largest sensitivity coefficients of the total strain energy density U . Cylindrical sandwich panels, with honeycomb core and composite eight-layer face sheets, subjected to combined pressure loading, prescribed edge displacement and temperature gradient through-the-thickness. Location of maximum values identified by a small solid circle. The contour plot of each sensitivity coefficient is divided by the maximum absolute value of that sensitivity coefficient.

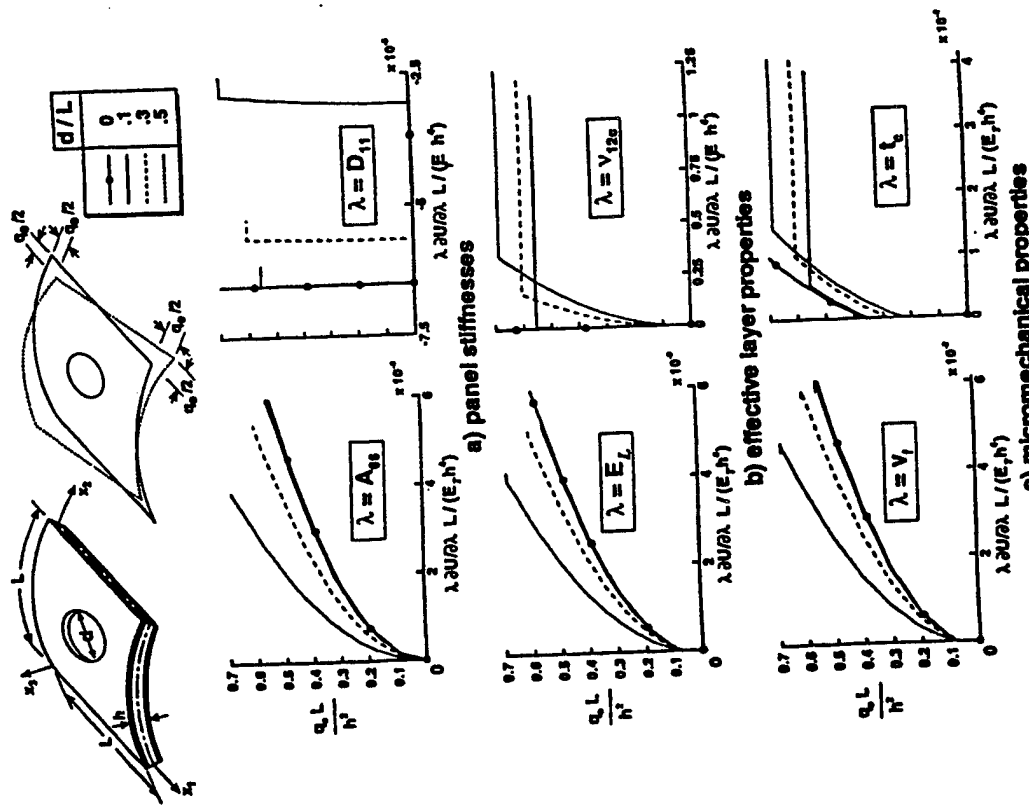


Figure 8. Effect of loading and hole diameter on the normalized sensitivity coefficients of the total strain energy U with respect to panel stiffnesses, effective layer properties and micromechanical properties. Cylindrical sandwich panels, with honeycomb core and composite eight-layer face sheets, subjected to combined pressure loading, edge shear and temperature gradient through-the-thickness.

creases, e.g., $d/L \geq 0.3$, the reductions become more pronounced (see Figure 4). On the other hand, the maximum surface principal strain ϵ_{max} and the maximum total strain energy density \bar{U} increase significantly if a small cutout is present. Sharp gradients of both ϵ_{max} and \bar{U} occur in the vicinity of the cutout. As d/L increases, both the maximum values and the gradients of ϵ_{max} and \bar{U} decrease. However, the accurate determination of ϵ_{max} and \bar{U} in the vicinity of the cutout requires more sophisticated models than the first-order shear deformation model used herein. Accurate transverse stresses and/or strains at the interfaces between the face sheets and core can be obtained by using a predictor-corrector iterative process to improve the accuracy of the response quantities generated by the first-order shear deformation model (see Reference [8]). The accurate prediction of the stresses and deformations in the core requires the use of detailed finite element models for the honeycomb core. For the case of edge shortening, the maximum value of the transverse shear strain energy per unit volume \bar{U}_{sh} at the location of maximum \bar{U}_{sh} decreases with the increase in d/L . The decrease is more pronounced for $d/L \geq 0.3$. An opposite situation occurs for the case of edge shear (see Figure 6).

Sensitivity Studies

Plots of the edge displacement q_e versus the sensitivity coefficients of the total strain energy U with respect to panel parameters, effective layer, and micromechanical parameters are shown in Figures 7 and 8 for panels with $d/L = 0, 0.1, 0.3$ and 0.5. Normalized contour plots for the maximum sensitivity coefficients of the total strain energy density \bar{U} with respect to each of the three sets of parameters are shown in Figure 9 for the panels with and without cutouts. The sensitivity studies can be summarized as follows:

- For a given value of the edge displacement q_e , the sensitivity coefficients of the total strain energy U decrease with the increase in d/L . The decrease becomes more pronounced for $d/L \geq 0.3$.
- Because of the relationship between the edge displacement q_e and the total edge force \bar{N} , for a given \bar{N} , the sensitivity coefficients of U increase with the increase in d/L .
- The distribution of the sensitivity coefficients of the total strain energy density \bar{U} for panels with no cutout is nearly uniform. The presence of a small cutout results in sharp gradients and nonuniform distribution of the sensitivity coefficients in the vicinity of the cutout. The maximum value of the strain energy density \bar{U} in the vicinity of the cutout is very sensitive to variations in the panel, effective layer and micromechanical parameters. An accurate evaluation of \bar{U} in the immediate vicinity of the cutout requires accurate determination of these param-

ters, as well as the use of three-dimensional continuum or detailed models for the face sheet layers and the honeycomb core.

- The temperature gradient has a much more pronounced effect on the sensitivity coefficients of U with respect to the effective and actual core parameters than on the face sheet parameters.

CONCLUDING REMARKS

A study is made of the nonlinear response of curved sandwich panels with composite face sheets subjected to a temperature gradient through the thickness combined with mechanical loadings. The panels are composed of perfectly bonded layers (face sheet layers and core), and the core is replaced by an equivalent homogeneous anisotropic layer. The analysis is based on a first-order shear-deformation Sanders-Budiansky type theory with the effects of large displacements, moderate rotations, average transverse shear deformation through the thickness, and laminated anisotropic material behavior included. A linear, Duhamel-Neumann type constitutive model is used and the material properties are assumed to be independent of temperature. The panels are discretized by using two-field mixed finite element models, with the fundamental unknowns consisting of the nodal displacements and stress resultant parameters. The stress resultants are allowed to be discontinuous at interelement boundaries.

Both the nonlinear response of the panel as well as the hierarchical sensitivity coefficients are generated. The hierarchical sensitivity coefficients measure the sensitivity of the different response quantities to variations in three sets of interrelated parameters; namely, panel stiffnesses, effective properties of the face sheet layers and the core, and micromechanical parameters of the face sheet layers and the core. An efficient multiple-parameter reduction method is used for generating the nonlinear response and evaluating the sensitivity coefficients.

The computational procedure for evaluating the hierarchical sensitivity coefficients consists of evaluating the sensitivity coefficients with respect to each of the panel stiffnesses, and then generating the sensitivity coefficients with respect to the effective layer and micromechanical parameters as linear combinations of the sensitivity coefficients with respect to the panel parameters. Hierarchical sensitivity coefficients can be used to assess the effects of variations in the panel, face sheet layers, core and micromechanical parameters on the nonlinear response. They can also help relate structural design and material development.

Numerical studies are presented which show the effects of variations in the loading and the hole diameter on the nonlinear response and the sensitivity coefficients of cylindrical sandwich panels with eight-layer quasi-isotropic face sheets and titanium honeycomb core with hexagonal cells. The loading on the panels con-

sisted of a sequence of mechanical and thermal loadings: uniform pressure loading, monotonically increasing edge displacement, and then a temperature gradient through-the-thickness. Two types of edge displacements were considered; namely, edge shortening and edge shear. In both cases, the stacking sequence of the face sheet layers did not have a noticeable effect on either the nonlinear response or the sensitivity coefficients, and the edge displacement had the most pronounced effect on the global response. The models used in the numerical studies are adequate for calculating the global response characteristics, such as the total strain energy U . However, the accurate determination of local response characteristics in the vicinity of the cutout requires the use of three-dimensional continuum or detailed models for the face sheets and core.

ACKNOWLEDGMENTS

This work was partially supported by NASA Grant No. NAG-1-1162 and AFOSR Grant No. F49620-96-1-0462. The numerical studies were performed on the CRAY C-90 computer at NASA Ames Research Center. The authors acknowledge the assistance of Thea Ganoos of the University of Virginia in preparing the final manuscript and improving the figures.

REFERENCES

1. Aboudi, J., 1991, *Mechanics of Composite Materials: A Unified Micromechanical Approach*, Elsevier, Amsterdam.
2. Bert, C. W., 1995, "Shear Deformation and Sandwich Configuration," *Buckling and Postbuckling of Composite Plates*, Turvey, G. J. and Marshall, I. H., eds., Chapman and Hall, London, pp. 157-189.
3. Burton, W. S. and Noor, A. K., 1997, "Assessment of Continuum Models for Sandwich Panel Honeycomb Cores," *Computer Methods in Applied Mechanics and Engineering*, Vol. 145, pp. 341-360.
4. Gibson, L. J. and Ashby, M. F., 1988, *Cellular Solids, Structures and Properties*, Pergamon Press, Oxford.
5. Hoff, N. J., 1986, *Monocoque, Sandwich, and Composite Aerospace Structures*, Technomic Publishing Co., Inc., Lancaster, PA.
6. Noor, A. K., 1994, *Buckling and Postbuckling of Composite Structures*, ASME International Mechanical Symposium on Buckling and Postbuckling of Composite Structures, ASME International Mechanical Engineering Congress and Exposition, Chicago, IL, Nov. 6-11, 1994, AD Vol. 41/PVP Vol. 293.
7. Noor, A. K. and Anderson, C. M., 1982, "Mixed Models and Reduced/Selective Integration Displacement Models for Nonlinear Shell Analysis," *International Journal for Numerical Methods in Engineering*, Vol. 18, pp. 1429-1454.
8. Noor, A. K., Burton, W. S. and Bert, C., 1996, "Computational Models for Sandwich Panels and Shells," *Applied Mechanics Reviews*, Vol. 49, No. 3, pp. 155-199.
9. Noor, A. K. and Peters, J. M., 1983a, "Multiple-Parameter Reduced Basis Technique for Bifurcation and Postbuckling Analyses of Composite Plates," *International Journal for Numerical Methods in Engineering*, Vol. 19, pp. 1783-1803.

10. Noor, A. K. and Peters, J. M., 1983b, "Recent Advances in Reduction Methods for Instability Analysis of Structures," *Computers and Structures*, Vol. 16, Nos. 1-4, pp. 67-80.
11. Noor, A. K. and Peters, J. M., 1992, "Reduced Basis Technique for Calculating Sensitivity Coefficients of Nonlinear Structural Response," *AIAA Journal*, Vol. 30, No. 7, pp. 1840-1847.
12. Noor, A. K., Starnes, Jr., J. H. and Peters, J. M., 1997, "Analysis of Curved Sandwich Panels Subjected to Combined Temperature Gradient and Mechanical Loads," *Proceedings, AIAA/ASME/ASCE/AHS 38th Structures, Structural Dynamics and Materials Conference*, April 7-10, 1997, Kissimmee, FL, Part 4, pp. 2446-2470.
13. Turvey, G. J. and Marshall, I. H. (eds.), 1995, *Buckling and Postbuckling of Composite Plates*, Chapman and Hall, London.
14. Zenkert, D., 1995, *An Introduction to Sandwich Construction*, Chameleon Press, London.

ANALYSIS OF COMPOSITE PANELS SUBJECTED TO THERMO-MECHANICAL LOADS

By Ahmed K. Noor¹ and Jeanne M. Peters²

ABSTRACT: The results of a detailed study of the effect of cutout on the nonlinear response of curved unstiffened panels are presented. The panels are subjected to combined temperature gradient through-the-thickness combined with pressure loading and edge shortening or edge shear. The analysis is based on a first-order, shear-deformation, Sanders-Budiansky-type shell theory with the effects of large displacements, moderate rotations, transverse shear deformation, and laminated anisotropic material behavior included. A mixed formulation is used with the fundamental unknowns consisting of the generalized displacements and the stress resultants of the panel. The nonlinear displacements, strain energy, principal strains, transverse shear stresses, transverse shear strain energy density, and their hierarchical sensitivity coefficients are evaluated. The hierarchical sensitivity coefficients measure the sensitivity of the nonlinear response to variations in the panel parameters, as well as in the material properties of the individual layers. Numerical results are presented for cylindrical panels and show the effects of variations in the loading and the size of the cutout on the global and local response quantities as well as their sensitivity to changes in the various panel, layer, and micromechanical parameters.

INTRODUCTION

In recent years, considerable work has been devoted to the study of nonlinear and postbuckling responses of laminated composite plates and shells subjected to combined mechanical and thermal loads. Attempts have been made to identify the differences between the isothermal and thermal responses. Reviews of recent contributions are contained in two survey papers (Noor and Burton 1992; Noor and Peters 1994) and two monographs (Noor 1994; Turvey and Marshall 1995). Only a few of the reported studies considered the nonlinear response of curved panels subjected to temperature gradient through-the-thickness (i.e., Librescu et al. 1995; Librescu and Souza 1993), and to the authors' knowledge, none considered boundary conditions other than simple supports. Since curved panels have many applications in aircraft structures, including fuselage, wing, and empennage components of high-speed aircraft, an understanding of their nonlinear and postbuckling responses when subjected to combined temperature gradient through-the-thickness and mechanical loading is desirable. Moreover, a study of the sensitivity of the nonlinear and postbuckling responses to variations in the material, lamination, and geometric parameters of these panels is needed to provide an indication of the effects of changes in these parameters on the structural response.

The present study focuses on understanding the detailed nonlinear response characteristics of cylindrical multilayered composite panels subjected to combined temperature gradient through-the-thickness and mechanical loading. Sensitivity coefficients are evaluated which measure the sensitivity of the various response quantities to variations in the panel stiffnesses, the effective layer properties, and the micromechanical parameters of the individual layers.

The unstiffened panels considered in the study consist of a number of perfectly bonded layers and are symmetrically laminated with respect to the middle surface. The individual layers are assumed to be homogeneous and anisotropic. A

plane of thermoelastic symmetry exists at each point of the panel, parallel to the middle surface. The loading is selected to simulate that of a typical fuselage panel of a high-speed aircraft.

MATHEMATICAL FORMULATION

The analytical formulation is based on a first-order, shear-deformation, Sanders-Budiansky-type shell theory with the effects of large displacements, moderate rotations, average transverse shear deformation through-the-thickness, and laminated anisotropic material behavior included. For simplicity, a linear Duhamel-Neumann-type constitutive model is used and the material properties are assumed to be independent of temperature. The constitutive relations for the panel are given in Noor and Peters (1983). A total Lagrangian formulation is used and the panel deformations, at different values of the applied load-

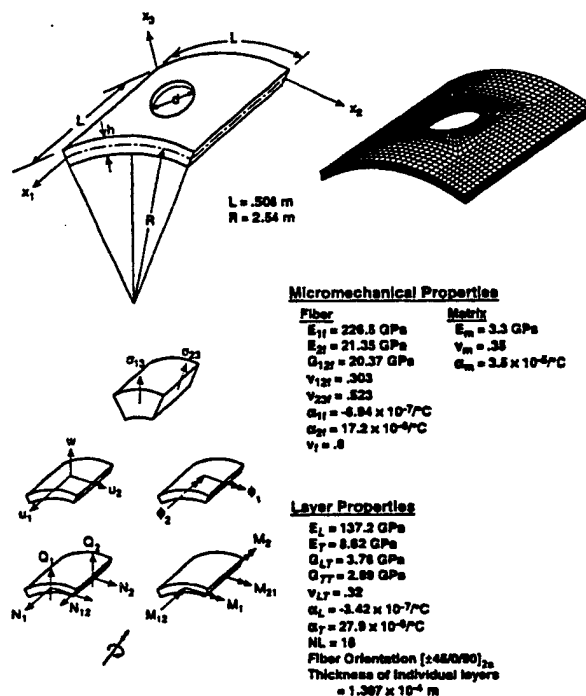


FIG. 1. Composite Panels Considered in Present Study and Sign Convention for Generalized Displacements and Stress Resultants

¹Prof., Ctr. for Advanced Computational Technol., Univ. of Virginia, NASA Langley Research Center, Hampton, VA 23681.

²Sr. Programming Analyst, Ctr. for Advanced Computational Technol., Univ. of Virginia, NASA Langley Research Center, Hampton, VA.

Note. Discussion open until June 1, 1999. To extend the closing date one month, a written request must be filed with the ASCE Manager of Journals. The manuscript for this paper was submitted for review and possible publication on April 13, 1998. This paper is part of the *Journal of Aerospace Engineering*, Vol. 12, No. 1, January, 1999. ©ASCE, ISSN 0893-1321/99/0001-0001-0007/\$8.00 + \$.50 per page. Paper No. 18218.

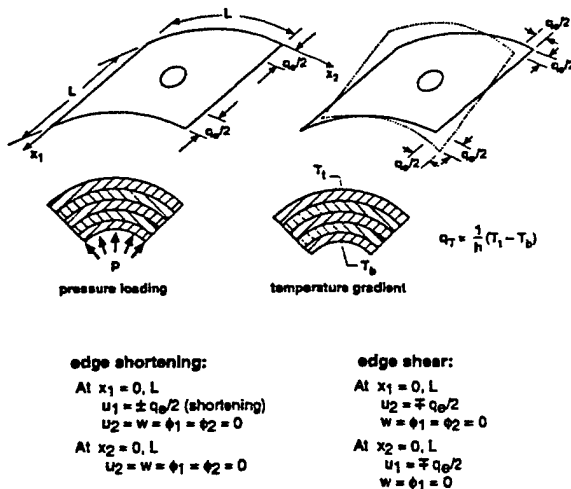


FIG. 2. Loadings and Boundary Conditions Considered in Numerical Studies

ing, are referred to the original undeformed configuration. The panel is discretized by using two-field mixed finite-element models. The fundamental unknowns consist of the nodal displacements and the stress-resultant parameters. The stress resultants are allowed to be discontinuous at interelement boundaries in the model. The sign convention for the generalized displacements and the stress resultants for the model are shown in Fig. 1. The external loading consists of a uniform pressure loading p ; monotonically increasing edge displacement q_e (either normal or tangential to the edge); and a temperature gradient through-the-thickness q_T [linear through-the-thickness temperature variation, $q_T = (T_t - T_b)/h$, where T_t and T_b are the changes in the top and bottom surface temperatures (see Fig. 2)].

Governing Finite-Element Equations

The governing equations for the response vector and its first-order sensitivity coefficients can be written in the following compact form:

$$\{f(Z)\} = [K]\{Z\} + \{G(Z)\} - p\{Q^{(1)}\} - q_e\{Q^{(2)}\} - q_T\{Q^{(3)}\} = 0 \quad (1)$$

$$\left[[K] + \left[\frac{\partial G_j}{\partial Z_j} \right] \right] \left\{ \frac{\partial Z}{\partial \lambda} \right\} = - \left[\frac{\partial K}{\partial \lambda} \right] \{Z\} + q_T \left\{ \frac{\partial Q^{(3)}}{\partial \lambda} \right\} \quad (2)$$

where $[K]$ = global linear structural matrix including the flexibility and the linear strain-displacement matrices; $\{Z\}$ = response vector including both unknown (free) nodal displacements and stress-resultant parameters; $\{G(Z)\}$ = vector of nonlinear terms; p , q_e , and q_T are the magnitudes of the internal pressure, applied edge displacement, and temperature gradient through-the-thickness; $\{Q^{(1)}\}$, $\{Q^{(2)}\}$, $\{Q^{(3)}\}$ are normalized vectors corresponding to unit values of p , q_e , and q_T , and λ = typical parameter of the sandwich panel. The range of the indices I and J is 1 to the total number of degrees of freedom in the model; and $\{Q^{(1)}\}$ and $\{Q^{(2)}\}$ are assumed to be independent of q_T . The form of the arrays $[K]$, $\{G(Z)\}$, $\{Q^{(1)}\}$, and $\{Q^{(2)}\}$ are given in Noor et al. (1997).

Eq. (1) is nonlinear in $\{Z\}$, but (2) is linear in $\{\partial Z/\partial \lambda\}$. Note that the matrix on the left-hand side of (2) is identical to that used in the Newton-Raphson iterative process. Therefore, if the Newton-Raphson technique is used in generating the nonlinear response, the evaluation of the sensitivity coefficients requires the generation of the right-hand side of

(2), and a forward-reduction/back-substitution operation only (no decomposition of the left-hand side matrix is required).

Evaluation of Transverse Shear Stresses

The transverse shear stresses are evaluated by using piecewise integration, in the thickness direction, of the three-dimensional equilibrium equations. For optimum accuracy, the transverse shear stresses are computed at the numerical quadrature points and then interpolated to the center of the element. The same procedure is used for evaluating the thickness distributions of the sensitivity coefficients of the transverse shear stresses.

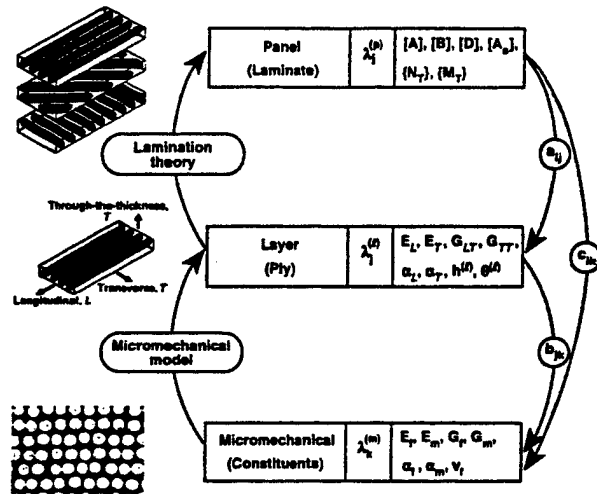


FIG. 3. Hierarchical Sensitivity Coefficients for Composite Panels

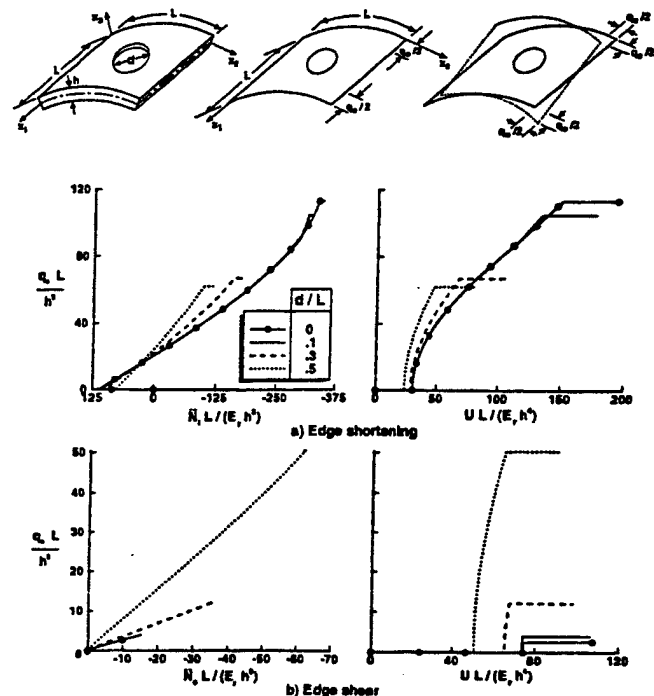


FIG. 4. Effect of Loading, Hole Diameter on Nonlinear Response of Composite Cylindrical Panels Subjected to Combined Pressure Loading, Prescribed Edge Displacement, and Temperature Gradient Through-the-Thickness

Hierarchical Sensitivity Coefficients

The nonlinear and postbuckling response characteristics of sandwich panels are dependent on a hierarchy of interrelated parameters, the kinds including panel, effective layer, and micromechanical. A study of the sensitivity of the response to variations in each of these parameters provides insight into the importance of the parameters and helps in the development of materials to meet certain performance requirements.

Three sets of sandwich parameters are considered herein—panel, effective layer, and micromechanical parameters. The panel parameters include the extensional; bending-extensional; bending and transverse shear stiffnesses (components of the matrices $[A]$, $[B]$, $[D]$, and $[A_e]$ —see Fig. 3); and the vectors of thermal effects $\{N_T\}$ and $\{M_T\}$ (see Noor et al. 1997). The effective layer parameters include the individual layer properties: elastic moduli E_L , E_T ; shear moduli G_{LT} , G_{TT} ; major Poisson's ratio ν_{LT} ; coefficients of thermal expansion α_L , α_T ; fiber-orientation angle $\theta^{(n)}$; layer thickness $h^{(n)}$, where subscripts L and T refer to the longitudinal (fiber) and transverse directions, respectively. The micromechanical parameters refer to the fiber and matrix material moduli E_{1f} , E_{2f} , E_m , G_{12f} , G_m ; Poisson's ratios ν_{12f} , ν_{23f} , ν_m ; coefficients of thermal expansion

α_{1f} , α_{2f} , α_m ; and the fiber volume fraction ν_f . The subscripts f and m denote the fiber and matrix property, respectively. The three sets of parameters will henceforth be referred to as $\lambda_i^{(p)}$, $\lambda_j^{(l)}$, $\lambda_k^{(m)}$ where superscripts p , l , and m refer to the panel, effective layer, and micromechanical parameters, respectively; and the indices i , j , and k range from 1 to the number of parameters in each category. In the present study, the Aboudi (1991) cell method is used to evaluate the effective properties of the layers.

The computational procedure consists of evaluating the sensitivity coefficients with respect to each of the panel parameters $\{\partial Z / \partial \lambda_i^{(p)}\}$ using (2). The sensitivity coefficients with respect to the effective layer parameters $\{\partial Z / \partial \lambda_j^{(l)}\}$ and micromechanical parameters $\{\partial Z / \partial \lambda_k^{(m)}\}$ are then obtained by forming linear combinations of them (see Noor et al. 1997).

NUMERICAL STUDIES

Numerical studies were performed to determine the effects of variations in the loading and the diameter of the cutout on both the response and the sensitivity coefficients of composite

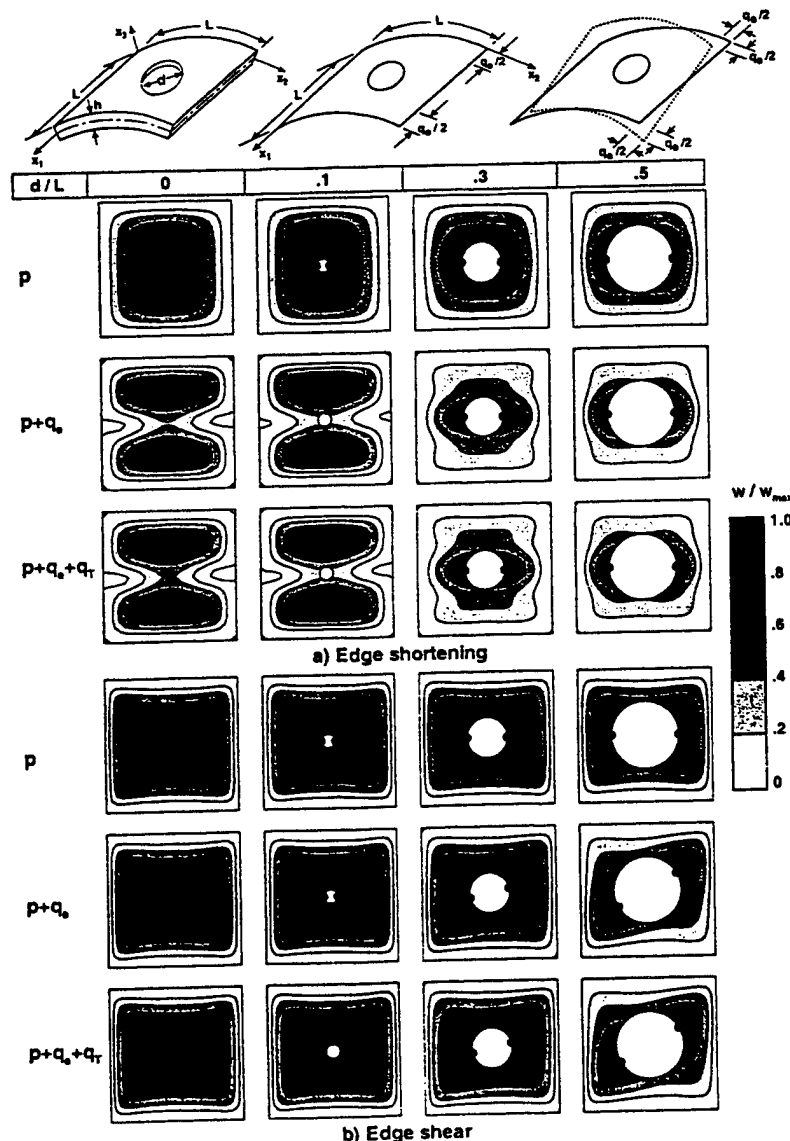


FIG. 5. Normalized Contour Plots Depicting Effects of Loading, Hole Diameter on Transverse Displacement w for Sixteen-Layer Composite Cylindrical Panels Subjected to Combined Pressure Loading, Prescribed Edge Displacement, Temperature Gradient Through-the-Thickness (Location of Maximum Values Identified by Small Solid Circle)

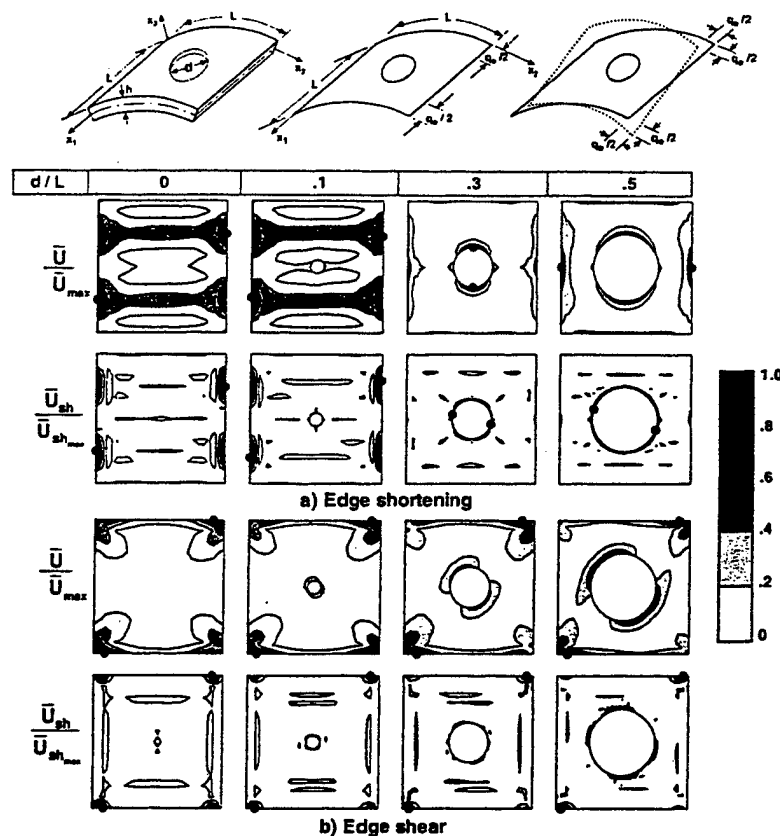


FIG. 6. Normalized Contour Plots Depicting Effect of Loading and Hole Diameter on Total Strain Energy Density \bar{U} and Transverse Shear Strain Energy Density \bar{U}_{sh} for Sixteen-Layer Composite Cylindrical Panels Subjected to Combined Pressure Loading, Prescribed Edge Displacement, Temperature Gradient Through-the-Thickness $p + q_n + q_T$ (Location of Maximum Values Identified by Small Solid Circle)

cylindrical panels with circular cutouts. The panels considered have sixteen layers and quasi-isotropic lamination. The material properties and geometric characteristics for the panels considered in the present study are given in Fig. 1. The material properties, the fiber orientation, and the stacking sequences selected are those typical of composite panels considered for high-speed aircraft applications. The loading on the panels consisted of a sequence of mechanical and thermal loadings: uniform pressure loading $p = 6.894 \times 10^6 \text{ Pa}$, followed by monotonically increasing edge displacement q_n , and then a temperature gradient through-the-thickness q_T (linear through-the-thickness temperature variation, $q_T = (T_t - T_b)/h$, where T_t and T_b are the changes in the top and bottom surface temperatures). The value of T_b was zero and T_t was increased to 137.8°C . Two different types of edge displacements were applied, namely, edge shortening and edge shear. The boundary conditions selected for the cases of edge shortening and edge shear are shown in Fig. 2. In each loading case, the maximum value of q_n was selected in such a way that the maximum principal strains on the surfaces do not exceed 0.005. Four different values of the cutout diameter are considered, namely, $d/L = 0, 0.1, 0.3$, and 0.5 . For each problem, hierarchical sensitivity coefficients are evaluated (see Fig. 3). The hierarchical sensitivity coefficients are the derivatives of the different response quantities with respect to panel stiffnesses, effective material parameters, and fiber angles of the individual layers—and micromechanical parameters of the layers.

Mixed finite-element models were used for the discretization of each panel. Biquadratic shape functions were used for approximating each of the generalized displacements, and bilinear shape functions were used for approximating each of the stress resultants. The characteristics of the finite-element model are given in Noor and Anderson (1982). For each panel,

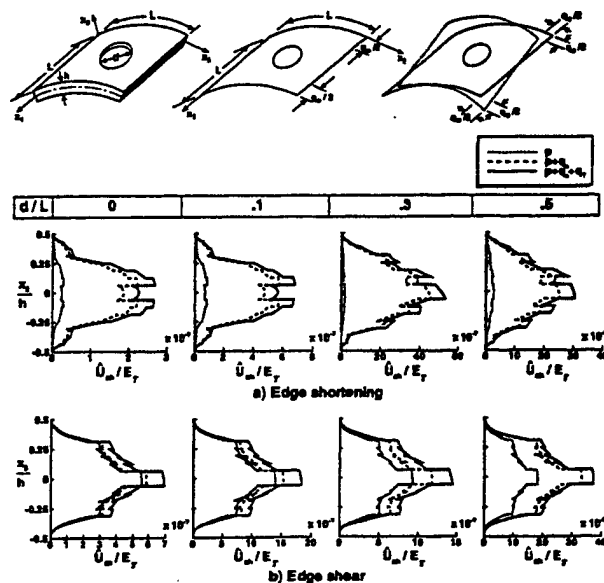


FIG. 7. Effect of Loading and Hole Diameter on Distribution of Transverse Shear Strain Energy Density Through-the-Thickness, at Point of Maximum Transverse Shear Strain Energy Density \bar{U}_{sh} (See Fig. 6); Cylindrical Panels Subjected to Combined Pressure Loading, Prescribed Edge Displacement, Temperature Gradient Through-the-Thickness

the multiple-parameter reduction methods described in Noor and Peters (1983a, b; 1992) were used in generating the nonlinear response and in evaluating the sensitivity coefficients. Results with an increasing number of elements were obtained to insure convergence of the solutions presented. Typical re-

sults are presented in Figs. 4–7 for the response studies and in Figs. 8–10 for the sensitivity coefficients. The numerical results presented show a complex interplay between the panel stiffnesses, effective layer and micromechanical parameters, and the loading. The effect of each of the individual parameters on the response cannot be easily delineated. However, some observations about the response and sensitivity studies presented in Figs. 4–7 and 8–10 are described subsequently.

Response Studies

Plots of the edge displacement q_e versus the total edge force \bar{N} , and the total strain energy U , are shown in Fig. 4 for the four panels with $d/L = 0, 0.1, 0.3$, and 0.5 . Normalized contour plots for the transverse displacement w at the end of each of the three loading stages— p , $p + q_e$, $p + q_e + q_T$, for panels with and without cutouts—are shown in Fig. 5. Normalized contour plots for the total strain energy density \bar{U} , and the transverse shear strain energy density \bar{U}_{sh} for panels with and without cutouts after the application of the total load $p + q_e + q_T$, are shown in Fig. 6. The thickness distributions of the transverse shear strain energy density per unit volume \bar{U}_{sh} , at the location of maximum \bar{U}_{sh} , for the panels with and without cutouts, are shown in Fig. 7. In Figs. 4–7 the two cases of edge shortening and edge shear are shown. The response studies can be summarized as follows:

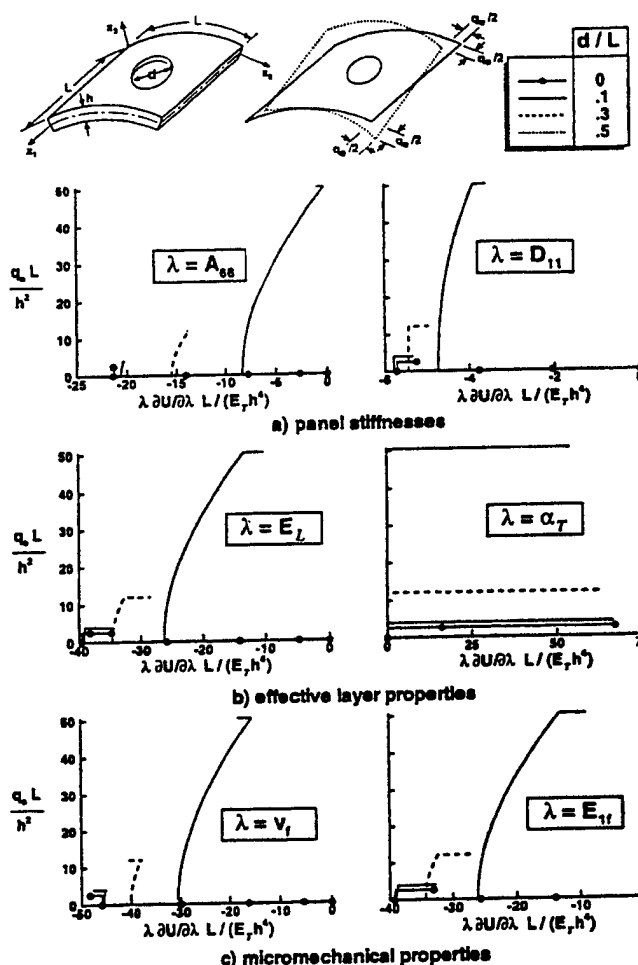


FIG. 9. Effect of Loading and Hole Diameter on Normalized Sensitivity Coefficients of Total Strain Energy U with Respect to Panel Stiffnesses, Effective Layer Properties, Micromechanical Properties; Cylindrical Panels Subjected to Combined Pressure Loading, Edge Shear, Temperature Gradient Through-the-Thickness

- For panels with small or no cutout, $d/L \leq 0.1$, the deformation pattern changes significantly after the application of $p + q_e$ (end shortening case) from that generated by p . As d/L increases, the change becomes less pronounced (see Fig. 5).
- The effects of the cutout on the global and local response characteristics of the panel are very different. The presence of a small cutout, $d/L \leq 0.1$, reduces slightly the total edge force \bar{N} and total strain energy U , and increases the strain energy density per unit volume \bar{U}_{sh} (see Fig. 7). As d/L increases, e.g., $d/L \geq 0.3$, the reductions in \bar{N} and U become more pronounced (see Fig. 4).
- The size of the cutout has a strong influence on the value of q_e , at which a maximum strain ϵ_{max} of 0.005 is reached. That value of q_e decreases rapidly as d/L increases from 0.1 to 0.3, and then decreases slowly as d/L becomes larger than 0.3.
- For the case of edge shear displacement, the maximum values of \bar{U} and \bar{U}_{sh} occur at the edges of the panel, irrespective of the value of d/L . By contrast, for the case of edge shortening, the locations of the maximum values of \bar{U} and \bar{U}_{sh} shift to the cutout for panels with $d/L = 0.3$. For panels with $d/L = 0.5$, the maximum values of \bar{U} shift back to the edges (see Fig. 6).
- The maximum transverse shear strain energy density per volume \bar{U}_{sh} is dominated by the contributions of q_e .

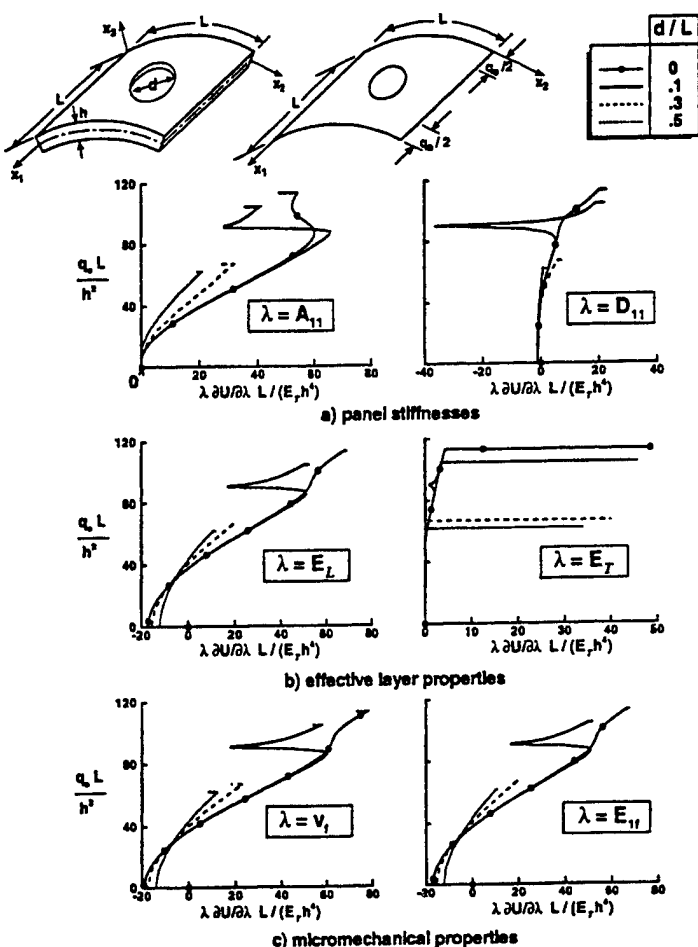


FIG. 8. Effect of Loading and Hole Diameter on Normalized Sensitivity Coefficients of Total Strain Energy U with Respect to Panel Stiffnesses, Effective Layer Properties, Micromechanical Properties; Cylindrical Panels Subjected to Combined Pressure Loading, Edge Shortening, Temperature Gradient Through-the-Thickness

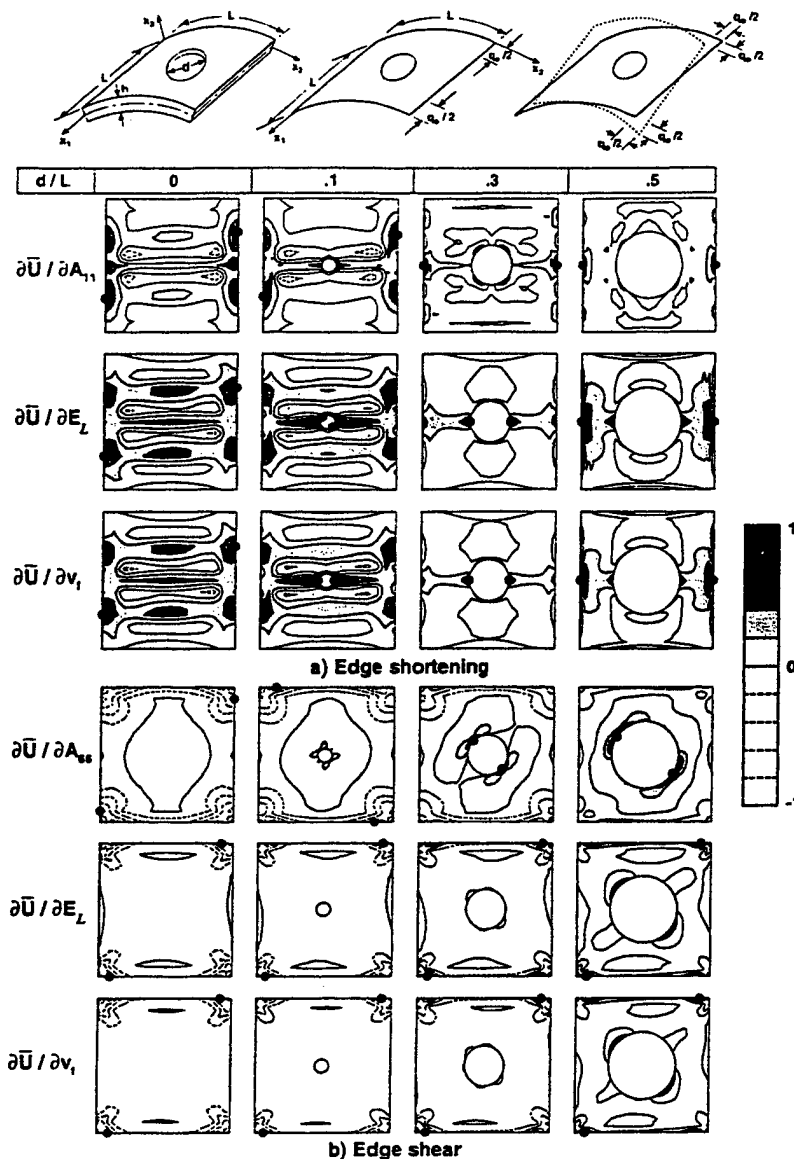


FIG. 10. Normalized Contour Plots Depicting Effect of Loading on Largest Sensitivity Coefficients of Strain Energy Density \bar{U} ; Cylindrical Panels Subjected to Combined Pressure Loading, Prescribed Edge Displacement, Temperature Gradient Through-the-Thickness (Location of Maximum Values Identified by Small Solid Circle; Contour Plot of Each Sensitivity Coefficient Divided by Maximum Absolute Value of that Sensitivity Coefficient)

for the edge shortening case, and by the contribution of p for the edge shear case. In the latter case, the contribution of q_r to \bar{U}_m increases with the increase in d/L (see Fig. 7).

Sensitivity Studies

Plots of the edge displacement q_r versus the sensitivity coefficients of the total strain energy \bar{U} with respect to panel stiffnesses, effective layer, and micromechanical parameters are shown in Figs. 8 and 9 for panels with $d/L = 0, 0.1, 0.3$, and 0.5 . Normalized contour plots for the maximum sensitivity coefficients of the total strain energy \bar{U} with respect to each of the three sets of parameters for panels with and without cutouts, after the application of the total load $p + q_r + q_T$, are shown in Fig. 10. The sensitivity studies can be summarized as follows:

- For a given value of the edge displacement q_r , the sensitivity coefficients of the total strain energy \bar{U} decrease with the increase in d/L . The decrease becomes more pronounced for $d/L \geq 0.3$.

- In the third loading phase, temperature gradient through-the-thickness, the total strain energy becomes very sensitive to variations in some of the parameters, such as the effective transverse layer properties E_T , α_T , and the matrix micromechanical parameters E_m , ν_m , α_m .
- The location of the maximum values of the sensitivity coefficients of the total strain energy depends on both the loading and boundary conditions, as well as on the size of the cutout. For the edge shortening case, the location of the maximum values of $\partial\bar{U}/\partial E_L$ and $\partial\bar{U}/\partial v_1$ shift from the edges to the cutout for panels with $0 < d/L \leq 0.3$ (see Fig. 10). The maximum values shift back to the edges for panels with $d/L = 0.5$. By contrast, for the edge shear case, the maximum values of $\partial\bar{U}/\partial E_L$ and $\partial\bar{U}/\partial v_1$ occur at the edges, regardless of the value of d/L .

ACKNOWLEDGMENTS

This work was partially supported by NASA Grant No. NAG-1-2016 and AFOSR Grant No. F49620-96-1-0462. The numerical studies were performed on the CRAY C-90 computer at NASA Ames Research Center.

The authors acknowledge the assistance of Thea Gano of the University of Virginia in preparing the final manuscript and improving the figures.

APPENDIX. REFERENCES

- Aboudi, J. (1991). *Mechanics of composite materials: A unified micro-mechanical approach*. Elsevier, Amsterdam.
- Librescu, L., Lin, W., Nemeth, M. P., and Starnes, J. H. Jr. (1995). "Thermomechanical postbuckling of geometrically imperfect flat and curved panels taking into account tangential edge constraints." *J. Thermal Stresses*, Vol. 18, 465-482.
- Librescu, L., and Souza, M. A. (1993). "Postbuckling of geometrically imperfect shear-deformable flat panels under combined thermal and compressive edge loadings." *J. Appl. Mech.*, Vol. 60, 526-533.
- Noor, A. K. (1994). "Buckling and Postbuckling of Composite Structures." *Proc., Symp. on Buckling and Postbuckling of Compos. Struct.*, ASME Int. Mech. Engrg. Congr. and Exposition, Chicago, Ill., AD Vol. 41/PVP Vol. 293.
- Noor, A. K., and Andersen, C. M. (1982). "Mixed models and reduced/selective integration displacement models for nonlinear shell analysis." *Int. J. for Numer. Methods in Engrg.*, Vol. 18, 1429-1454.
- Noor, A. K., and Burton, W. S. (1992). "Computational models for high-temperature multilayered composite plates and shells." *Appl. Mech. Rev.*, Vol. 45, No. 10, 419-446.
- Noor, A. K., and Peters, J. M. (1983). "Multiple-parameter reduced basis technique for bifurcation and postbuckling analyses of composite plates." *Int. J. Numer. Methods in Engrg.*, Vol. 19, 1783-1803.
- Noor, A. K., and Peters, J. M. (1983). "Recent advances in reduction methods for instability analysis of structures." *Comp. and Struct.*, Vol. 16(1-4), 67-80.
- Noor, A. K., and Peters, J. M. (1992). "Reduced basis technique for calculating sensitivity coefficients of nonlinear structural response." *AIAA Journal*, Vol. 30(7), 1840-1847.
- Noor, A. K., and Peters, J. M. (1994). "Finite element buckling and postbuckling solutions for multilayered composite panels." *Finite Elements in Anal. and Des.*, Vol. 15, 343-367.
- Noor, A. K., Starnes, J. H. Jr., and Peters, J. M. (1997). "Analysis of curved sandwich panels subjected to combined temperature gradient and mechanical loads." *Proc., AIAA/ASME/ASCE/AHS 38th Struct., Struct. Dyn. and Mat. Conf.*, April 7-10, 1997, Kissimmee, FL, Part 4, 2446-2470.
- Turvey, G. J., and Marshall, I. H. (eds.) (1995). *Buckling and postbuckling of composite plates*. Chapman and Hall, London.

JOURNAL OF AEROSPACE ENGINEERING

Volume 12

Number 1

January 1999

TECHNICAL PAPERS

Analysis of Composite Panels Subjected to Thermo-Mechanical Loads Ahmed K. Noor and Jeanne M. Peters	1
Imperfection Sensitivity of Moderately Thick Laminated Cylindrical Shells G. J. Simitses and S. S. Hsiung	8
Second-Order Sensitivity of Smart Structures Xiaojian Liu and David William Begg	15
PVDF Film Sensor and Its Applications in Damage Detection H. Luo and S. Hanagud	23
REVIEWERS OF THE <i>Journal of Aerospace Engineering</i>	31



ELSEVIER SCIENCE S.A. [DTD 4.1.0]

JOURNAL CMA ARTICLE No. 2199

PAGES 01-20 DISPATCH 19 July 1999

in all correspondence
concerning this
paper refer to: CMA 2199

PROD. TYPE: KEYED

A



ELSEVIER

Comput. Methods Appl. Mech. Engrg. 000 (1999) 000-000

Computer methods
in applied
mechanics and
engineering

www.elsevier.com/locate/cma

Uncertainty analysis of composite structures

Ahmed K. Noor^{*}, James H. Starnes Jr.[†], Jeanne M. Peters

Center for Advanced Computational Technology, University of Virginia, NASA Langley Research Center, Mail Stop 201, Hampton, VA 23681, USA

Accepted 26 March 1999

Abstract

A two-phase approach and a computational procedure are presented for predicting the variability in the nonlinear response of composite structures associated with variations in the geometric and material parameters of the structure. In the first phase, hierarchical sensitivity analysis is used to identify the major parameters, which have the most effect on the response quantities of interest. In the second phase, the major parameters are taken to be fuzzy parameters, and a fuzzy set analysis is used to determine the range of variation of the response, associated with preselected variations in the major parameters. The effectiveness of the procedure is demonstrated by means of a numerical example of a cylindrical panel with four T-shaped stiffeners and a circular cutout. © 1999 Elsevier Science S.A. All rights reserved.

Nomenclature

$[A]$, $[B]$, $[D]$, $[A_s]$

a_{ij} , c_{ik}

b_{jk}

E_L , E_T

E_{1f} , E_{2f}

E_m

$[F]$

G_{Lr} , G_{Tr}

G_{12f} , G_m

$\{G(Z)\}$

$\{H\}$

h_1 , h_{l-1}

h

$[K]$

L_1 , L_2

M_1 , M_2 , M_{12} , M_{21}

matrices of the extensional, coupling, bending and transverse shear stiffnesses of the panel, see Eqs. (A.10) and (A.11) – Appendix A

coefficients relating laminate stiffnesses to effective properties of individual plies, and micromechanical (constituent) properties, respectively – see Eqs. (3) and (4)

coefficients relating effective ply properties to the micromechanical properties – see Eq. (4)

effective elastic moduli of the individual plies in the direction of fibers and normal to it, respectively

elastic moduli of the fibers in the longitudinal and transverse directions

elastic modulus of the matrix

linear flexibility matrix of the panel, see Eq. (B.2) – Appendix B

effective shear moduli of the individual plies in the plane of the fibers and normal to it, respectively

shear moduli of the fibers and matrix

vector of nonlinear terms of the panel, see Eq. (1)

vector of stress-resultant parameters

distances from the top and bottom surfaces of the l th ply to the middle surface

total thickness of the skin

global linear structural matrix, see Eq. (1)

side lengths of the panel in the x_1 and x_2 coordinate directions

bending stress resultants

43/68

^{*} Corresponding author. Tel.: +1-757-864-1978; fax: +1-757-864-8089; e-mail: a.k.noor@larc.nasa.gov

$\{M(X, \bar{X}_e)\}$	subvectors of nonlinear terms, Eq. (B.3) – Appendix B
$\{N(H, X, \bar{X}_e)\}$	
N_t	total axial force on the curved panel
N_1, N_2, N_{12}	in-plane (extensional) stress resultants
NL	total number of layers in the panel
$\{N\}, \{M\}$	vectors of in-plane and bending stress resultants, see Eq. (A.1) – Appendix A
$\{N_T\}, \{M_T\}$	vectors of thermal forces and moments in the panel, see Eq. (A.1) – Appendix A
p	intensity of uniform pressure loading
Q_1, Q_2	transverse shear stress resultants
$\{Q\}$	vector of transverse shear stress resultants
$\{Q^{(1)}\}, \{Q^{(2)}\},$	vectors of normalized mechanical loads, mechanical strains and thermal strains,
$\{Q^{(3)}\}$	see Eq. (1)
$[\bar{Q}]^{(l)}, [\bar{Q}_e]^{(l)}$	matrices of the extensional and transverse shear stiffnesses of the l th ply
	(referred to the x_1, x_2, x_3 coordinate system)
q_e	applied edge displacement
q_T	thermal strain parameter associated with $\{Q^{(3)}\}$
R	radius of curvature of the reference surface of the panel
$[S_1], [S_2]$	linear strain displacement matrices associated with the free nodal displacements
	$\{X\}$, and the constrained (prescribed nonzero) edge displacements $q_e\{\bar{X}_e\}$
T_t, T_b	top and bottom surface temperature changes
U	total strain energy of the panel
$U_{skin}, U_{flange}, U_{rib}$	total strain energy in the panel skin, the stiffener flanges (including adjacent
	skin) and the ribs
\bar{U}	strain energy density (energy per unit surface area) of the panel
\bar{U}_{sh}	transverse shear strain energy density per unit surface area
\bar{U}_{sh}	transverse shear strain energy density per unit volume
u_1, u_2, w	displacement components in the coordinate directions, see Fig. 1
v_f	fiber volume fraction
$\{X\}$	vector of free (unknown) nodal displacements
$\{\bar{X}_e\}$	normalized vector of constrained (prescribed nonzero) edge displacements
x_1, x_2, x_3	orthogonal coordinate system (x_3 is normal to the reference surface of the panel)
$\{Z\}$	response vector of the panel
α_{1f}, α_{2f}	coefficients of thermal expansion of the fibers in the longitudinal and transverse
	directions
α_L, α_T	effective coefficients of thermal expansion of the individual plies in the direction
	of the fibers and normal to it, respectively
α_m	coefficient of thermal expansion of the matrix
$\{\alpha\}^{(l)}$	vector of coefficients of thermal expansion of the l th ply of the panel (referred to
	the x_1, x_2, x_3 coordinate system)
$\{\gamma\}$	vector of transverse shear strain components of the panel, see Eq. (A.1) –
	Appendix A
$\{\epsilon\}$	vector of extensional strain components of the panel, see Eq. (A.1) – Appendix
	A
$\{\epsilon_T\}$	thermal strain subvector, see Eq. (B.5) – Appendix B
θ	fiber orientation angles of the individual plies
$\{\kappa\}$	vector of bending strain components of the panel, see Eq. (A.1) – Appendix A
λ	typical panel, laminate, effective ply or micromechanical parameter
ν_{12f}, ν_{23f}	Poisson's ratios of the fibers
ν_{LT}	effective major Poisson's ratio of the individual plies
ν_m	Poisson's ratio of the matrix
ϕ_1, ϕ_2	rotation components of the middle surface of the panel

Subscripts $\bar{I}, \bar{J} = 1$

to the total number of degrees of freedom (free nodal displacements and stress-resultant parameters) in the model

 $I' = 1$ to the total number of stress-resultant parameters in the model (components of the vector $\{H\}$) $I, J = 1$ to the total number of free nodal displacement components in the model (components of the vector $\{X\}$) L

direction of fibers

 $l = 1$ to the total number of plies, NL $i = 1$

to the total number of laminate parameters

 $j = 1$

to the total number of ply parameters

 $k = 1$

to the total number of micromechanical parameters

 f

fiber

 m

matrix

 T

transverse direction

 T nodal idation

thermal

 β

1, 2

Superscripts l

denotes laminate property

 m

denotes micromechanical property

 p

denotes ply (layer) property

 t

denotes transposition

1. Introduction

has evolved.

A significant numerical simulation capability now exists for studying the various phenomena associated with the response, failure and performance of multilayered composite panels and shells. The phenomena involved cover a wide range of length scales from local to global structural response. The modeling approaches used for multilayered panels can be divided into four different categories: detailed micromechanical models, three-dimensional continuum models, quasi-three-dimensional models, and a two-dimensional plate and shell models. Within each category ~~has evolved~~ a number of models with several levels of sophistication. The four categories are described in review paper [1,2] and monographs [3,4]. Recent applications to composite panels subjected to variety of mechanical and thermal loadings are reported in Refs. [5-7].

Since current measurement technology does not allow the accurate determination of the material parameters that are used in the analytical models, stochastic models and probabilistic analysis methods have been proposed. These methods assume random variations of the material parameters and require new codes to be developed. The present study aims at assessing the effects of variability of composite material properties on the response and failure of composite structures. An attempt is made to develop a tool kit, in the form of pre- and post-processors, that can be attached to any deterministic analysis program to generate the bounds of variation of response functions and quantities governing failure initiation. This approach is demonstrated in the present paper by analyzing composite cylindrical panels subjected to mechanical, thermal and pressure loads.

The cylindrical panels considered in the present paper have a number of T-shaped stiffeners. The panel skin, flange and rib of each stiffener consist of a number of perfectly bonded plies (layers). The individual plies are assumed to be homogeneous and anisotropic. A plane of thermoelastic symmetry exists at each point of the skin and the stiffener sections (parallel) to the reference surface of the section.

2. Basic idea of proposed approach

The proposed approach for uncertainty analysis consists of two major phases. In the first phase, hierarchical sensitivity analysis is used to evaluate the sensitivity coefficients with respect to a hierarchy of parameters, ranging from micromechanical to component parameters, and to identify the major parameters for the response quantities of interest. It is also used to identify the major parameters for the quantities governing failure initiation. In the second phase, the major parameters are taken to be fuzzy parameters, and a fuzzy set analysis is used to determine the range of variation of the response quantities of interest, associated with preselected variations of the fuzzy parameters.

A brief description of the fuzzy set analysis is given in Appendix C. The approach can be implemented by developing pre- and post-processors that can be attached to any deterministic analysis program to generate the bounds of variation of response functions, as well as of quantities governing failure initiation (see Fig. 16).

3. Mathematical formulation

3.1. Finite element equations governing the response

The analytical formulation is based on a first-order shear deformation type theory for each element of the stiffened panels, with the effects of large displacements, moderate rotations, average through-the-thickness transverse shear deformation, and laminated anisotropic material behavior included. For simplicity, a linear Duhamel–Neumann type constitutive model is used and the material properties are assumed to be independent of temperature. The thermoelastic constitutive relations used in the present study are given in Appendix A. The skin and each section of the stiffeners are discretized by using two-field mixed finite element models. The fundamental unknowns consist of the nodal displacements and the stress resultant parameters. The stress resultants are allowed to be discontinuous at interelement boundaries in the model. The sign convention for the generalized displacements, stress resultants and transverse stresses, is shown in Fig. 1. The external loading consists of a uniform pressure loading p , monotonically increasing edge displacement q_e (either end shortening or end extension), and a through-the-thickness temperature gradient q_T (with piecewise linear variation through the skin and flange thicknesses, and the stiffener blades, $q_T = (T_t - T_b)/h$, where T_t and T_b are the changes in the top and bottom surface temperatures, see Fig. 2). The skin and each section of the stiffener are modeled as two-dimensional shell elements.

The governing finite element equations describing the nonlinear response of the panel can be written in the following compact form

$$\{f(\mathbf{z})\} = [\mathbf{K}]\{\mathbf{z}\} + \{\mathbf{G}(\mathbf{z})\} - p\{\mathbf{Q}^{(1)}\} - q_e\{\mathbf{Q}^{(2)}\} - q_T\{\mathbf{Q}^{(3)}\} = 0, \quad (1)$$

where $[\mathbf{K}]$ is the global linear structural matrix which includes the flexibility and linear strain-displacement matrices; $\{\mathbf{z}\}$ is the response vector which includes both unknown (free) nodal displacements and stress-resultant parameters; $\{\mathbf{G}(\mathbf{z})\}$ is the vector of nonlinear terms; p , q_e and q_T are the magnitudes of the internal pressure, applied edge displacement and through-the-thickness temperature gradient; $\{\mathbf{Q}^{(1)}\}$, $\{\mathbf{Q}^{(2)}\}$, $\{\mathbf{Q}^{(3)}\}$ are normalized vectors corresponding to unit values of p , q_e and q_T . The form of the arrays $\{\mathbf{K}\}$, $\{\mathbf{G}(\mathbf{z})\}$, $\{\mathbf{Q}^{(2)}\}$ and $\{\mathbf{Q}^{(3)}\}$ is given in Appendix B.

The standard approach for the solution of Eq. (1) is to fix the value of two of the three parameters p , q_e and q_T and to vary the third, or to choose a functional relationship between the three parameters which is dependent on a single parameter q . In either case, the solution corresponding to the chosen combination of p , q_e and q_T (which is effectively dependent on a single parameter) constitutes a curve on the equilibrium surface of the panel.

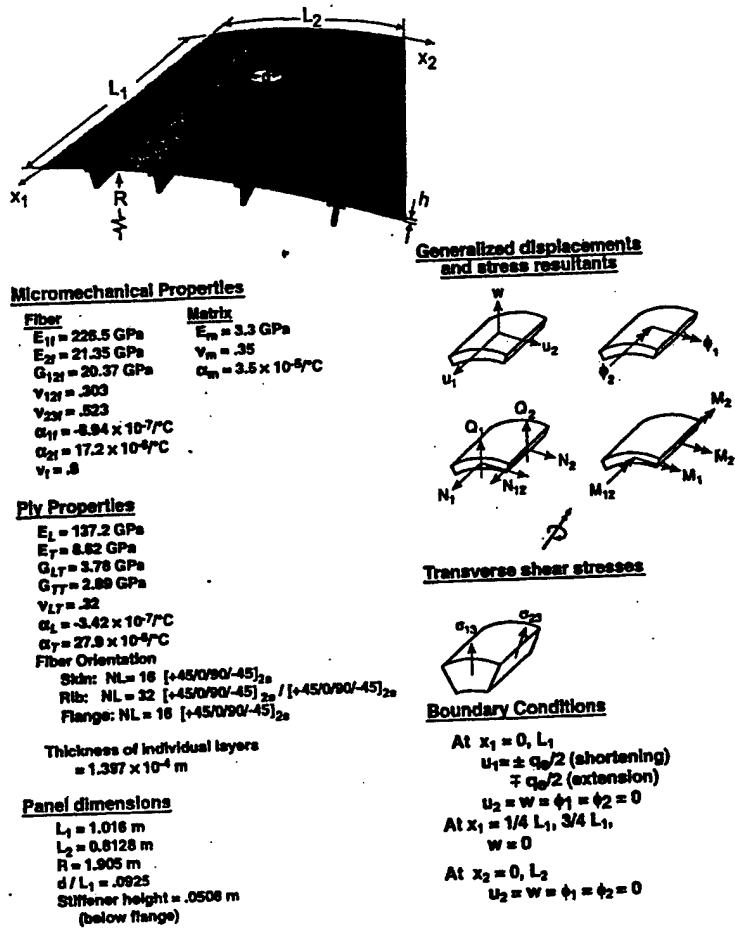


Fig. 1. Panel considered in the present study and sign convention for generalized displacements, stress resultants and transverse shear stresses.

3.2. Governing equations for the sensitivity coefficients

The sensitivity coefficients are the derivatives of the various response quantities with respect to the different material, lamination and geometric parameters of the panel. They can be used to study the sensitivity of the nonlinear and post-buckling responses to variations in the different parameters. The governing equations for the sensitivity coefficients are obtained by differentiating Eq. (1) with respect to a typical parameter λ . The resulting linear algebraic equations have the following form

$$\left[[K] + \left[\frac{\partial G_I}{\partial Z_J} \right] \right] \left\{ \frac{\partial Z}{\partial \lambda} \right\} = - \left[\frac{\partial K}{\partial \lambda} \right] \{Z\} + q_T \left\{ \frac{\partial Q^{(3)}}{\partial \lambda} \right\}, \quad (2)$$

where the range of the indices I and J is 1 to the total number of degrees of freedom in the model; and $\{Q^{(1)}\}$ and $\{Q^{(2)}\}$ are assumed to be independent of λ . Note that the matrix on the left-hand side of Eq. (2) is identical to that used in the Newton-Raphson iterative process. Therefore, if the Newton-Raphson technique is used in generating the nonlinear response, the evaluation of the sensitivity coefficients requires the generation of the right-hand side of Eq. (2), and a forward-reduction/back-substitution operation only (no decomposition of the left-hand side matrix is required). The form of the arrays

$$\left[\frac{\partial G_I}{\partial Z_J} \right], \left\{ \frac{\partial K}{\partial \lambda} \right\} \text{ and } \left\{ \frac{\partial Q^{(3)}}{\partial \lambda} \right\}$$

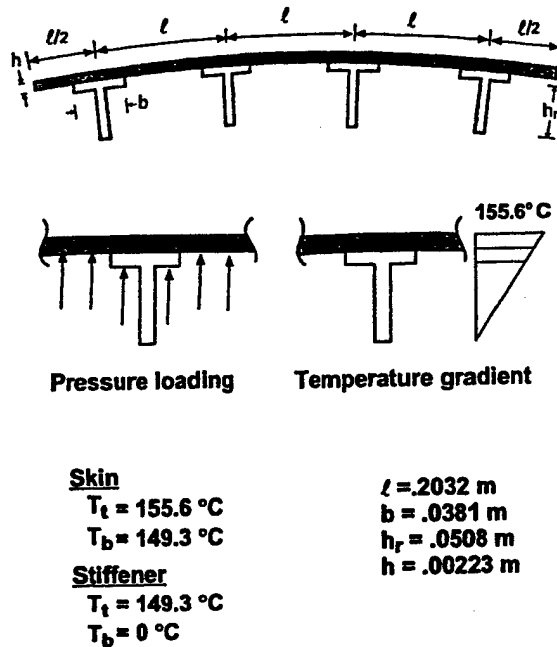


Fig. 2. Loading conditions considered in the numerical studies.

is given in Appendix B.

3.3. Evaluation of the transverse shear stresses

The transverse shear stresses are evaluated by using piecewise integration, in the thickness direction, of the three-dimensional equilibrium equations. For optimum accuracy, the transverse shear stresses are computed at the numerical quadrature points and then interpolated to the center of the element. The same procedure is used for evaluating the thickness distributions of the sensitivity coefficients of the transverse shear stresses.

3.4. Hierarchical sensitivity coefficients

The nonlinear response of composite structures is dependent on a hierarchy of interrelated geometric and material parameters at five different levels, namely:

- component (e.g., fuselage barrel section);
- subcomponent (e.g., stiffened panel);
- laminate;
- ply (layer);
- micromechanical (constituents – fiber, matrix, interface/interphase).

A study of the sensitivity of the response to variations in the parameters at each level provides insight into the importance of the parameters and helps in the development of materials to meet certain performance requirements. In the present study only the last four levels are considered. The subcomponent parameters include geometric characteristics such as stiffener spacing l , stiffener dimensions b and h_r , dimensions of cutouts and other discontinuities (e.g., diameter of the circular cutout d), and material characteristics such as skin and stiffener stiffnesses. The laminate parameters include the extensional, bending-extensional, bending and transverse shear stiffnesses (components of the matrices $[A]$, $[B]$, $[D]$ and $[A_s]$ – see Eqs. (A.10) and (A.11), Appendix A); and the vectors of thermal effects $\{N_T\}$ and $\{M_T\}$ – see Eq. (A.12), Appendix A. The ply parameters include the effective properties of individual plies: elastic moduli E_L , E_T ; shear moduli G_{LT} , G_{TT} ; major Poisson's ratio ν_{LT} ; coefficients of thermal expansion α_L , α_T ; ply thickness $h^{(i)}$; and fiber-

orientation angle $\theta^{(l)}$, where subscripts L and T refer to the longitudinal (fiber) and transverse directions, respectively. The micromechanical parameters refer to the fiber, matrix and interface/interphase material moduli E_{1f} , E_{2f} , E_m , E_p , G_{12f} , G_m , G_p ; Poisson's ratios ν_{12f} , ν_{23f} ; coefficients of thermal expansion α_{1f} , α_{2f} , α_m , α_p ; the fiber volume fraction v_f of the layers. The subscripts f , m , and p denote the fiber, matrix and interface/interphase property, respectively. The three sets of laminate, ply and micromechanical parameters will henceforth be referred to as $\lambda_i^{(l)}$, $\lambda_j^{(p)}$, $\lambda_k^{(m)}$, where superscripts l , p and m refer to the panel, effective ply (layer) and micromechanical parameters, respectively; and the indices i , j and k range from 1 to the number of parameters in each category.

The computational procedure consists of evaluating the sensitivity coefficients with respect to each of the laminate parameters $\{\partial Z / \partial \lambda_i^{(l)}\}$ using Eq. (2). The sensitivity coefficients with respect to the effective ply and micromechanical parameters are then obtained by forming the following linear combinations:

$$\left\{ \frac{\partial Z}{\partial \lambda_j^{(p)}} \right\} = \sum_i a_{ij} \left\{ \frac{\partial Z}{\partial \lambda_i^{(l)}} \right\} \quad (3)$$

and

$$\left\{ \frac{\partial Z}{\partial \lambda_k^{(m)}} \right\} = \sum_j b_{jk} \left\{ \frac{\partial Z}{\partial \lambda_j^{(p)}} \right\} = \sum_i c_{ik} \left\{ \frac{\partial Z}{\partial \lambda_i^{(l)}} \right\}, \quad (4)$$

where

$$a_{ij} = \left\{ \frac{\partial \lambda_i^{(l)}}{\partial \lambda_j^{(p)}} \right\}, \quad (5)$$

$$b_{jk} = \left\{ \frac{\partial \lambda_j^{(p)}}{\partial \lambda_k^{(m)}} \right\}, \quad (6)$$

$$c_{ik} = \left\{ \frac{\partial \lambda_i^{(l)}}{\partial \lambda_k^{(m)}} \right\} = \sum_j a_{ij} b_{jk}. \quad (7)$$

The a_{ij} coefficients relate the laminate stiffnesses to the effective properties of the individual plies and are obtained from lamination theory. The b_{jk} coefficients relate the effective ply properties to the constituent properties and are obtained from the micromechanical model; and the c_{ik} coefficients relate the panel stiffnesses to the micromechanical properties (see Fig. 3). If the laminate stiffnesses are uniform, and the constitutive relations of the laminate, ply, and the constituents are linear, then a_{ij} , b_{jk} , c_{ik} coefficients are constants and need to be generated only once for each panel, even when the response is nonlinear.

4. Numerical studies

Numerical studies were performed to assess the effectiveness of the proposed computational procedure for predicting the variability in the nonlinear response of a typical aircraft composite structure. The structure considered is a cylindrical composite panel with four T-shaped stiffeners and a circular cutout. The material properties and geometric characteristics for the panel are given in Fig. 1. The material properties, the fiber orientation and the stacking sequence selected for the panel and stiffeners are those typical of fuselage panels considered for high-speed aircraft applications. The loading on the panel consisted of a sequence of mechanical and thermal loads: uniform pressure load $p = 6.894 \times 10^4$ Pa., followed by monotonically increasing edge displacement q_e , and then a through-the-thickness temperature gradient q_T (linear temperature variation through the skin, and through the stiffener flange and rib, $q_T = (T_t - T_b)/h$, where T_t and T_b are the changes in the top and bottom surface temperatures and h is the distance between the top and bottom surfaces - see Fig. 2). Two different types of edge displacements were applied, namely,

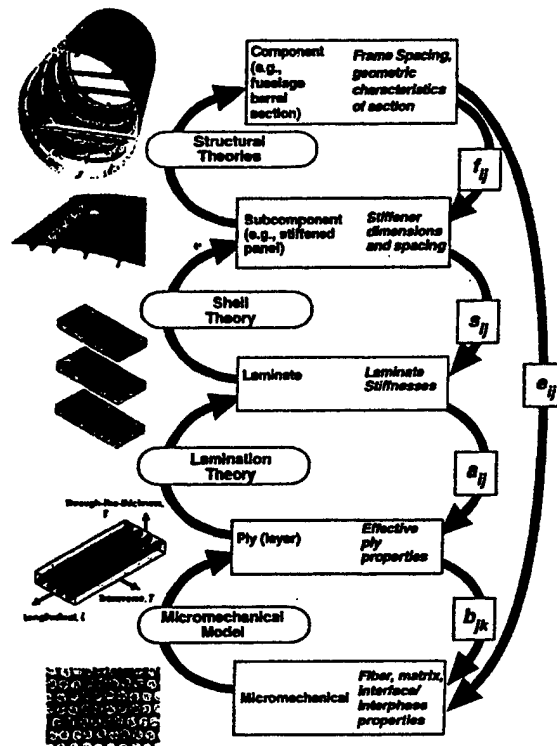


Fig. 3. Hierarchical sensitivity coefficients for composite structures.

end shortening and end extension. The boundary conditions selected for the cases of end shortening and extension are shown in Fig. 2. The transverse displacement w is set equal to zero at $x_1 = L_1/4$ and $3L_1/4$ simulating the presence of frames at these locations. For each load case, the maximum value of q_c was selected in such a way that the magnitude of the maximum principal strains on the surfaces do not exceed 0.005. For each load case, global and detailed response quantities were generated. In addition, the hierarchical sensitivity coefficients are evaluated. The hierarchical sensitivity coefficients are derivatives of the different response quantities with respect to subcomponent parameters, laminate stiffnesses, material parameters and fiber angles of the individual plies, and the micromechanical parameters.

Mixed finite element models were used for the discretization of the skin and each section of the stiffener sections. Biquadratic shape functions were used for approximating each of the generalized displacements, and bilinear shape functions were used for approximating each of the stress resultants. The characteristics of the finite element model are given in Ref. [8]. For each panel, the multiple parameter reduction methods described in Refs. [9-11] were used in generating the nonlinear response and evaluating the sensitivity coefficients. Typical results are presented in Figs. 4-8 for the response studies, in Figs. 9-11 for the sensitivity studies, and in Figs. 12-15 for the variability of the nonlinear response, and are described subsequently.

4.1. Response studies

The global and detailed response characteristics of the panel are shown in Figs. 4-8. Plots of the total strain energy U and the total axial force N_1 versus the applied end shortening or extension q_c are shown in Fig. 4. The total strain energy obtained by the present model is in close agreement with that obtained by the STAGS general shell analysis code [12]. The variations of the strain energy in the skin, stiffener flanges (including adjacent skin) and ribs, and their ratios to the total strain energy of the panel, with loading are shown in Fig. 5. Typical contour plots for the transverse displacement w and the strain energy density \bar{U} in the skin and stiffener flanges, after each loading stage, are shown in Fig. 6. Through-the-thickness distri-

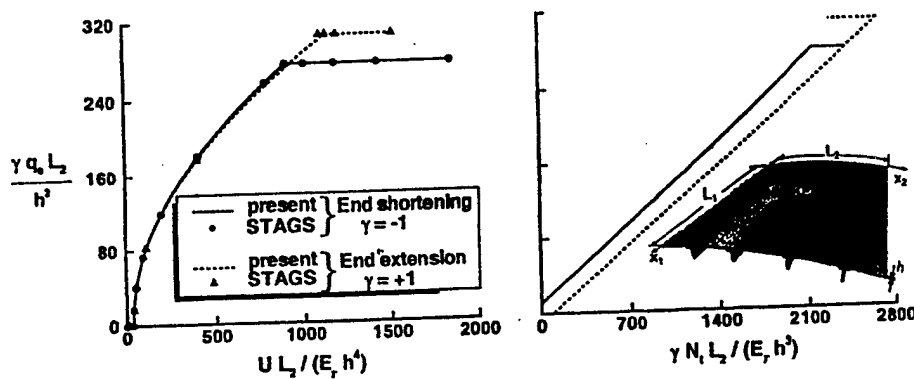


Fig. 4. Effect of loading conditions on the response of stiffened cylindrical panel with circular cutout subjected to combined pressure load, end shortening or extension and through-the-thickness temperature gradient.

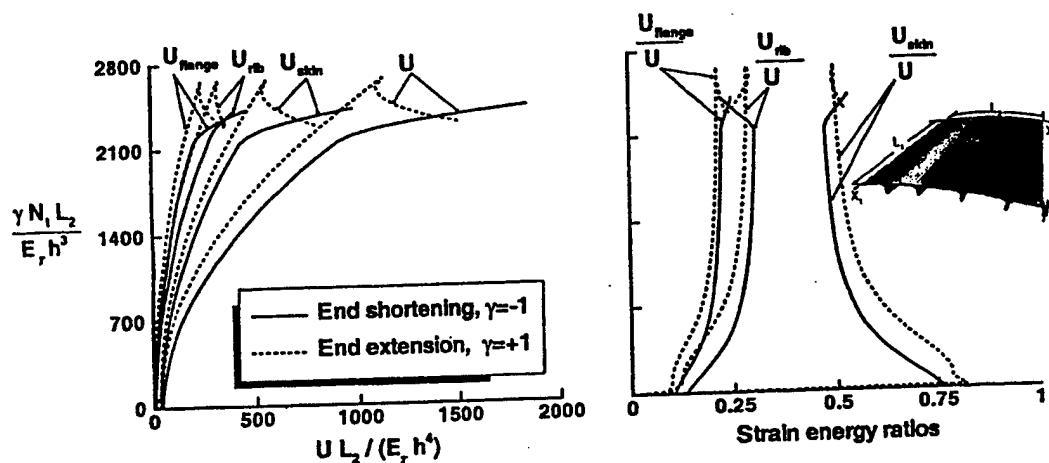


Fig. 5. Effect of loading on the total strain energy in the skin, stiffener flanges and ribs. Stiffened cylindrical panel with circular cutout subjected to combined pressure load, end shortening or extension and through-the-thickness temperature gradient. The skin section adjacent to (above) each flange is considered to be part of the flange.

butions of the transverse shear strain energy density (per unit volume) \hat{U}_{sh} , at the location of the maximum \bar{U}_{sh} (transverse shear strain energy per unit surface area), are shown in Fig. 7. The distributions of \hat{U}_{sh} at the interfaces between the skin and flanges, at the locations of maximum \bar{U}_{sh} , is shown in Fig. 8. An examination of Figs. 4-8 reveals:

1. The pressure load p has the least effect on the global panel response, and the edge displacement q_e has the most effect on that response (see Figs. 4 and 5). By contrast, the temperature gradient has the most effect on the transverse shear strain energy density \hat{U}_{sh} (see Fig. 7).
2. For the pressure load, over 78% of the total strain energy is in the skin (not including the section adjacent to the flanges), i.e., $U_{skin}/U > 0.78$. At the end of the second loading stage ($p + q_e$), the ratios U_{skin}/U , U_{flange}/U and U_{rib}/U are 0.47, 0.22, 0.30 for the end shortening case and 0.50, 0.21, 0.29 for the end extension case. The corresponding ratios at the end of the third loading stage ($p + q_e + q_r$) are (0.53, 0.25, 0.22) and (0.52, 0.24 and 0.24) for the end shortening and end extension cases, respectively.
3. For the two load cases no mode change occurs from the first to the second and third loading stages (p , $p + q_e$, $p + q_e + q_r$). However, the distribution of the strain energy density \bar{U} in the panel changes significantly after the application of each of the second and third loadings.

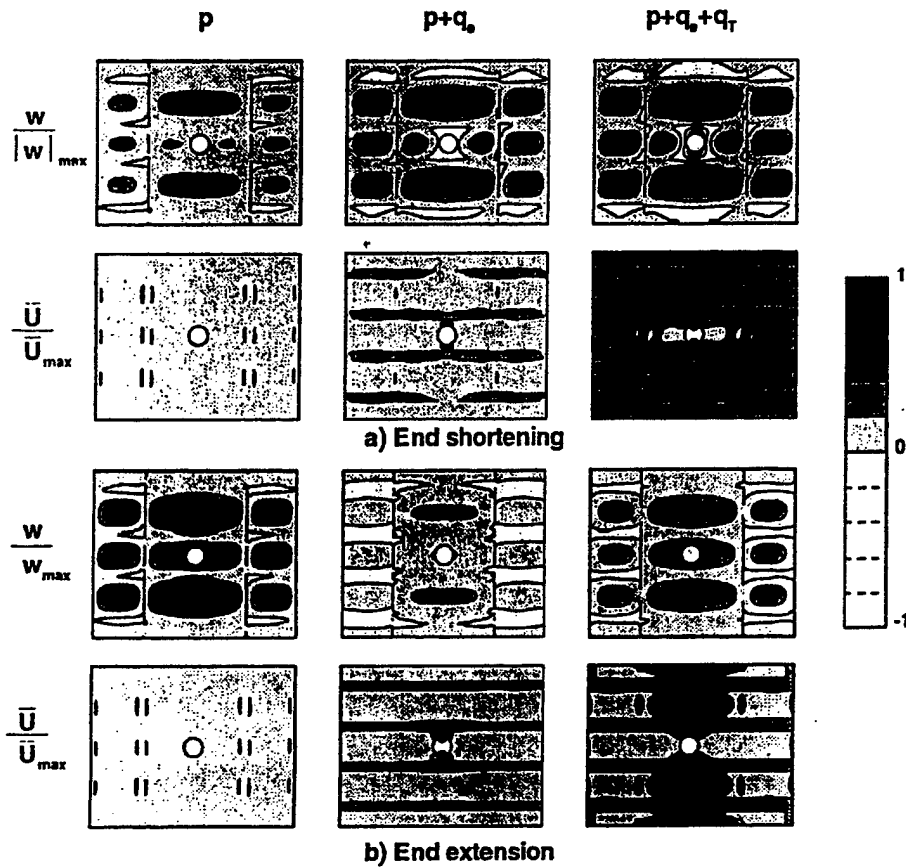


Fig. 6. Normalized contour plots depicting the effect of loading conditions on the transverse displacement w and the strain energy density \bar{U} in the skin and the stiffener flanges. Cylindrical panel with circular cutout subjected to combined pressure, end shortening or extension and through-the-thickness temperature gradient.

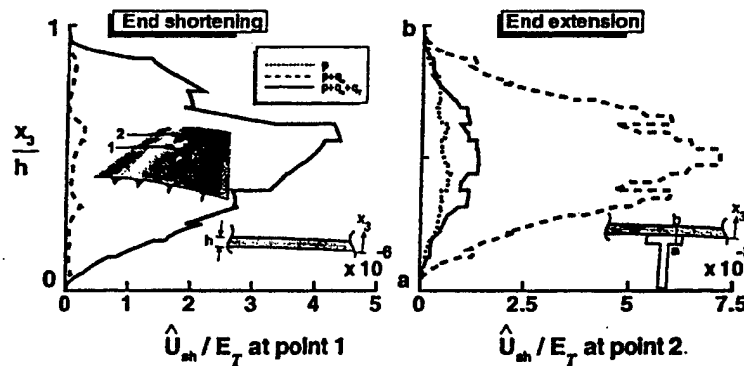


Fig. 7. Effect of loading conditions on the through-the-thickness distributions of the transverse shear strain energy density (per unit volume) \hat{U}_{sh} at the location of the maximum \hat{U}_{sh} (transverse shear strain energy per unit surface area). Stiffened cylindrical panel with circular cutout subjected to combined pressure load, end shortening or extension and through-the-thickness temperature gradient.

4. The maximum strain energy density occurs at the cutout. For the end shortening case, \bar{U}_{max} is associated with the $p + q_c + q_T$ loading condition. By contrast, for the end extension case, \bar{U}_{max} is associated with the $p + q_c$ loading condition.

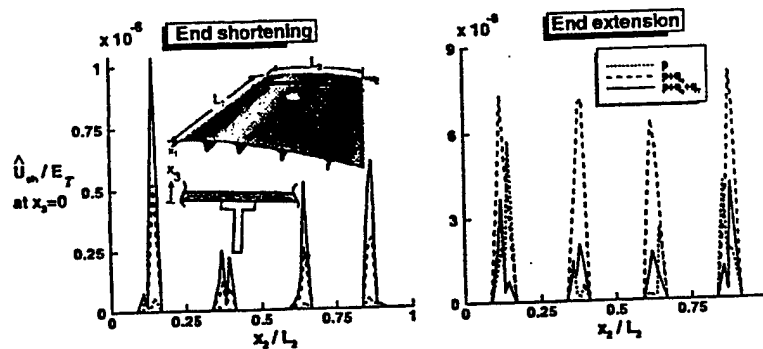


Fig. 8. Effect of loading conditions on the distributions of the transverse shear strain energy density (per unit volume) \bar{U}_{sh} at the interface between the skin and stiffener flanges. Stiffened cylindrical panel with circular cutout subjected to combined pressure load, end shortening or extension and through-the-thickness temperature gradient.

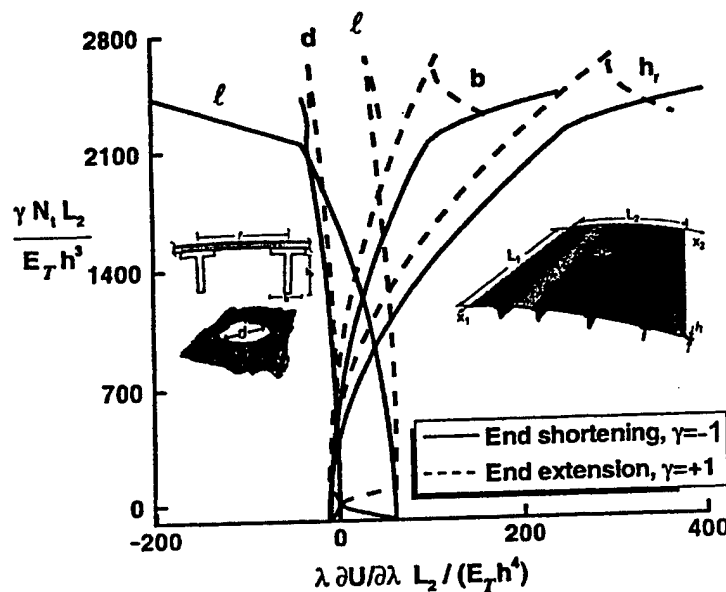


Fig. 9. Effect of loading conditions on the normalized sensitivity coefficients of the total strain energy U with respect to subcomponent parameters. Stiffened cylindrical panel with circular cutout subjected to combined pressure load, end shortening or extension and through-the-thickness temperature gradient.

5. The maximum \bar{U}_{sh} for the end shortening case occurs at the cutout and is associated with the $p + q_c + q_T$ loading condition. By contrast, the maximum \bar{U}_{sh} for the end extension case occurs at the frames and is associated with the $p + q_c$ loading condition. The transverse shear strain energy density \bar{U}_{sh} for the end shortening case is almost two orders of magnitude larger than that for the end extension case.

4.2. Sensitivity studies

Sensitivity studies were conducted to identify which of the subcomponent parameters, laminate parameters, effective ply properties, and micromechanical parameters most affect the nonlinear response. Typical results showing the sensitivity of the total strain energy U with respect to the subcomponent parameters, l , b , h , and d , are shown in Fig. 9. Sensitivity coefficients of U with respect to the extensional and bending stiffnesses of the panel skin, the stiffener flanges and ribs are presented in Fig. 10. Sensitivity co-

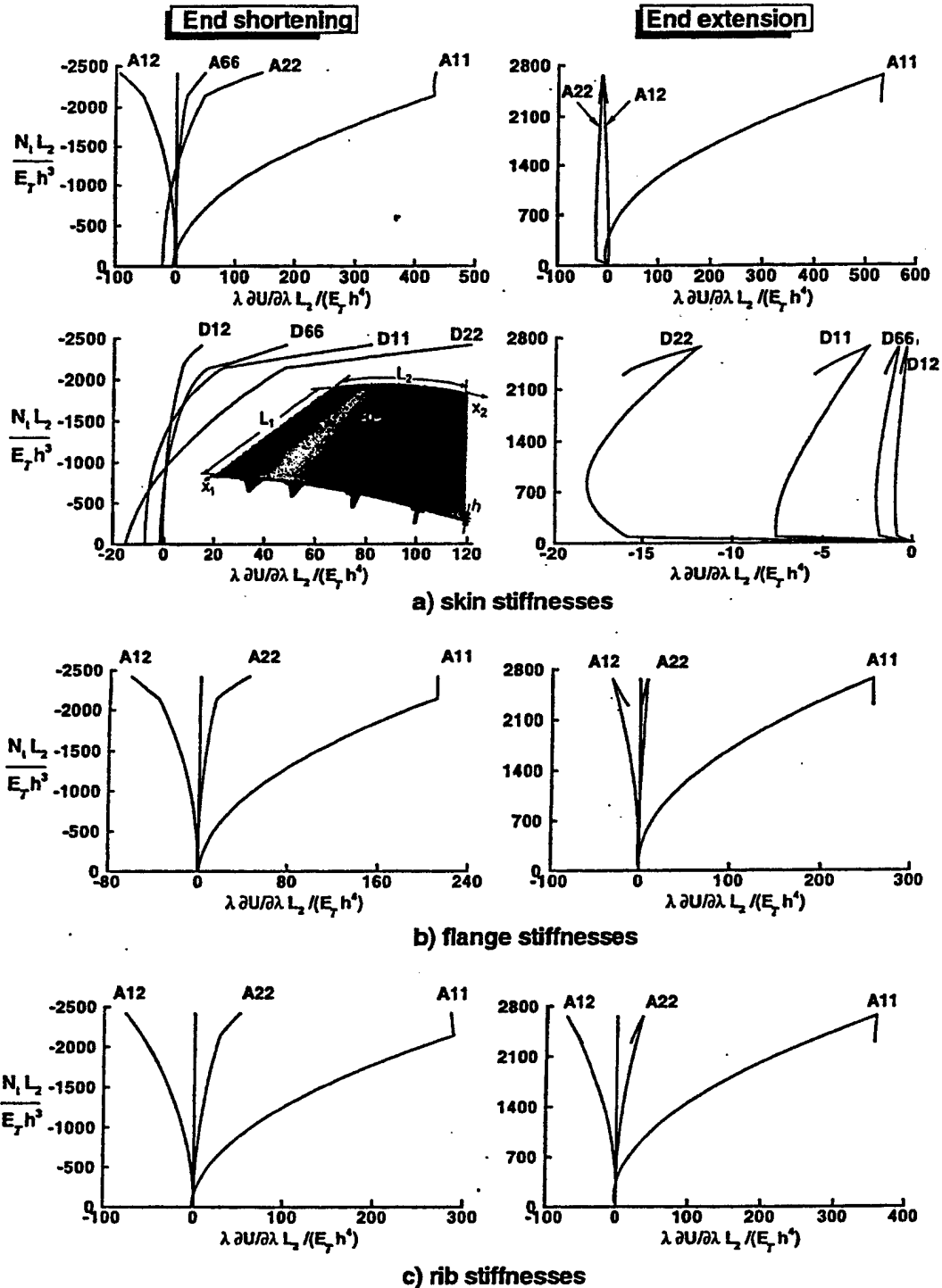


Fig. 10. Effect of loading conditions on the normalized sensitivity coefficients of the total strain energy U with respect to skin, flange and rib stiffnesses. Stiffened cylindrical panel with circular cutout subjected to combined pressure load, end shortening or extension and through-the-thickness temperature gradient. The skin section adjacent to (above) each flange is considered to be part of the flange.

efficients of U with respect to the fiber angles of the skin, flange and rib, the effective material properties of individual plies and the micromechanical parameters are shown in Fig. 11.

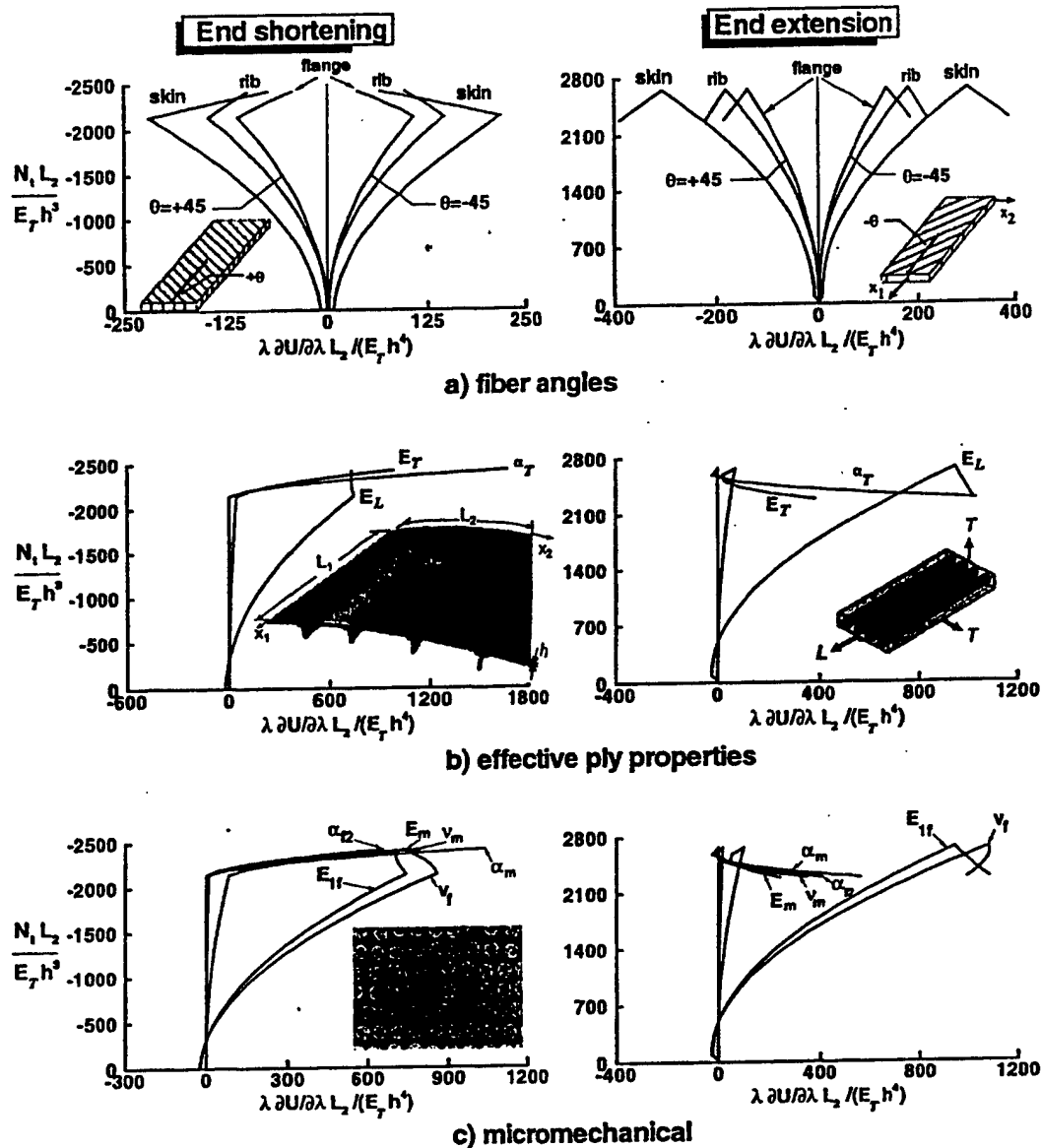


Fig. 11. Effect of loading conditions on the normalized sensitivity coefficients with respect to fiber angles, effective ply and micro-mechanical parameters. Stiffened cylindrical panel with circular cutout subjected to combined pressure load, end shortening or extension and through-the-thickness temperature gradient. The skin section adjacent to (above) each flange is considered to be part of the flange.

An examination Figs. 9 and 11 reveals:

1. For the pressure loading, the total strain energy U is considerably more sensitive to variations in the stiffener spacing l than to variations in the other parameters. After application of q_e , U becomes considerably more sensitive to variations in the stiffener dimensions b and h_r than to variations in l and d . The same is true after application of the temperature gradient q_T .
2. The total strain energy U is considerably more sensitive to variations in A_{11} for the skin than to variations in the other extensional stiffnesses for the skin, stiffener, ribs and flanges. The sensitivity of U to variations in the bending stiffness D_{22} of the skin is more pronounced than that for variations in other bending stiffnesses.

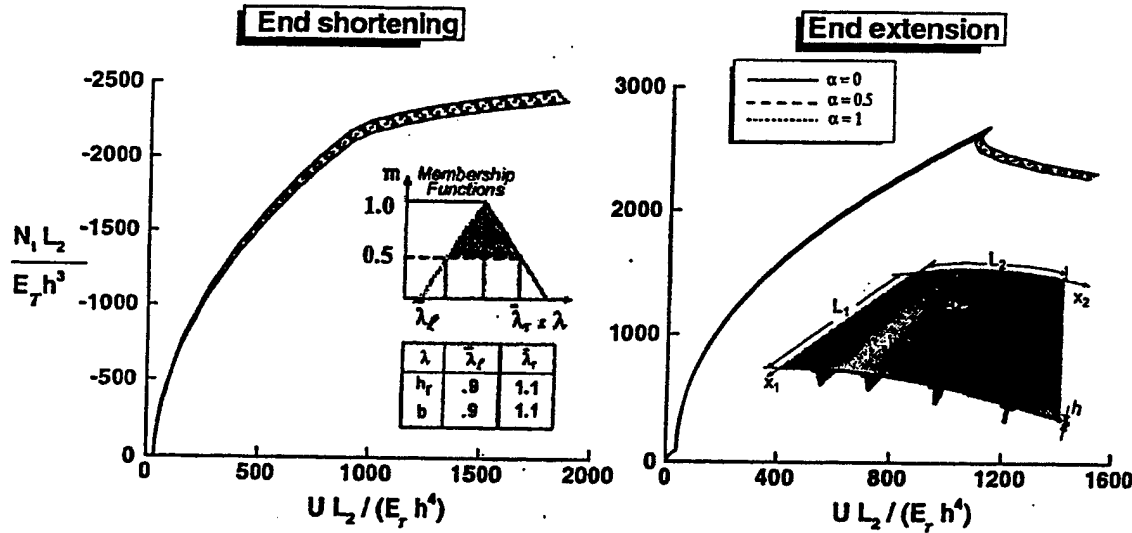


Fig. 12. Effect of variability in the subcomponent parameters b and h , on the total strain energy U of stiffened cylindrical panel with circular cutout subjected to combined pressure load, end shortening or extension and through-the-thickness temperature gradient.

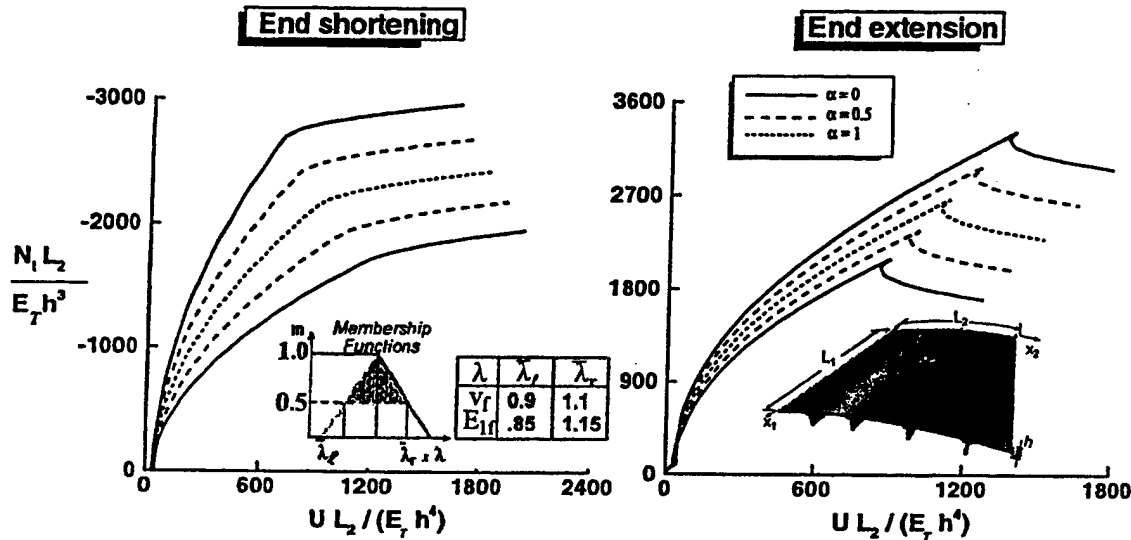


Fig. 13. Effect of variability in the micromechanical parameters v_f and E_f on the total strain energy U of stiffened cylindrical panel with circular cutout subjected to combined pressure load, end shortening or extension and through-the-thickness temperature gradient.

3. The sensitivity of U to variations in A_{11} increases with the increase in q_c . The addition of the temperature gradient does no change the sensitivity with respect to A_{11} , but increases the sensitivity with respect to D_{22} .
4. The total strain energy is considerably more sensitive to variations in the following parameters than to each of the other parameters in the same category: (a) the effective elastic moduli of the individual plies E_L and E_T , and the effective coefficient of thermal expansion α_T ; (b) the fiber angles $+45^\circ$ and -45° ; and (c) the micromechanical parameters v_f , E_{f1} , α_m , E_m , v_m and α_{f2} . The sensitivity of U with respect to E_L , fiber angles $+45^\circ$, -45° , v_f and E_{f1} increases with the increase in q_c . For the end shortening case, the additions of q_T increases the sensitivity to variations in α_T , E_T , fiber angles $+45^\circ$, -45° , α_m , E_m , v_m and α_{f2} , and slightly decreases the sensitivity with respect to E_L , v_f and E_{f1} . For the edge extension case, the addition of q_T has an opposite effect to that described for edge shortening.

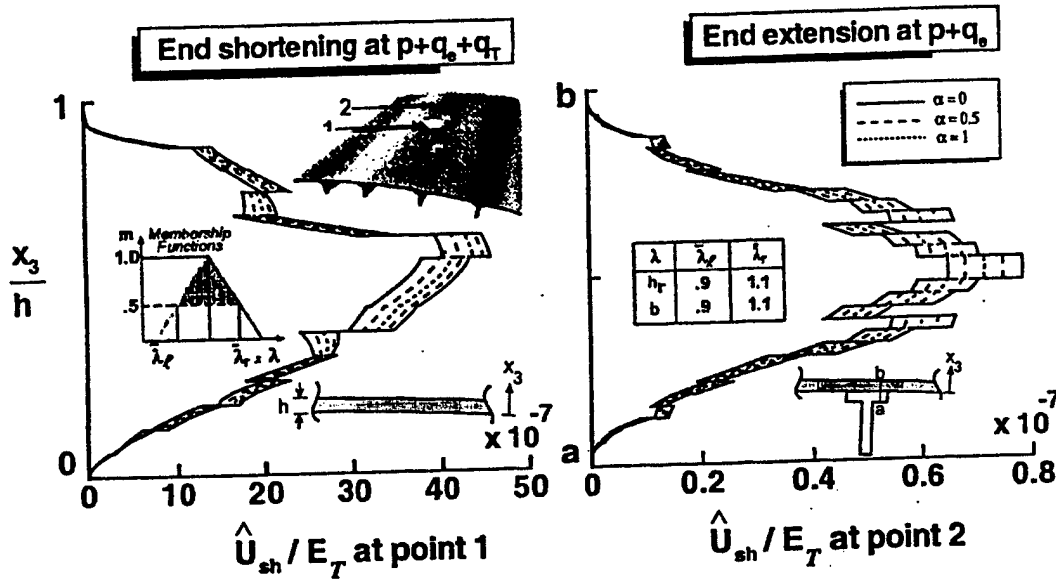


Fig. 14. Effect of variability in the subcomponent parameters b and h_r on the through-the-thickness distribution of the transverse shear strain energy density \hat{U}_{sh} . Stiffened cylindrical panel with circular cutout subjected to combined pressure load, end shortening or extension and through-the-thickness temperature gradient.

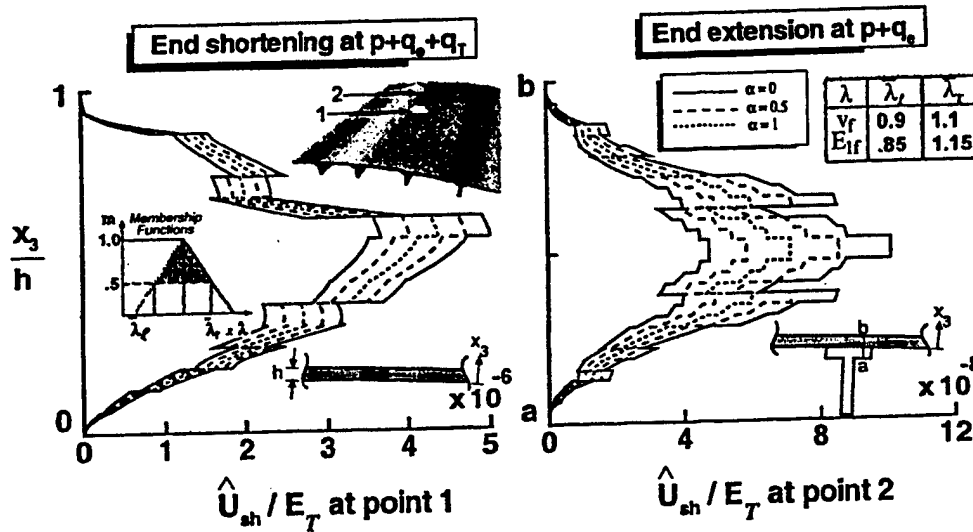


Fig. 15. Effect of variability in the micromechanical parameters v_r and E_{1r} on the through-the-thickness distribution of the transverse shear strain energy density \hat{U}_{sh} . Stiffened cylindrical panel with circular cutout subjected to combined pressure load, end shortening or extension and through-the-thickness temperature gradient.

4.3. Variability of response

Studies were conducted to assess the effect of variation of two major parameters at each of the subcomponent and micromechanical levels (b , h_r) and (v_r , E_{1r}) on the total strain energy of the panel U , and the transverse shear strain energy per unit volume \hat{U}_{sh} at the location of the maximum \hat{U}_{sh} .

Each pair of parameters (b , h_r) and (v_r , E_{1r}) were taken to be fuzzy parameters with triangular membership functions. The nominal values of b and h_r were changed by $\pm 10\%$, and the nominal values of v_r and E_{1r} were changed by $\pm 10\%$ and $\pm 15\%$, respectively. The variations of the upper and lower bounds of U with loading due to variations in each pair of parameters (b , h_r) and (v_r , E_{1r}), are shown in Figs. 12 and 13,

respectively. The corresponding variations of the through-the-thickness distributions of the upper and lower bounds of \bar{U}_{sh} (at the location of the maximum \bar{U}_{sh}) are shown in Figs. 14 and 15. For the end shortening case, the variations in b and h_r resulted in less than 2% change in the values of U and N_i (from their values associated with the nominal b and h_r after the application of $p + q_c + q_T$). The variations in v_r and E_{1f} resulted in changes of (–9%, +10%) and (+22%, –19%) in the magnitudes of the same two response quantities. For the end extension case, the corresponding changes in the values of U were $\pm 1.1\%$ and (–16%, +18%), and in the values of N_i were $\pm 1\%$ and (–26%, +29%).

The changes in the maximum values of \bar{U}_{sh} resulting from the variations in (b , h_r) and (v_r , E_{1f}) were less than (+5%, –8%) and (+15%, –17%) for the end shortening case. The corresponding changes for the end extension case were less than $\pm 10\%$ and (+42%, –34%).

5. Concluding remarks

A two-phase computational procedure is presented for studying the effects of variability of composite material properties on the response and failure of composite structures. In the first phase, hierarchical sensitivity analysis is used to identify the major parameters for the response quantities of interest, as well as for the quantities governing failure initiation. In the second phase, the major parameters are taken to be fuzzy parameters, and a fuzzy set analysis is used to determine the range of variation of the response quantities of interest, associated with preselected variations of the fuzzy parameters. The approach can be implemented by developing a tool kit, in the form of pre- and post-processors that can be attached to any deterministic analysis program to generate the bounds of variation of response functions as well as of quantities governing failure initiation.

The procedure was applied to a composite cylindrical panel with four T-shaped stiffeners and a circular cutout. The external loads applied to the panel consisted of a uniform pressure load, monotonically increasing edge displacement (either edge shortening or edge extension), and a through-the-thickness temperature gradient. The panel skin, flange and rib of each stiffener consisted of a number of perfectly bonded layers and were modeled as two-dimensional shell elements.

Both the geometrically nonlinear response of the panel as well as the hierarchical sensitivity coefficients are generated. The hierarchical sensitivity coefficients measure the sensitivity of the different response quantities to variations in three sets of interrelated parameters; namely, panel and stiffener stiffnesses, effective ply properties; and micromechanical parameters. The effect of variation of two major subcomponent parameters and two major micromechanical parameters on the variability of the total strain energy, and the transverse shear strain energy per unit volume for the panel are studied.

Acknowledgements

The work was partially supported by NASA Grant NAG-1-2016 and Air Force Office of Scientific Research Grant F49620-96-1-0462. The authors acknowledge the help of Dr. Charles C. Rankin and the staff of the Lockheed Martin Advanced Technology Center in Palo Alto, California, in using the STAGS general shell analysis program.

Appendix A. Thermoelastic constitutive relations for the laminate

The thermoelastic model used in the present study is based on the following assumptions:

1. The laminates are composed of a number of perfectly bonded plies (skin, stiffener, flange and blade).
2. The Aboudi cell method is used to evaluate the effective properties of the individual layers [13].
3. The reference surfaces for the skin and the stiffener flange are chosen to be the bottom surface of the skin. The reference surface for the stiffener is chosen to be its middle surface.
4. Every point of the laminate is assumed to possess a single plane of thermoelastic symmetry parallel to the reference surface of the laminate.
5. The material properties are independent of temperature.

6. The constitutive relations for the laminate are described by lamination theory and can be written in the following compact form:

$$\begin{Bmatrix} N \\ M \\ Q \end{Bmatrix} = \begin{bmatrix} [A] & [B] & 0 \\ [B]^t & [D] & 0 \\ 0 & 0 & [A_s] \end{bmatrix} \begin{Bmatrix} \varepsilon \\ \kappa \\ \gamma \end{Bmatrix} - \begin{Bmatrix} N_T \\ M_T \\ 0 \end{Bmatrix}, \quad (\text{A.1})$$

where $\{N\}$, $\{M\}$, $\{Q\}$, $\{\varepsilon\}$, $\{\kappa\}$, $\{\gamma\}$, $\{N_T\}$ and $\{M_T\}$ are the vectors of extensional, bending and transverse shear stress resultants, strain components and thermal effects of the panel, and are given by:

$$\{N\}^t = [N_1 \quad N_2 \quad N_{12}] \quad (\text{A.2})$$

$$\{M\}^t = [M_1 \quad M_2 \quad M_{12}] \quad (\text{A.3})$$

$$\{Q\}^t = [Q_1 \quad Q_2] \quad (\text{A.4})$$

$$\{\varepsilon\}^t = [\varepsilon_1 \quad \varepsilon_2 \quad 2\varepsilon_{12}] \quad (\text{A.5})$$

$$\{\kappa\}^t = [\kappa_1 \quad \kappa_2 \quad 2\kappa_{12}] \quad (\text{A.6})$$

$$\{\gamma\}^t = [2\varepsilon_{31} \quad 2\varepsilon_{32}] \quad (\text{A.7})$$

$$\{N_T\}^t = [N_{T1} \quad N_{T2} \quad N_{T12}] \quad (\text{A.8})$$

and

$$\{M_T\}^t = [M_{T1} \quad M_{T2} \quad M_{T12}] \quad (\text{A.9})$$

The matrices $[A]$, $[B]$, $[D]$ and $[A_s]$ contain the extensional, coupling, bending and transverse shear stiffnesses of the panel which can be expressed in terms of the effective ply stiffnesses as follows:

$$\begin{aligned} [[A][B][D]] &= \sum_{l=1}^{NL} \int_{h_{l-1}}^{h_l} [\bar{Q}]^{(l)} [I] x_3 [I] (x_3)^2 [I] dx_3 \\ &= \sum_{l=1}^{NL} \int_{h_{l-1}}^{h_l} [\bar{Q}]^{(l)} [I] x_3 [I] (x_3)^2 [I] dx_3, \end{aligned} \quad (\text{A.10})$$

$$[A_s] = \sum_{l=1}^{NL} \int_{h_{l-1}}^{h_l} [\bar{Q}_s]^{(l)} dx_3, \quad (\text{A.11})$$

where $[\bar{Q}]^{(l)}$ and $[\bar{Q}_s]^{(l)}$ are the extensional and transverse shear stiffnesses of the l th ply (referred to the x_1, x_2, x_3 coordinate system); $[I]$ is the identity matrix; h_l and h_{l-1} are the distances from the top and bottom surfaces of the l th ply to the middle surface; and NL is the total number of plies in the laminate. The expressions for the different coefficients of the matrices $[\bar{Q}]^{(l)}$ and $[\bar{Q}_s]^{(l)}$ in terms of the material and geometric properties of the constituents of the composite face sheets (fiber and matrix) are given in Refs. [14,15].

The vectors of thermal effects, $\{N_T\}$ and $\{M_T\}$, are given by:

$$[\{N_T\} \quad \{M_T\}] = \sum_{l=1}^{NL} \int_{h_{l-1}}^{h_l} [\bar{Q}]^{(l)} \{\alpha\}^{(l)} [1] x_3 T dx_3, \quad (\text{A.12})$$

where $\{\alpha\}^{(l)}$ is the vector of coefficients of thermal expansion of the l th ply (referred to the coordinates x_1, x_2, x_3 ; see, for example, Refs. [16,17]).

Appendix B. Form of the arrays in the governing discrete equations of the panel

The governing discrete equations of the panel, Eq. (1), consist of both the constitutive relations and the equilibrium equations.

The response vector $\{Z\}$ can be partitioned into subvectors of stress-resultant parameters $\{H\}$, and free (unconstrained) nodal displacements $\{X\}$, as follows:

$$\{Z\} = \begin{Bmatrix} H \\ X \end{Bmatrix}. \quad (B.1)$$

The different arrays in Eqs. (1) and (2) can be partitioned as follows:

$$[K] = \begin{bmatrix} F & S_1 \\ S_1^t & 0 \end{bmatrix}, \quad (B.2)$$

$$\{G(Z)\} = \begin{Bmatrix} M(X, \bar{X}_e) \\ N(H, X, \bar{X}_e) \end{Bmatrix}, \quad (B.3)$$

$$\{Q^{(2)}\} = \begin{Bmatrix} -[S_2]\{\bar{X}_e\} \\ 0 \end{Bmatrix}, \quad (B.4)$$

$$\{Q^{(3)}\} = \begin{Bmatrix} \varepsilon_T \\ 0 \end{Bmatrix}, \quad (B.5)$$

$$\left[\frac{\partial G_I}{\partial Z_I} \right] = \begin{bmatrix} 0 & \frac{\partial M_I}{\partial X_I} \\ \text{Sym} & \frac{\partial N_I}{\partial X_I} \end{bmatrix}, \quad (B.6)$$

$$\left[\frac{\partial K}{\partial \lambda} \right] = \begin{bmatrix} -\left[\frac{\partial F}{\partial \lambda} \right] & 0 \\ 0 & 0 \end{bmatrix}, \quad (B.7)$$

$$\left\{ \frac{\partial Q^{(3)}}{\partial \lambda} \right\} = \begin{Bmatrix} \frac{\partial \varepsilon_T}{\partial \lambda} \\ 0 \end{Bmatrix}, \quad (B.8)$$

where $[F]$ is the linear flexibility matrix; $[S_1]$ and $[S_2]$ are the linear strain-displacement matrices associated with the free nodal displacements $\{X\}$, and the constrained (prescribed nonzero) edge displacements $q_e\{\bar{X}_e\}$; $\{M(X, \bar{X}_e)\}$ and $\{N(H, X, \bar{X}_e)\}$ are the subvectors of nonlinear terms; $\{\varepsilon_T\}$ is the subvector of normalized thermal strains; 0 is a null matrix or vector; and superscript t denotes transposition. The explicit form of $\{\varepsilon_T\}$ is given in Ref. [18].

For the purpose of obtaining analytic derivatives with respect to lamination parameters (e.g., fiber orientation angles of different layers), it is convenient to express $\partial[F]/\partial\lambda$ in terms of $\partial[F]^{-1}/\partial\lambda$ as follows:

$$\frac{\partial[F]}{\partial\lambda} = -[F] \frac{\partial[F]^{-1}}{\partial\lambda} [F]. \quad (B.9)$$

The explicit forms of $\partial[F]^{-1}/\partial\lambda$ and $\{\partial\varepsilon_T/\partial\lambda\}$ are given in Ref. [18].

Analytic expressions are given in Ref. [19] for the laminate stiffnesses $[A]$, $[B]$, $[D]$ and $[A_s]$, the vectors of thermal effects $\{N_T\}$ and $\{M_T\}$, and their derivatives with respect to each of the material properties of the individual plies and fiber orientation angles.

Appendix C. Fuzzy-set analysis

Concepts of fuzzy logic that are pertinent to the present work are briefly reviewed herein. Detailed reviews of the subject can be found in monographs (e.g., Ref. [20]).

Variability (fuzziness) in a parameter λ is introduced by specifying a membership function (possibility distribution) $\mu(\lambda)$. For convenience, the membership functions of the fuzzy parameters are assumed to be triangular, as shown schematically in Fig. 16. The response quantities are also fuzzy. The analysis used in the present study aims at constructing possibility distributions of the fuzzy response quantities by using the "vertex" method [21] to numerically implement the extension principle.

The membership functions of all fuzzy parameters λ_i ($i = 1, 2, \dots, N$) are discretized by a number of α -cuts. An α -cut of a fuzzy variable λ denotes the interval in which the possibility of λ is at least equal to α (see Fig. 16). Different binary combinations are formed by the left and right end points of the α -cut intervals for

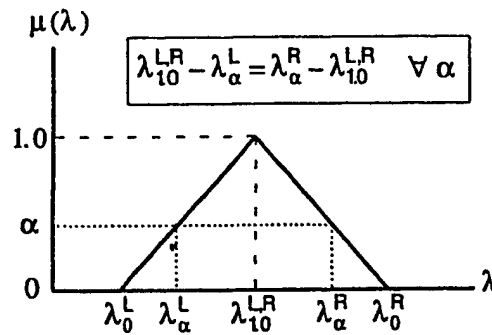


Fig. 16. - Membership function.

all the fuzzy material parameters [21]. For the triangular membership functions of Fig. 16, the number of these combinations per α -cut, $N_{c/\alpha}$, is:

$$N_{c/\alpha} = \begin{cases} 2^N & \text{for } 0 \leq \alpha < 1; \\ 1 & \text{for } \alpha = 1, \end{cases} \quad (\text{C.1})$$

where N is the number of fuzzy parameters. These combinations will be referred to henceforth as $C_{\alpha,j}$ ($j = 1, 2, \dots, N_{c/\alpha}$).

For an output response quantity η which is a function of the fuzzy parameters, $\eta = F(\lambda_1, \lambda_2, \dots, \lambda_N)$, the corresponding α -cut interval is then obtained.

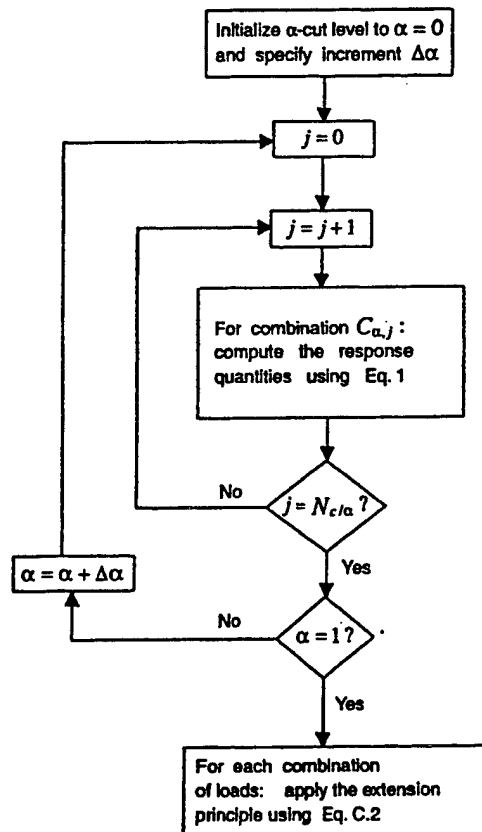


Fig. 17. - Flow chart for the implementation of the Wiley method.

$$[\eta_a^L, \eta_a^R] = [\min_{i,j} \{F(C_{i,j})\}, \max_{i,j} \{F(C_{i,j})\}];$$

$$\zeta \geq \alpha; j = 1, 2, \dots, N_{c/\alpha}. \quad (C.2)$$

The possibility distribution of η is constructed by applying Eq. (C.2) to a sweep of α -cuts at different possibility levels. The accuracy of the distribution is directly proportional to the number of α -cuts. The procedure for numerical implementation of the vertex method is summarized by the flow chart in Fig. 17.

References

- [1] A.K. Noor, W.S. Burton, Computational models for high-temperature multilayered composite plates and shells, *Applied Mechanics Reviews*, ASME 45 (10) (1992) 419-446.
- [2] A.K. Noor, J.M. Peters, Finite element buckling and postbuckling solutions for multilayered composite panels, *Finite Elements in Analysis and Design* 15 (1994) 343-367.
- [3] A.K. Noor (Ed.), Buckling and postbuckling of composite structures, in: *Proceedings of the Symposium on Buckling and Postbuckling of Composite Structures*, ASME Int. Mech. Eng. Congress and Exposition, Chicago, IL, Nov. 6-11, 1994, AD vol. 41/PVP vol. 293, 1994.
- [4] G.J. Turvey, I.H. Marshall, *Buckling and Postbuckling of Composite Plates*, Chapman & Hall, London, 1995.
- [5] L. Librescu, W. Lin, M.P. Nemeth, J.H. Starnes Jr, Thermomechanical postbuckling of geometrically imperfect flat and curved panels taking into account tangential edge constraints, *Journal of Thermal Stresses* 18 (1995) 465-482.
- [6] A.K. Noor, J.H. Starnes, J.M. Peters, Thermomechanical buckling and postbuckling responses of composite panels with skewed stiffeners, *Finite Elements in Analysis and Design* 27 (2) (1997) 193-214.
- [7] A.K. Noor, J.H. Starnes, J.M. Peters, Curved sandwich panels subjected to temperature gradient and mechanical loads, *Journal of Aerospace Engineering*, ASCE 10 (4) (1997) 143-161.
- [8] A.K. Noor, C.M. Andersen, Mixed models and reduced selective integration displacement models for nonlinear shell analysis, *International Journal for Numerical Methods in Engineering* 18 (1982) 1429-1454.
- [9] A.K. Noor, J.M. Peters, Multiple-parameter reduced basis technique for bifurcation and postbuckling analyses of composite plates, *International Journal for Numerical Methods in Engineering* 19 (1983) 1783-1803.
- [10] A.K. Noor, J.M. Peters, Recent advances in reduction methods for instability analysis of structures, *Computers and Structures* 16 (1-4) (1983) 67-80.
- [11] A.K. Noor, J.M. Peters, Reduced basis technique for calculating sensitivity coefficients of nonlinear structural response, *AIAA Journal* 30 (7) (1992) 1840-1847.
- [12] F.A. Brogan, C.C. Rankin, H.D. Cabiness, STAGS users manual, Lockheed Palo Alto Research Laboratory, Palo Alto, CA, Report LMSC P032594, 1994.
- [13] J. Aboudi, *Mechanics of Composite Materials: A Unified Micromechanical Approach*, Elsevier, Amsterdam, 1991.
- [14] R.M. Jones, *Mechanics of Composite Materials*, McGraw-Hill, New York, 1975.
- [15] S.W. Tsai, H.T. Hahn, *Introduction to Composite Materials*, Technomic Publishing Co, Westport, CT, 1980.
- [16] J. Padovan, Anisotropic thermal stress analysis, in: R.B. Hetnarski (Ed.), *Thermal Stresses I*, Elsevier, Amsterdam, 1986, pp. 143-262.
- [17] C.W. Bert, Analysis of plates: 7 structural design and analysis, Part I, in: C.C. Chamis (Ed.), *Composite Materials*, Academic Press, New York, 1975, pp. 149-206.
- [18] A.K. Noor, J.H. Starnes Jr, J.M. Peters, Thermomechanical buckling of multilayered composite panels with cutouts, *AIAA Journal* 32 (7) (1994) 1507-1519.
- [19] A.K. Noor, L.H. Tenek, Stiffness and thermal coefficients for composite laminates, *Journal of Composite Structures* 21 (1) (1992) 57-66.
- [20] T.J. Ross, *Fuzzy logic with engineering applications*, McGraw-Hill, New York, 1995.
- [21] W. Dong, H.C. Shah, Vertex method for computing functions of fuzzy variables, *Fuzzy Sets and Systems* 24 (1987) 65-78.

Reprinted from

Computer methods in applied mechanics and engineering

Comput. Methods Appl. Mech. Engrg. 178 (1999) 431-443

**Accurate determination of transverse normal stresses in
sandwich panels subjected to thermomechanical loadings**

Ahmed K. Noor *, Moinuddin Malik

Center for Advanced Computational Technology, University of Virginia, NASA Langley Research Center, Hampton, VA 23681, USA

Received 1 October 1998



COMPUTER METHODS IN APPLIED MECHANICS AND ENGINEERING
EDITORS: J.H. ARGYRIS, STUTTGART and LONDON
T.J.R. HUGHES, STANFORD, CA
J.T. ODEN, AUSTIN, TX

W. PRAGER
Founding Editor
(deceased 1980)

EDITORIAL ADDRESSES

John H. ARGYRIS
Institut für Computer Anwendungen
Pfaffenwaldring 27
D-70569 STUTTGART
Germany
(Editorial Office)

Thomas J.R. HUGHES
Division of
Applied Mechanics
Durand Building
Room No. 281
Stanford University
STANFORD
CA 94305-4040, USA

J. Tinsley ODEN
The University of Texas
The Texas Institute for
Computational and
Applied Mathematics
Taylor Hall 2.400
AUSTIN
TX 78712, USA

ASSOCIATE EDITORS

K. APPA, Lake Forest, CA
I. BABUŠKA, Austin, TX
A.J. BAKER, Knoxville, TN
T.B. BELYTSCHKO, Evanston, IL
F. BREZZI, Pavia
P.G. CIARLET, Paris
L. DEMKOWICZ, Austin, TX
R.E. EWING, College Station, TX
R. GLOWINSKI, Houston, TX

R.W. LEWIS, Swansea
J.L. LIONS, Paris
F.L. LITVIN, Chicago, IL
H. LOMAX, Moffet Field, CA
L.S.D. MORLEY, Farnborough
N. OLSHOFF, Aalborg
E. ONATE, Barcelona
M. PAPADRAKAKIS, Athens

J. PLANCHARD, Clamart
E. RAMM, Stuttgart
G. STRANG, Cambridge, MA
R.L. TAYLOR, Berkeley, CA
S.Ø. WILLE, Oslo
G. YAGAWA, Tokyo
D. ZHU, Xi'an
O.C. ZIENKIEWICZ, Swansea

ADVISORY EDITORS

M.P. ARNAL, Baden
J.S. ARORA, Iowa City, IA
K.J. BATHE, Cambridge, MA
P.G. BERGAN, Høvik
J.F. BESSELING, Delft
M.O. BRISTEAU, Le Chesnay
C. CANUTO, Turin
J.L. CHENOT, Valbonne
Y.K. CHEUNG, Hong Kong
T.J. CHUNG, Huntsville, AL
T.A. CRUSE, Nashville, TN
E.R. DE ARANTES E OLIVEIRA, Lisbon
J. DONEA, Ispra
A. ERIKSSON, Stockholm
C. FARHAT, Boulder, CO
C.A. FELIPPA, Boulder, CO
C.J. FITZSIMONS, Baden-Dattwil
M. GERADIN, Liège
R. GRUBER, Manno
H.-Å. HÄGGBLAD, Luleå
E.J. HAUG, Iowa City, IA

J.C. HEINRICH, Tucson, AZ
U. HEISE, Aachen
J. HELLESLAND, Oslo
C. HOEN, Oslo
M. HOGGE, Liège
S. IDELSOHN, Santa Fe
L. JOHANSSON, Linköping
C. JOHNSON, Göteborg
M. KAWAHARA, Tokyo
S.W. KEY, Albuquerque, NM
A. KLARBRING, Linköping
M. KLEIBER, Warsaw
P. LADEVEZE, Chachan
A. LEGER, Clamart
B.P. LEONARD, Akron, OH
P. LE TALLEC, Paris
W.K. LIU, Evanston, IL
G. MAIER, Milan
H.A. MANG, Vienna
A. NEEDLEMAN, Providence, RI
M.P. NIELSEN, Lyngby

A.K. NOOR, Hampton, VA
R. OHAYON, Paris
J. PERIAUX, Saint Cloud
QIAN Ling-xi (L.H. Tsien), Dalian
A.K. RAO, Hyderabad
B.D. REDDY, Rondebosch
J.N. REDDY, College Station, TX
E. RIKS, Delft
G.I.N. ROZVANY, Essen
W. SCHIEHLEN, Stuttgart
M.S. SHEPHARD, Troy, NY
E. STEIN, Hannover
P.K. SWEET, Reading
M. TANAKA, Nagano
T.E. TEZDUYAR, Houston, TX
C.W. TROWBRIDGE, Kidlington
H. VAN DER VORST, Utrecht
J.R. WHITEMAN, Uxbridge
K.J. WILLAM, Boulder, CO
T. ZIMMERMANN, Lausanne

Editorial Secretary: Marlies PARSONS

Advertising information. Advertising orders and enquiries can be sent to: Europe and ROW: Rachel Gresle-Farthing, Elsevier Science Ltd., Advertising Department, The Boulevard, Langford Lane, Kidlington, Oxford OX5 1GB, UK; phone: (+44) (1865) 843565; fax: (+44) (1865) 843976; e-mail: r.gresle-farthing@elsevier.co.uk. USA and Canada: Elsevier Science Inc., Mr Tino DeCarlo, 655 Avenue of the Americas, New York, NY 10010-5107, USA; phone: (+1) (212) 633 3815; fax: (+1) (212) 633 3820; e-mail: t.decarlo@elsevier.com. Japan: Elsevier Science K.K., Advertising Department, 9-15 Higashi-Azabu 1-chome, Minato-ku, Tokyo 106, Japan; phone: (+81) (3) 5561-5033; fax: (+81) (3) 5561 5047.

© The paper used in this publication meets the requirements of ANSI/NISO Z39.48-1992 (Permanence of Paper).



ELSEVIER

Comput. Methods Appl. Mech. Engrg. 178 (1999) 431–443

**Computer methods
in applied
mechanics and
engineering**

www.elsevier.com/locate/cma

Accurate determination of transverse normal stresses in sandwich panels subjected to thermomechanical loadings

Ahmed K. Noor*, Moinuddin Malik

Center for Advanced Computational Technology, University of Virginia, NASA Langley Research Center, Hampton, VA 23681, USA

Received 1 October 1998

Abstract

A two-stage computational procedure is presented for the accurate determination of transverse normal stresses in sandwich panels subjected to thermomechanical loadings. The procedure involves the use of a first-order shear deformation model in the first stage, and an iterative process for successive improvement of the accuracy of the displacement and stress fields in the second stage. The effectiveness of the procedure is demonstrated by means of numerical studies of thin and moderately thick flat rectangular sandwich panels. Two sets of boundary conditions are considered; namely, one with all edges simply supported, and the other with two opposite edges simply supported and the remaining two clamped. The displacement components and the transverse shear and normal stresses obtained by the proposed computational procedure are found to be in close agreement with the solutions of the three-dimensional (3-D) continuum models. Published by Elsevier Science S.A.

1. Introduction

Considerable work has been devoted to the development of computational models for studying the various phenomena associated with the response, failure and performance of sandwich panels and shells. The phenomena involved cover a wide range of length scales from local behavior to global structural response. Within each category has evolved a number of models with several levels of sophistication, for each of the core, face sheets, and adhesive layers, as well as for the entire sandwich panel. The modeling approaches used for sandwich panels can be divided into four categories: detailed models; three-dimensional (3-D) continuum models; 2-D plate and shell models; and simplified models. The four categories are described in three survey papers [3,5,13] and two monographs [10,20]. The detailed models and 3-D continuum models are computationally expensive, and the simplified models are inadequate for the accurate determination of transverse normal stresses. Since transverse shear and normal stresses are important for predicting the onset of some of the damage mechanisms in sandwich panels, accurate determination of these stresses is needed. Experience with higher-order 2-D models has shown that unless the 3-D equilibrium equations are used in evaluating the thickness distribution of the transverse stresses, the resulting stresses are inaccurate (see, for example, Refs. [8,11,16]). Because the finite element models based on the first-order shear deformation model are considerably less expensive than those based on higher-order 2-D models, their use in conjunction with post-processing techniques has received increasing attention in recent years (see Refs. [6,12,14,15,17,18]). However, none of the cited references considered transverse normal stresses in thermally loaded sandwich panels.

* Corresponding author. Tel.: +1-757-864-1978; fax: +1-757-864-8089; e-mail: a.k.noor@larc.nasa.gov

In the present paper, the predictor-corrector computational procedure presented by Noor et al. [14] is extended to the determination of transverse normal stresses in sandwich panels subjected to mechanical and thermal loads. The procedure uses an iterative process to correct the through-thickness variation of displacements obtained by the first-order shear deformation model. The effectiveness of the proposed procedure is demonstrated by means of numerical examples of rectangular sandwich panels with composite face sheets. The basis of comparison is taken to be the solutions obtained by using 3-D continuum models for the core and each of the face sheet layers.

2. Basic idea of the computational procedure

The geometry of a sandwich panel, coordinate axes and sign convention for various response quantities are shown in Fig. 1. The basic equations of the first-order shear deformation theory are given in Appendix A. A flow chart of the two-stage computational procedure used herein is shown in Fig. 2. The procedure is based on *a posteriori* generation of through-the-thickness coordinate functions for the displacement components and then the determination of their amplitudes by the Rayleigh–Ritz technique. In the first stage, a first-order shear deformation model is used to calculate the displacements, strains, and in-plane stress components. Subsequently, the transverse stresses are determined by through-the-thickness integration of 3-D equilibrium equations. In the second stage, the transverse strains are determined by using the 3-D constitutive relations. The transverse strains are then integrated in the thickness-direction to generate through-the-thickness distributions of the three displacement components. Numerical experiments have shown that the through-the-thickness shapes of the displacement components so obtained resemble the shapes of the corresponding components obtained by the 3-D model. The differences can be significantly reduced by adjusting the amplitudes and/or adding a linear function in the thickness direction. Consequently, the coordinate functions for each displacement component are generated by decomposing the corresponding through-the-thickness distributions into four components: (a) uniform, (b) linear antisymmetric, (c) nonlinear symmetric and (d) nonlinear antisymmetric, where the symmetry and antisymmetry of these components is defined with respect to the middle plane of the panel (see Fig. 3). The amplitudes of the coordinate functions are determined by using the Rayleigh–Ritz technique. The resulting displacement field is used in conjunction with the 3-D kinematic and constitutive equations to calculate more accurate in-plane stresses. The transverse stresses are then calculated using the 3-D equilibrium equations. The second

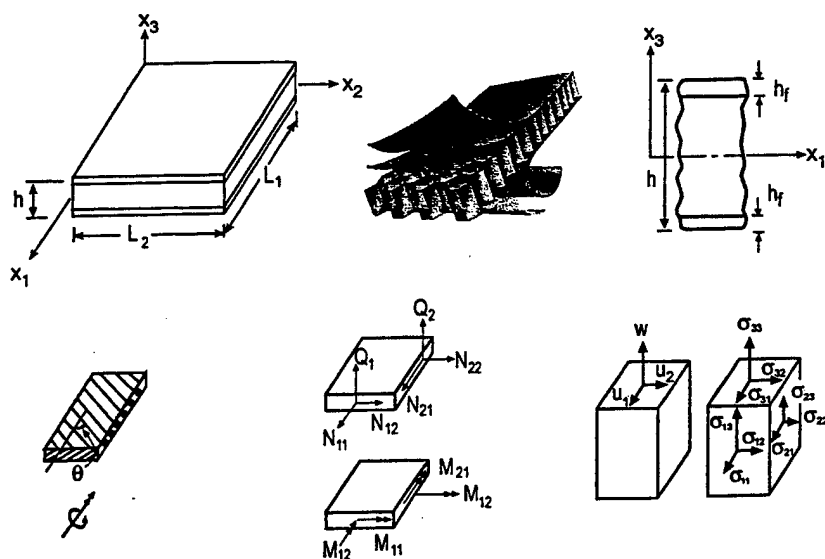


Fig. 1. Sandwich panel: geometry, coordinate axes, and sign convention for generalized displacements, stresses and stress resultants.

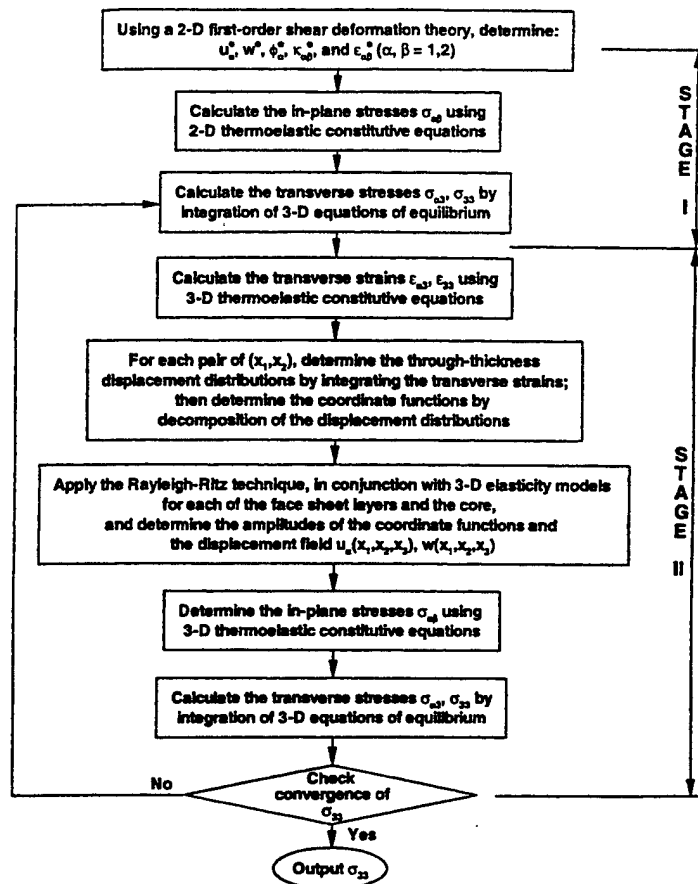
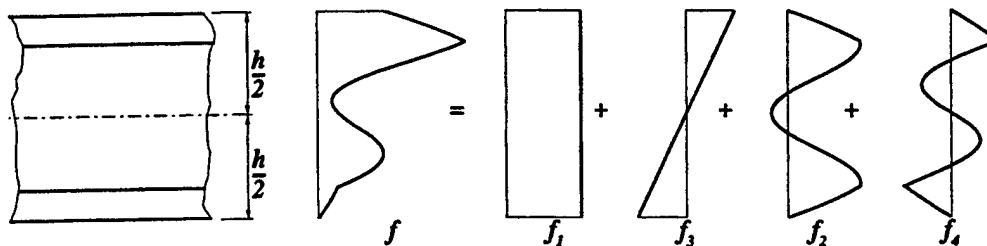


Fig. 2. Flow chart of the computational procedure.

Fig. 3. Decomposition of a through-thickness displacement distribution into four coordinate functions; f refers to any of the displacement components.

stage of the computational procedure is repeated until convergence of the transverse normal stresses is achieved to the desired accuracy.

3. Numerical studies

To assess the effectiveness of the foregoing computational procedure for calculating the transverse normal stresses, several sandwich panels with composite face sheets were analyzed. The panels were subjected to transverse static loading or to a thermal loading, in the form of either a uniform temperature change or a temperature gradient in the thickness direction. Solutions obtained by the foregoing procedure

were compared with those obtained by using 3-D continuum models for each of the face sheet layers and the core. Typical results are presented herein for two problem sets of flat rectangular panels. These problems are: (1) panels with all edges simply supported and (2) panels with two opposite edges simply supported and the other two clamped. Henceforth, the two sets of panels will be referred to as SSSS and SCSC panels. Each panel had a honeycomb metallic core with hexagonal cells and an eight-layer cross-ply face sheet laminate. The face sheet layers are arranged such that the sandwich is symmetric with respect to the middle plane and the 90° layers are adjacent to the core. The effective physical properties of the face sheet layers and core are given in Table 1. The shear correction factors used in conjunction with the first-order shear deformation models are calculated assuming cylindrical bending in each of the x_1 and x_2 directions ([7,19]). The face sheet thickness ratio for the panels, h_f/h , is selected to be 0.1. Two aspect ratios, $L_2/L_1 = 1$ and 2, and two thickness ratios, $h/L_1 = 0.1$ and 0.2, are considered.

Each of the transverse loading, uniform temperature through the thickness, and temperature gradient through the thickness had a double sinusoidal variation in the $x_1 - x_2$ plane, namely,

$$\begin{Bmatrix} p \\ \Delta T_0 \\ \Delta T_1 \end{Bmatrix} = \begin{Bmatrix} p_0 \\ T_0 \\ T_1 \end{Bmatrix} \sin \frac{\pi x_1}{L_1} \sin \frac{\pi x_2}{L_2}. \quad (1)$$

In the presence of both ΔT_0 and ΔT_1 , the total temperature change is given by

$$\Delta T = \Delta T_0 + x_3 \Delta T_1. \quad (2)$$

The selected loading, boundary conditions, and face sheet laminations allowed exact analytic or semi-analytic solutions to be obtained for the governing differential equations of the problems considered. The numerical discretization for the semi-analytic solutions was performed by the differential quadrature method (Refs. [2,4]). Convergence studies were performed for the differential quadrature solutions to insure that the displacements and stresses presented are the converged values.

The coordinate functions of each displacement component were obtained by decomposing its through-the-thickness distributions into four components. A total of twelve coordinate functions were needed for the SSSS panels. In case of the SCSC panels, a set of twelve coordinate functions were generated at each discrete point in the x_2 -direction of the panel.

Typical results for the SSSS and SCSC panels are presented in Figs. 4 and 5 for the displacements; in Figs. 6 and 7 for the transverse shear stresses; and in Figs. 8–10 for the transverse normal stresses. The following designation is used for the curves in these figures. The designation 3-D refers to the solutions obtained from the 3-D continuum model for the face sheets and the core. RRM-1 and RRM-2 refer to the

Table 1
Effective properties of the core and face sheet layers^a

Physical property	Core	Face sheet layer	Units
E_1	0.4328	137.2×10^3	MPa
E_2	0.2864	8.618×10^3	MPa
E_3	2396.8	8.618×10^3	MPa
G_{23}	393.62	2.892×10^3	MPa
G_{13}	521.19	3.758×10^3	MPa
G_{12}	7.9205	3.758×10^3	MPa
ν_{23}	0.37×10^{-4}	0.49	
ν_{13}	0.56×10^{-4}	0.32	
ν_{12}	1.23	0.32	
α_1	0.91×10^{-5}	-0.34×10^{-6}	°C
α_2	0.91×10^{-5}	0.28×10^{-4}	°C
α_3	0.91×10^{-5}	0.28×10^{-4}	°C

^a E , G = Effective elastic and shear moduli; ν , α = Effective Poisson ratios and coefficients of thermal expansion. Subscripts 1, 2, 3 refer to directions x_1, x_2, x_3 (see Fig. 1); c, f refer to core and face sheets.

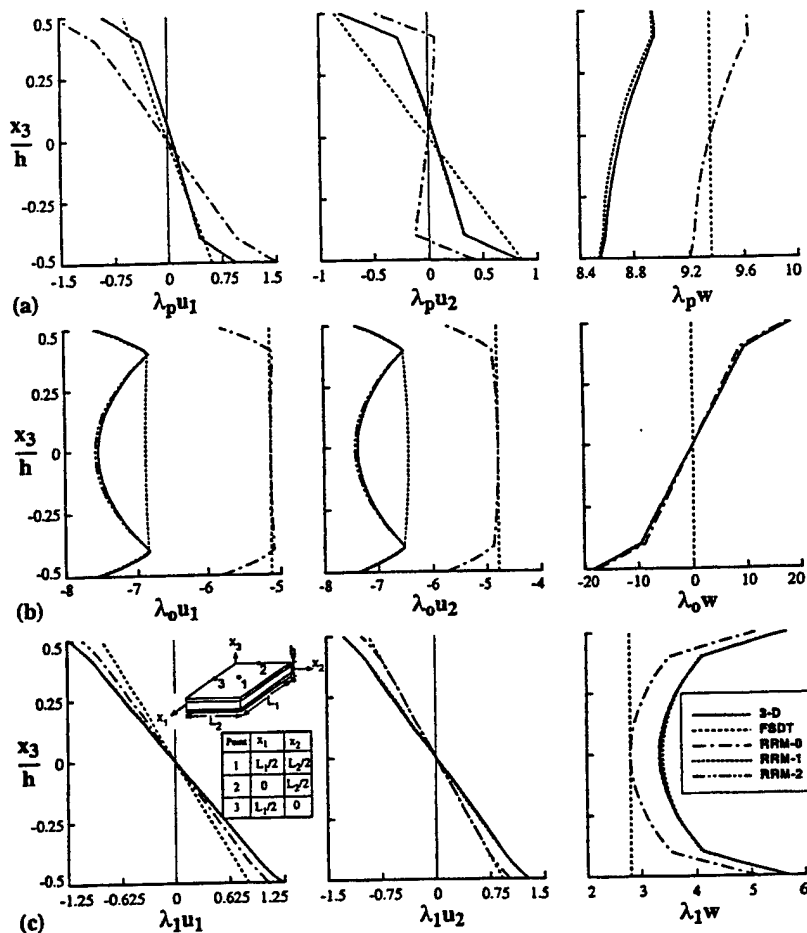


Fig. 4. Through-the-thickness variation of displacement components in an SSSS panel for (a) mechanical, (b) T_0 , and (c) T_1 loadings; the variations of the displacement components w , u_1 , and u_2 are at points 1, 2, and 3, respectively. ($L_2/L_1 = 1$, $h_f/h = 0.1$, $h/L_1 = 0.2$, $\lambda_p = E_{3c}/(p_0 h)$, $\lambda_0 = 10^2 E_{3c} \alpha_{3c} T_0/h$, $\lambda_1 = 10^3 E_{3c} \alpha_{3c} T_1$.)

response quantities obtained after one and two applications of the Rayleigh–Ritz technique. The designation RRM-0 refers to the response quantities obtained at the end of Stage I. In Figs. 4 and 5, the FSDT values are the displacement components obtained from the first-order shear deformation model, and the RRM-0 values are the through-the-thickness displacement distributions from which coordinate functions are generated for the first application of the Rayleigh–Ritz technique. The results presented in Figs. 4–10 are discussed subsequently.

3.1. Through-the-thickness variation of the displacement components

An examination of the through-the-thickness variations of the displacement components shown in Figs. 4 and 5 reveals the following:

1. The displacements obtained by the FSDT model are significantly different from those obtained by the 3-D model both in magnitude and through-the-thickness variations.
2. In almost all cases, the shapes of the through-the-thickness displacement distributions, shown by the RRM-0 curves, are close to the corresponding distributions obtained by the 3-D model. The RRM-0 in-plane displacement components for the mechanical and the T_1 loadings and the RRM-0 transverse components for the T_0 loading differ from the corresponding 3-D components by a multiplier and/or a linear function. The RRM-0 transverse displacements for the mechanical and the T_1 loadings differ from the 3-D components by a multiplier. Although the shapes of the RRM-0 and 3-D curves of the in-plane

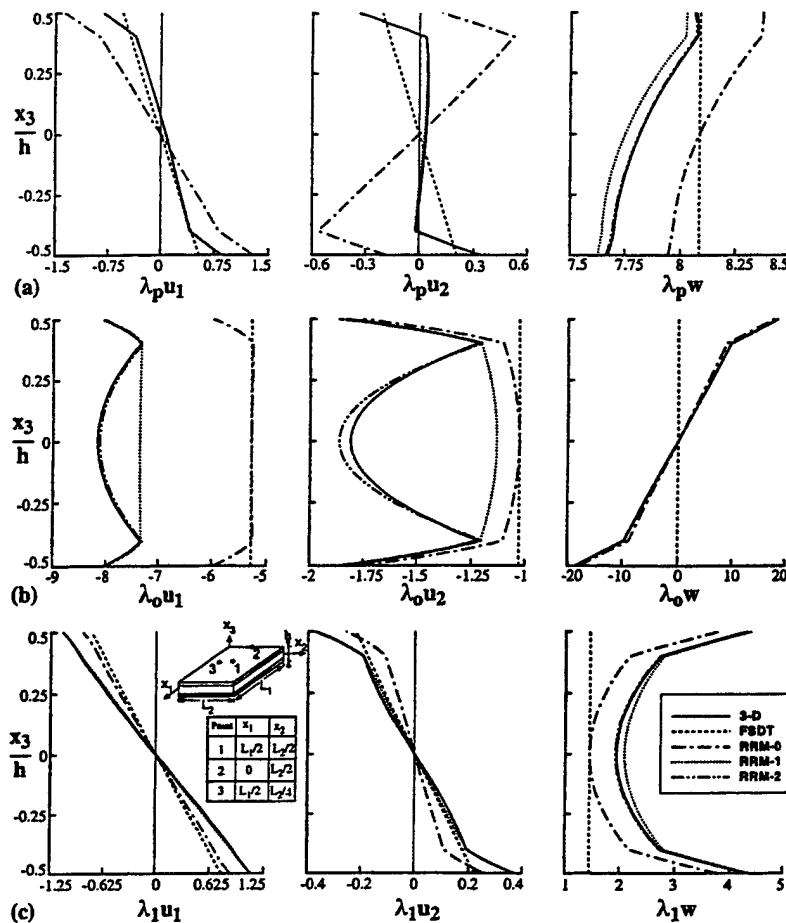


Fig. 5. Through-the-thickness variation of displacement components in an SCSC panel for (a) mechanical, (b) T_0 , and (c) T_1 loadings; the variations of the displacement components w , u_1 , and u_2 are at points 1, 2, and 3, respectively. ($L_2/L_1 = 1$, $h_f/h = 0.1$, $h/L_1 = 0.2$, $\lambda_p = E_{3c}/(p_0 h)$, $\lambda_0 = 10^2 E_{3c} \alpha_{3c} T_0/h$, $\lambda_1 = 10^3 E_{3c} \alpha_{3c} T_1$.)

displacement components for the T_0 loading are very similar in the face sheet regions, the differences in the core region are noticeable.

3. The observations concerning the differences between the through-thickness shapes of the RRM-0 and 3-D displacement components provide the rationale for generating the coordinate functions by decomposition of the through-thickness displacement distributions as illustrated in Fig. 3. With the exception of the in-plane displacement components for the T_0 loading, the displacement components obtained after the first application of the Rayleigh–Ritz technique, i.e., the RRM-1 solutions, are in close agreement with the corresponding 3-D displacement components. The second application of the Rayleigh–Ritz technique yields RRM-2 displacements which are almost indistinguishable from the 3-D displacements.

3.2. Through-the-thickness variation of the transverse shear stresses

An examination of Figs. 6 and 7 reveals that the RRM-0 transverse shear stresses are grossly in error, particularly in the core of the panels. Since the transverse shear stresses are obtained by the integration of the 3-D equilibrium equations, the accuracy of these stresses is directly linked with those of the in-plane stresses. When the accuracy of the in-plane stresses is improved in the second stage of the computational procedure, highly accurate transverse shear stresses are obtained.

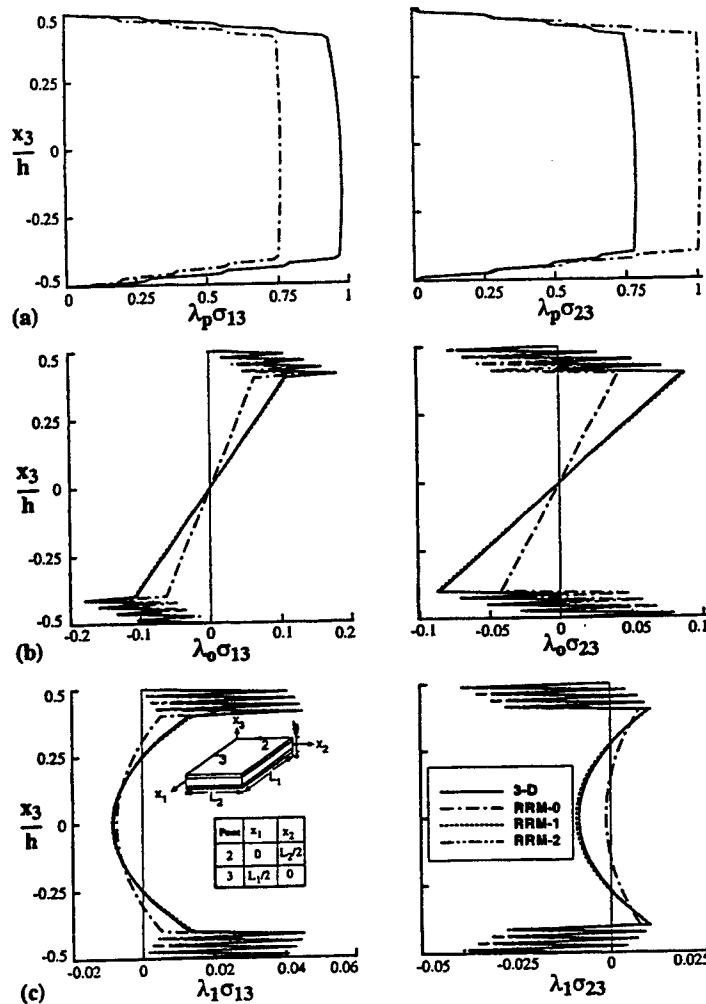


Fig. 6. Through-the-thickness variation of transverse shear stresses in an SSSS panel for (a) mechanical, (b) T_0 , and (c) T_1 loadings; the variations of the stress components σ_{13} and σ_{23} are at points 2 and 3, respectively. ($L_2/L_1 = 1$, $h_f/h = 0.1$, $h/L_1 = 0.2$, $\lambda_p = 1/p_0$, $\lambda_0 = 1/(E_{3c}\alpha_{3c}T_0)$, $\lambda_1 = 1/(E_{3c}\alpha_{3c}T_1h)$.)

3.3. Through-the-thickness variation of the transverse normal stresses

An examination of Figs. 8–10 reveals the following:

1. For the case of the mechanical loading, there is no noticeable difference between the RRM-0 and 3-D predictions of the transverse normal stresses. This can be attributed to the compensating errors in the RRM-0 values of the transverse shear stresses σ_{13} and σ_{23} ; see Figs. 6(a) and 7(a). Therefore, for mechanical loading the second stage of the computational procedure is not needed.
2. For the thermal loadings T_0 and T_1 , the RRM-0 transverse normal stresses are considerably in error. However, the application of the Rayleigh–Ritz technique in the second stage improves the accuracy of the transverse normal stresses. This is demonstrated by the close agreement between the RRM-1 and RRM-2 solutions and the predictions of the 3-D model.

On the basis of the numerical studies conducted, two observations can be noted. First, the through-the-thickness shapes of the displacement components do not vary throughout the panel. This is obviously true for the SSSS panels, and is also true for the SCSC panels. Second, the through-the-thickness shapes for the corresponding displacement components of the SSSS and SCSC panels are similar (see Figs. 4 and 5). These two observations indicate the possibility that the coordinate functions generated for the SSSS panels can be

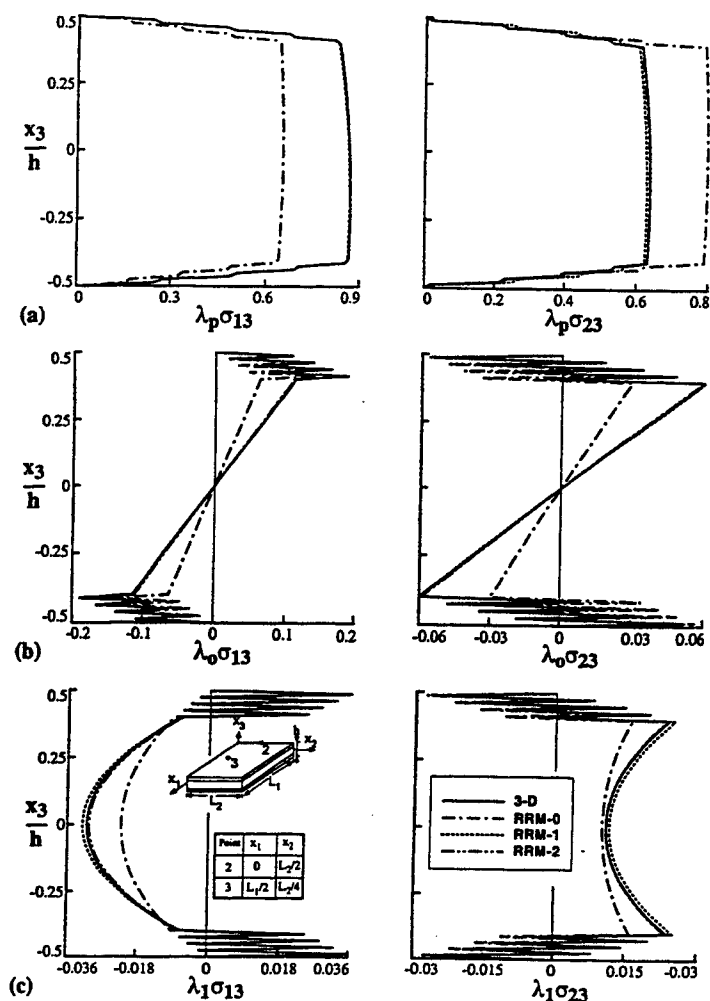


Fig. 7. Through-the-thickness variation of transverse shear stresses in an SCSC panel for (a) mechanical, (b) T_0 , and (c) T_1 loadings; the variations of the stress components σ_{13} and σ_{23} are at points 2 and 3, respectively. ($L_2/L_1 = 1$, $h_f/h = 0.1$, $h/L_1 = 0.2$, $\lambda_p = 1/p_0$, $\lambda_0 = 1/(E_{3c}\alpha_{3c}T_0)$, $\lambda_1 = 1/(E_{3c}\alpha_{3c}T_1h)$.)

used for the SCSC panels, and possibly, for panels with other types of boundary conditions. However, investigation of this possibility was beyond the scope of the present study.

4. Concluding remarks

A two-stage computational procedure, based on *a posteriori* determination of the shape of the displacement variation in the thickness direction, is described for the accurate determination of transverse normal stresses in sandwich panels subjected to thermomechanical loadings. In the first stage, a first-order shear deformation theory is used for evaluating the average through-the-thickness displacements and strains as well as the in-plane stress components. The 3-D equilibrium equations are then used to evaluate the transverse shear and normal stresses. In the second stage, the transverse normal and shear strains are calculated, and are integrated to obtain the distributions of the displacement components in the thickness direction which, in turn, are used to generate the coordinate functions. The Rayleigh–Ritz technique is applied to determine the amplitudes of the coordinate functions. The in-plane stresses are calculated and the transverse shear and normal stresses are determined from the equations of equilibrium. The second

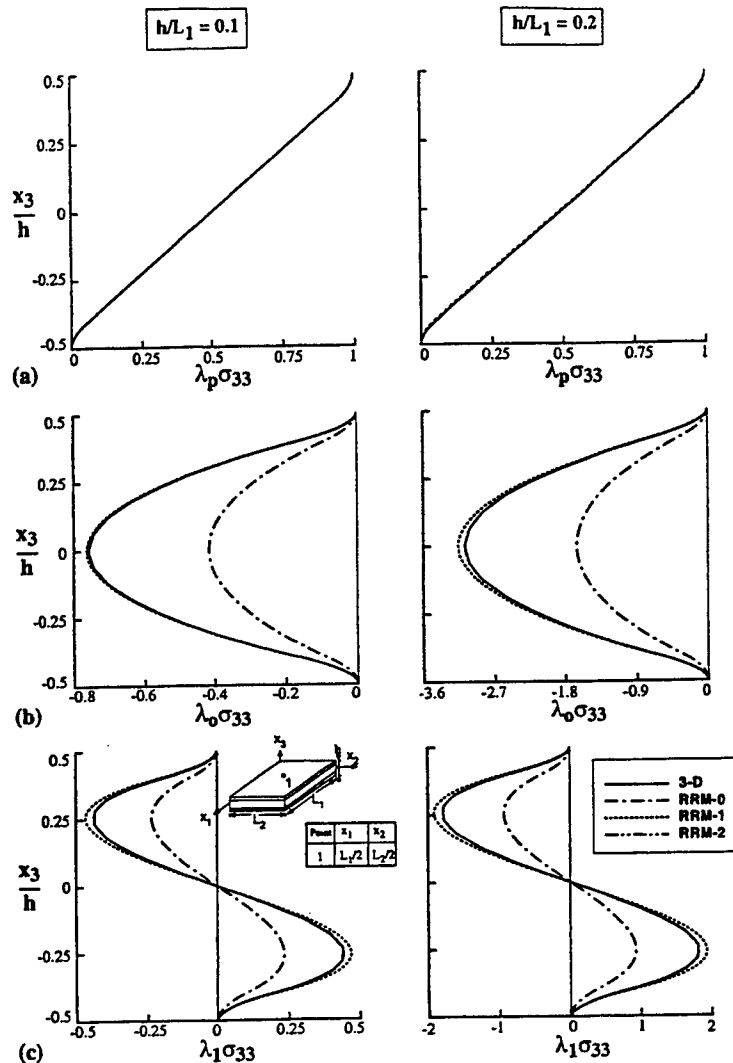


Fig. 8. Through-the-thickness variation of transverse normal stresses in an SSSS panel for (a) mechanical, (b) T_0 , and (c) T_1 loadings; the variation of the stress component σ_{33} is at point 1. ($L_2/L_1 = 1$, $h_f/h = 0.1$, $\lambda_p = 1/p_0$, $\lambda_0 = 10^2/(E_{3c}\alpha_{3c}T_0)$, $\lambda_1 = 10^3/(E_{3c}\alpha_{3c}T_1h)$.)

stage is repeated until convergence of the transverse normal stresses is achieved. All the calculations in the second stage are carried out using solely the 3-D elasticity equations.

The effectiveness of the procedure is demonstrated by means of numerical examples of flat rectangular sandwich panels with composite face sheets. The panels have two opposite edges simply supported and the other two either simply supported or clamped. The panels are subjected to transverse mechanical loading and thermal loadings in the forms of uniform temperature change and temperature gradient through the thickness. The results obtained by using the foregoing computational procedure, with a single application of Rayleigh–Ritz technique, were found to be in close agreement with those obtained by using the 3-D continuum models for each of the face sheet layers and the core.

The computational procedure can be extended to provide an adaptive shape function refinement strategy for the finite element analyses of the sandwich structures. In the present work, due to the particular type of laminates chosen for the composite face sheets, the types of boundary conditions considered, and the forms of the loading functions selected, the coordinate functions were only needed at a limited number of points in the plane of the panel. For more complicated panel geometries, boundary conditions, and loadings, coordinate functions may have to be generated at a larger number of points in the plane of the panel.

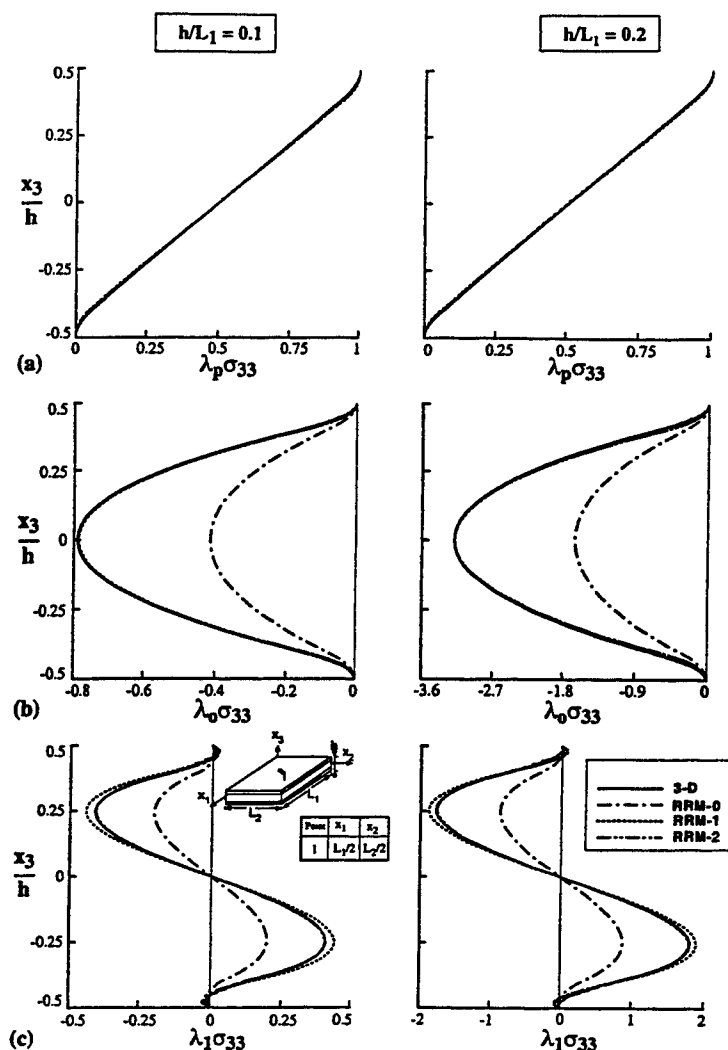


Fig. 9. Through-the-thickness variation of transverse normal stresses in an SCSC panel for (a) mechanical, (b) T_0 , and (c) T_1 loadings; the variation of the stress component σ_{33} is at point 1. ($L_2/L_1 = 1$, $h_f/h = 0.1$, $\lambda_p = 1/p_0$, $\lambda_0 = 10^2/(E_{3c}\alpha_{3c}T_0)$, $\lambda_1 = 10^3/(E_{3c}\alpha_{3c}T_1h)$.)

However, in practical analysis of sandwich panels with complex geometry, the accurate determination of interlaminar stresses is needed only in the critical zones of the structure. This can be done effectively by using as starting values the coordinate functions from the displacement field of a panel with simple types of boundary conditions (e.g., simply supported edges).

Acknowledgements

This work was partially supported by Air Force Office of Scientific Research Grant F49620-96-1-0462 and NASA Grant NAG-1-2016. The authors acknowledge the help of Jeanne Peters and Thea Ganoe, both of the University of Virginia, in various stages of this work.

Appendix A. Fundamental equations of the first-order shear deformation theory used in the present study

The first-order shear deformation model used in the present study is based on the following assumptions:

1. The panels are composed of a number of perfectly bonded layers (face sheet layers and core).
2. A honeycomb core with hexagonal cells is used.

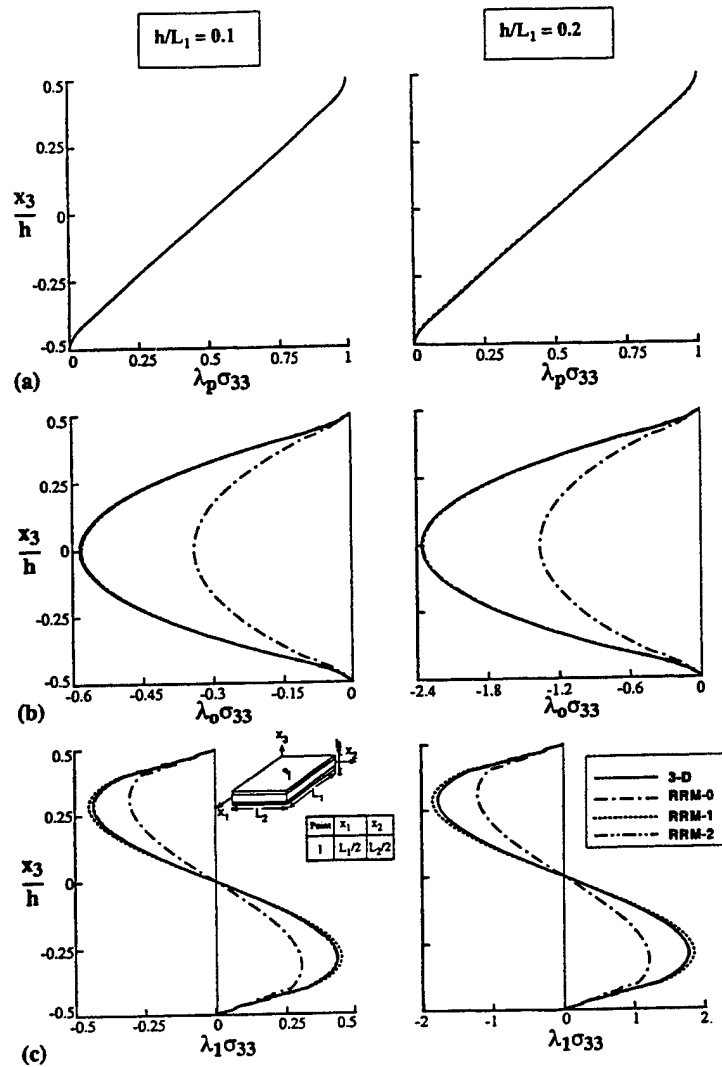


Fig. 10. Through-the-thickness variation of transverse normal stresses in an SCSC panel for (a) mechanical, (b) T_0 , and (c) T_1 loadings; the variation of the stress component σ_{33} is at point 1. ($L_2/L_1 = 2$, $h_f/h = 0.1$, $\lambda_p = 1/p_0$, $\lambda_0 = 10^2/(E_{3c}\alpha_{3c}T_0)$, $\lambda_1 = 10^3/(E_{3c}\alpha_{3c}T_1h)$.)

3. The Aboudi cell method ([1]) is used to evaluate effective properties of the face sheet layers, and an upper-bound energy approach is used to evaluate the effective core properties ([5,9]).

4. Every point of the panel is assumed to possess a single plane of thermoelastic symmetry parallel to the middle surface of the panel.

5. The strains are linear in the thickness direction, i.e.

$$\varepsilon_{x\beta} = \varepsilon_{x\beta}^0 + x_3 \kappa_{x\beta}^0, \quad (3)$$

where $\varepsilon_{x\beta}^0$ and $\kappa_{x\beta}^0$ are extensional strains and curvature changes of the middle surface.

6. The material properties are independent of temperature.

7. The temperature change has a linear variation in the thickness direction as given by Eq. (2).

8. The extensional stresses $\sigma_{x\beta}$ and strains $\varepsilon_{x\beta}$ are related by the generalized plane stress constitutive relations

$$\sigma_{x\beta} = \bar{C}_{x\beta;\gamma\delta} (\varepsilon_{\gamma\delta} - \alpha_{\gamma\delta} \Delta T) \quad (4)$$

where $\bar{C}_{\alpha\beta;\gamma}$ are the generalized plane-stress stiffness coefficients, $\alpha_{;\gamma}$ are the coefficients of thermal expansion, and a repeated index denotes summation over its range (1, 2).

The constitutive relations for the panel are described by the lamination theory, and can be written in the following compact form:

$$\begin{Bmatrix} N_{\alpha\beta} \\ M_{\alpha\beta} \\ Q_z \end{Bmatrix} = \begin{bmatrix} A_{\alpha\beta;\gamma} & B_{\alpha\beta;\gamma} & 0 \\ B_{\alpha\beta;\gamma} & D_{\alpha\beta;\gamma} & 0 \\ 0 & 0 & A_{z3\beta3} \end{bmatrix} \begin{Bmatrix} \epsilon_{;\gamma}^0 \\ \kappa_{;\gamma}^0 \\ 2\epsilon_{\beta3} \end{Bmatrix} - \begin{Bmatrix} N_{\alpha\beta}^{\text{th}} \\ M_{\alpha\beta}^{\text{th}} \\ 0 \end{Bmatrix}, \quad (5)$$

where the A 's, D 's, and B 's with Greek subscripts are the extensional, bending, and bending-extensional coupling coefficients of the panel; $A_{\alpha3\beta3}$ are the transverse shear coefficients of the panel; and $N_{\alpha\beta}^{\text{th}}$ and $M_{\alpha\beta}^{\text{th}}$ are thermal extensional and bending stress resultants given by:

$$\begin{Bmatrix} N_{\alpha\beta}^{\text{th}} \\ M_{\alpha\beta}^{\text{th}} \end{Bmatrix} = \begin{bmatrix} A_{\alpha\beta}^{\text{th}} & B_{\alpha\beta}^{\text{th}} \\ B_{\alpha\beta}^{\text{th}} & D_{\alpha\beta}^{\text{th}} \end{bmatrix} \begin{Bmatrix} \Delta T_0 \\ \Delta T_1 \end{Bmatrix} \quad (6)$$

with

$$\begin{Bmatrix} A_{\alpha\beta}^{\text{th}} \\ B_{\alpha\beta}^{\text{th}} \\ D_{\alpha\beta}^{\text{th}} \end{Bmatrix} = \sum_{k=1}^n \int_{h_{k-1}}^{h_k} \bar{C}_{\alpha\beta;\gamma} \alpha_{;\gamma} \begin{Bmatrix} 1 \\ x_3 \\ x_3^2 \end{Bmatrix} dx_3 \quad (7)$$

where n is the total number of layers of the panel (including both face sheet layers and core) and h_{k-1} , h_k are the distances from the middle surface to the top and bottom faces of the k th layer.

References

- [1] J. Aboudi, *Mechanics of Composite Materials: A Unified Micromechanical Approach*, Elsevier, Amsterdam, 1991.
- [2] R. Bellman, B.G. Kashef, J. Casti, Differential quadrature: A technique for the rapid solution of nonlinear partial differential equations, *Journal of Computational Physics* 10 (1972) 40–52.
- [3] C.W. Bert, Shear deformation and sandwich configuration, in: G.J. Turvey, I.H. Marshall (Eds.), *Buckling and Postbuckling of Composite Plates*, Chapman & Hall, London, 1995, pp. 157–189.
- [4] C.W. Bert, M. Malik, Differential quadrature method in computational mechanics: A review, *Applied Mechanics Reviews* 49 (1996) 1–28.
- [5] W.S. Burton, A.K. Noor, Assessment of continuum models for sandwich panel honeycomb cores, *Computer Methods in Applied Mechanics and Engineering* 145 (1997) 341–360.
- [6] C. Byun, R.K. Kapania, Prediction of interlaminar stresses in laminated plates using global orthogonal interpolation polynomials, *AIAA Journal* 30 (1992) 2740–2749.
- [7] T.S. Chow, On the propagation of flexural waves in an orthotropic laminated plate and its response to an impulsive load, *Journal of Composite Materials* 5 (1971) 306–319.
- [8] J.J. Engblom, O.O. Ochoa, Through-the-thickness stress predictions for laminated plates of advanced composite materials, *International Journal for Numerical Methods in Engineering* 21 (1985) 1759–1776.
- [9] L.J. Gibson, M.F. Ashby, *Cellular Solids: Structure and Properties*, Cambridge University Press, Cambridge, 1997.
- [10] N.J. Hoff, *Monocoque, Sandwich and Composite Aerospace Structures*, Technomic, Lancaster, PA, 1986.
- [11] T. Kant, B. Pandya, A simple finite element formulation of a higher-order theory for unsymmetrically laminated composite plates, *Composite Structures* 9 (1988) 215–246.
- [12] A.K. Noor, Buckling and postbuckling of composite structures, in: *Proceedings of the Symposium on Buckling and Postbuckling of Composite Structures*, ASME International Mechanical Engineering Congress and Exposition, Chicago, AD Vol. 41/PVP Vol. 293, 1994.
- [13] A.K. Noor, W.S. Burton, C.W. Bert, Computational models for sandwich panels and shells, *Applied Mechanics Reviews* 49 (1996) 155–199.
- [14] A.K. Noor, W.S. Burton, J.M. Peters, Predictor-corrector procedures for stress and free vibration analyses of multilayered composite plates and shells, *Computer Methods in Applied Mechanics and Engineering* 82 (1990) 341–363.
- [15] C.W. Pryor Jr., R.M. Barker, A finite-element analysis including transverse shear effects for applications to laminated plates, *AIAA Journal* 9 (1971) 912–923.
- [16] J.N. Reddy, A simple higher-order theory for laminated composite plates, *ASME Journal of Applied Mechanics* 51 (1984) 745–752.

- [17] R. Rolfes, A.K. Noor, H. Sparr, Evaluation of transverse thermal stresses in composite plates based on first-order shear deformation theory, *Computer Methods in Applied Mechanics and Engineering* 167 (1998) 355-368.
- [18] R. Rolfes, K. Rohwer, Improved transverse shear stresses in composite finite elements based on first order shear deformation theory, *International Journal for Numerical Methods in Engineering* 40 (1997) 51-60.
- [19] J.M. Whitney, Shear correction factors for orthotropic laminates under static load, *ASME Journal of Applied Mechanics* 40 (1973) 302-307.
- [20] D. Zenkert, *An Introduction to Sandwich Constructions*, Chameleon Press, London, 1995.

INFORMATION FOR CONTRIBUTORS

Manuscripts should be sent in triplicate to one of the Editors. All manuscripts will be refereed. Manuscripts should preferably be in English. They should be typewritten, double-spaced, first copies (or clear Xerox copies thereof) with a wide margin. Abstracts, footnotes and lists of references should also be double-spaced. All pages should be numbered (also those containing references, tables and figure captions). Upon acceptance of an article, author(s) will be asked to transfer copyright of the article to the publisher. This transfer will ensure the widest possible dissemination of information.

Abstracts

The text of a paper should be preceded by a summary in English. This should be short, but should mention all essential points of the paper.

Figures and tables

The drawings for the figures must be originals, drawn in black India ink in large size and carefully lettered, or printed on a high-quality laser printer. The lettering as well as the details should have proportionate dimensions, so as not to become illegible or unclear after the usual reduction by the printers; in general, the figures should be designed for a reduction factor of two or three. Mathematical symbols should be entered in italics, where appropriate. Each figure should have a number and a caption; the captions should be collected on a separate sheet. The appropriate place of a figure should be indicated in the margin. Tables should be typed on separate sheets. Each table should have a number and a title. The appropriate places for the insertion of tables should be indicated in the margin. Colour illustrations can be included and will be printed in colour at no charge if, in the opinion of the Editors, the colour is essential. If this is not the case, the figures will be printed in black and white unless the author is prepared to pay the extra costs arising from colour reproduction.

Formulae

Displayed formulae should be numbered and typed or clearly written by hand. Symbols should be identified in the margin, where they occur for the first time.

References

In the text, reference to other parts of the paper should be made by section (or equation) number, but not by page number. References should be listed on a separate sheet in the order in which they appear in the text.

COMPLETE INSTRUCTIONS TO AUTHORS are published in every last issue of a volume, and copies can also be obtained from the Editors and the Publisher, Elsevier Science B.V., P.O. Box 1991, 1000 BZ Amsterdam, The Netherlands.

Instructions for LaTeX manuscripts

The LaTeX files of papers that have been accepted for publication may be sent to the Publisher by e-mail or on a diskette (3.5" or 5.25" MS-DOS). If the file is suitable, proofs will be produced without rekeying the text. The article should be encoded in Elsevier-LaTeX, standard LaTeX, or AMS-LaTeX (in document style "article"). The Elsevier-LaTeX package, together with instructions on how to prepare a file, is available from the Publisher. This package can also be obtained through the Elsevier WWW home page (<http://www.elsevier.nl/>), or using anonymous FTP from the Comprehensive TeX Archive Network (CTAN). The host-names are: <ftp.dante.de>, <ftp.tex.ac.uk>, <ftp.shsu.edu>; the CTAN directories are: [/pub/tex/macros/latex209/contrib/elsevier](#), [/pub/archive/macros/latex209/contrib/elsevier](#), [/tex-archive/macros/latex209/contrib/elsevier](#), respectively. No changes from the accepted version are permissible, without the explicit approval of the Editor. The Publisher reserves the right to decide whether to use the author's file or not. If the file is sent by e-mail, the name of the journal should be mentioned in the "subject field" of the message to identify the paper. Authors should include an ASCII table (available from the Publisher) in their files to enable the detection of transmission errors.

Publication information:

Computer Methods in Applied Mechanics and Engineering (ISSN 0045-7825). For 1999 volumes 164–176 are scheduled for publication. Subscription prices are available upon request from the Publisher. Subscriptions are accepted on a prepaid basis only and are entered on a calendar year basis. Issues are sent by surface mail except to the following countries where Air delivery via SAL mail is ensured: Argentina, Australia, Brazil, Canada, Hong Kong, India, Israel, Japan, Malaysia, Mexico, New Zealand, Pakistan, PR China, Singapore, South Africa, South Korea, Taiwan, Thailand, USA. For all other countries airmail rates are available upon request. Claims for missing issues should be made within six months of our publication (mailing) date.

Orders, claims, and product enquiries: please contact the Customer Support Department at the Regional Sales Office nearest you:

New York: Elsevier Science, PO Box 945, New York, NY 10159-0945, USA; phone: (+1) (212) 633 3730 [toll free number for North American customers: 1-888-4ES-INFO (437-4636)]; fax: (+1) (212) 633 3680; e-mail: usinfo-f@elsevier.com

Amsterdam: Elsevier Science, PO Box 211, 1000 AE Amsterdam, The Netherlands; phone: (+31) 20 4853757; fax: (+31) 20 4853432; e-mail: nlinfo-f@elsevier.nl

Tokyo: Elsevier Science, 9-15 Higashi-Azabu 1-chome, Minato-ku, Tokyo 106, Japan; phone: (+81) (3) 5561 5033; fax: (+81) (3) 5561 5047; e-mail: info@elsevier.co.jp

Singapore: Elsevier Science, No. 1 Temasek Avenue, #17-01 Millenia Tower, Singapore 039192; phone: (+65) 434 3727; fax: (+65) 337 2230; e-mail: asiainfo@elsevier.com.sg

Rio de Janeiro: Elsevier Science, Rua Sete de Setembro 111/16 Andar, 20050-002 Centro, Rio de Janeiro – RJ, Brazil; phone: (+55) (21) 509 5340; fax: (+55) (21) 507 1991; e-mail: elsevier@campus.com.br [Note (Latin America): for orders, claims and help desk information, please contact the Regional Sales Office in New York as listed above]

INTERNATIONAL JOURNAL FOR NUMERICAL METHODS IN ENGINEERING
Int. J. Numer. Meth. Engrg. 47, 000-000 (2000)

Accurate determination of transverse normal stresses in hybrid laminated panels subjected to electro-thermo-mechanical loadings

Moinuddin Malik and Ahmed K. Noor*

*University of Virginia Center for Advanced Computational Technology, NASA Langley Research Center,
 Hampton, VA 23681, U.S.A.*

should be

panels

SUMMARY

A computational procedure is presented for the accurate determination of transverse normal stresses in hybrid laminated panels consisting of fibre-reinforced composite and piezoelectric layers, and subjected to mechanical, thermal and electrical loadings. The three key elements of the procedure are: (a) using through-the-thickness distributions of the response quantities of a simpler problem to effect a dimensional reduction in the given problem, (b) adaptive improvement of the thickness distributions of the response quantities through successive applications of the Rayleigh-Ritz technique, in conjunction with the three-dimensional electro-thermo-elasticity equations for each layer, and (c) using three-dimensional divergence equations for evaluating the transverse stresses and the transverse component of the electric field.

The effectiveness of the procedure is demonstrated by means of two numerical examples of rectangular, hybrid laminated panels. The panels had two opposite edges clamped and the other two either simply supported or clamped. In both cases, the simpler panels were the panels of the same lamination and geometry as the example problems but with all edges simply supported. Published in 2000 by John Wiley & Sons, Ltd. This article is a U.S. government work and is in the public domain in the United States.

KEY WORDS: interlaminar transverse stresses; hybrid composite piezoelectric panels; smart structures; differential quadrature method

1. INTRODUCTION

The potential of combining piezoelectric layers and fibre-reinforced composite structures to alter the structural response through sensing, actuation and control has stimulated interest in the development of theories and computational models for hybrid panels consisting of fibre-reinforced composite and piezoelectric layers. Some of the computational models developed for the hybrid panels are similar to those used for laminated composite panels, and include: (1) three-dimensional piezoelectricity models [1, 2], and two-dimensional models, which can be classified into: (a) global through-the-thickness approximation models [3-8], and (b) discrete-layer models based on piece-wise displacement/stress approximations in the thickness direction [9-11].

delete

* Correspondence to: Ahmed K. Noor, NASA Langley Research Center, University of Virginia, Mailstop 201, Hampton, VA 23681, U.S.A. E-mail: a.k.noor@larc.nasa.gov

Contract grant sponsor: Air Force Office of Scientific Research; Contract grant number: F49620-96-1-0462
 Contract grant sponsor: NASA; Contract grant number: NAG-1-2016

This article is a U.S. government work and is in the public domain in the United States.

CCC 0029-5981/99/000000-00\$17.50

Published in 2000 by John Wiley & Sons, Ltd.

Received 8 February 1999

insert comma, therefore,

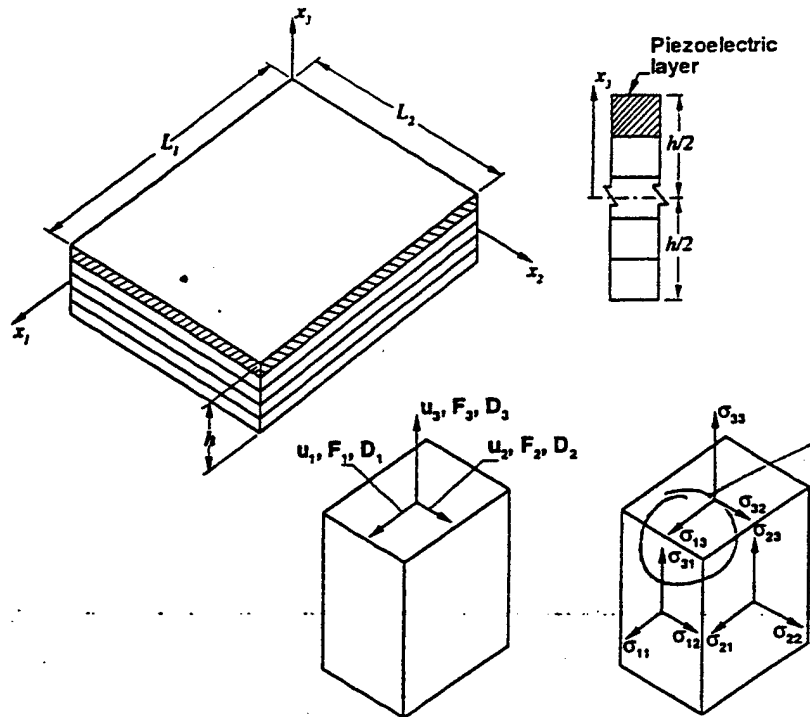


Figure 1. Hybrid panel: geometry, co-ordinate axes, and sign convention for displacements, stresses, and electric response quantities

should be switched (see enclosure - new original figure)

The use of three-dimensional models for predicting the electroelastic response characteristics of panels with complicated geometry and loadings is computationally expensive and, therefore, may not be feasible for practical problems. Experience with two-dimensional models has shown them to be inadequate for the accurate determination of transverse response quantities, which are used for predicting the onset of some of the damage mechanisms in multilayered structures. This is particularly true for the models based on lower-order approximations of the response quantities in the thickness direction. Several post-processing techniques have been proposed, in conjunction with two-dimensional models, for the accurate determination of transverse stresses in multilayered composite panels which can be applied to hybrid panels as well. These are based on the use of: (a) three-dimensional equilibrium equations [12-14], (b) simplifying assumptions [15, 16], and (c) predictor-corrector approaches [17-19]. Although accurate transverse shear stresses can be generated by the first two techniques, the accuracy of the transverse normal stresses generated by these techniques is not adequate. This is particularly true for thermal loadings. see, for instance [16].

The objective of this work is to present a computational procedure for the accurate determination of transverse normal stresses in hybrid panels, having perfectly bonded fibre-reinforced composite and piezoelectric layers, and subjected to mechanical, thermal, and electrical loadings. The procedure proposed herein has evolved from the ideas presented in an earlier work of the present authors [19]. The effectiveness of the proposed procedure is demonstrated by means of numerical examples. The geometry of a hybrid panel and the sign convention of the displacements, stresses, and electric response quantities are shown in Figure 1.

delete
S

Corrected
Figure 1

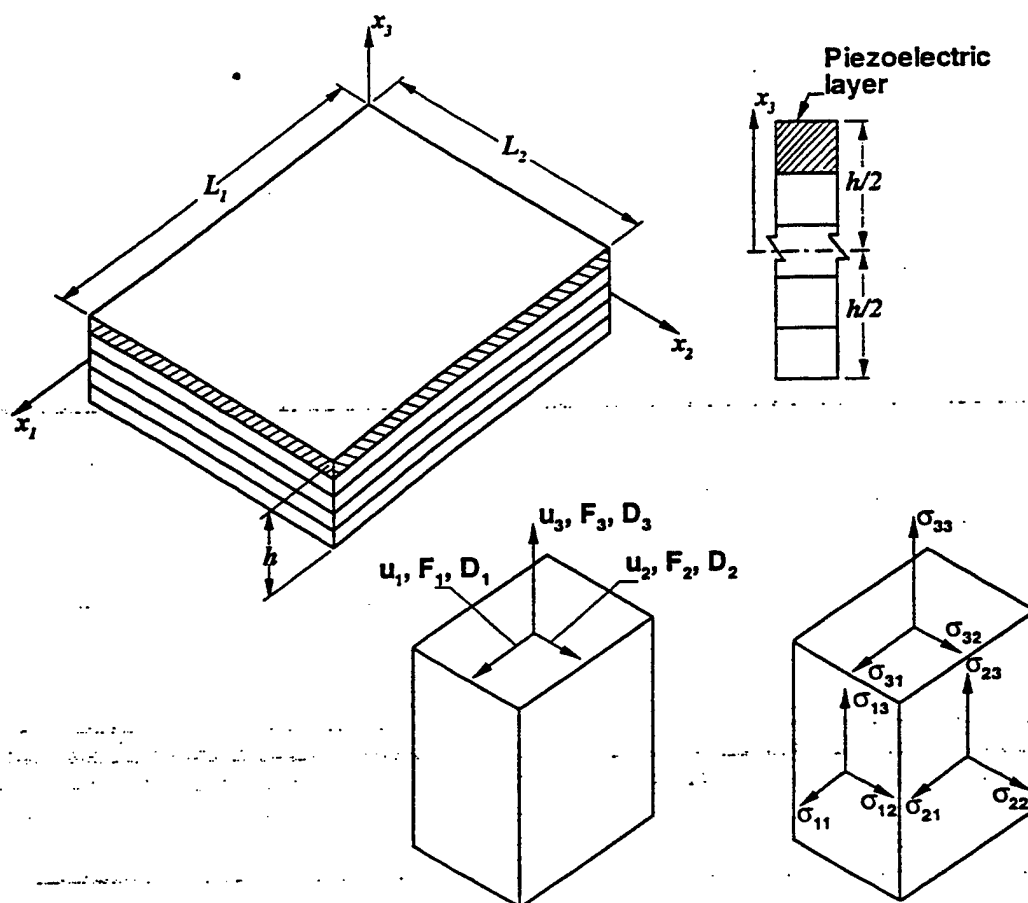


Figure 1

2. BASIC IDEA

The basic idea of the proposed computational procedure is to generate the response of a given panel through successive improvements of the response of a simpler panel, having the same lamination as the given panel, but simpler boundary conditions, loading distribution, and/or geometry. It is convenient to select the simpler panel such that exact, analytical, semianalytical, or inexpensive numerical solutions can be obtained for the three-dimensional continuum equations. The three key elements of the procedure are: (a) using through-the-thickness distributions of the response quantities of a simpler problem to effect a dimensional reduction in the given problem, (b) adaptive improvement of the thickness distributions of the response quantities through successive applications of the Rayleigh–Ritz technique, in conjunction with the three-dimensional electro-thermo-elasticity equations for each layer, and (c) using three-dimensional divergence equations for evaluating the transverse stresses and the transverse component of the electric field.

The rationale of the above idea is that extensive numerical studies have demonstrated that through-the-thickness distributions of the displacement components and electric potential in hybrid composite/piezoelectric panels are more sensitive to the lamination parameters and loading type than to the boundary conditions and geometry of the panel. This is particularly true in the interior of the panel. To verify this observation, each of the thickness distributions of the three displacements u_1, u_2, u_3 and the electric potential ϕ , obtained from the full three-dimensional solutions, are decomposed into four components: uniform, linear antisymmetric, non-linear symmetric, and non-linear antisymmetric (where the symmetry and antisymmetry are defined with respect to the middle plane of the panel). Each of the components is normalized by dividing by its maximum value. Henceforth, these normalized components will be referred to as (through-the-thickness) co-ordinate functions. The non-linear symmetric and antisymmetric co-ordinate functions of u_1, u_2, u_3 and ϕ at different (x_1, x_2) locations of a fully clamped panel with four cross-ply layers and one piezoelectric layer are shown in Figure 2 along with the corresponding co-ordinate functions of a simply supported panel. The panels are subjected to transverse loading with sinusoidal variations in both the x_1 - and x_2 -directions.

An examination of Figure 2 reveals that, with the exception of the non-linear antisymmetric u_2 and symmetric u_3 components, the remaining non-linear co-ordinate functions of the displacements and electric potential of the clamped panel are similar to those of the simply supported panel. The distributions of the non-linear co-ordinate functions for the thermal and electric loadings were found to be similar to those of Figure 2 for mechanical loading. Therefore, it is reasonable to use the co-ordinate functions of the displacements and electric potential of a simply supported panel to effect a dimensional reduction in a panel with different boundary conditions.

For thin and medium-thick panels, the amplitudes of the uniform and linear antisymmetric co-ordinate functions of u_1, u_2, u_3 and ϕ are found to be larger, by an order of magnitude or more than those of the non-linear co-ordinate functions. This justifies the use of first-order shear deformation theory for predicting the global response characteristics of thin and medium-thick panels. However, the non-linearities of the co-ordinate functions of the displacement components in Figure 2 can have significant effect on the transverse stresses, and possibly on the in-plane stresses, in the panel. This is particularly true for the thermal loadings. As to be expected, the amplitudes of the non-linear co-ordinate functions increase, and subsequently, their effect on the overall state of stresses, with increase in the panel thickness.

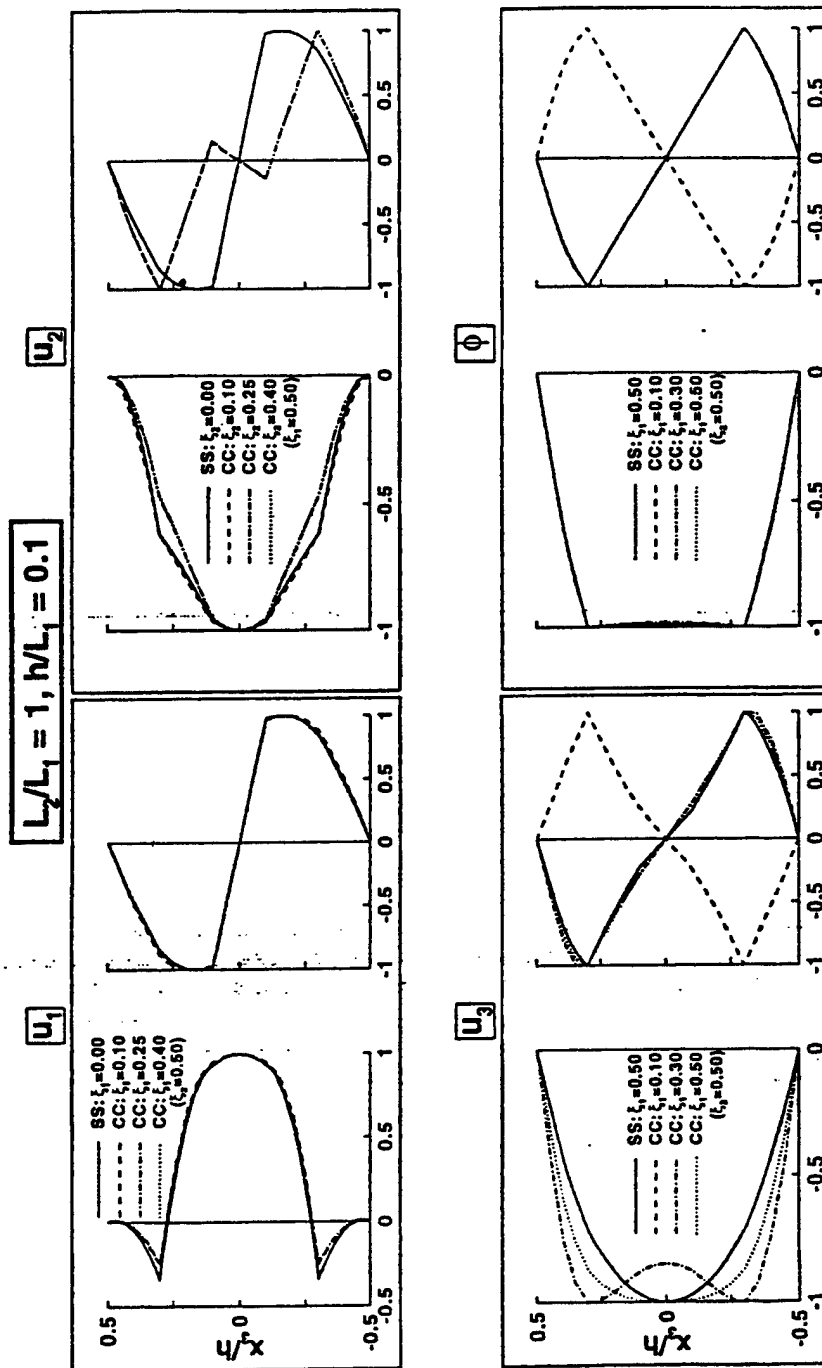


Figure 2. Normalized, symmetric and antisymmetric, non-linear co-ordinate functions of the displacement components and electric potential for Clamped (CC) and Simply Supported (SS) panels subjected to sinusoidal transverse loading ($\xi_2 = \eta_2/L_2$; $x = 1, 2$)

DETERMINATION OF TRANSVERSE NORMAL STRESSES

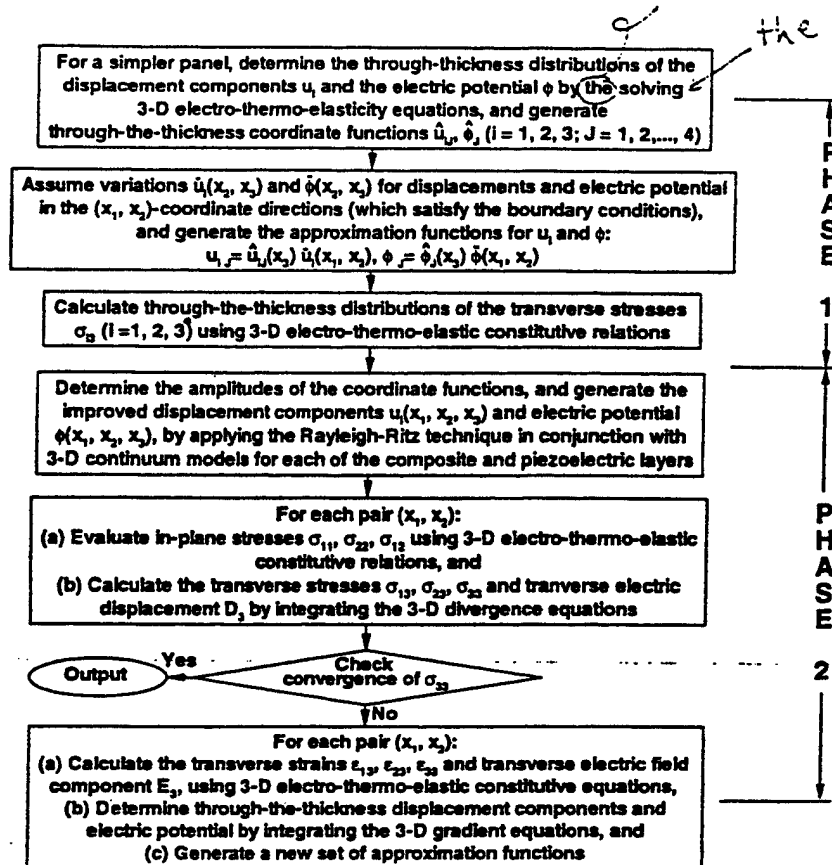


Figure 3. Flowchart of the computational procedure

3. THE COMPUTATIONAL PROCEDURE

A flow chart of the computational procedure for evaluating the transverse stresses is shown in Figure 3. The procedure can be conveniently divided into two distinct phases:

(a) *Initial phase*: This phase consists of the following steps.

1. Generation of through-the-thickness distributions of the displacements and electric potential for a simpler panel, having the same lamination as the original panel, but with simpler boundary conditions, loading distributions, and/or geometry.
2. Generation of approximation functions for the displacement components and electric potential, by multiplying each of through-the-thickness co-ordinate functions of the simpler panel by the functions of the in-plane co-ordinates, which satisfy the boundary conditions of the original panel.

1000000
Figure 3

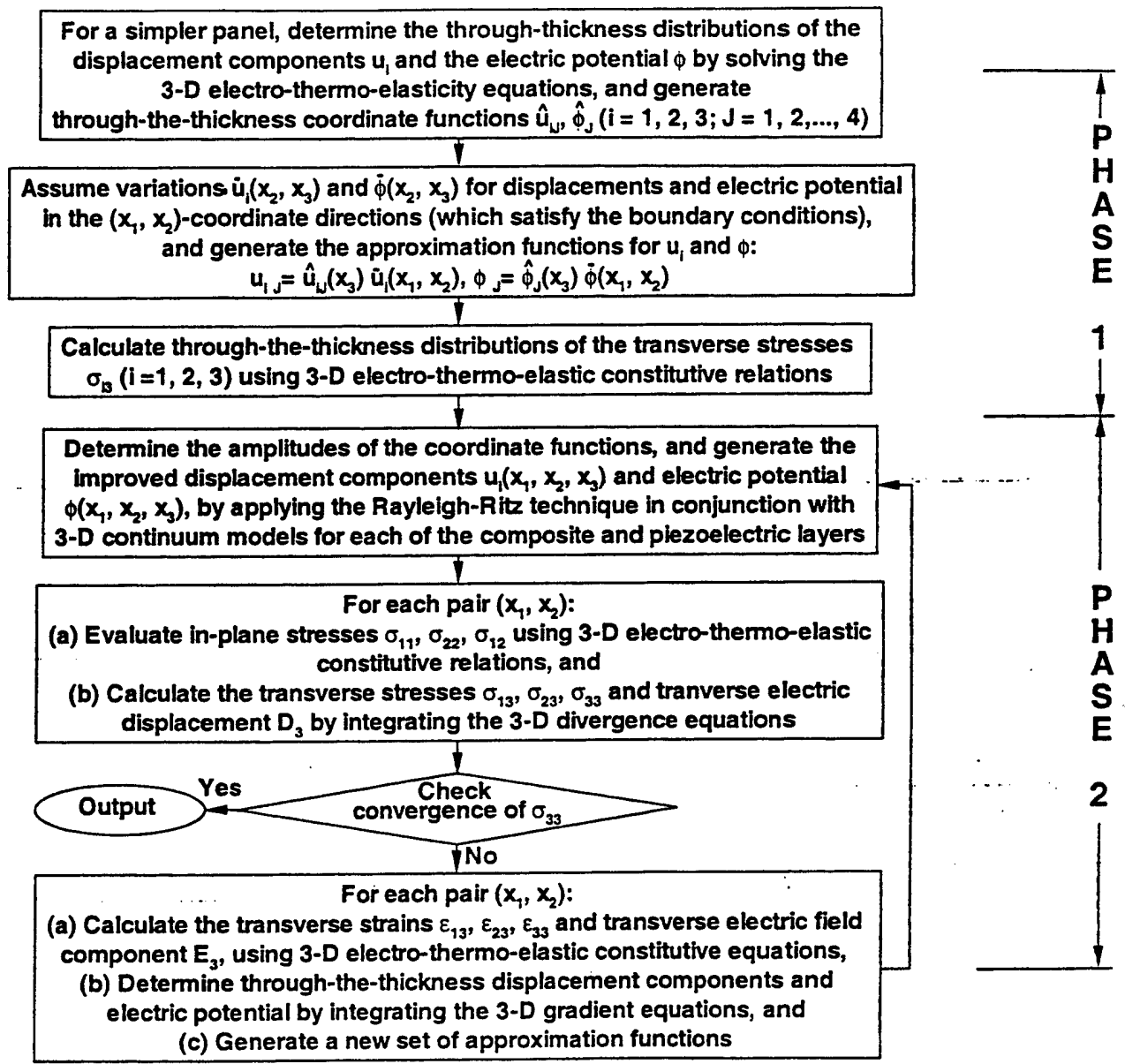


Figure 3

(b) *Successive improvement phase*: This phase consists of the following steps.

1. Determination of the amplitudes of the co-ordinate functions by using the Rayleigh–Ritz technique in conjunction with the three-dimensional equations of electro-thermo-elasticity (see the appendix).
2. Determination of the in-plane stresses and in-plane electric displacements using three-dimensional constitutive relations.
3. Evaluation of transverse stresses and transverse component of electric displacement using the three-dimensional divergence equations.
4. Generation of improved through-the-thickness distributions of the displacements and electric potential from the three-dimensional gradient relations for successive applications of the Rayleigh–Ritz technique.

4. NUMERICAL STUDIES

To assess the effectiveness of the foregoing computational procedure for calculating the transverse normal stresses, several flat, rectangular, hybrid composite/piezoelectric laminated panels were analysed. The panels analysed consisted of four graphite-epoxy cross-ply layers with fibre orientations $[90^\circ/0^\circ/90^\circ/0^\circ]$ and one PZT-5A piezoelectric layer at the top. The effective properties for the fibre-reinforced and piezoelectric layers are given in Table I. Two aspect ratios, $L_2/L_1 = 1$ and 2, and two thickness ratios, $h/L_1 = 0.1$ and 0.2, are considered. The layers are assumed to have equal thicknesses. Each of the panels is subjected to four types of loadings, namely, (1) transverse static load (p) at the bottom surface, (2) uniform temperature change (ΔT_0) through the panel thickness, (3) linear temperature gradient through the panel thickness (ΔT_1), and (4) electric potential at the bottom surface (ϕ). Henceforth, these loadings are referred to as p -, T_0 -, T_1 - and ϕ -loadings, respectively. Each of these loadings has a sinusoidal variation in both the x_1 - and x_2 -directions, namely,

$$\begin{Bmatrix} p \\ \Delta T_0 \\ \Delta T_1 \\ \phi \end{Bmatrix} = \begin{Bmatrix} p_0 \\ T_0 \\ x_3 T_1 \\ \phi_0 \end{Bmatrix} \sin \frac{\pi x_1}{L_1} \sin \frac{\pi x_2}{L_2} \quad (1)$$

insert comma

Typical results are presented herein for two sets of panels, namely: (1) panels with two edges simply supported and the other two clamped, and (2) panels with all edges clamped. For both sets of panels, the simpler panel is taken to be the corresponding panel with the same lamination and geometry, but with all edges simply supported. Henceforth, the two sets of panels and the simpler panel will be referred to as SC, CC and SS panels, respectively.

The individual layers of each panel are assumed to be homogeneous orthotropic with the principal material directions coincident with the co-ordinate directions. For the selected loading, full three-dimensional solutions were obtained for the simpler (SS) panel. For the SC and CC panels, numerical discretization, using the differential quadrature method [20, 21], had to be used in the x_2 - and (x_1, x_2) -directions, respectively. A set of 16 co-ordinate functions were generated at each discrete point in the x_2 -direction for the SC panel, and at each discrete point in the (x_1, x_2) -plane for the CC panel. The standard of comparison in each case was taken to be the solution, obtained using the differential quadrature method, for the full three-dimensional continuum models of each

Table I. Material properties of the graphite-epoxy and the PZT-5A layers used in the present study

Physical constant	Graphite-epoxy layer	PZT-5A layer
E_1 (10^9 Pa)	181.0	61.0
E_2 (10^9 Pa)	10.3	61.0
E_3 (10^9 Pa)	10.3	53.2
G_{12} (10^9 Pa)	7.17	22.6
G_{13} (10^9 Pa)	7.17	21.1
G_{23} (10^9 Pa)	2.87	21.1
ν_{12}	0.28	0.35
ν_{13}	0.28	0.38
ν_{23}	0.33	0.38
α_{11} ($10^{-6}/^\circ\text{C}$)	0.02	1.5
α_{22} ($10^{-6}/^\circ\text{C}$)	22.5	1.5
α_{33} ($10^{-6}/^\circ\text{C}$)	22.5	2.0
d_{111} (10^{-12} m/V)	0	-171.0
d_{222} (10^{-12} m/V)	0	-171.0
d_{333} (10^{-12} m/V)	0	374.0
d_{313} (10^{-12} m/V)	0	584.0
d_{323} (10^{-12} m/V)	0	584.0
κ_{11} (10^{-8} Farad/m)	1.53	1.53
κ_{22} (10^{-8} Farad/m)	1.53	1.53
κ_{33} (10^{-8} Farad/m)	1.53	1.50
r_3 (Coulomb/m ² /°C)	0	0.0007

Note: The crystal class of the PZT-5A layer is orthorhombic mm^2 . Herein, only the non-zero values of the various material properties are tabulated.

delete A

2 is not a superscript
add period

of the composite and piezoelectric layers. Convergence studies were performed to insure that the response characteristics presented are the converged values.

Typical results for the displacements in the SC and CC panels are presented in Figures 4 and 5; in Figure 6 for the electric response quantities, namely, the electric potential and transverse components of the electric field and electric displacement; in Figures 7 and 8 for the transverse shear stresses; and in Figures 9–11 for the transverse normal stresses. The following designation is used in these figures: 3-D refers to the solutions obtained using the full three-dimensional models; RR-1, RR-2, ..., RR-4 refer to the predictions of the proposed computational procedure obtained after one, two, ..., four applications of the Rayleigh–Ritz technique. As to be expected, the convergence of the response quantities, obtained by the foregoing procedure, in the interior of the panel was faster than that for the corresponding quantities near the boundaries. The results presented in Figures 4–11 are discussed subsequently.

4.1. Through-the-thickness variation of the displacement components

An examination of the through-the-thickness variations of the displacement components shown in Figures 4 and 5 reveals:

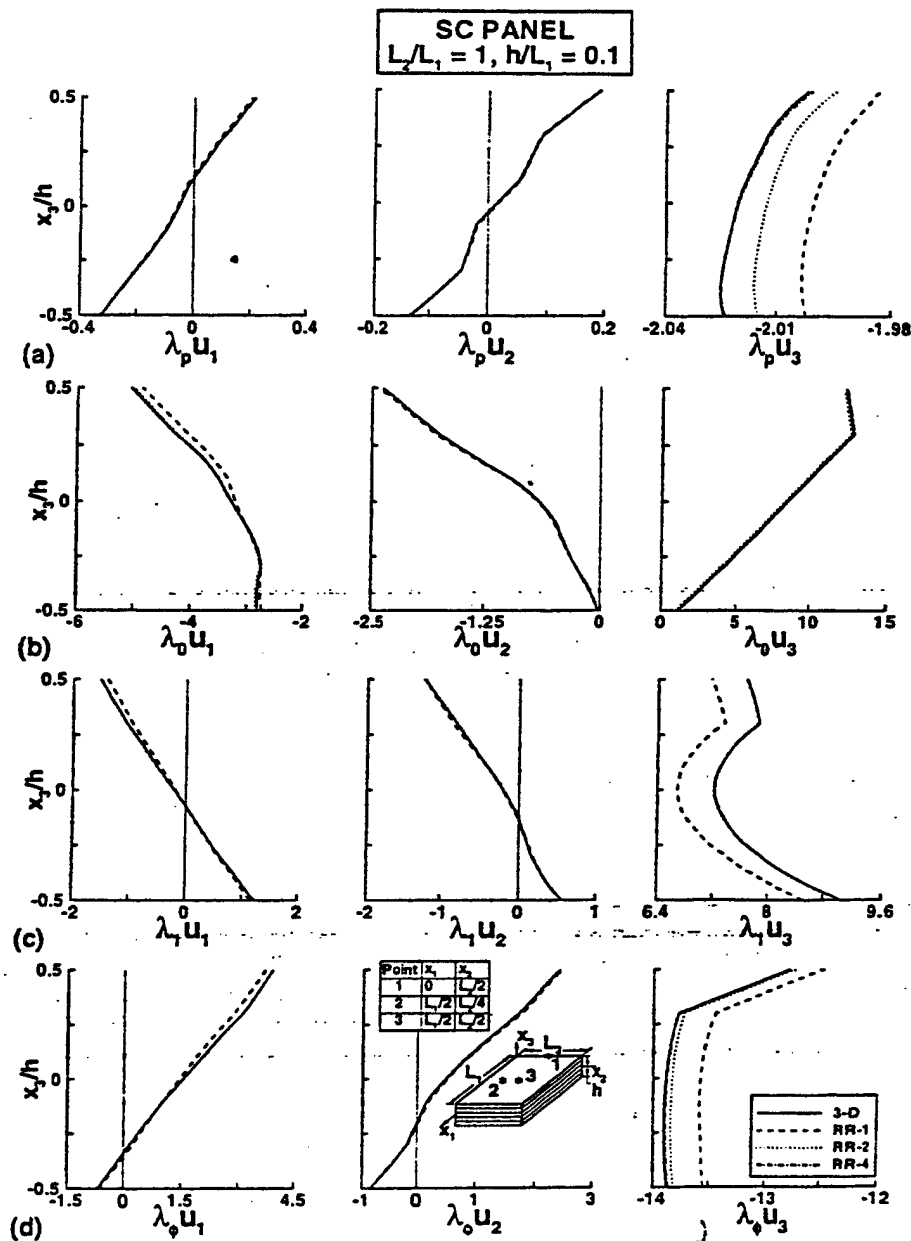


Figure 4. Through-the-thickness variations of displacement components u_1 , u_2 , and u_3 at the points 1, 2, and 3, respectively, in an SC panel subjected to (a) p -, (b) T_0 -, (c) T_1 -, and (d) ϕ -loadings; $\lambda_p = 10^{-2} E_3^p / (p_0 h)$, $\lambda_0 = 10^{-2} h / (x_{33}^p T_0)$, $\lambda_1 = 10^{-2} / (x_{33}^p T_1)$, $\lambda_\phi = 10 / (d_{33}^p \phi_0)$ (Superscript p denotes the values of physical constants for the piezoelectric layer.)

↑ insert period

↑ insert comma

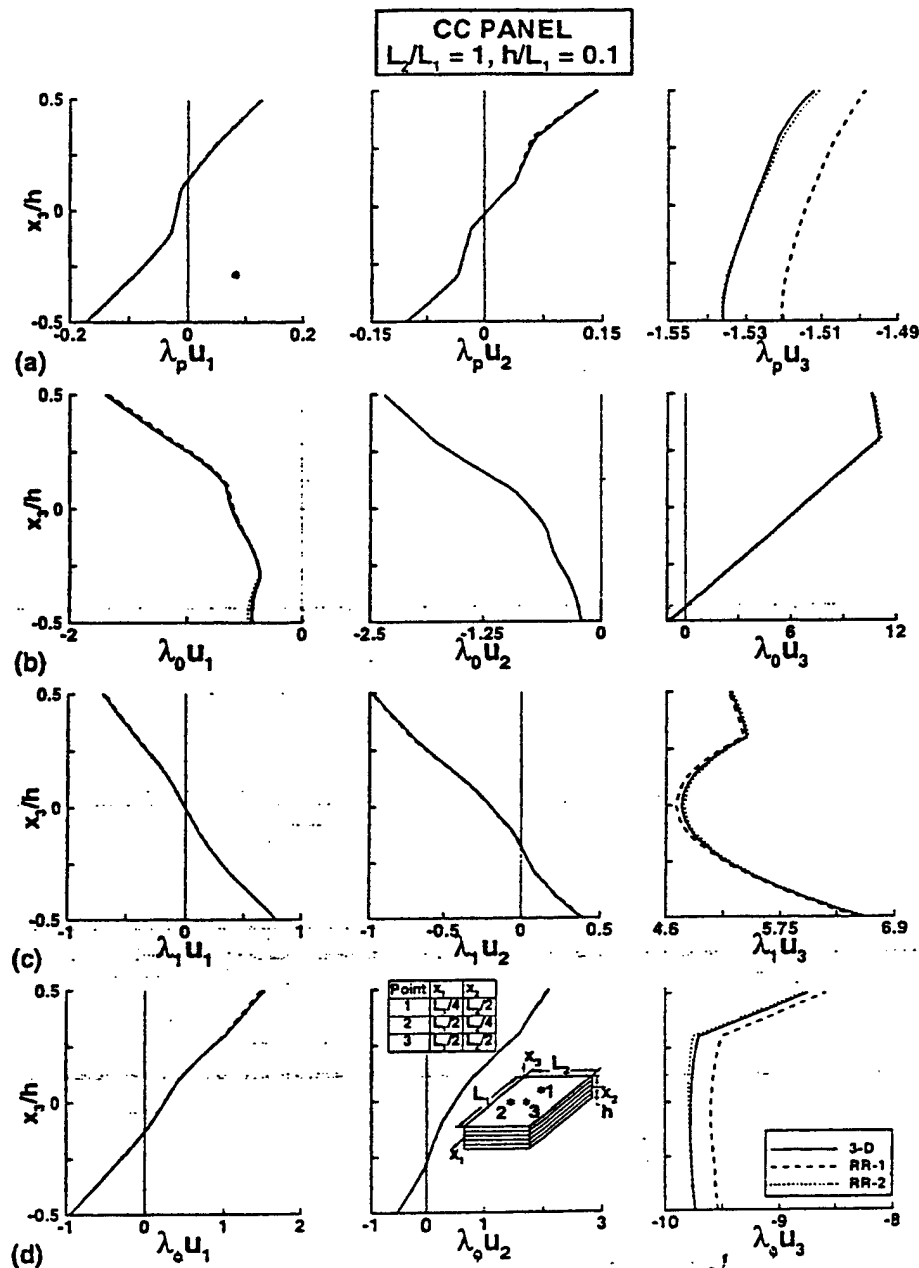


Figure 5. Through-the-thickness variations of displacement components u_1 , u_2 , and u_3 at the points 1, 2, and 3, respectively, in a CC panel subjected to (a) p -, (b) T_0 -, (c) T_1 -, and (d) ϕ -loadings; $\lambda_p = 10^{-2} E_3^p (p_0 h)$, $\lambda_0 = 10^2 h / (x_{33}^p T_0)$, $\lambda_1 = 10^2 / (x_{33}^p T_1)$, $\lambda_\phi = 10 / (d_{33}^p \phi_0)$ (Superscript p denotes the values of physical constants for the piezoelectric layer.)

insert
period

insert
comma

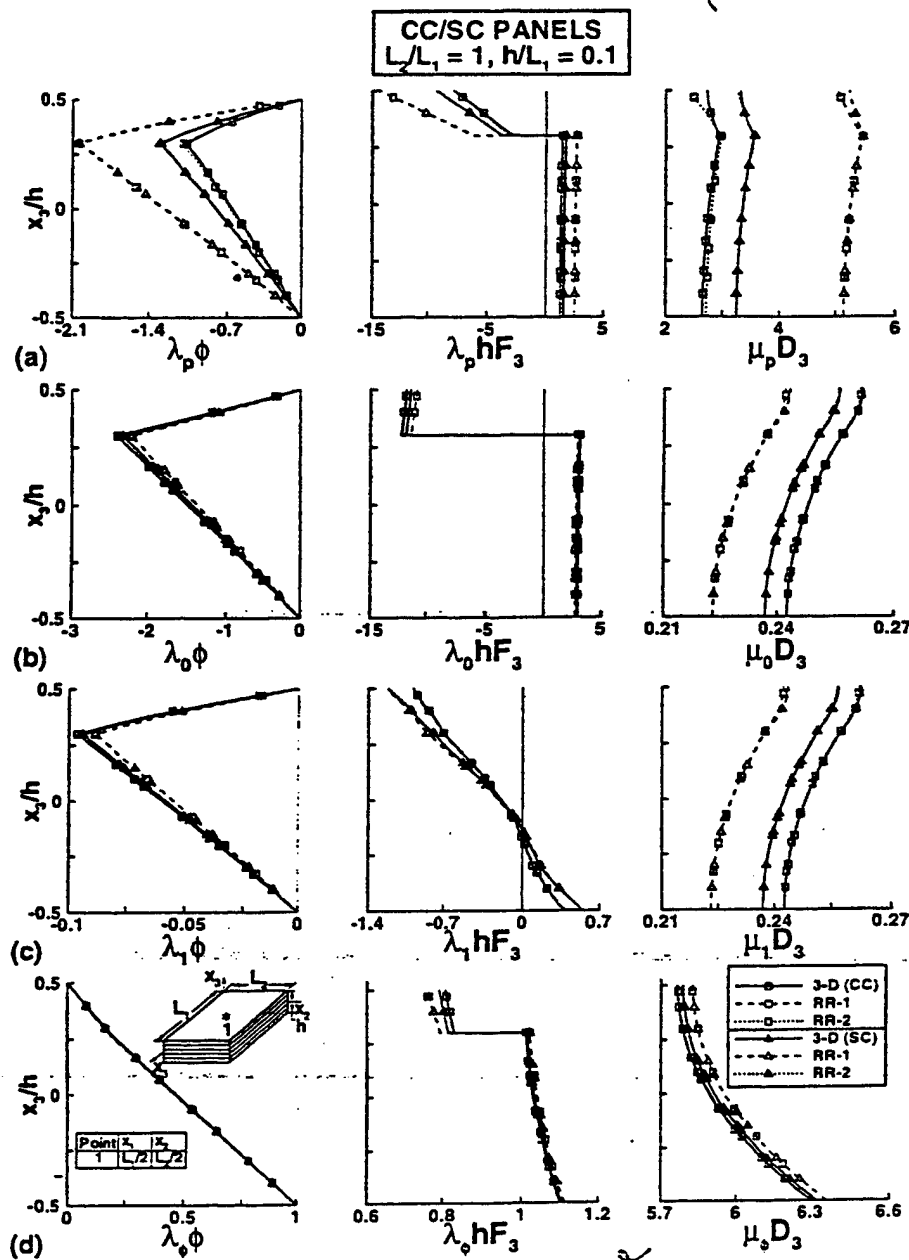


Figure 6. Through-the-thickness variations of electric response quantities, at the point 1, in SC and CC panels subjected to (a) p -, (b) T_0 -, (c) T_1 -, and (d) ϕ -loadings; $\lambda_p = 10^{11} d_{333}^p/h$, $\mu_p = 10^{11}/(E_3^p d_{333}^p)$, $\lambda_0 = \lambda_1 = 10^6 d_{333}^p/h$, $\mu_0 = \mu_1 = 10^6/(E_3^p d_{333}^p)$, $\lambda_\phi = \mu_\phi = 10^{18} d_{333}^p/h$, $\phi_0 = \phi_1 = 10^{18}/(E_3^p d_{333}^p)$. (Superscript p denotes the values of physical constants for the piezoelectric layer.)

insert
comma

insert period

1. In almost all cases, a single application of the Rayleigh-Ritz technique yields displacement components (RR-1) very close, in both magnitude and shape, to the corresponding components of the full three-dimensional model. The displacements obtained after the second application of the Rayleigh-Ritz technique (RR-2) are almost indistinguishable from that of the 3-D components.
2. For p - and ϕ -loadings, the variations of the displacement component u_3 in the thickness direction is considerably smaller than the corresponding variations in the thermal loading cases. The scales selected in Figure 4 amplify the differences between the u_3 predicted by the foregoing procedure and those predicted by the full 3-D model. As an example, for the case of p -loading, the RR-1, RR-2 and RR-4 values of u_3 differ by less than 1.2, 0.7 and 0.02 per cent, respectively, from the 3-D values.

delete comma

4.2. Through-the-thickness variations of electric response quantities

An examination of the through-thickness variations of the electric response quantities shown in Figure 6 reveals:

1. In all cases, one or two applications of the Rayleigh-Ritz technique result in through-the-thickness distributions of electric response quantities which are almost indistinguishable from the corresponding distributions of the three-dimensional models.
2. The shapes of through-thickness distributions of the electric response quantities for the SC and CC panels are similar. For p -loading, the magnitudes of electric potential ϕ are different in the SC and CC panels, and for both mechanical and thermal loadings, the magnitudes of the electric displacement D_3 differ in the two panels.

change to that

add s ?

4.3. Through-the-thickness variation of the transverse shear stresses

An examination of Figures 7 and 8 reveals that the proposed computational procedure yields transverse shear stresses sufficiently close to those obtained by the three-dimensional model after two applications of the Rayleigh-Ritz technique.

add s ?

4.4. Through-the-thickness variation of the transverse normal stresses

An examination of Figures 9-11 reveals:

1. For the case of the mechanical loading, one application of Rayleigh-Ritz technique yields transverse normal stresses which are very close to those obtained by the full three-dimensional model.
2. For the thermal and electric loading, the transverse normal stresses obtained after one application of the Rayleigh-Ritz technique may be considerably in error. However, one more application of the Rayleigh-Ritz technique results in significant improvement in the accuracy of the transverse normal stresses. In all the cases shown in Figures 9-11, the transverse normal stresses obtained after two applications of the Rayleigh-Ritz technique (RR-2) solutions are within 2 per cent of those obtained by the full 3-D model.

change to that

be consistent

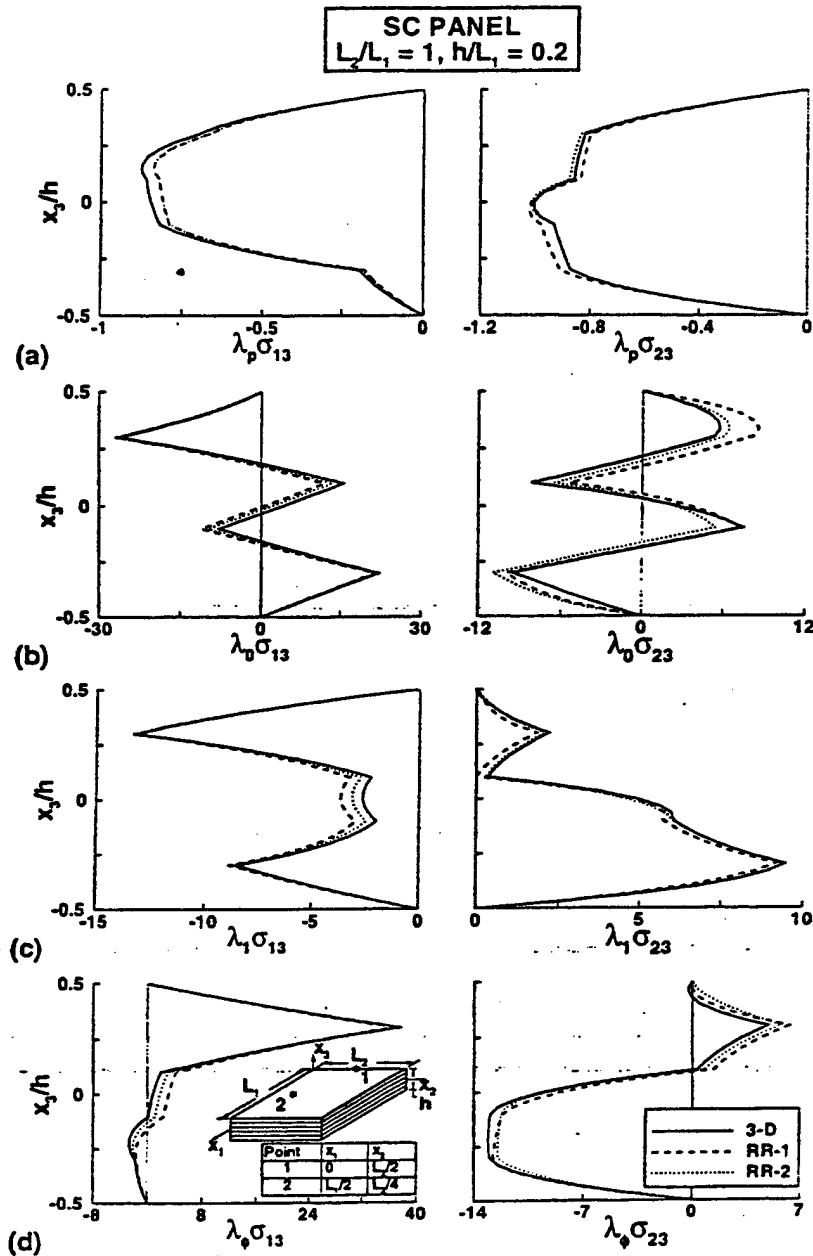


Figure 7. Through-the-thickness variations of transverse shear stresses σ_{13} and σ_{23} at the points 1 and 2, respectively, in an SC panel subjected (a) p -, (b) T_0 -, (c) T_1 -, and (d) ϕ -loadings; $\lambda_p = 1/p_0$, $\lambda_0 = 10^2/(E_3^p x_{33}^p T_0)$, $\lambda_1 = 10^2/(E_3^p x_{33}^p T_1 h)$, $\lambda_\phi = 10^3 h/(E_3^p d_{33}^p \phi_0)$. (Superscript p denotes the values of physical constants for the piezoelectric layer.)

insert
period

insert
comma

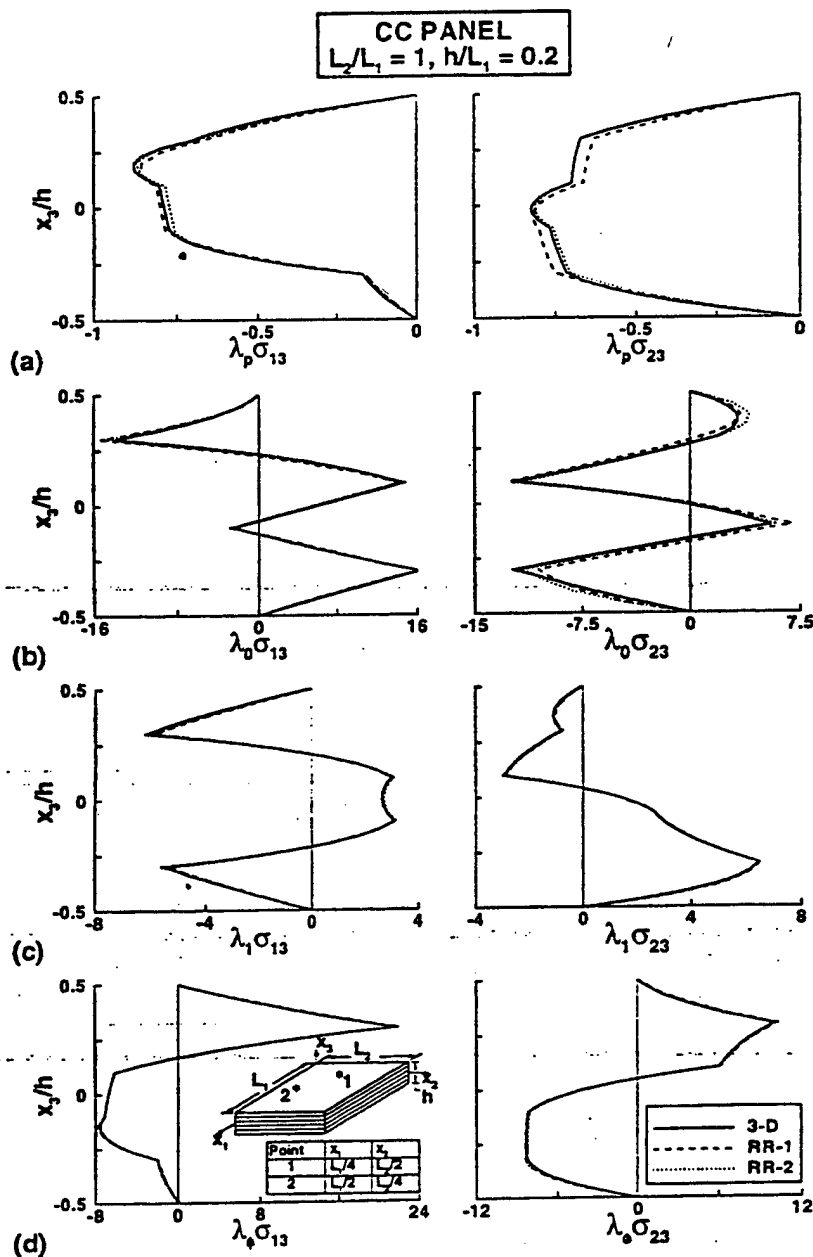


Figure 8. Through-the-thickness variations of transverse shear stresses σ_{13} and σ_{23} at the points 1 and 2, respectively, in a CC panel subjected (a) p -, (b) T_0 -, (c) T_1 -, and (d) ϕ -loadings; $\lambda_p = 1/p_0$, $\lambda_0 = 10^{-2} \cdot (E_3^p x_{33}^p T_0)$, $\lambda_1 = 10^{-2} \cdot (E_3^p x_{33}^p T_1 h)$, $\lambda_\phi = 10^3 h / (E_3^p d_{333}^p \phi_0)$. (Superscript p denotes the values of physical constants for the piezoelectric layer.)

↑ insert period
↑ insert comma

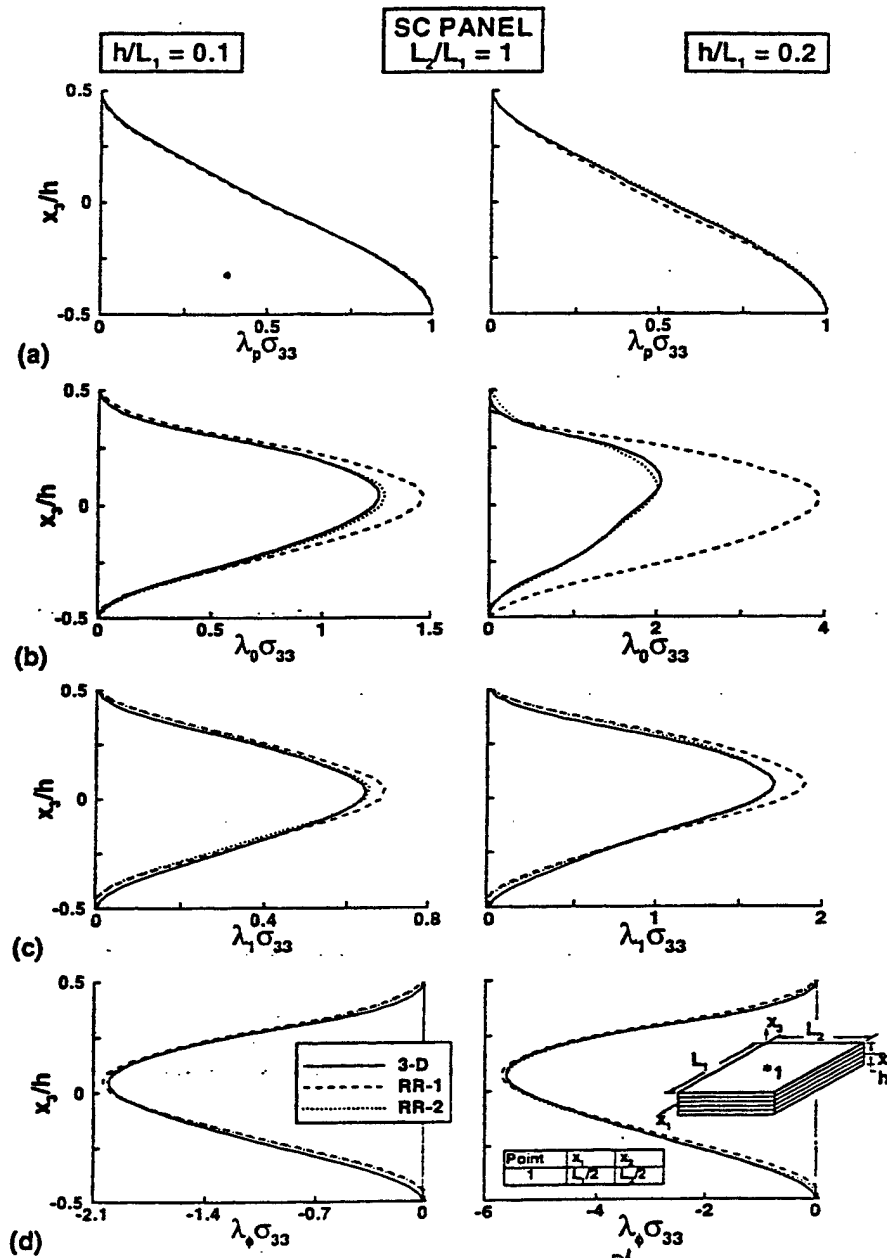


Figure 9. Through-the-thickness variation of transverse normal stress σ_{33} , at the point 1, in SC panels subjected to (a) p -, (b) T_0 -, (c) T_1 - and (d) ϕ -loadings; $\lambda_p = 1/p_0$, $\lambda_0 = 10^2/(E_3^p x_3^p T_0)$, $\lambda_1 = 10^2/(E_3^p x_3^p T_1 h)$, $\lambda_\phi = 10^3 h/(E_3^p d_{333}^p \phi_0)$. (Superscript p denotes the values of physical constants for the piezoelectric layer.)

insert
comma

add
period

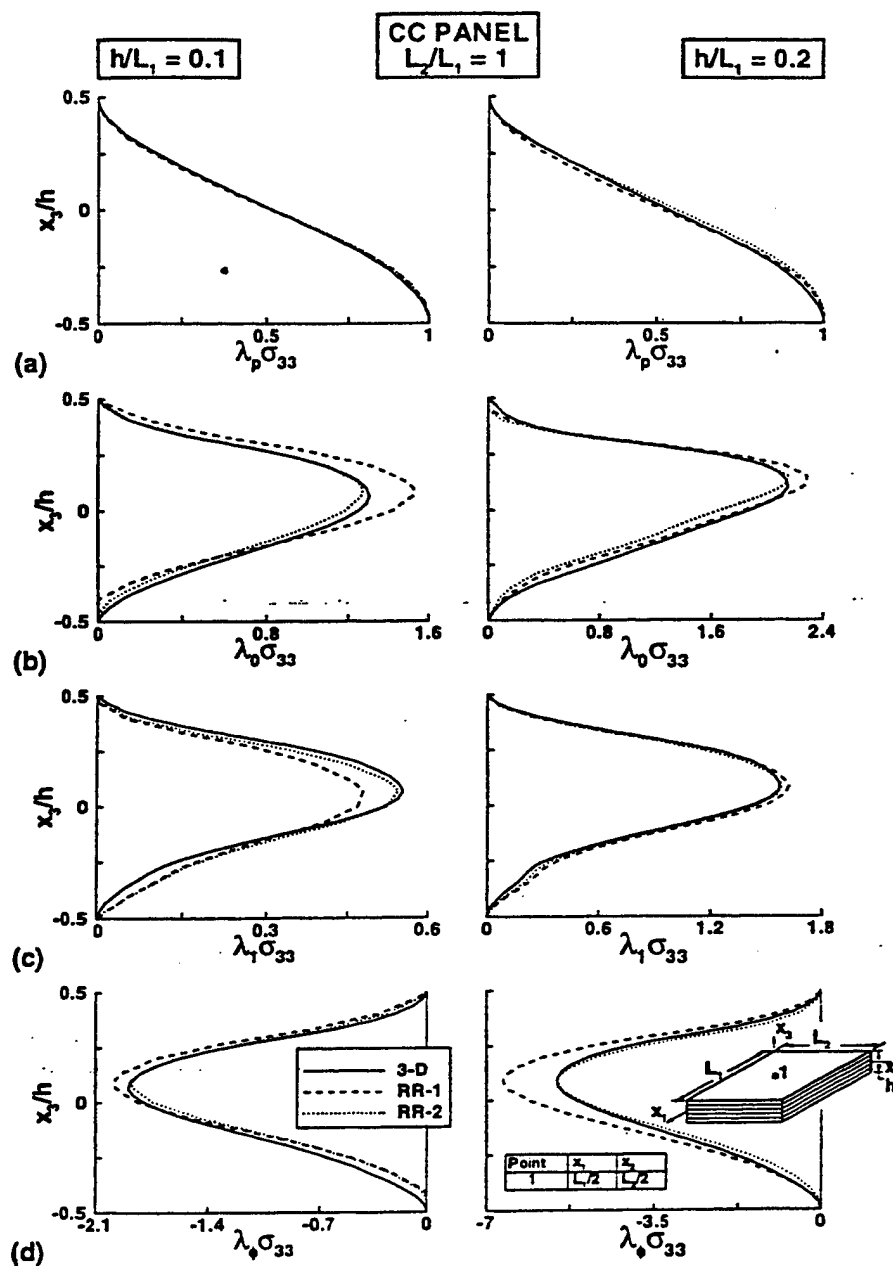


Figure 10. Through-the-thickness variation of transverse normal stress σ_{33} , at the point 1, in CC panels subjected to (a) p , (b) T_0 , (c) T_1 , and (d) ϕ -loadings; $\lambda_p = 1/p_0$, $\lambda_0 = 10^2/(E_3^p x_{33}^p T_0)$, $\lambda_1 = 10^2/(E_3^p x_{33}^p T_1 h)$, $\lambda_\phi = 10^3 h/(E_3^p d_{33}^p \phi_0)$. (Superscript p denotes the values of physical constants for the piezoelectric layer.)

insert
comma

add
period

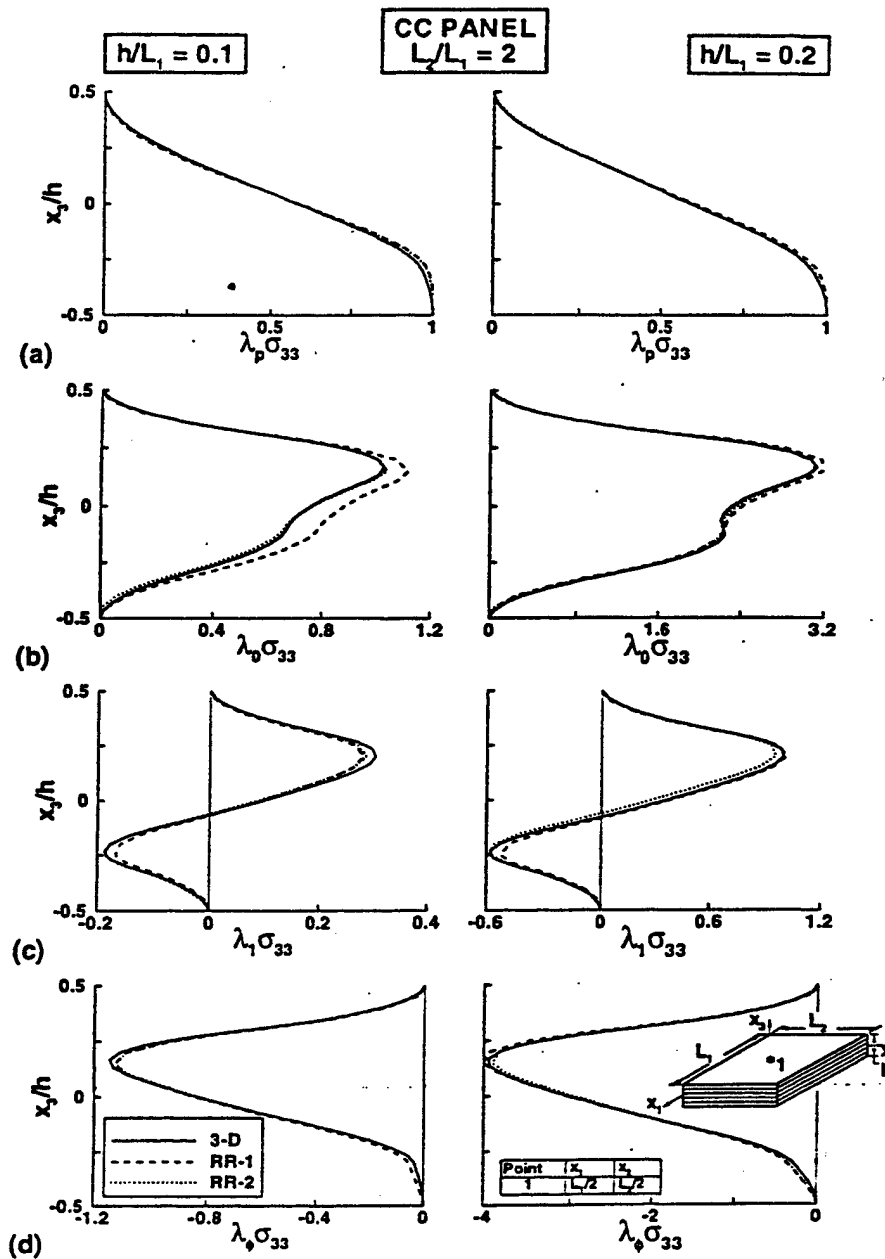


Figure 11. Through-the-thickness variation of transverse normal stress σ_{33} , at the point 1, in CC panels subjected to (a) p -, (b) T_0 -, (c) T_1 - and (d) ϕ -loadings; $\lambda_p = 1/p_0$, $\lambda_0 = 10^2/(E_3^p x_{33}^p T_0)$, $\lambda_1 = 10^2/(E_3^p x_{33}^p T_1 h)$, $\lambda_\phi = 10^3 h/(E_3^p d_{33}^p \phi_0)$. (Superscript p denotes the values of physical constants for the piezoelectric layer.)

insert comma

add period

5. CONCLUDING REMARKS

A computational procedure is presented for the accurate determination of transverse normal stresses in hybrid laminated panels consisting of fibre-reinforced composite and piezoelectric layers, subjected to mechanical, thermal and electrical loadings. The basic idea of the procedure is to generate the response of the panel through successive improvements of the response of a simpler panel, having the same lamination as the given panel, but simpler boundary conditions, loading distribution, and/or geometry. The computational procedure can be conveniently divided into two distinct phases: (a) An initial phase, in which through-the-thickness distributions of the response quantities of the simpler panel are used to effect a dimensional reduction of the original problem, and to generate approximation functions for the response quantities of the original panel, and (b) successive improvement phase, which involves adaptive improvement of through-the-thickness distributions of the response quantities through successive applications of the Rayleigh–Ritz technique in conjunction with the three-dimensional electro-thermo-elasticity equations for each layer; and use of the three-dimensional divergence equations for evaluating the transverse stresses and the transverse component of the electric displacement.

The effectiveness of the procedure is demonstrated by means of numerical studies on two types of flat rectangular hybrid panels: panels having two opposite edges simply supported and the other two clamped, and panels with all edges clamped. In each case, the simpler problem is taken to be a panel with all edges simply supported. The panels are subjected to transverse mechanical loading, thermal loadings in the forms of uniform temperature change and temperature gradient through the thickness, and electric loading due to an applied electric potential. The results obtained by using the foregoing computational procedure, with one or two applications of Rayleigh–Ritz technique, were found to be in close agreement with those obtained by using the three-dimensional models for each of the composite and piezoelectric layers.

The co-ordinate functions used in conjunction with the Rayleigh–Ritz technique were generated by integrating numerically the three-dimensional gradient relations, and were defined in terms of their values at discrete points in the thickness direction. The computational procedure can be extended to provide adaptive refinement strategies of the shape function in the other co-ordinate directions.

APPENDIX

1.1 Fundamental equations of three-dimensional electro-thermo-elasticity

The equations of steady-state linear electro-thermo-elasticity can be grouped into three categories of equations, namely, divergence equations, gradient relations, and constitutive relations, as follows [22]:

1. Divergence equations:

$$\sigma_{ij,i} = 0 \quad (2)$$

$$D_{i,i} = 0 \quad (3)$$

2. Gradient relations:

$$\varepsilon_{ij} = \frac{1}{2}(u_{i,j} + u_{j,i}) \quad (4)$$

$$E_i = -\phi_{,i} \quad (5)$$

3. Constitutive relations:

$$\sigma_{ij} = C_{ijk} (\epsilon_{kl} - d_{mk} F_m - \alpha_{kl} \Delta T) \quad (6)$$

$$D_m = C_{ijk} d_{mk} \epsilon_{ij} + \kappa_{mn} F_n + r_m \Delta T \quad (7)$$

In equations (2)–(7), σ_{ij} is the stress tensor, ϵ_{ij} the strain tensor, C_{ijk} the elastic constitutive tensor, u_i the elastic displacement vector, D_i the electric displacement vector, F_i the electric field vector, d_{ijk} the piezoelectric tensor, κ_{ij} the permittivity tensor, α_{ij} the thermal expansion coefficients tensor, r_i the pyroelectric coefficients vector, and ΔT the temperature change. The range of indices is 1, 2, 3.

Note that only partial coupling is considered since the coupling between the electric, thermal, and elastic fields is included only in the constitutive relations. The functional used in the Rayleigh–Ritz technique is

$$\Pi = \int_V H dV - \int_S (n_i \sigma_{ij} u_j + n_i D_i \phi) dS \quad (8)$$

where

$$H = C_{ijk} (\frac{1}{2} \epsilon_{ij} \epsilon_{kl} - d_{mk} F_m \epsilon_{ij} - \epsilon_{ij} \alpha_{kl} \Delta T) - \frac{1}{2} \kappa_{ij} F_i F_j - E_i r_i \Delta T \quad (9)$$

and, V is the volume, S the surface area, and n_i is unit outward normal.

ACKNOWLEDGEMENTS

The work was partially supported by Air Force Office of Scientific Research Grant F49620-96-1-0462 and NASA Grant NAG-1-2016. The authors acknowledge the help of Jeanne Peters of the University of Virginia in various stages of this work.

REFERENCES

1. Tzou HS, Tseng CI. Distributed piezoelectric sensor/actuator design for dynamic measurement/control of distributed parameter systems: a piezoelectric finite element approach. *Journal of Sound Vibration* 1990; 138:17–34.
2. Chandrashekhara K, Agarwal AN. Active vibration control of laminated composite plates using piezoelectric devices: a finite element approach. *Journal of Intel. Material System Structures* 1993; 4:496–508.
3. Gaudenzi P, Bathe KJ. An iterative finite element procedure for the analysis of piezoelectric continua. *Journal of Intel. Material System Structures* 1995; 6:266–273.
4. Shah DK, Chan WS, Joshi SP. Finite element analysis of plates with piezoelectric layers. *AIAA-93-1678-CP*, 1993; pp. 3189–3197.
5. Hwang WS, Park HC, Hwang W. Vibration control of a laminated plate with piezoelectric sensor/actuator: Finite element formulation and modal analysis. *Journal of Intel. Material System Structures* 1993; 4:317–329.
6. Jonnalagadda KD, Blandford GE, Tauchert TR. Higher-order displacement formulation for a piezothermoelastic laminate. *Mechanical and Electromagnetic Material Structures ASME*. AMD-161, MD-42 (1993) 145–159.
7. Jonnalagadda KD, Blandford GE, Tauchert TR. Piezothermoelastic composite plate analysis using first-order shear deformation theory. *Computers and Structures* 1994; 51:79–89.
8. Rogacheva NN. *The Theory of Piezoelectric Shells and Plates*. CRC Press: Boca Raton, 1994.
9. Robbins DH, Reddy JN. Analysis of piezoelectrically actuated beams using a layer-wise displacement theory. *Computers and Structures* 1991; 41:265–279.
10. Heyliger P, Ramirez G, Saravanan D. Coupled discrete-layer finite elements for laminated piezoelectric plates. *Communications in Numerical Methods in Engineering* 1994; 10:971–981.
11. Saravanan DA. Mixed laminate theory and finite element for smart piezoelectric composite shell structures. *AIAA Journal* 1997; 35:1327–1333.
12. Pryor Jr CW, Barker RM. A finite-element analysis including transverse shear effects for applications to laminated plates. *AIAA Journal* 1971; 9:912–923.

change to
This

delete e

change to the
REFERENCES
should be
systems and

Intelli-
gent

A.A.
Pl. provide & check
journal name's
full form

A.A.
Pl. check journal
name full form

This is
a journal
it is a
proceeding
title

13. Engblom JJ, Ochoa OO. Through-the-thickness stress predictions for laminated plates of advanced composite materials. *International Journal for Numerical Methods in Engineering* 1985; 21:1759-1776.
14. Noor AK, Kim YH, Peters JM. Transverse shear stresses and their sensitivity coefficients in multilayered panels. *AIAA Journal* 1994; 32:1259-1269.
15. Rolfes R, Rohwer K. Improved transverse shear stresses in composite finite elements based on first order shear deformation theory. *International Journal for Numerical Methods in Engineering* 1997; 40:51-60.
16. Rolfes R, Noor AK, Sparr H. Evaluation of transverse thermal stresses in composite plates based on first-order shear deformation theory. *Computer Methods in Applied Mechanics and Engineering* 1998; 167:355-368.
17. Noor AK, Burton WS, Peters JM. Predictor-corrector procedures for stress and free vibration analyses of multilayered composite plates and shells. *Computer Methods in Applied Mechanics and Engineering* 1990; 82:341-363.
18. Tang YY, Noor AK, Xu K. Assessment of computational models for thermoelectroelastic multilayered plates. *Computers and Structures* 1996; 61:915-933.
19. Noor AK, Malik M. Accurate determination of transverse normal stresses in sandwich panels subjected to thermomechanical loadings. *Computer Methods in Applied Mechanics and Engineering*, to be published.
20. Bellman R, Kashef BG, Casti J. Differential quadrature: a technique for the rapid solution of nonlinear partial differential equations. *Journal of Computational Physics* 1972; 10:40-52.
21. Bert CW, Malik M. Differential quadrature method in computational mechanics: a review. *Applied Mechanics Review* 1996; 49:1-28.
22. Mindlin RD. Equations of high frequency vibrations of thermopiezoelectric crystal plates. *International Journal of Solids Structures* 1974; 10:625-637.

not
published
yet

A-2.
Pl. update

add
and

An Assessment of Five Modeling Approaches for Thermo-mechanical Stress Analysis of Laminated Composite Panels

Ahmed K. Noor and Moinuddin Malik
Center for Advanced Computational Technology
University of Virginia
NASA Langley Research Center
Hampton, VA 23681

Abstract A study is made of the effects of variation in the lamination and geometric parameters, and boundary conditions of multi-layered composite panels on the accuracy of the detailed response characteristics obtained by five different modeling approaches. The modeling approaches considered include four two-dimensional models, each with five parameters to characterize the deformation in the thickness direction, and a predictor-corrector approach with twelve displacement parameters. The two-dimensional models are first-order shear deformation theory, third-order theory; a theory based on trigonometric variation of the transverse shear stresses through the thickness, and a discrete layer theory. The combination of the following four key elements distinguishes the present study from previous studies reported in the literature: a) the standard of comparison is taken to be the solutions obtained by using three-dimensional continuum models for each of the individual layers; 2) both mechanical and thermal loadings are considered; 3) boundary conditions other than simply supported edges are considered; and 4) quantities compared include detailed through-the-thickness distributions of transverse shear and transverse normal stresses.

Based on the numerical studies conducted, the predictor-corrector approach appears to be the most effective technique for obtaining accurate transverse stresses, and for thermal loading, none of the two-dimensional models is adequate for calculating

transverse normal stresses, even when used in conjunction with three-dimensional equilibrium equations.

1 Introduction

A significant numerical simulation capability now exists for studying the various phenomena associated with the response, life, failure and performance of multi-layered composite panels and shells. The phenomena involved cover a wide range of length scales from local to global structural response. The modeling approaches used for multi-layered panels can be divided into four different categories: detailed micro-mechanical models, three-dimensional continuum models, quasi-three-dimensional models (with simplifying assumptions made regarding the stress or strain state in the laminate or in the individual layers), and two-dimensional plate and shell models. Within each category has evolved a number of models with several levels of sophistication. The four categories are described in survey papers (see, for example, Leissa, 1987; Grigolyuk and Kulikov, 1988; Noor and Burton, 1989; Kapania, 1989; Noor and Burton, 1990, 1992; Reddy and Robbins, 1994; and Robbins and Reddy, 1996) and monographs (see, for example, Ambartsumian, 1974; Bolotin and Novichkov, 1980; Khoroshun et al, 1988; Turvey and Marshall, 1995; Chao, 1996; and Reddy, 1997). The use of detailed models, three-dimensional continuum models and quasi-three-dimensional models for predicting the response of panels with complicated geometry is computationally expensive, and therefore, may not be feasible for practical composite panels.

Experience with the two-dimensional first-order shear deformation model has shown it to be inadequate for calculating the inter-laminar stresses that are used in predicting the onset of some of the damage mechanisms in multi-layered composite

panels. Therefore, various higher-order shear deformation models and post-processing techniques have been proposed for the accurate determination of transverse stresses in laminated panels. The higher-order models can be divided into (see, for example, Noor and Burton, 1989, 1990): a) global approximation models, based on global through-the-thickness displacement, strain or stress approximation, and b) discrete layer models based on layer-by-layer approximations of the response quantities in the thickness direction. The post-processing techniques proposed for the evaluation of transverse stresses are based on the use of: a) three-dimensional equilibrium equations (Chaudhuri, 1986; Chaudhuri and Seide, 1987; Engblom and Ochoa, 1985; Kant and Pandya, 1988; Reddy, Barbero and Teply, 1989); b) predictor-corrector approaches (Noor, Burton and Peters, 1990; and Noor and Malik, 1999); and c) simplifying assumptions (Rolfes and Rohwer, 1997; and Rolfes, Noor and Sparr, 1998). Most of the reported studies considered the case of mechanical loading only. The few studies that considered thermal loading, such as Reddy (1997); Rolfes, Noor and Sparr (1998); and Noor and Malik (1999); did not assess the effectiveness of the various modeling approaches for calculating transverse stresses. The establishment of reliable, efficient and practical modeling approaches and computational procedures for predicting transverse stresses in multi-layered composites subjected to thermo-mechanical loadings remains a challenging task and is the focus of the present study. Specifically, the objective of this paper is to assess the accuracy of five modeling approaches for calculating the detailed response characteristics, including transverse stresses, of composite panels subjected to thermo-mechanical loading.

The composite panels considered herein consist of a number of perfectly bonded layers. The individual layers are assumed to be homogeneous and anisotropic, and are

anti-symmetrically laminated with respect to the middle plane of the panel. At each point of the panel, a plane of elastic symmetry exists, parallel to the middle plane. The sign convention for the different displacement and stress components is shown in Fig. 1. The panels are subjected to mechanical and thermal loads. The basis of comparison is taken to be the solutions obtained by using three-dimensional continuum models for each of the individual layers. The effects of the different lamination and geometric parameters and boundary conditions of the panel on the accuracy of the detailed response characteristics obtained by the different modeling approaches are studied.

2

Modeling approaches used in the present study

The five computational models considered in the study are: first-order shear deformation theory; third-order theory; a theory based on trigonometric variation of the transverse shear stresses through-the-thickness; a discrete layer theory; and a predictor-corrector approach. The predictor-corrector approach is a slightly modified version of the one presented in Noor and Malik (1999), and is briefly described in the succeeding section. The first four models can be considered as special cases of a general two-dimensional theory based on the following through-the-thickness displacement assumption:

$$u_{\alpha}(x_{\beta}, x_3) = u_{\alpha}^o(x_{\beta}) + U_{\alpha}(x_{\beta}, x_3) \quad (1)$$

$$u_3(x_{\beta}, x_3) = w^o(x_{\beta}) \quad (2)$$

where u_{α}^o and w^o are the displacement components of the reference (middle) plane of the plate ($x_3 = 0$), U_{α} are functions of x_3 which vanish at $x_3 = 0$ and $\alpha, \beta = 1, 2$. The functional dependence of U_{α} on x_3 , along with the characteristics of the four models, is

given in Table 1. The in-plane stresses for the four two-dimensional models were calculated by assuming a state of generalized plane stress to exist in each layer. The transverse stresses were calculated by piecewise integration of the three-dimensional equilibrium equations. The following comments can be made about the four two-dimensional modeling approaches.

1. The first-order shear deformation theory is an extension of the Reissner-Bolles-Mindlin type theories for isotropic plates. Since in these theories the transverse shear strains or stresses are assumed to be constant within each layer, correction factors have to be used in order to adjust the transverse shear stiffnesses and match the response predicted by the two-dimensional theory with that of the three-dimensional elasticity theory. The range of validity of the first-order shear deformation theory is strongly dependent on the factors used in adjusting the transverse shear stiffnesses of the plate. In the present study the shear correction factors were calculated by assuming cylindrical bending type of deformation in each of the x_1 and x_2 directions (see Chow, 1971; and Whitney, 1973). The use of these composite correction factors was found to result in fairly accurate gross response characteristics for a wide range of lamination and geometric parameters of the panel (see Noor and Burton, 1989 and 1990).

2. The third-order shear deformation theory is based on using a cubic in-plane displacement approximation, and a constant transverse displacement, in the thickness direction. To reduce the number of displacement parameters to five, the conditions of zero transverse shear stresses (and strain) at the top and bottom surfaces of the laminate are imposed. This approach was introduced for homogeneous isotropic plates by Panc (1975), and later applied by a number of researchers to laminated plates (see, for

example, Kaczkowski, 1980; Bhimaraddi and Stevens, 1984; Reddy, 1984; Pandya and Kant, 1987; and Krishna Murty and Vellaichamy, 1987). Reddy used the same kinematic assumptions and applied Hamilton's principle to obtain an energy consistent set of equations for the plate (see Reddy, 1984).

3. Model 3 was proposed by Touratier (1991) and is based on assuming trigonometric variation of the transverse shear stresses through the thickness, which satisfies the free shear stress boundary conditions at the top and bottom surfaces of the panel. This is accomplished by augmenting the thickness distribution of the in-plane displacements of the classical theory with a trigonometric function whose derivative with respect to x_3 vanishes at the top and bottom surfaces of the laminate. The use of trigonometric functions in the thickness coordinate for the in-plane displacements was previously proposed in a number of publications (see, for example, Kilchevskii, 1961; and Stein, 1986).

4. The discrete layer theory (model 4) is based on piecewise linear variation of the in-plane displacements, and constant transverse displacement, in the thickness coordinate. The imposition of the continuity of the transverse stresses at layer interfaces is used to reduce the total number of displacement parameters to 5. Di Sciuva (1986, 1987) proposed this model. Other discrete layer models were previously proposed in a number of publications (see, for example, Ambartsumian, 1987; and Whitney, 1969).

3

Predictor-corrector approach

The predictor-corrector approach is based on using the through-the-thickness displacement field for the three-dimensional continuum model of a simpler panel having the same lamination as the original panel, but with simply supported edges, to generate

coordinate functions for the Rayleigh-Ritz technique, and then adaptively improving these coordinate functions. The computational procedure can be conveniently divided into two stages. In the first stage, coordinate functions are generated using the three-dimensional continuum model of a simply supported panel. The coordinate functions for each displacement component are obtained by decomposing the corresponding through-the-thickness distribution into four components: a) uniform, b) linear antisymmetric, c) nonlinear symmetric, and d) nonlinear antisymmetric, where the symmetry and antisymmetry of these components are defined with respect to the middle plane of the panel. The amplitudes of the coordinate functions are determined by using the Rayleigh-Ritz technique. The resulting displacements are used in conjunction with three-dimensional kinematic and constitutive relations to calculate the strains and the in-plane stress components. Subsequently, the transverse stresses are determined by through-the-thickness, piecewise integration of three-dimensional equilibrium equations. In the second stage, the transverse strains are determined by using the three-dimensional constitutive relations. The transverse strains are then integrated in the thickness direction to generate more accurate through-the-thickness distributions of the displacement components, from which improved coordinate functions, displacements, strains and stresses are obtained. A flow chart of the computational procedure is shown in Fig. 2. Other predictor-corrector approaches are presented in Noor, Burton and Peters (1990), and Noor and Burton (1990).

4

Numerical studies

The accuracy of the different response quantities of multi-layered composite panels subjected to thermo-mechanical loading, predicted by different modeling approaches is dependent on a number of parameters, including:

- Lamination parameters (viz., number of layers, stacking sequence, degree of orthotropy, and fiber orientation of different layers).
- Geometric parameters (e.g., panel geometry, thickness ratio, presence or absence of discontinuities).
- Type and rate of variation of thermal and mechanical loading.
- Boundary (or support) conditions.

Due to the large number of these parameters and the fact that closed form (or analytic) solutions are only obtainable for panels with simple geometries, loading and boundary conditions, it is impractical to present quantitative results of a general nature. Although several attempts have been made to assess the accuracy of the response of composite panels and shells predicted by different modeling approaches (see, for example, Di Sciuva, 1986; Noor and Burton, 1989; Touratier, 1991; and Reddy, 1997) the combination of the following four key elements distinguishes the present study from previous studies reported in the literature: 1) the standard of comparison is taken to be the solutions obtained by using three-dimensional continuum models for each of the individual layers; 2) both mechanical and thermal loadings are considered; 3) quantities compared include detailed through-the-thickness distributions of transverse shear and transverse normal stresses; and 4) boundary conditions other than simply supported edges are considered;.

Herein the results of parametric studies for flat multi-layered rectangular panels are presented. These studies were conducted to provide some insight into the effects of variation in the lamination, geometric parameters and boundary conditions of composite panels on the accuracy of the five modeling approaches described in the preceding section (see Table 1). The modeling approaches will henceforth be referred to as models 1 to 5.

The composite panels considered in this study are rectangular with side lengths in the x_1 and x_2 directions equal to L_1 and L_2 , respectively, and L_1 is taken to be 1.0. Cross ply lamination with the fiber orientation selected to be $[0/90/0/90/\dots]$, where the fibers of the top layer are parallel to the x_1 direction. The material characteristics of the individual layers are taken to be those typical of high-modulus fibrous composites, namely:

$$E_L / E_T = 25, \quad G_{LT} / E_T = 0.5, \quad G_{TT} / E_T = 0.2, \\ \nu_{LT} = 0.25, \quad \nu_{TT} = 0.25, \quad \alpha_T / \alpha_L = 3, \quad \alpha_L = 1.0$$

The panels are subjected to transverse static loading p , or to a thermal loading in the form of either a constant temperature change ΔT_0 , or a temperature gradient in the thickness direction ΔT_1 . Each of the three loadings had a double sinusoidal variation in the x_1 - x_2 plane, namely:

$$\begin{Bmatrix} p \\ \Delta T_0 \\ \Delta T_1 \end{Bmatrix} = \begin{Bmatrix} p_0 \\ \bar{T}_0 \\ x_3 \bar{T}_1 \end{Bmatrix} \sin \frac{\pi x_1}{L_1} \sin \frac{\pi x_2}{L_2} \dots \quad (3)$$

The amplitudes of the transverse loading, uniform temperature and temperature gradient $(p_0, \bar{T}_0, \bar{T}_1)$ were chosen to be one.

Four parameters were varied: namely, the thickness ratio h/L_1 ; the aspect ratio L_1/L_2 ; the lamination; and the boundary conditions. The thickness ratio was varied between 0.01 and 0.2; the aspect ratio was varied between 1 and 3; the number of layers was varied between 2 and 10. Both symmetric and anti-symmetric laminations (with respect to the middle plane) were considered. Three types of boundary conditions were considered; namely, all edges simply supported; two opposite edges simply supported and the other two clamped; and all edges clamped.

For panels with all edges simply supported, analytic solutions were obtained for all five models, as well as for the three-dimensional model (used as a standard for comparison). For panels with other types of boundary conditions, the numerical discretization was performed by using the differential quadrature method (see Bellman, et al, 1973; Bert and Malik, 1996; and Chen, et al, 1997). The predictions of the two-dimensional models were validated by comparing them with those published in the literature, for both a version of model 1 with different composite correction factors and model 2 (Reddy, 1997), model 3 (Touratier, 1991), and model 4 (Di Sciuva, 1986). For panels with two opposite edges clamped or all edges clamped, convergence studies were performed for the three-dimensional model to insure that the results presented herein are converged solutions.

Typical results are presented in Fig. 3 for a two-layer panel with two opposite edges simply supported and the other two clamped, and in Figs. 4-14 for panels with all edges clamped. Figures 3-14 show the through-the-thickness distributions of the in-plane stresses ($\sigma_{11}, \sigma_{22}, \sigma_{12}$), the transverse shear stresses (σ_{13}, σ_{23}), and the transverse normal stresses σ_{33} predicted by the five models, along with those predicted by the three-

dimensional continuum model. The description of the boundary conditions, lamination, geometric parameters and loading used in each of the figures is summarized in Table 2. The results are described subsequently for the three loading cases.

4.1

Case of mechanical loading

Typical results for the case of mechanical loading are presented in Figs. 3-6. An examination of the results obtained reveals:

1. For thin panels ($h/L_1 \leq 0.01$) with simply supported edges, all the two-dimensional models predict accurate stresses. For panels with two or all edges clamped, the stresses predicted by models 1, 3, 4 and 5 are in close agreement with those of the three-dimensional continuum model. However, the predictions of model 2 show a pronounced difference (15% for the in-plane normal stresses, 6% for the in-plane shear stress, 22% for the transverse shear stresses, and 13% for the transverse normal stress, see Fig. 4).
2. As expected, an increase in the thickness ratio h/L_1 results in increasing the differences between the predictions of the two-dimensional and three-dimensional continuum models. This effect is more pronounced for the transverse shear stresses predicted by models 2, 3 and 4; and for the in-plane shear stress predicted by model 1 (see Figs. 3, 5 and 6).
3. As the aspect ratio of the panel L_2/L_1 increases, the differences between the maximum values of each pair of stresses (σ_{13}, σ_{23}) increases. The errors in the smaller stress predicted by each of the two-dimensional models increases

with the increase in L_2 / L_1 . This effect is more pronounced for σ_{23} predicted by model 2 (see Fig. 6).

4. For two-layered panels, the transverse shear stresses predicted by models 1, 2 and 3 have comparable accuracy. The corresponding stresses predicted by model 4 are less accurate. As the number of layers increases, the accuracy of the transverse stresses predicted by the two-dimensional models increases. The increase is more pronounced for the stresses predicted by model 1.
5. The accuracy of the transverse shear stresses predicted by the different models is sensitive to the boundary conditions of the panel. As an example, for a square two-layered simply supported panel with $h / L_1 = 0.2$, the maximum errors in the transverse shear stresses predicted by models 1, 2, 3 and 4 were 7.3, 13.0, 13.7 and 17.6%, respectively. For the corresponding panels with two opposite edges simply supported and the other two clamped, the errors increased to 7.6, 19.3, 20.6 and 31.6%, respectively.
6. For all the panels considered, the stresses obtained by the predictor-corrector approach (model 5 – with one iteration in stage 2) are highly accurate (within 0.5% of the three-dimensional continuum model predictions). When a second iteration is used in stage 2, the predictions of model 5 become indistinguishable from those of the three-dimensional continuum model.

4.2

Case of uniform temperature change through the thickness

Typical results for the case of ΔT_0 loading are presented in Figs. 7-10. The results can be summarized as follows:

1. The accuracy of the stresses predicted by the different two-dimensional models is sensitive to variations in the thickness ratio and the lamination, and is insensitive to the boundary conditions of the panel. This can be seen by comparing the corresponding results shown in Figs. 8-10.
2. For thin panels ($h/L_1 \leq 0.01$) with simply supported edges, the in-plane normal stresses (σ_{11}, σ_{22}) and transverse shear stresses (σ_{13}, σ_{23}) predicted by the four two-dimensional models are fairly accurate. The same is true for the in-plane normal stresses and transverse shear stresses predicted by models 1, 3 and 4 in panels with two or all edges clamped. By contrast, the in-plane shear stresses σ_{12} and transverse normal stresses σ_{33} predicted by all the two-dimensional models are grossly in error. For panels with two or all edges clamped, the transverse shear stresses predicted by model 2 are less accurate than those predicted by the other models (see Fig. 8).
3. As the thickness ratio increases, the accuracy of the stresses predicted by all the two-dimensional models decreases. This is particularly true for the transverse shear stresses.
4. In all the cases considered, the transverse normal stresses predicted by all the two-dimensional models were highly inaccurate.
5. As for the case of mechanical loading, the stresses obtained by the predictor-corrector approach, with one iteration in stage 2, are fairly accurate. For thick panels ($h/L_1 = 0.2$), the maximum error in the transverse normal stresses predicted by this model was about 5% (see Fig. 10). When a second iteration is used in stage 2, the corresponding error reduces to less than 1%.

4.3

Case of temperature gradient through the thickness

Typical results for the case of ΔT_1 loading are presented in Figs. 11-14, and can be summarized as follows:

1. As for the p_0 case, the in-plane and transverse stresses predicted by the two-dimensional models are fairly accurate for the simply supported panels ($h/L_1 \leq 0.01$). When two or all edges of the panel are clamped, the in-plane and transverse shear stresses predicted by models 1, 3 and 4 are still accurate. The accuracy of the transverse normal stresses deteriorate with the increase in the number of layers. The predictions of model 2 show a pronounced difference from those of the three-dimensional model, regardless of the number of layers (see, for example, Fig. 11).
2. For medium thick and thick panels ($h/L_1 = 0.1$ to 0.2) the accuracy of the in-plane stresses predicted by the two-dimensional models increases with restraining the edges of the panel. This observation applies to panels with two and ten layers. For example, for two-layered panels with $h/L_1 = 0.2$ and with two opposite edges clamped and the other two simply supported, the maximum errors in the in-plane stresses predicted by models 1, 2, 3 and 4 were 28.9, 22.0, 25.2 and 41.5% (see Fig. 11). The corresponding maximum errors in panels with all edges clamped were (6.1, 5.1, 5.1, and 1.9%), respectively. For the corresponding panels with ten layers, the maximum errors were (78.5, 31.8, 28.9 and 73.4%) and (7.6, 0.6, 0.9 and 4.8%) for the

cases of two opposite edges clamped and all edges clamped, respectively (see Fig. 13).

3. The transverse stresses in medium thick and thick panels ($h/L_1 = 0.1$ and 0.2) predicted by the two-dimensional models are grossly in error. Although the through-the-thickness distributions of transverse stresses predicted by the four two-dimensional models are in close agreement with those predicted by the three-dimensional model for the simply supported panels, the differences become pronounced when two or all edges are clamped, as can be seen in Figs. 11 and 12. None of the four two-dimensional models is adequate for predicting the transverse stresses in panels with two or all edges clamped.
4. By contrast to the p and ΔT_0 loading cases, for the ΔT_1 loading case, the aspect ratio (L_2/L_1) has a significant effect on the accuracy of the predicted response characteristics of the two-dimensional models. As the aspect ratio increases, both the in-plane and transverse stresses increase, but the transverse stresses show orders of magnitude more increase. At the same time, the errors in the transverse stresses decrease by orders of magnitude. As an example, for a square, ten-layer antisymmetrically laminated panel with clamped edges and $h/L_1 = 0.2$, the transverse stresses predicted by all the two-dimensional models were grossly in error. By contrast, for rectangular panels with $L_2/L_1 = 3$, the maximum errors in the transverse shear and transverse normal stresses predicted by models 1, 2, 3 and 4 were (17.9, 26.7, 32.4 and 31.5%) and (27.4, 44.3, 34.4 and 42.5%), respectively (see Fig. 14).

5. The stresses obtained by model 5 with one iteration in stage 2 were highly accurate. For all the panels considered, the maximum errors in the in-plane and transverse stresses obtained by using one iteration in stage 2 were found to be less than 0.1 and 1%, respectively.

5

Concluding remarks

A study is made of the effects of variation in the lamination and geometric parameters, and boundary conditions of multilayered composite panels on the accuracy of the detailed response characteristics obtained by five different modeling approaches. The modeling approaches considered include four two-dimensional shear deformation models, each with five parameters to characterize the deformation in the thickness direction; and a predictor-corrector approach with twelve parameters. The two-dimensional models are first-order theory, third-order theory, a theory based on trigonometric variation of the transverse shear stresses through the thickness, and a discrete layer theory. The predictor-corrector approach is based on using the through-the-thickness displacement field for the three-dimensional model of a panel with the same lamination, but with simply supported edges, to generate coordinate functions for the Rayleigh-Ritz technique, and then adaptively refining the coordinate functions and the through-the-thickness displacement field.

Parametric studies are conducted for flat multi-layered rectangular panels to provide some insight into the effects of variation in the lamination, geometric parameters and boundary conditions on the accuracy of the five modeling approaches. The panels are subjected to transverse static loading, or to a thermal loading in the form of either a constant temperature change or a temperature gradient in the thickness direction.

The combination of the following four key elements distinguishes the present study from previous studies reported in the literature: a) the standard of comparison is taken to be the solution obtained by using three-dimensional continuum models for each of the individual layers; 2) both mechanical and thermal loadings are considered; 3) boundary conditions other than simply supported edges are considered; and 4) quantities compared include detailed through-the-thickness distributions of transverse shear and transverse normal stresses.

Based on the numerical studies conducted, the following general observations can be made:

1. For thin panels with simply supported edges subjected to mechanical loading, the in-plane stresses predicted by all the two-dimensional models are accurate. The transverse stresses calculated by using the three-dimensional equilibrium equations are reasonably accurate. For thermal loading, the transverse normal stresses predicted by the four models are inaccurate. The accuracy of model 2 decreases when two or four edges are clamped.
2. As expected, the accuracy of the four two-dimensional models deteriorates with the increase in the thickness ratio. The deterioration is more pronounced when two or four edges of the panel are clamped.
3. For all the panels considered, the stresses obtained by the predictor-corrector approach with one iteration in stage 2 are in close agreement with those obtained by using the three-dimensional models for each layer of the panel.

The foregoing predictor-corrector approach can be used in conjunction with finite element models for the accurate determination of the transverse stresses in the critical regions of panels with arbitrary lamination and geometry.

Acknowledgments

The work was partially supported by Air Force Office of Scientific Research Grant F49620-96-1-0462 and NASA Grant NAG-1-2016. The authors acknowledge the help of Jeanne Peters of the University of Virginia, in various stages of the work.

References

Ambartsumian SA (1987) Theory of anisotropic plates. Nauka, Moscow (in Russian).

English translation, Hemisphere Publishing Corp., New York.

Ambartsumian SA (1974) General theory of anisotropic shells. Izdatel'stvo Nauka, Moscow (in Russian).

Bellman R, Kashef BG and Casti J (1972) Differential quadrature: a technique for the rapid solution of nonlinear partial differential equations. J. Comput. Phys. 10:4-52.

Bert CW and Malik M (1996) Differential quadrature method in computational mechanics: a review. Applied Mechanics Reviews 49:1-28.

Bhimaraddi A, Stevens LK (1984) A higher-order theory for free vibration of orthotropic, homogeneous and laminated rectangular plates. J. Appl. Mech. 51:195-198.

Bolotin VV, Novichkov YuN (1980) Mechanics of multilayered structures. Izdatel'stvo Mashinostroenie, Moscow (in Russian).

Chao CC (1996) Three-dimensional consistent higher-order theory of laminated plates and shells. Ministry of Education, Republic of China.

- Chaudhuri RA (1986)** An equilibrium method for prediction of transverse shear stresses in a thick laminated plate. *Computers and Structures* 23:139-146.
- Chaudhuri RA, Seide P (1987)** An approximate semi-analytical method for prediction of inter-laminar shear stresses in an arbitrarily laminated thick plate. *Computers and Structures* 25:627-636.
- Chen W, Striz AG and Bert CW (1997)** A new approach to the differential quadrature method for fourth-order equations. *Journal title missing* 40:1941-1956.
- Chow TS (1971)** On the propagation of flexural waves in an orthotropic laminated plate and its response to an impulsive load. *J. Composite Mat.* 5:306-319.
- Di Sciuva M (1987)** An improved shear deformation theory for moderately thick multilayered anisotropic shells and plates. *J. Appl. Mech.* 54:589-596.
- Di Sciuva M (1986)** Bending, vibration and buckling of simply supported thick multilayered orthotropic plates: an evaluation of a new displacement model. *J. Sound Vibr.* 105:425-442.
- Engblom JJ, Ochoa OO (1985)** Through the thickness stress predictions for laminated plates of advanced composite materials. *Int. J. Num. Meth. Eng.* 21:1759-1776.
- Grigolyuk EI, Kulikov GM (1988)** General direction of development of the theory of multilayered shells. *Mekhanika Kompozitnykh Materialov* 24(2):287-298. English translation in *Mechanics of Composite Materials* 24(2),1988:231-241.
- Kaczkowski Z (1980)** *Płyty obliczenia statyczne*. Arkady, Warsaw, second edition (in Polish).
- Kant T, Pandya BN (1988)** A simple finite element formulation of a higher-order theory for unsymmetrically laminated composite plates. *Composite Struct.* 9: 215-246.

- Kapania RK** (1989) A review of the analysis of laminated shells. ASME J. Press. Vess. Tech. 111:88-90.
- Khoroshun PL, Kozlov SV, Ivanov YuA., Koshevoi IK** (1988) Generalized theory of nonhomogeneous, in the thickness direction, plates and shells. Izdatel'stvo Naukova Dumka, Kiev (in Russian).
- Kilchevskii NA** (1961) Analysis of various methods of reducing three-dimensional problems in the theory of elasticity to two-dimensional ones and analysis of formation of boundary-value problems in the theory of shells. In Theory of Plates and Shells (Proc. Second All-Union Conf., Lvov, Sept. 1961). Izdatel'stvo Akad Nauk Ukrainian SSR Kiev, 1962, pp. 58-69 (in Russian).
- Krishna Murty AV, Vellaichamy S** (1987) On higher-order shear deformation theory of laminated composite panels. Composite Structures 8:247-270.
- Leissa AW** (1987) A review of laminated composite plate buckling. Appl. Mech. Revs. 40(5):575-591.
- Noor AK, Burton WS** (1992) Computational models for high-temperature multilayered composite plates and shells. Appl. Mech.Revs. 45(10):419-446.
- Noor AK, Burton WS** (1990) Assessment of computational models for multilayered anisotropic plates. Composite Structures 14:233-265.
- Noor AK, Burton WS** (1989) Assessment of shear deformation theories for multilayered composite plates. Appl. Mech. Revs. 41(1):1-13.
- Noor AK, Burton WS, Peters JM** (1990) Predictor-corrector procedure for stress and free vibration analyses of multilayered composite plates and shells. Comp. Meth. Appl. Mech. Eng. 82:341-364.

- Noor AK, Malik M** (1999) Accurate determination of transverse normal stresses in sandwich panels subjected to thermomechanical loadings. *Comp. Meth. Appl. Mech. Eng.* (to appear).
- Panc V** (1975) Theories of elastic plates. Noordhoff, Leyden, Netherlands (translated from Czech).
- Pandya BN, Kant T** (1987) A consistent refined theory for flexure of a symmetric laminate. *Mech Res Commun* 14(2):107-113.
- Reddy JN** (1997) Mechanics of laminated composite plates - theory and analysis. CRC Press, Boca Raton, FL.
- Reddy JN** (1984) A simple higher-order theory for laminated composite plates. *J. Appl. Mech.* 51:745-752.
- Reddy JN, Barbero EJ, Teply JL** (1989) A plate bending element based on a generalized laminate plate theory. *Int. J. Num. Meth. Eng.* 28:2275-2292.
- Reddy JN, Robbins DH** (1994) Structural theories and computational models for composite laminates. *Appl. Mech. Revs.* 47(6), Pt. 1:147-170.
- Robbins DH, Reddy JN** (1996) Variable kinematic modeling of laminated composite plates. *Int. J. Num. Meth. Eng.* 39:2283-2317.
- Rolfes R, Noor AK, Sparr H** (1998) Evaluation of transverse thermal stresses in composite plates based on first-order shear deformation theory. *Comp. Meth. Appl. Mech. Eng.* 167:355-368.
- Rolfes R, Rohwer K** (1997) Improved transverse shear stresses in composite finite elements based on first-order shear deformation theory. *Int. J. Num. Meth. Eng.* 40: 51-60.

Stein M (1986) Nonlinear theory for plates and shells including the effects of transverse shearing. *AIAA J.* 24(9):1537-1544

Touratier M (1991) An efficient standard plate theory. *Inter. Eng. Sci.* 29:901-916.

Turvey GJ, Marshall IH (1995) Buckling and postbuckling of composite plates. Chapman & Hall, London.

Whitney JM (1973) Shear correction factors for orthotropic laminates under static load. *J. Appl. Mech.* 40:302-304.

Whitney JM (1969) The effect of transverse shear deformation on the ending of laminated plates. *J. Compos. Mat.* 3:534-547.

Table 1 – Two-dimensional modeling approaches used in the numerical studies.

Model	Description	Through-the-Thickness In-Plane Displacement Assumptions (U_α in Eqs. 1)	Constraint Conditions on Stresses	Reference
1	First-order shear deformation theory	$x_3 \phi_\alpha$	$\sigma_{33} = 0$	
2	Third-order shear deformation theory	$-x_3 \partial_\alpha w^o$ $+ x_3 \left[1 - \frac{4}{3} \left(\frac{x_3}{h} \right)^2 \right] \phi_\alpha^o$	$\sigma_{33} = 0$ throughout the thickness, and $\sigma_{\alpha 3} = 0$ at top and bottom surfaces	Reddy, 1984
3	Higher-order shear deformation theory	$-x_3 \partial_\alpha w^o$ $+ \frac{h}{\pi} \sin \frac{\pi x_3}{h} \gamma_\alpha^o$		Touratier, 1991
4	Discrete layer theory	$\sum_{i=1}^K U_\alpha^{(\kappa)} \phi(\kappa, i)$ $\phi(\kappa, i) = 1$ for $\kappa = i$ $= \frac{x_3 - h_{\kappa-1}}{h_\kappa - h_{\kappa-1}}$ for $\kappa = i$	$\sigma_{33} = 0$ and $\sigma_{\alpha 3}$ are continuous at layer interfaces	Di Sciuva, 1986

Notes:

The transverse displacement w in the four models is assumed to be constant throughout the thickness of the laminate; total number of independent displacement parameters in each model = 5; the composite shear correction factors in the first-order shear deformation are obtained by using the procedure described in Chow, 1971, and Whitney, 1973; κ is the layer number $1 \leq \kappa \leq NL$; $h_{\kappa-1}, h_\kappa$ are the distances from the reference surface to the bottom and top surfaces of the κ th layer; the parameters $\phi_\alpha^o, \gamma_\alpha^o$ and $U_\alpha^{(\kappa)}$ are

functions of x_α only (see Eq. (1)), and $\partial_\alpha \equiv \frac{\partial}{\partial x_\alpha}$ ($\alpha = 1, 2$).

Table 2 – Types of panels and loadings for the results presented.

Panel Boundary Conditions	Lamination	Aspect Ratio, L_2 / L_1	Thickness Ratio, h / L_1	Figure for Loading Type		
				p	ΔT_0	ΔT_1
Clamped-Simply Supported	2-layer [0/90] antisymmetric	1	0.2	3	7	11
Fully Clamped	10-layer [0/90/.../0/90] antisymmetric	1	0.01	4	8	12
	10-layer [0/90/.../90/0] symmetric	1	0.1	5	9	13
	10-layer [0/90/.../0/90] antisymmetric	3	0.2	6	10	14

Clamped simply supported panel has the edges $x_1 = 0, L_1$ clamped and the other two supply supported. Clamped panel $p, \Delta T_0, \Delta T_1 = (p_0, \bar{T}_0, x_3 \bar{T}_1) \sin \frac{\pi x_1}{L_1} \sin \frac{\pi x_2}{L_2}, \bar{T}_0 = 1, \bar{T}_1 = 1$.

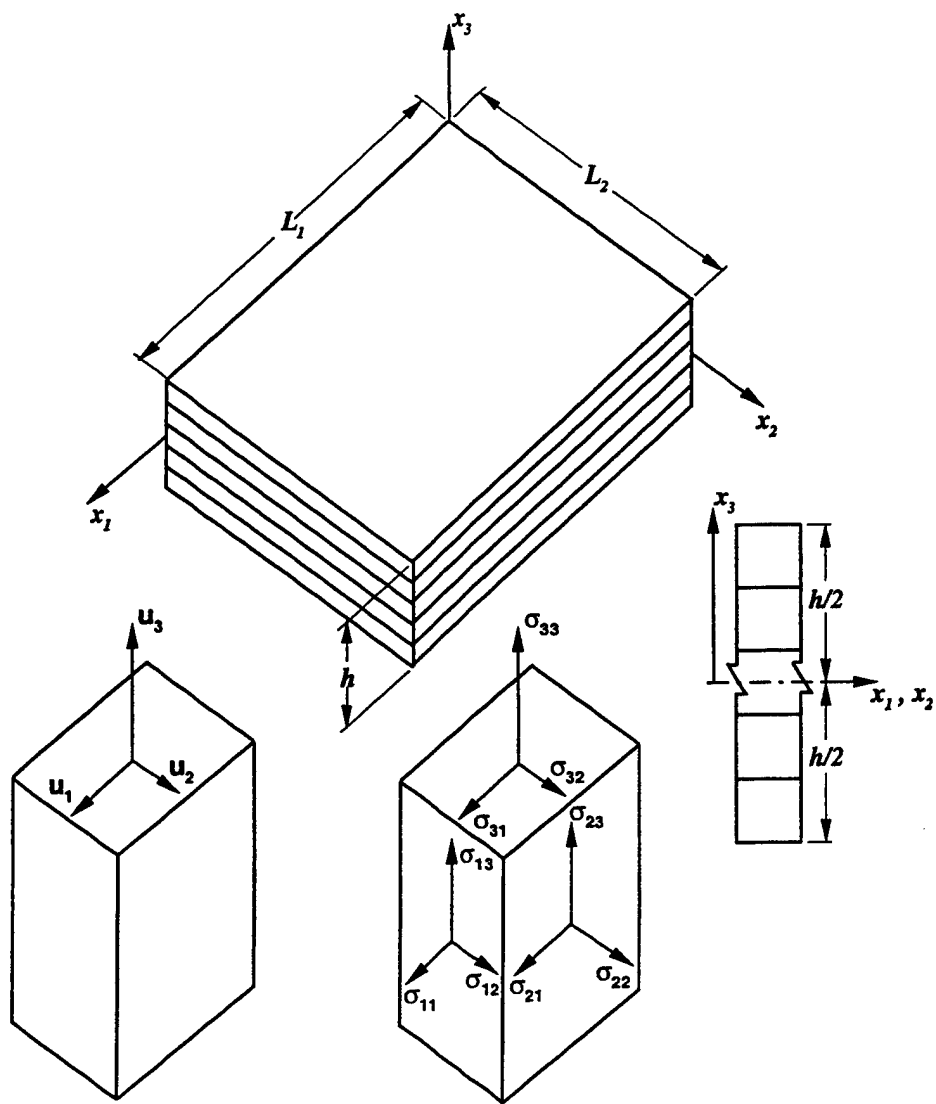


Figure 1

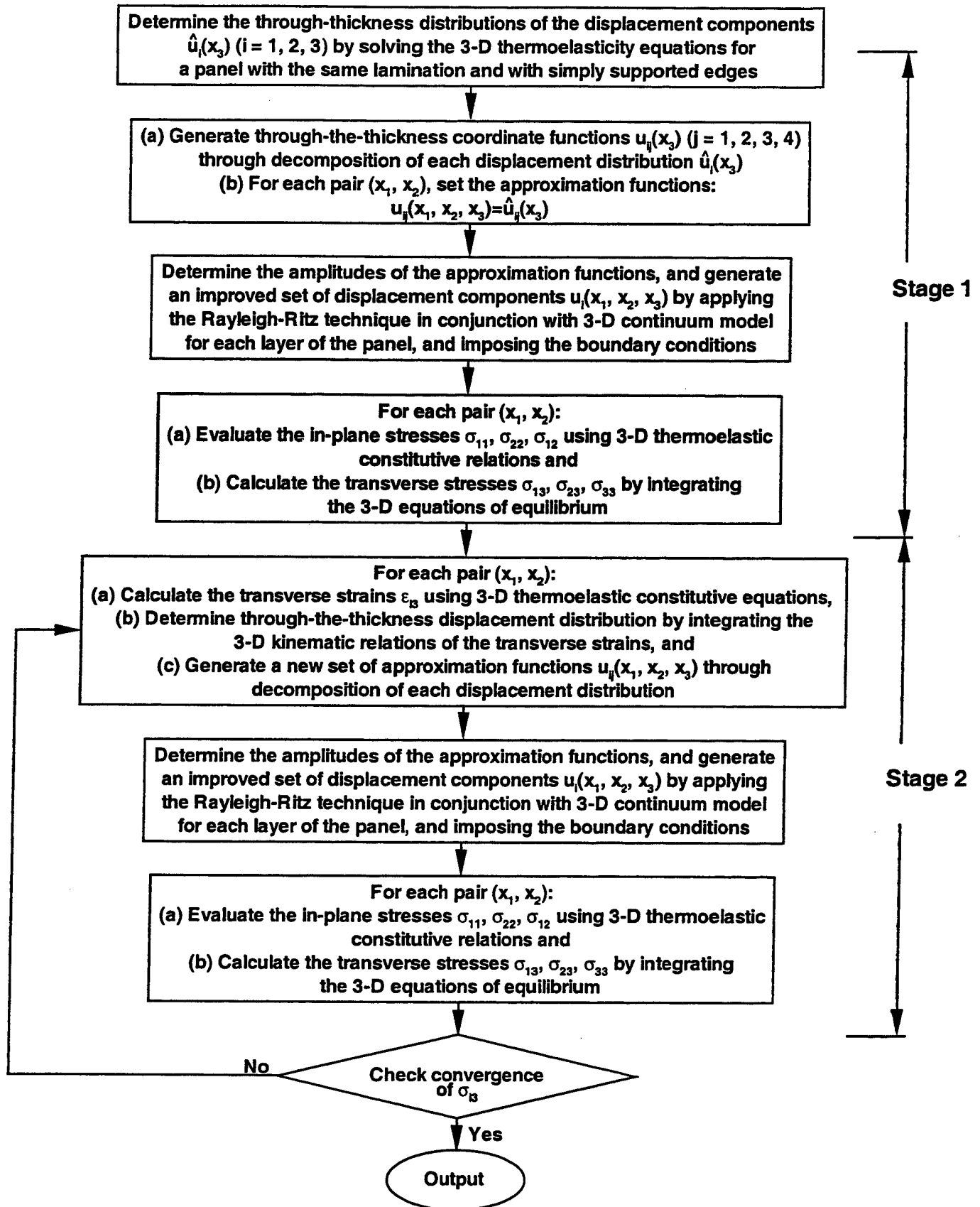


Figure 2

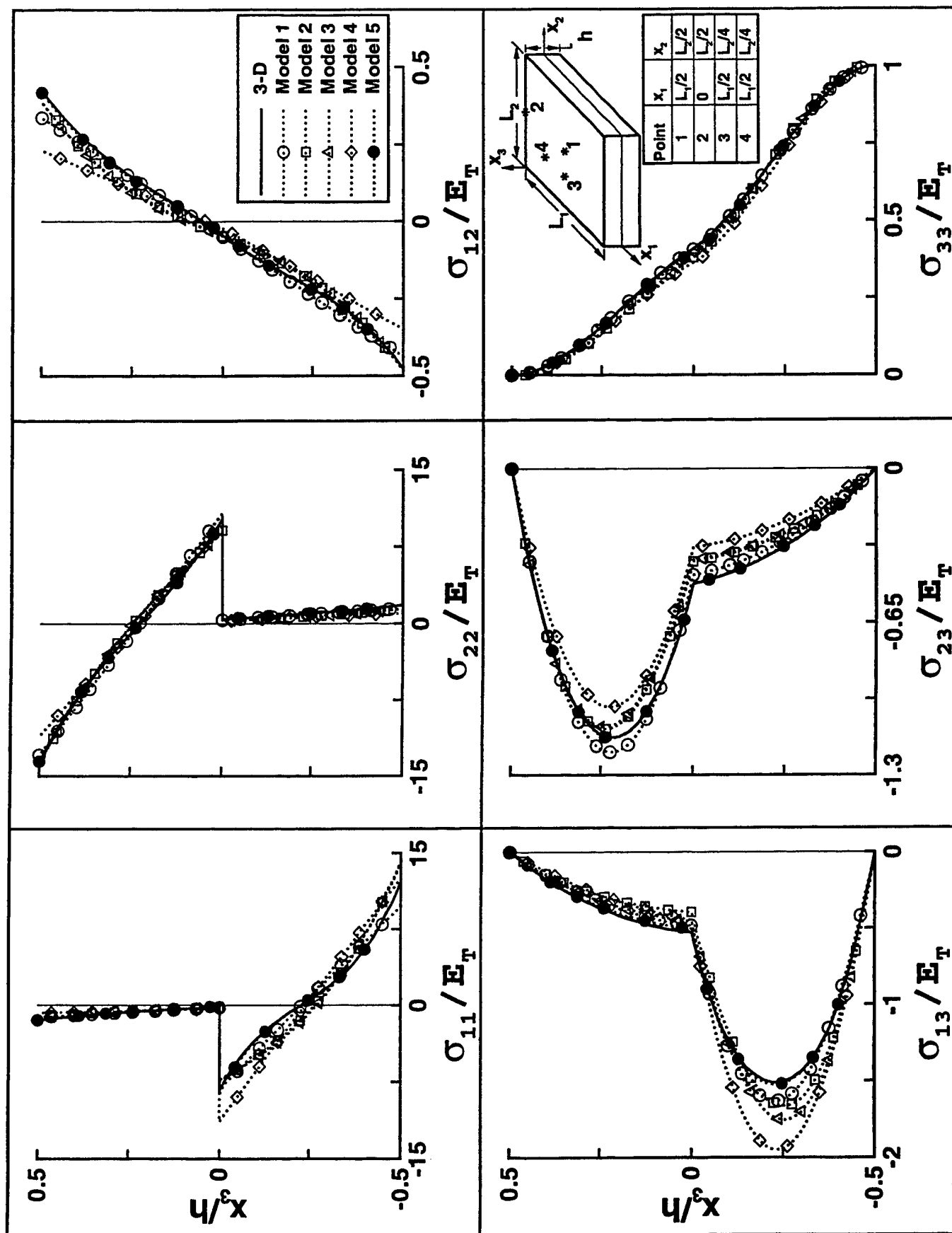


Figure 3

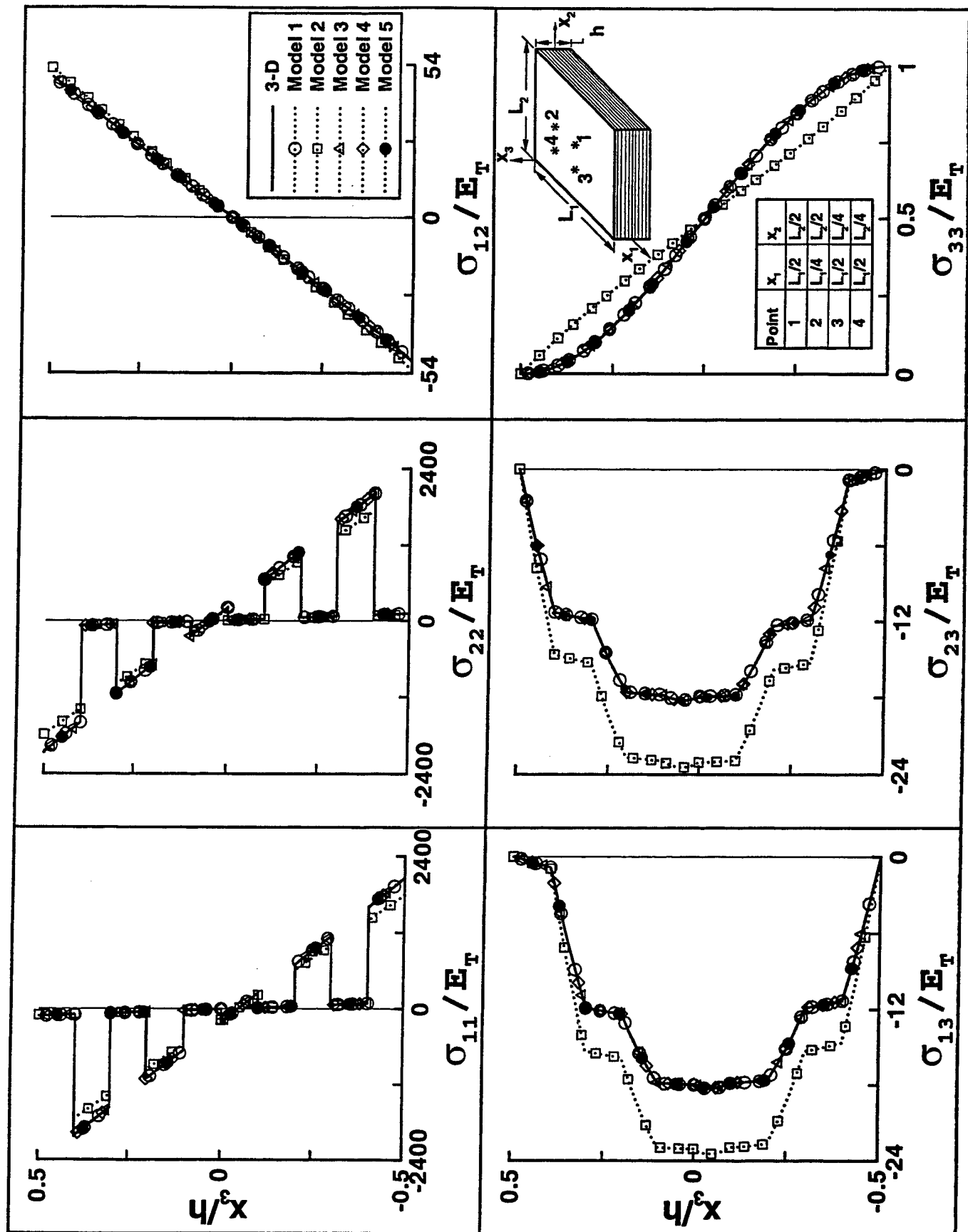


Figure 4

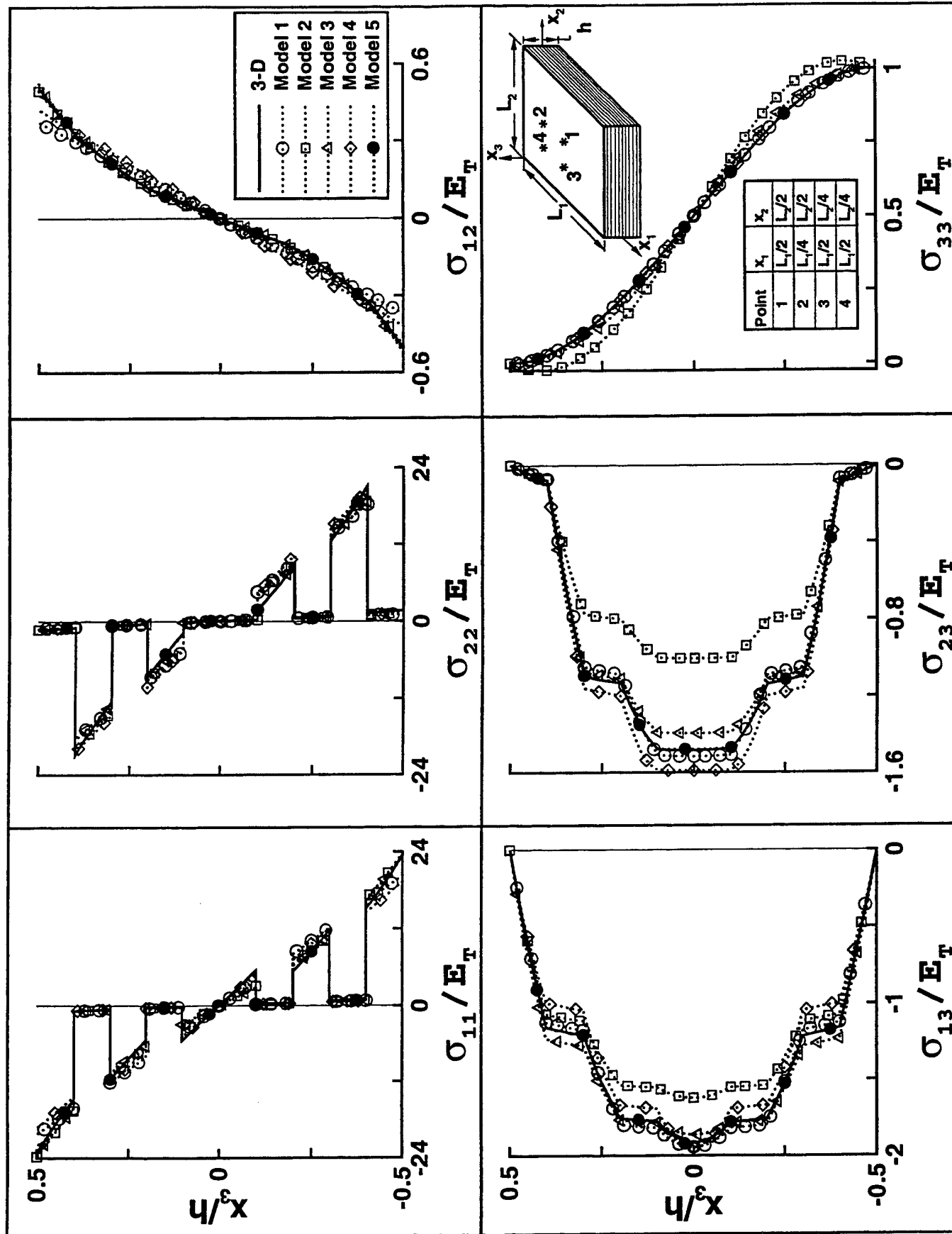


Figure 5

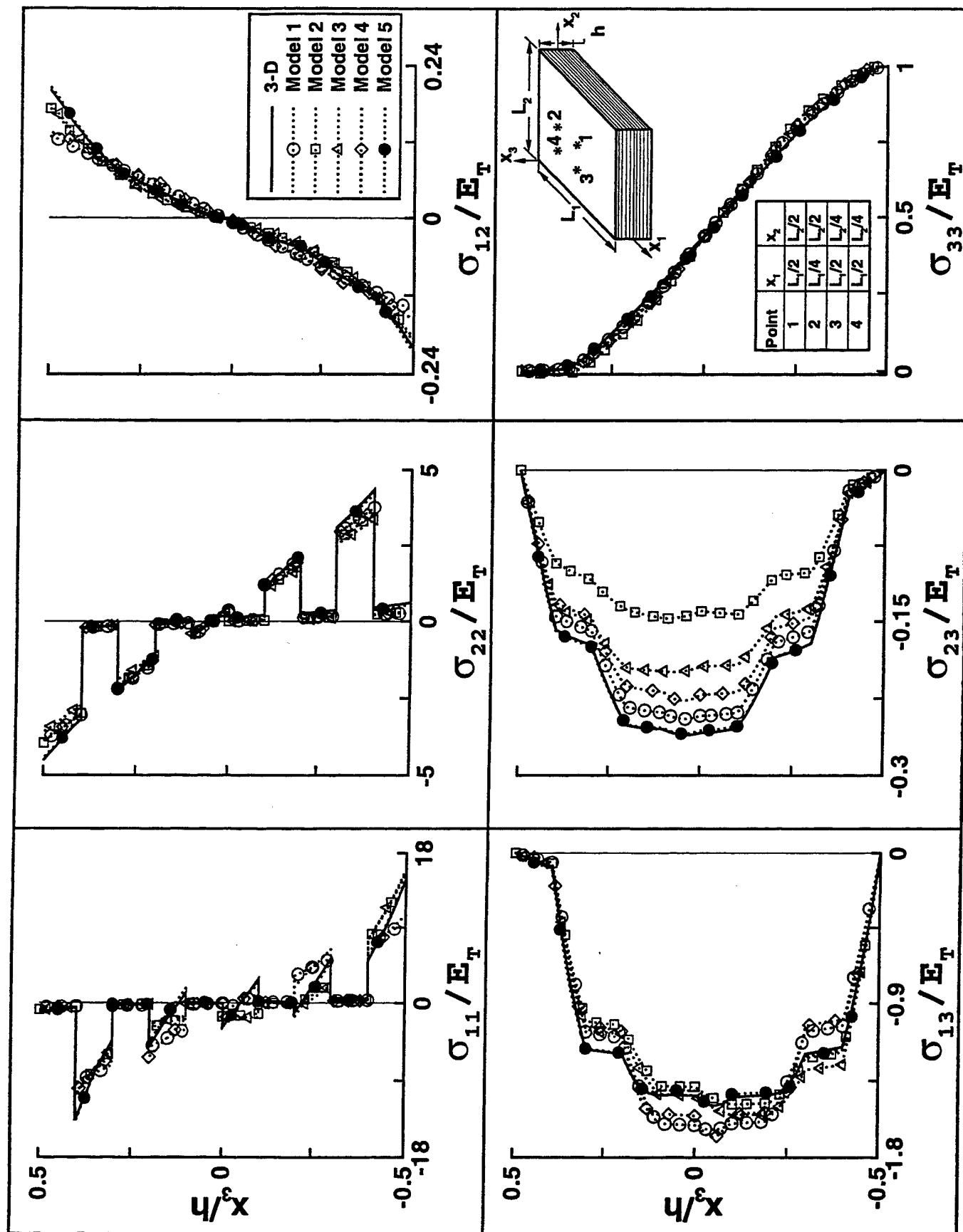


Figure 6

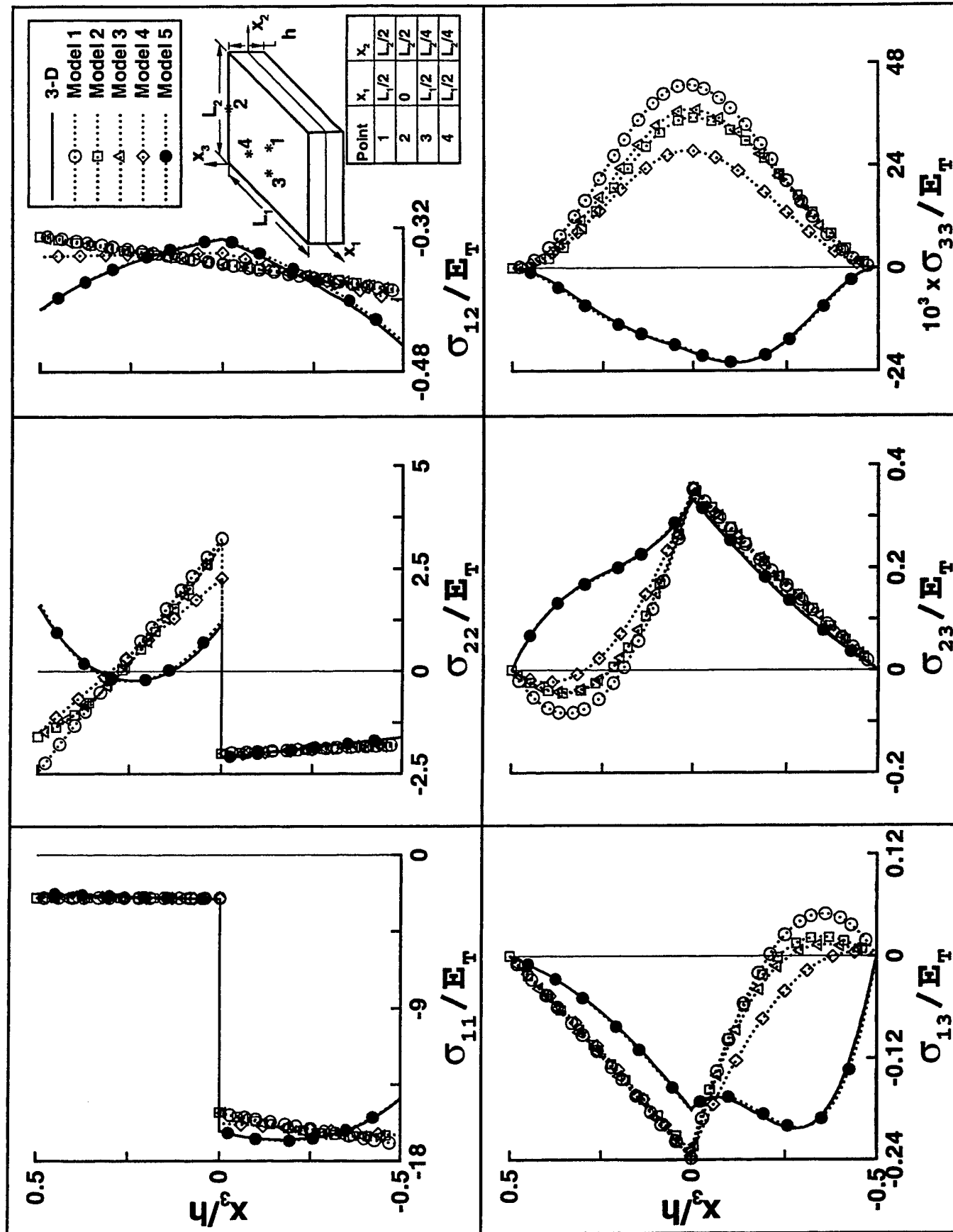


Figure 7

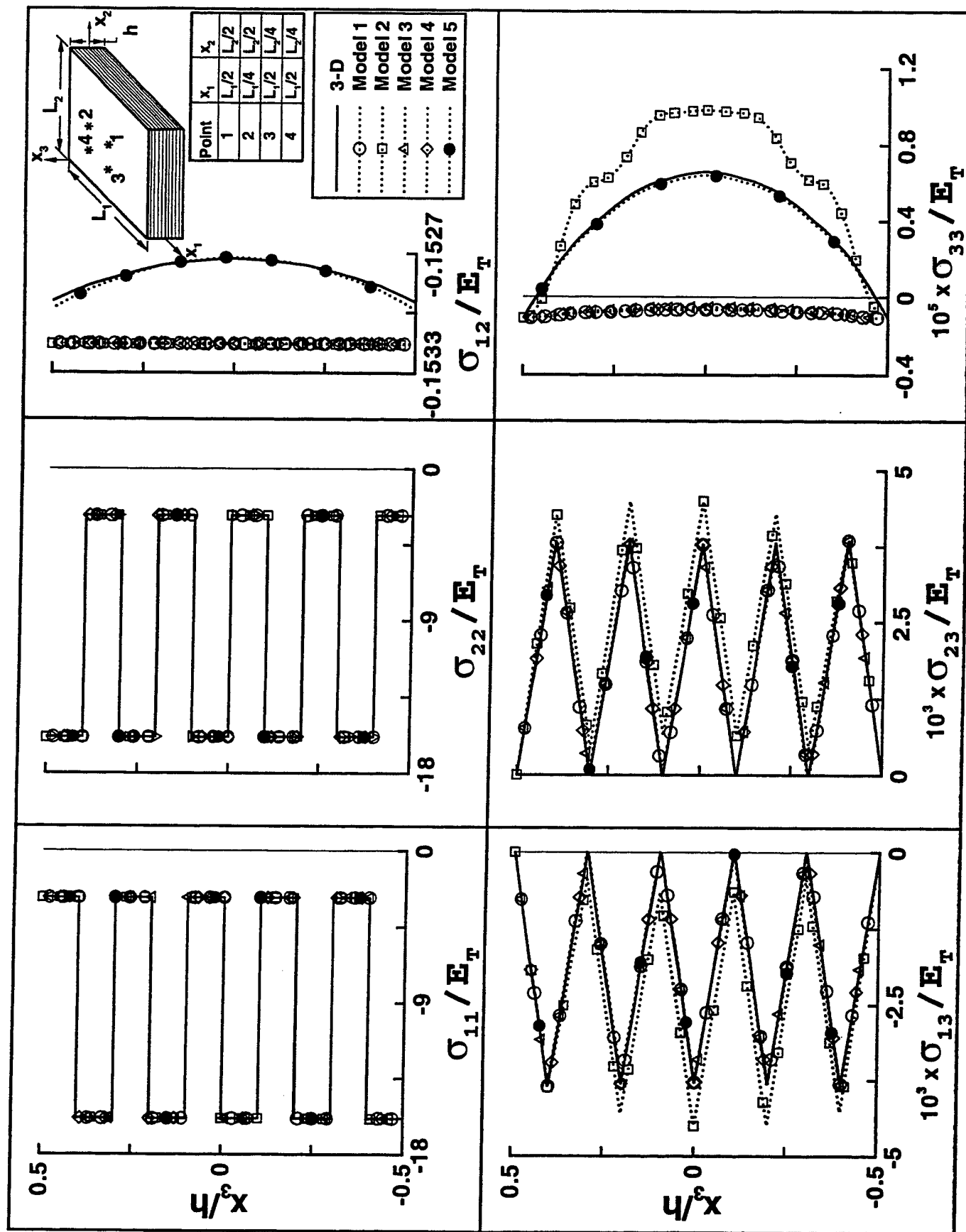


Figure 8

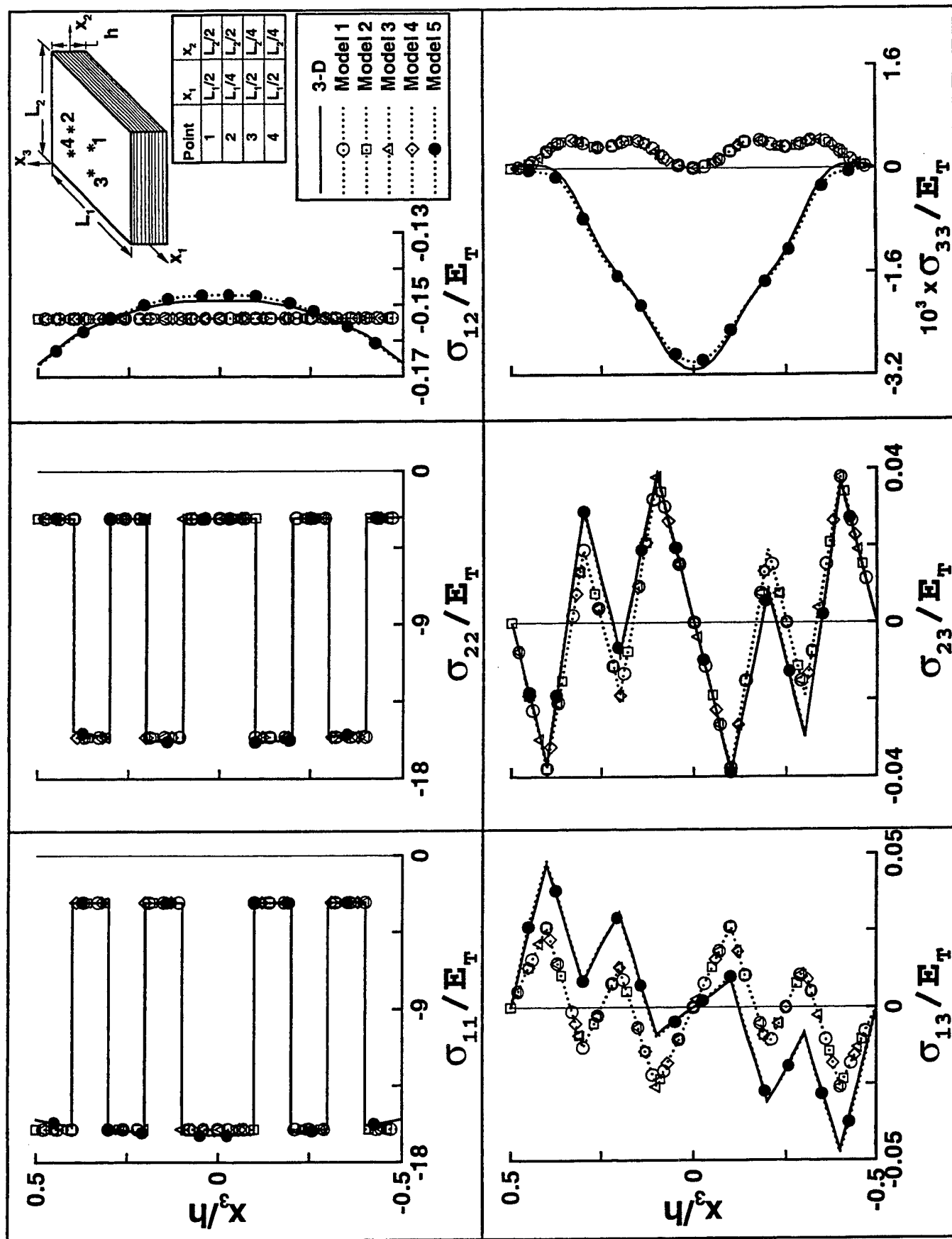


Figure 9

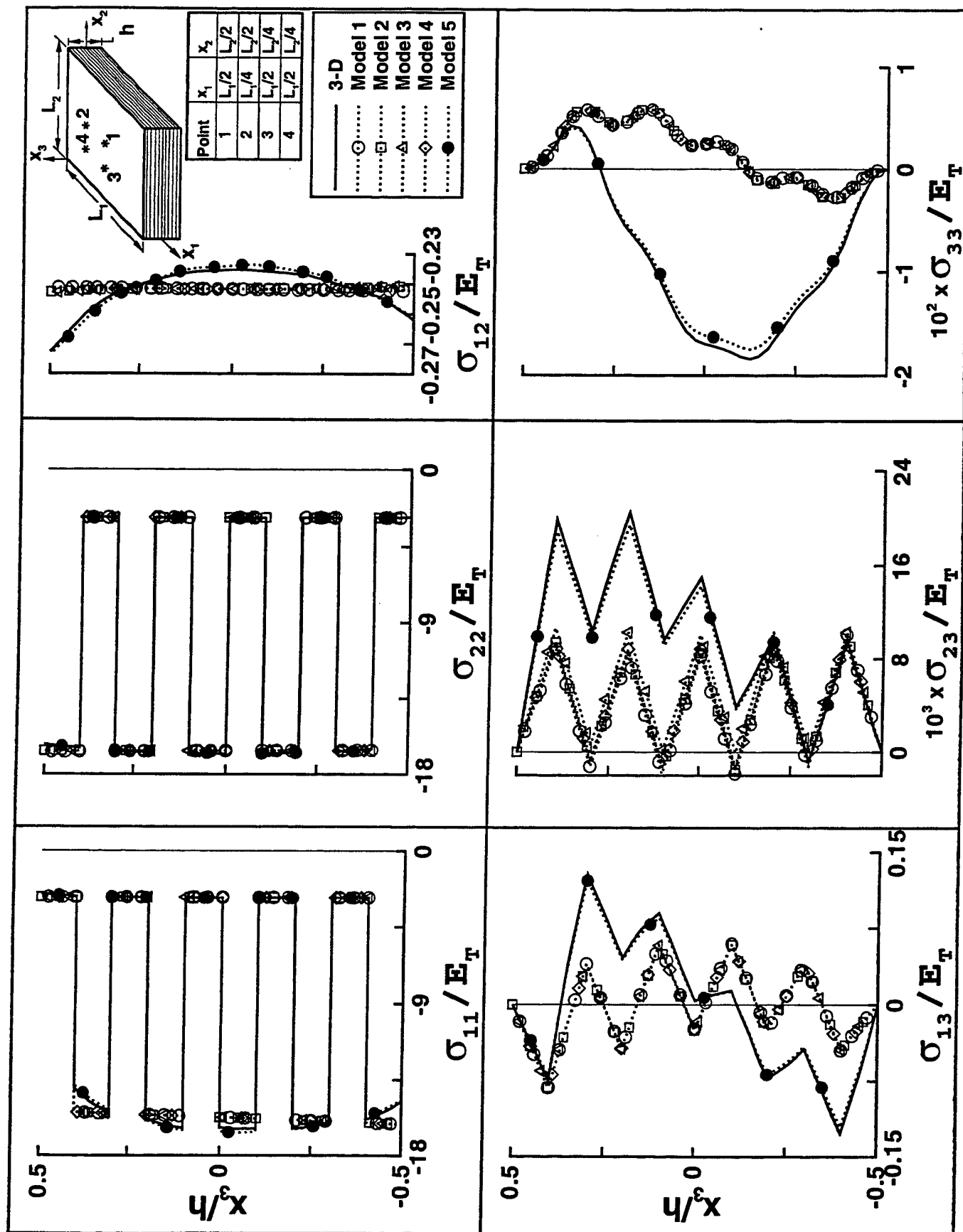


Figure 10

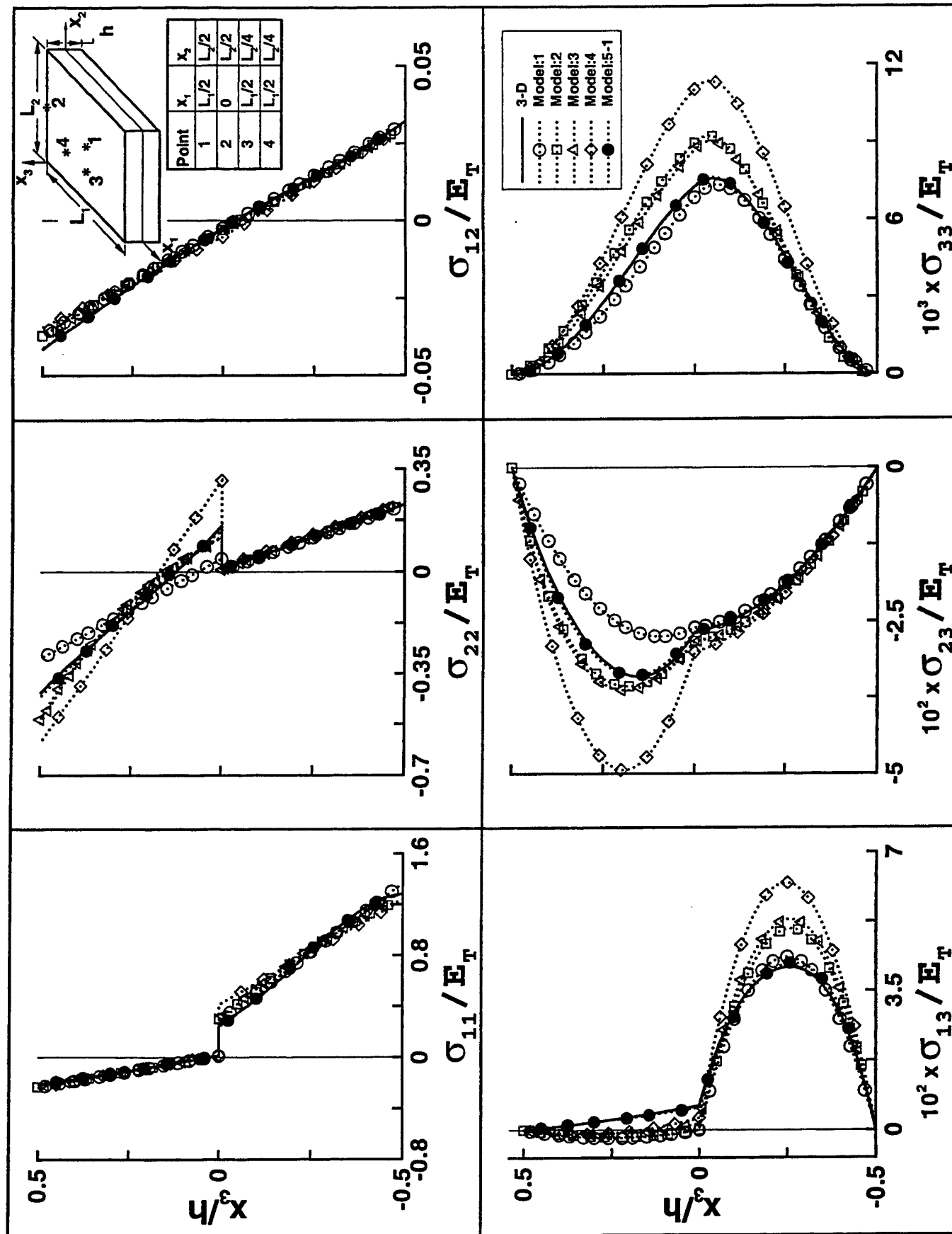


Figure 11

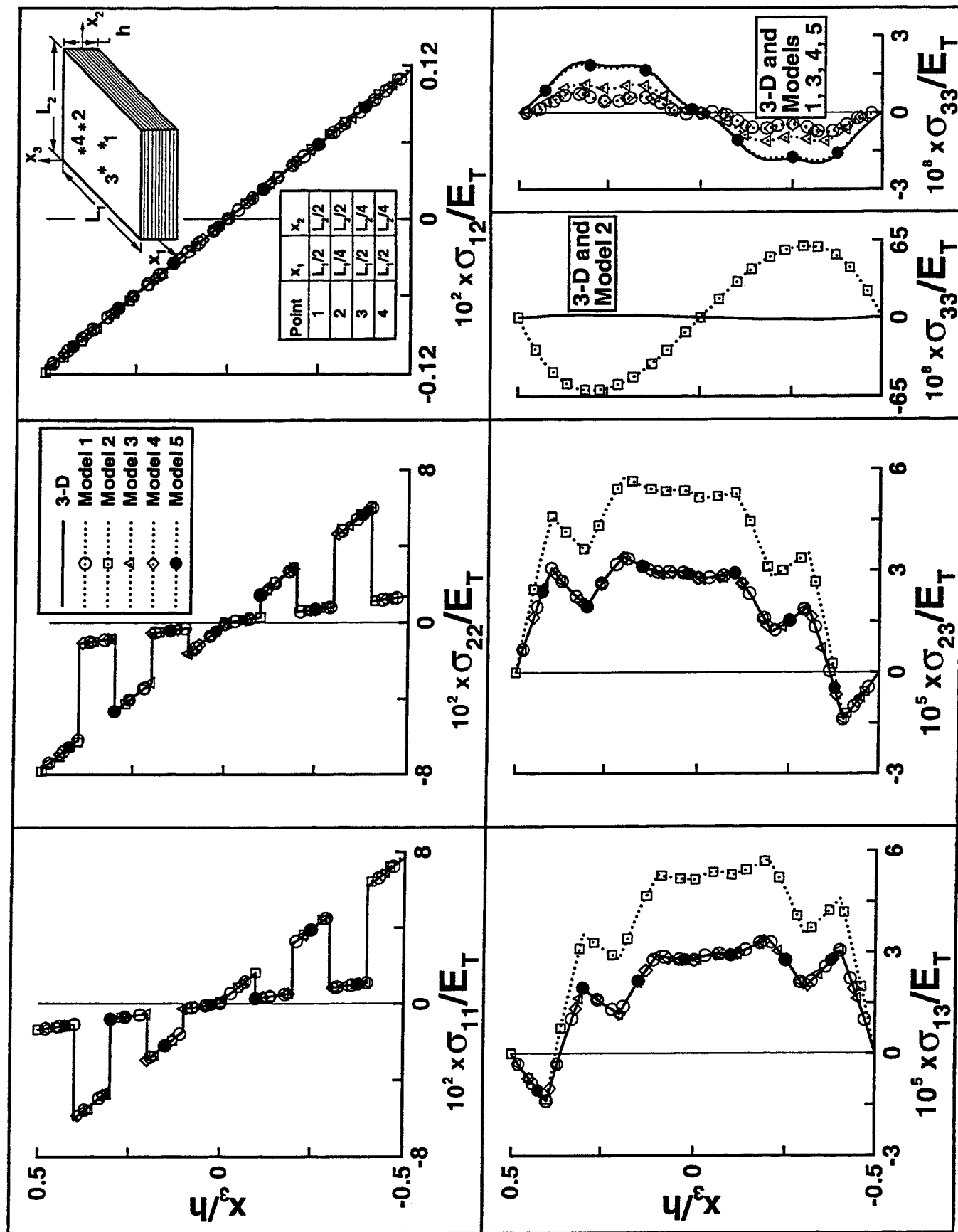


Figure 12

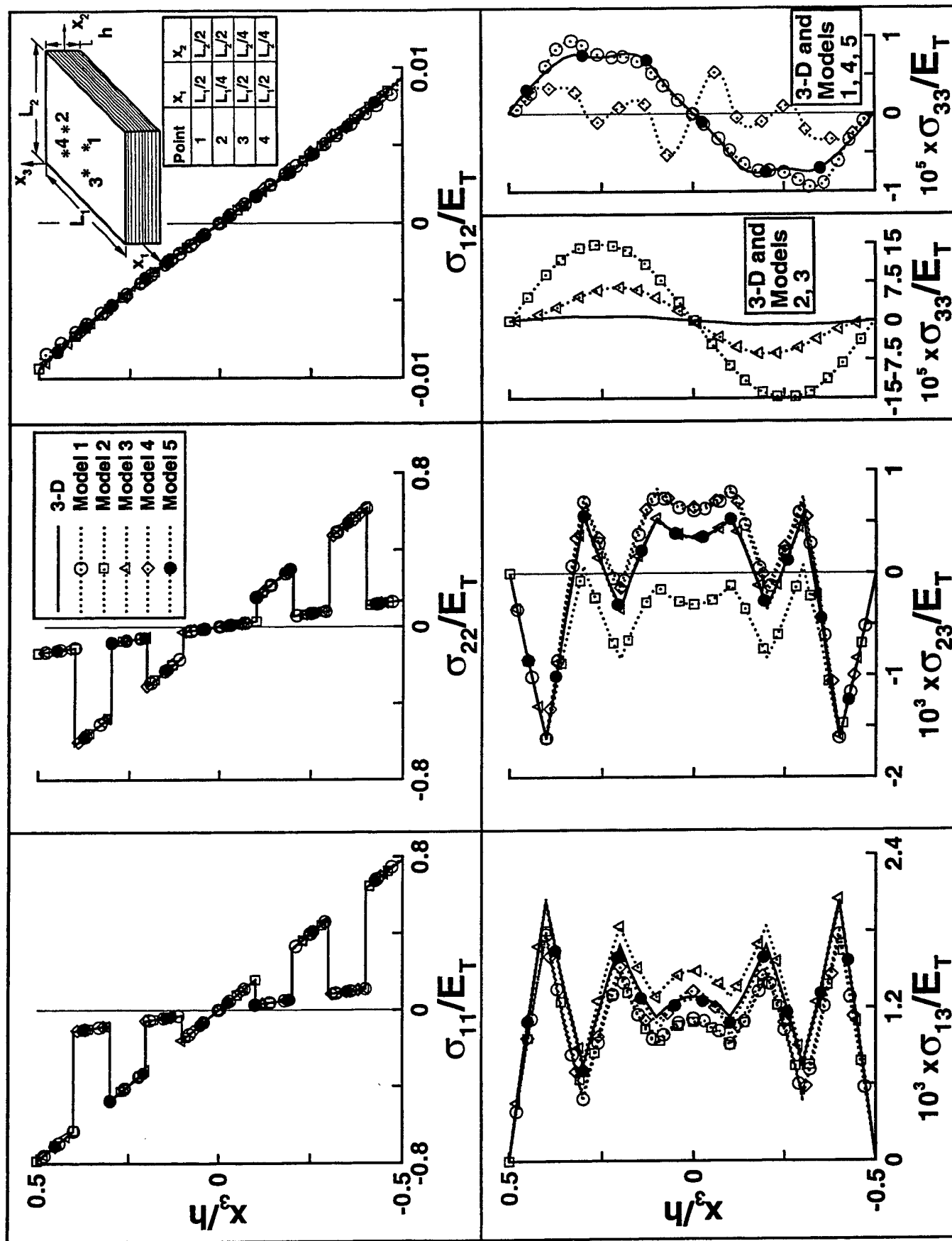


Figure 13

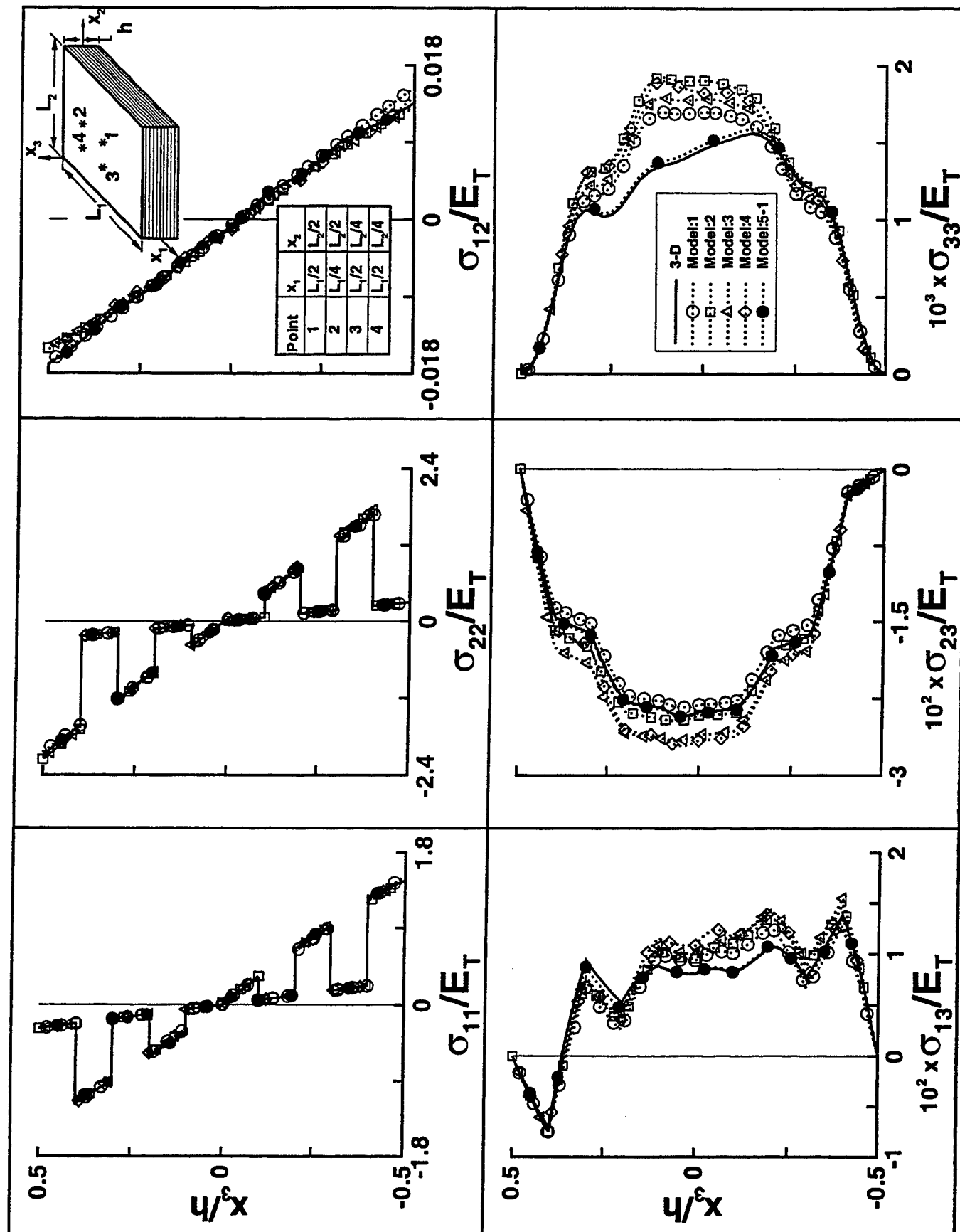


Figure 14

LIST OF FIGURES

Fig. 1 Laminated panel: geometry, coordinate axes, and sign convention for displacements and stresses.

Fig. 2 Flowchart of the computational procedure based on the predictor-corrector approach.

Fig. 3 Accuracy of stress components obtained by different models. Square, two-layer cross-ply panel, with two opposite edges simply supported and the other two clamped, subjected to the static loading $p = p_0 \sin \frac{\pi x_1}{L_1} \sin \frac{\pi x_2}{L_2}$, $h/L_1 = 0.2$. Stress components are shown at different locations: $\sigma_{11}, \sigma_{22}, \sigma_{33}$ at the point 1; σ_{13} at the point 2; σ_{23} at the point 3; and σ_{12} at the point 4.

Fig. 4 Accuracy of stress components obtained by different models. Square, ten-layer antisymmetrically laminated cross-ply panel with all edges clamped, subjected to static loading $p = p_0 \sin \frac{\pi x_1}{L_1} \sin \frac{\pi x_2}{L_2}$, $h/L_1 = 0.01$. Stress components are shown at different locations: $\sigma_{11}, \sigma_{22}, \sigma_{33}$ at the point 1; σ_{13} at the point 2; σ_{23} at the point 3; and σ_{12} at the point 4.

Fig. 5 Accuracy of stress components obtained by different models. Square, ten-layer symmetrically laminated cross-ply panel with all edges clamped, subjected to static loading $p = p_0 \sin \frac{\pi x_1}{L_1} \sin \frac{\pi x_2}{L_2}$, $h/L_1 = 0.1$. Stress components are shown at different locations: $\sigma_{11}, \sigma_{22}, \sigma_{33}$ at the point 1; σ_{13} at the point 2; σ_{23} at the point 3; and σ_{12} at the point 4.

Fig. 6 Accuracy of stress components obtained by different models. Rectangular, ten-layer antisymmetrically laminated cross-ply panel with all edges clamped, subjected to static loading $p = p_0 \sin \frac{\pi x_1}{L_1} \sin \frac{\pi x_2}{L_2}$, $L_2 / L_1 = 3$, $h / L_1 = 0.2$. Stress components are shown at different locations: $\sigma_{11}, \sigma_{22}, \sigma_{33}$ at the point 1; σ_{13} at the point 2; σ_{23} at the point 3; and σ_{12} at the point 4.

Fig. 7 Accuracy of stress components obtained by different models. Square, two-layer cross-ply panel with all edges clamped, subjected to uniform temperature change $\Delta T_0 = T_0 \sin \frac{\pi x_1}{L_1} \sin \frac{\pi x_2}{L_2}$, $h / L_1 = 0.2$. Stress components are shown at different locations: $\sigma_{11}, \sigma_{22}, \sigma_{33}$ at the point 1; σ_{13} at the point 2; σ_{23} at the point 3; and σ_{12} at the point 4.

Fig. 8 Accuracy of stress components obtained by different models. Square, ten-layer antisymmetrically laminated cross-ply panel with all edges clamped, subjected to uniform temperature change: $\Delta T_0 = T_0 \sin \frac{\pi x_1}{L_1} \sin \frac{\pi x_2}{L_2}$, $h / L_1 = 0.01$. Stress components are shown at different locations: $\sigma_{11}, \sigma_{22}, \sigma_{33}$ at the point 1; σ_{13} at the point 2; σ_{23} at the point 3; and σ_{12} at the point 4.

Fig. 9 Accuracy of stress components obtained by different models. Square, ten-layer symmetrically laminated cross-ply panel with all edges clamped, subjected to uniform temperature change: $\Delta T_0 = T_0 \sin \frac{\pi x_1}{L_1} \sin \frac{\pi x_2}{L_2}$, $h / L_1 = 0.1$. Stress

components are shown at different locations: $\sigma_{11}, \sigma_{22}, \sigma_{33}$ at the point 1; σ_{13} at the point 2; σ_{23} at the point 3; and σ_{12} at the point 4.

Fig. 10 Accuracy of stress components obtained by different models. Rectangular, ten-layer antisymmetrically laminated cross-ply panel with all edges clamped, subjected to uniform temperature change $\Delta T_0 = T_0 \sin \frac{\pi x_1}{L_1} \sin \frac{\pi x_2}{L_2}$, $L_2 / L_1 = 3$, $h / L_1 = 0.2$.

Stress components are shown at different locations: $\sigma_{11}, \sigma_{22}, \sigma_{33}$ at the point 1; σ_{13} at the point 2; σ_{23} at the point 3; and σ_{12} at the point 4.

Fig. 11 Accuracy of stress components obtained by different models. Square, two-layer cross-ply panel with all edges clamped, subjected to temperature gradient

$$\Delta T_1 = x_3 T_1 \sin \frac{\pi x_1}{L_1} \sin \frac{\pi x_2}{L_2}, \quad h / L_1 = 0.2. \text{ Stress components are shown at different}$$

locations: $\sigma_{11}, \sigma_{22}, \sigma_{33}$ at the point 1; σ_{13} at the point 2; σ_{23} at the point 3; and σ_{12} at the point 4.

Fig. 12 Accuracy of stress components obtained by different models. Square, ten-layer antisymmetrically laminated cross-ply panel with all edges clamped, subjected to

$$\text{temperature gradient } \Delta T_1 = x_3 T_1 \sin \frac{\pi x_1}{L_1} \sin \frac{\pi x_2}{L_2}, \quad h / L_1 = 0.01. \text{ Stress components}$$

are shown at different locations: $\sigma_{11}, \sigma_{22}, \sigma_{33}$ at the point 1; σ_{13} at the point 2; σ_{23} at the point 3; and σ_{12} at the point 4.

Fig. 13 Accuracy of stress components obtained by different models. Square, ten-layer symmetrically laminated cross-ply panel with all edges clamped, subjected to

temperature gradient: $\Delta T_1 = x_3 T_1 \sin \frac{\pi x_1}{L_1} \sin \frac{\pi x_2}{L_2}$, $h/L_1 = 0.1$. Stress components

are shown at different locations: $\sigma_{11}, \sigma_{22}, \sigma_{33}$ at the point 1; σ_{13} at the point 2; σ_{23} at the point 3; and σ_{12} at the point 4.

Fig. 14 Accuracy of stress components obtained by different models. Rectangular, ten-layer antisymmetrically laminated cross-ply panel with all edges clamped, subjected to temperature gradient $\Delta T_1 = x_3 T_1 \sin \frac{\pi x_1}{L_1} \sin \frac{\pi x_2}{L_2}$, $L_2/L_1 = 3$, $h/L_1 = 0.2$. Stress components are shown at different locations: $\sigma_{11}, \sigma_{22}, \sigma_{33}$ at the point 1; σ_{13} at the point 2; σ_{23} at the point 3; and σ_{12} at the point 4.

DISTRIBUTION LIST

- 1 - 3 Major Brian Sanders
 Department of the Air Force
 Air Force Office of Scientific Research
 801 North Randolph Street, Room 732
 Washington, DC 20011
- 4 - 5 SEAS Postaward Research Administration
- 6 - 7 A. K. Noor
 Center for Advanced Computation Technology
 University of Virginia
 NASA Langley Research Center, MS 201
 Hampton, VA 23681
- 8 N. J. Garber
- 9 - 10 M. Rodeffer, Clark Hall
- 11 SEAS Preaward Research Administration File

JO#0202:ph